NASA Contractor Report 3516

Rotary Balance Data for an F-15 Model With Conformal Fuel Tanks for an Angle-of-Attack Range of 8° to 90°

Billy Barnhart

CONTRACT NAS1-16205
MAY 1982

NASA

NASA Contractor Report 3516

Rotary Balance Data for an F-15 Model With Conformal Fuel Tanks for an Angle-of-Attack Range of 8° to 90°

Billy Barnhart
Bihrle Applied Research, Inc.
Jericho, New York

Prepared for
Langley Research Center
under Contract NAS1-16205

National Aeronautics
and Space Administration

Scientific and Technical
Information Branch

1982

SUMMARY

Aerodynamic characteristics obtained in a rotational flow environment, utilizing a rotary balance located in the Langley Spin Tunnel, are presented in plotted form for a 1/12-scale F-15 airplane model with conformal fuel tanks. The configurations tested included the build-up of airplane components and the basic airplane with various control deflections. Data are presented for all configurations without analysis for an angle-of-attack range of 8^{o} to 90^{o}, and clockwise and counter-clockwise rotations covering an $\Omega b/2V$ range from 0 to 0.4. Selected configurations are presented over an extended $\Omega b/2V$ range from 0 to 0.9. Analysis of these data is presented in another report.

INTRODUCTION

The NASA Langley Research Center is conducting an investigation to determine the influence of the addition of conformal fuel tanks on the spin and recovery characteristics of the Air Force/McDonnell Douglas F-15 airplane. As a part of this effort, rotary balance wind tunnel force tests of the F-15 airplane were conducted to establish a data base for the analysis of the free-spinning model results. A rotary balance is used to measure the forces and moments acting on an airplane while it is subjected to steady rotational flow conditions.

A 1/12-scale model of the F-15 was tested with and without conformal fuel tanks on the rotary balance located in the Langley Spin Tunnel. Data were obtained for the basic airplane with various control settings and for build-up of airplane components. This report presents the data obtained for these configurations for the CFT configured model, without analysis. Reference 1 presents an analysis of the influence of conformal fuel tanks on the aerodynamic characteristics of the basic airplane, as presented herein, as well as the effect of control deflections, component build-up, and predicted spin modes. Reference 2 contains the data measured for the airplane without CFT's.

SYMBOLS

The units for physical quantities used herein are presented in the International System of Units and U.S. Customary Units. The measurements were all made in the U.S. Customary Units; equivalent dimensions were determined by using the conversion factors found in reference 3.

b wing span, m (ft)

$\bar{c}$ mean aerodynamic chord, m (ft)

C_A axial-force coefficient, $\frac{\text{Axial force}}{qS}$

C_N normal-force coefficient, $\frac{\text{Normal force}}{qS}$

C_Y side-force coefficient, $\frac{\text{Side force}}{qS}$

C_ℓ rolling-moment coefficient, $\frac{\text{Rolling moment}}{qSb}$

C_m pitching-moment coefficient, $\frac{\text{Pitching moment}}{q S \bar{c}}$

C_n yawing-moment coefficient, $\frac{\text{Yawing moment}}{qSb}$

q free-stream dynamic pressure, N/m^2 (lb/ft^2)

S wing area, m^2 (ft^2)

V free-stream velocity, m/sec (ft/sec)

α angle of attack, deg

β angle of sideslip, deg

Ω angular velocity about spin axis, rad/sec

$\frac{\Omega b}{2V}$ spin coefficient, positive for clockwise spin

δ_a aileron deflection, positive when right aileron is down $(\delta_{a_{right}} - \delta_{a_{left}})/2$, deg

δ_d differential horizontal tail deflection, positive when right surface is down, $(\delta_{d_{right}} - \delta_{d_{left}})/2$, deg

δ_e symmetrical horizontal tail deflection, positive when trailing edge is down, deg

δ_r rudder deflection, positive when trailing edge is to the left, deg

Abbreviations:

CFT conformal fuel tanks

cg center of gravity

rpm revolutions per minute

SR spin radius

TE trailing edge

TEST EQUIPMENT

A rotary balance measures the forces and moments acting on a model while it is subjected to rotational flow conditions. The historical background for this apparatus is discussed in reference 4. A photograph and sketch of the rotary balance apparatus installed in the Langley Spin Tunnel are shown in figures 1 and 2, respectively. The system's rotary arm, which rotates about a vertical axis at the tunnel center, is supported by a horizontal boom and is driven by a motor mounted external to the test section.

The test model is mounted on a strain gauge balance affixed to the bottom of the rotary balance apparatus. Controls located outside of the tunnel are used to activate motors on the rig, which position the model to the desired attitude. The angle-of-attack range of the rig is 0 to 90 degrees, and the sideslip angle range is ±15 degrees. Spin radius and lateral displacement motors are used to position the moment center of the balance on, or a specific distance from, the spin axis. (This is done for each combination of angle of attack and sideslip angle.) It is customary to mount the balance to the model such that its moment center is at the location about which the aerodynamic moments are desired. Electrical current from the balance and to the motors on the rig is conducted through slip-rings located in the rig head. Figure 2 shows how the rig is positioned in angle of attack and sideslip.

The rig is capable of rotating up to 90 rpm in either direction. A range of $\frac{\Omega b}{2V}$ values can be obtained by adjusting rotational speed and/or tunnel air flow velocity. (Static aerodynamic forces and moments are obtained when $\Omega=0$.)

A NASA six-component strain gauge balance, mounted inside the model, is used to measure the normal, lateral, and longitudinal forces, and the yawing, rolling, and pitching moments acting about the model body axis.

The data acquisition, reduction, and presentation system is composed of a 12-channel scanner/ voltmeter, a mini-computer, a plotter, and a CRT display. This equipment permits data to be presented via on-line digital print-outs and/or graphical plots.

TEST PROCEDURES

Rotary aerodynamic data are obtained in two steps. First, the inertial forces and moments (tares) acting on the model at different attitudes and rotational speeds are measured. To accomplish this, the model is enclosed in a sealed spherical structure, which rotates with the model without touching it. In this manner, the air immediately surrounding the model is constrained to rotate with it, thus eliminating any aerodynamic forces and moments as would be present if the model were moving through a stationary air mass. As the rig is rotated at the desired attitude and rate, the inertial forces and moments generated by the model are measured and stored on

magnetic tape for later use.

The second step is to record force and moment data with the air on and with the enclosure removed. The tares, measured in step one, are then subtracted from these data, leaving only the aerodynamic forces and moments, which are converted to coefficient form and stored on magnetic tape.

MODEL

A 1/12-scale model of the Air Force/McDonnell Douglas F-15 fighter airplane was constructed of balsa and plywood. A three-view drawing of the model is shown in figure 3, dimensional characteristics of the basic model are listed in Table I, and a photograph of the model installed on the rotary balance located in the Langley Spin Tunnel is presented in figure 1.

The model was constructed such that the various airplane components were removable for component build-up tests. The model control surfaces could be set at any position prior to testing. The maximum deflections for the control surfaces were:

Rudder, deg	30 right, 30 left
Horizontal tail (TE)	25 up, 15 down
Aileron	20 up, 20 down

TEST CONDITIONS

The tests were conducted in the spin tunnel at a free-stream velocity of 7.62 m/sec (25 ft/sec), which corresponds

to a Reynolds number of approximately 211,000 based on model wing chord. All the configurations were tested through an angle-of-attack range of 8° to 90°, unless noted otherwise in Table II. The component build-up tests were all performed at a zero sideslip angle, while the basic airplane tests were performed at both zero and ten degrees sideslip angles. For all tests, the spin axis passed through the full-scale airplane nominal cg location for angles of attack above 30°. For angles of attack below 35°, the spin axis was set 0.28 b/2 forward of the cg location. For each angle of attack, data were obtained for $\frac{\Omega b}{2V}$ values of 0.1, 0.2, 0.3, and 0.4 in both clockwise and counter-clockwise directions, as well as for $\frac{\Omega b}{2V} = 0$ (static value). In addition, data were obtained for an $\frac{\Omega b}{2V}$ range through 0.9 for selected configurations.

DATA PRESENTATION

Table II identifies the configurations tested and the corresponding appendix figure numbers which present the aerodynamic data. The body-axis aerodynamic coefficients, plotted as a function of $\frac{\Omega b}{2V}$, are presented for each configuration in six sequentially numbered figures in the following order: C_n, C_ℓ, C_m, C_N, C_Y, C_A. Each figure, in turn, consists of four pages, which present the subject aerodynamic coefficient versus $\frac{\Omega b}{2V}$ for the following angles of attack and spin radii, unless noted otherwise in Table II.

a) α=8, 10, 12, 14, 16 deg SR=0.28 b/2

b) α=18, 20, 25, 30, 35 deg SR=0.28 b/2

c) α=30, 35, 40, 45, 50 deg SR=0

d) α=55, 60, 70, 80, 90 deg SR=0

All the moment data are presented for a cg position of $0.26\bar{c}$.

REFERENCES

1. Barnhart, B.: Analysis of Rotary Balance Data for the F-15 Airplane Including the Effect of Conformal Fuel Tanks. NASA CR-3479, 1982.
2. Barnhart, B.: F-15 Rotary Balance Data for an Angle-of-Attack Range of 8° to 90°. NASA CR-3478, 1982.
3. Standard for Metric Practice. E 380-79, American Society for Testing and Materials, c.1980.
4. Bihrle, William, Jr.; Bowman, James S., Jr.: The Influence of Wing, Fuselage, and Tail Design on Rotational Flow, Journal of Aircraft, Vol. 18, November 1981.

TABLE I.- DIMENSIONAL CHARACTERISTICS OF THE BASIC MODEL

Overall length, m (ft)	1.59 (5.21)
Wing:	
Area, m^2 (ft^2)	0.39 (4.16)
Span, m (ft)	1.09 (3.57)
Mean aerodynamic chord, m (ft)	0.41 (1.33)
Leading edge of $\bar{c}$, distance rearward of leading edge of theoretical root chord, m (ft)	0.22 (0.71)
Aspect ratio	3.01
Taper ratio	0.25
Leading edge sweep, deg	45
Dihedral, deg	-1
Incidence, deg	0
Airfoil section:	
Root	NACA 64A006.6
Tip	NACA 64A203
Ailerons:	
Area (each), m^2 (ft^2)	0.009(0.092)
Span (percent b/2)	25.3
Horizontal tails:	
Area (each), m^2 (ft^2)	0.036 (0.39)
Span (each), m (ft)	0.21 (0.68)
Mean aerodynamic chord, m (ft)	0.21 (0.69)
Aspect ratio	2.05
Taper ratio	0.34
Leading edge sweep, deg	50
Dihedral, deg	0
Hinge-line location, percent root chord	60.9
Airfoil section:	
Root	NACA 0005.5-64(Mod)
Tip	NACA 0002.5-64
Vertical tails:	
Area (each), m^2 (ft^2)	0.04 (0.43)
Span, m (ft)	0.26 (0.86)
Taper ratio	0.27
Leading edge sweep, deg	36.57
Airfoil section:	
Root	NACA 0005-64
Tip	NACA 0003.5-64
Rudders:	
Area (each), m^2 (ft^2)	0.006 (0.069)
Hinge-line location, percent chord	71.75

TABLE II.- CONFIGURATIONS TESTED AND FIGURE INDEX

(Unless noted otherwise, all configurations tested through α= 8 to 90°.)

FIGURE NO.	CONFIGURATION	β deg	δ_e deg	δ_d deg	δ_a deg	δ_r deg	REMARKS
A1-A6	Body alone	0	off	off	off	off	
A7-A12	Body, wing	↓	↓	↓	0	↓	
A13-A18	Body, wing, vertical tail	↓	↓	↓	↓	0	
A19-A24	Body, wing, horizontal tail	↓	0	0	↓	↓	
A25-A30	Basic	↓	↓	↓	↓	↓	
A31-A36	↓	+10	↓	↓	↓	↓	
A37-A42	↓	-10	↓	↓	↓	↓	
A43-A48	↓	0	-25	↓	↓	↓	*α= 30 to 90° only
A49-A54	↓	+10	↓	↓	↓	↓	* ↓
A55-A60	↓	0	0	+6	↓	↓	
A61-A66	↓	+10	↓	↓	↓	↓	
A67-A72	↓	0	↓	+11	↓	↓	
A73-A78	↓	+10	↓	↓	↓	↓	
A79-A84	↓	0	↓	+6	+20	↓	*α= 30 to 90° only
A85-A90	↓	+10	↓	↓	↓	↓	* ↓
A91-A96	↓	0	↓	↓	↓	-15	↓
A97-A102	↓	+10	↓	↓	↓	↓	↓
A103-A108	↓	0	↓	-6	-20	+30	↓
A109-A114	↓	+10	↓	↓	↓	↓	↓

*Not tested at α=35° and 45° with SR=0.

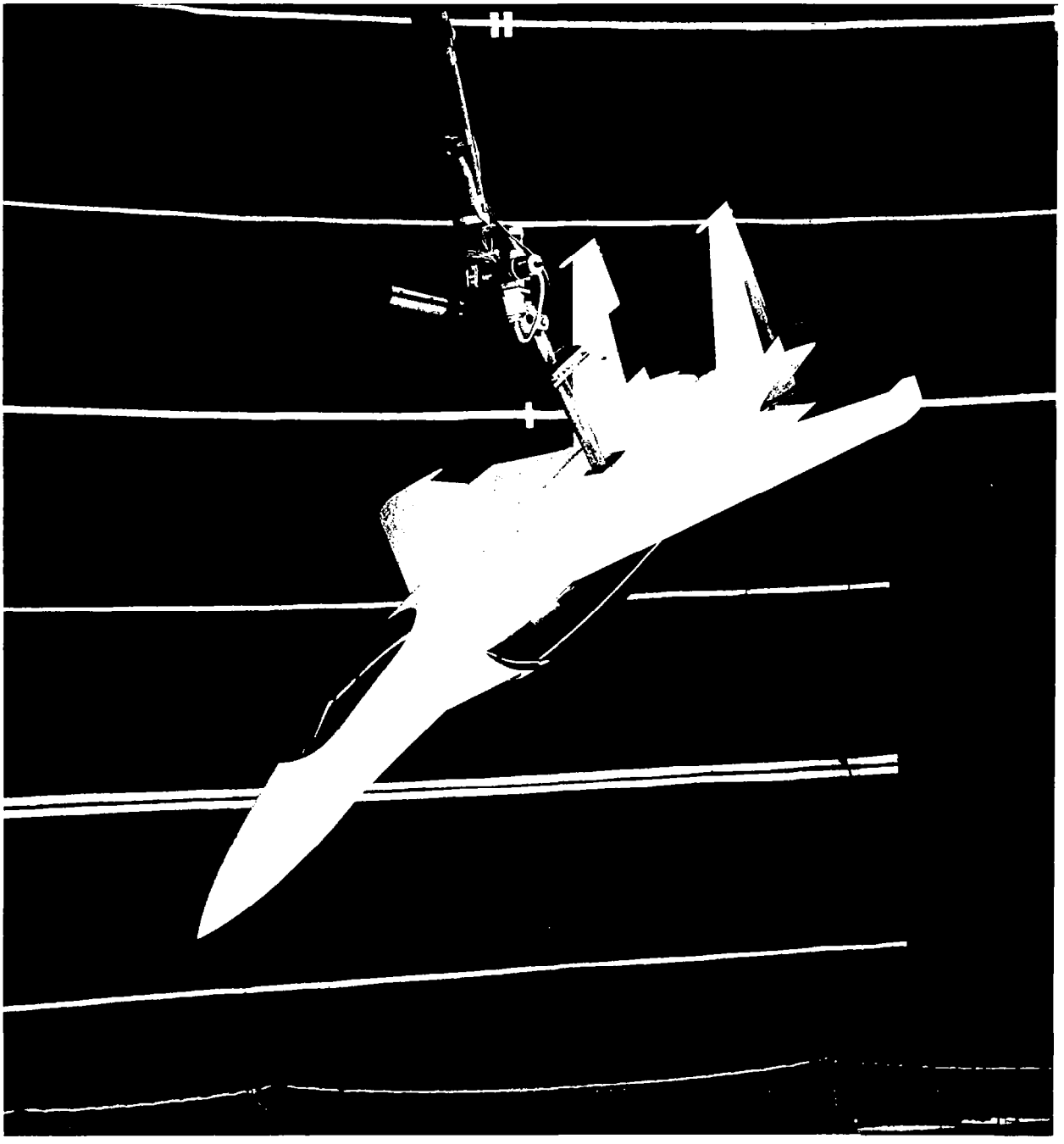

Figure 1.– Photograph of 1/12–scale model installed on rotary balance apparatus.

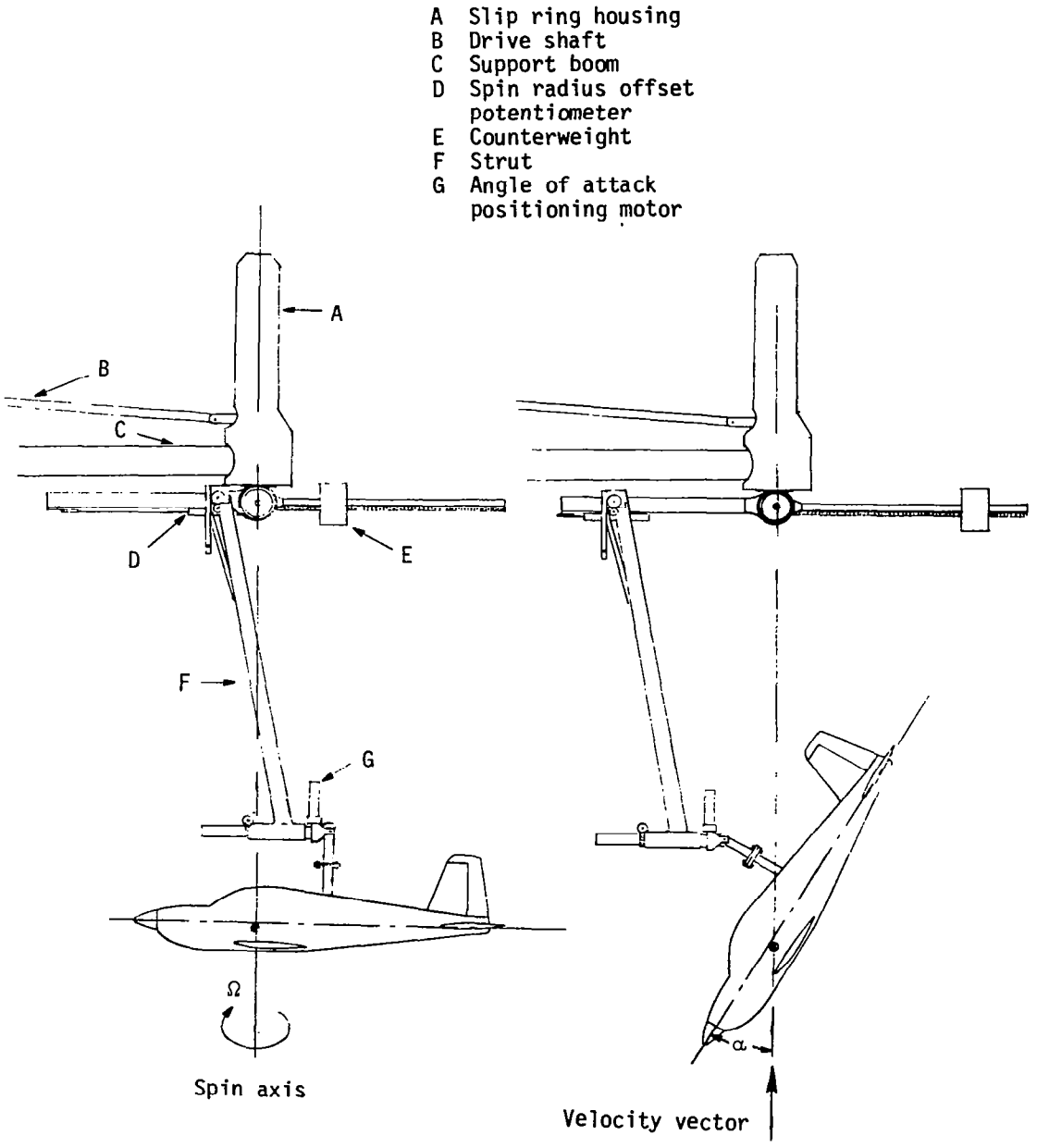

(a) Side view of model.

Figure 2.- Sketch of rotary balance apparatus.

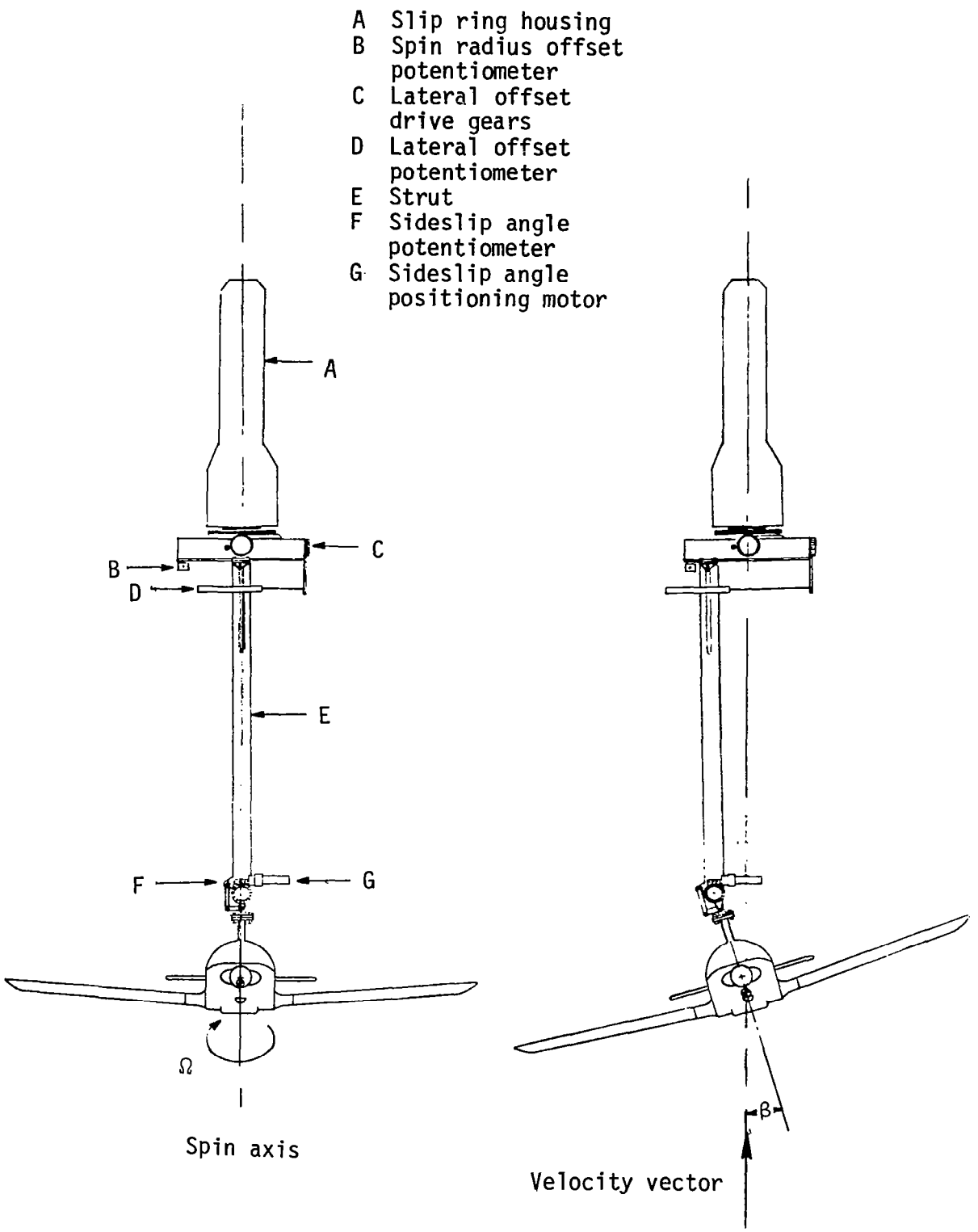

(b) Front view of model.

Figure 2.- Concluded.

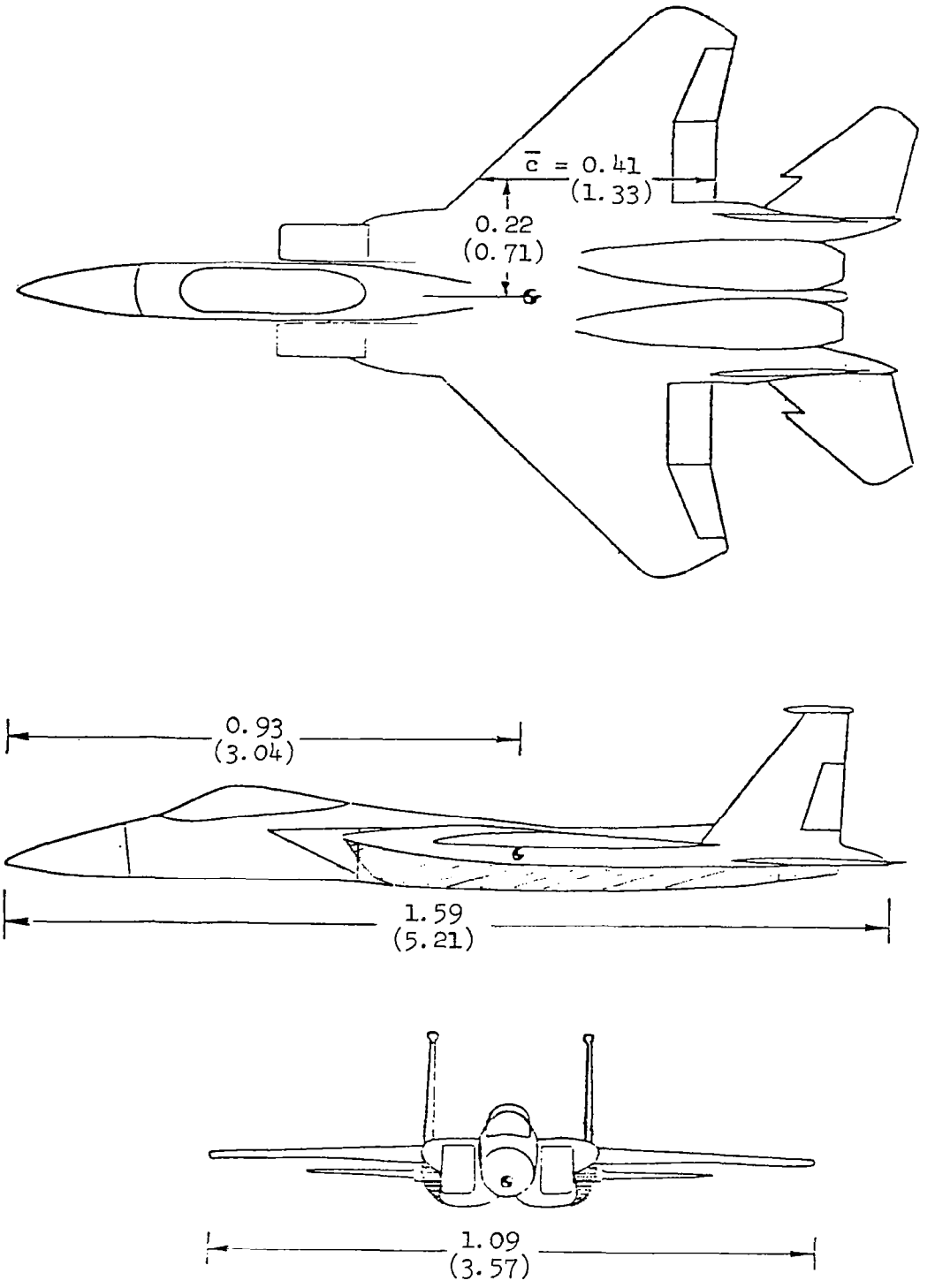

Figure 3.– Three–view sketch of 1/12–scale model. Dimensions are given in meters(feet).

APPENDIX

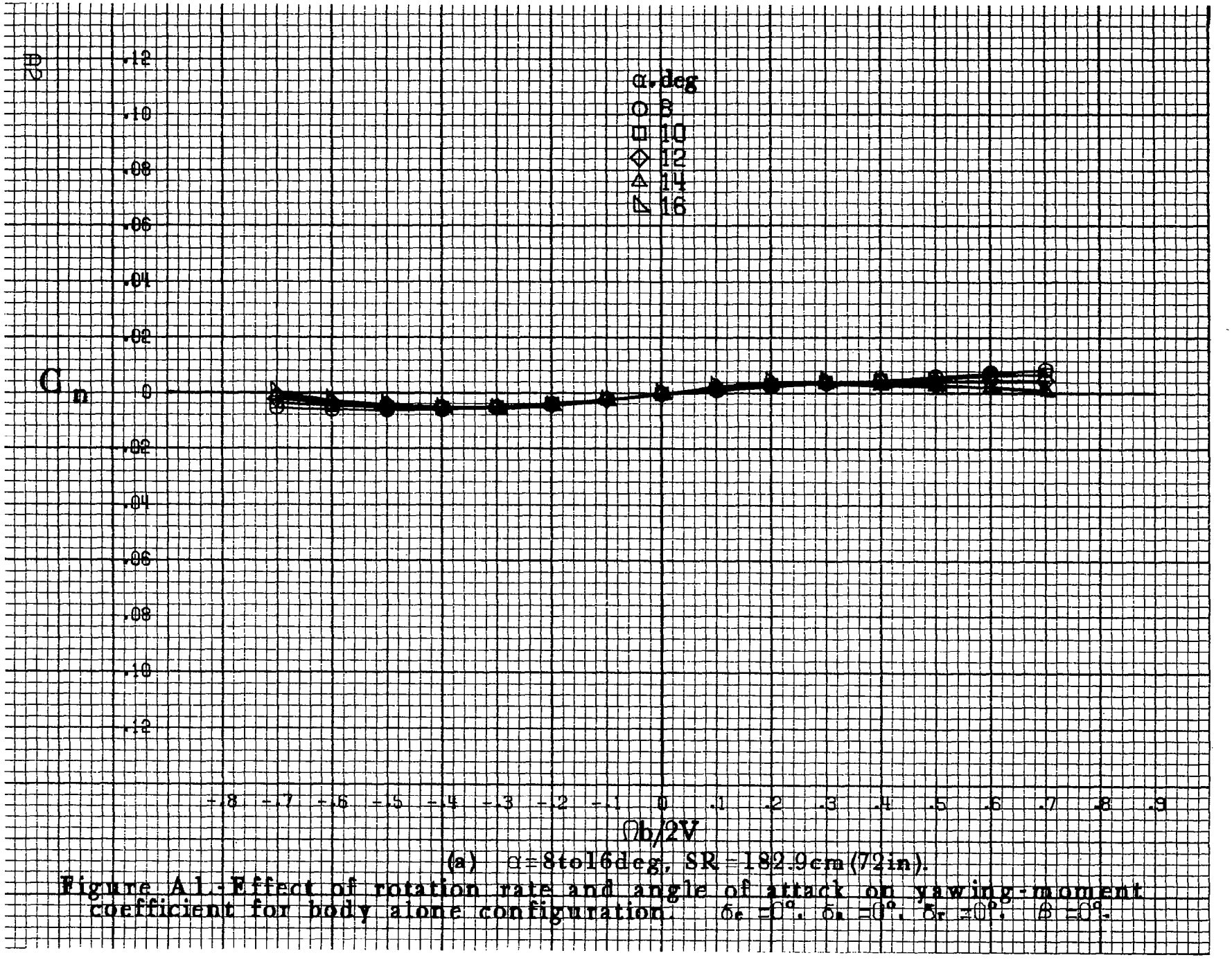

(a) $\alpha = 8$ to 16 deg, SR = 182.9 cm (72 in).

Figure A1.- Effect of rotation rate and angle of attack on yawing-moment coefficient for body alone configuration. $\delta_e = 0°$, $\delta_a = 0°$, $\delta_r = 0°$, $\beta = 0°$.

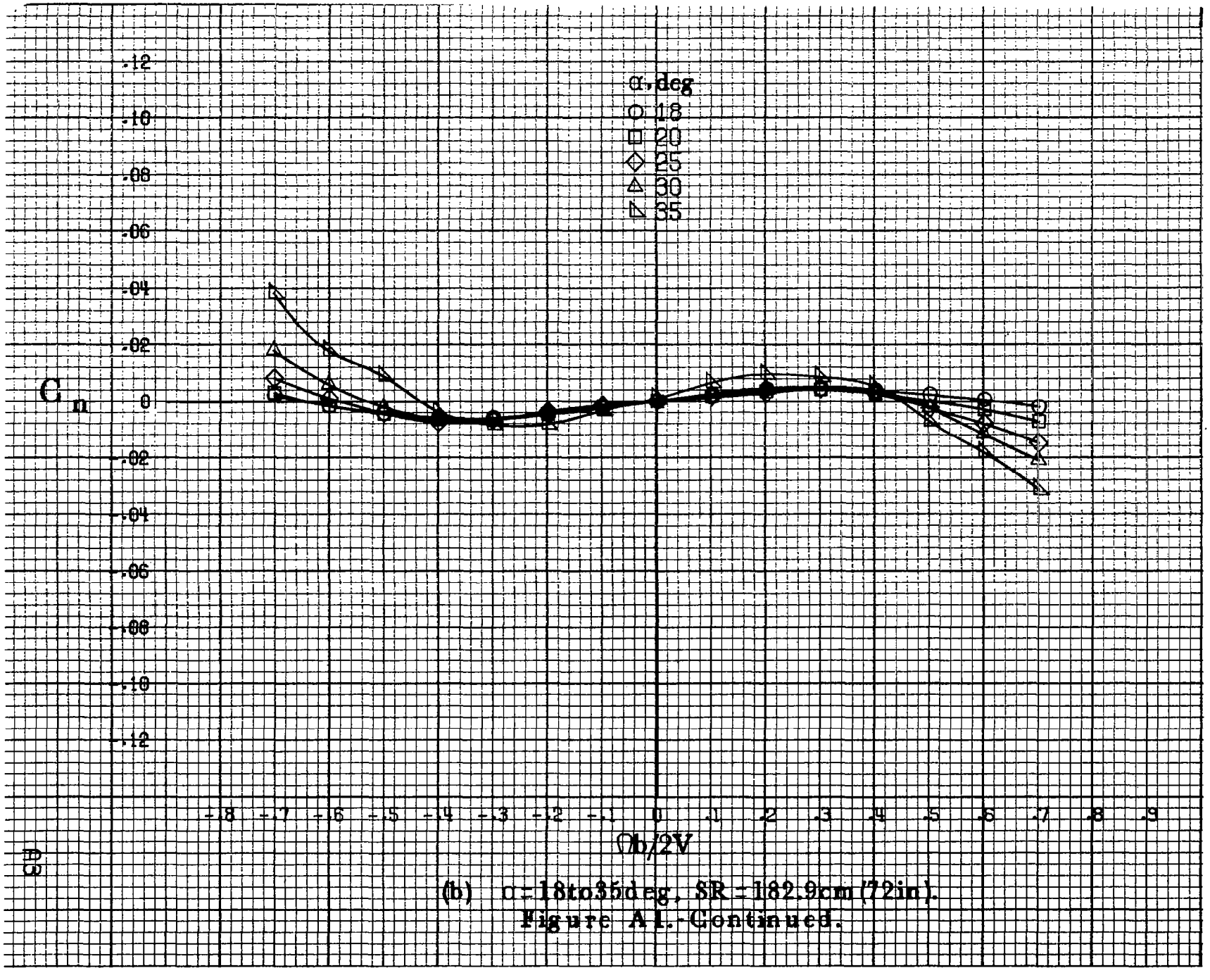

(b) α = 18 to 35 deg, SR = 182.9 cm (72 in.).

Figure A1.- Continued.

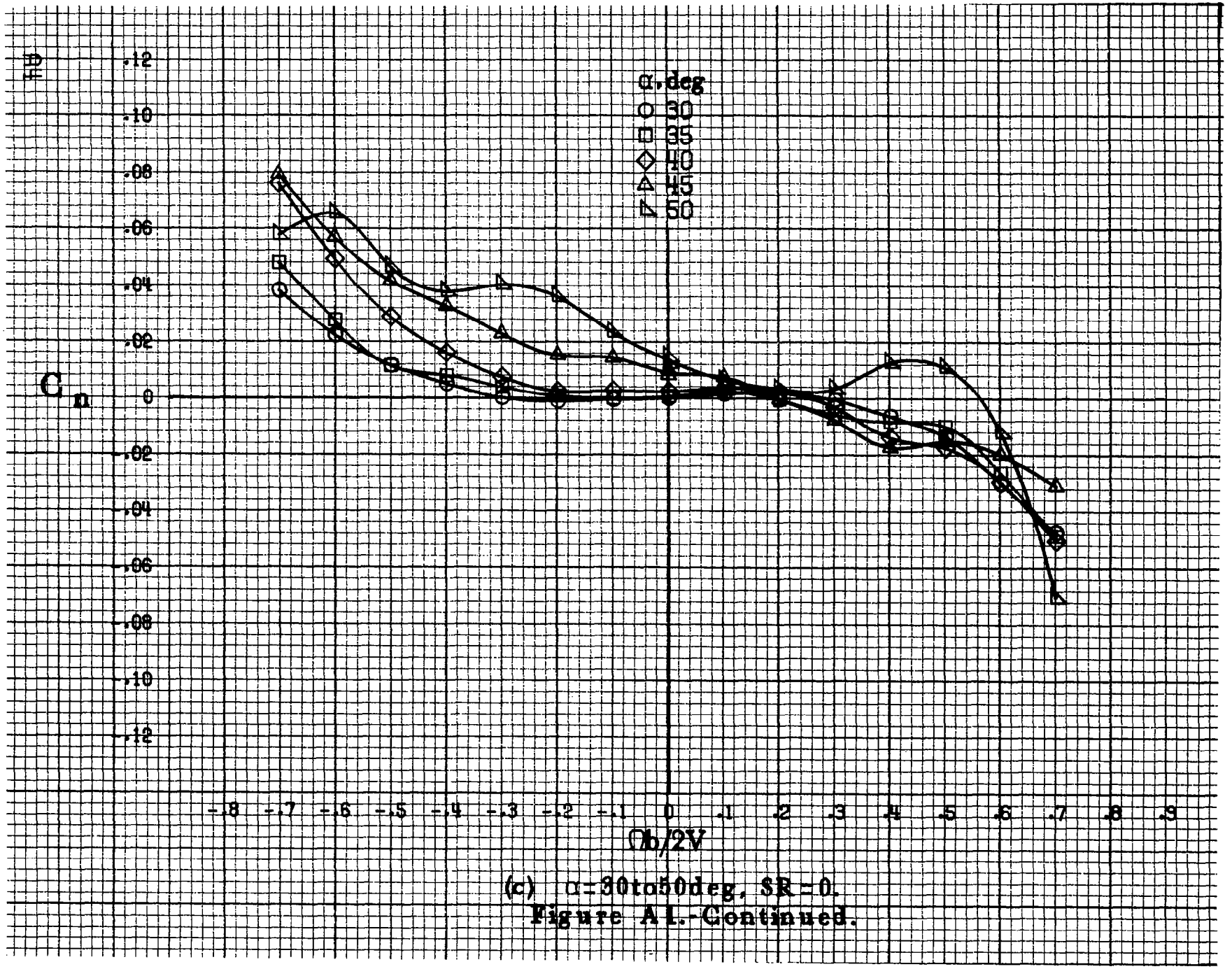

(c) α=30 to 50 deg, $R=0.

Figure A1.-Continued.

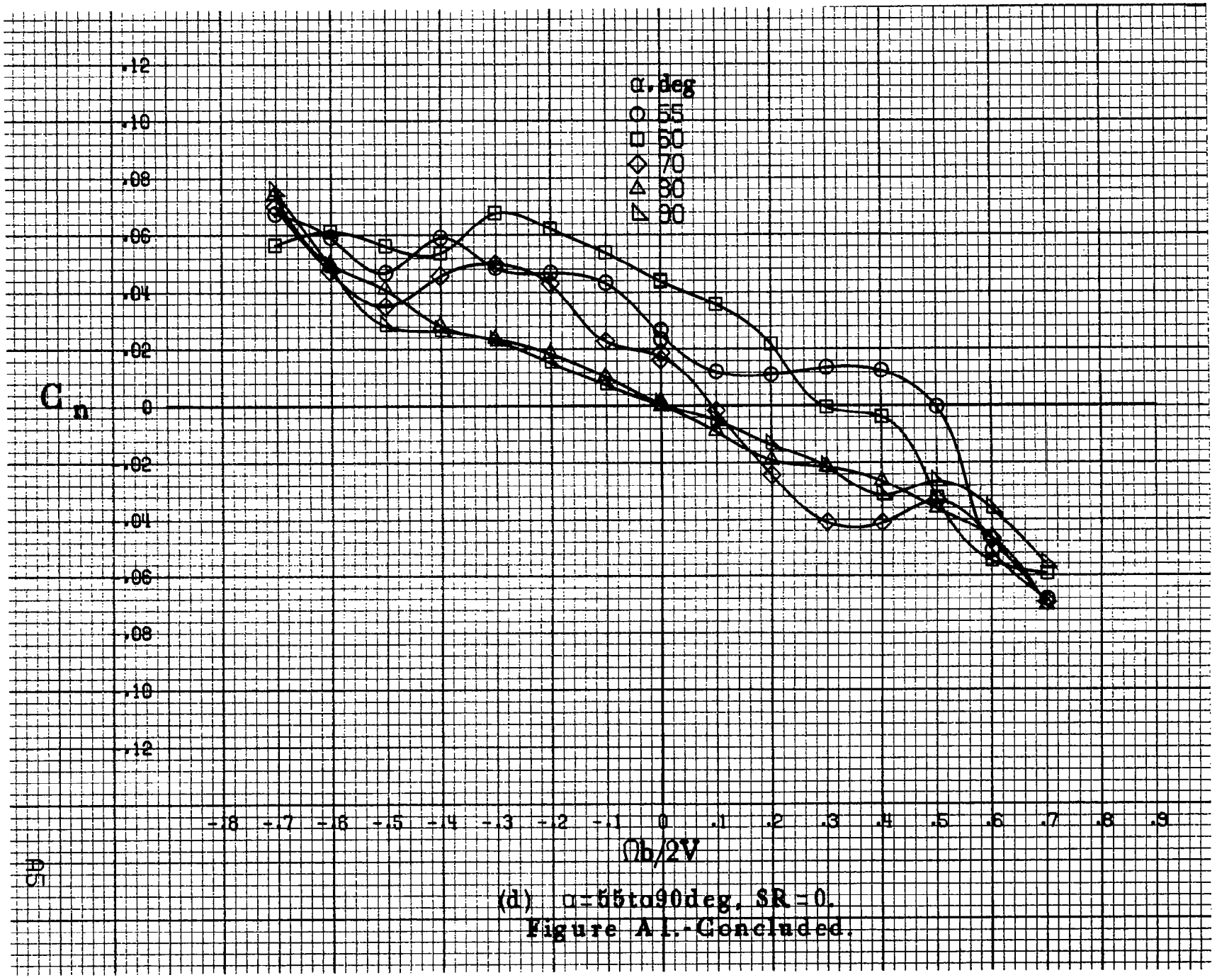

(d) $\alpha = 55$ to 90 deg, $SR = 0$.

Figure A1.- Concluded.

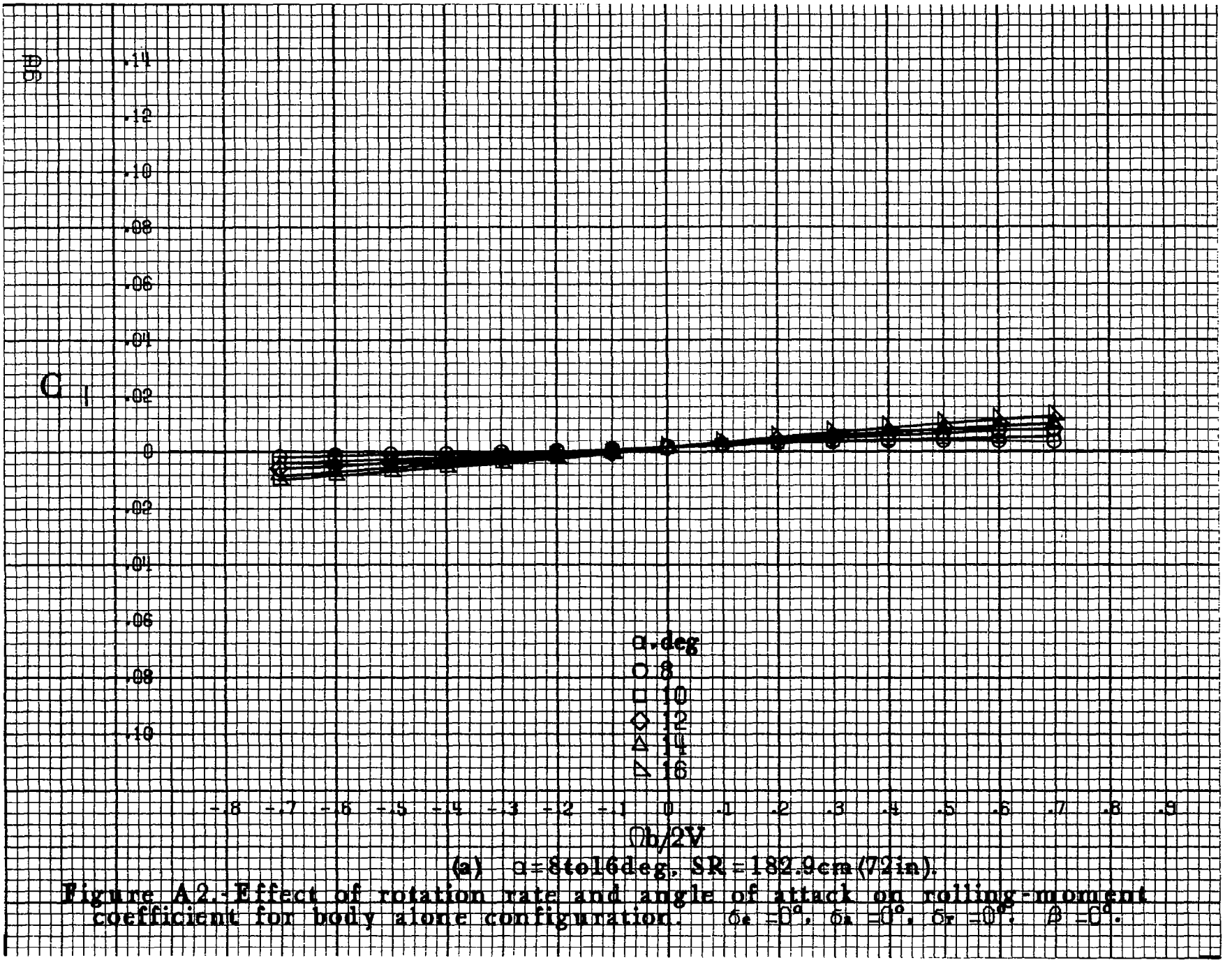

(a) $\alpha = 8$ to 16 deg, SR = 182.9 cm (72 in).

Figure A2.- Effect of rotation rate and angle of attack on rolling-moment coefficient for body alone configuration. $\delta_e = 0°$, $\delta_a = 0°$, $\delta_r = 0°$, $\beta = 0°$.

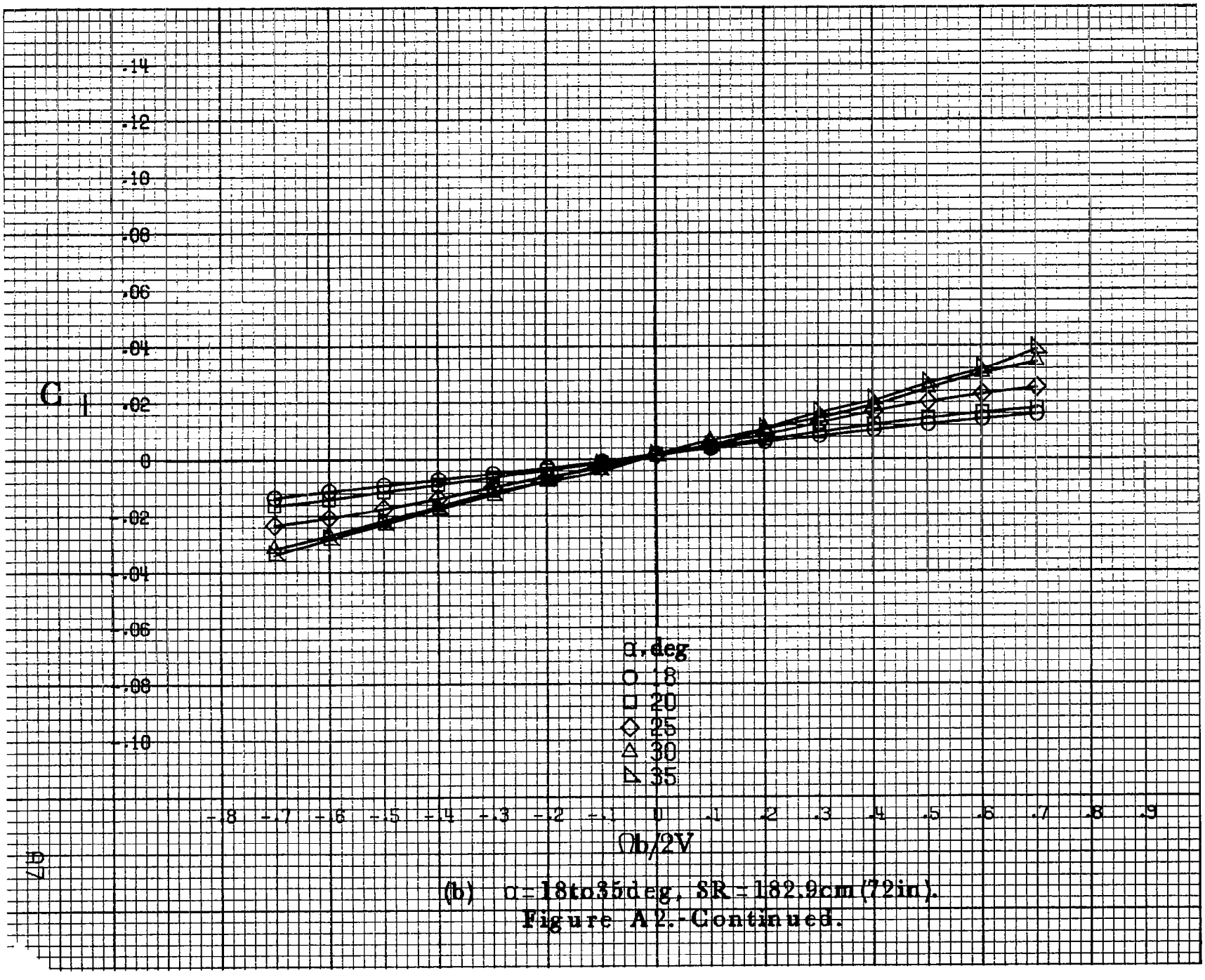

(b) $\alpha = 18$ to 35 deg, SR = 182.9 cm (72 in.).

Figure A2.- Continued.

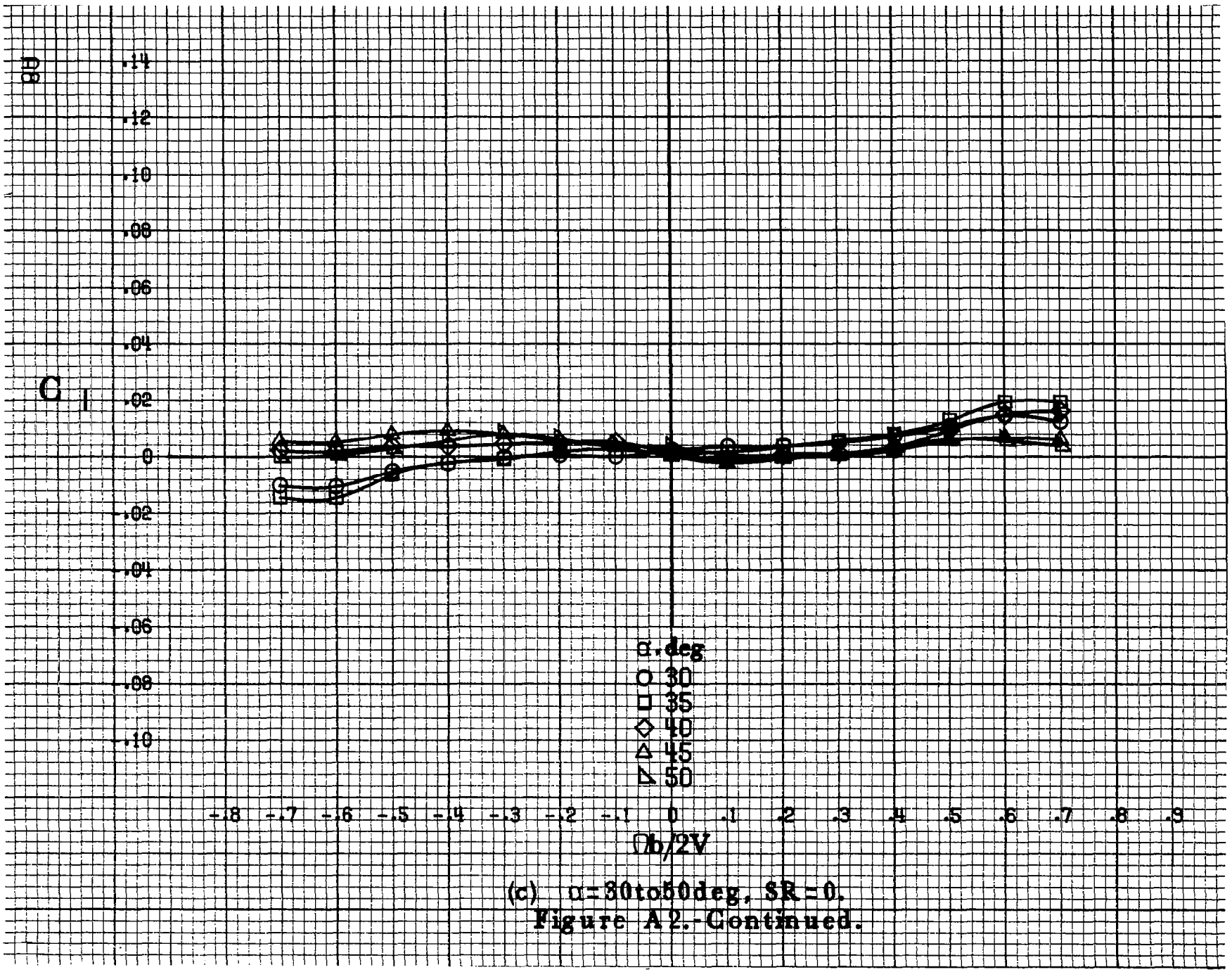

(c) α=30to50deg, SR=0.

Figure A2.-Continued.

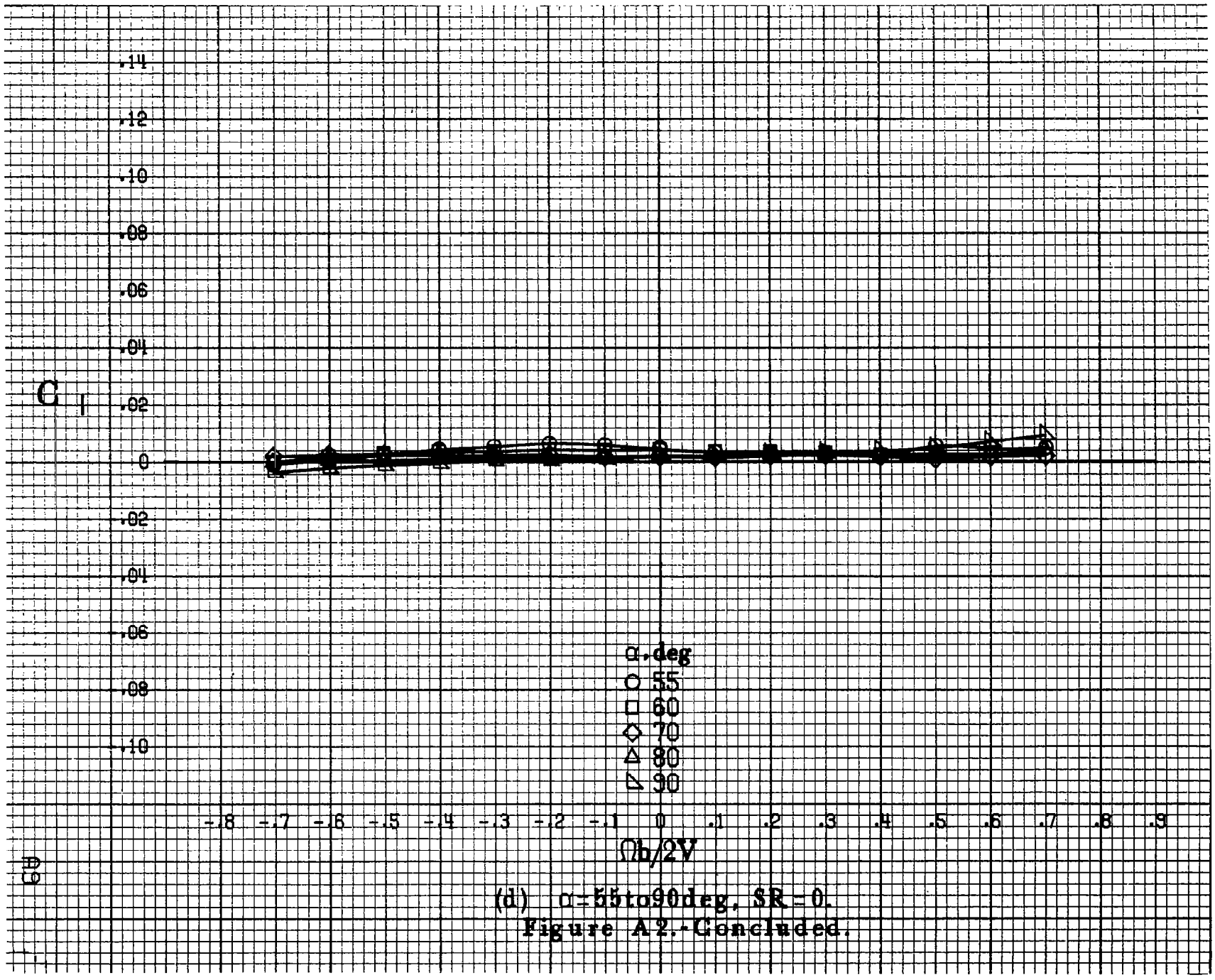

(d) α=55to90deg, SR=0.

Figure A2.-Concluded.

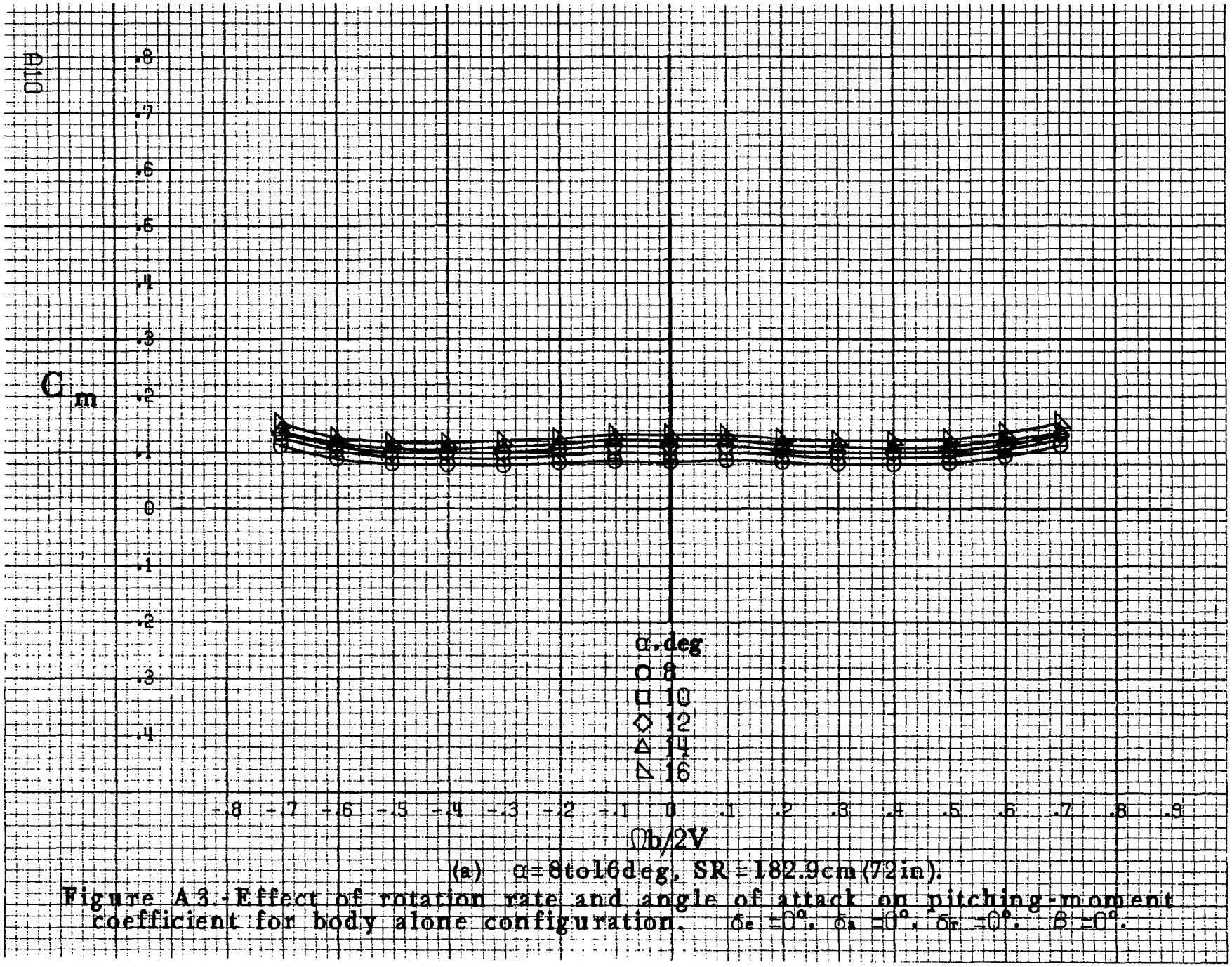

(a) $\alpha = 8$ to 16 deg, SR = 182.9 cm (72 in).

Figure A3.- Effect of rotation rate and angle of attack on pitching-moment coefficient for body alone configuration. $\delta_e = 0°$, $\delta_a = 0°$, $\delta_r = 0°$, $\beta = 0°$.

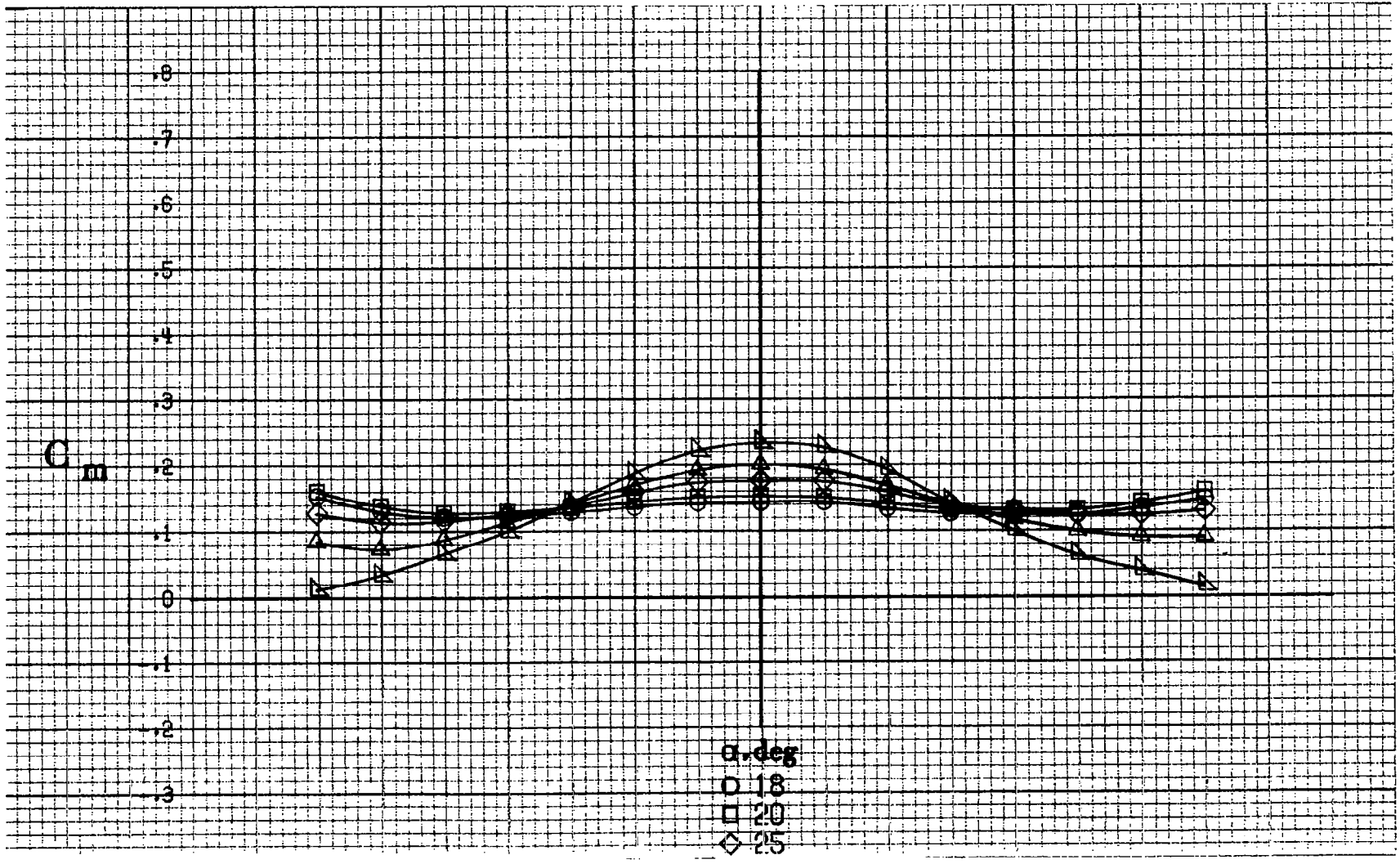
.8
.7
.6
.5
.4
.3
.2
.1
0
-.1
-.2
-.3
C_m
α, deg
18
20
25

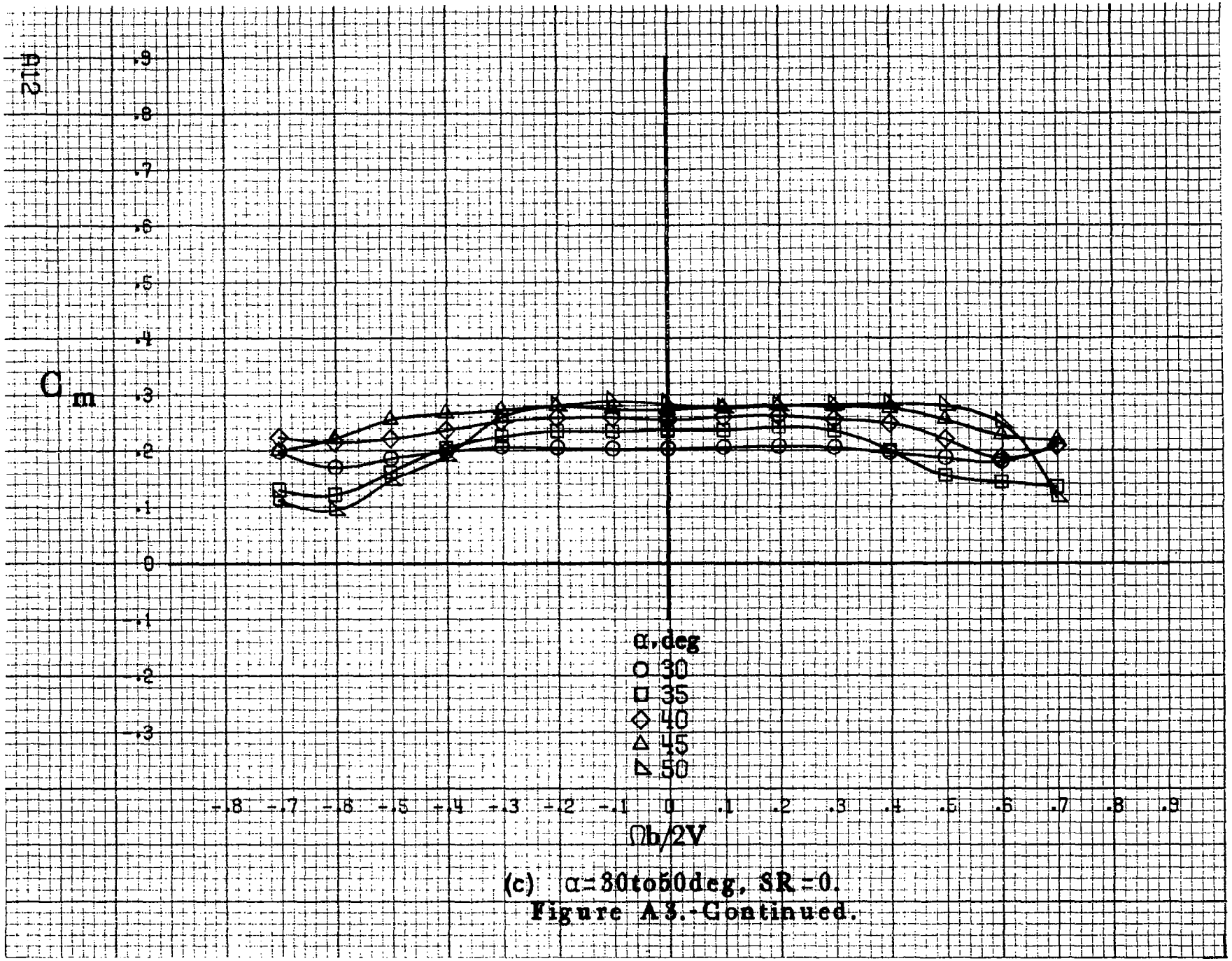

(c) α=30to50deg, SR=0.

Figure A3.-Continued.

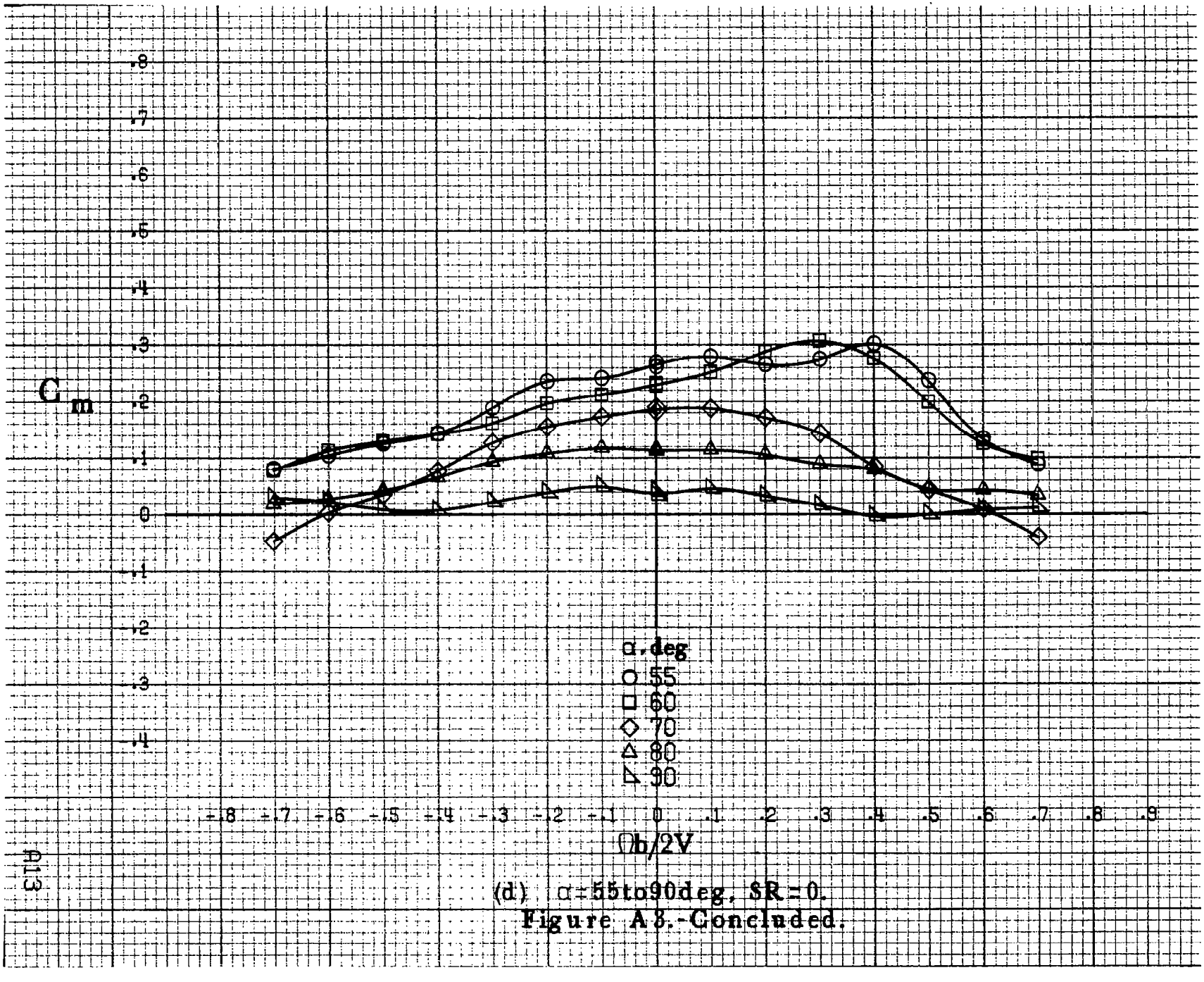

(d) α=55to90deg, SR=0.

Figure A8.-Concluded.

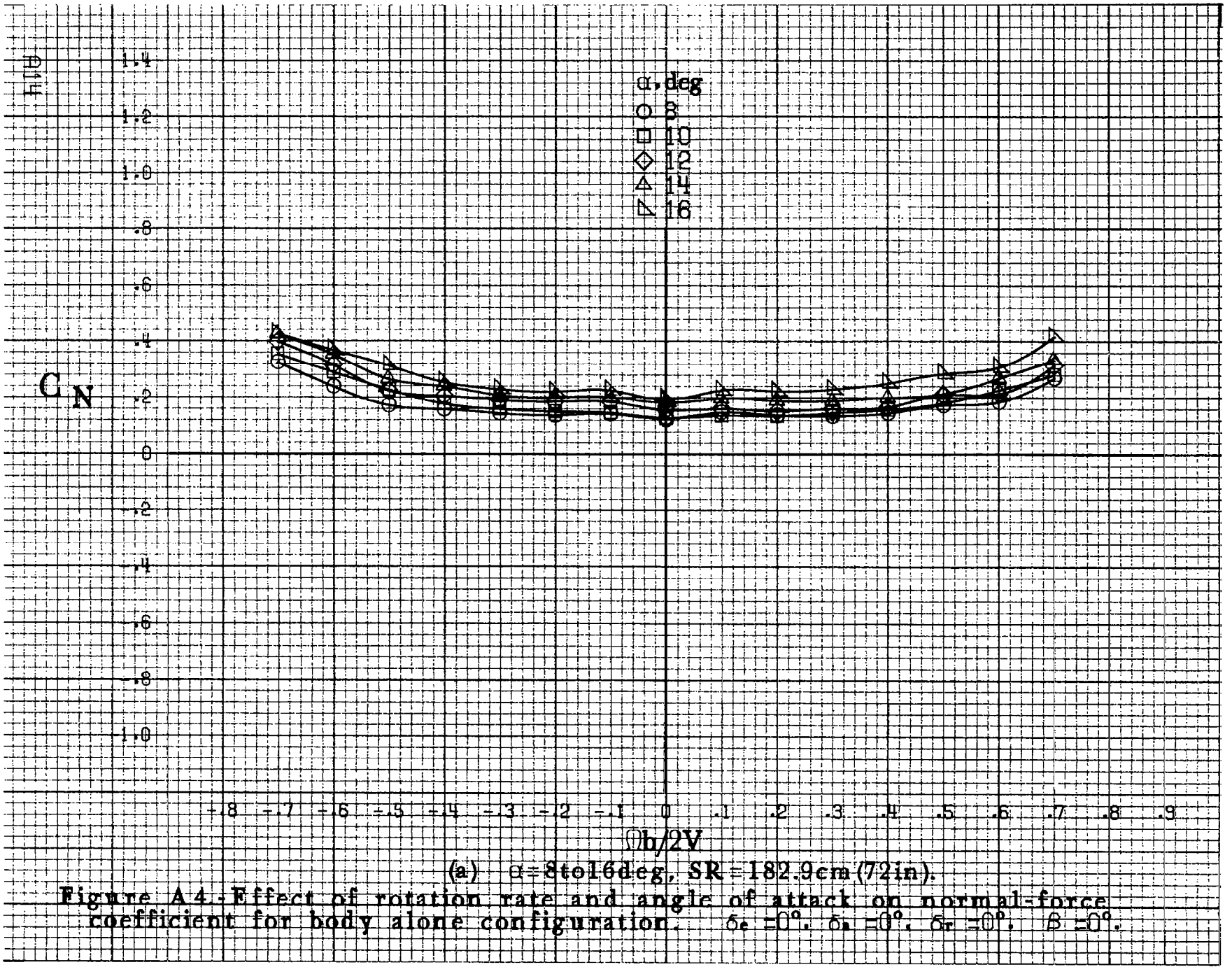

(a) $\alpha = 8$ to 16 deg, SR = 182.9 cm (72 in).

Figure A4.- Effect of rotation rate and angle of attack on normal-force coefficient for body alone configuration. $\delta_e = 0°$, $\delta_a = 0°$, $\delta_r = 0°$, $\beta = 0°$.

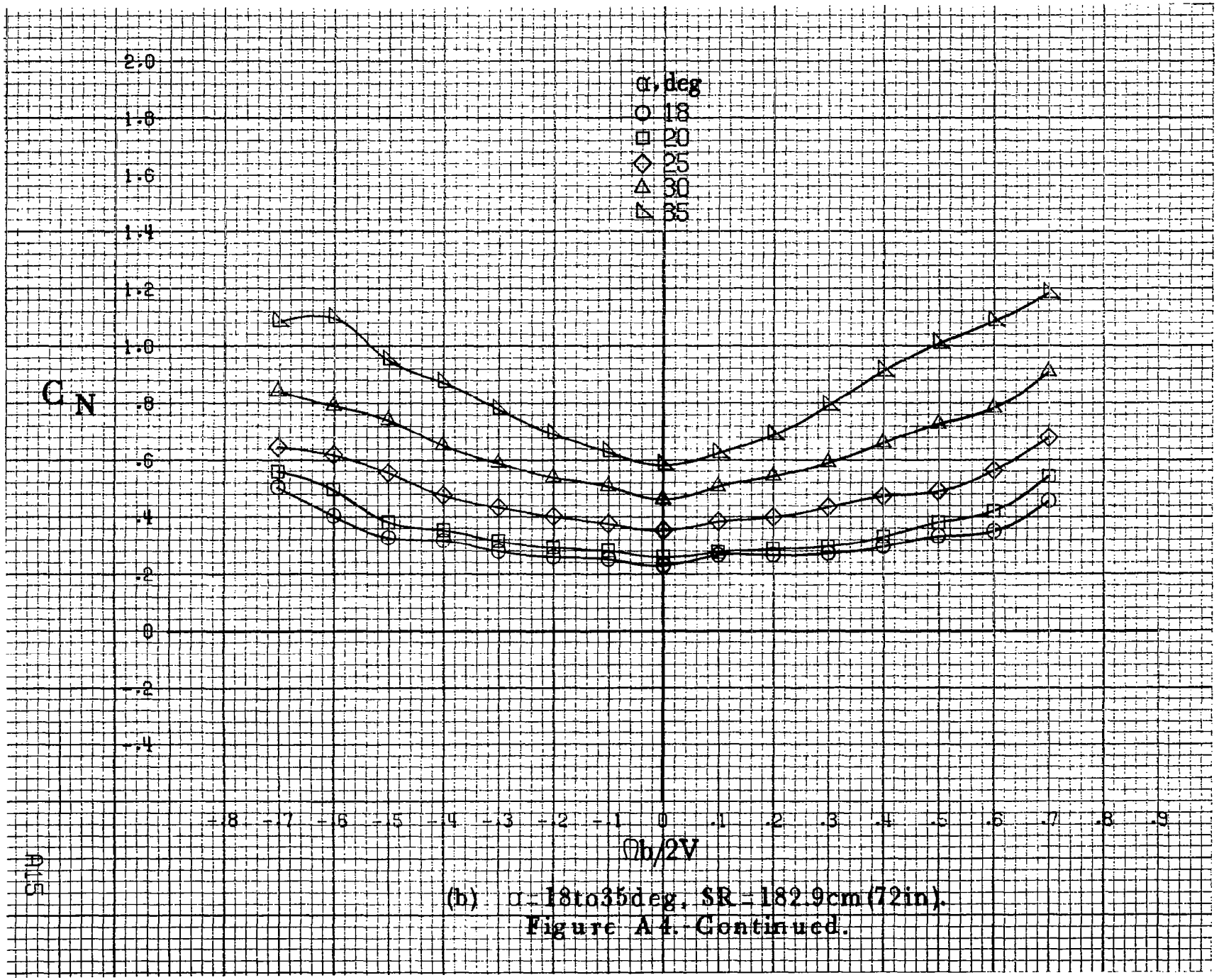

(b) α = 18 to 35 deg, SR = 182.9 cm (72 in).

Figure A4. - Continued.

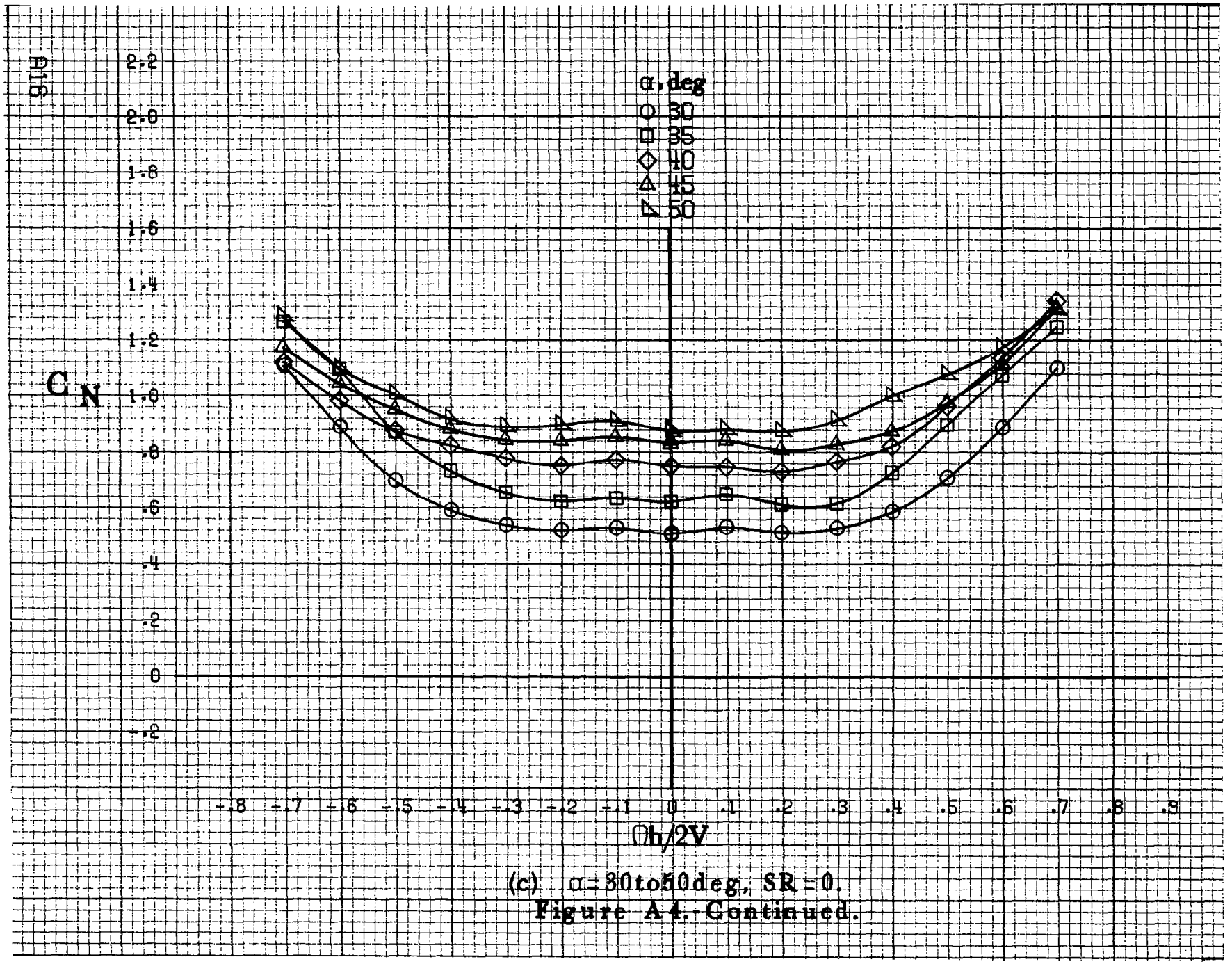

(c) α = 30 to 50 deg, SR = 0.

Figure A4.- Continued.

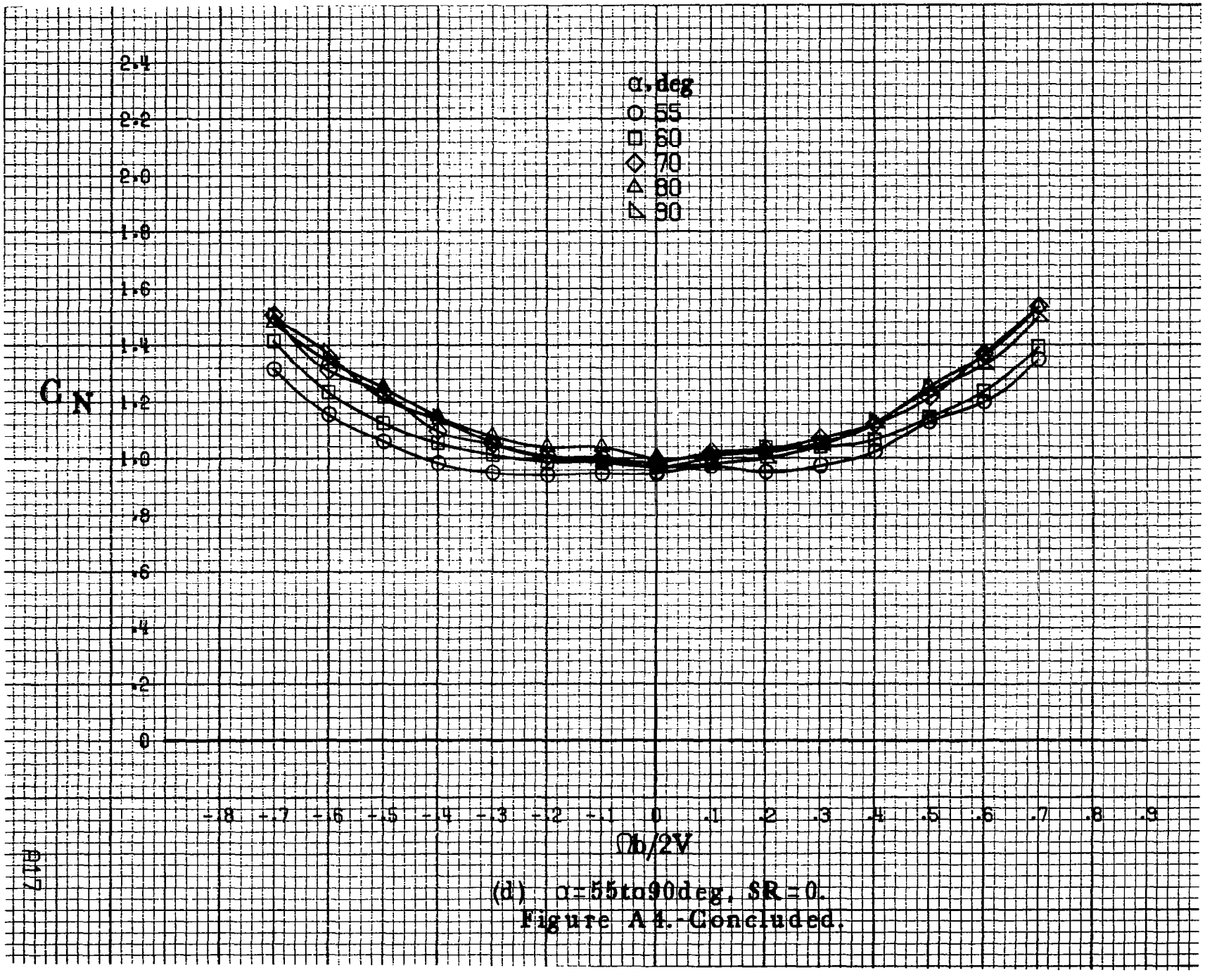

(d) $\alpha = 55$ to 90 deg, $\$R = 0$.

Figure A1.- Concluded.

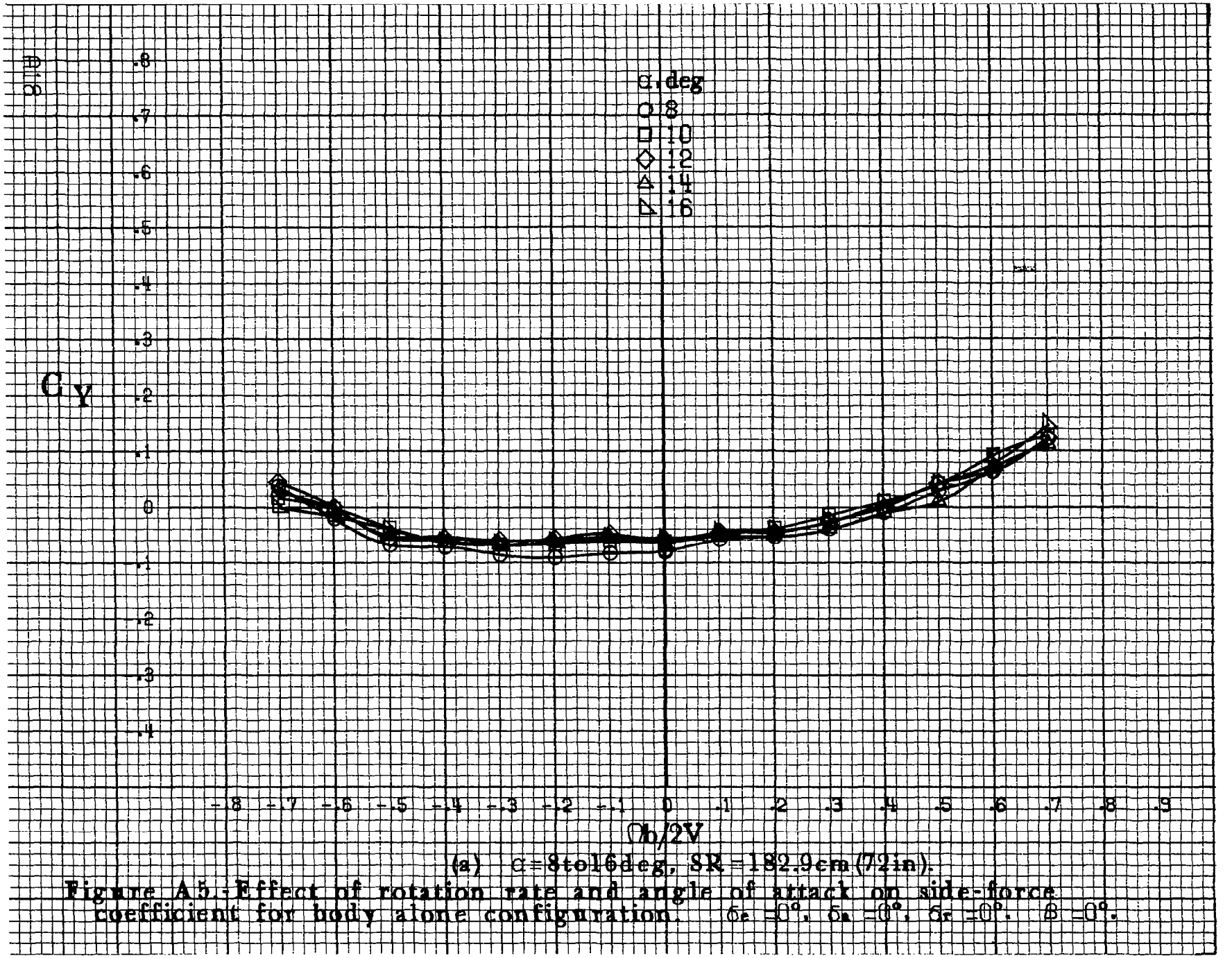

(a) $\alpha = 8$ to 16 deg, $S_R = 182.9$ cm (72 in).

Figure A5.- Effect of rotation rate and angle of attack on side-force coefficient for body alone configuration. $\delta_e = 0°$, $\delta_a = 0°$, $\delta_r = 0°$, $\beta = 0°$.

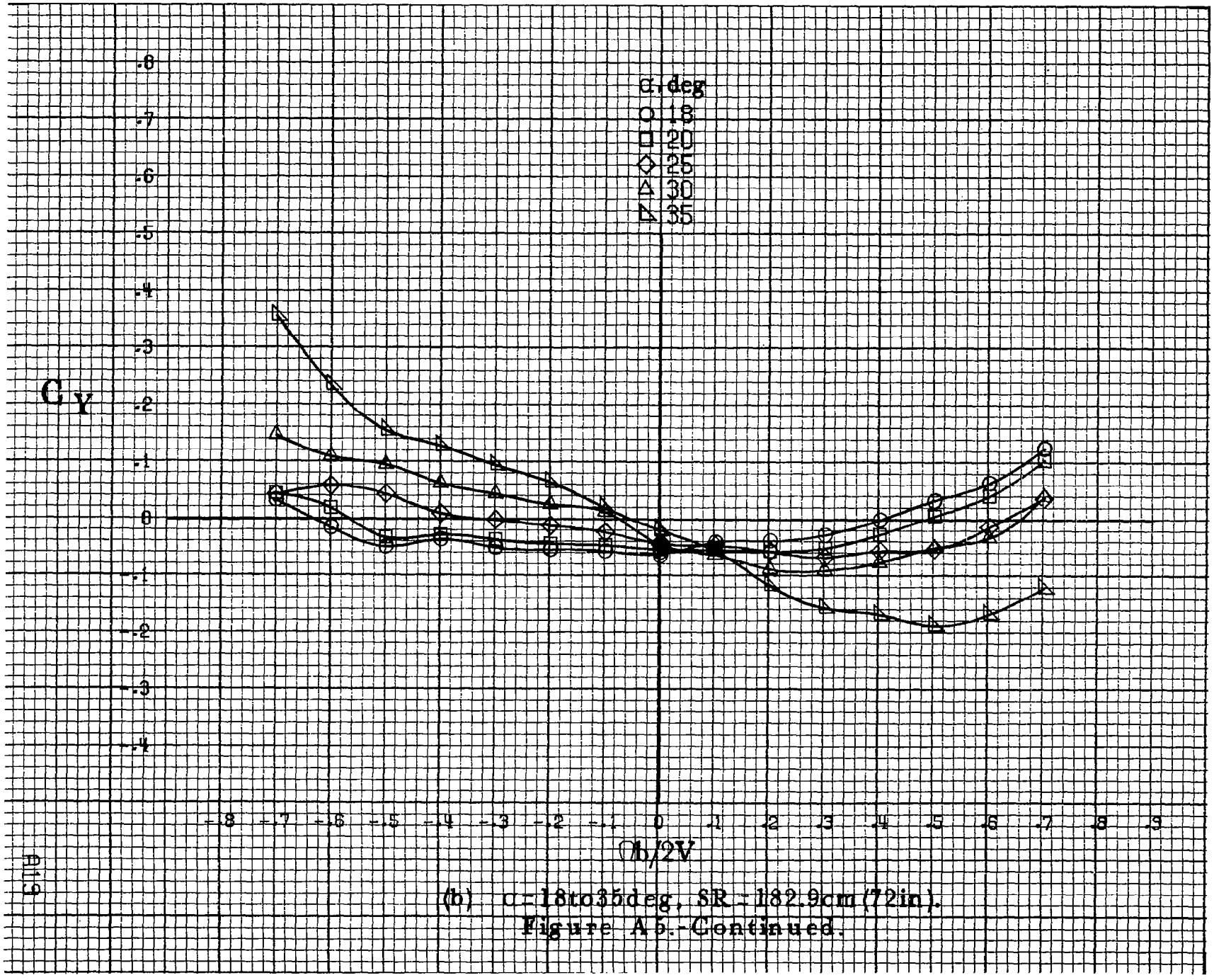

(b) α = 18 to 35 deg, SR = 182.9 cm (72 in.).

Figure A5.- Continued.

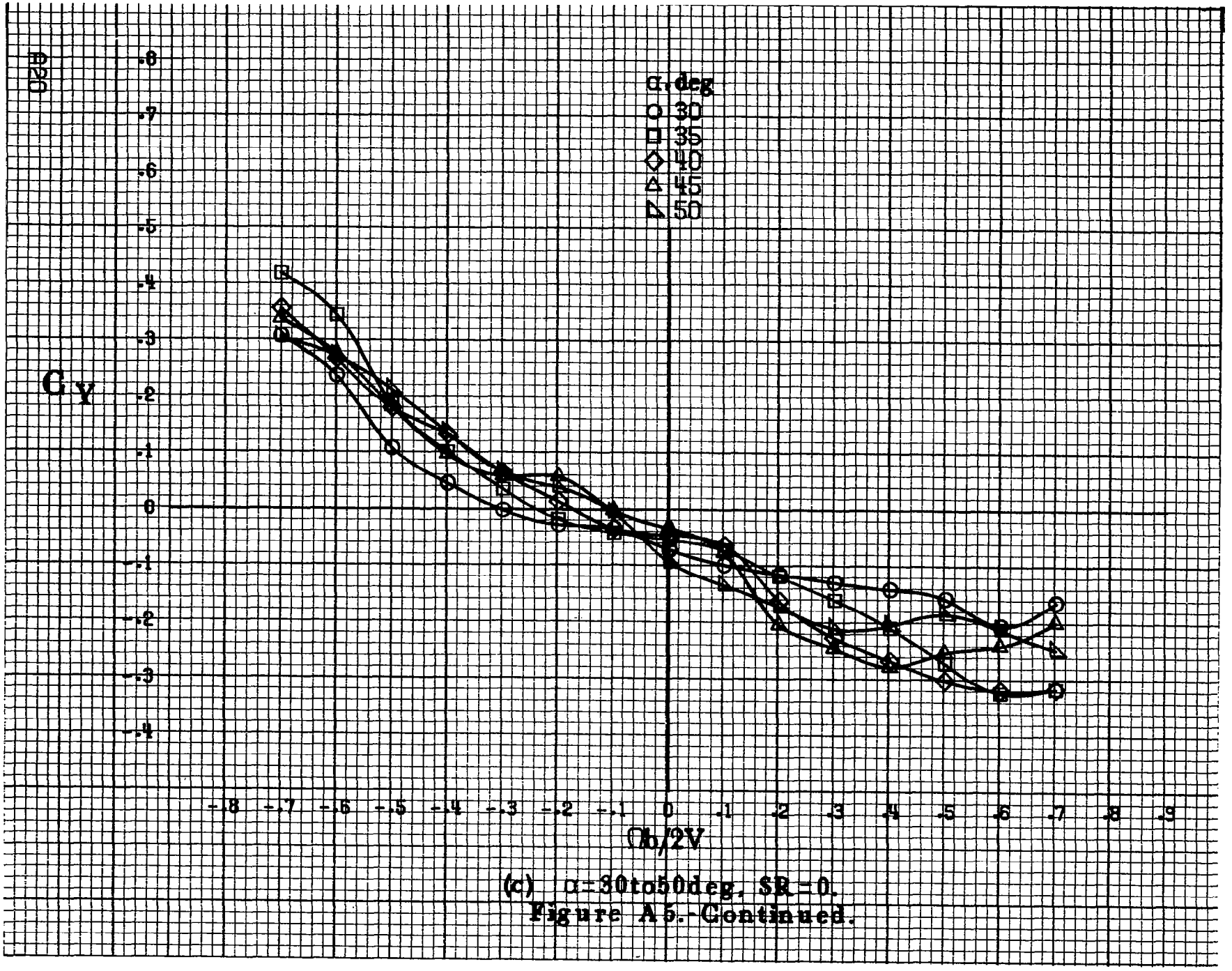

(c) α=30to50deg. δ_R=0.

Figure A5.-Continued.

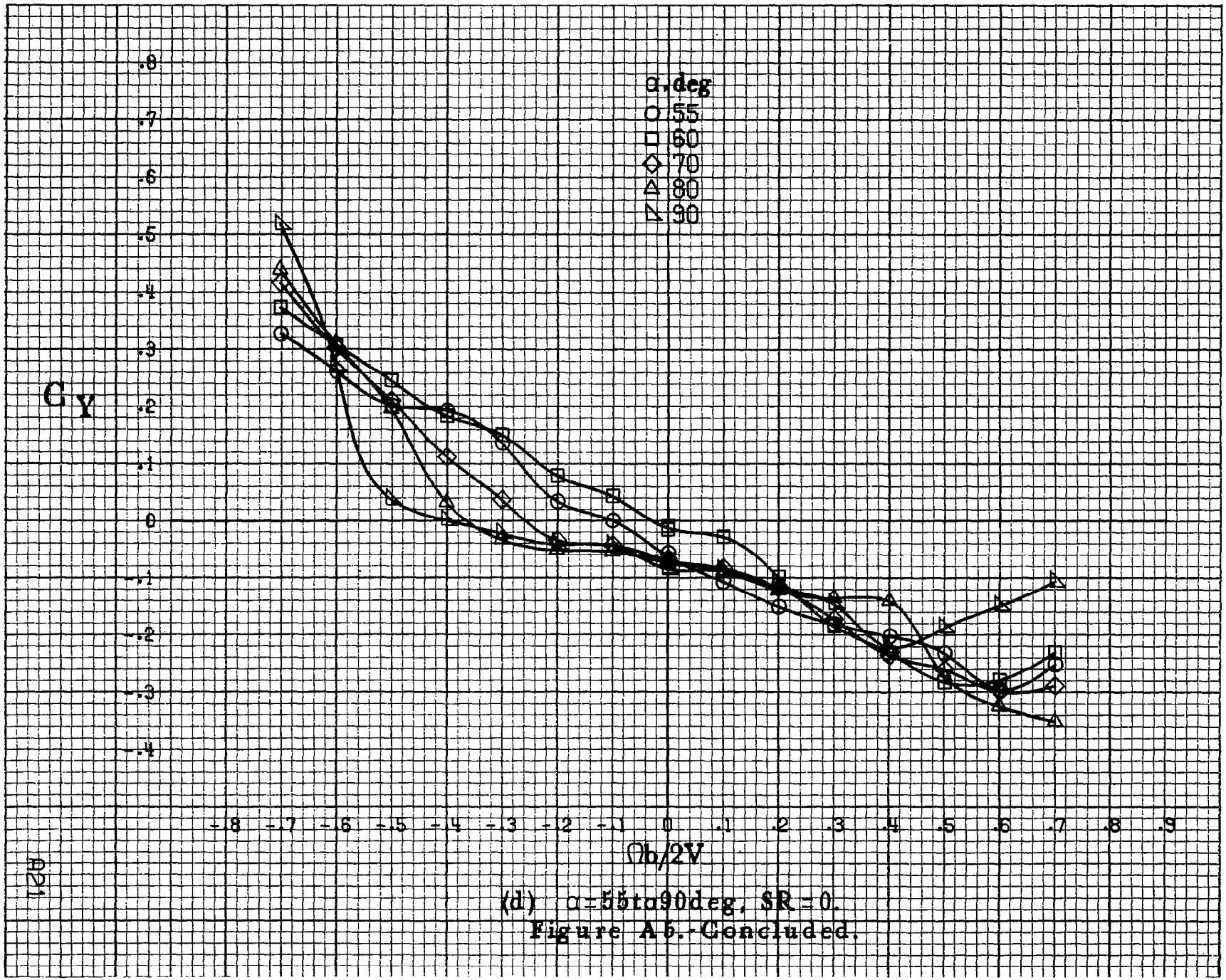

(d) $\alpha = 55$ to 90 deg, SR = 0.

Figure A6.-Concluded.

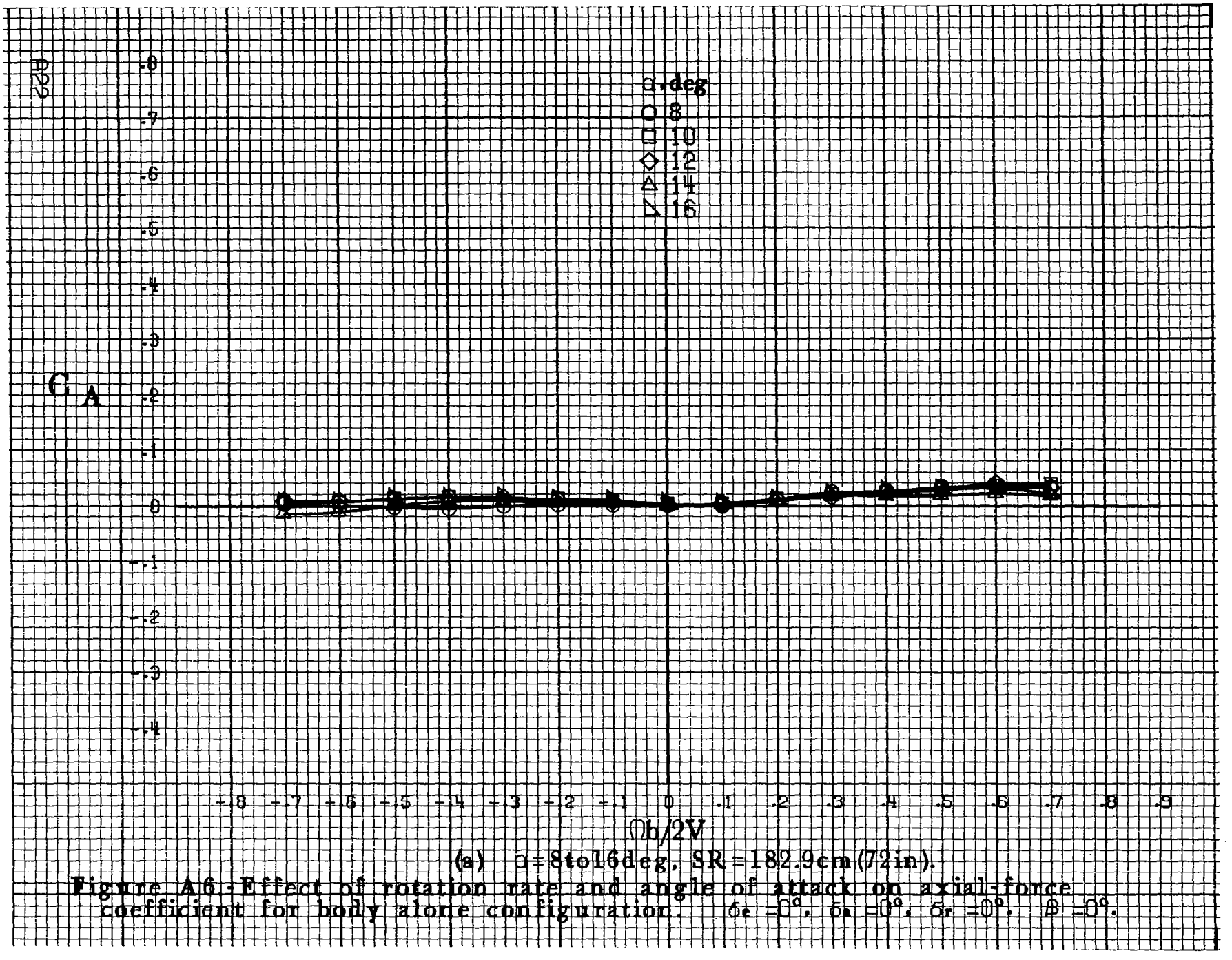

(a) α = 8 to 16 deg, SR = 182.9 cm (72 in).

Figure A6.- Effect of rotation rate and angle of attack on axial-force coefficient for body alone configuration. $\delta_e = 0°$, $\delta_a = 0°$, $\delta_r = 0°$, $\beta = 0°$.

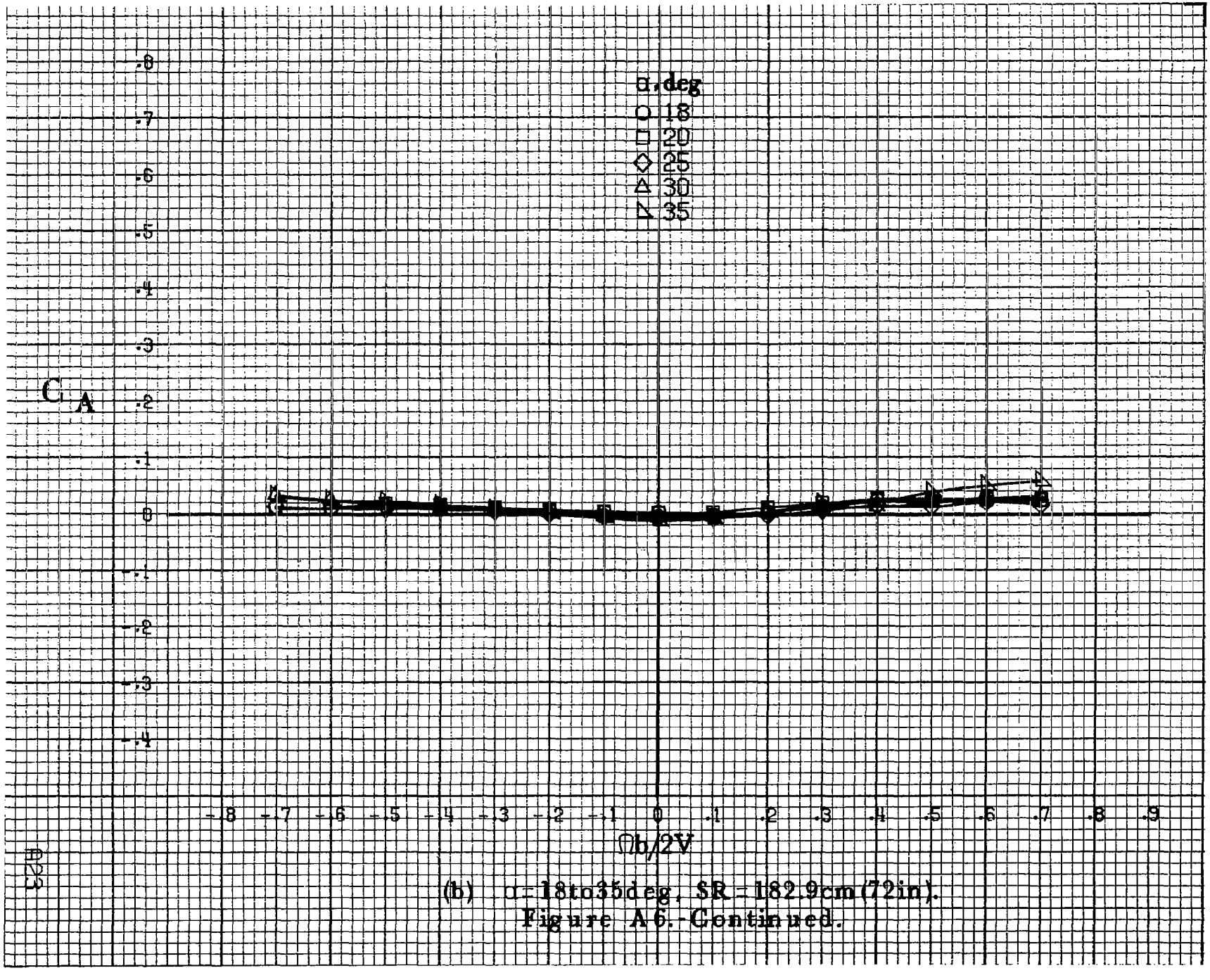

(b) α = 18 to 35 deg, SR = 182.9 cm (72 in).

Figure A6.- Continued.

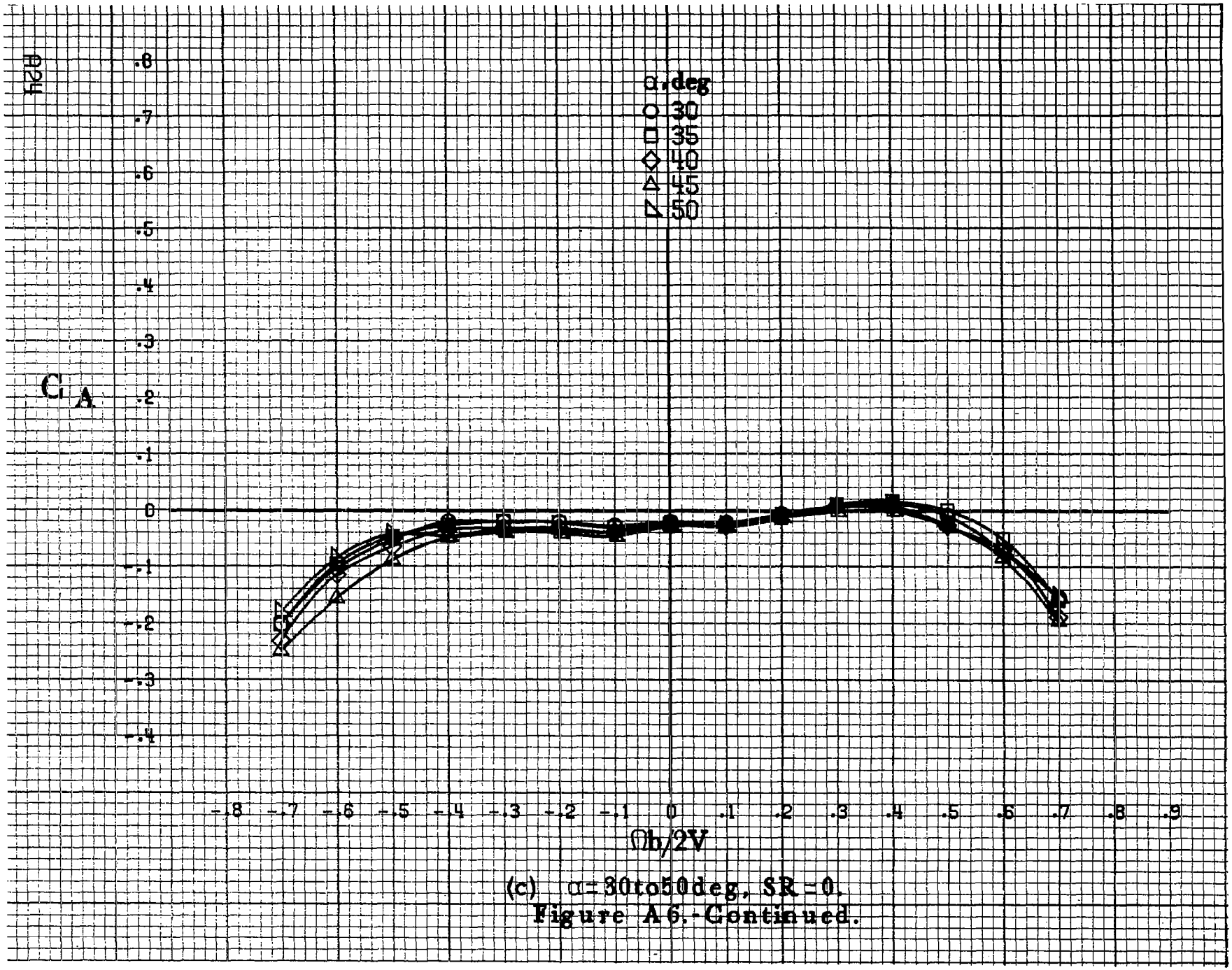

(c) α = 30 to 50 deg, SR = 0.

Figure A6.- Continued.

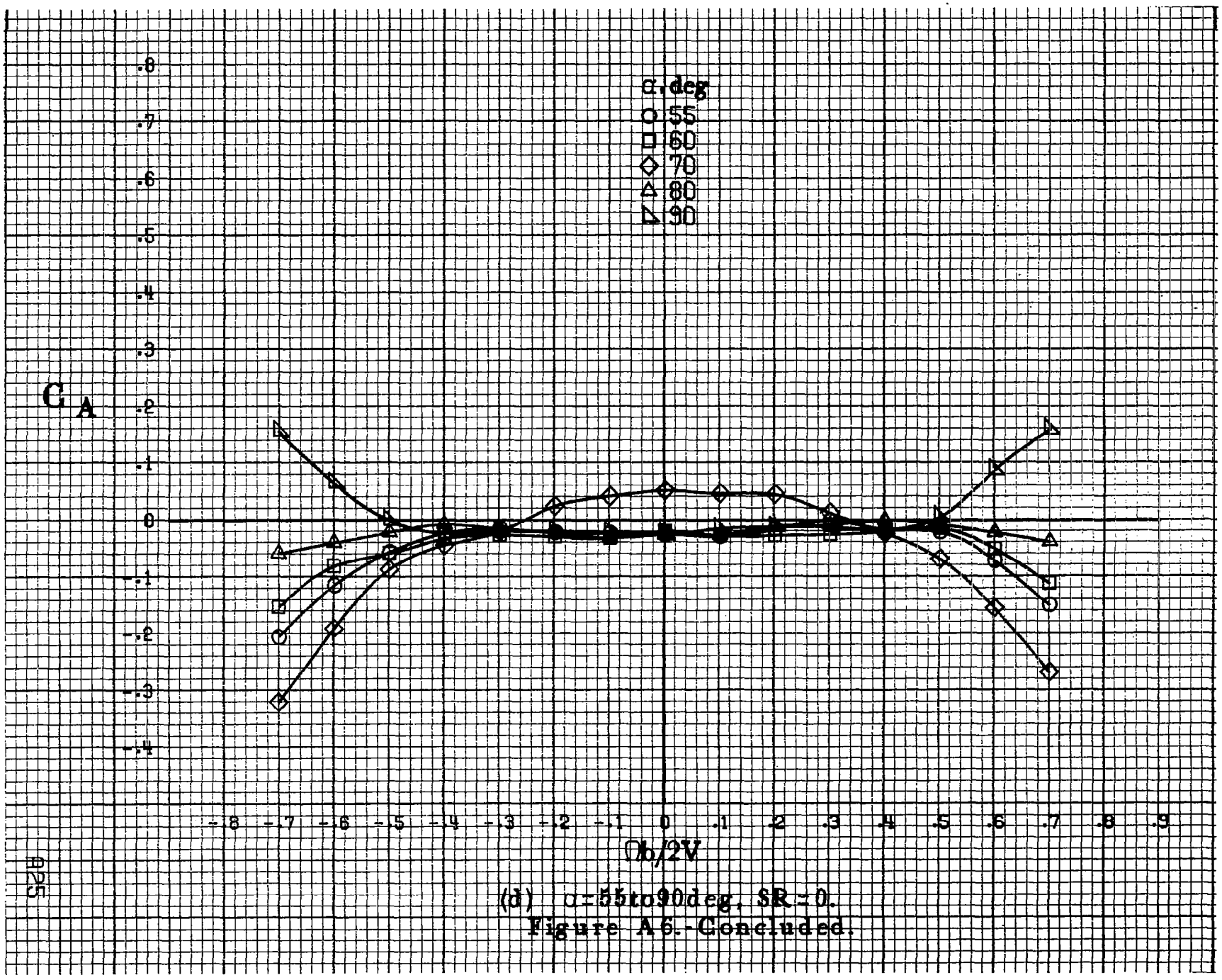

(d) $\alpha = 55$ to 90 deg, $SR = 0$.

Figure A6.- Concluded.

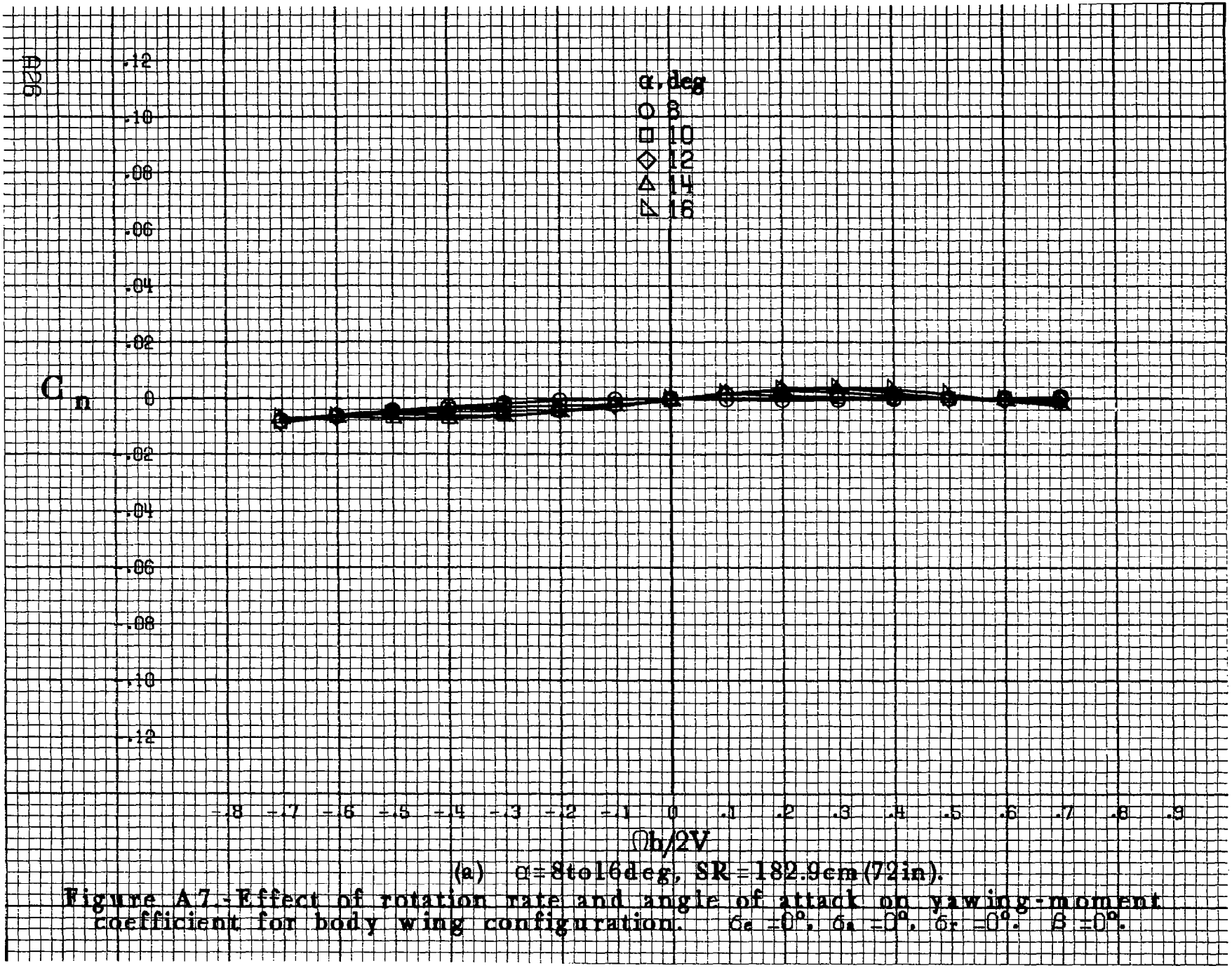

(a) $\alpha = 8$ to 16 deg, SR = 182.9 cm (72 in).

Figure A7.- Effect of rotation rate and angle of attack on yawing-moment coefficient for body wing configuration. $\delta_e = 0°$, $\delta_a = 0°$, $\delta_r = 0°$, $\beta = 0°$.

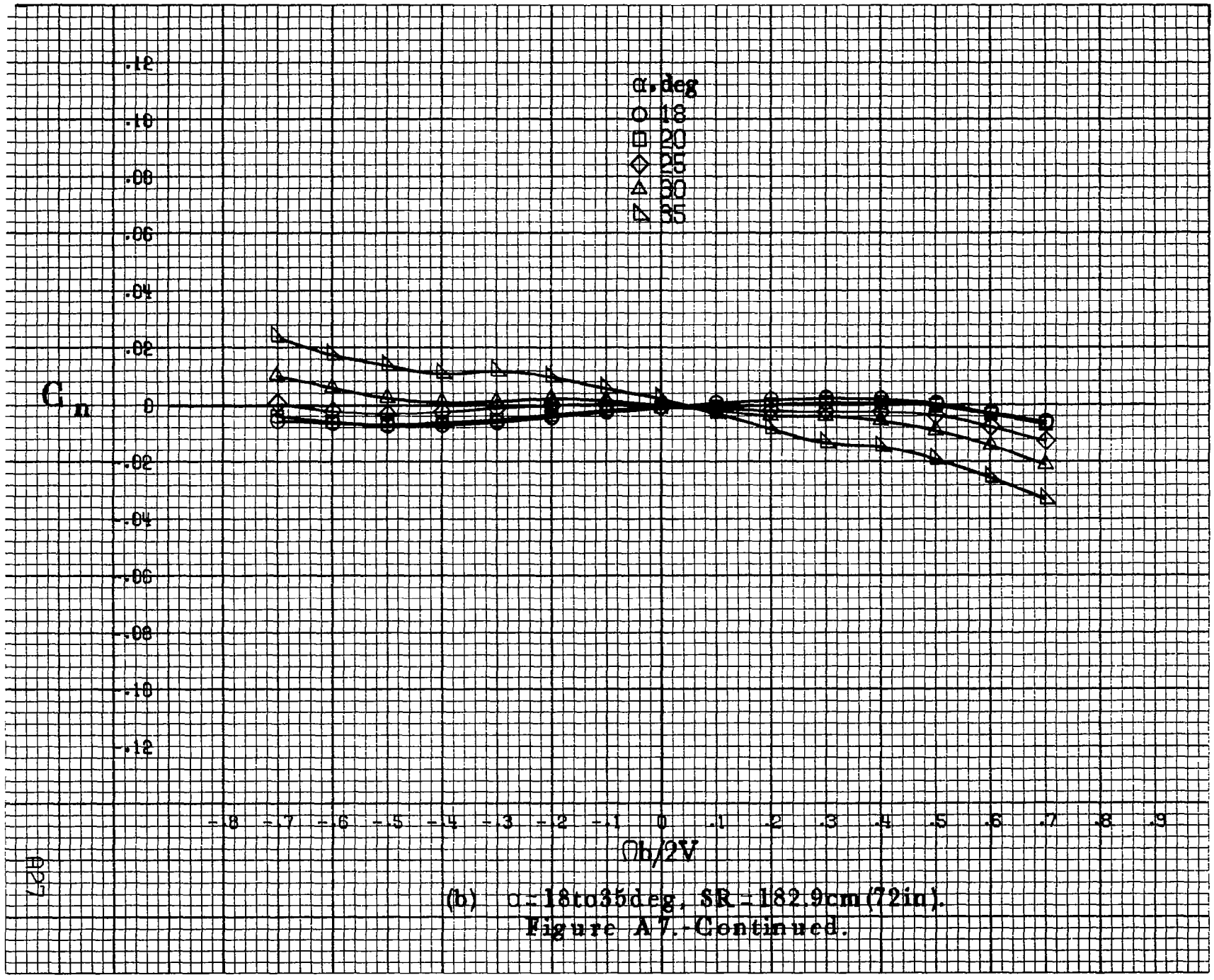

(b) α = 18 to 35 deg, SR = 182.9 cm (72 in.).

Figure A7.- Continued.

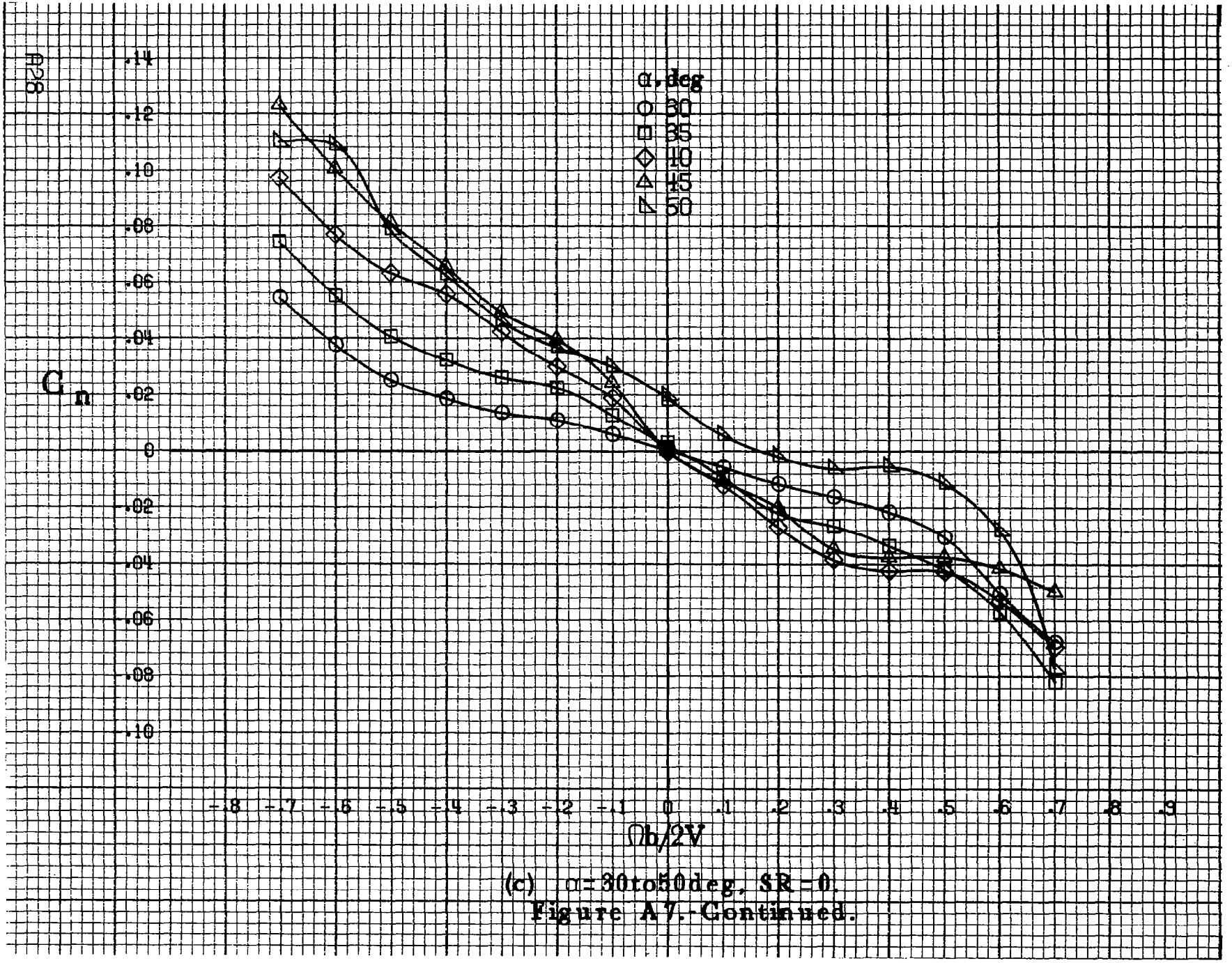

(c) $\alpha = 30$ to 50 deg, $SR = 0$.

Figure A7.- Continued.

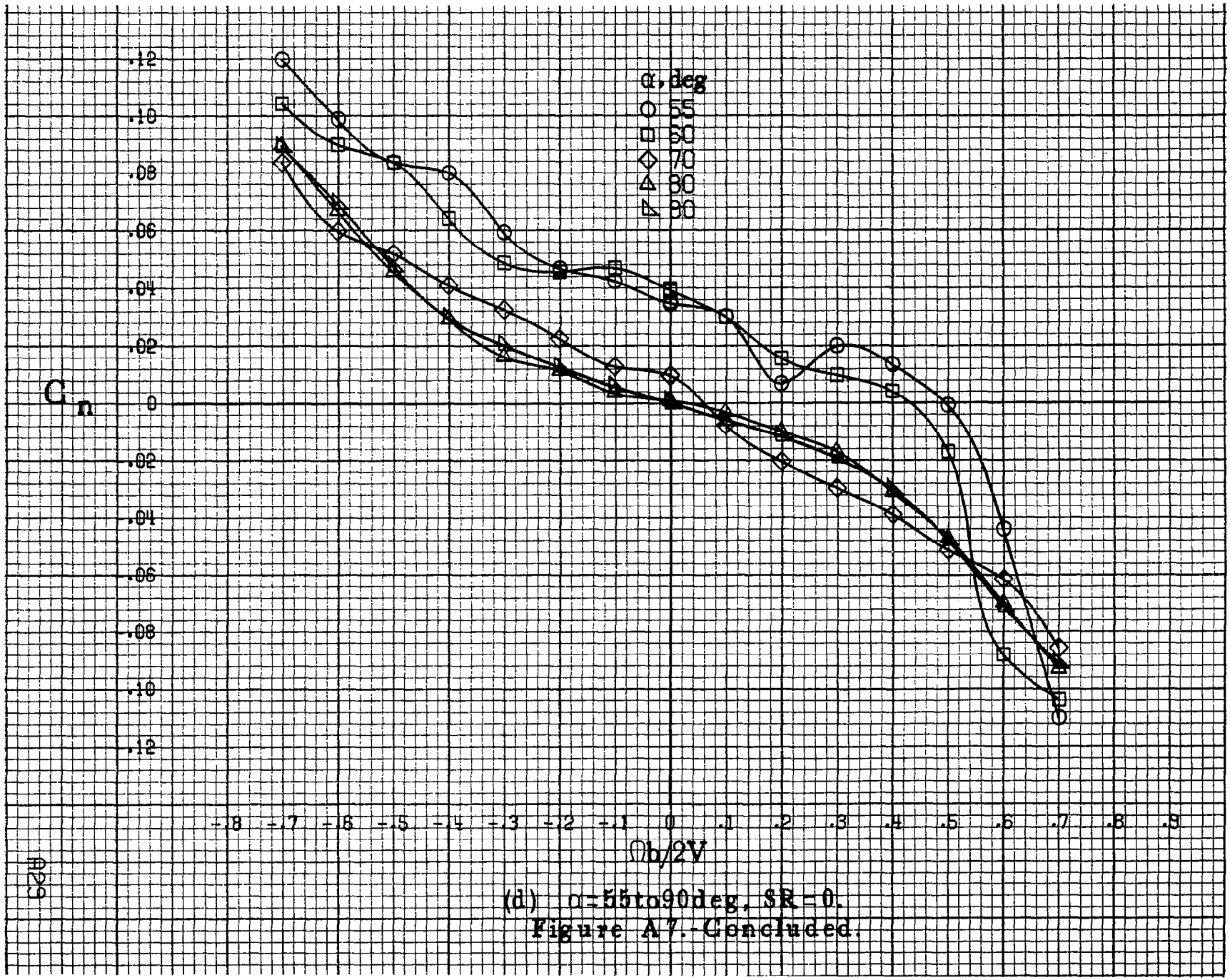

(d) α=55to90deg, SR=0.

Figure A7.-Concluded.

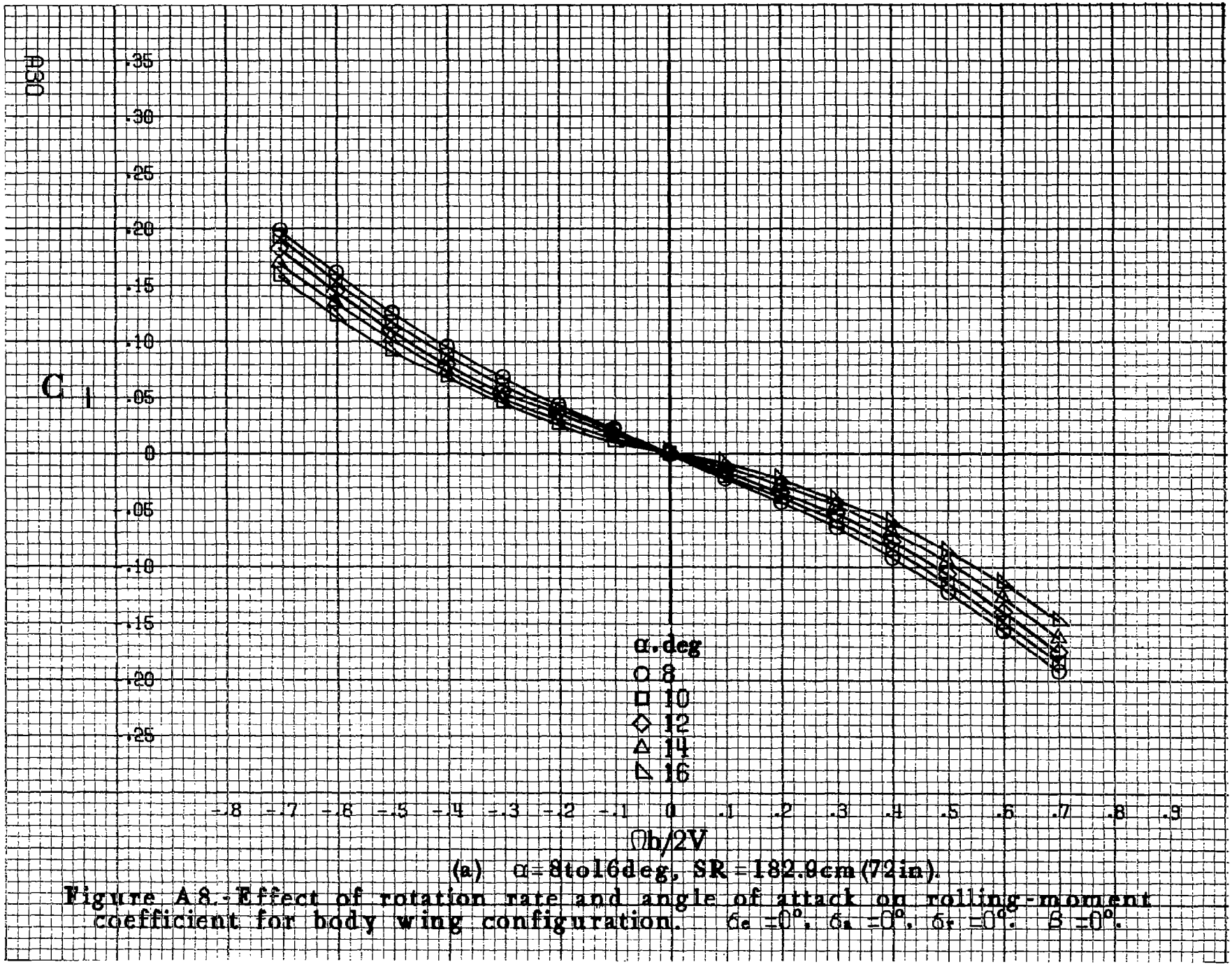

(a) $\alpha = 8$ to 16 deg, SR = 182.9 cm (72 in).

Figure A8.- Effect of rotation rate and angle of attack on rolling-moment coefficient for body wing configuration. $\delta_e = 0°$, $\delta_a = 0°$, $\delta_r = 0°$, $\beta = 0°$.

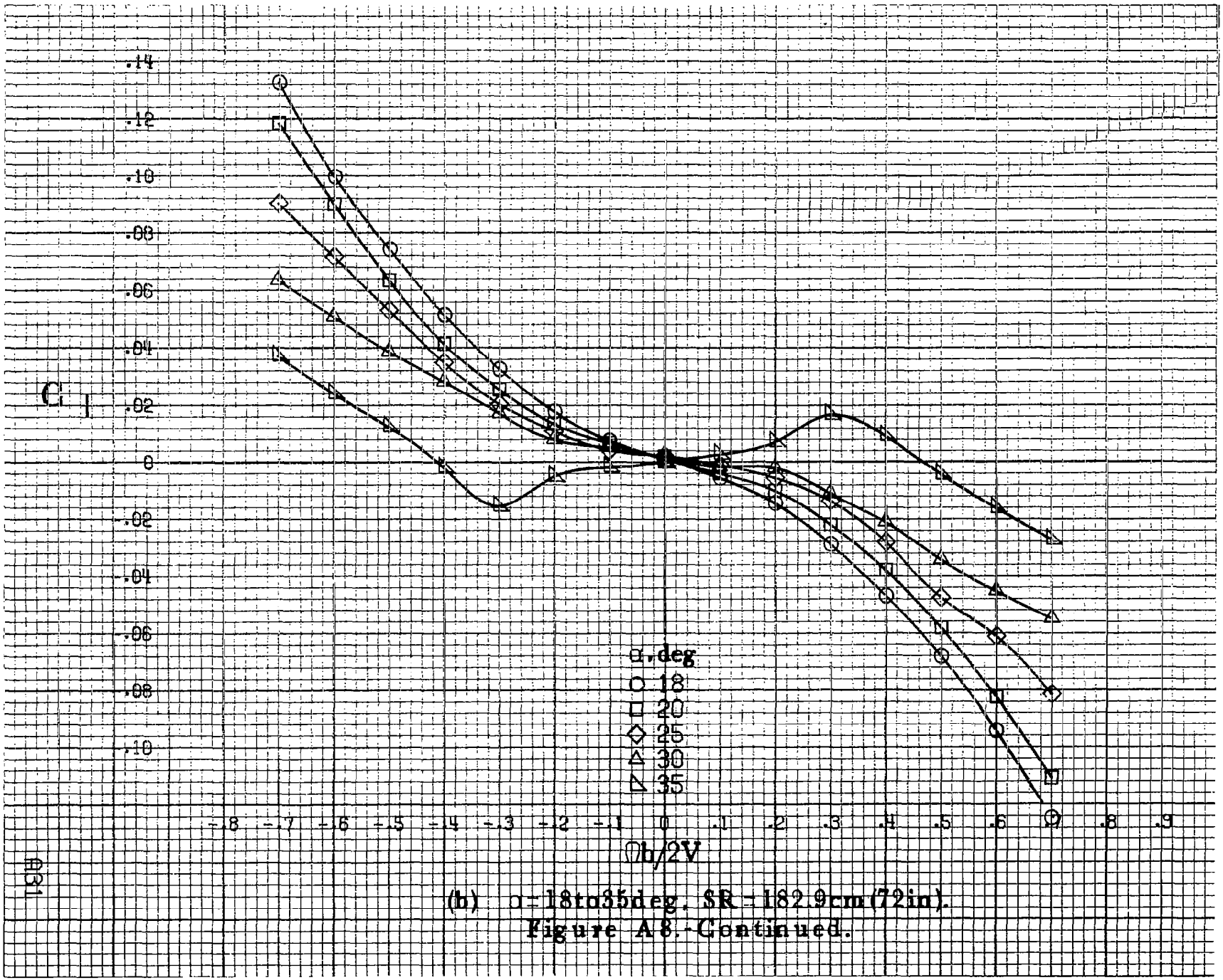

(b) α = 18 to 35 deg. SR = 182.9 cm (72 in).

Figure A8.-Continued.

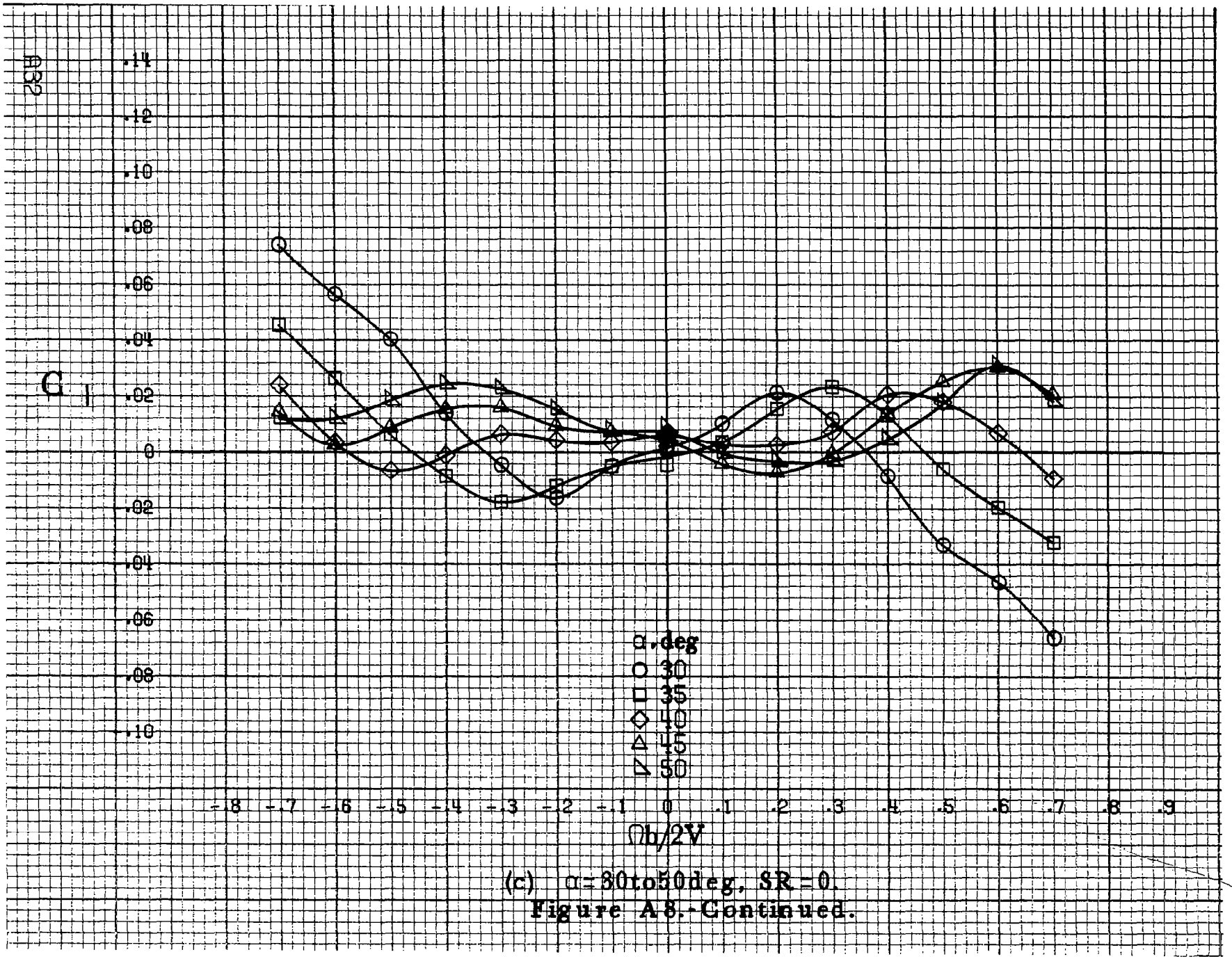

(c) $\alpha = 30$ to 50 deg, SR = 0.

Figure A8.- Continued.

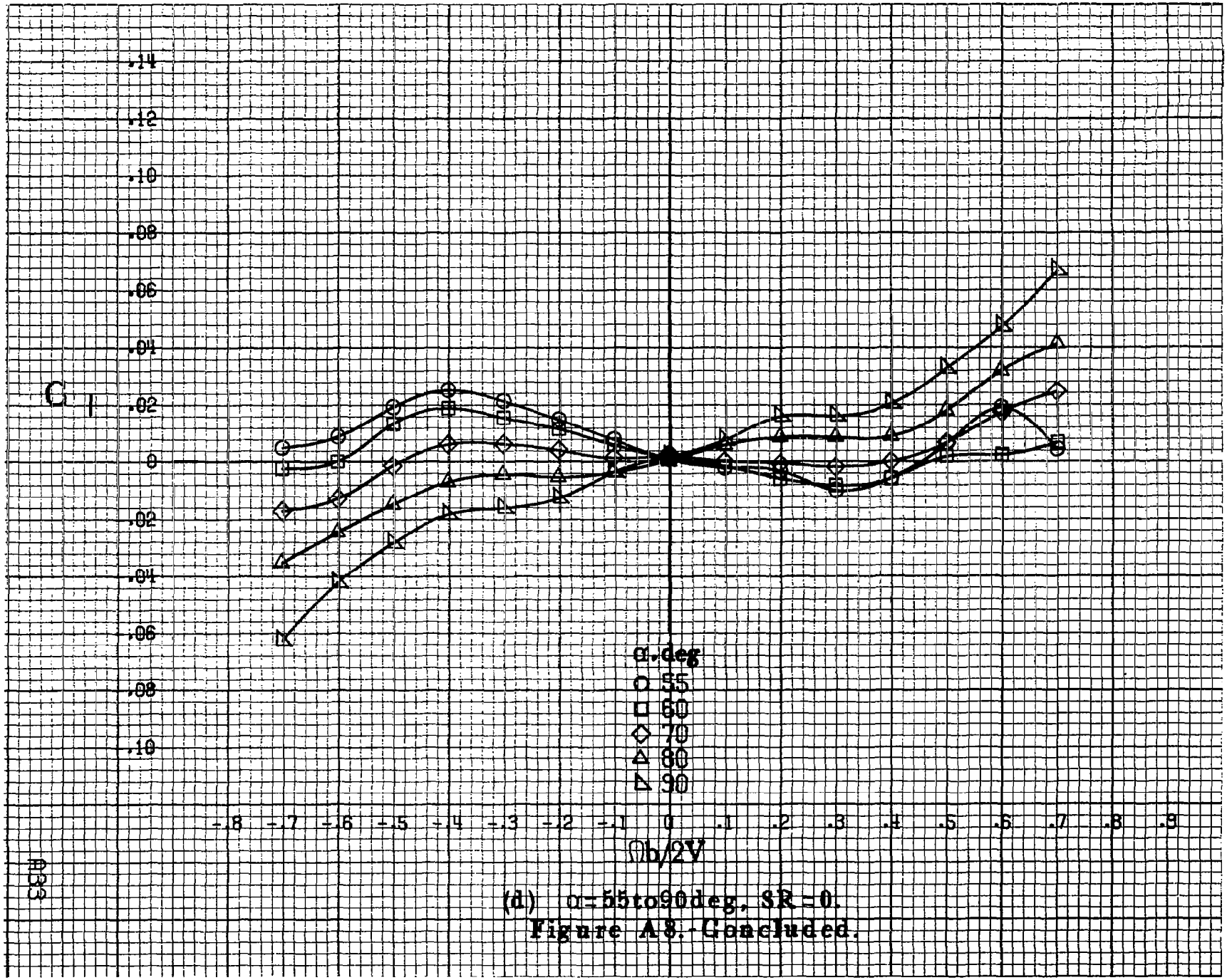

(d) α = 55 to 90 deg, SR = 0.

Figure A8.- Concluded.

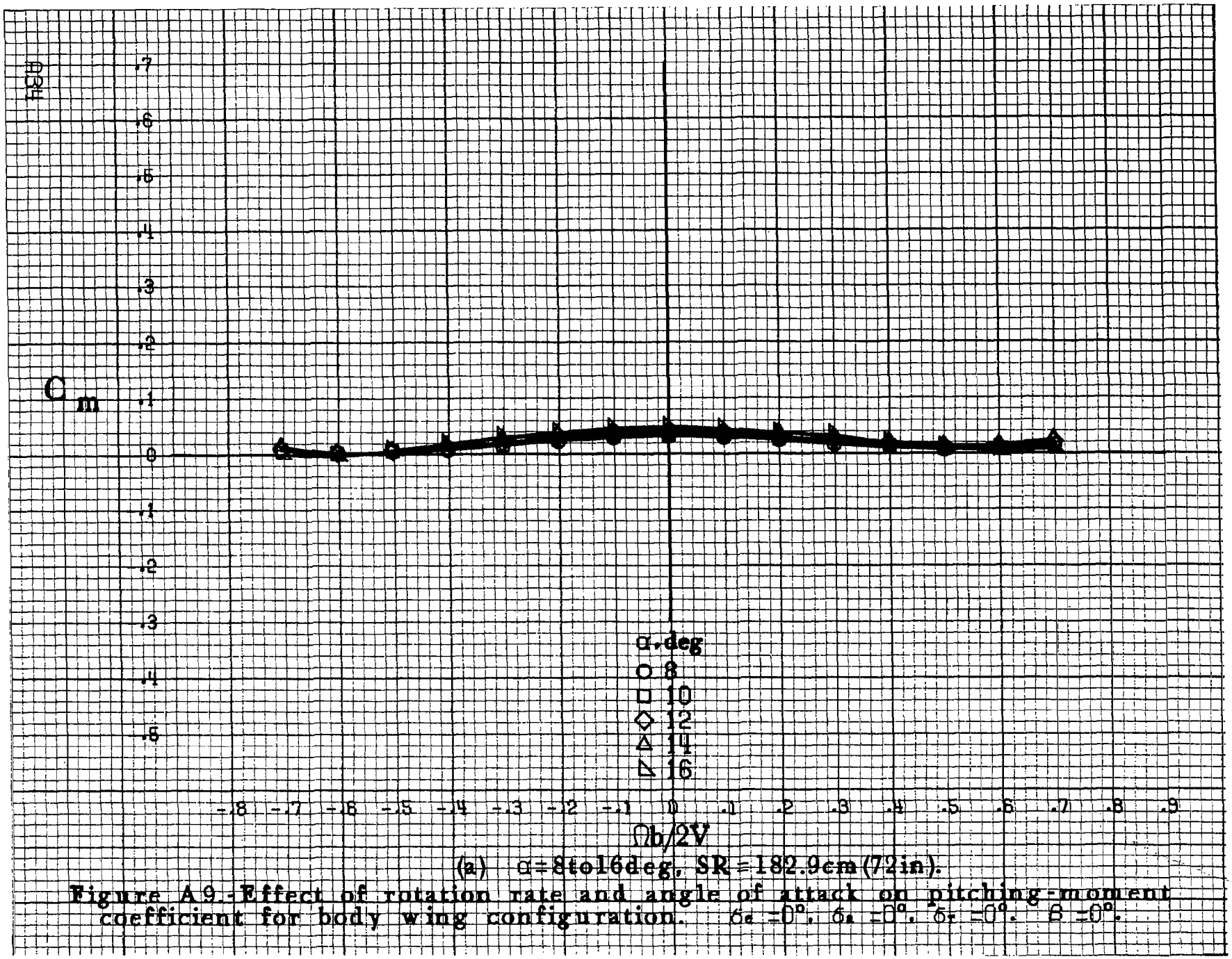

(a) $\alpha = 8$ to 16 deg, SR = 182.9 cm (72 in).

Figure A9.- Effect of rotation rate and angle of attack on pitching-moment coefficient for body wing configuration. $\delta_e = 0°$, $\delta_a = 0°$, $\delta_r = 0°$, $\beta = 0°$.

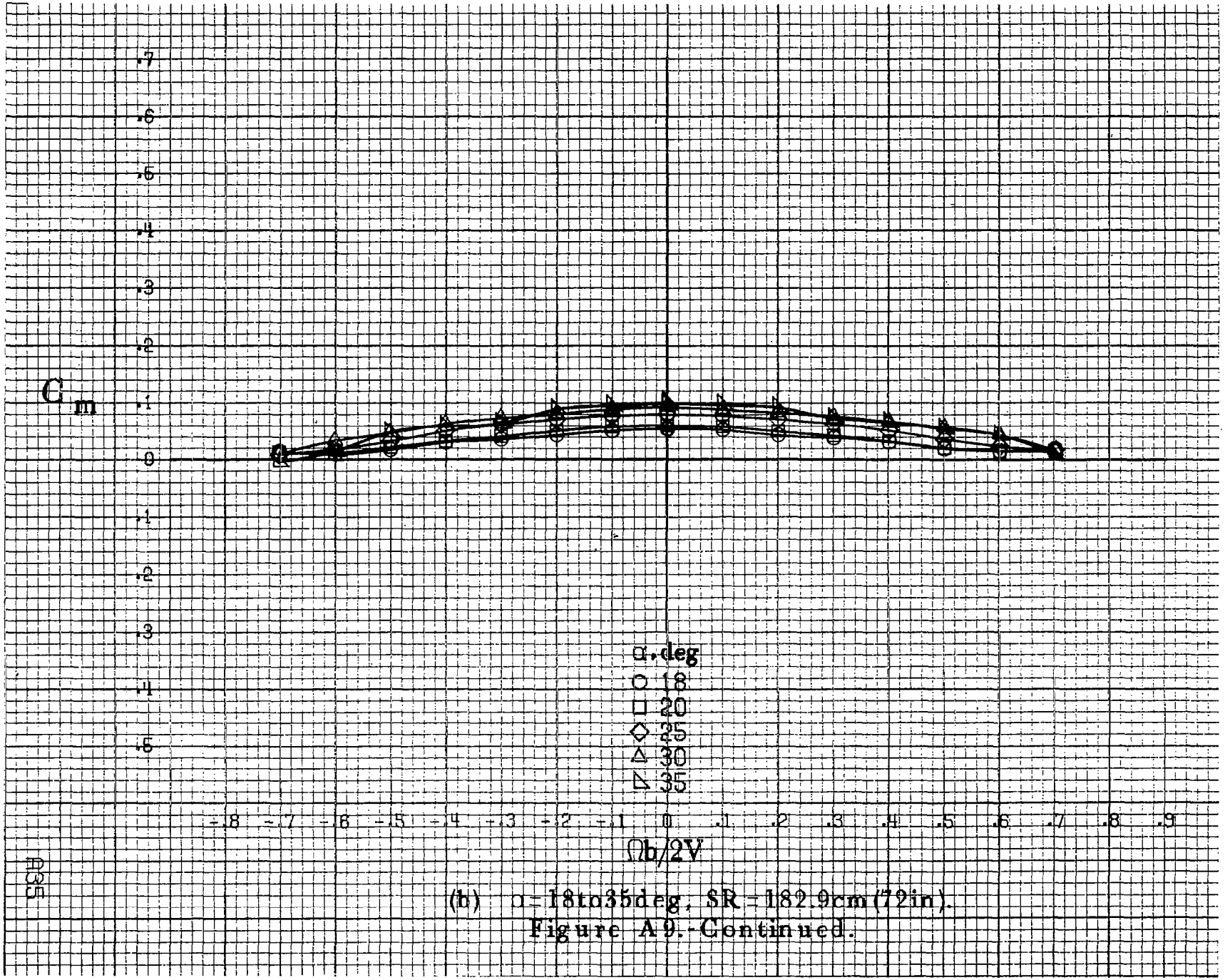

(b) α = 18 to 35 deg, SR = 182.9 cm (72 in).

Figure A9.- Continued.

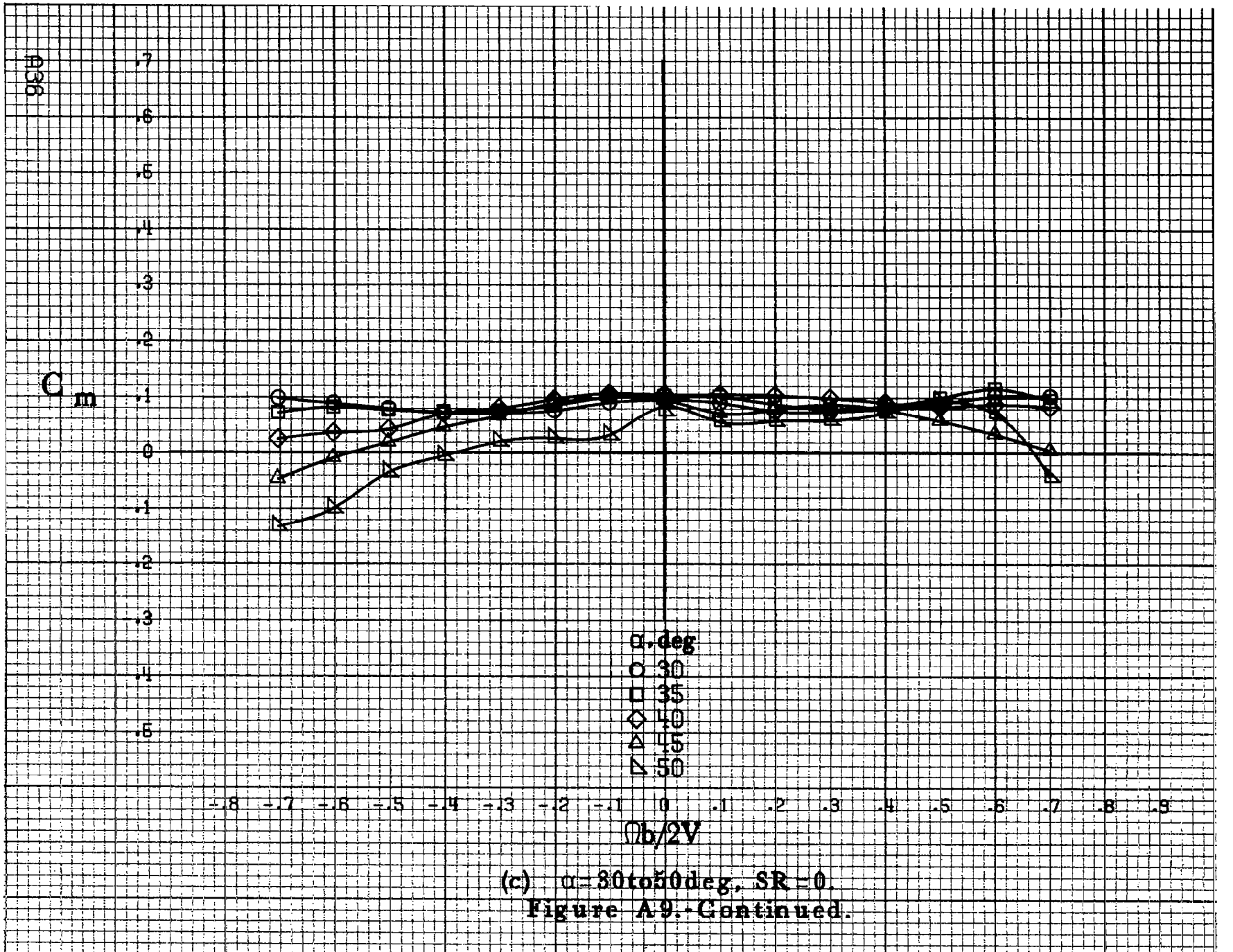

(c) α=30to50deg, SR=0.

Figure A9.-Continued.

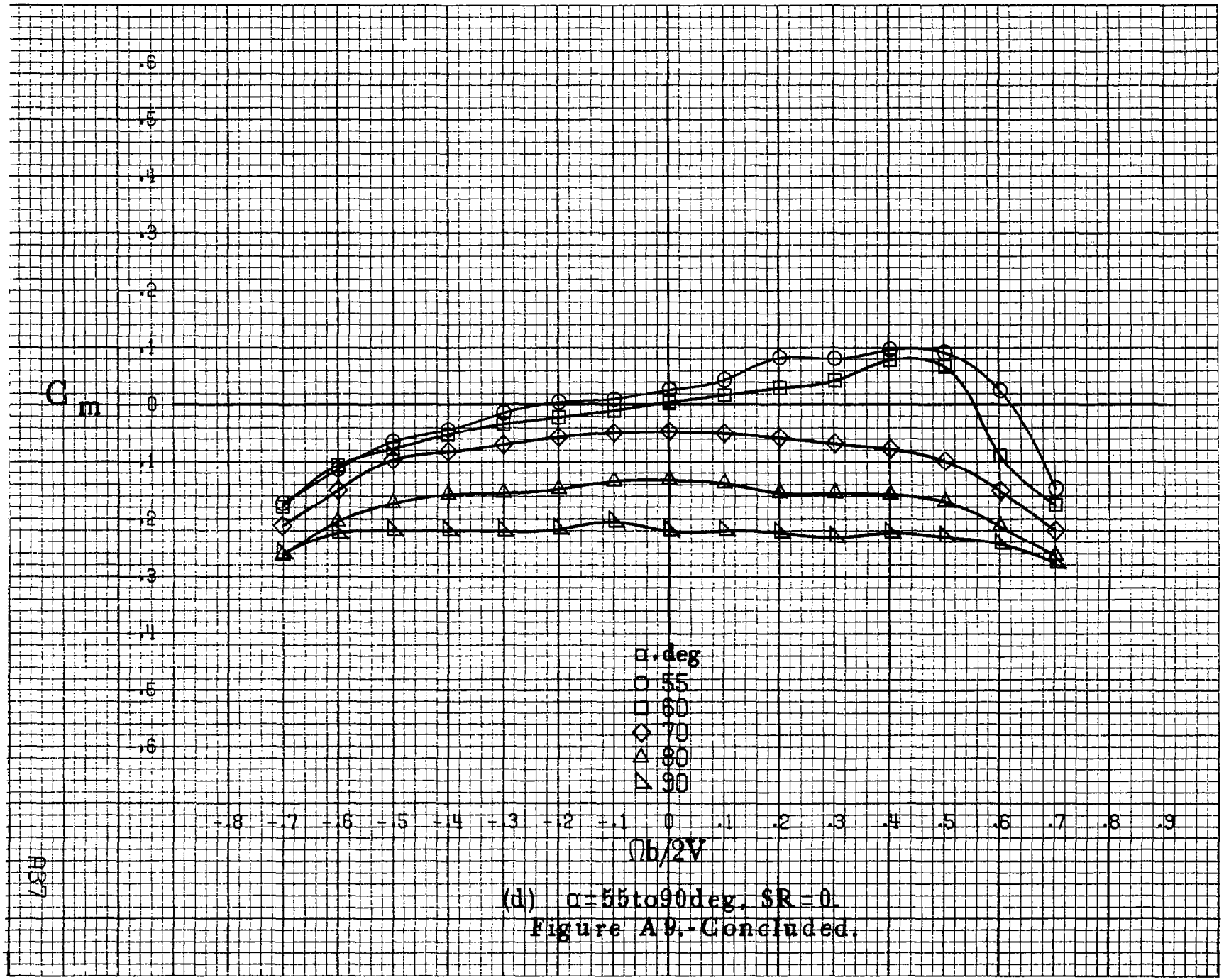

(d) α = 55 to 90 deg, SR = 0.

Figure A9.- Concluded.

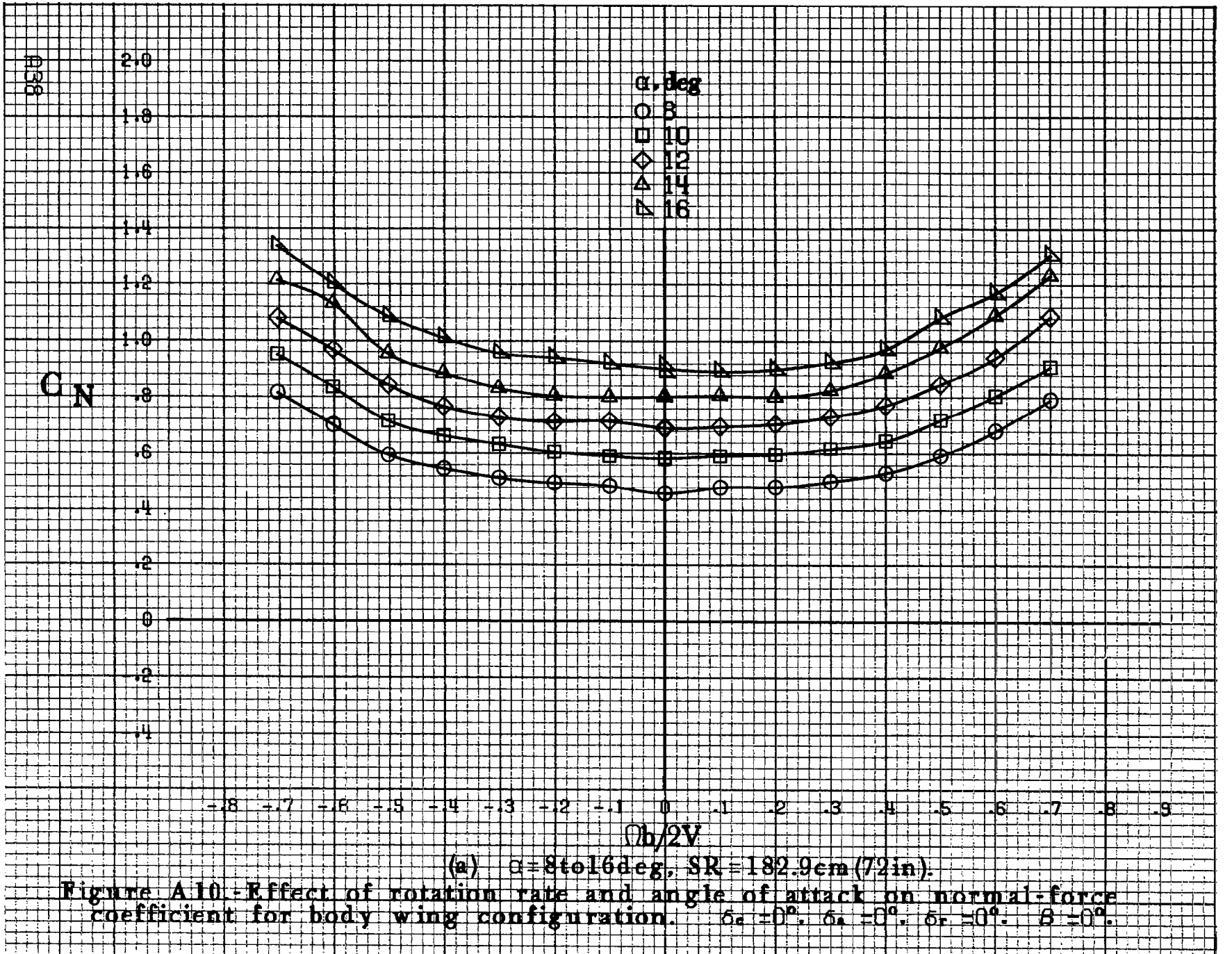

(a) $\alpha = 8$ to 16 deg, SR = 182.9 cm (72 in).

Figure A10.- Effect of rotation rate and angle of attack on normal-force coefficient for body wing configuration. $\delta_e = 0°$, $\delta_a = 0°$, $\delta_r = 0°$, $\beta = 0°$.

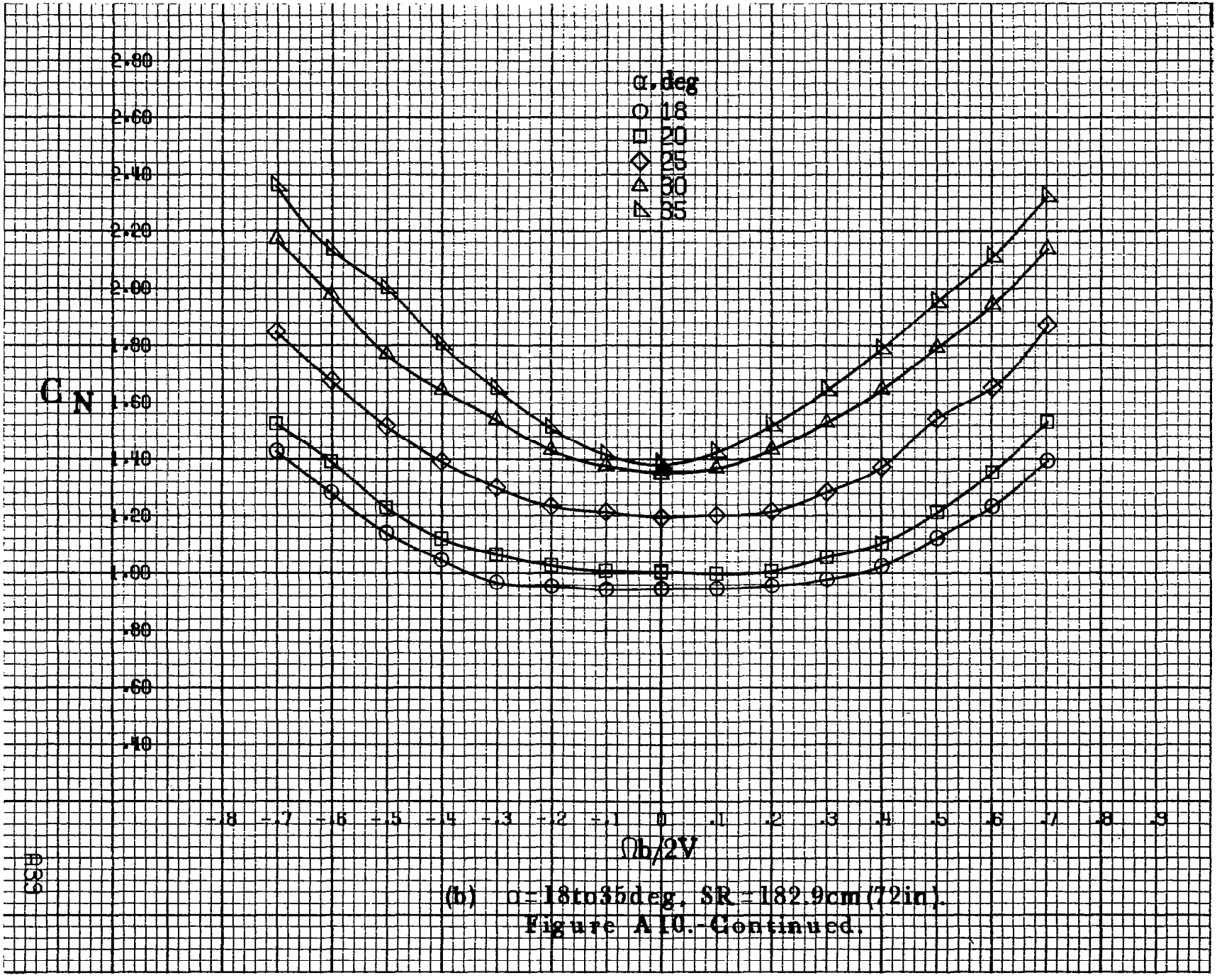

(b) α = 18 to 35 deg, SR = 182.9 cm (72 in).

Figure A10.-Continued.

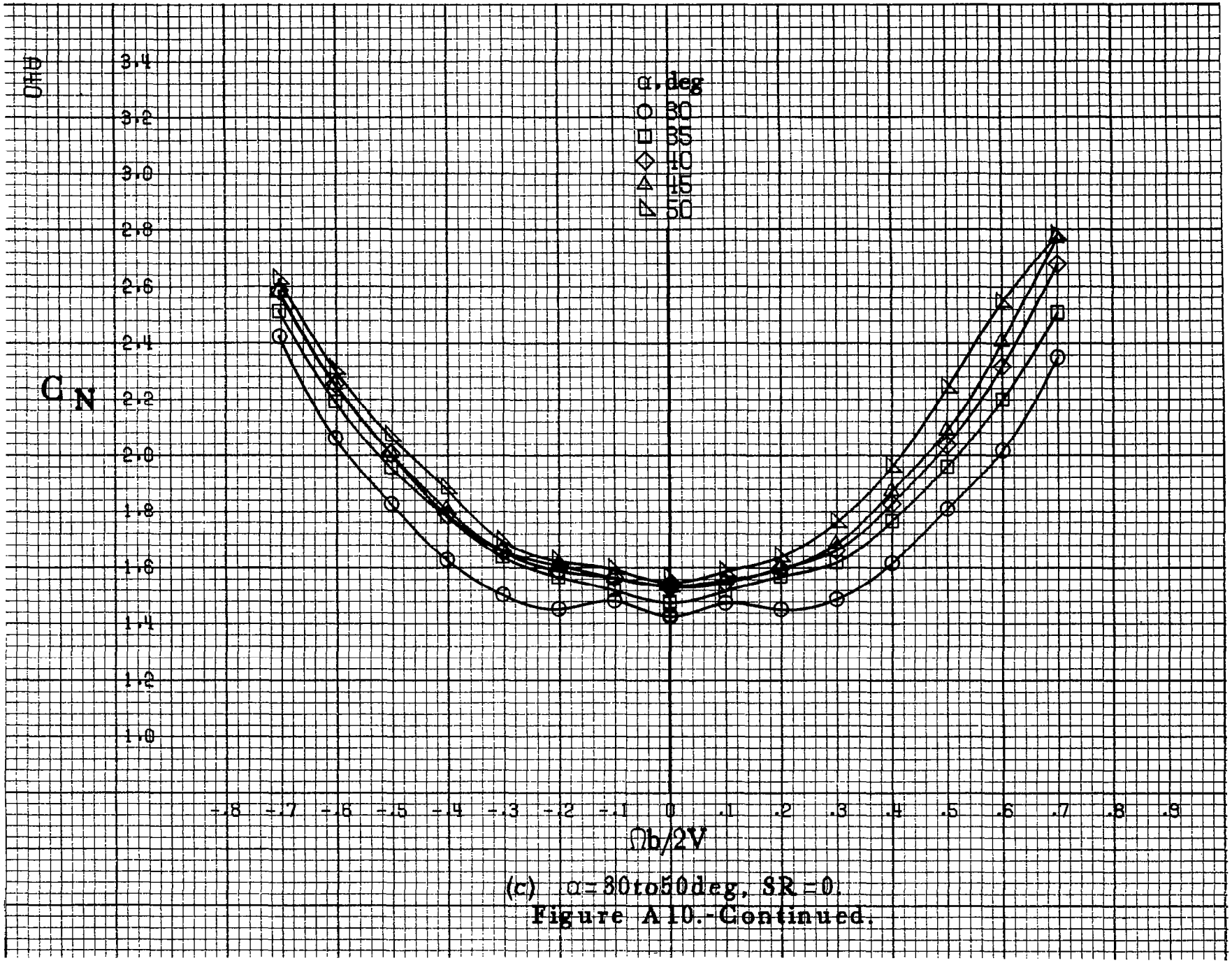

(c) $\alpha = 30$ to 50 deg, $SR = 0$.

Figure A10.-Continued.

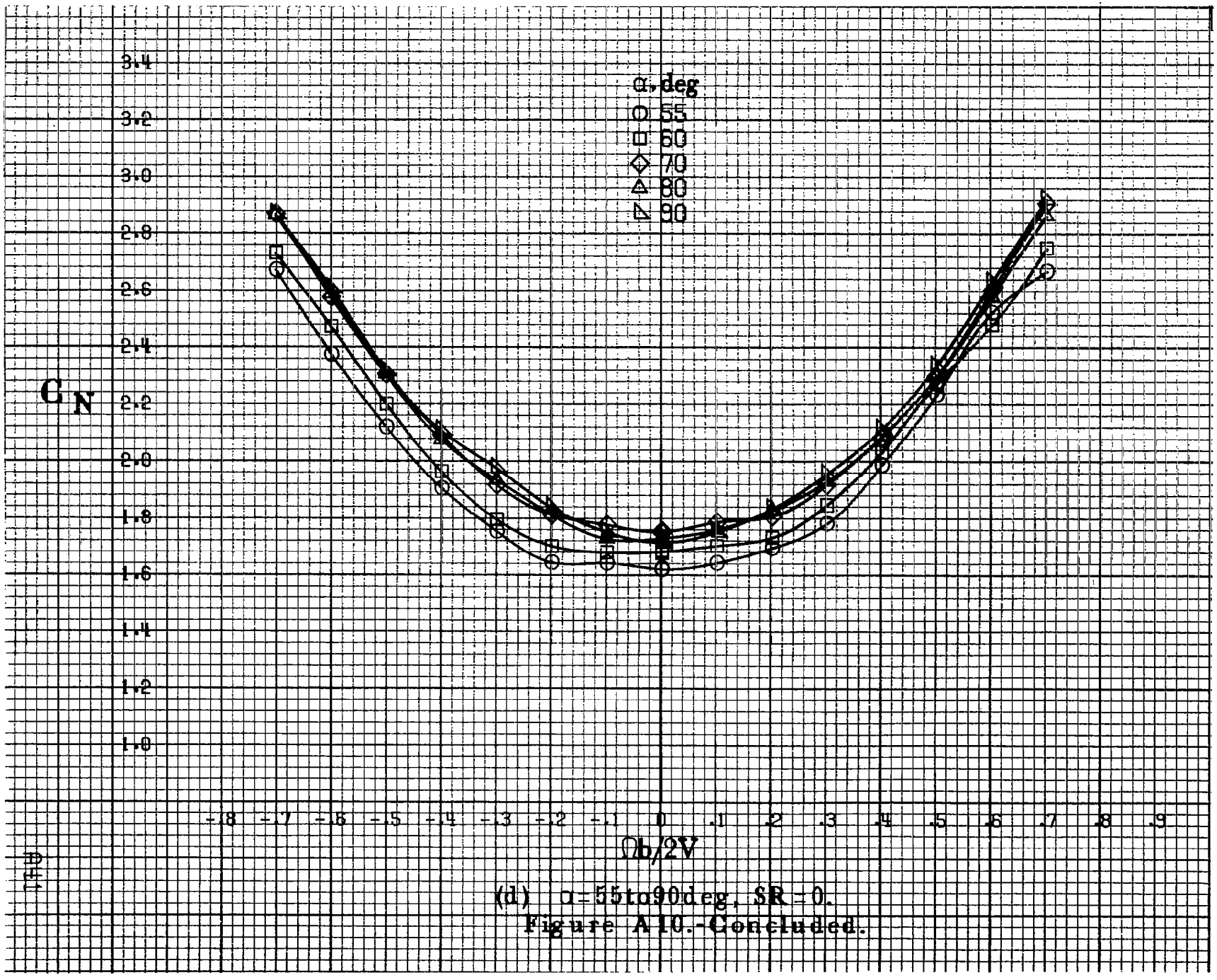

(d) $\alpha = 55$ to 90 deg, $SR = 0$.

Figure A10.-Concluded.

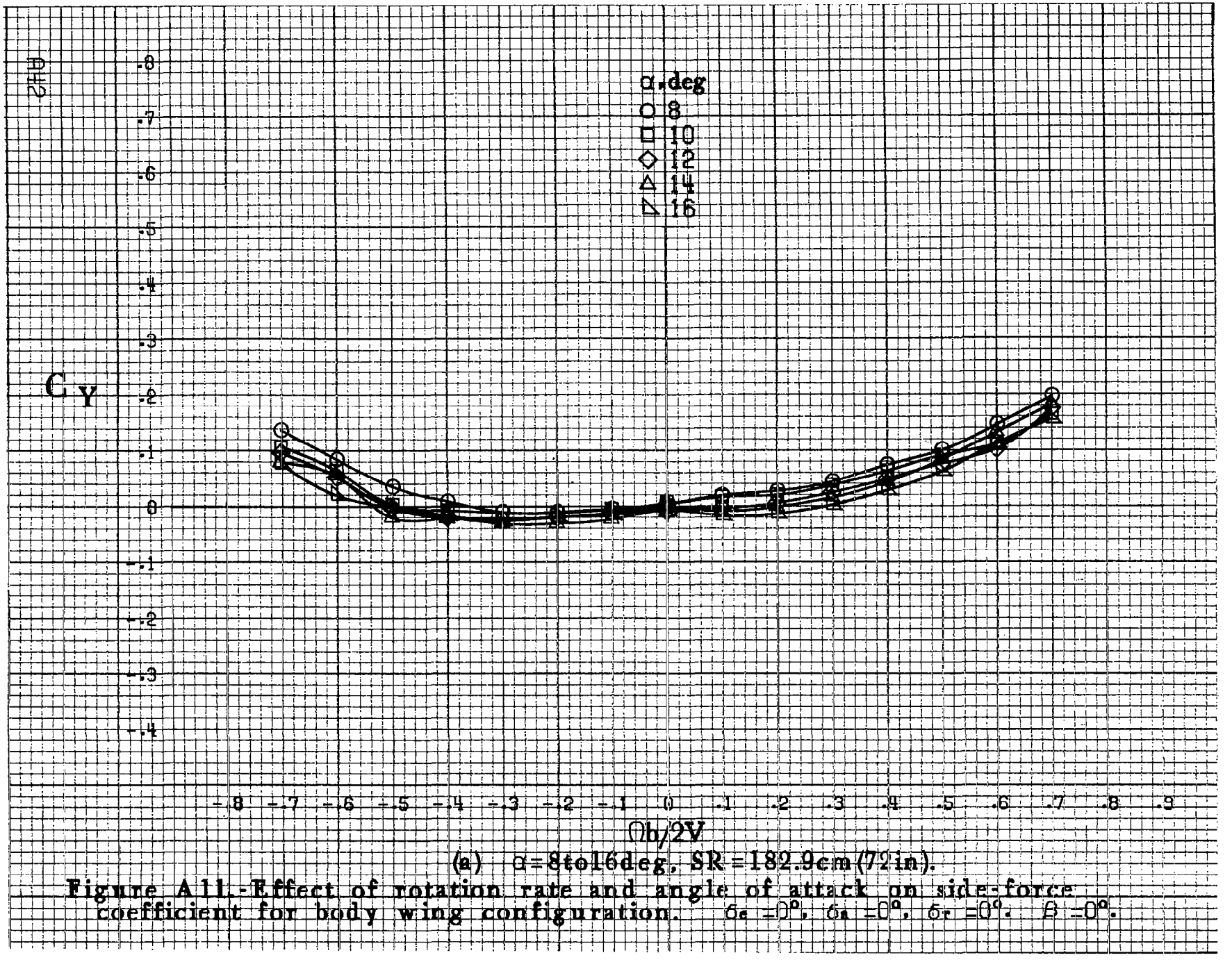

(a) α = 8 to 16 deg, SR = 182.9 cm (72 in.).

Figure A11.-Effect of rotation rate and angle of attack on side-force coefficient for body wing configuration. $\delta_e = 0°$, $\delta_a = 0°$, $\delta_r = 0°$, $\beta = 0°$.

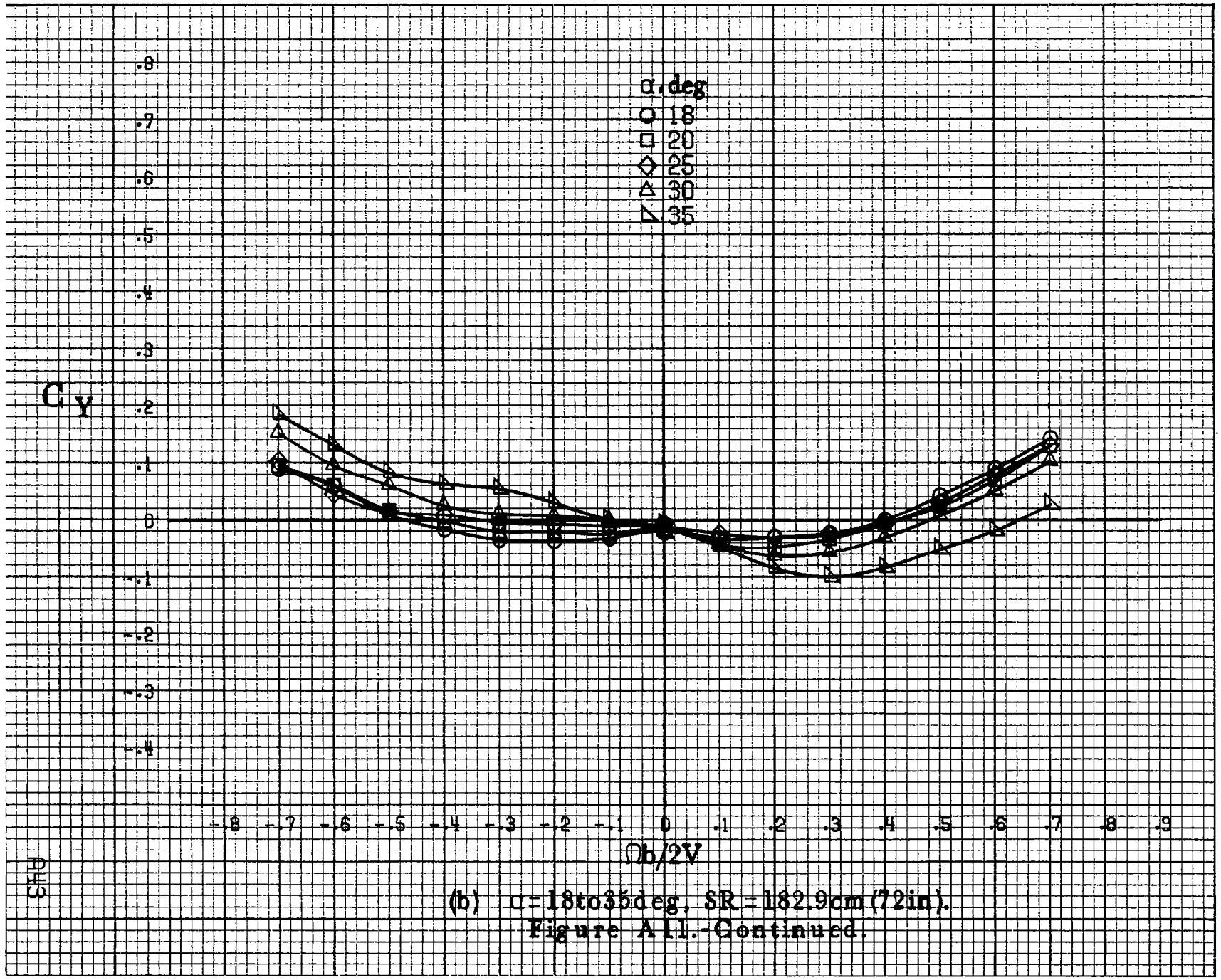

(b) $\alpha = 18$ to 35 deg, SR = 182.9 cm (72 in).

Figure A11.-Continued.

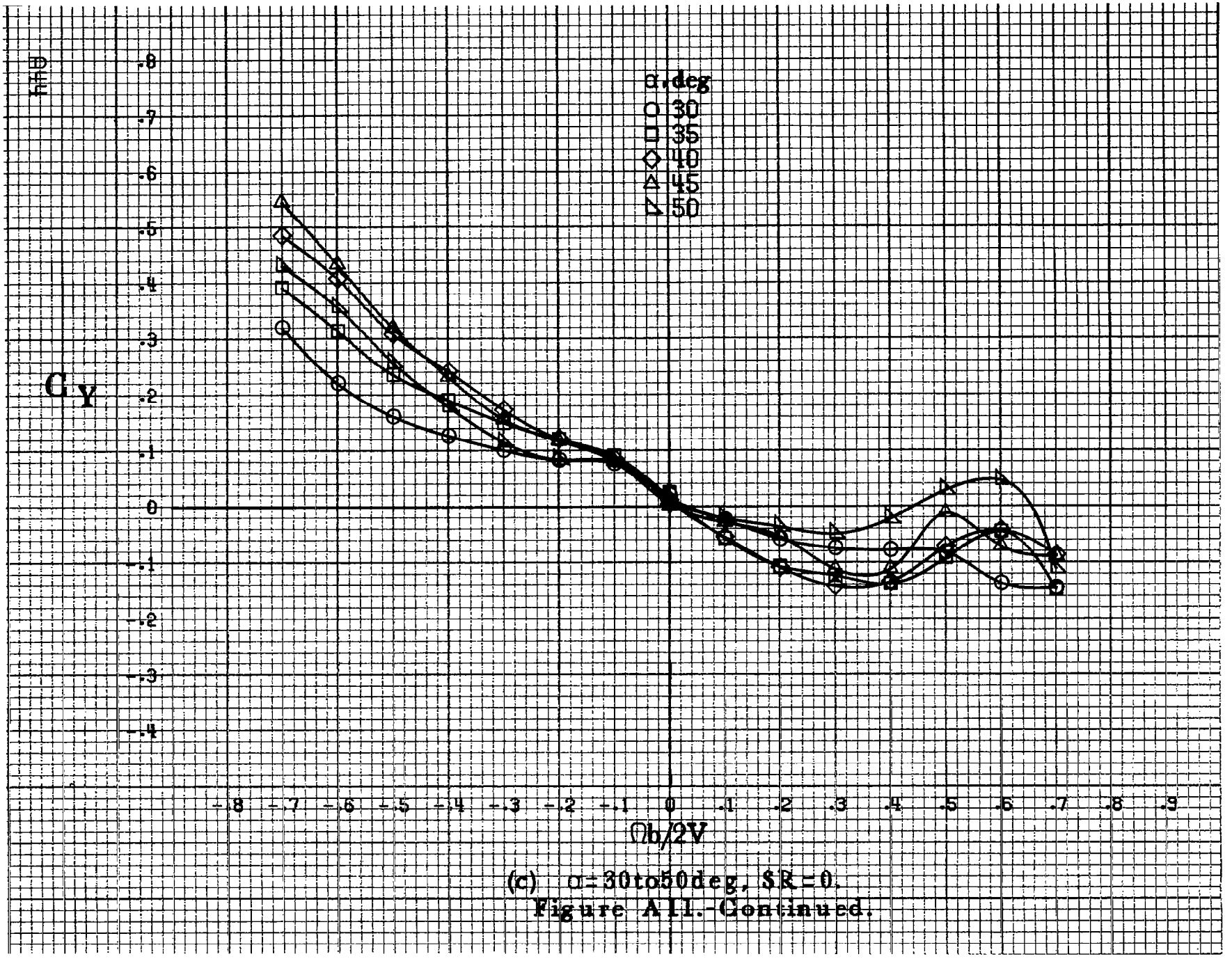

(c) $\alpha = 30$ to 50 deg, $\$R = 0$.

Figure A11.-Continued.

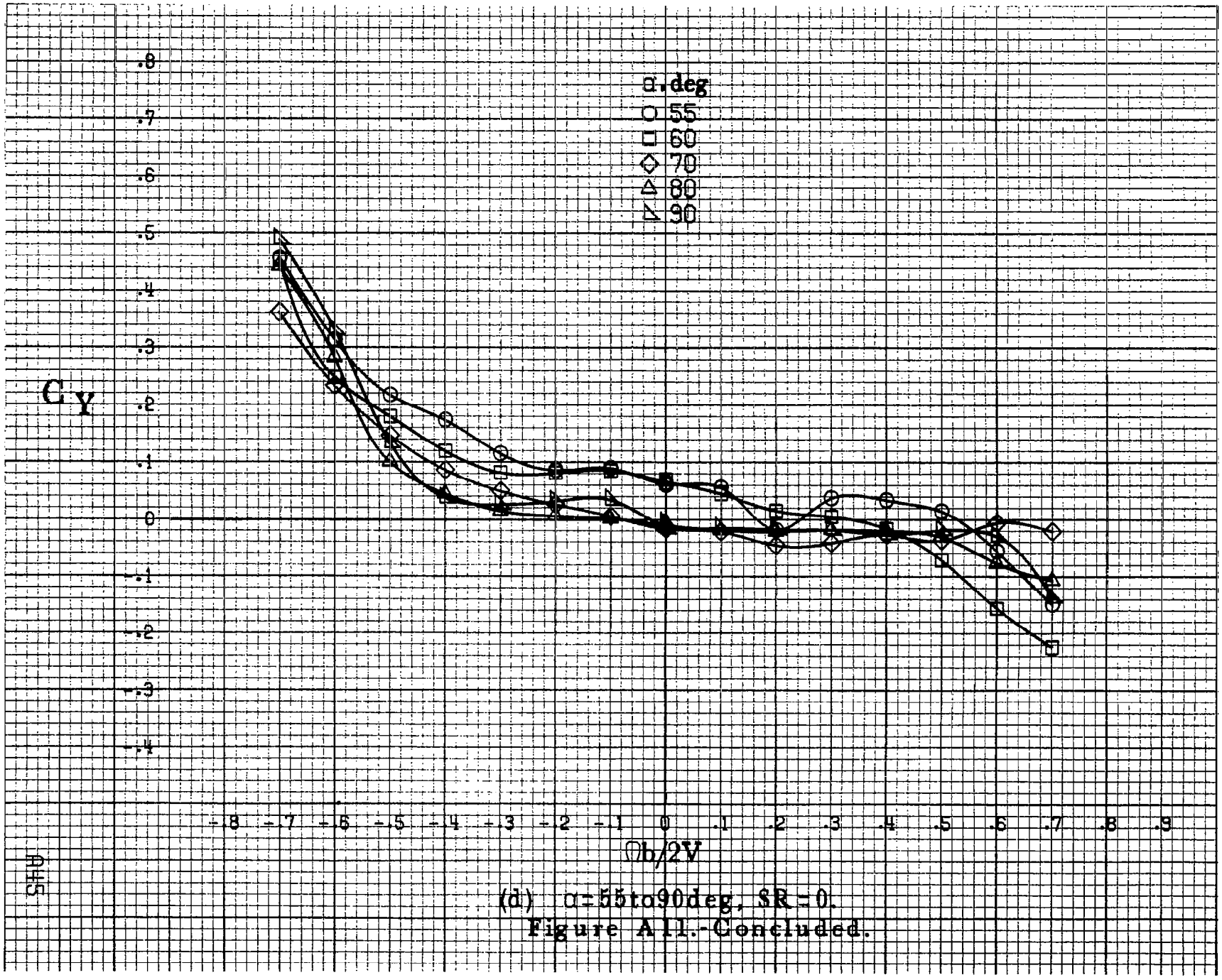

(d) α = 55 to 90 deg, SR = 0.

Figure A11.- Concluded.

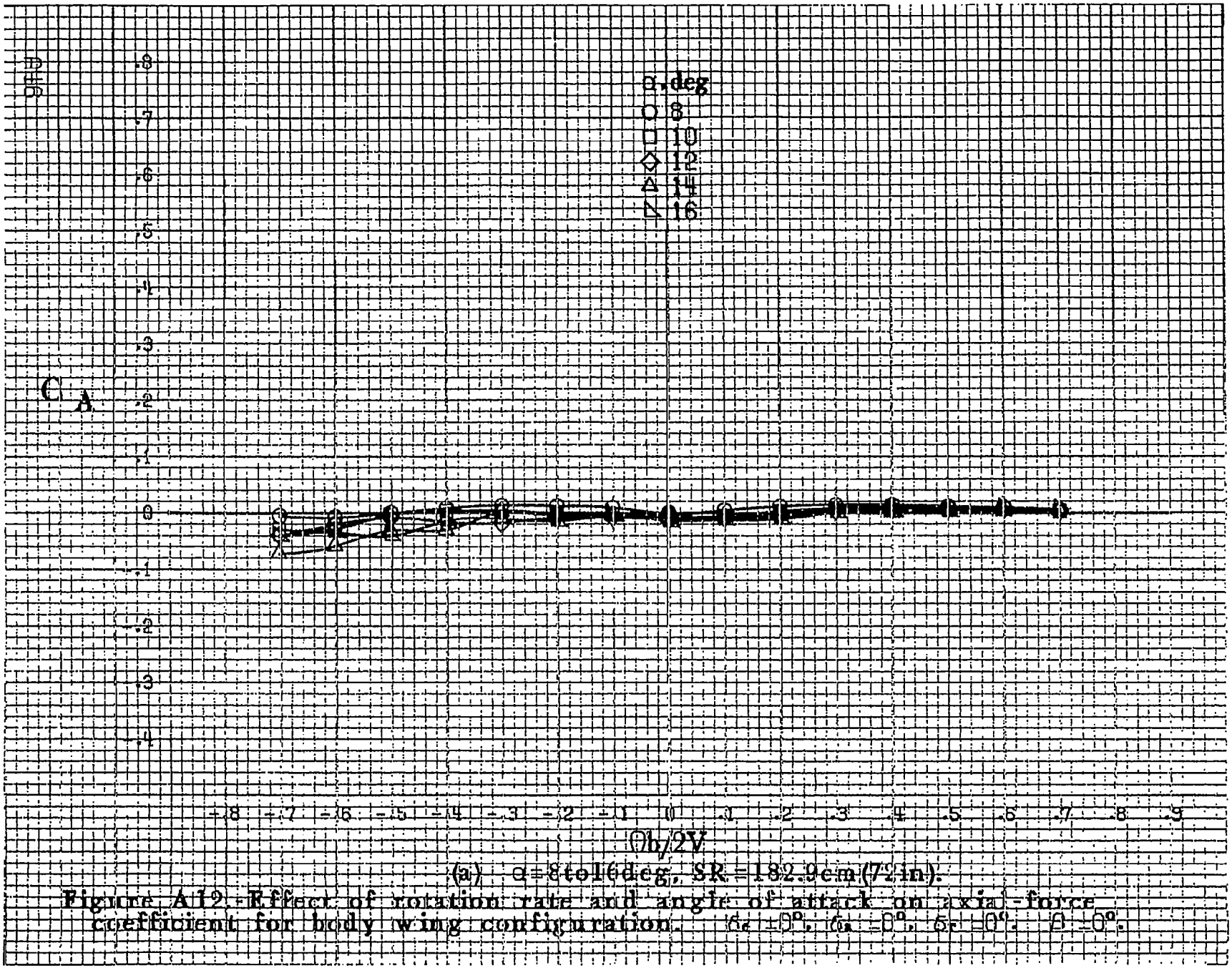

(a) $\alpha = 8$ to 16 deg, SR = 182.9 cm (72 in.).

Figure A12.- Effect of rotation rate and angle of attack on axial-force coefficient for body wing configuration. $\delta_f = 0°$, $\delta_a = 0°$, $\delta_r = 0°$, $\beta = 0°$.

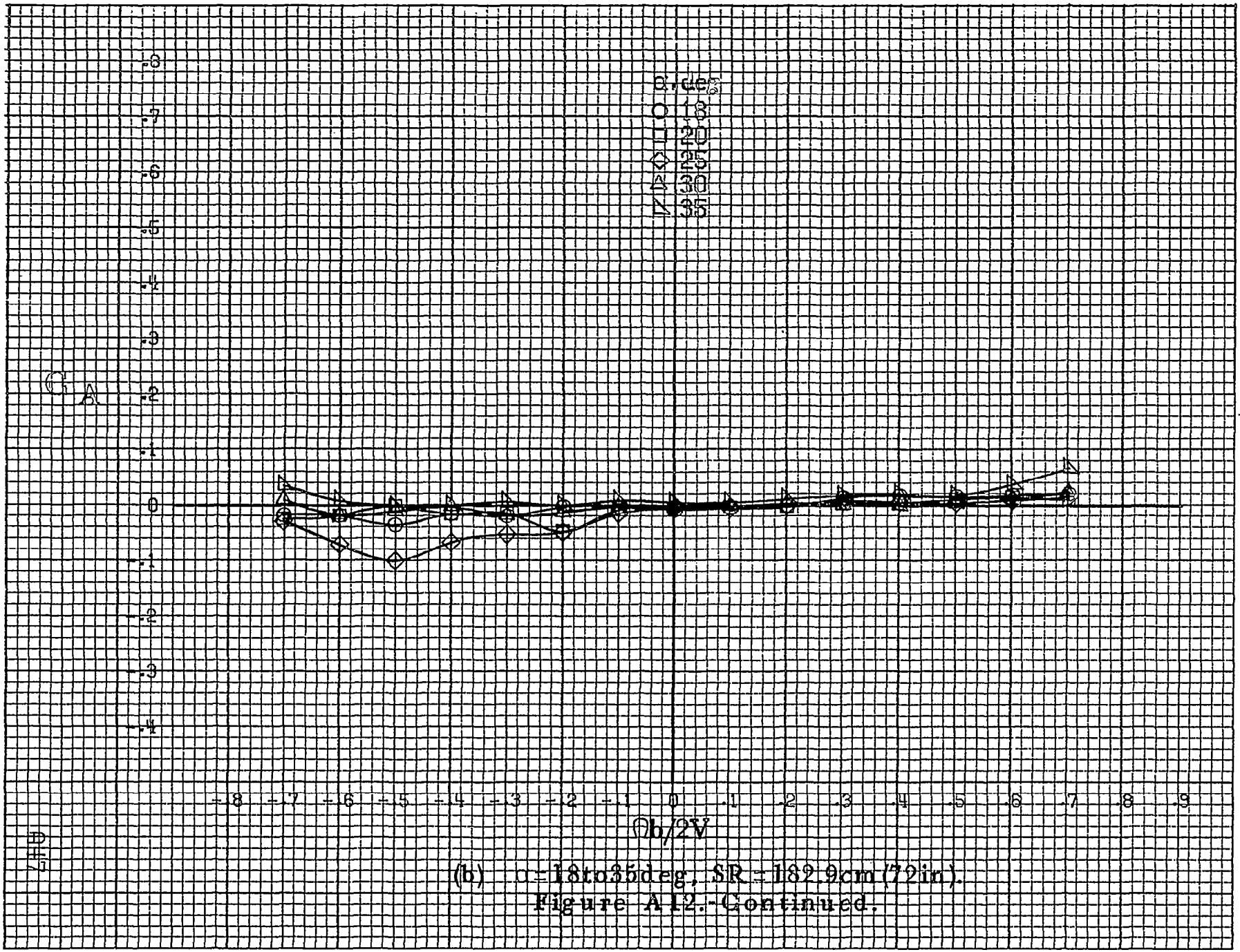

(b) α=18to35deg, SR=182.9cm(72in).

Figure A12.-Continued.

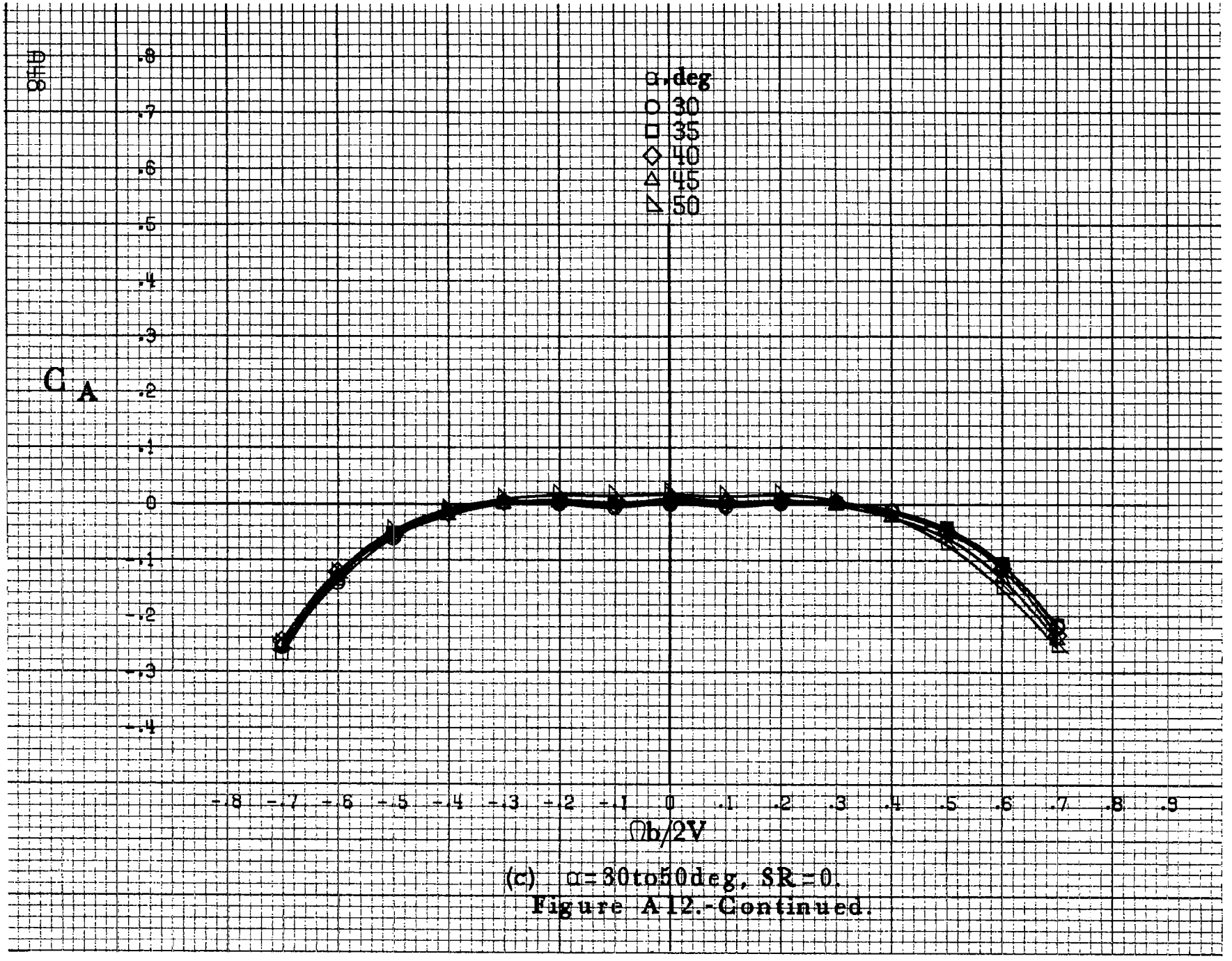

(c) $\alpha = 30$ to 50 deg, SR = 0.

Figure A12.-Continued.

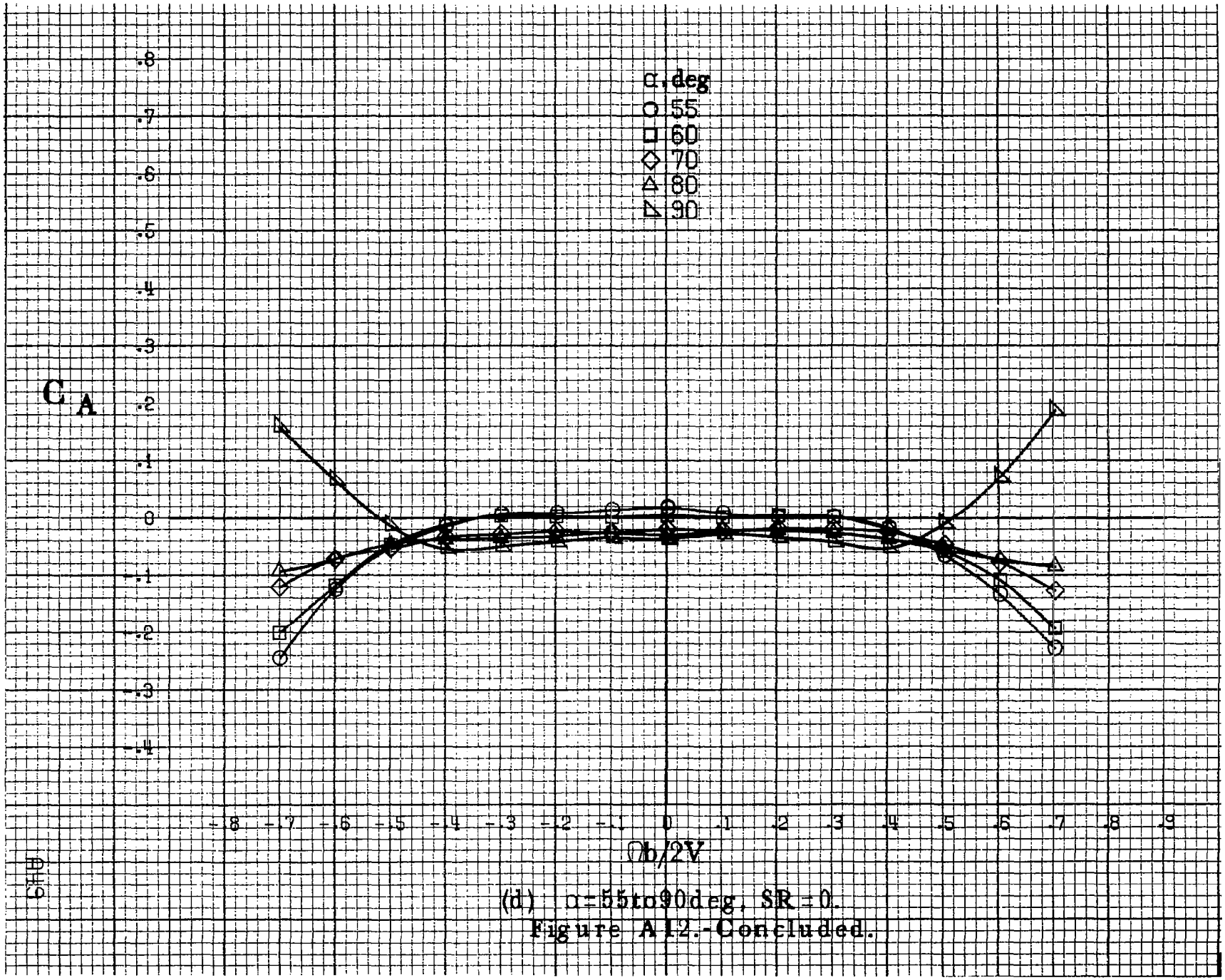

(d) α=55to90deg, SR=0.

Figure A12.-Concluded.

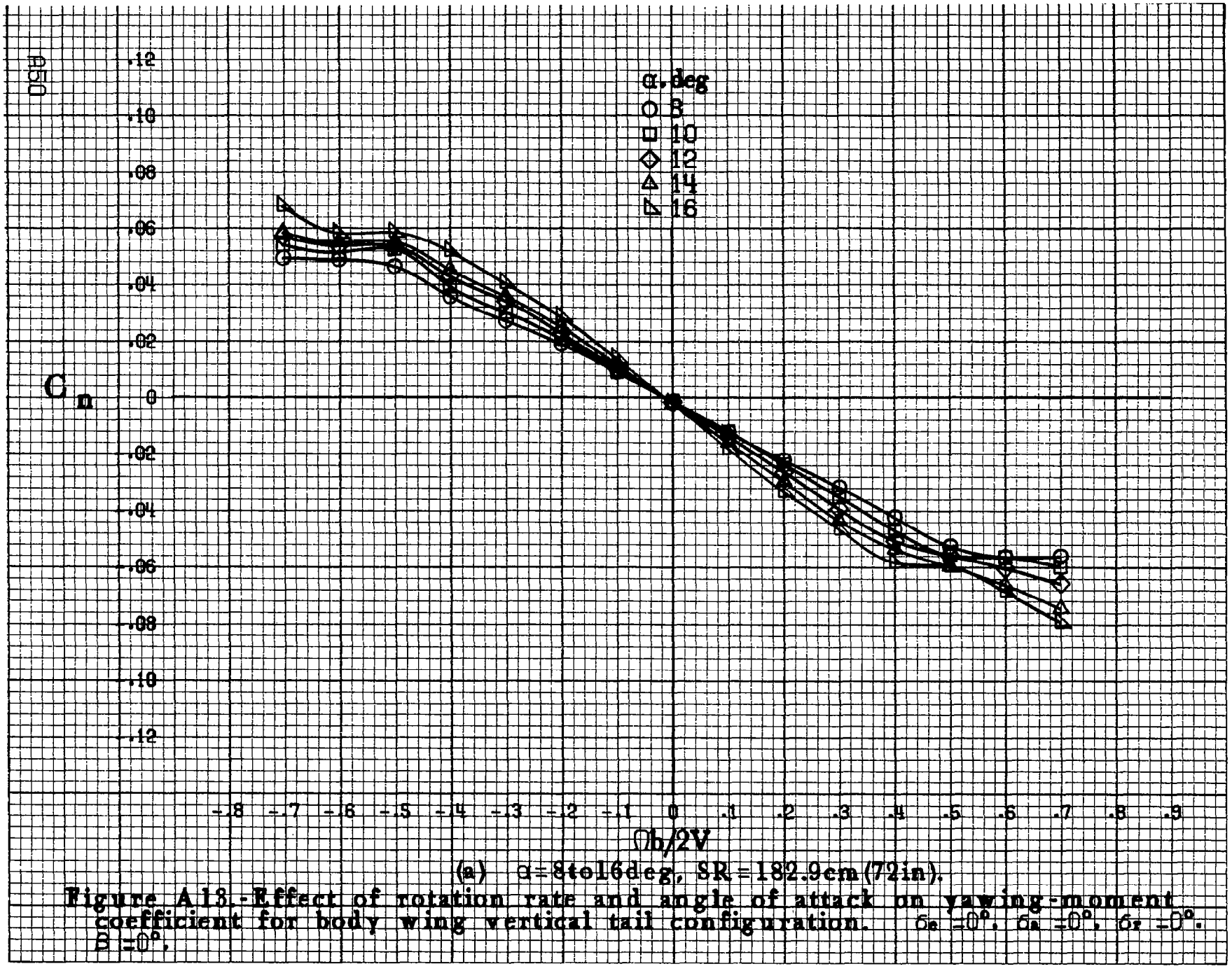

(a) $\alpha = 8$ to 16 deg, SR = 182.9 cm (72 in).

Figure A13.- Effect of rotation rate and angle of attack on yawing-moment coefficient for body wing vertical tail configuration. $\delta_e = 0°$, $\delta_a = 0°$, $\delta_r = 0°$, $\beta = 0°$.

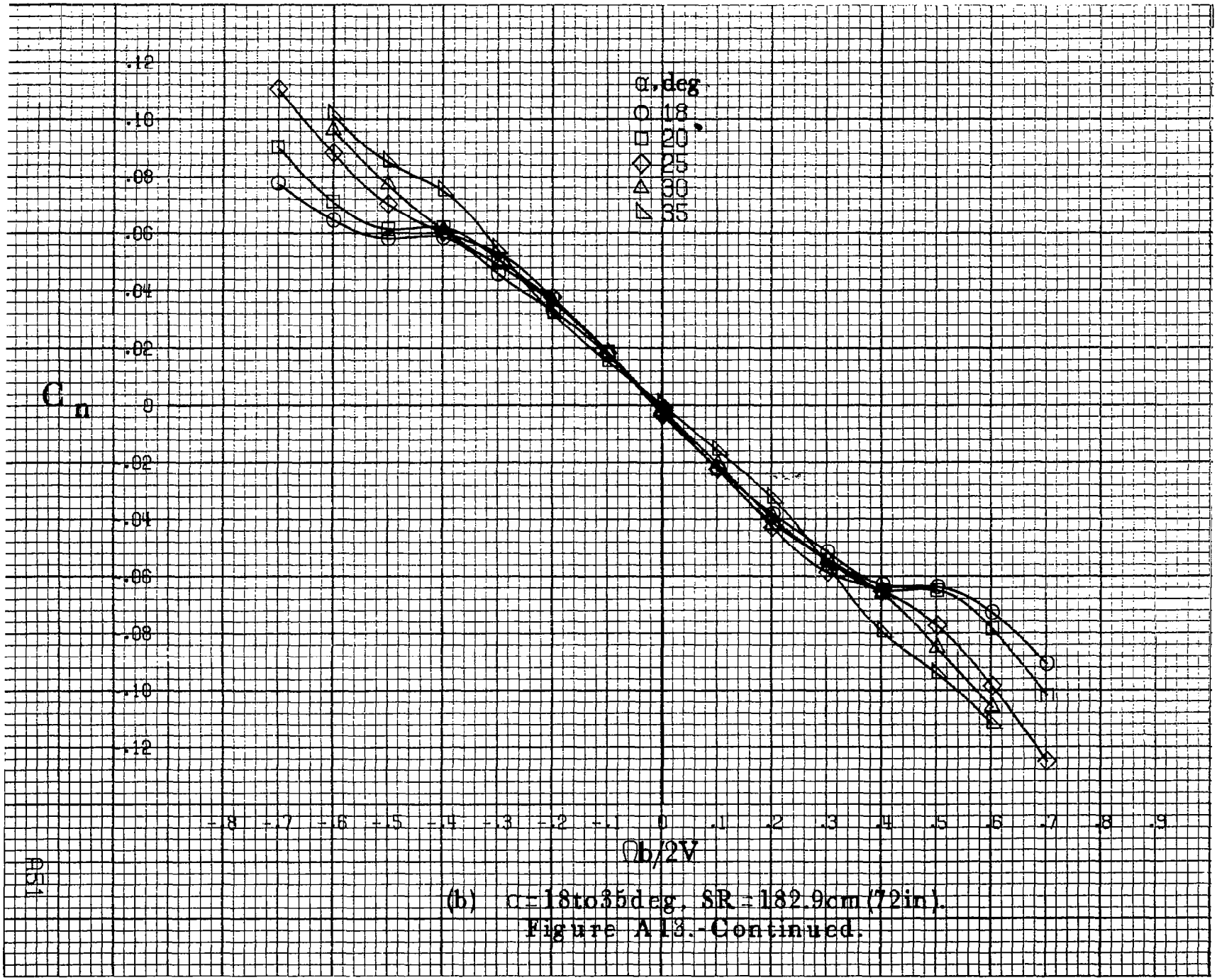

(b) $\alpha = 18$ to 35 deg, SR = 182.9 cm (72 in).

Figure A13.- Continued.

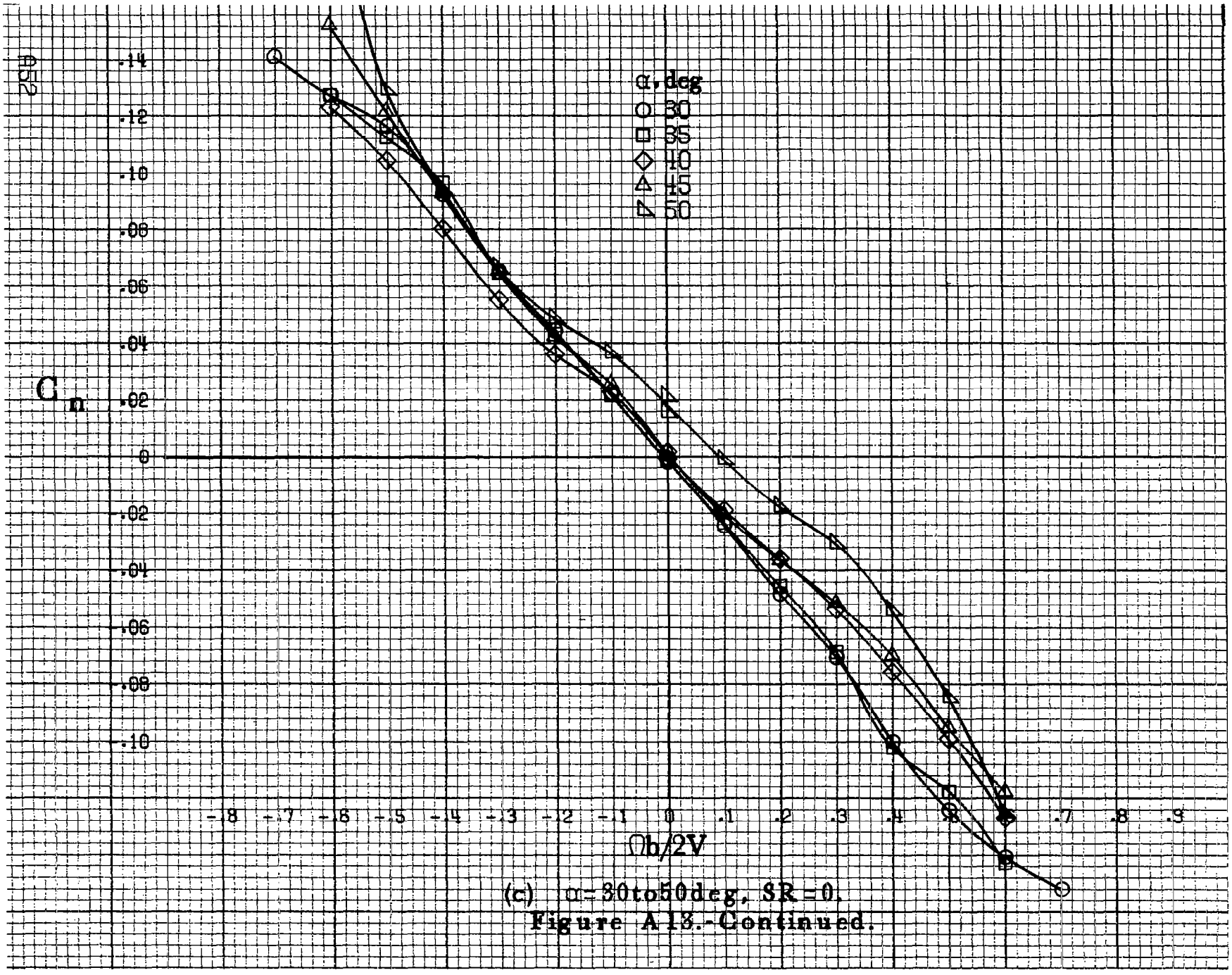

(c) α = 30 to 50 deg, SR = 0.

Figure A 13.- Continued.

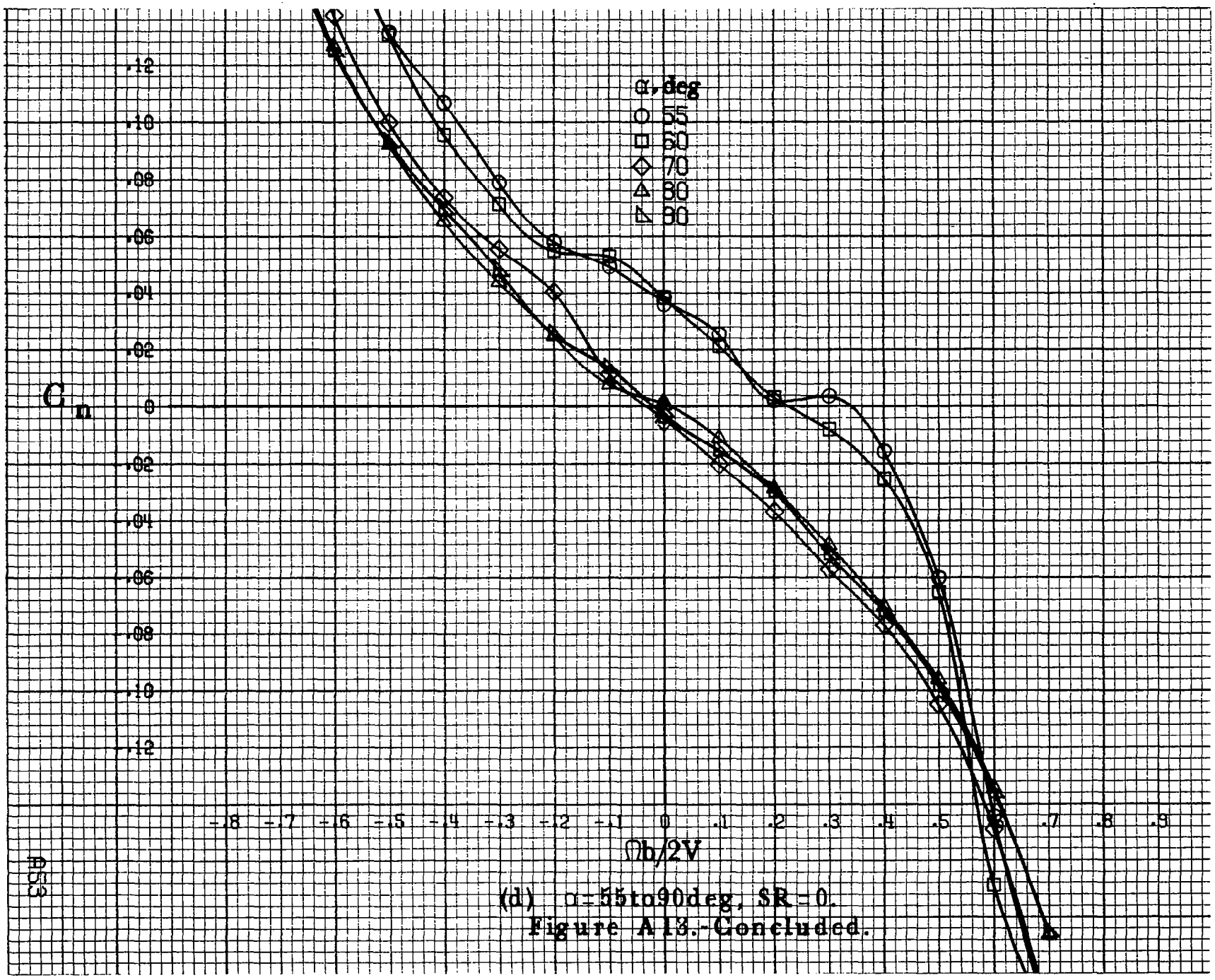

(d) α=55to90deg, SR=0.

Figure A13.-Concluded.

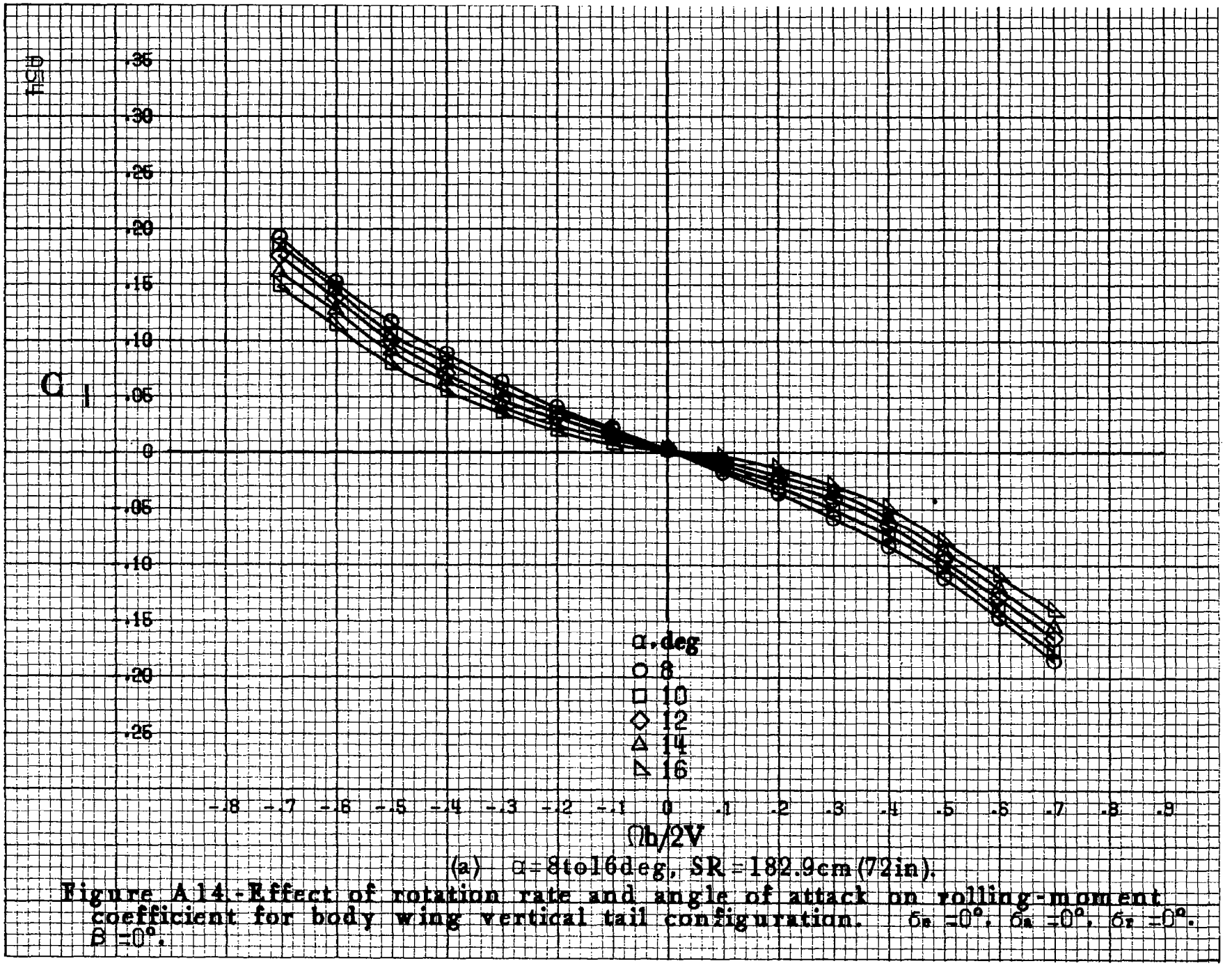

(a) $\alpha = 8$ to 16 deg, SR = 182.9 cm (72 in).

Figure A14.- Effect of rotation rate and angle of attack on rolling-moment coefficient for body wing vertical tail configuration. $\delta_e = 0°$, $\delta_a = 0°$, $\delta_r = 0°$, $\beta = 0°$.

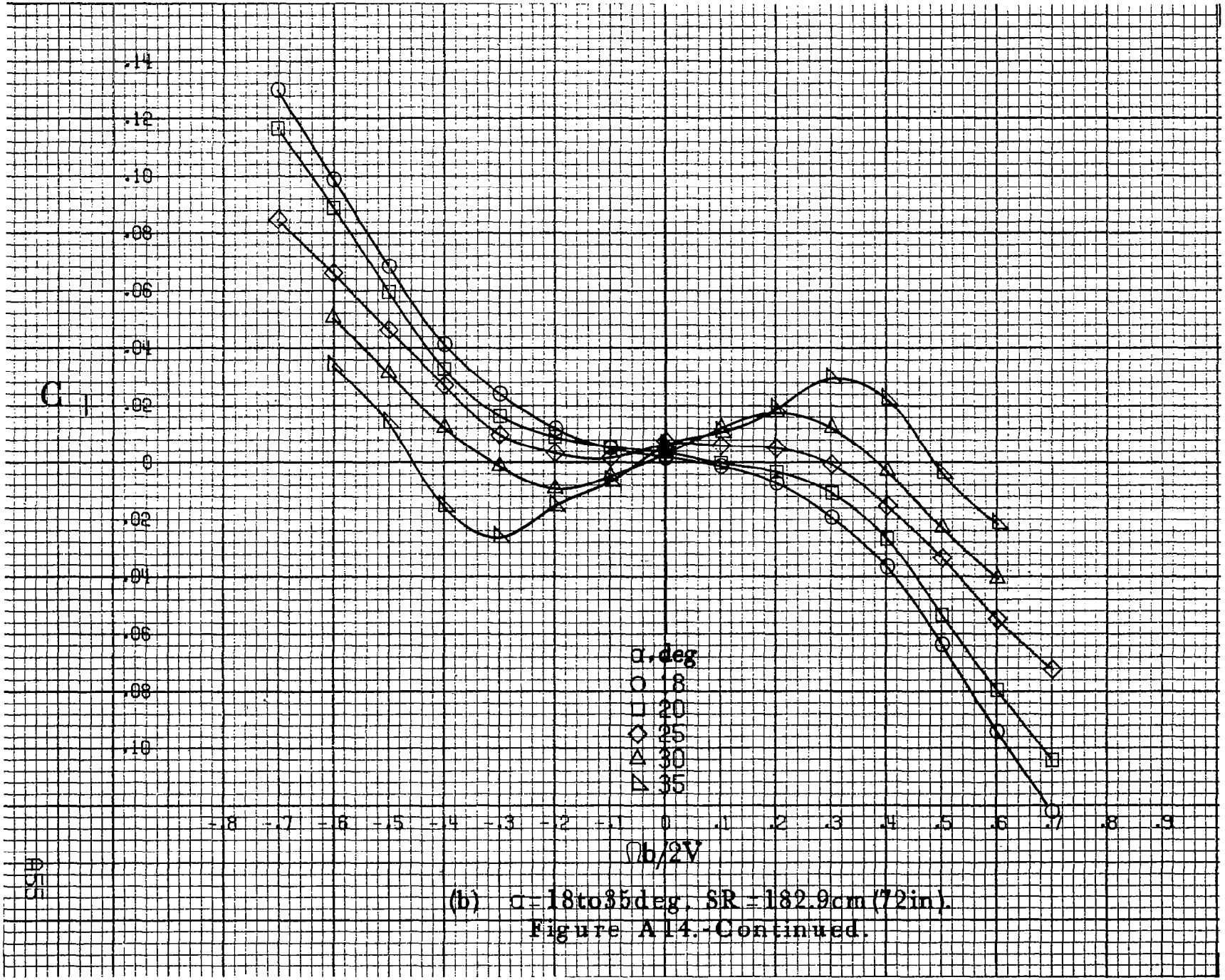

(b) $\alpha = 18$ to 35 deg. SR = 182.9 cm (72 in).

Figure A14.-Continued.

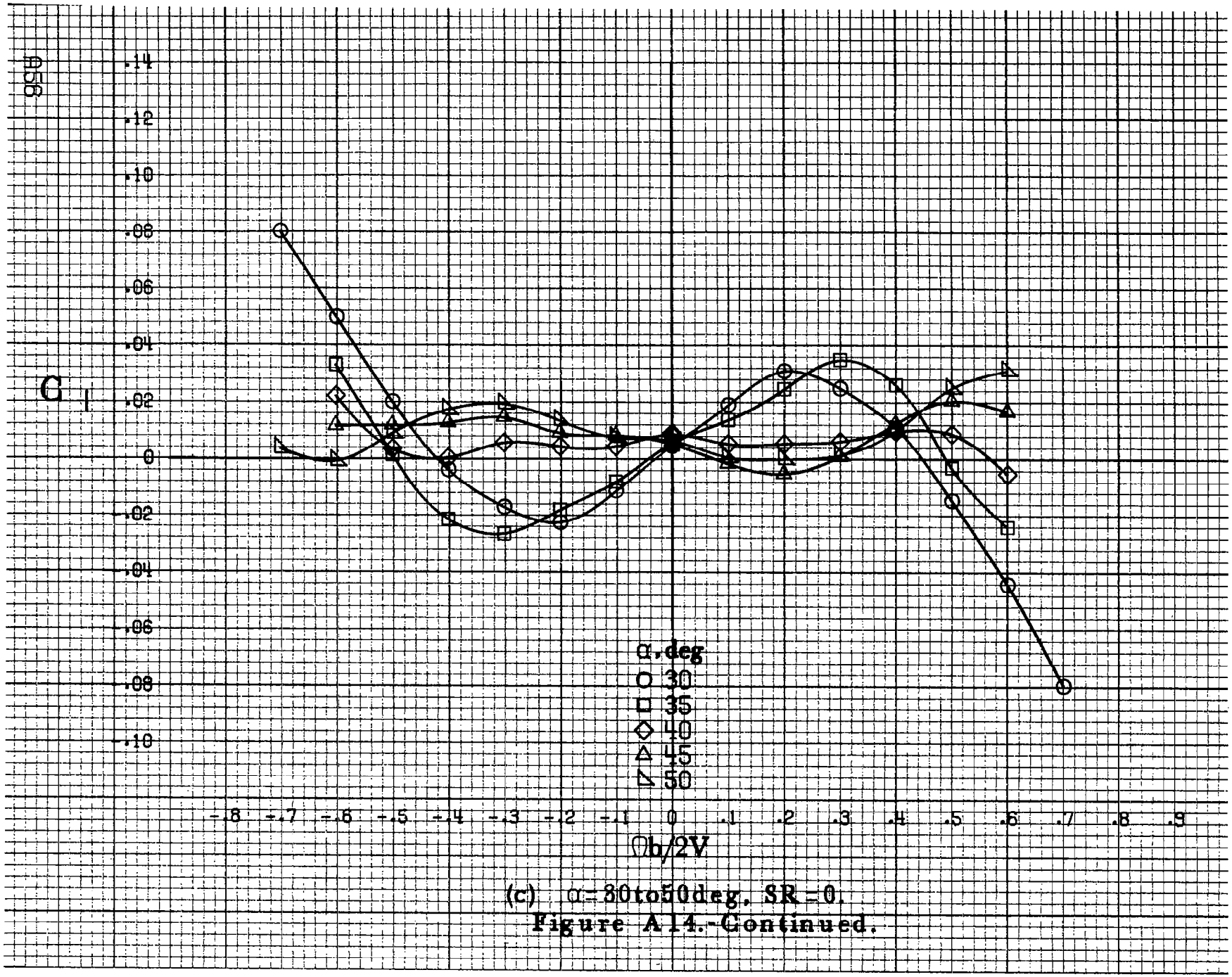

(c) $\alpha = 30$ to 50 deg, SR = 0.

Figure A14.-Continued.

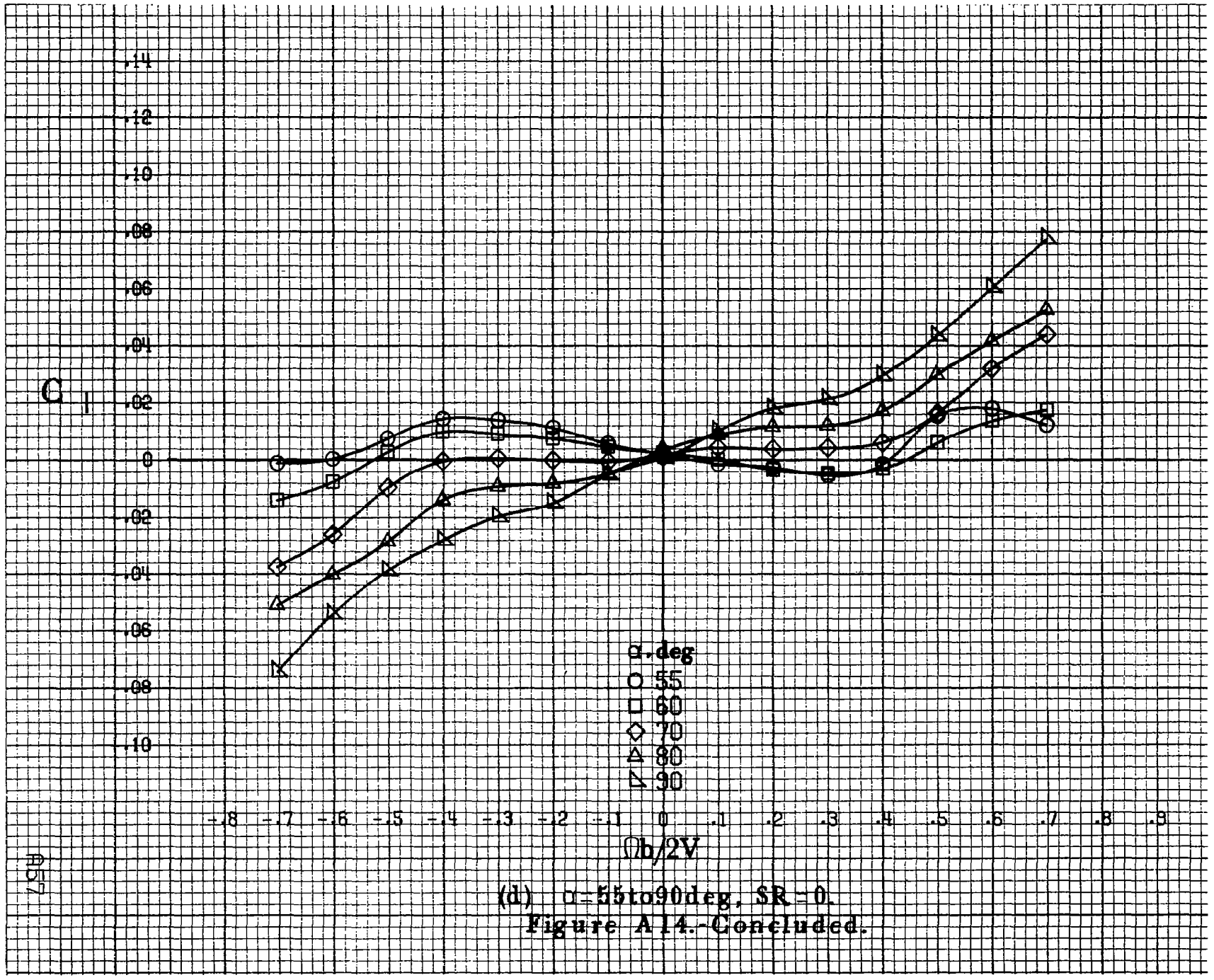

(d) α = 55 to 90 deg, SR = 0.

Figure A14.-Concluded.

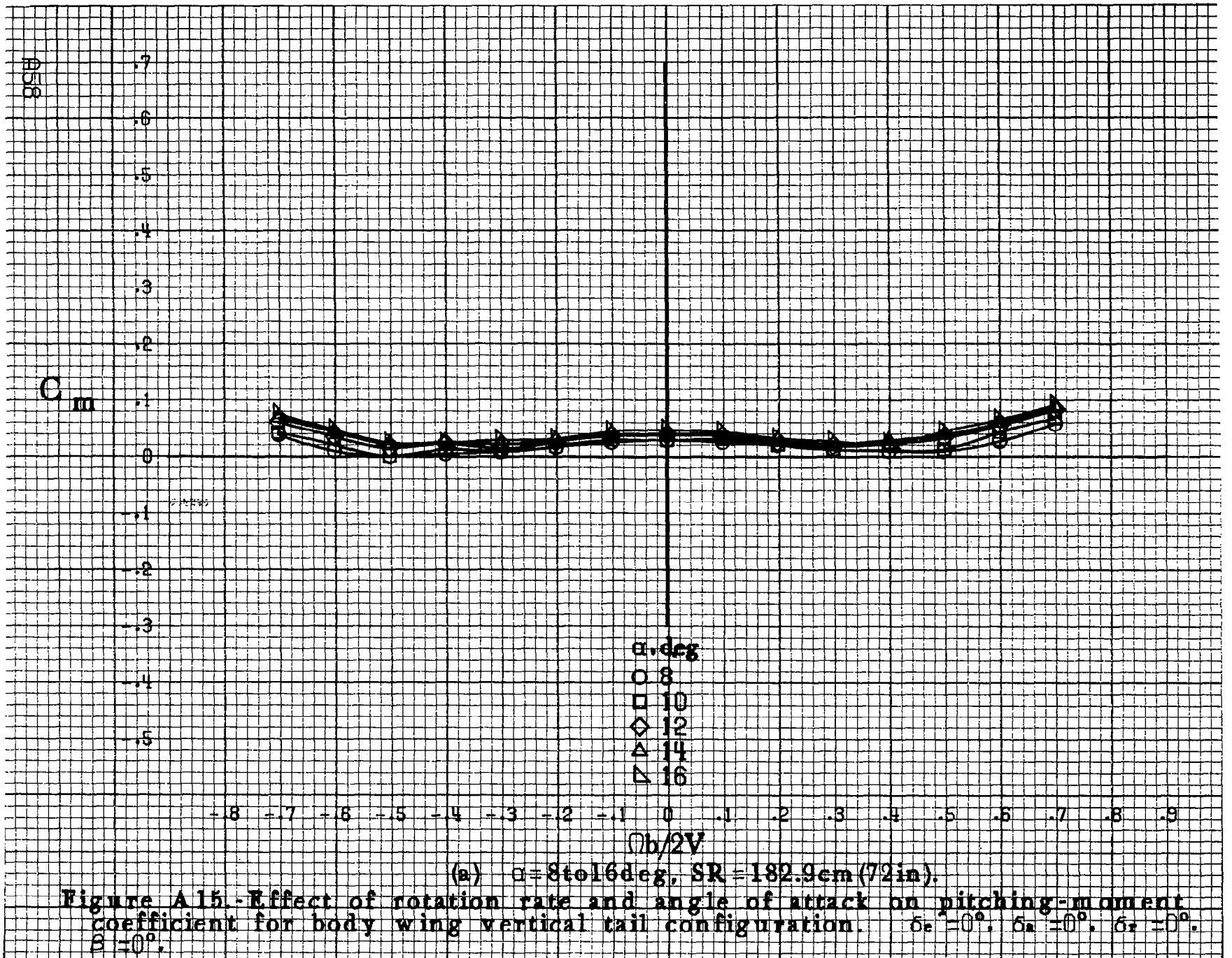

(a) α = 8 to 16 deg, SR = 182.9 cm (72 in).

Figure A15.- Effect of rotation rate and angle of attack on pitching-moment coefficient for body wing vertical tail configuration. $\delta_e = 0°$, $\delta_a = 0°$, $\delta_r = 0°$, $\beta = 0°$.

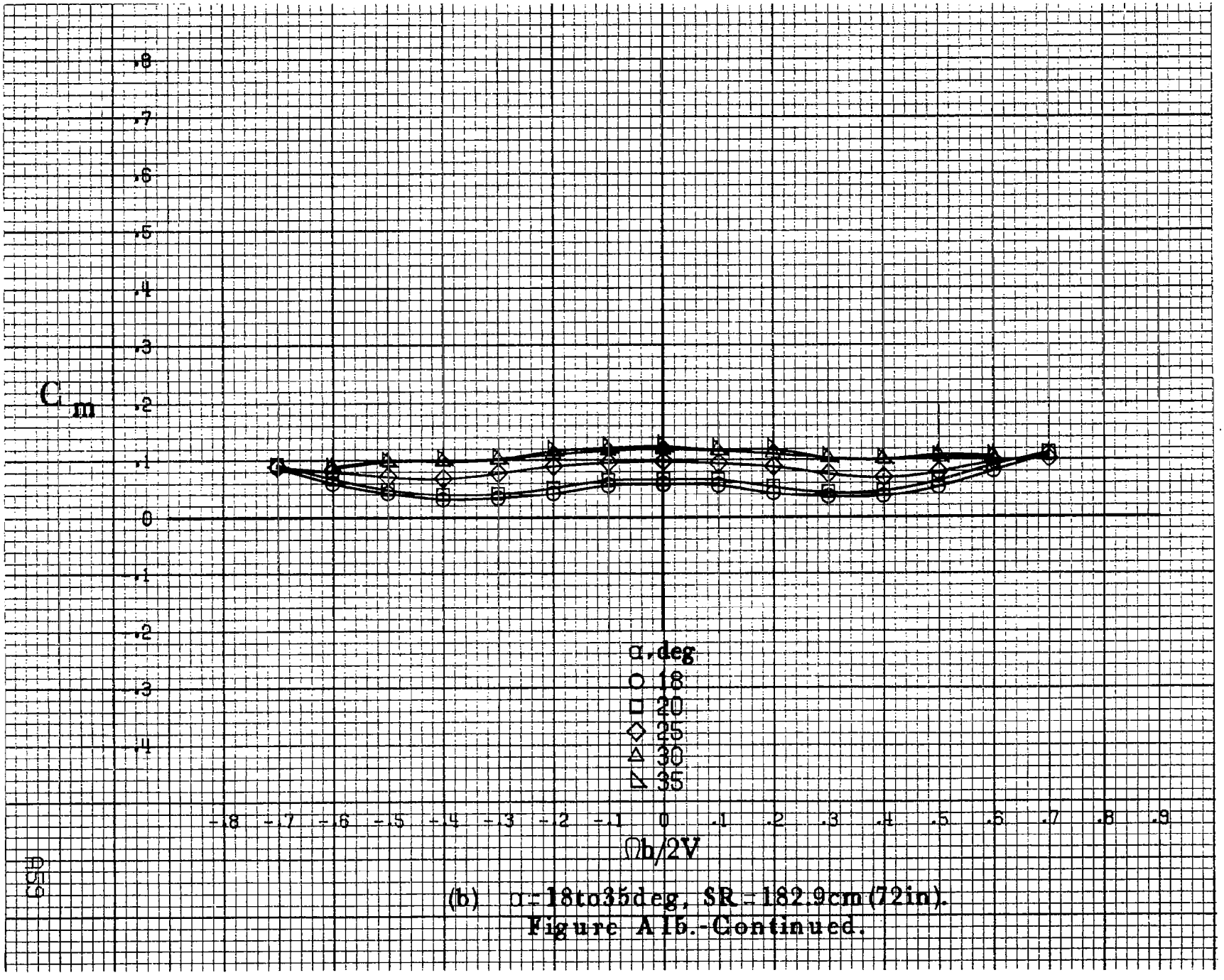

(b) α = 18 to 35 deg, SR = 182.9 cm (72 in).

Figure A1b.-Continued.

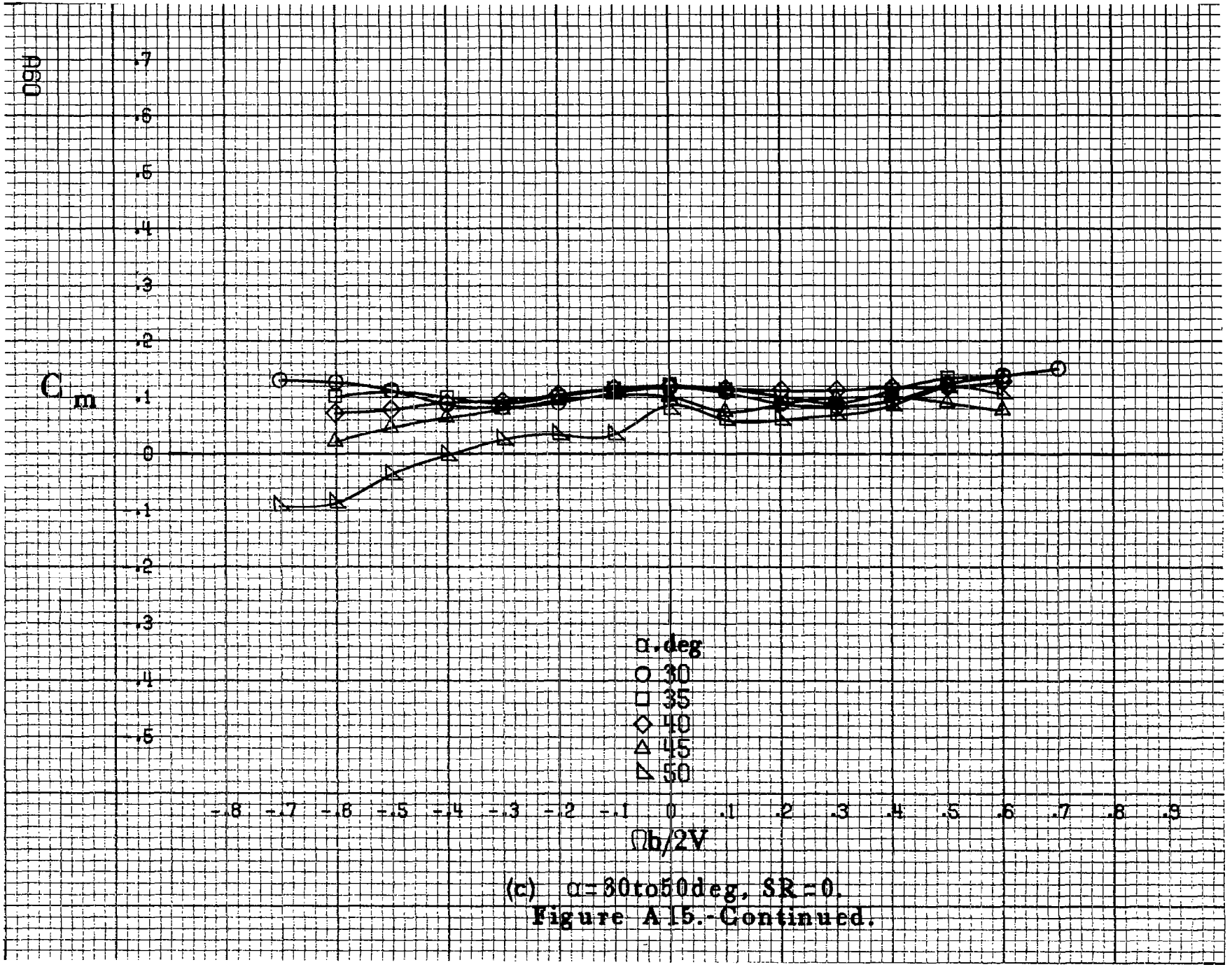

(c) $\alpha = 30$ to 50 deg, SR = 0.

Figure A15.- Continued.

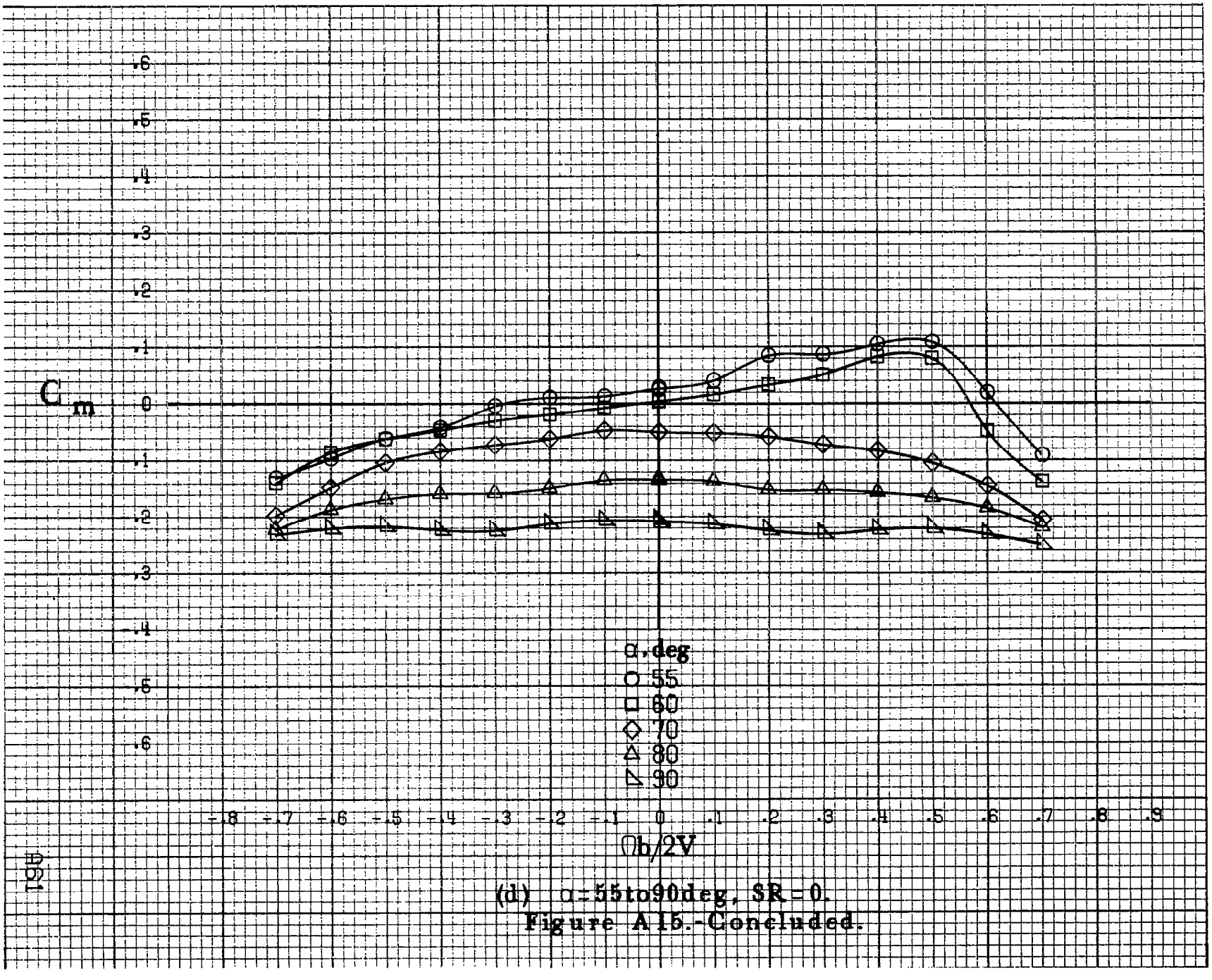

(d) $\alpha = 55$ to 90 deg, $SR = 0$.

Figure A15.-Concluded.

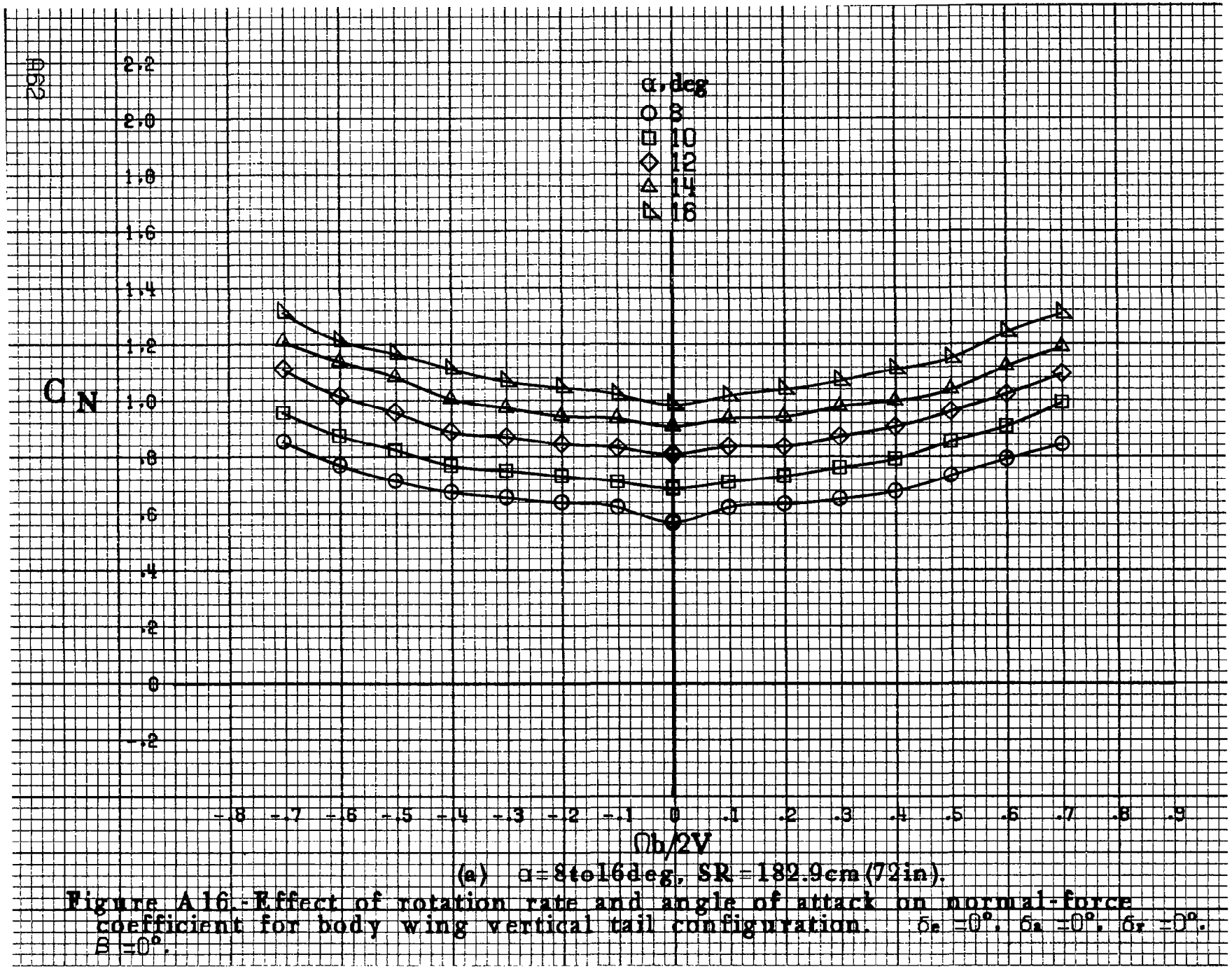

(a) $\alpha = 8$ to 16 deg, SR = 182.9 cm (72 in).

Figure A16.- Effect of rotation rate and angle of attack on normal-force coefficient for body wing vertical tail configuration. $\delta_e = 0°$, $\delta_a = 0°$, $\delta_r = 0°$, $\beta = 0°$.

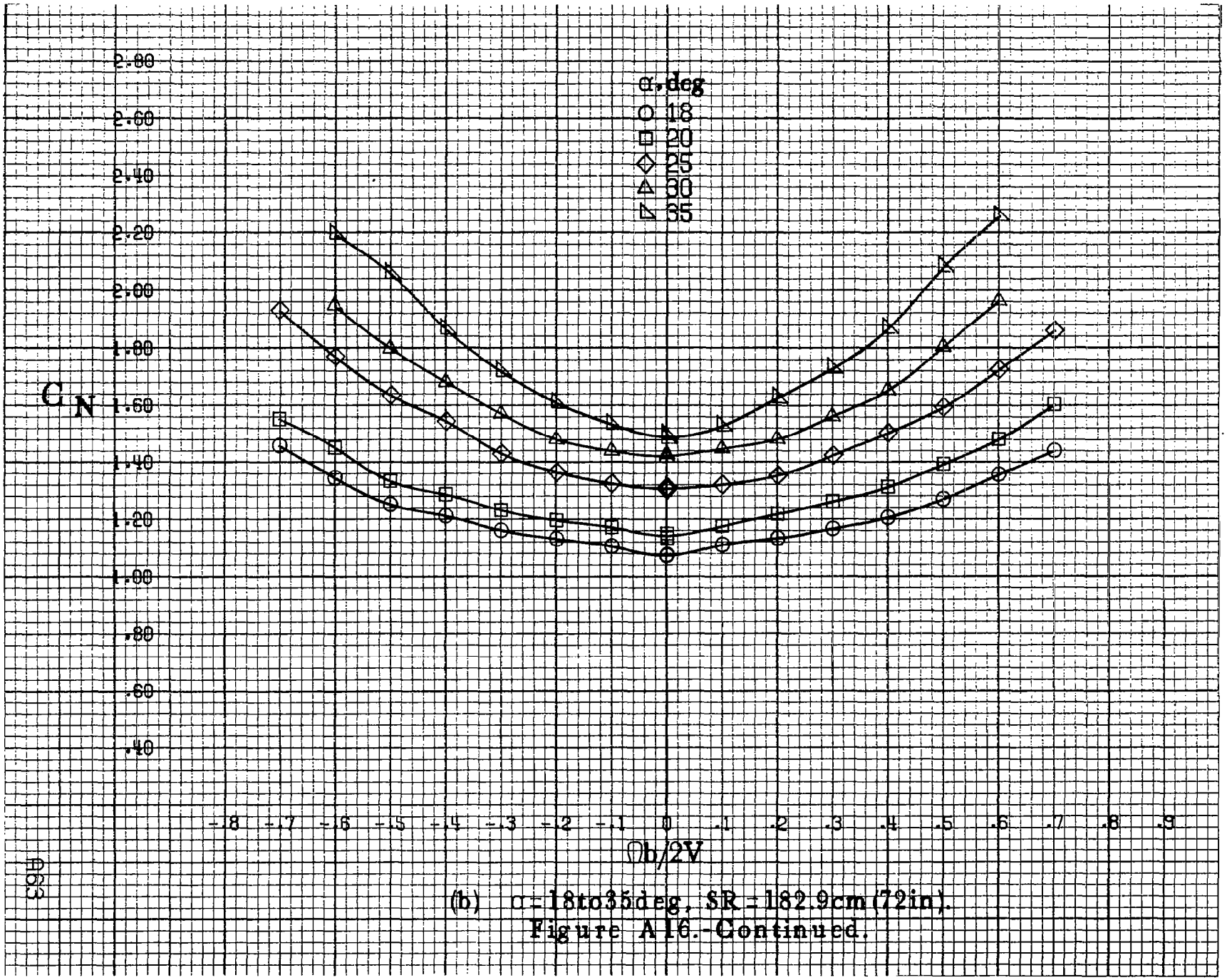

(b) $\alpha = 18$ to 35 deg, SR = 182.9 cm (72 in).

Figure A16.-Continued.

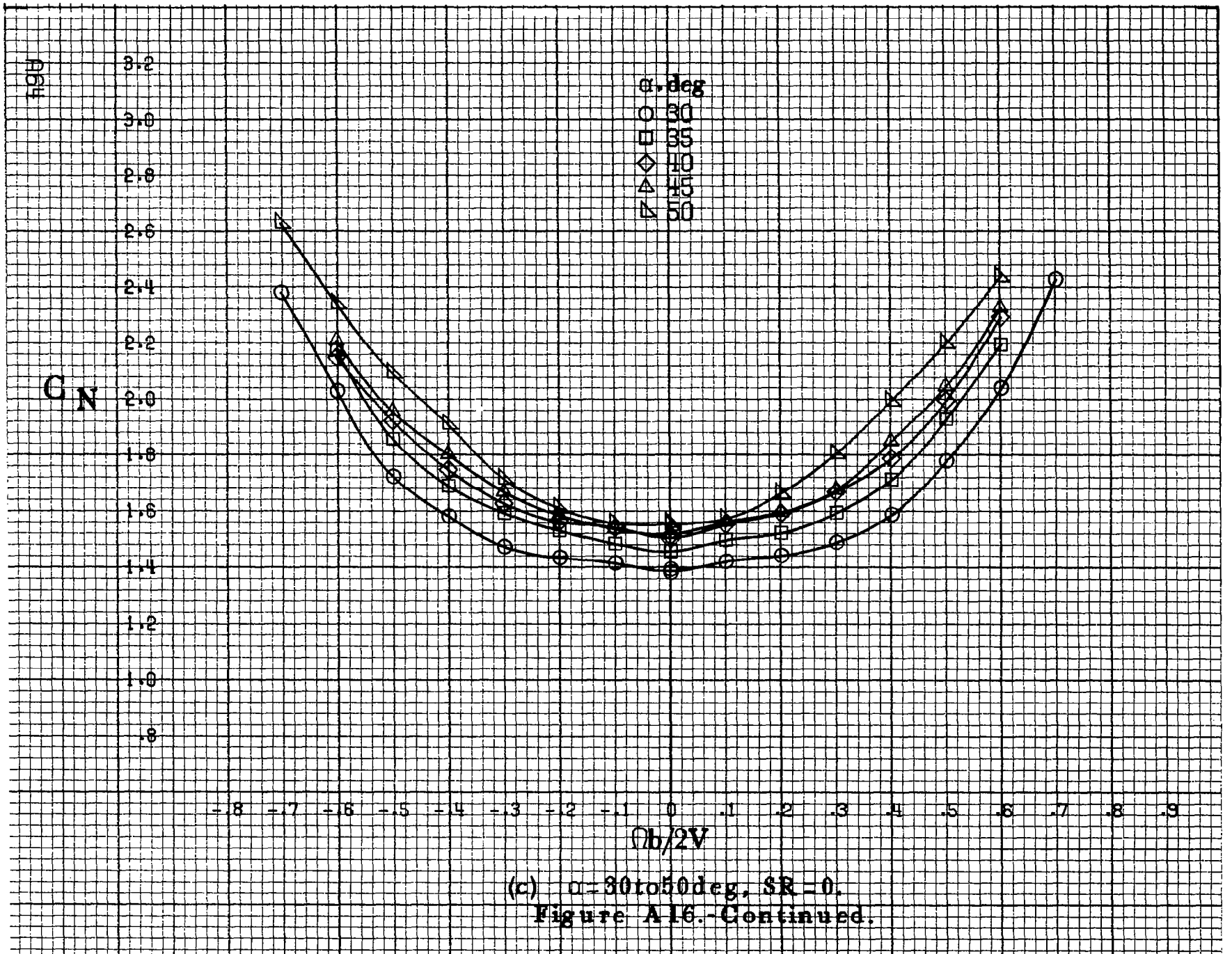

(c) α = 30 to 50 deg, SR = 0.

Figure A16.-Continued.

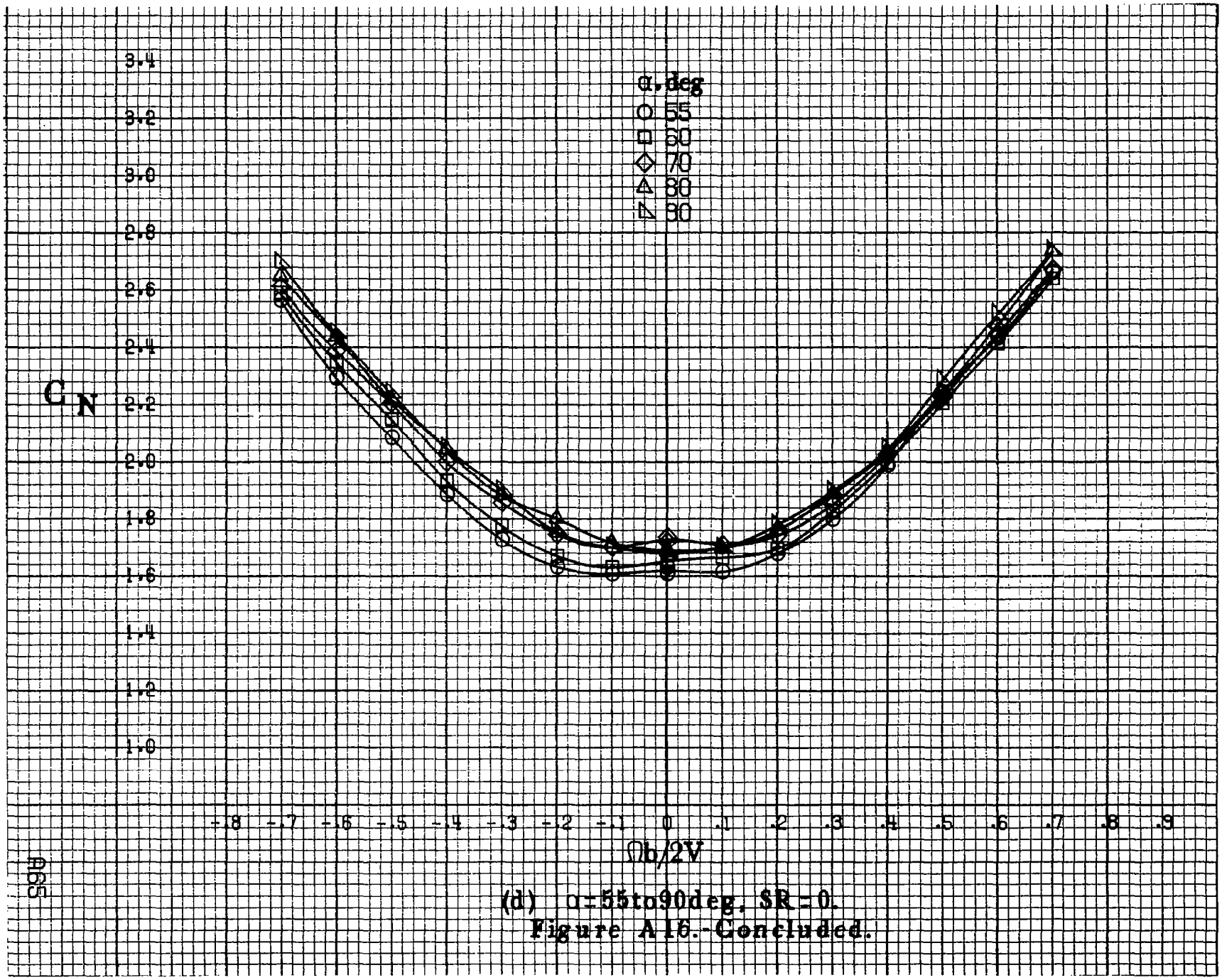

(d) α=55to90deg, SR=0.

Figure A16.-Concluded.

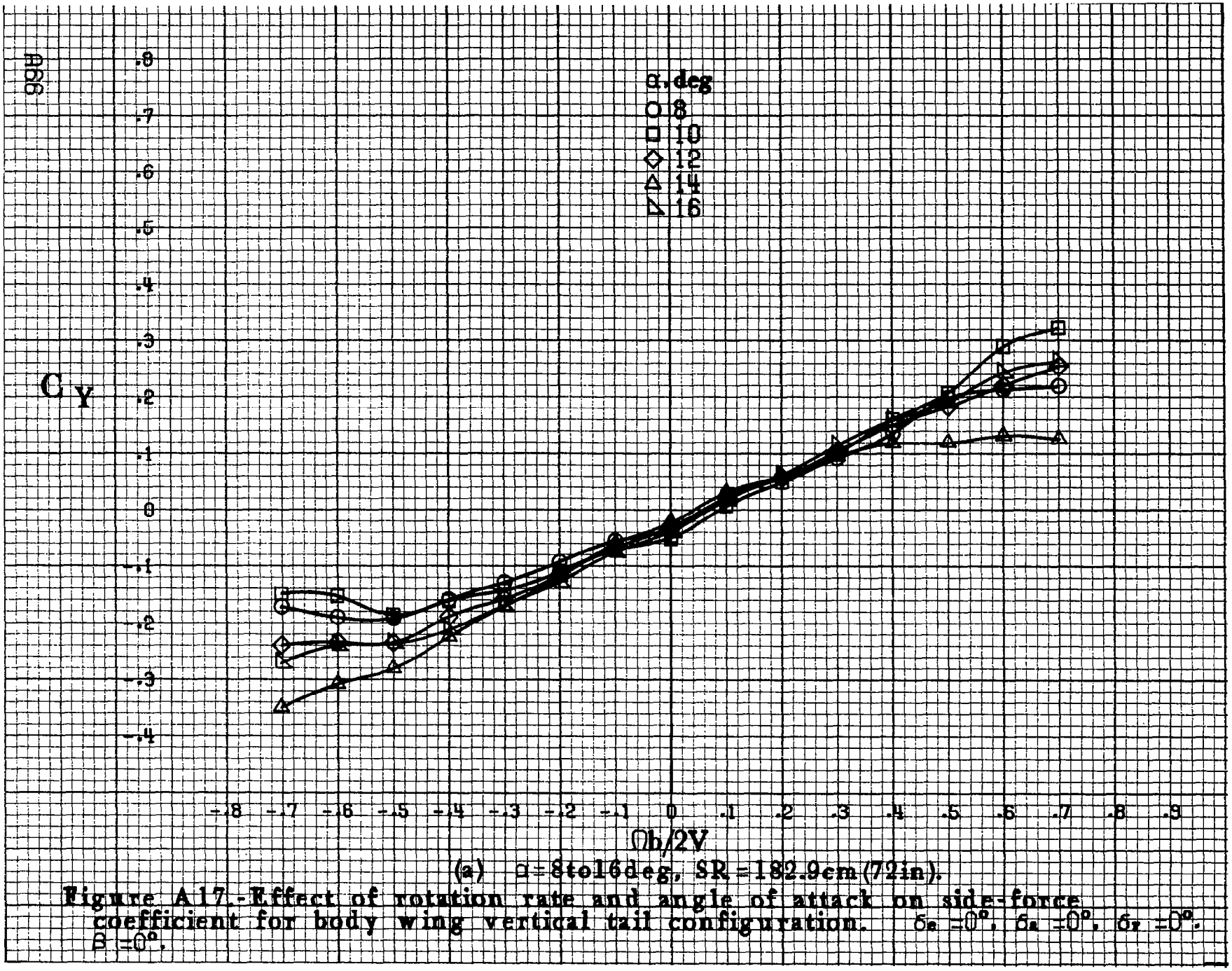

(a) $\alpha = 8$ to 16 deg, SR = 182.9 cm (72 in).

Figure A17.- Effect of rotation rate and angle of attack on side-force coefficient for body wing vertical tail configuration. $\delta_e = 0°$, $\delta_a = 0°$, $\delta_r = 0°$, $\beta = 0°$.

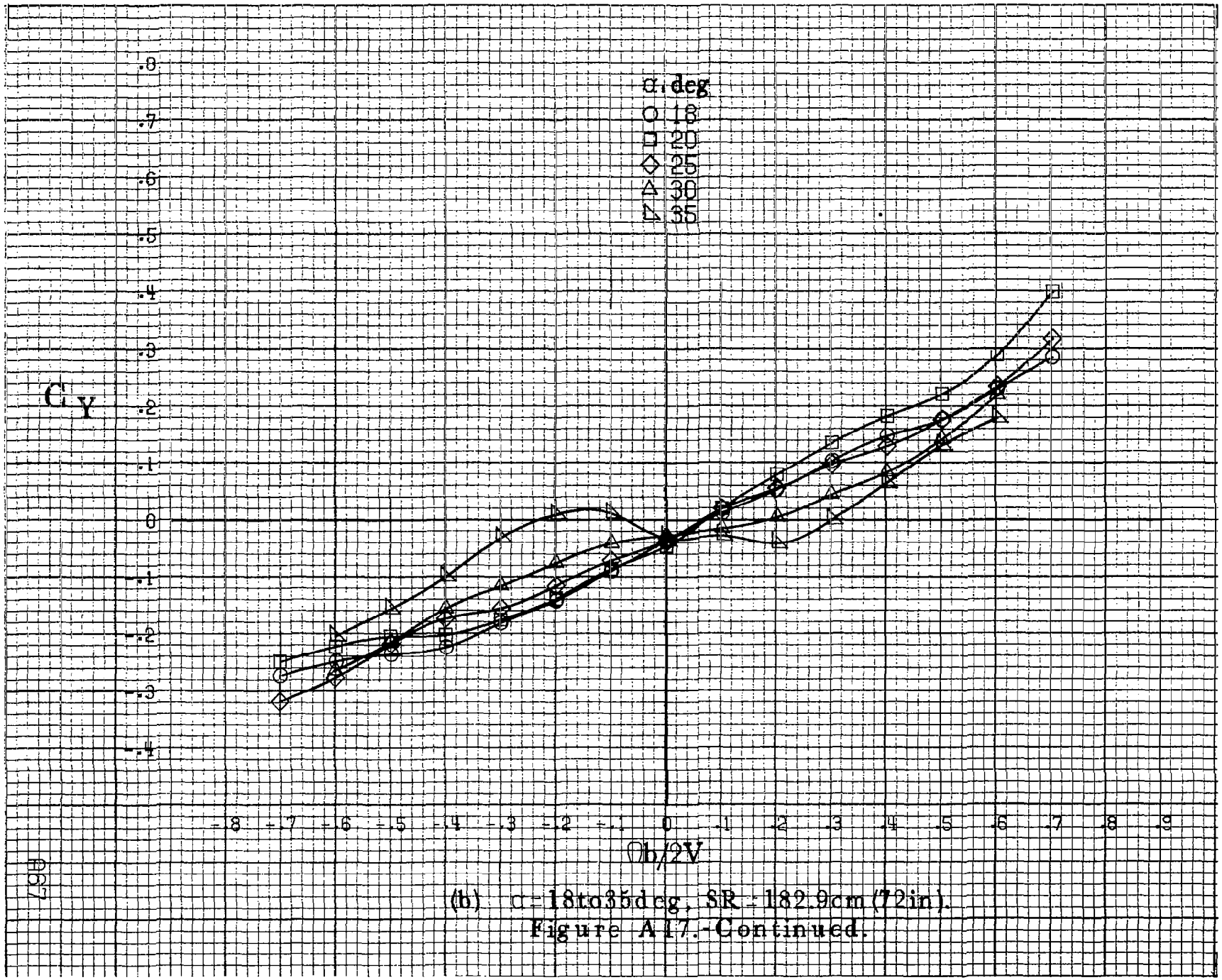

(b) $\alpha = 18$ to 35 deg, SR = 182.9 cm (72 in).

Figure A17.-Continued.

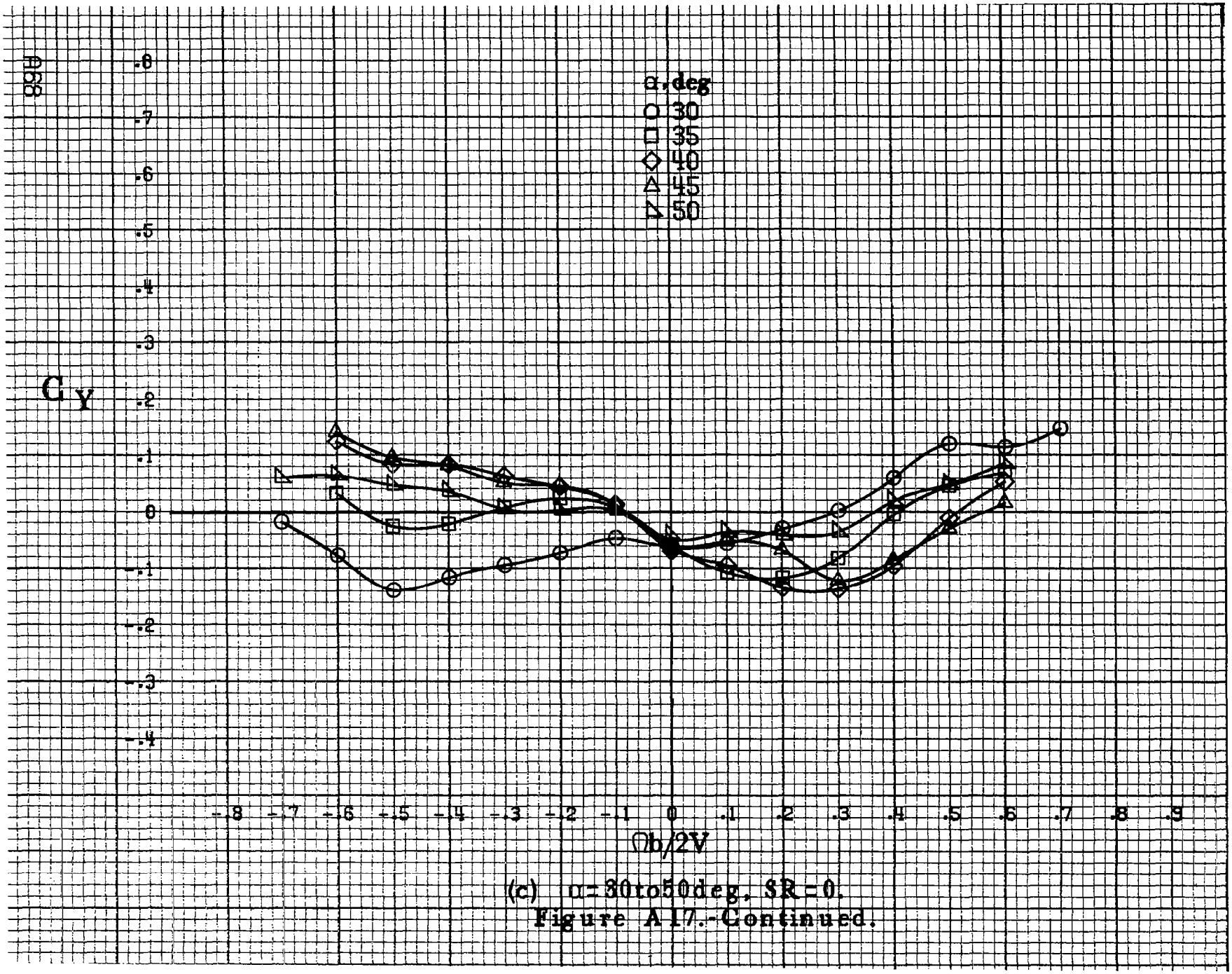

(c) $\alpha = 30$ to 50 deg, SR = 0.

Figure A17.- Continued.

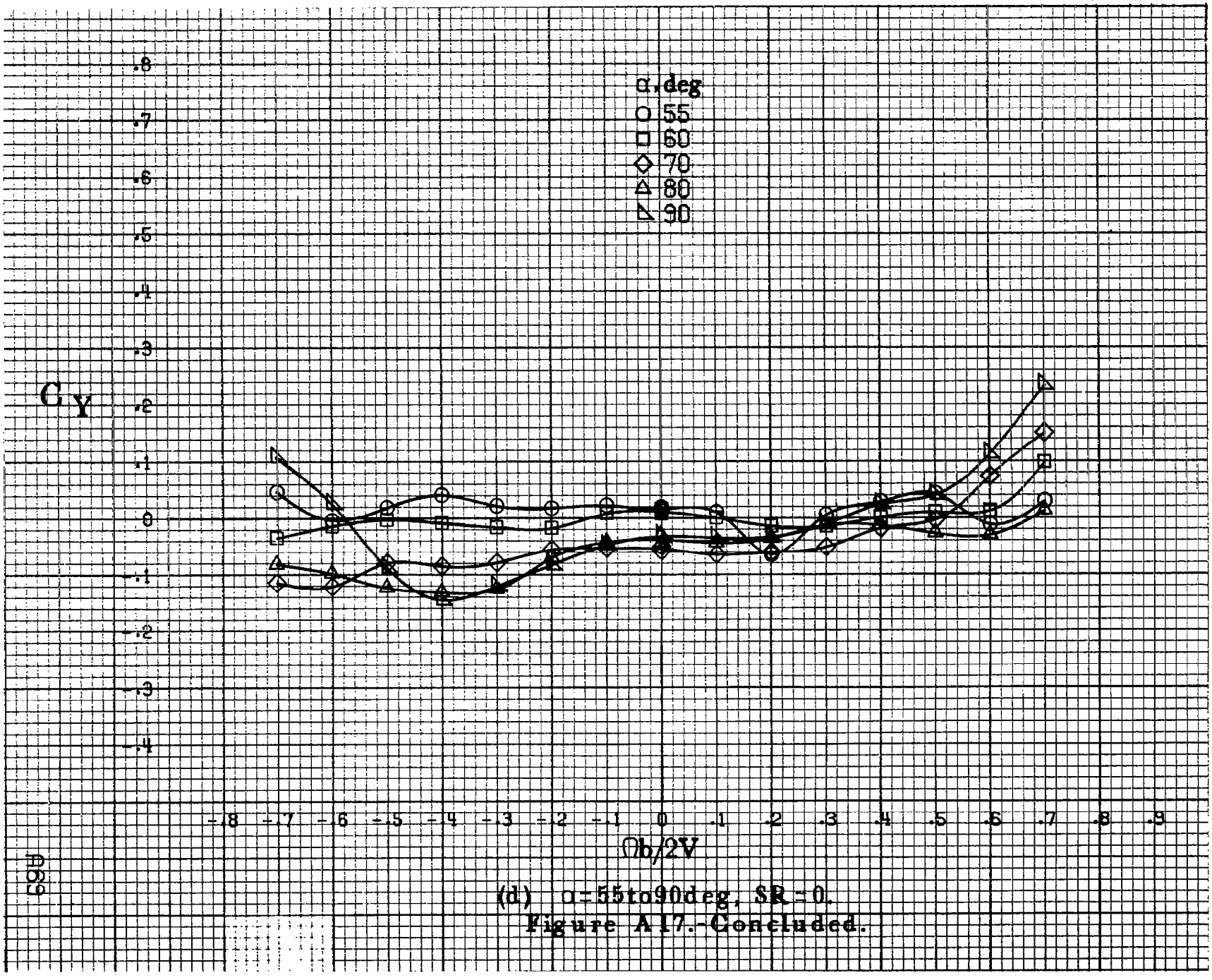

(d) $\alpha = 55$ to 90 deg, SR = 0.

Figure A17.-Concluded.

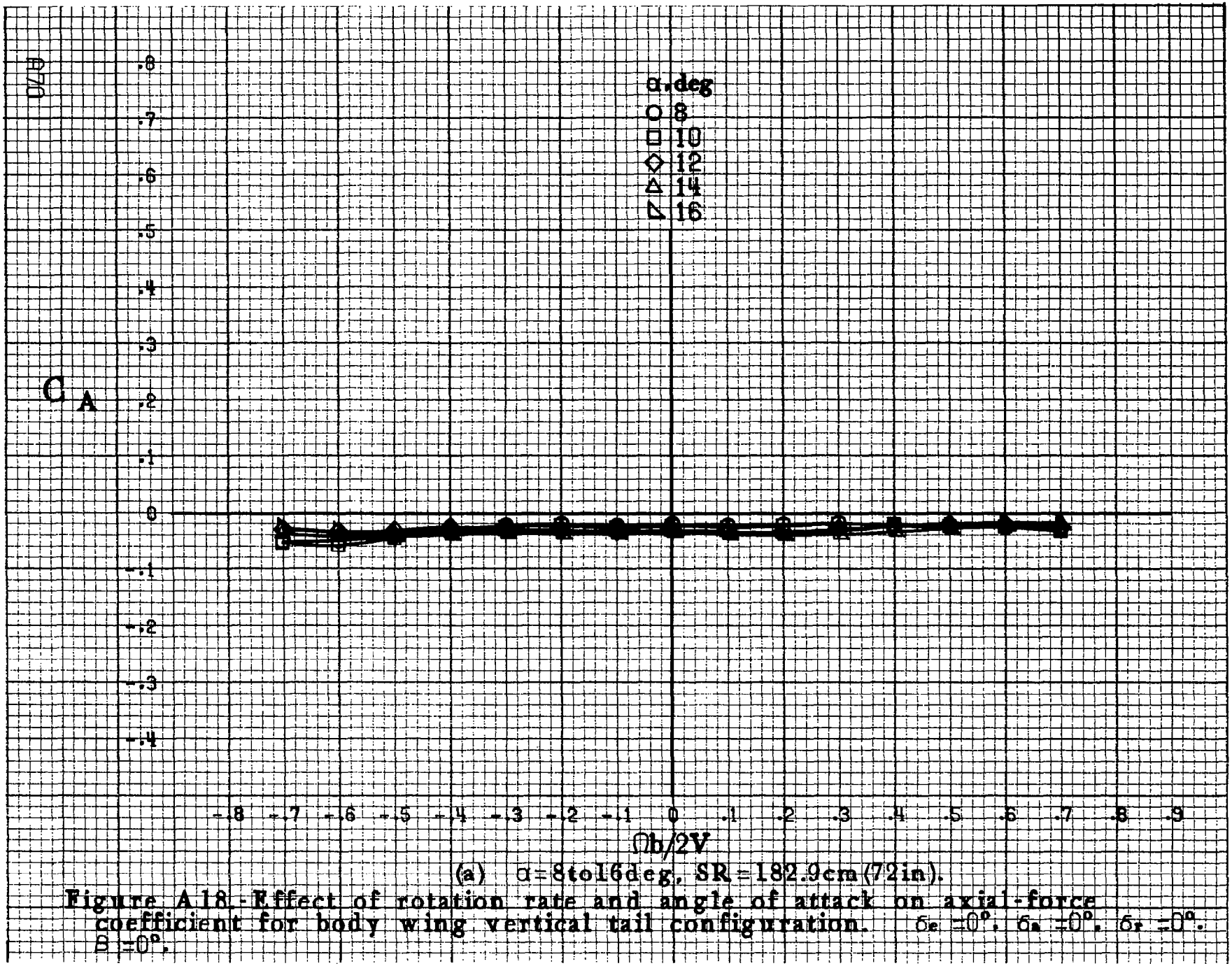

(a) $\alpha = 8$ to 16 deg, SR = 182.9 cm (72 in).

Figure A18.-Effect of rotation rate and angle of attack on axial-force coefficient for body wing vertical tail configuration. $\delta_e = 0°$, $\delta_a = 0°$, $\delta_r = 0°$, $\beta = 0°$.

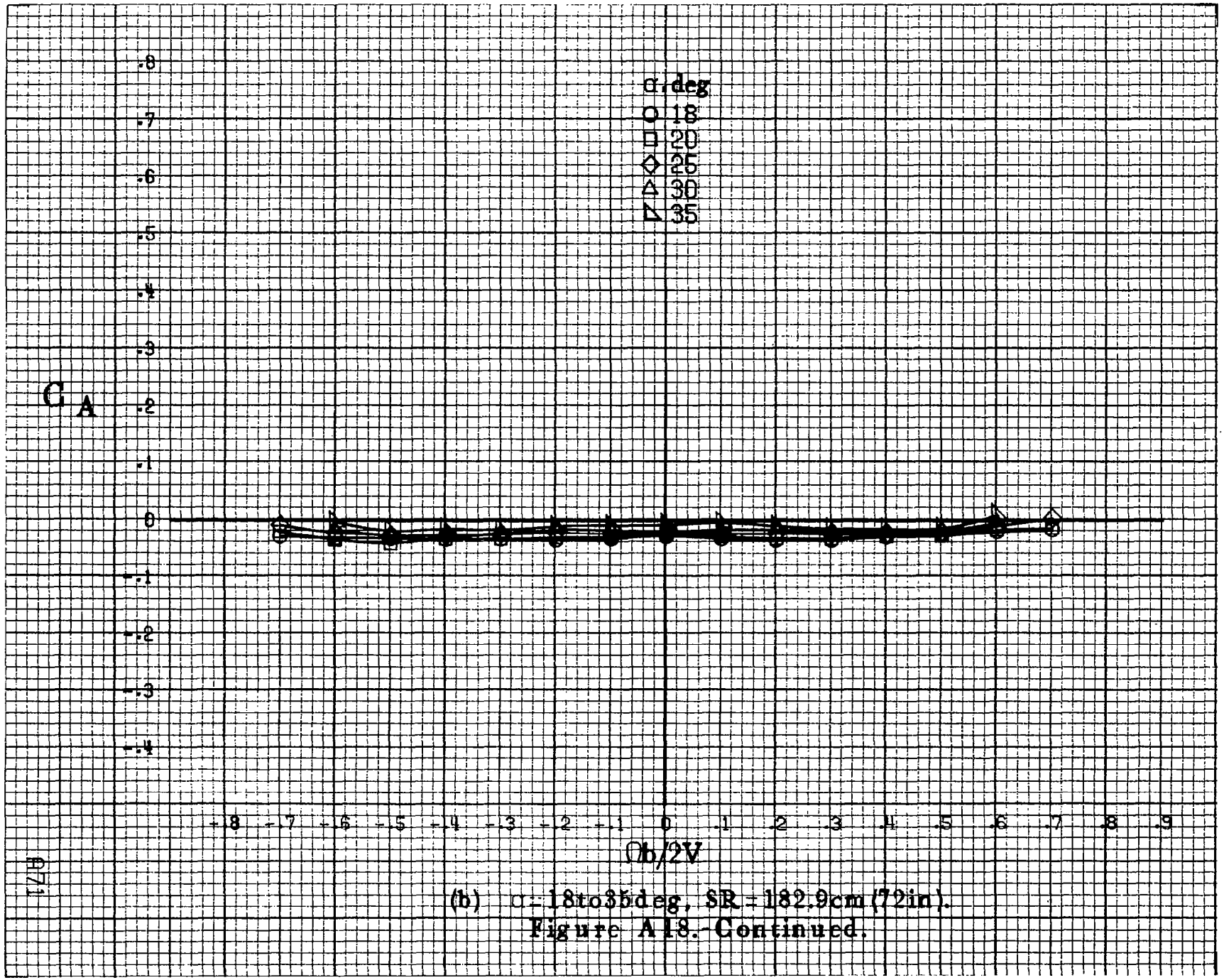

B71

(b) α = 18 to 35 deg, SR = 182.9 cm (72 in.).

Figure A18.- Continued.

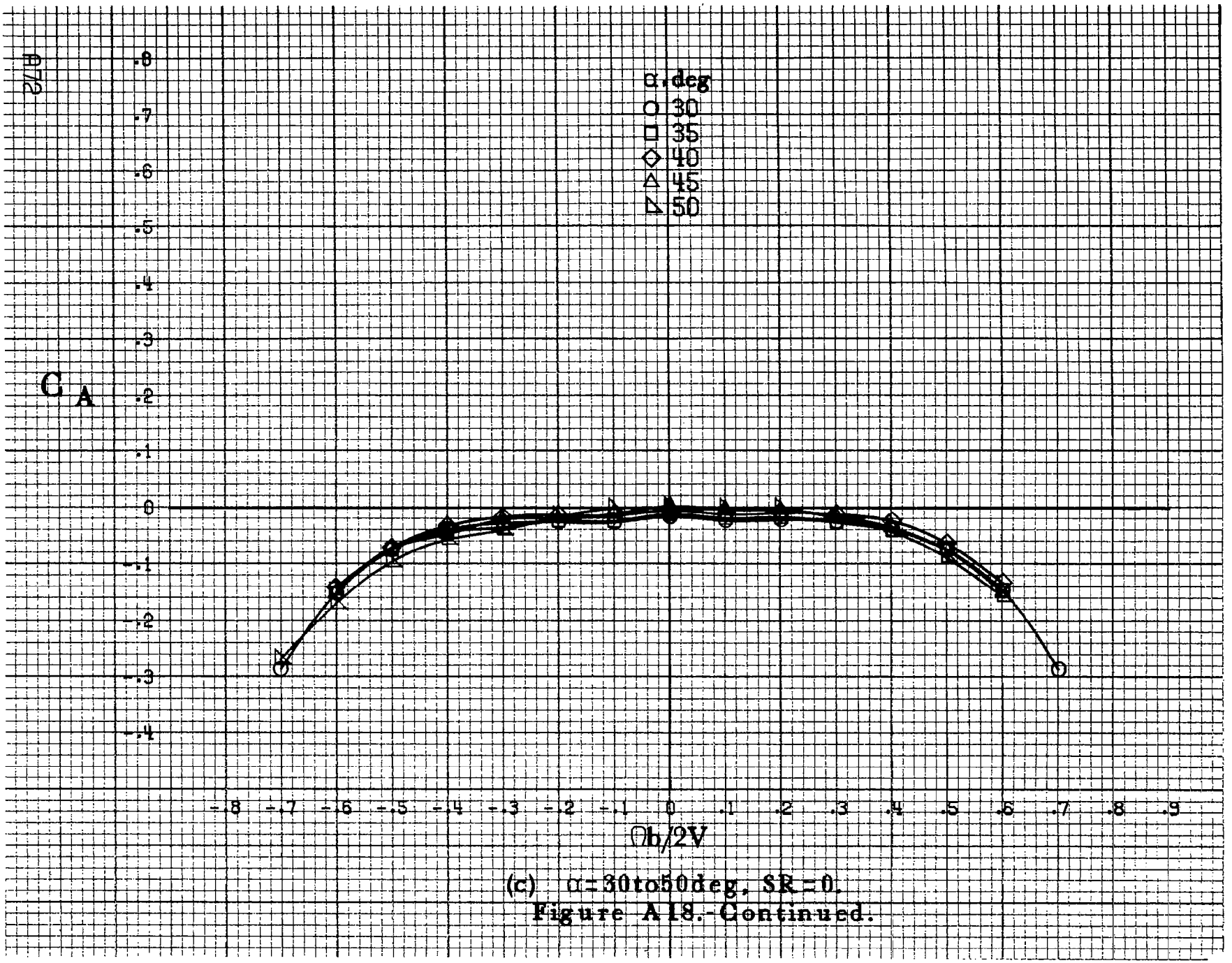

(c) $\alpha = 30$ to 50 deg, SR = 0.

Figure A18.-Continued.

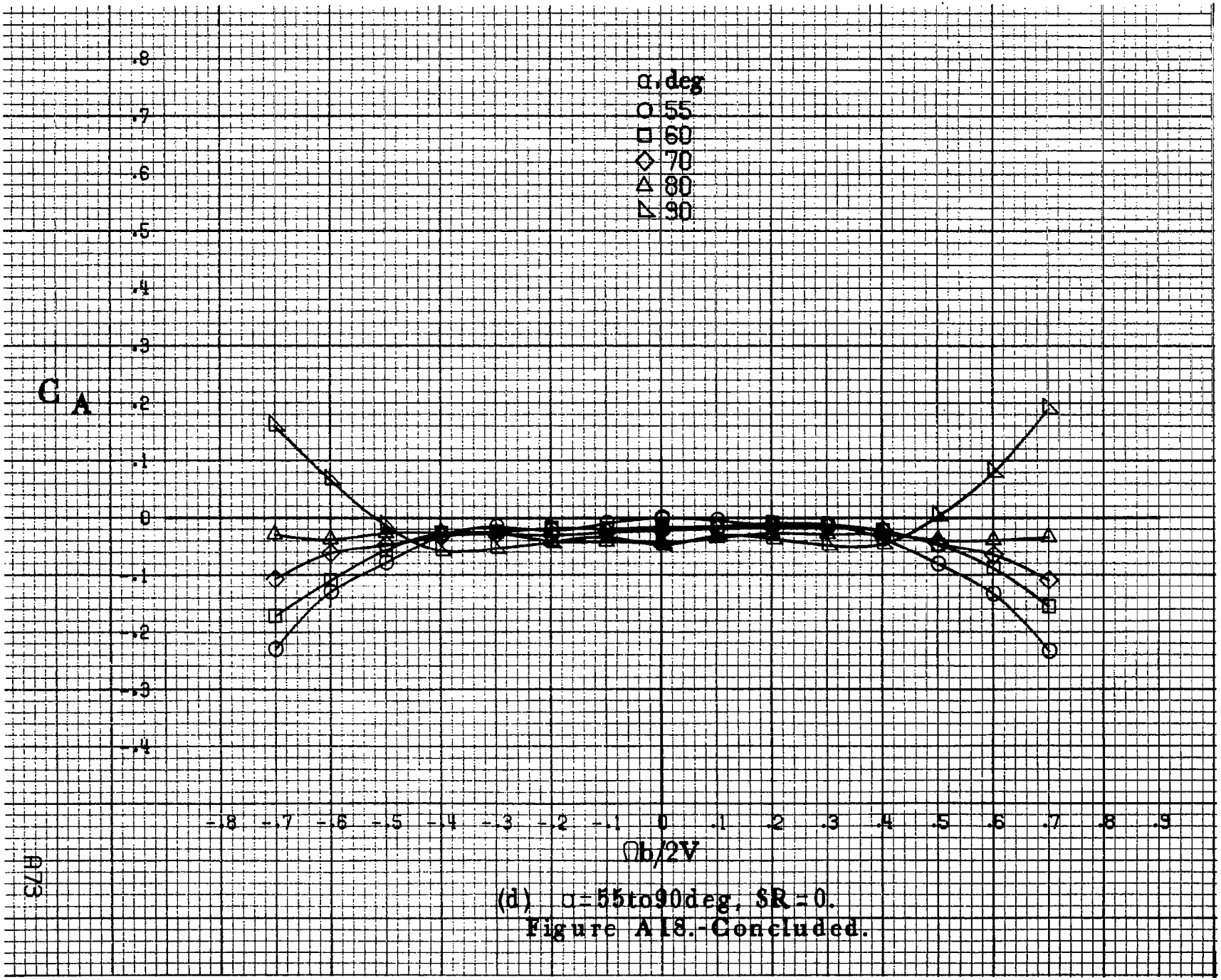

(d) α = 55 to 90 deg, $R = 0.

Figure A18.- Concluded.

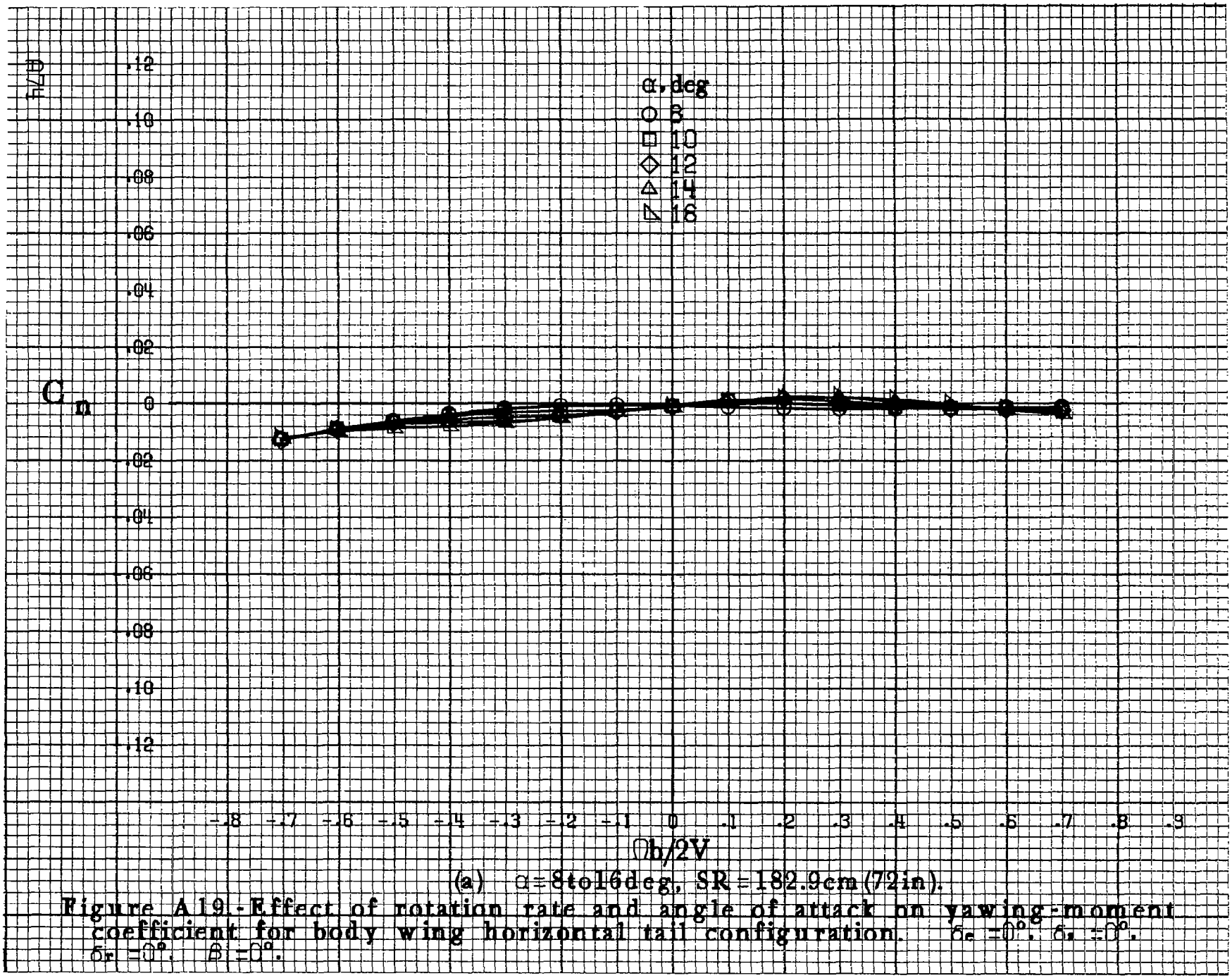

(a) α = 8 to 16 deg, SR = 182.9 cm (72 in).

Figure A19.- Effect of rotation rate and angle of attack on yawing-moment coefficient for body wing horizontal tail configuration. $\delta_e = 0°$, $\delta_a = 0°$, $\delta_r = 0°$, $\beta = 0°$.

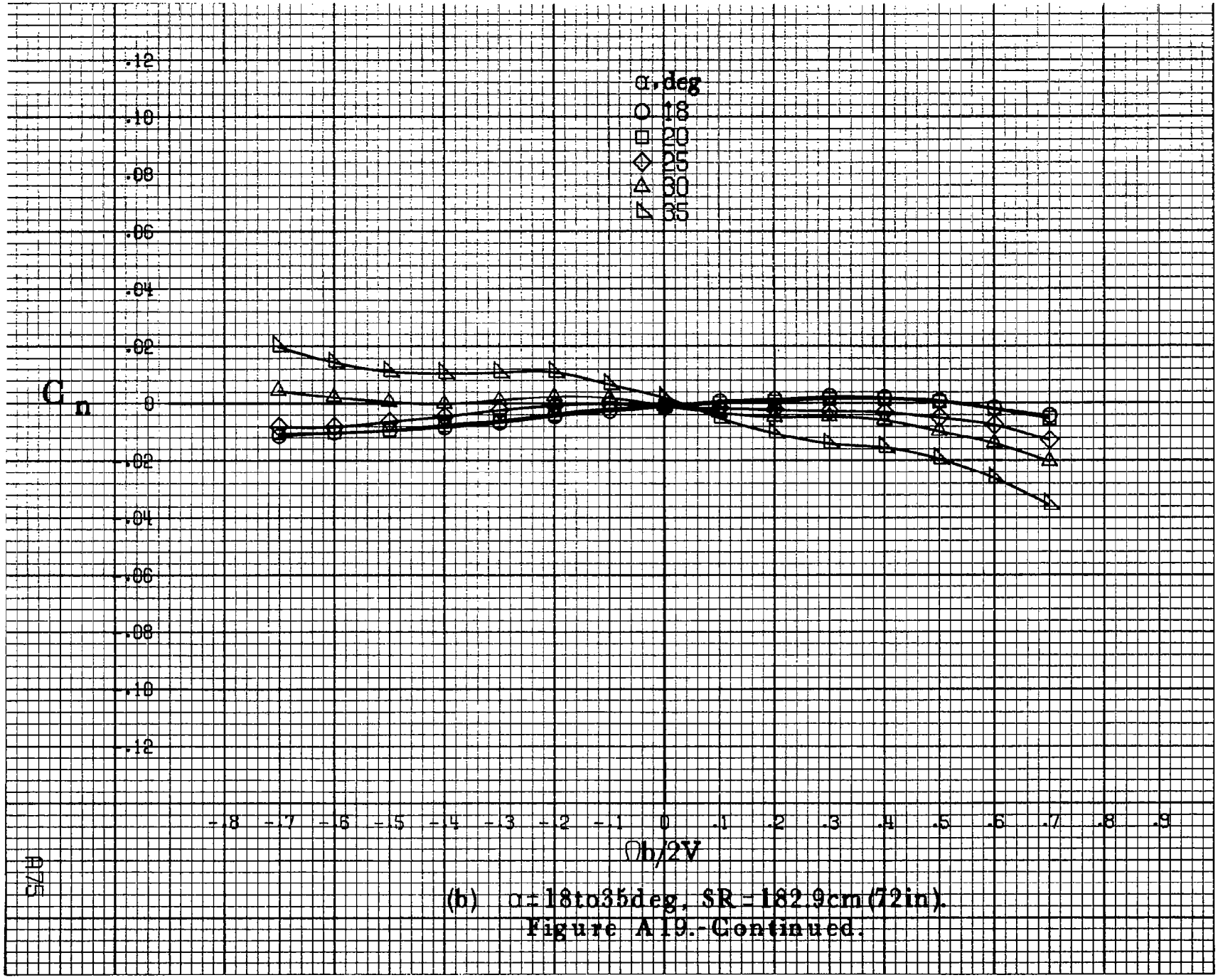

(b) α = 18 to 35 deg, S_R = 182.9 cm (72 in).

Figure A19.- Continued.

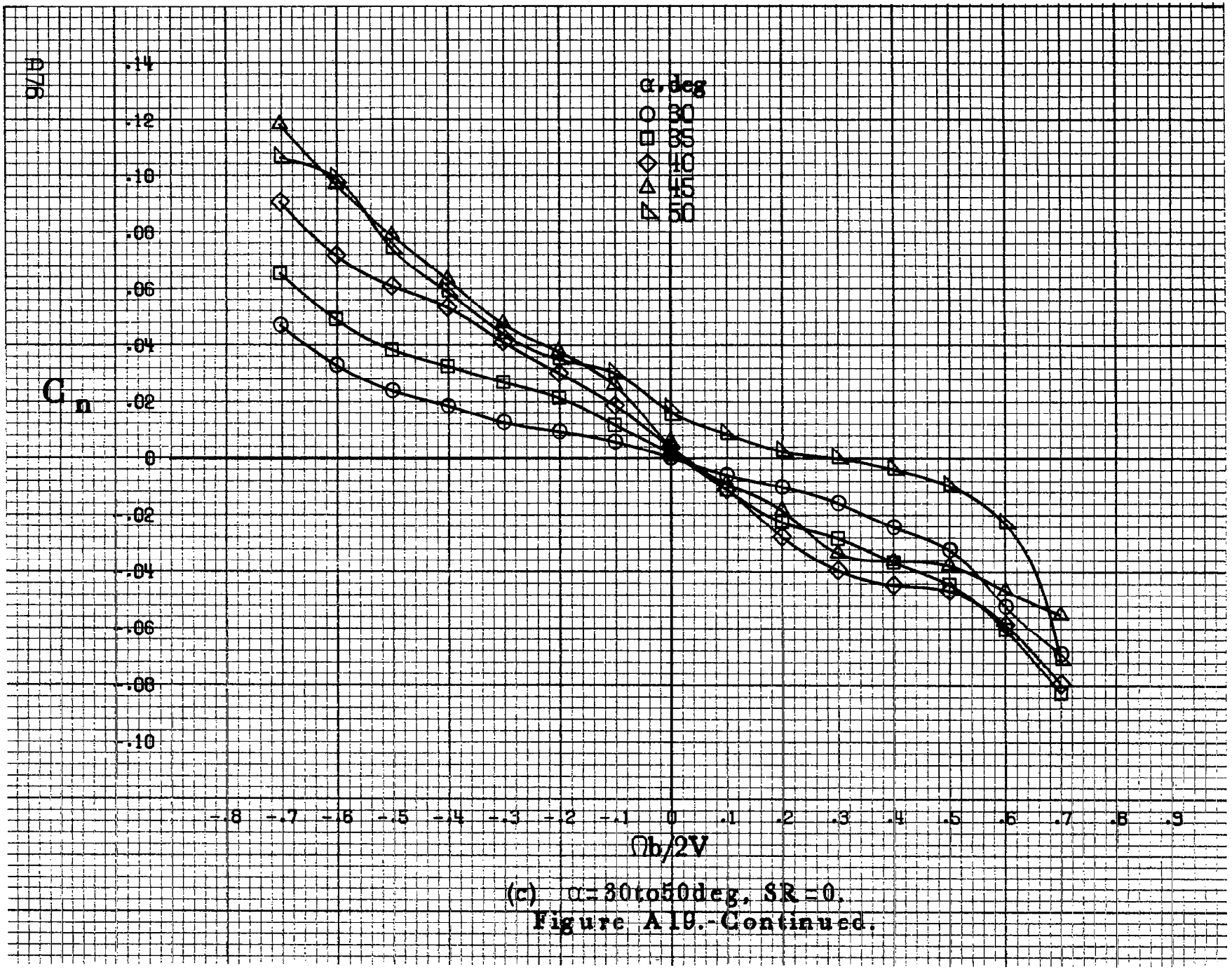

(c) $\alpha = 30$ to 50 deg, SR = 0.

Figure A19.- Continued.

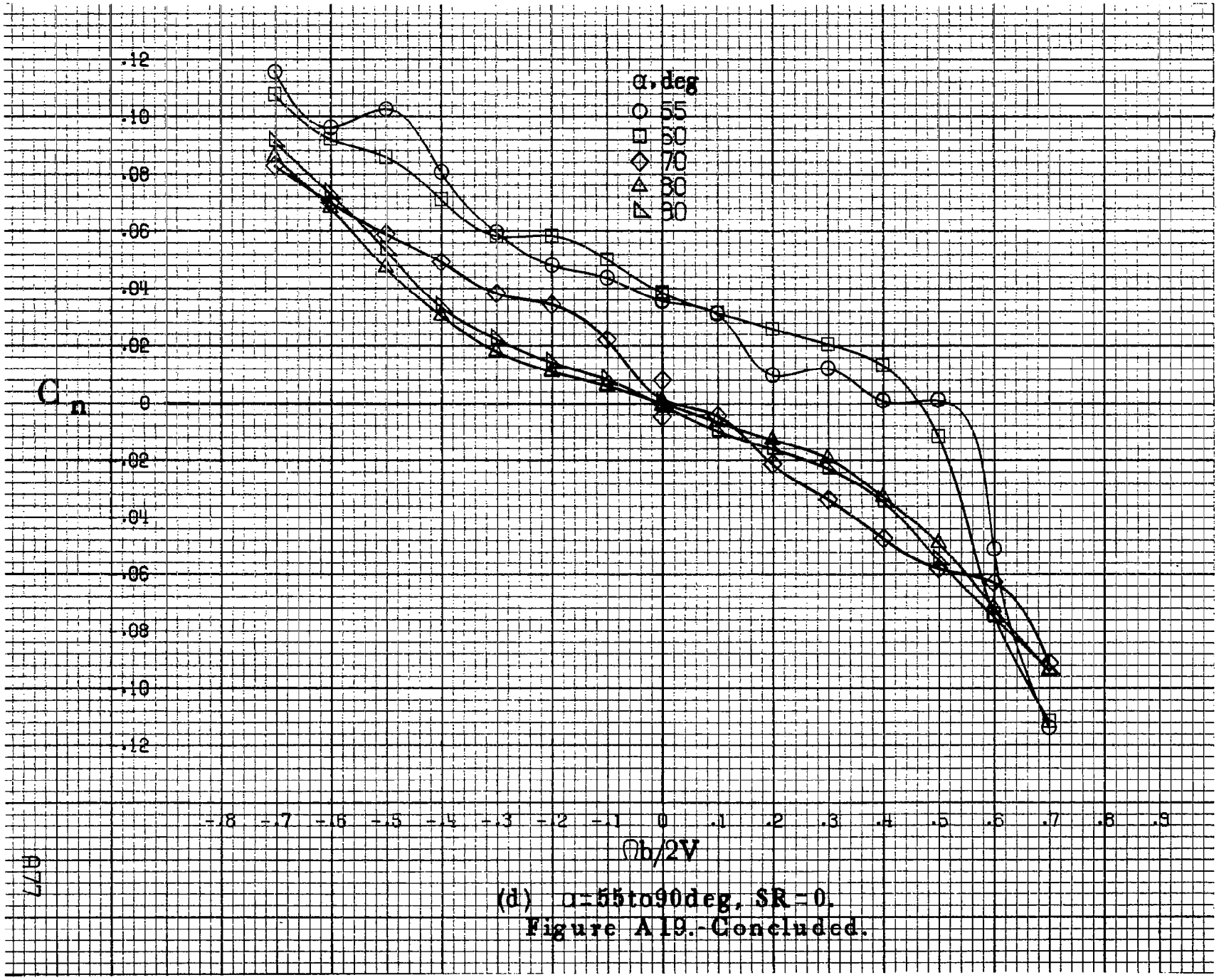

(d) α=55to90deg, SR=0.

Figure A19.-Concluded.

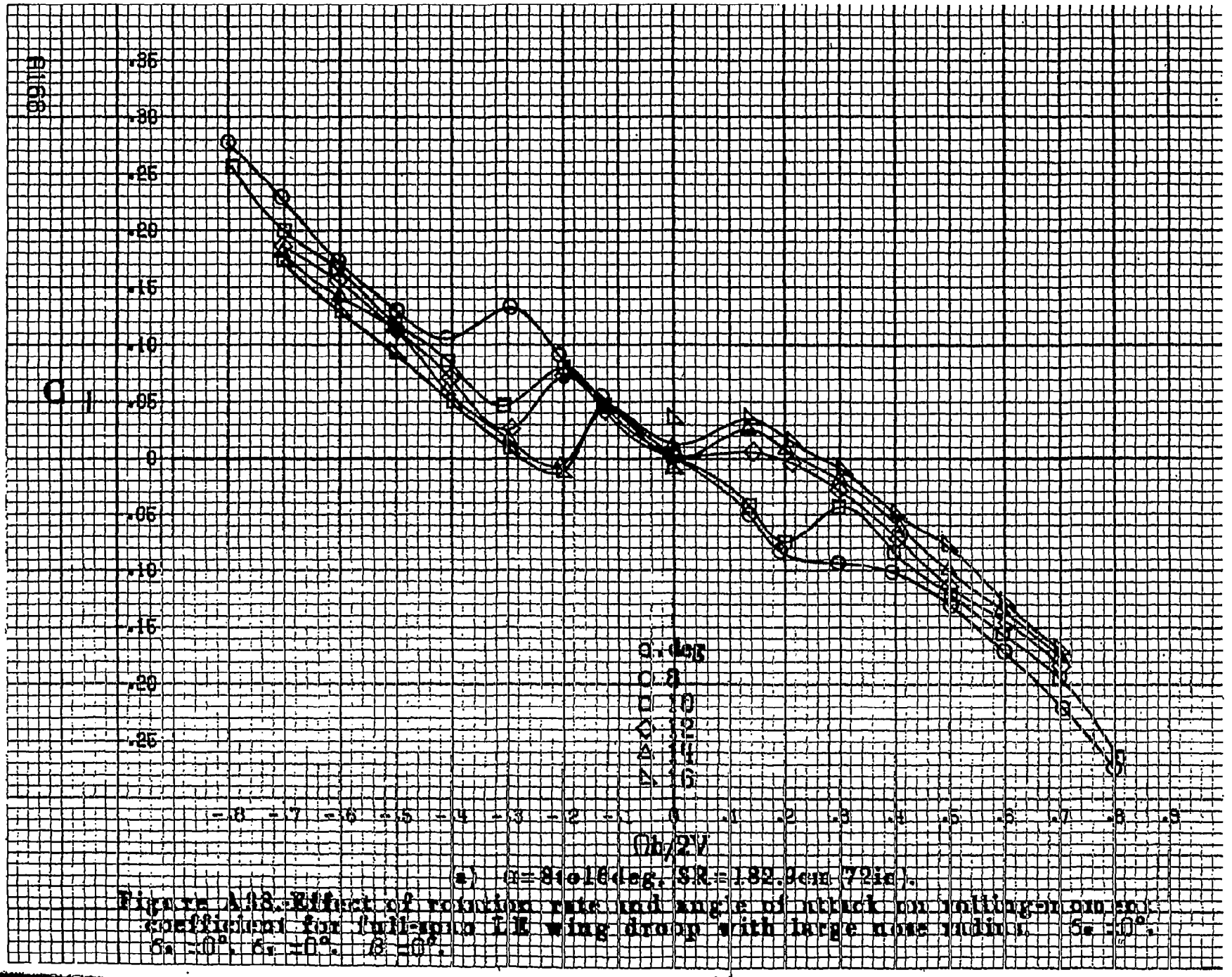

a) $\alpha = 8 \pm 16$ deg. S.R. = 182.3 cm (72 in.).

Figure A18. Effect of rotation rate and angle of attack on rolling-moment coefficient for full-span LE wing droop with large nose radius. $\delta_a = 0°$, $\delta_r = 0°$, $\beta = 0°$.

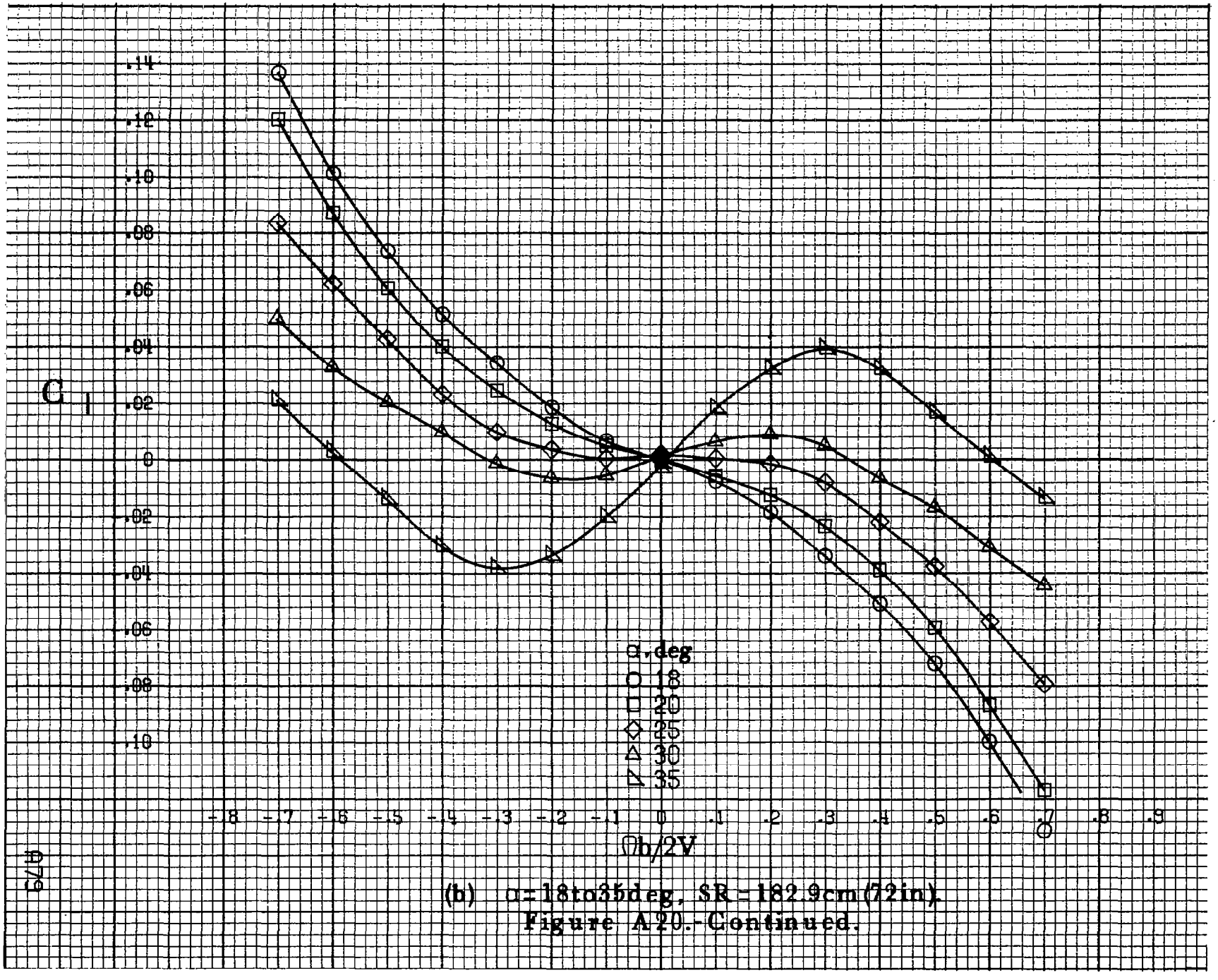

(b) α = 18 to 35 deg, SR = 182.9 cm (72 in).

Figure A20.- Continued.

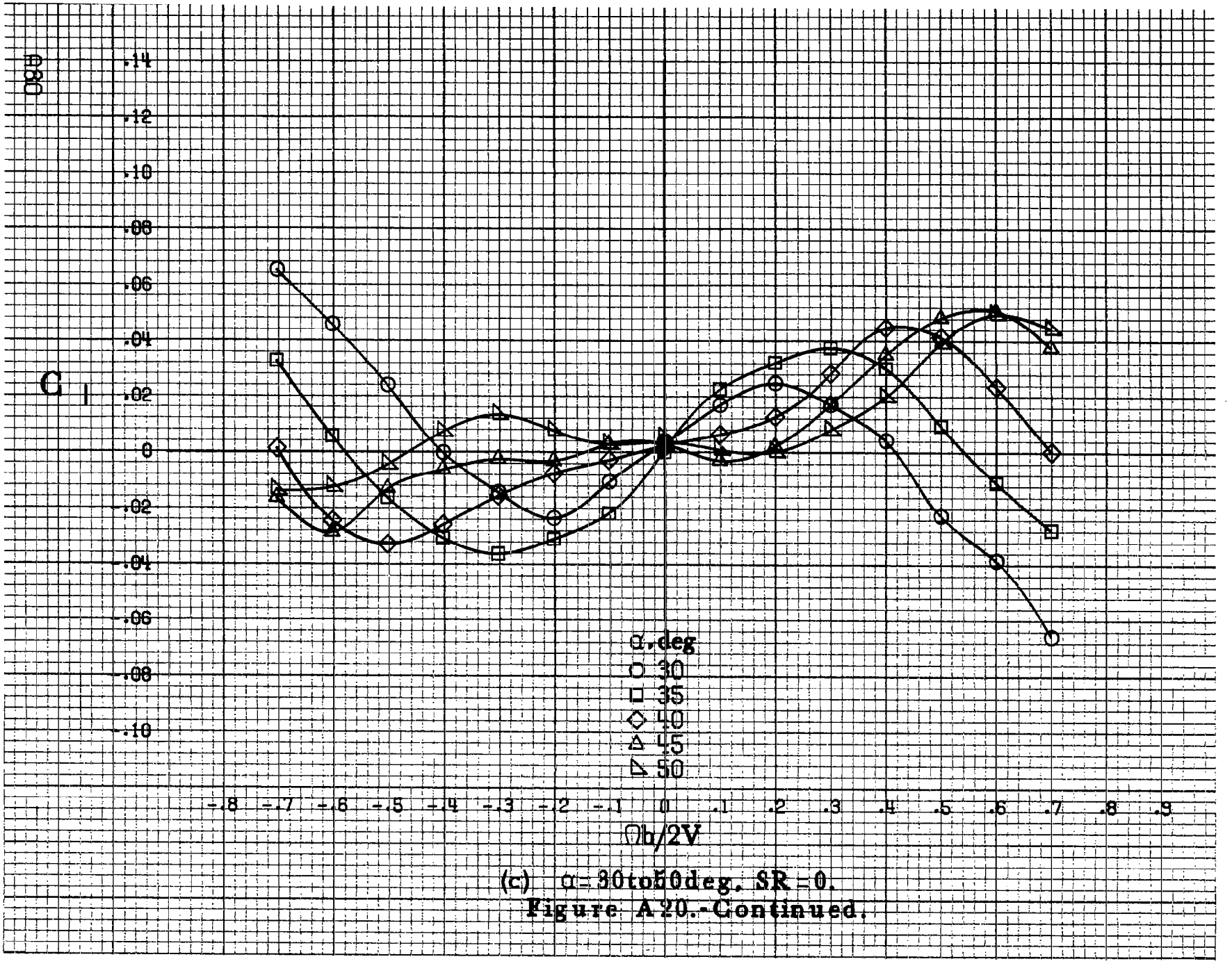

(c) $\alpha = 30$ to 50 deg. SR = 0.

Figure A20.-Continued.

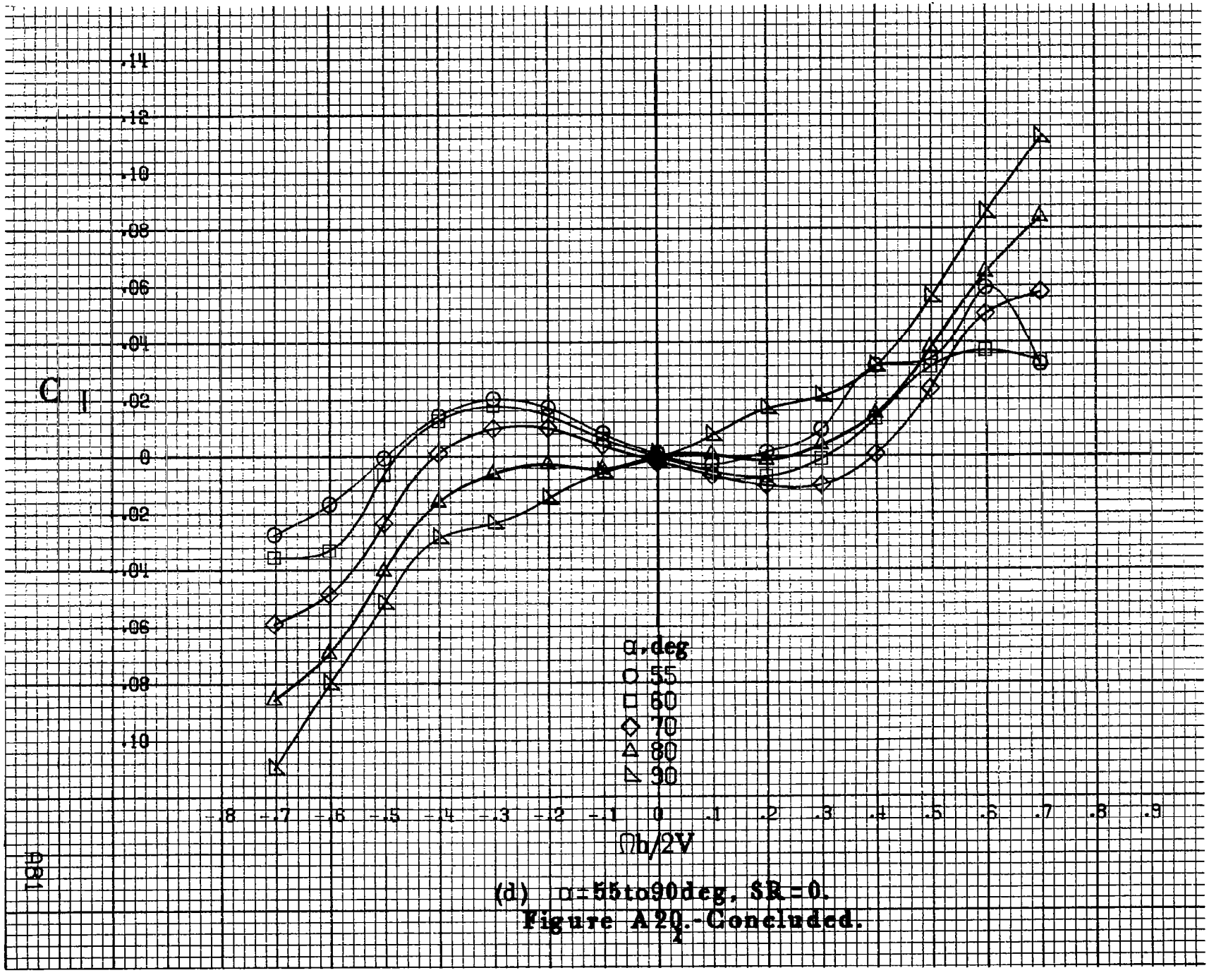

(d) $\alpha = 55$ to 90 deg, $\delta R = 0$.

Figure A20.- Concluded.

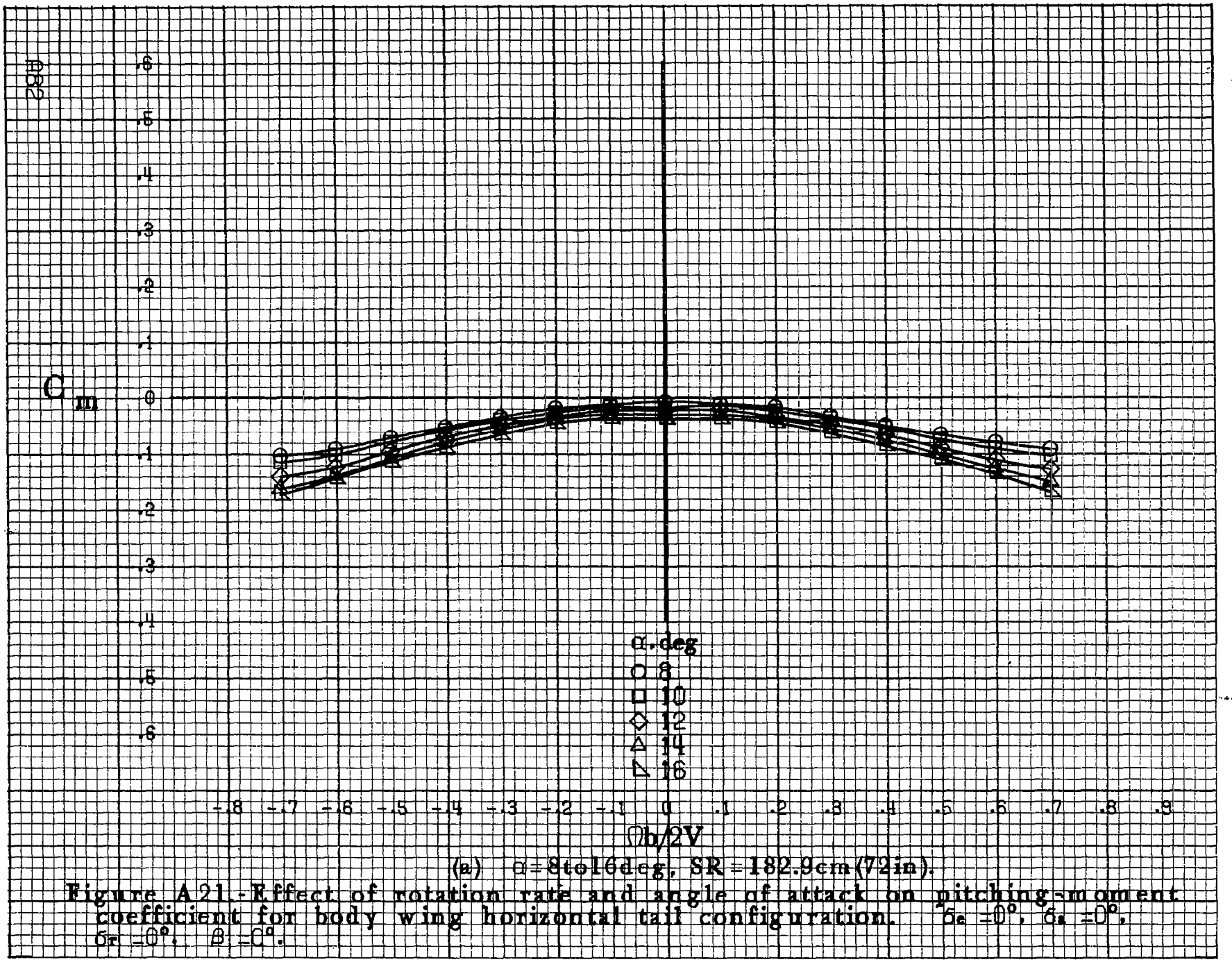

(a) $\alpha = 8$ to 16 deg, SR = 182.9 cm (72 in).

Figure A21.- Effect of rotation rate and angle of attack on pitching-moment coefficient for body wing horizontal tail configuration. $\delta_e = 0°$, $\delta_a = 0°$, $\delta_r = 0°$, $\beta = 0°$.

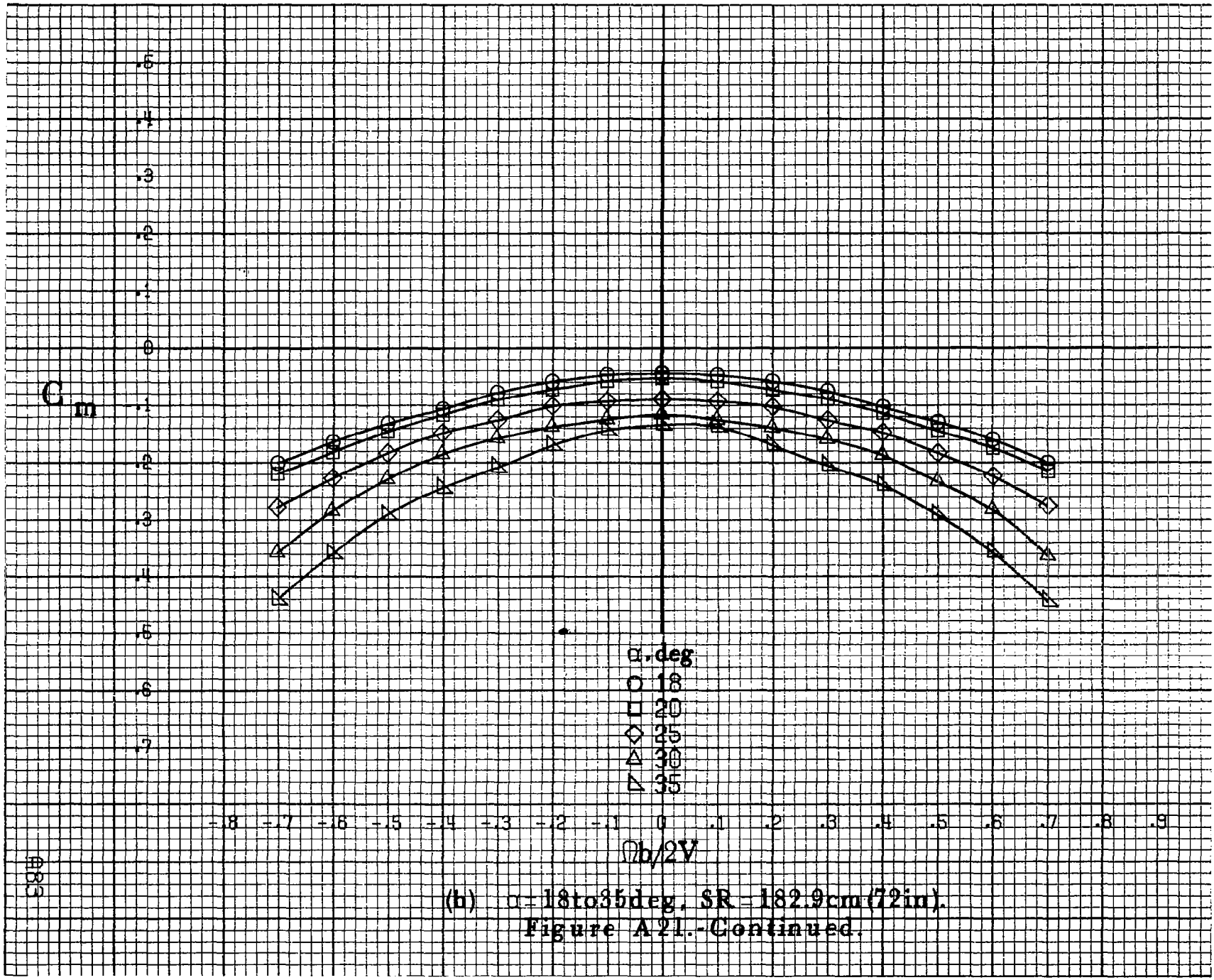

(b) α = 18 to 35 deg, SR = 182.9 cm (72 in).

Figure A21.-Continued.

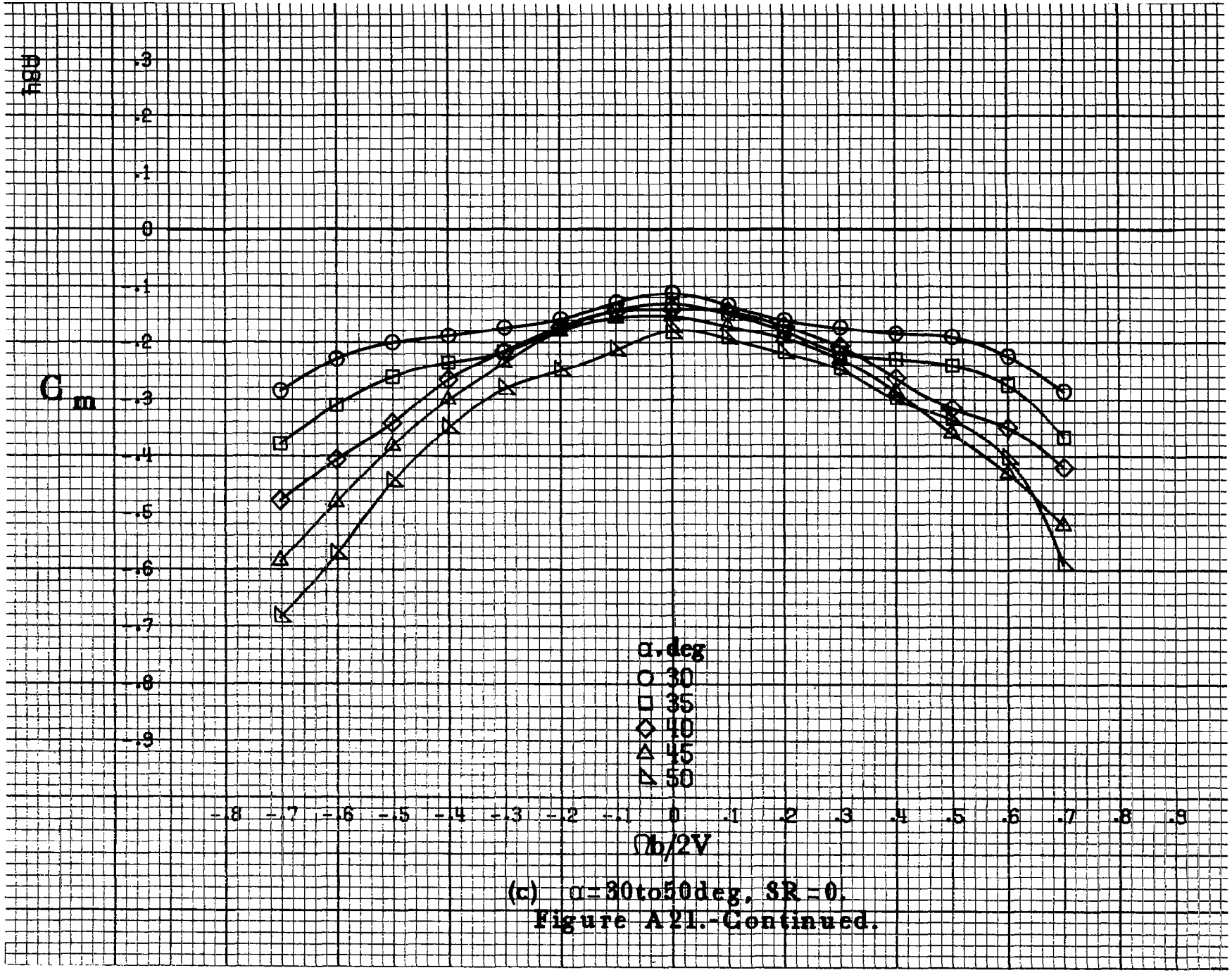

(c) α=30to50deg, SR=0.

Figure A21.-Continued.

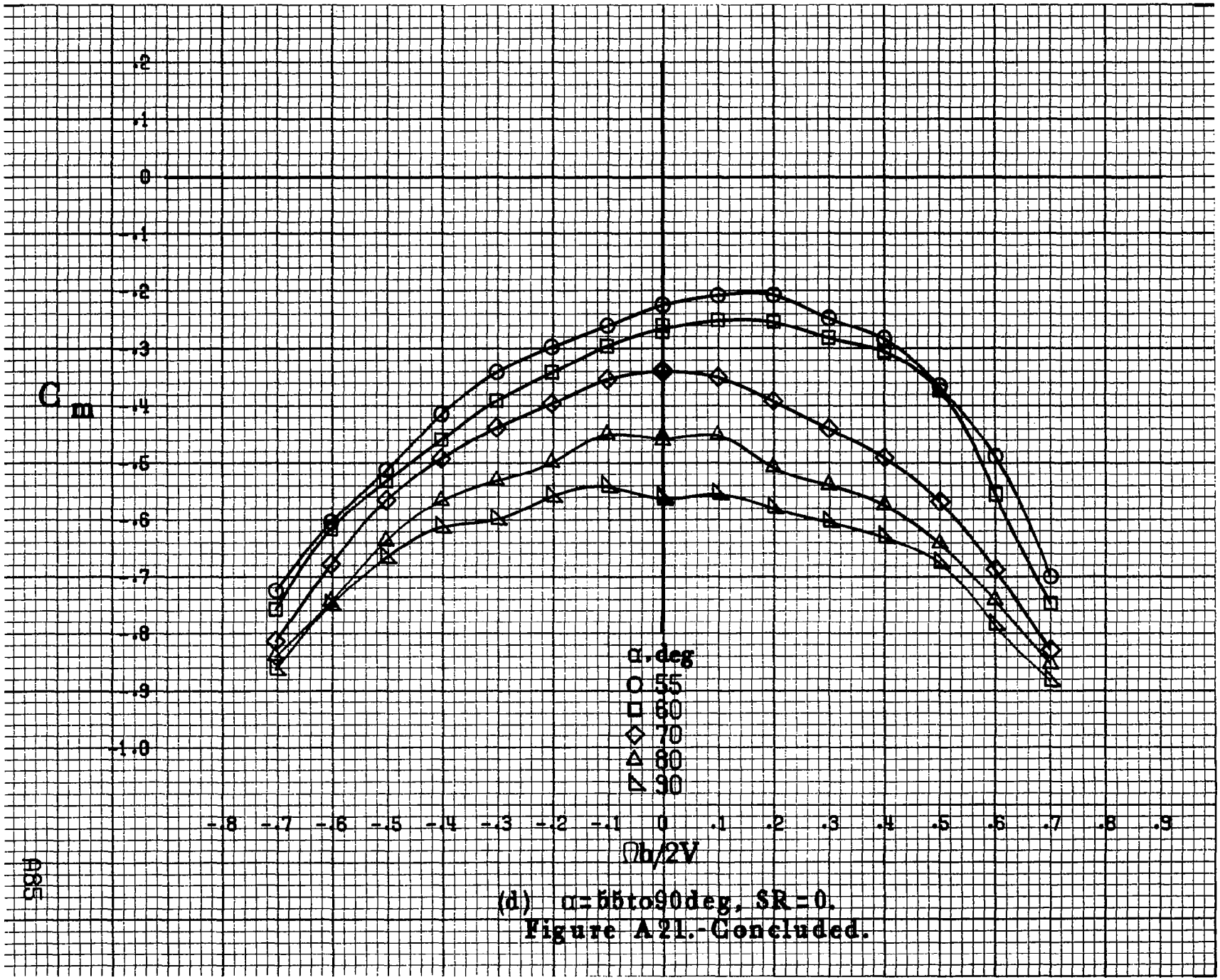

(d) α = 55 to 90 deg, $\delta_R = 0$.

Figure A21.- Concluded.

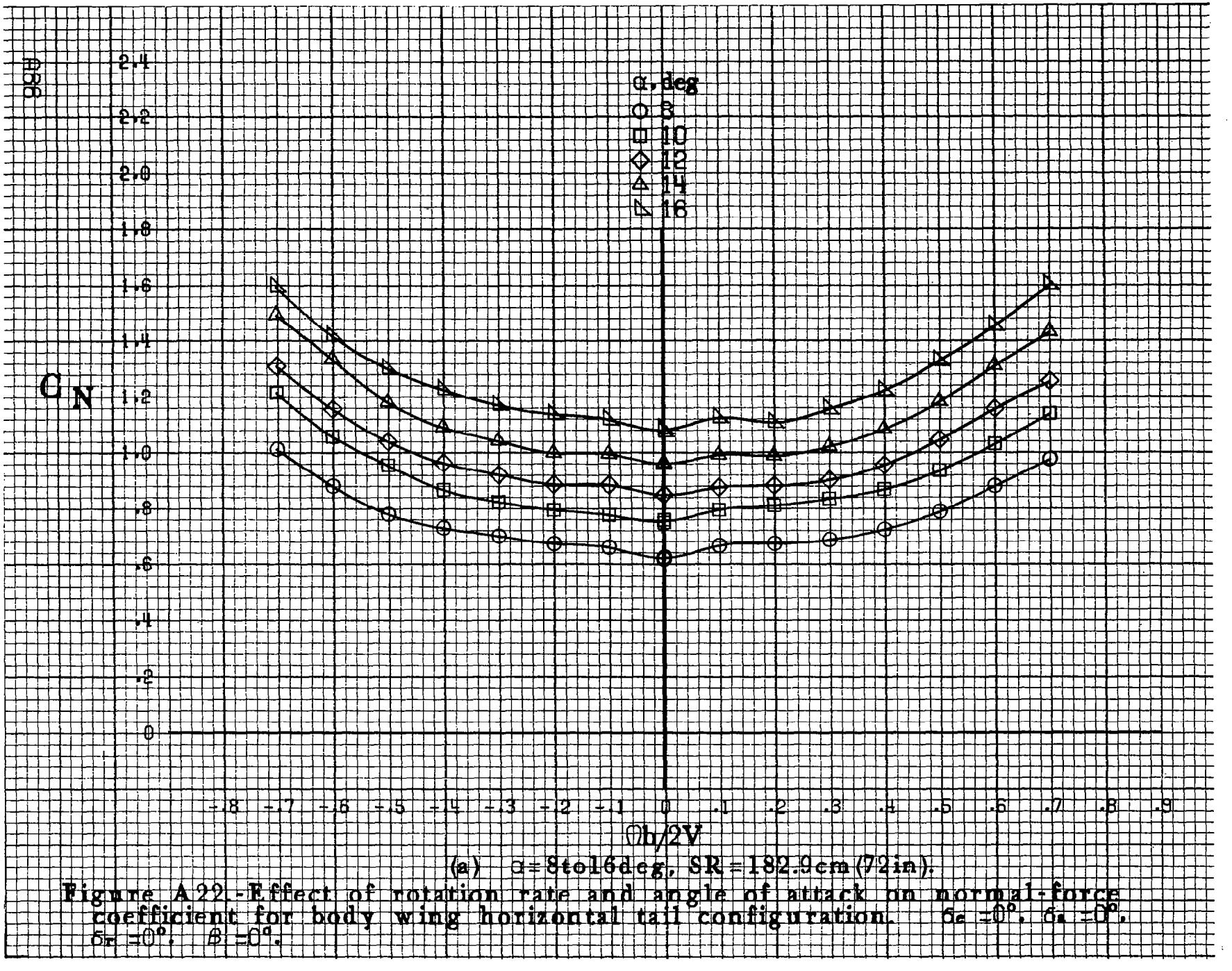

(a) α = 8 to 16 deg, SR = 182.9 cm (72 in).

Figure A 22.- Effect of rotation rate and angle of attack on normal-force coefficient for body wing horizontal tail configuration. $\delta_e = 0°$, $\delta_a = 0°$, $\delta_r = 0°$, $\beta = 0°$.

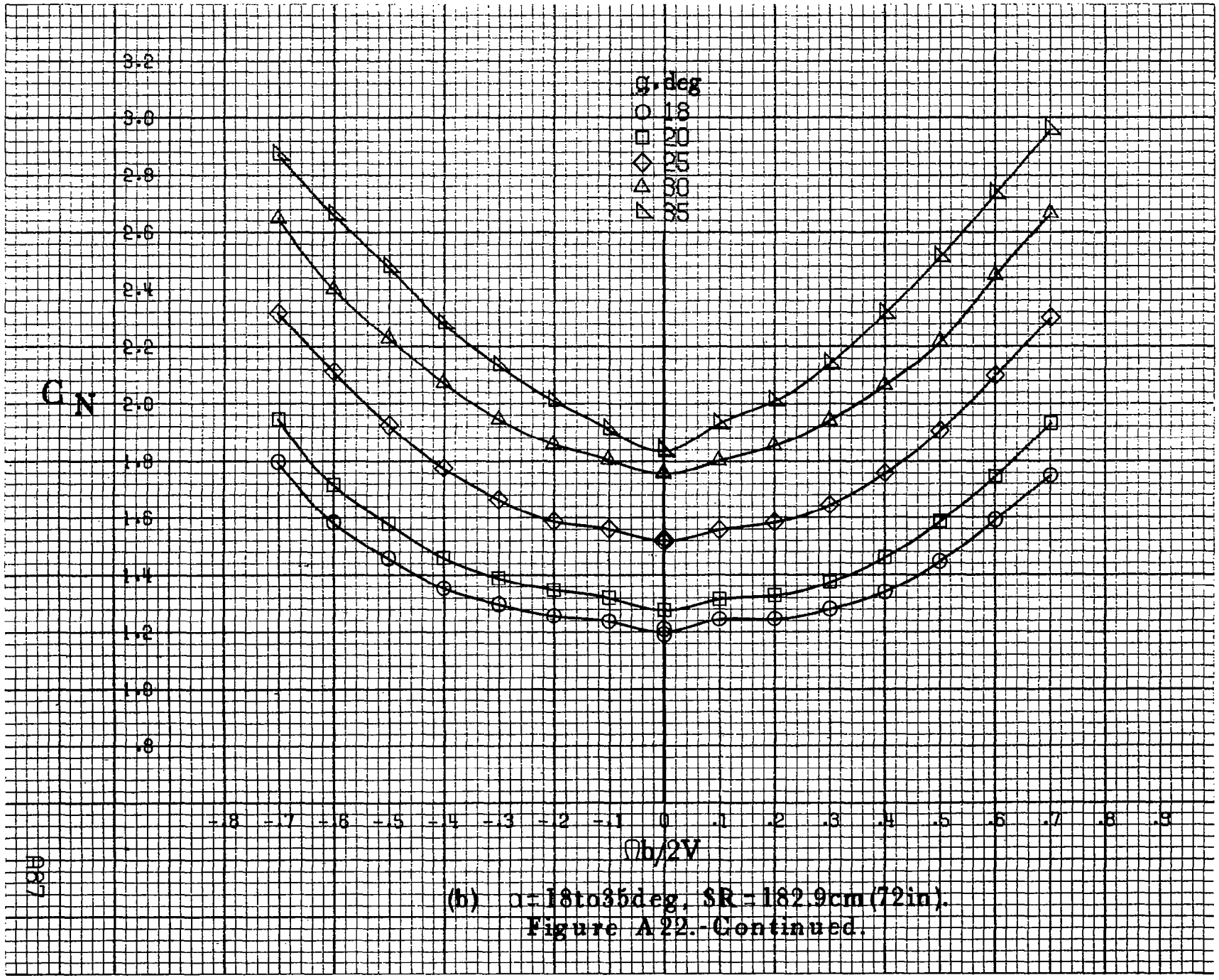

(b) α = 18 to 35 deg, SR = 182.9 cm (72 in).

Figure A22.-Continued.

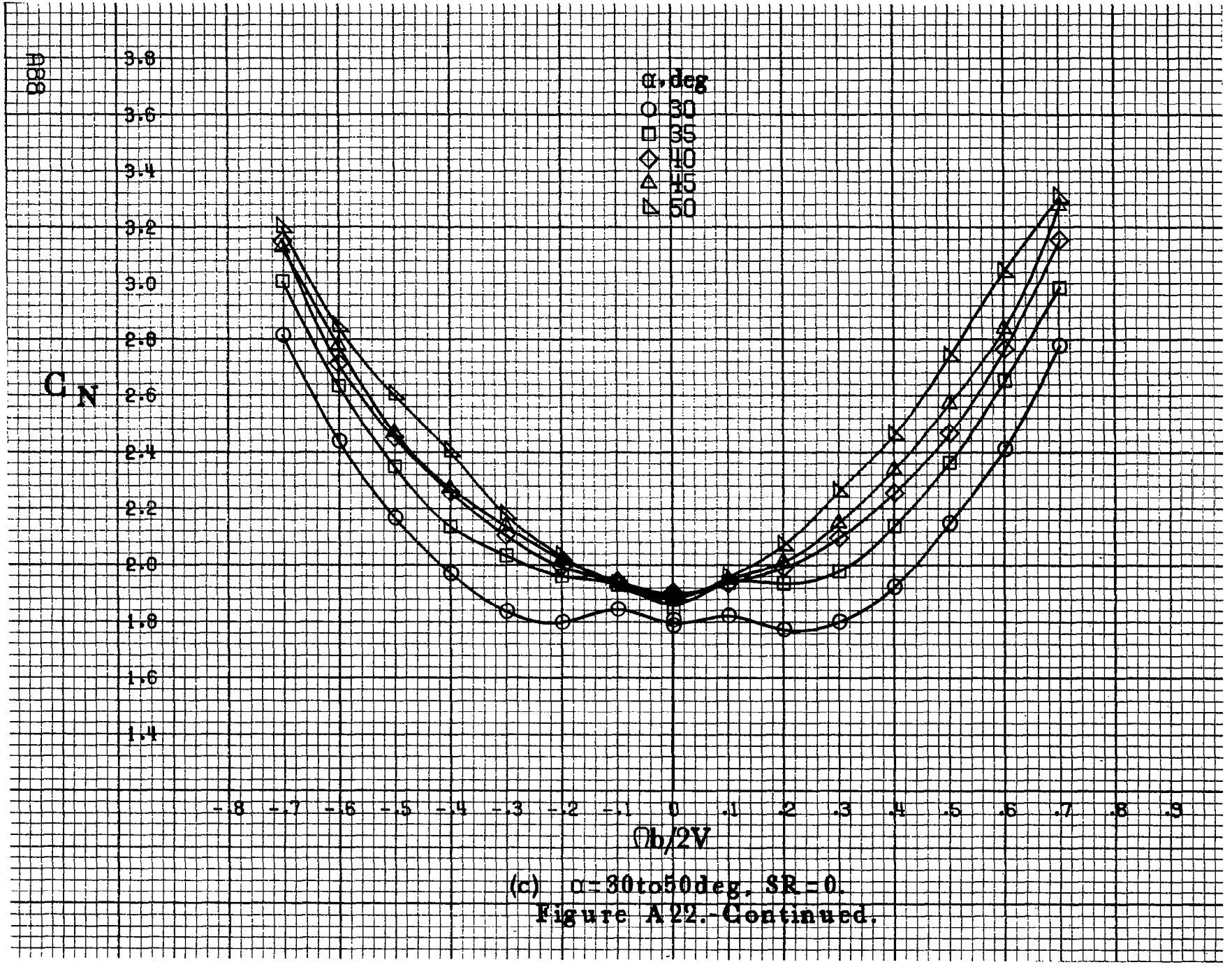

(c) $\alpha = 30$ to 50 deg, $SR = 0$.

Figure A22.- Continued.

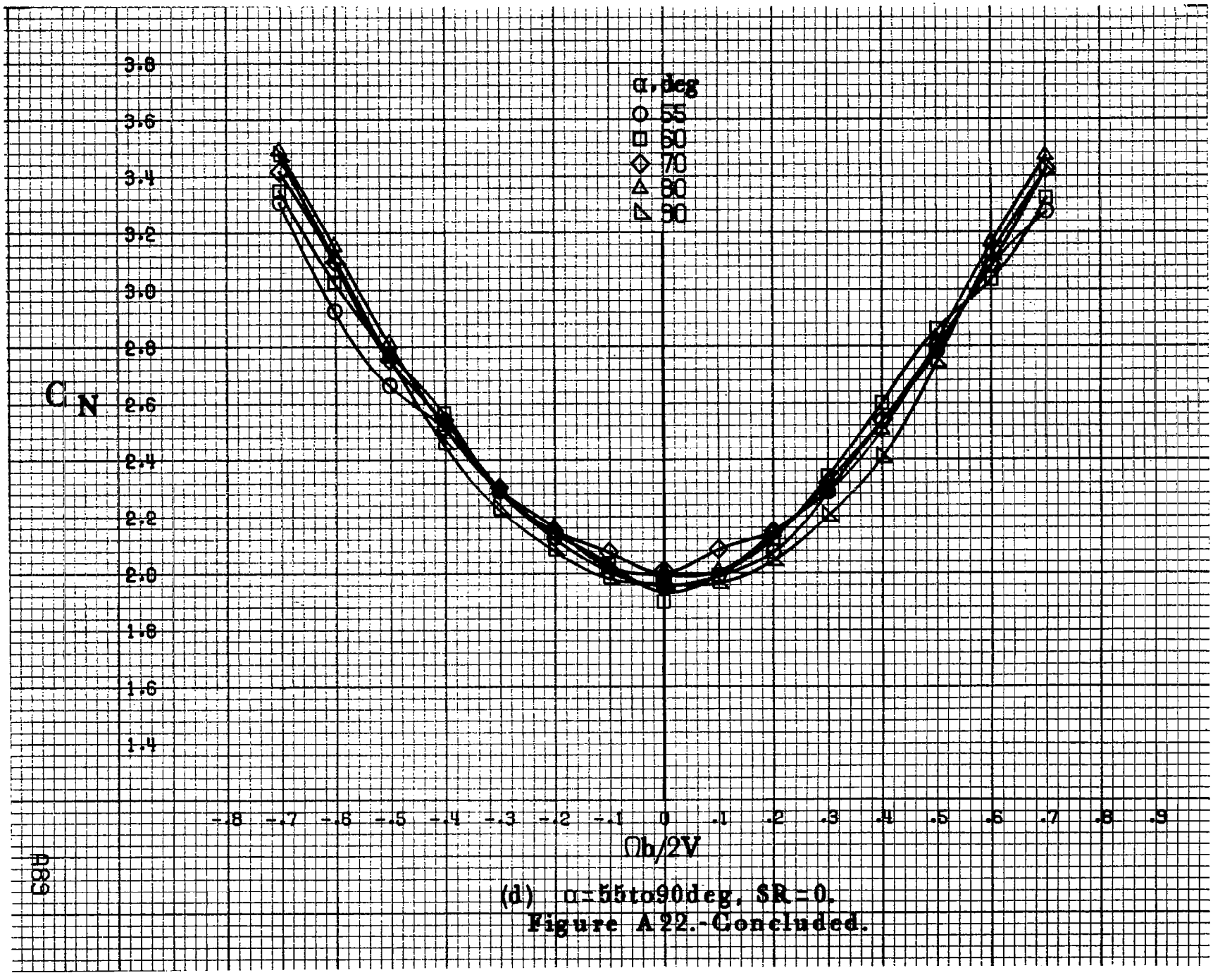

(d) $\alpha = 55$ to 90 deg, $\$R = 0$.

Figure A22.- Concluded.

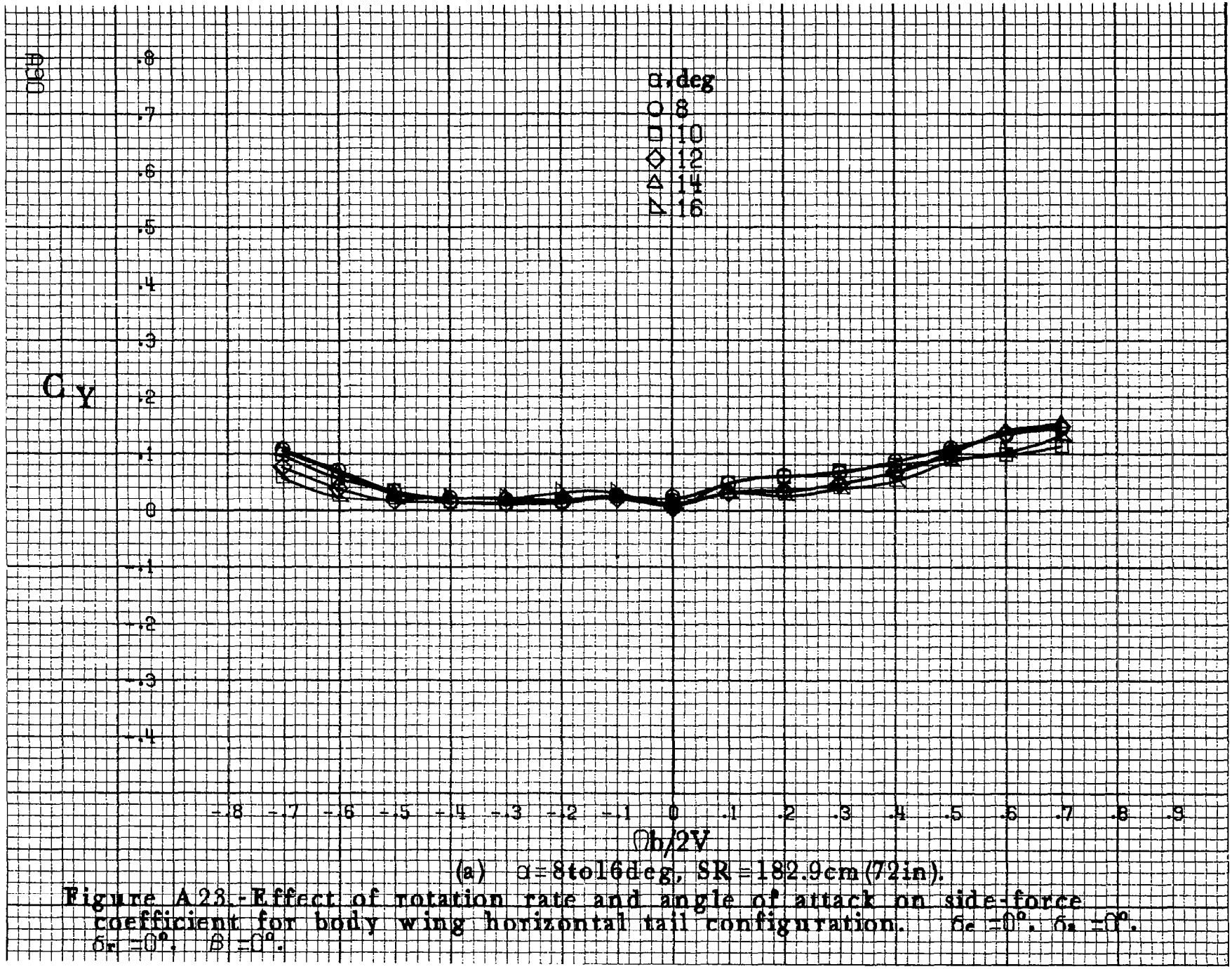

(a) $\alpha = 8$ to 16 deg, SR = 182.9 cm (72 in).

Figure A23.- Effect of rotation rate and angle of attack on side-force coefficient for body wing horizontal tail configuration. $\delta_e = 0°$, $\delta_a = 0°$, $\delta_r = 0°$, $\beta = 0°$.

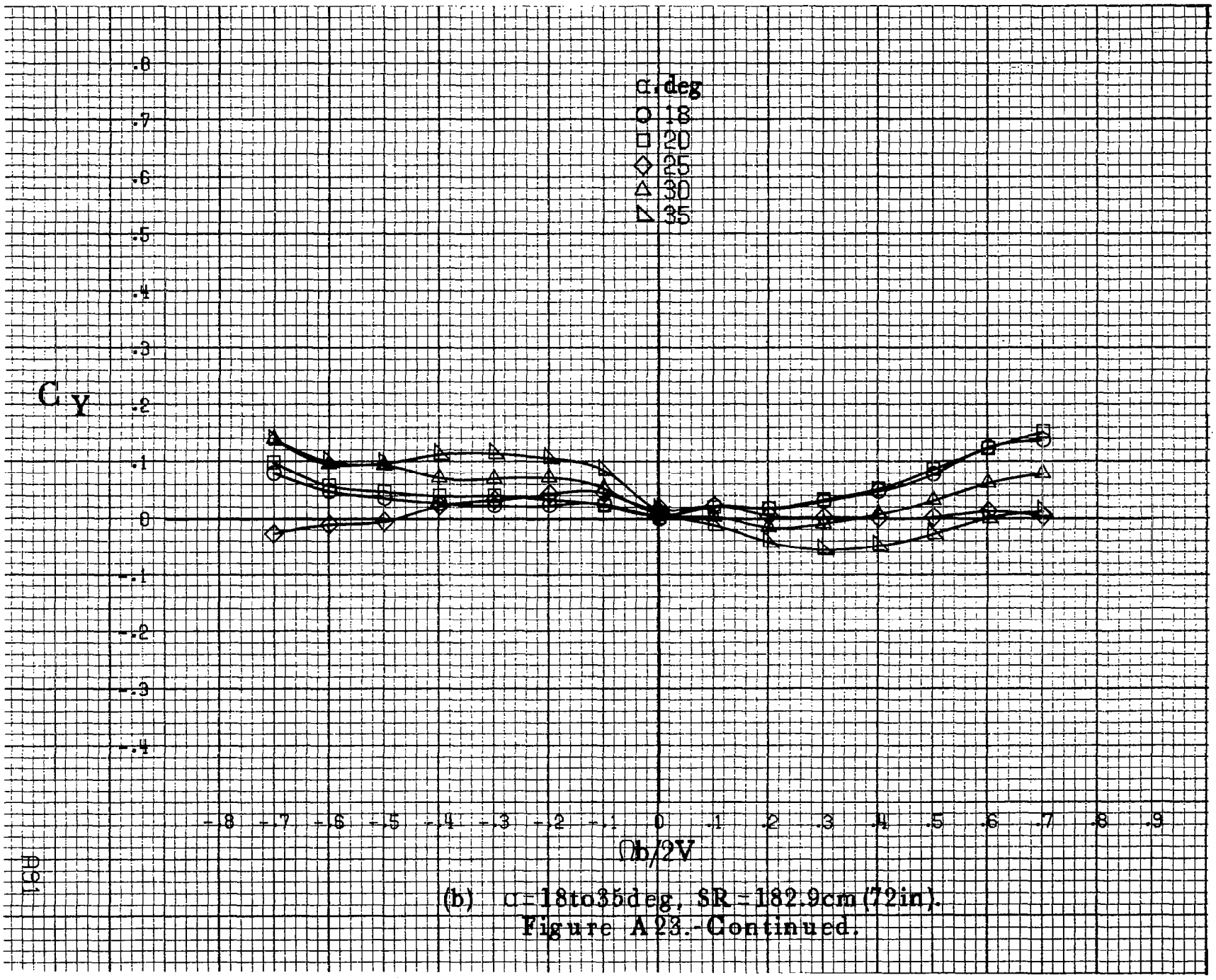

(b) α = 18 to 35 deg, SR = 182.9 cm (72 in).

Figure A23.- Continued.

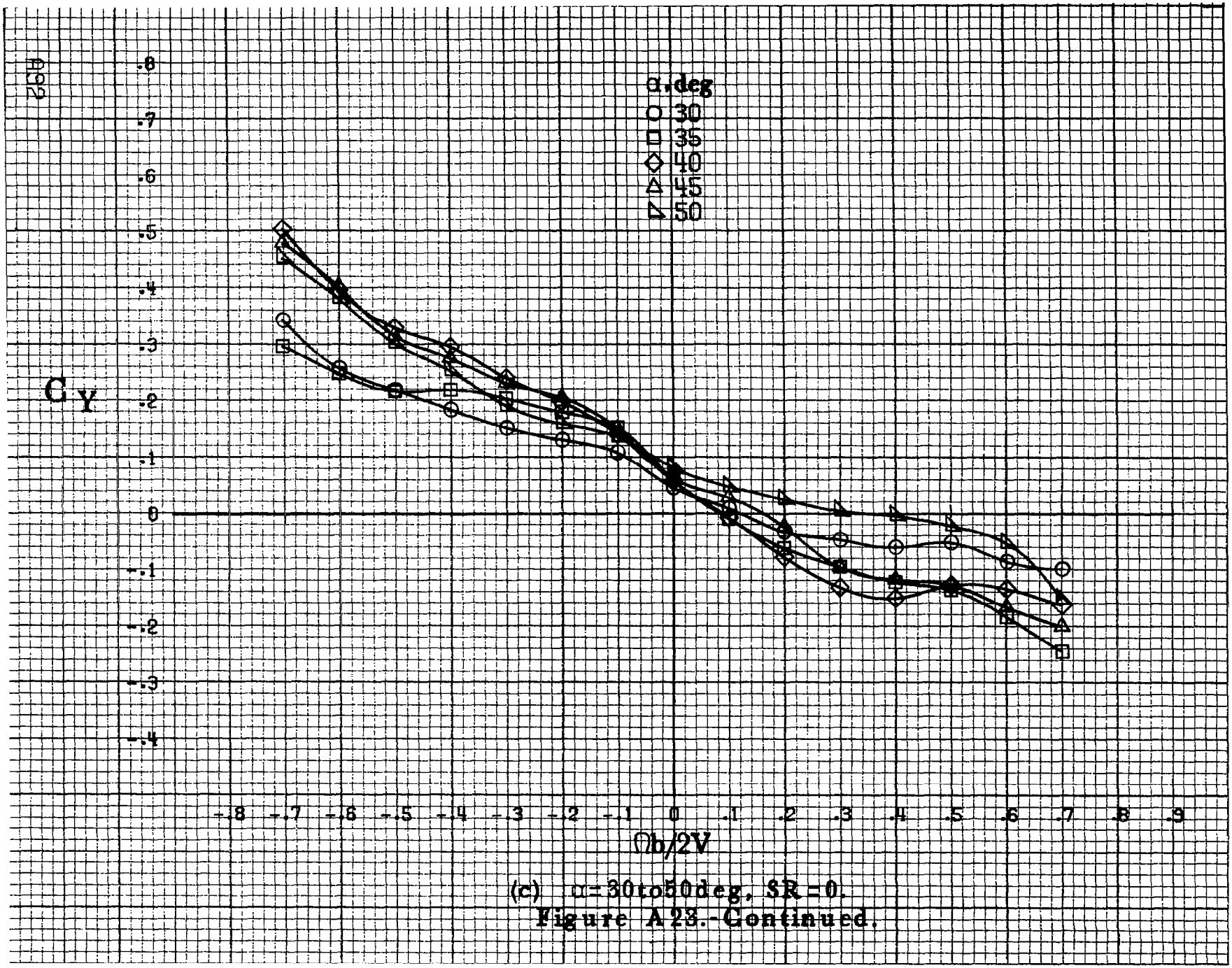

(c) α = 30 to 50 deg, SR = 0.

Figure A23.- Continued.

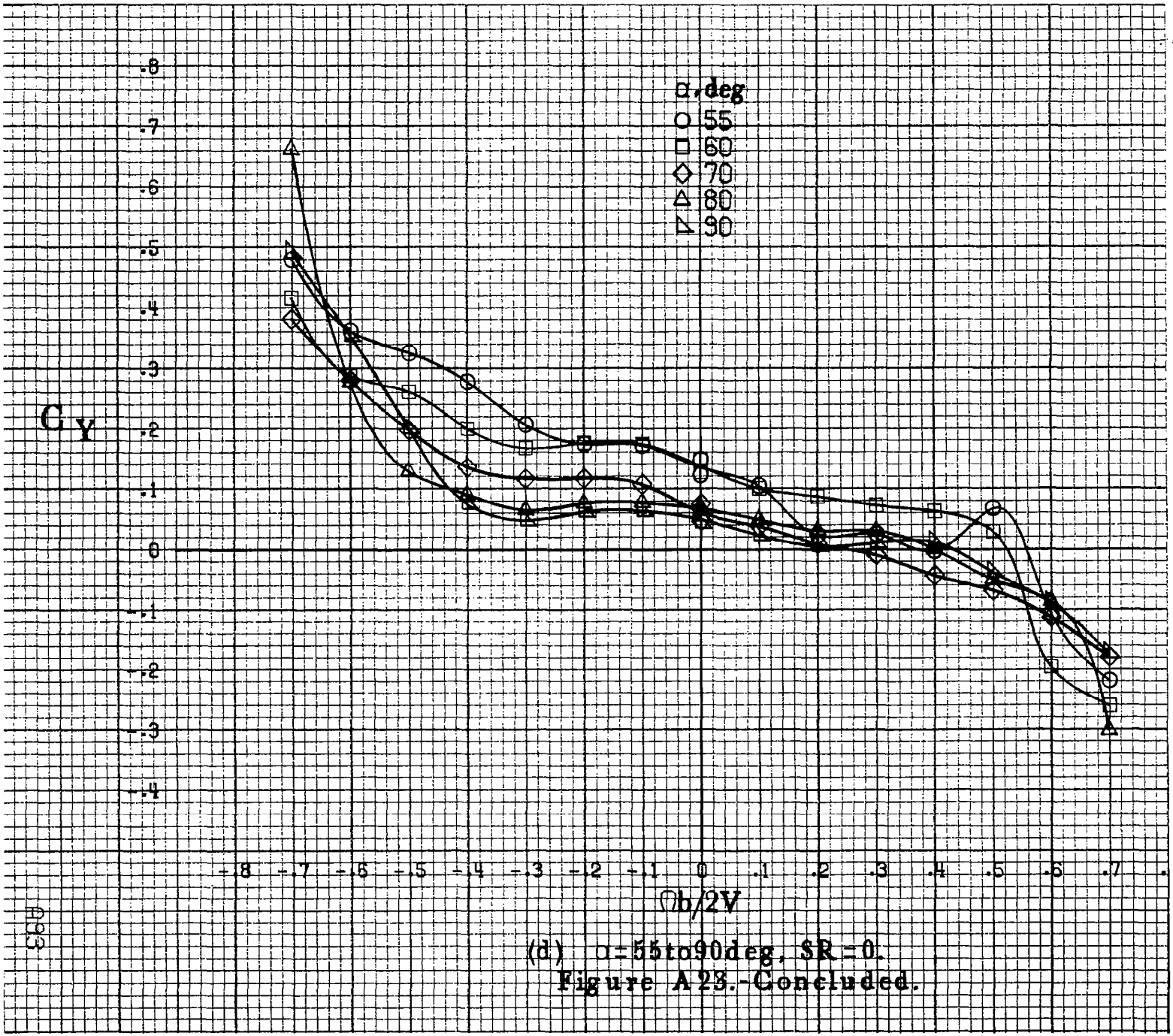

(d) $\alpha = 55$ to 90 deg, SR = 0.

Figure A23.-Concluded.

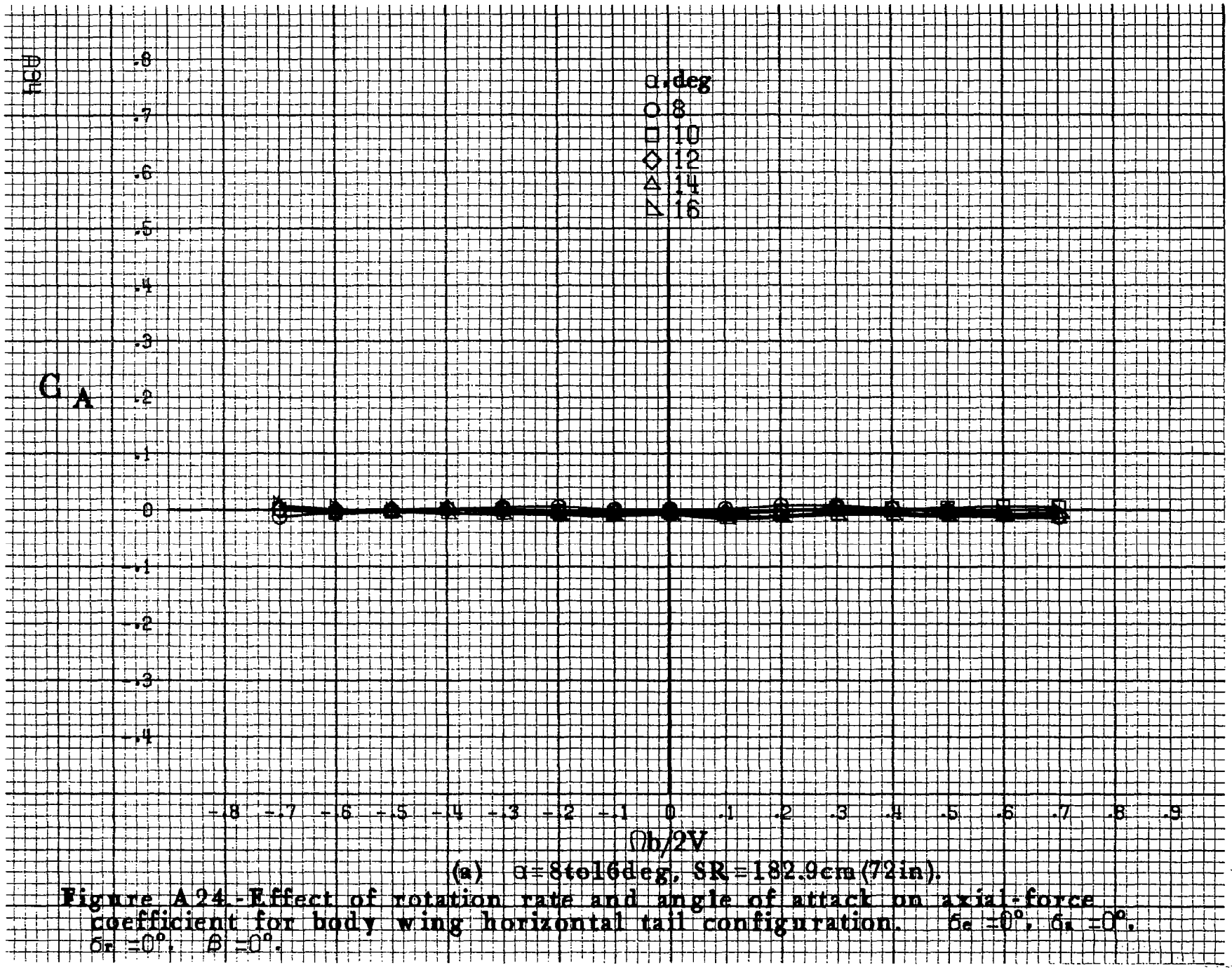

(a) α = 8 to 16 deg, SR = 182.9 cm (72 in).

Figure A24.-Effect of rotation rate and angle of attack on axial-force coefficient for body wing horizontal tail configuration. $\delta_e = 0°$, $\delta_a = 0°$, $\delta_r = 0°$, $\beta = 0°$.

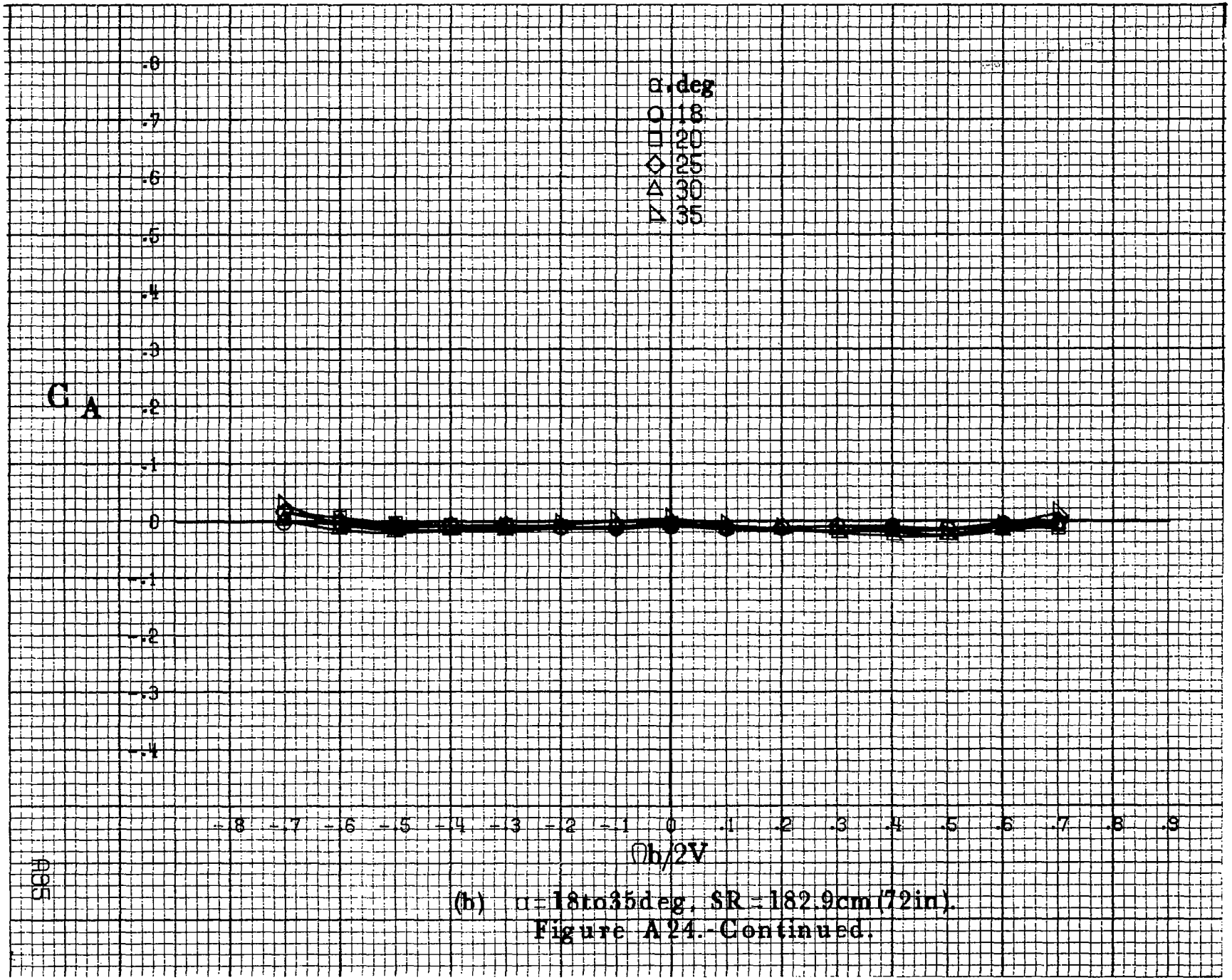

(b) α = 18 to 35 deg, SR = 182.9 cm (72 in).

Figure A24.-Continued.

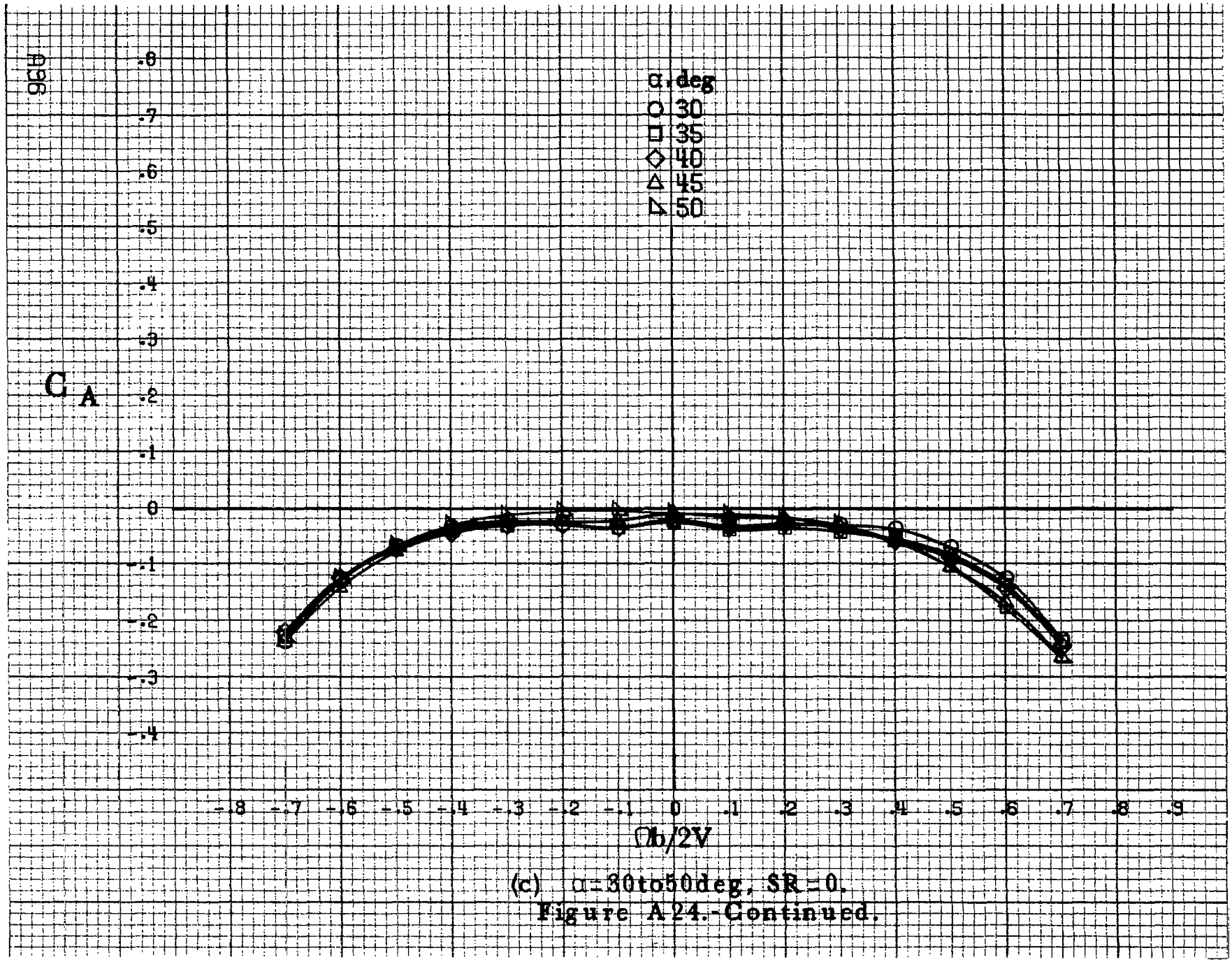

(c) α=30to50deg, SR=0.

Figure A24.-Continued.

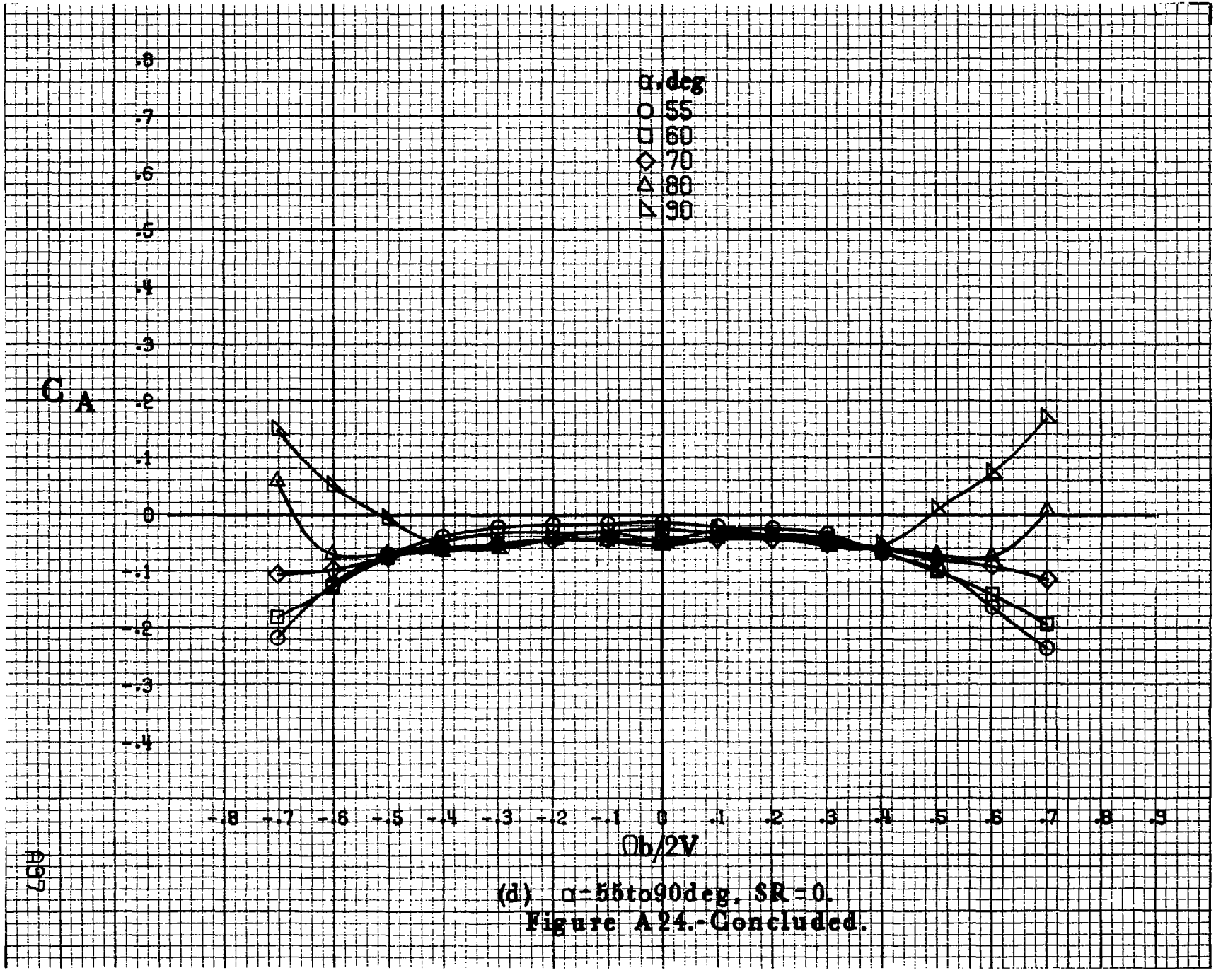

(d) α=55to90deg, $R=0.

Figure A24.-Concluded.

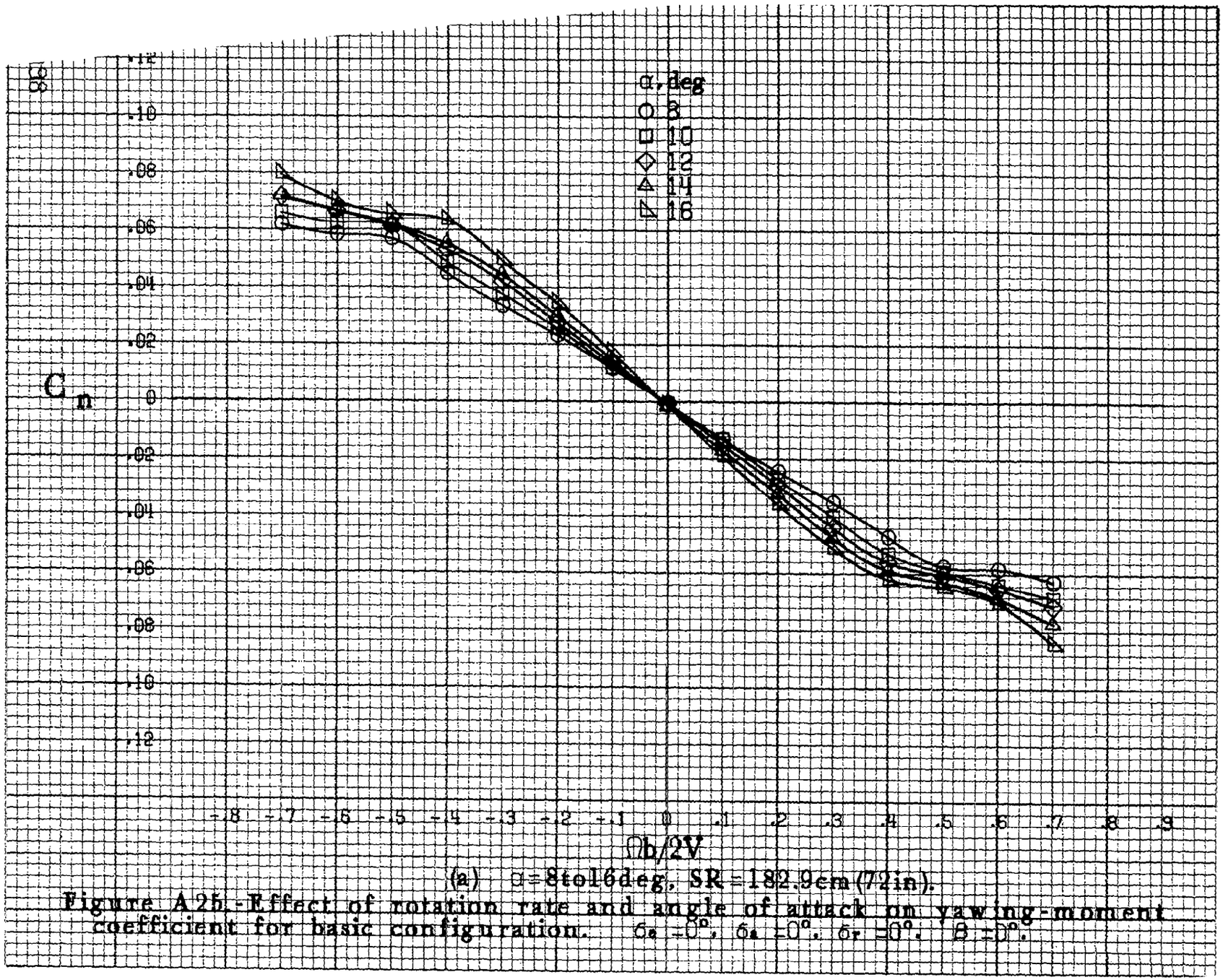

(a) $\alpha = 8$ to 16 deg, SR = 182.9 cm (72 in.).

Figure A.25.- Effect of rotation rate and angle of attack on yawing-moment coefficient for basic configuration. $\delta_e = 0°$, $\delta_a = 0°$, $\delta_r = 0°$, $\beta = 0°$.

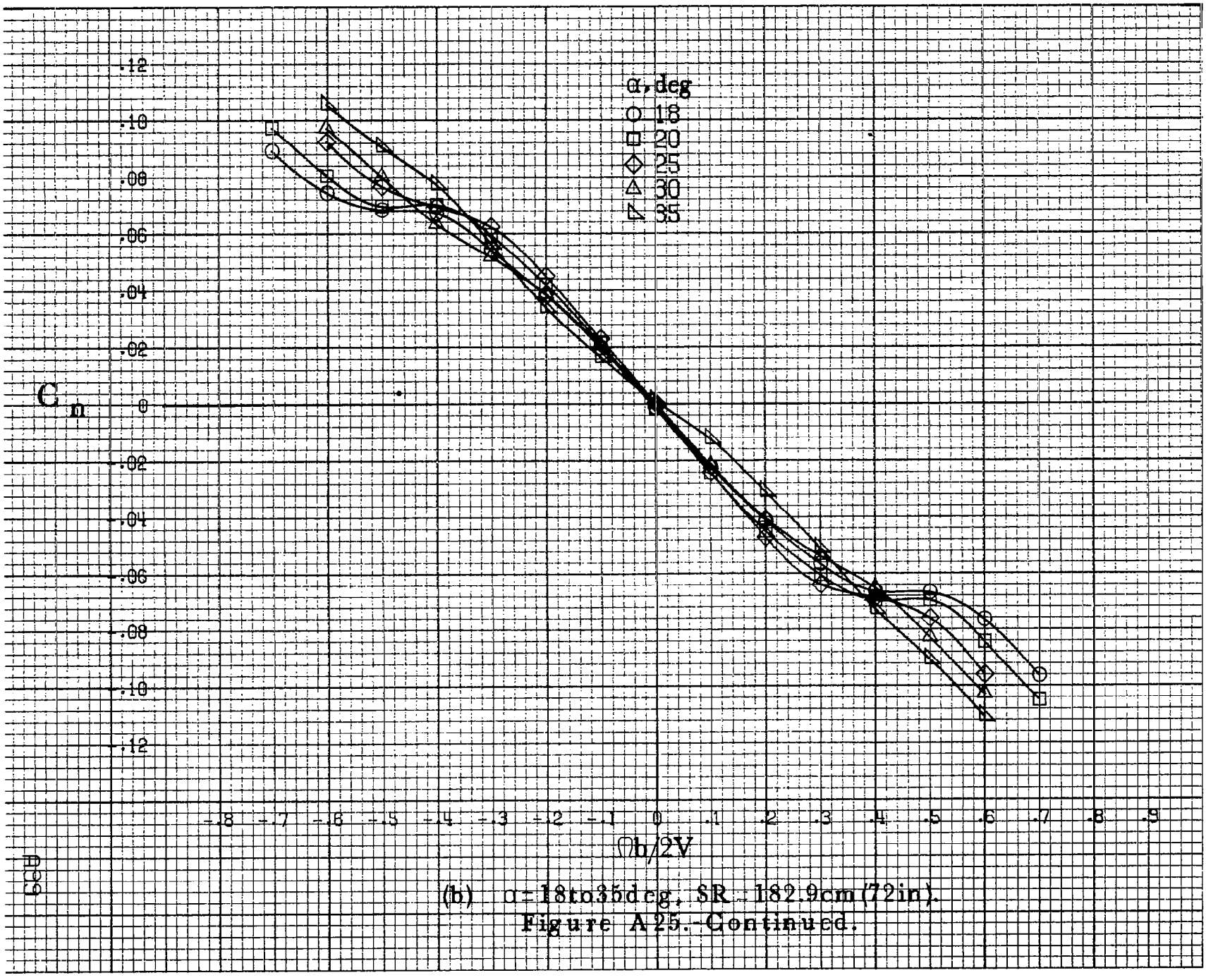

(b) α = 18 to 35 deg, SR = 182.9 cm (72 in).

Figure A25.-Continued.

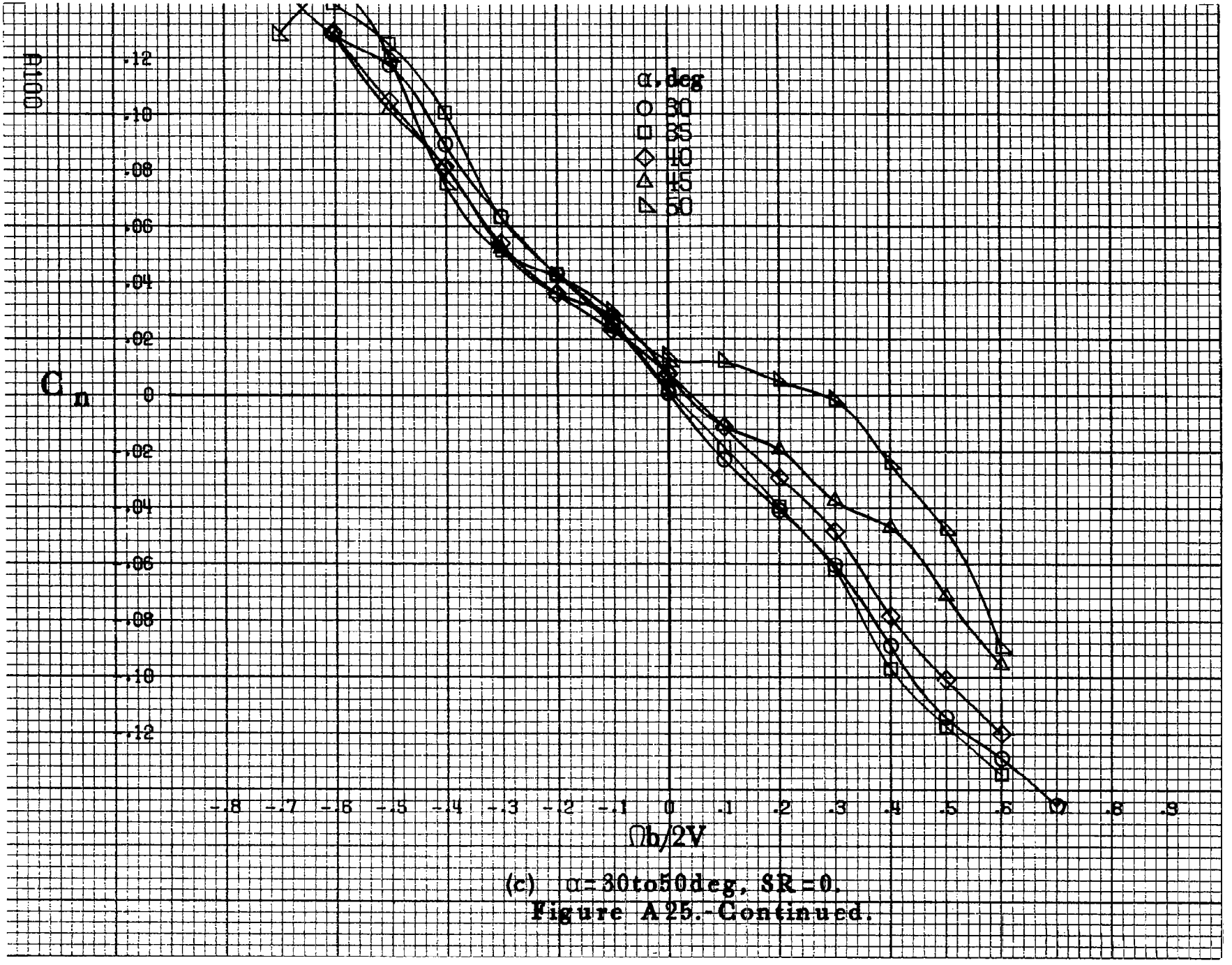

(c) $\alpha = 30$ to 50 deg, SR = 0.

Figure A25.-Continued.

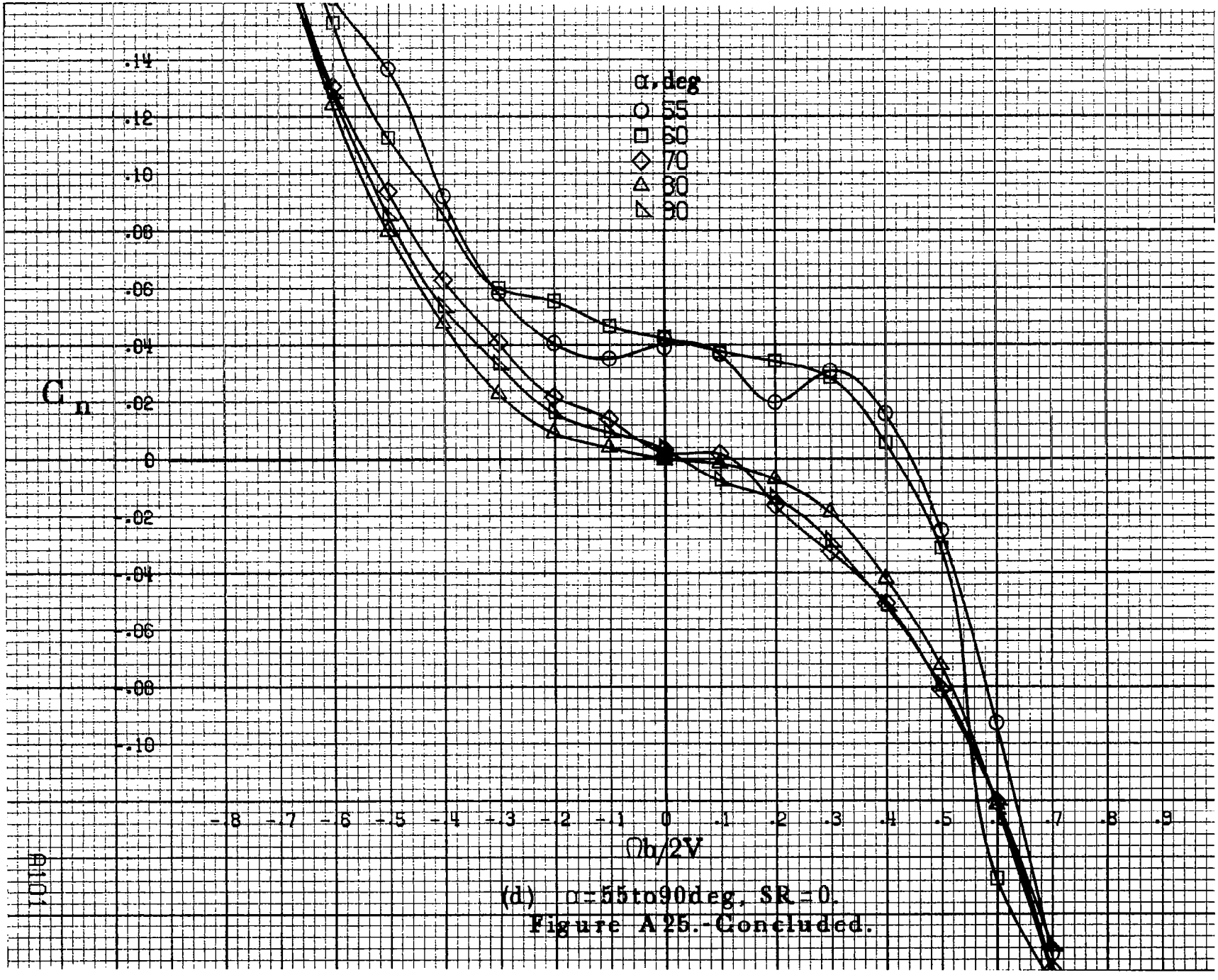

(d) $\alpha = 55$ to 90 deg, $SR = 0$.

Figure A25.- Concluded.

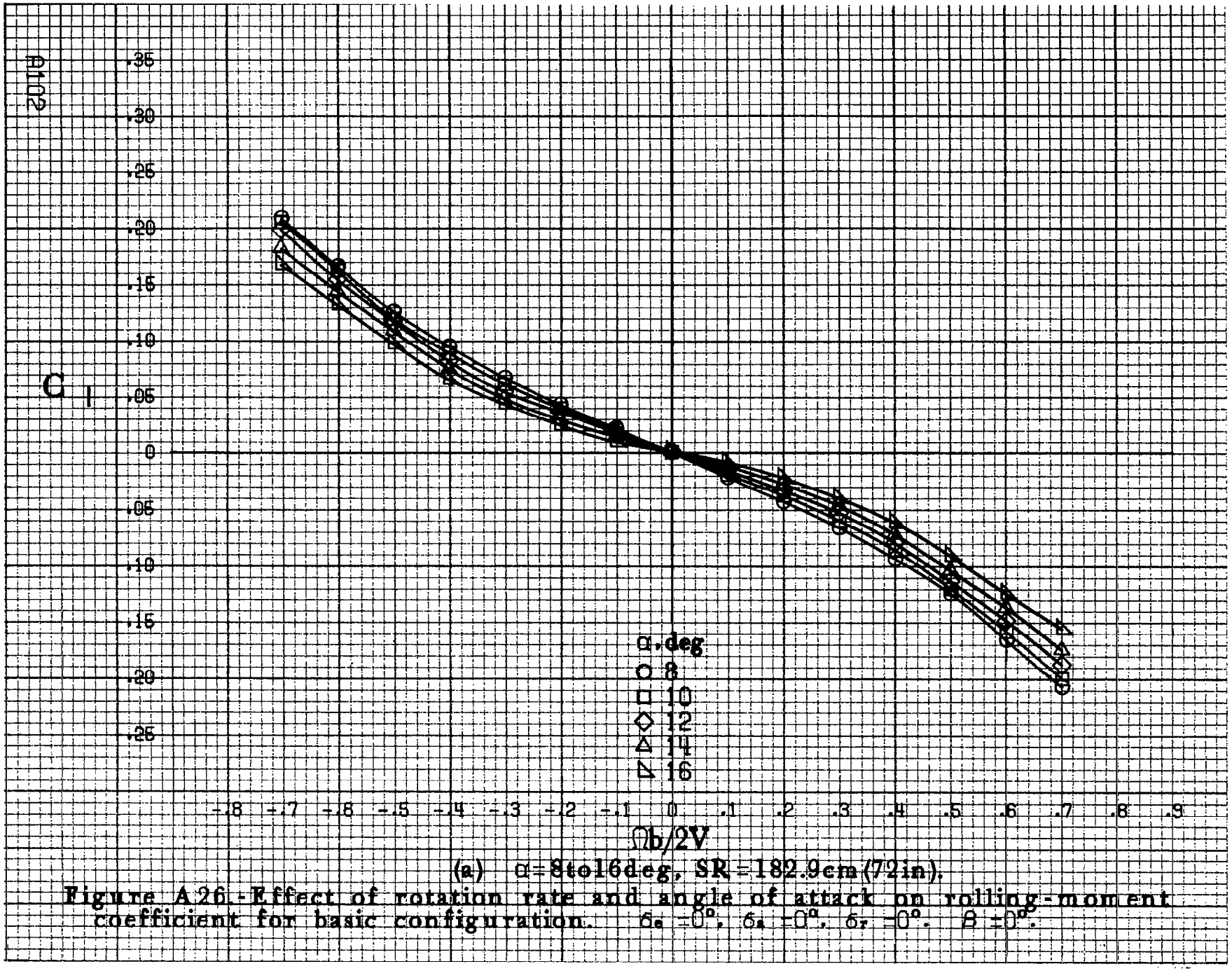

(a) $\alpha = 8$ to 16 deg, SR = 182.9 cm (72 in).

Figure A26.- Effect of rotation rate and angle of attack on rolling-moment coefficient for basic configuration. $\delta_e = 0°$, $\delta_a = 0°$, $\delta_r = 0°$, $\beta = 0°$.

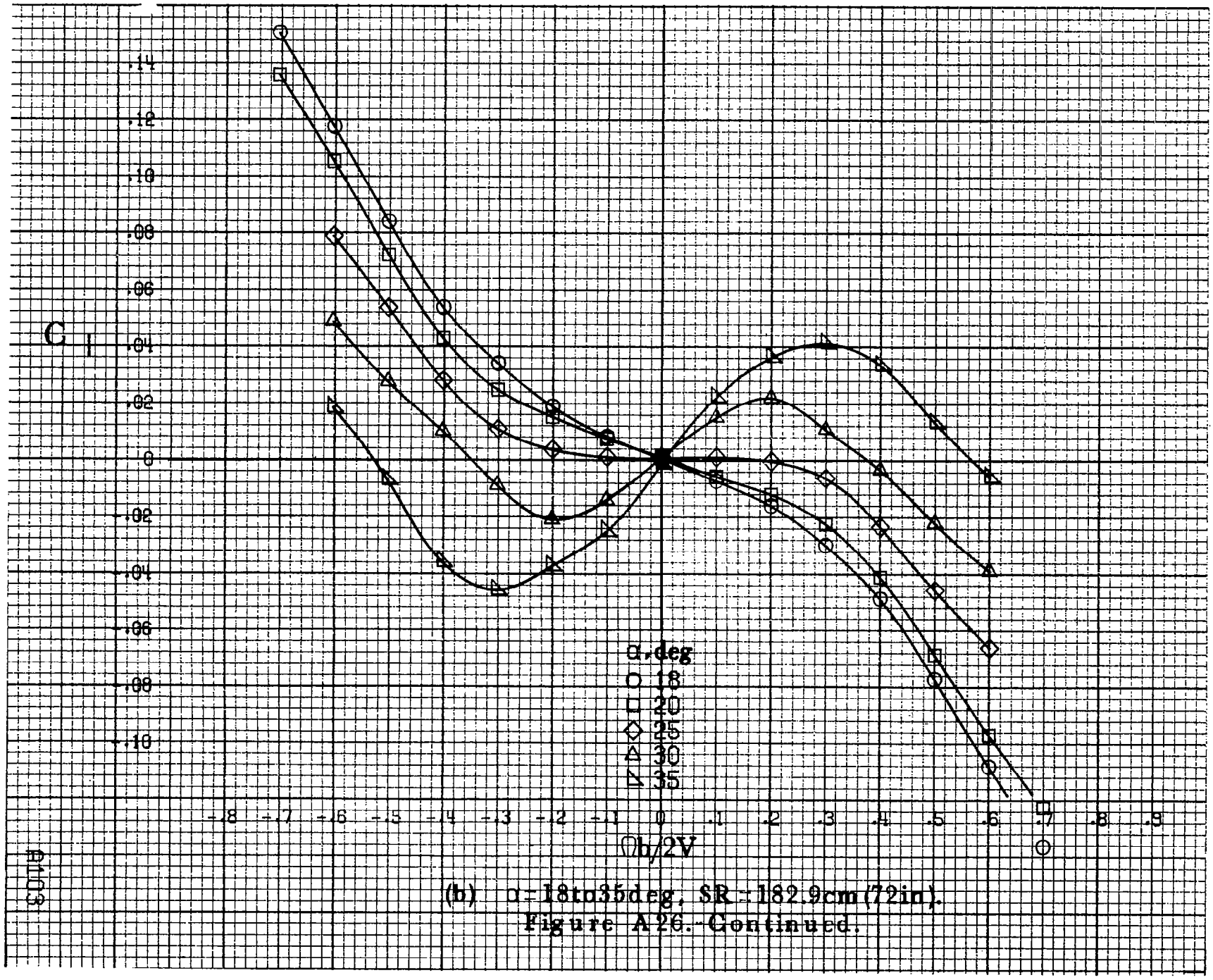

(b) α = 18 to 35 deg, SR = 182.9 cm (72 in).

Figure A26.- Continued.

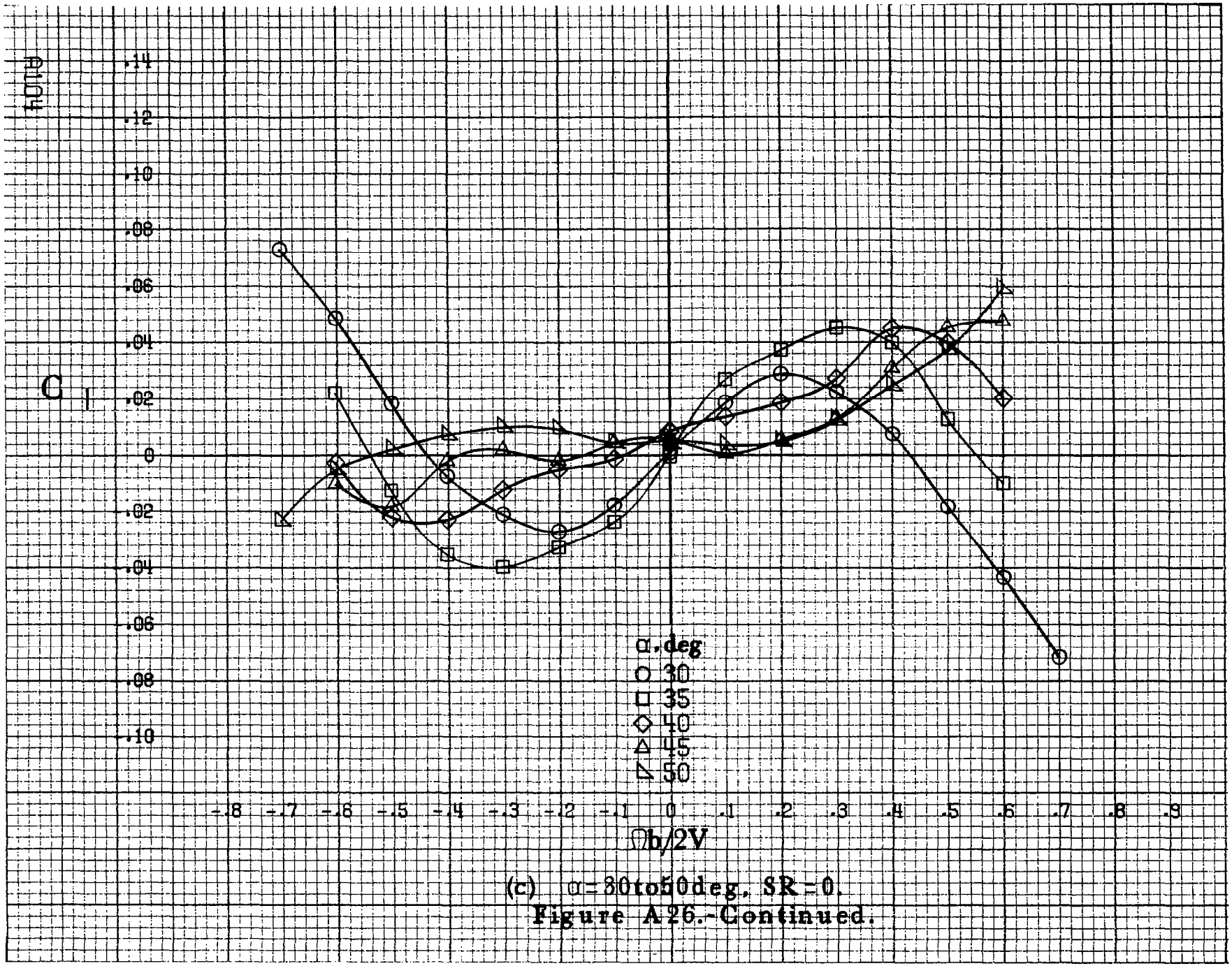

(c) $\alpha = 30$ to 50 deg, SR = 0.

Figure A26.-Continued.

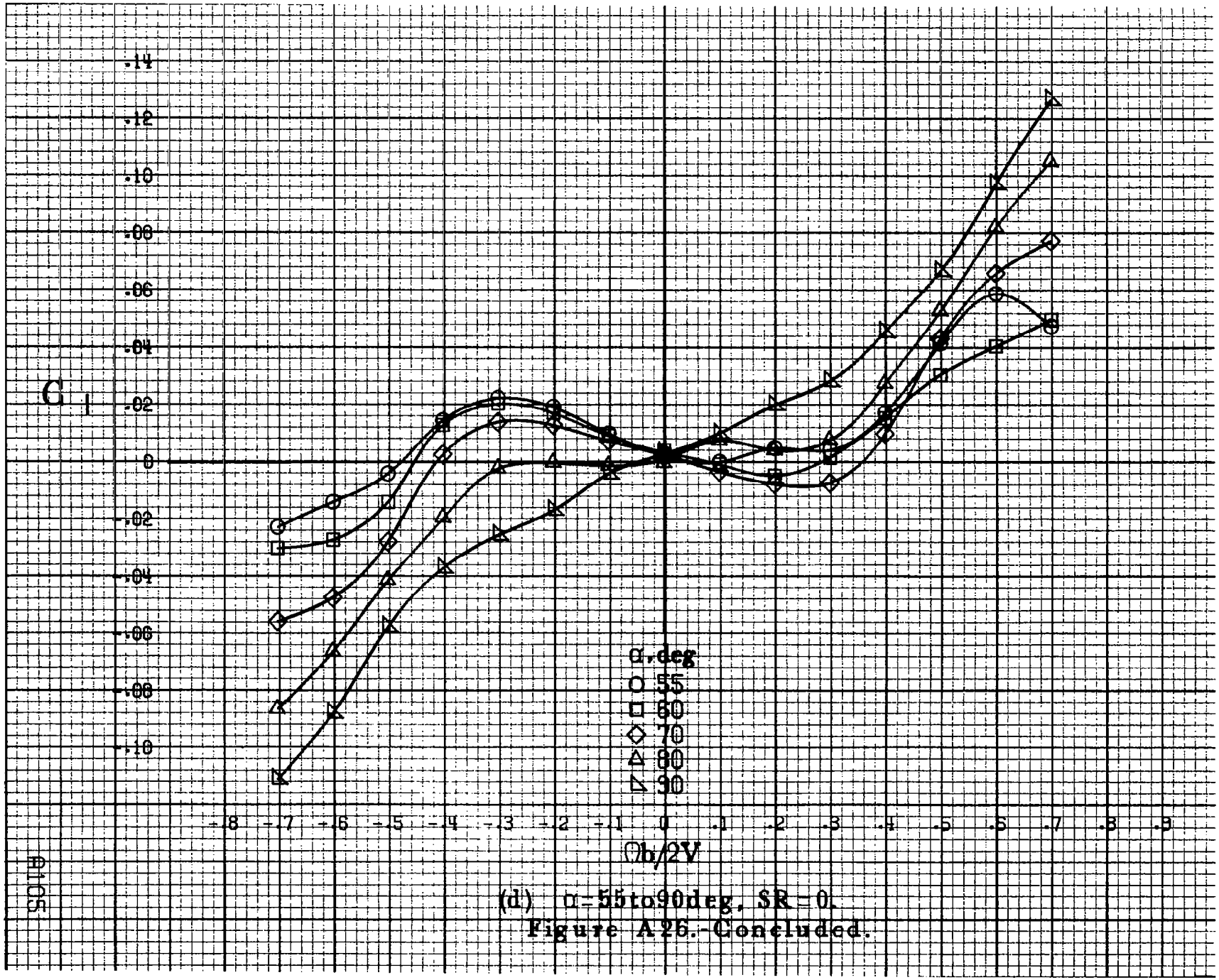

(d) $\alpha = 55$ to 90 deg, SR = 0.

Figure A26.- Concluded.

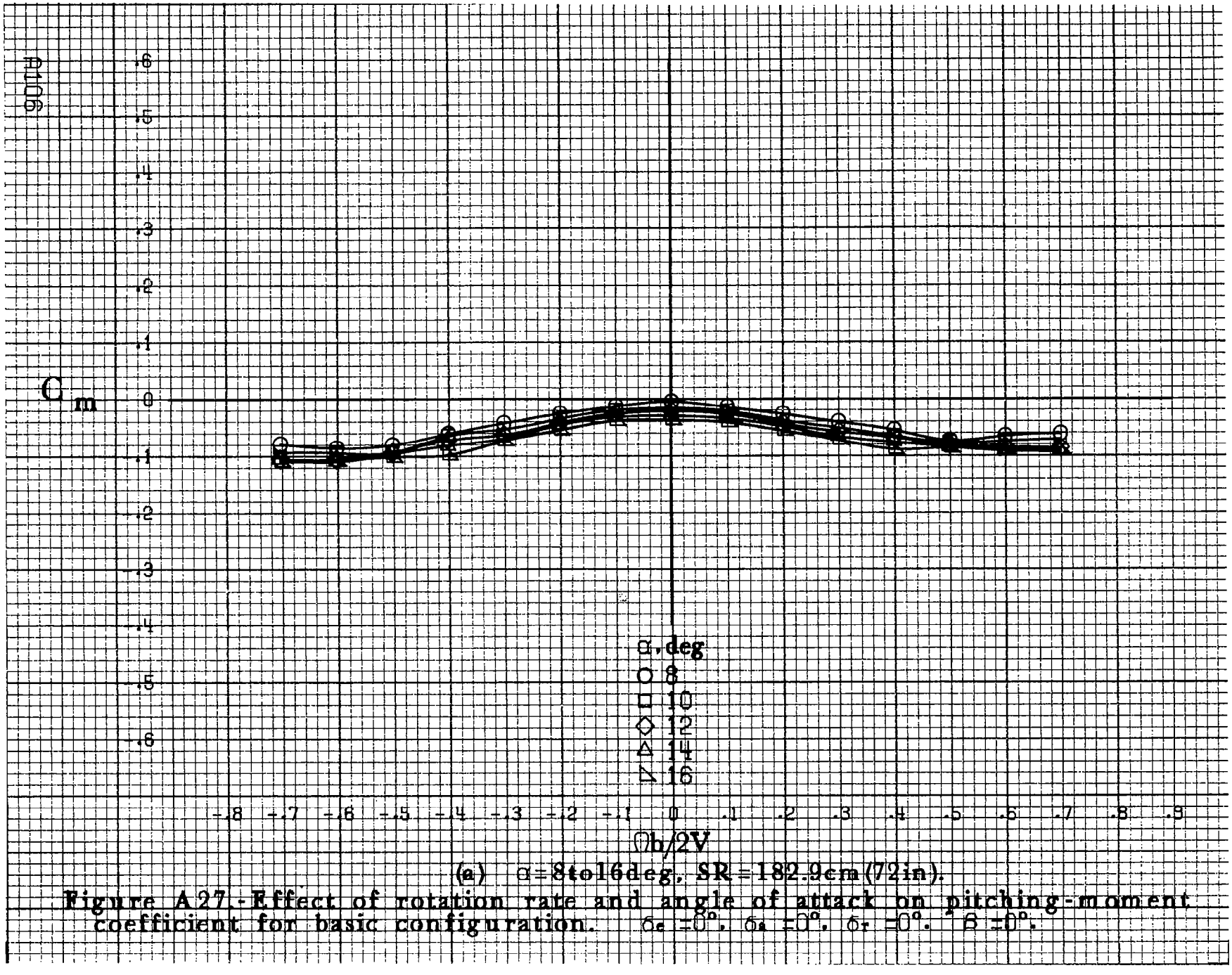

(a) $\alpha = 8$ to 16 deg, SR = 182.9 cm (72 in).

Figure A27.- Effect of rotation rate and angle of attack on pitching-moment coefficient for basic configuration. $\delta_e = 0°$, $\delta_a = 0°$, $\delta_r = 0°$, $\beta = 0°$.

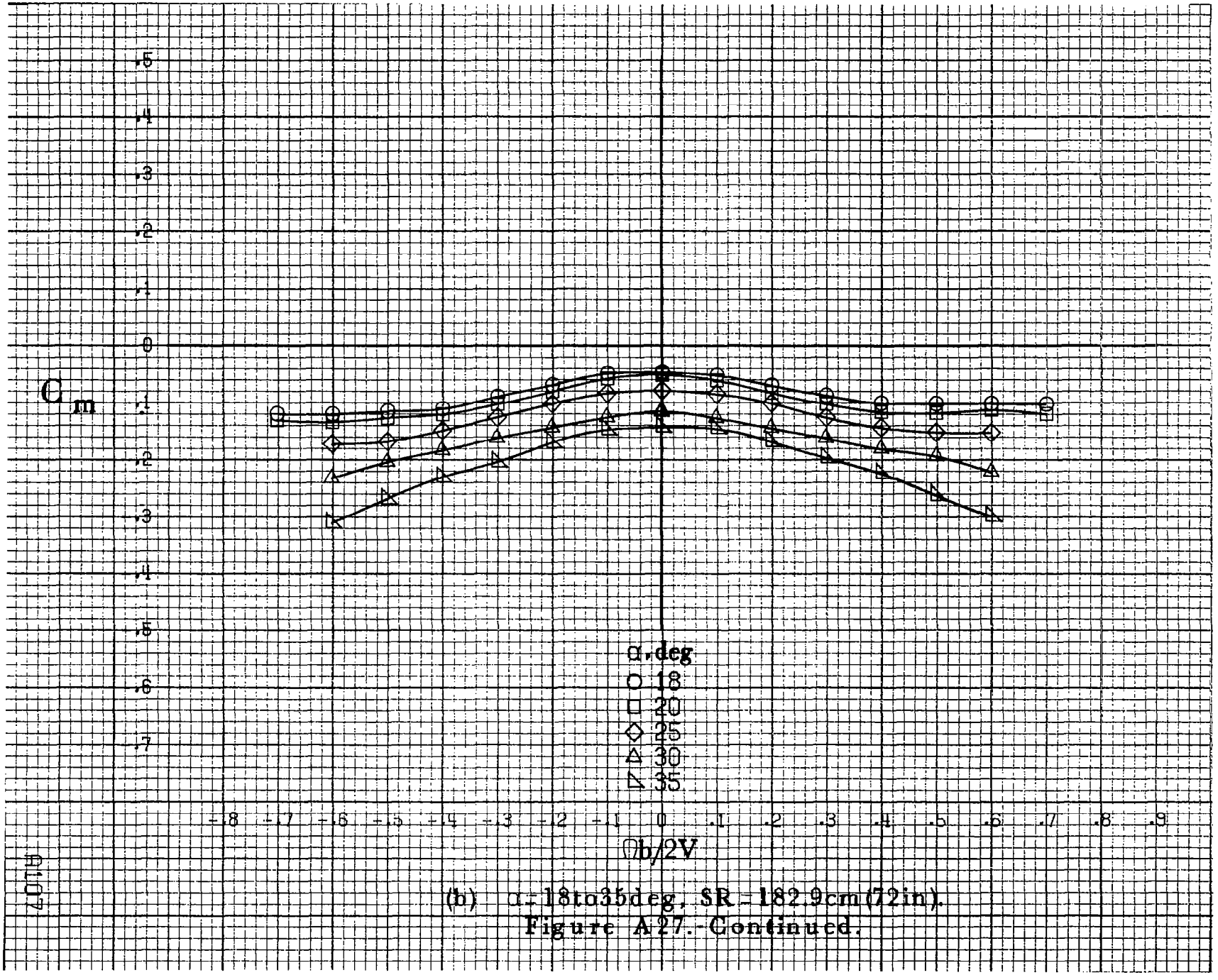

(b) α = 18 to 35 deg, SR = 182.9 cm (72 in).

Figure A27. Continued.

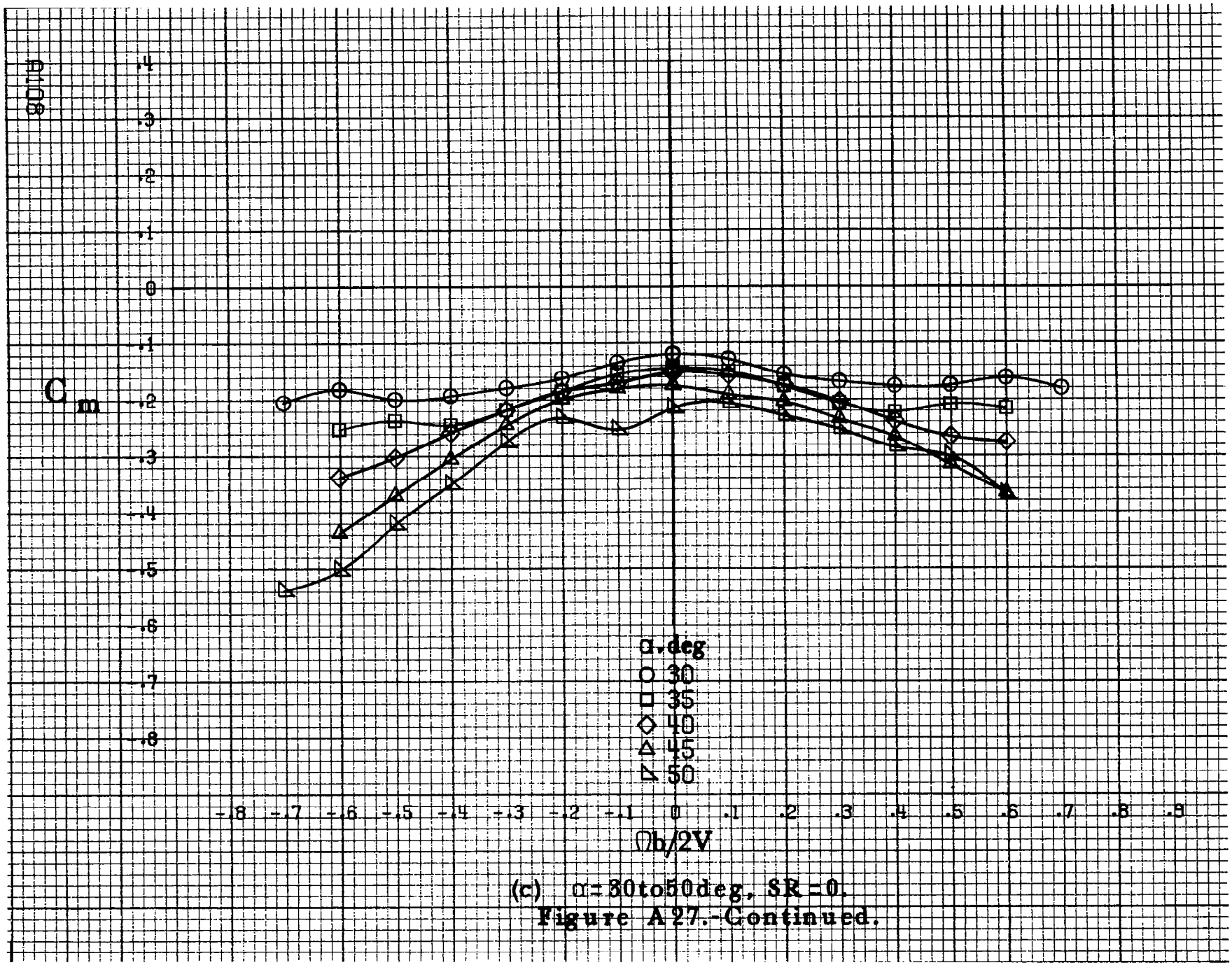

(c) $\alpha = 30$ to 50 deg, SR = 0.

Figure A27.-Continued.

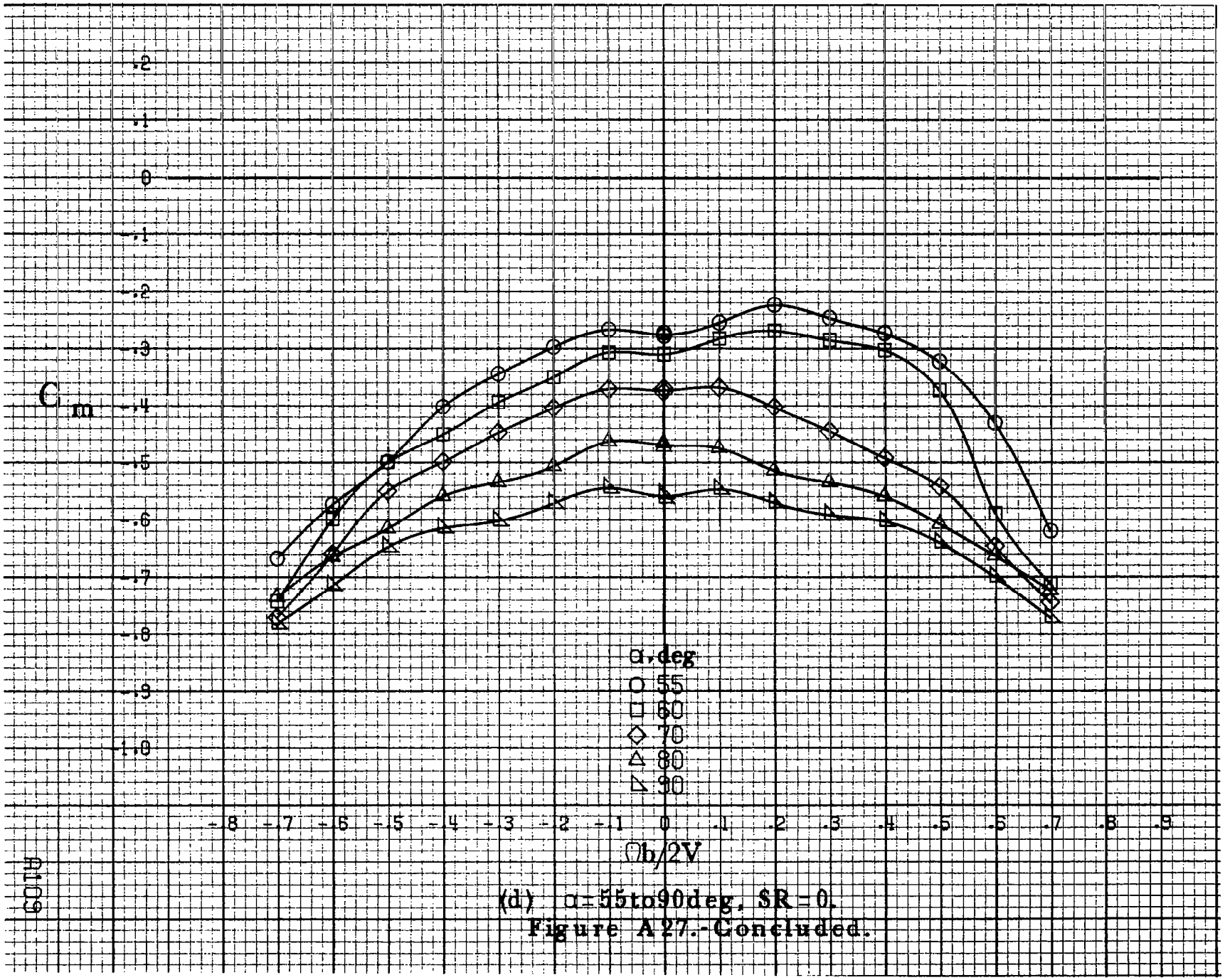

(d) α=55to90deg, $R=0.

Figure A27.-Concluded.

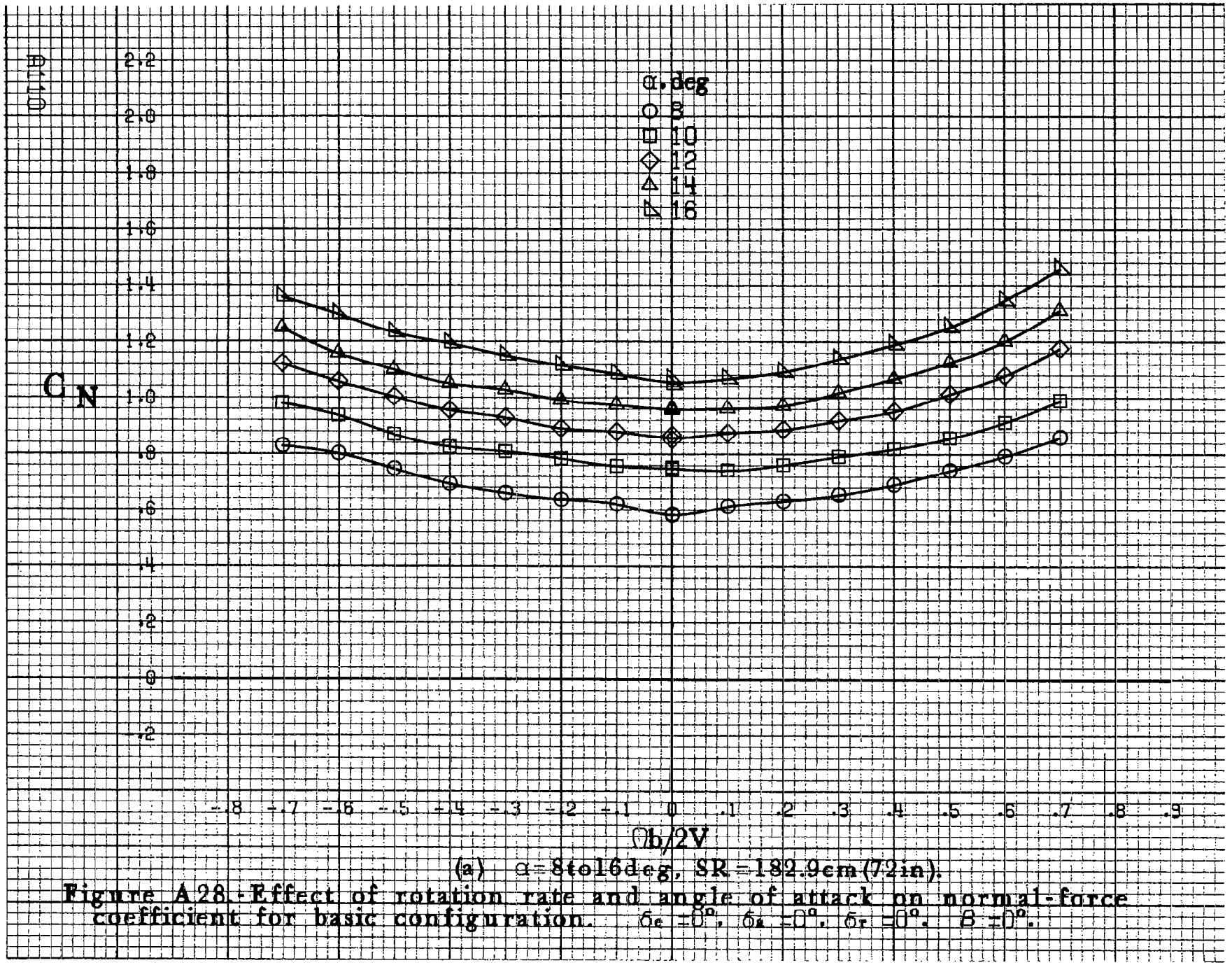

(a) $\alpha = 8$ to 16 deg, SR = 182.9 cm (72 in).

Figure A28.- Effect of rotation rate and angle of attack on normal-force coefficient for basic configuration. $\delta_e = 0°$, $\delta_a = 0°$, $\delta_r = 0°$, $\beta = 0°$.

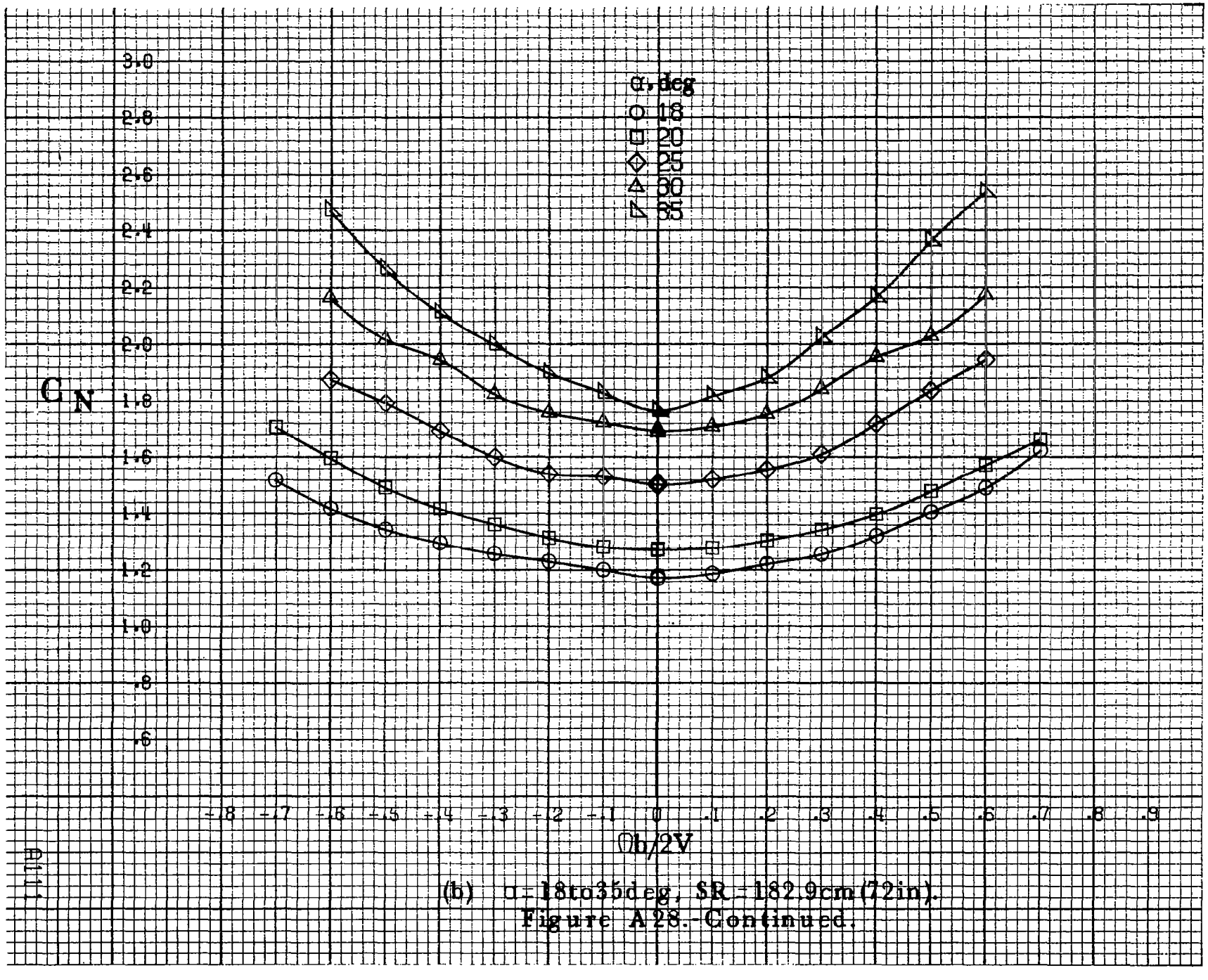

(b) α = 18 to 35 deg, SR = 182.9 cm (72 in).

Figure A28.- Continued.

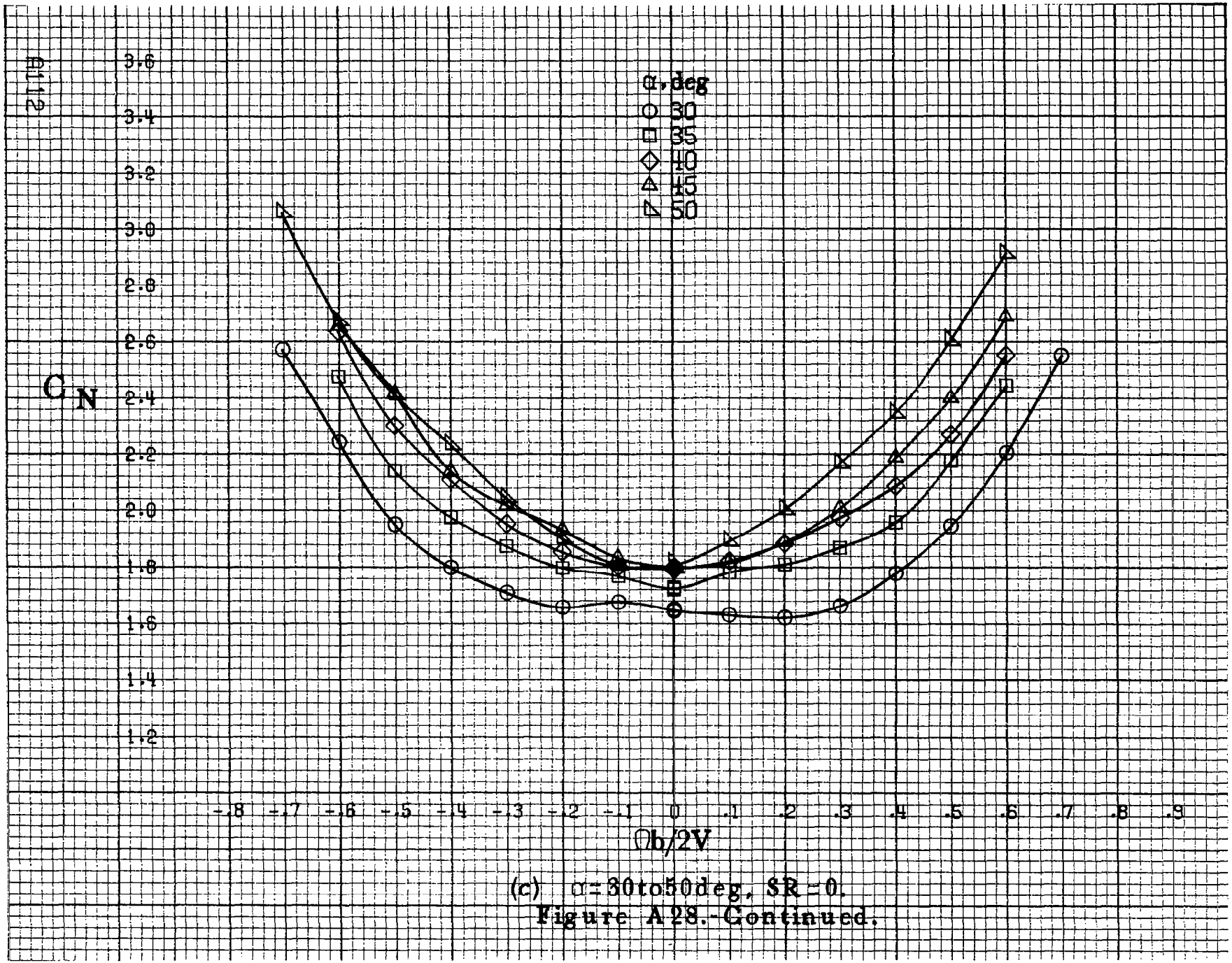

(c) $\alpha = 30$ to 50 deg, $SR = 0$.

Figure A28.- Continued.

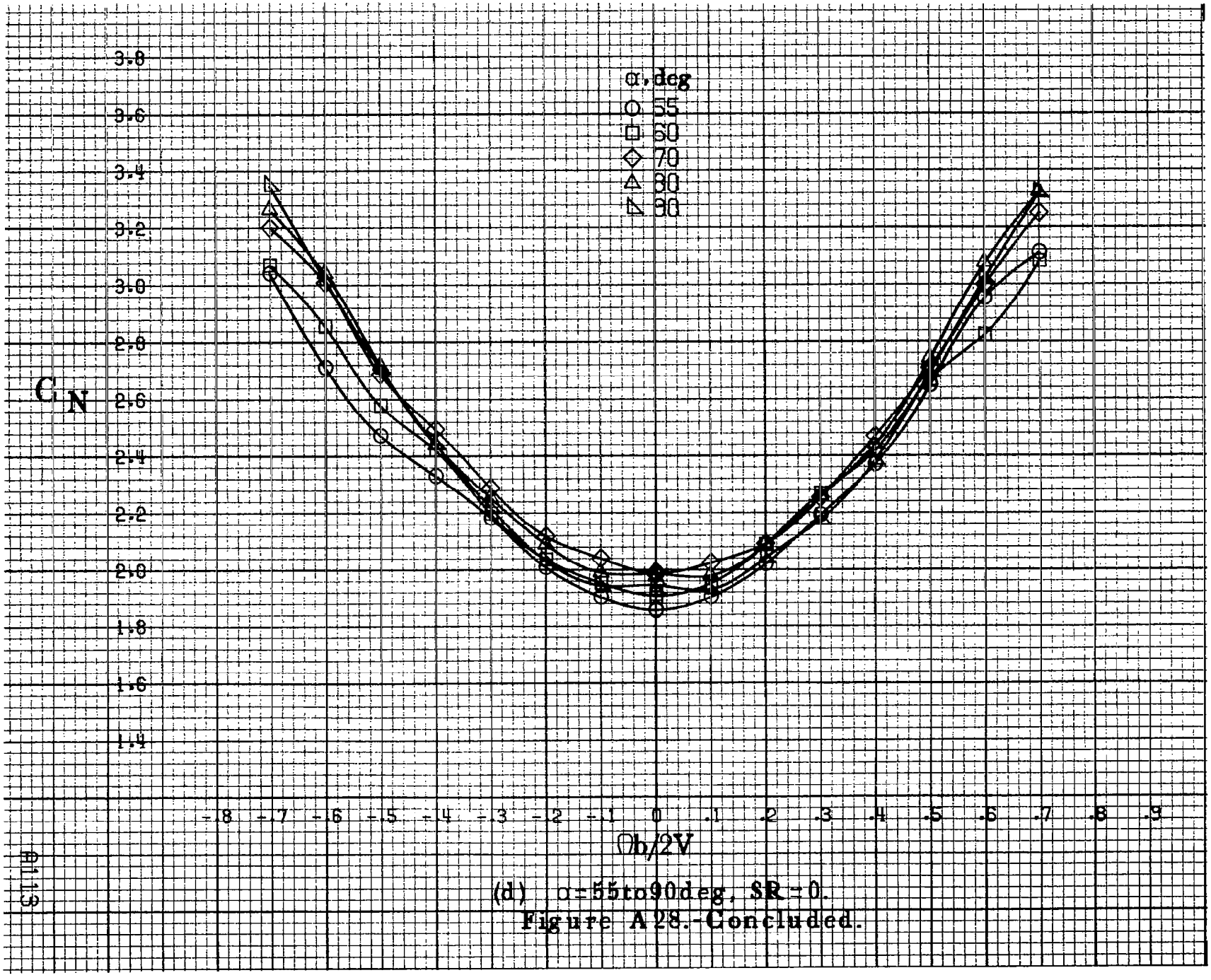

(d) $\alpha = 55$ to 90 deg, $SR = 0$.

Figure A28.-Concluded.

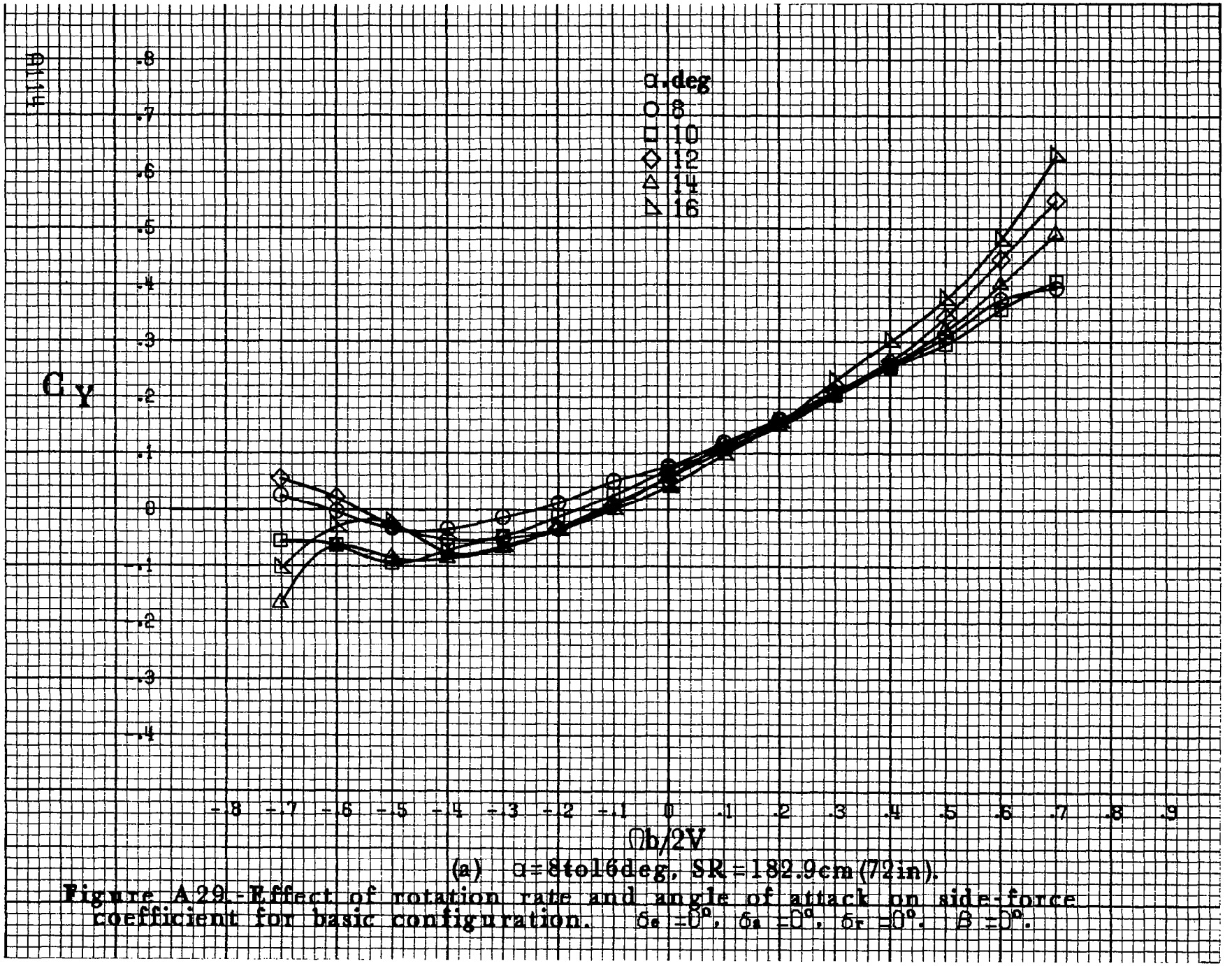

(a) $\alpha = 8$ to 16 deg, SR = 182.9 cm (72 in).

Figure A29.- Effect of rotation rate and angle of attack on side-force coefficient for basic configuration. $\delta_e = 0°$, $\delta_a = 0°$, $\delta_r = 0°$, $\beta = 0°$.

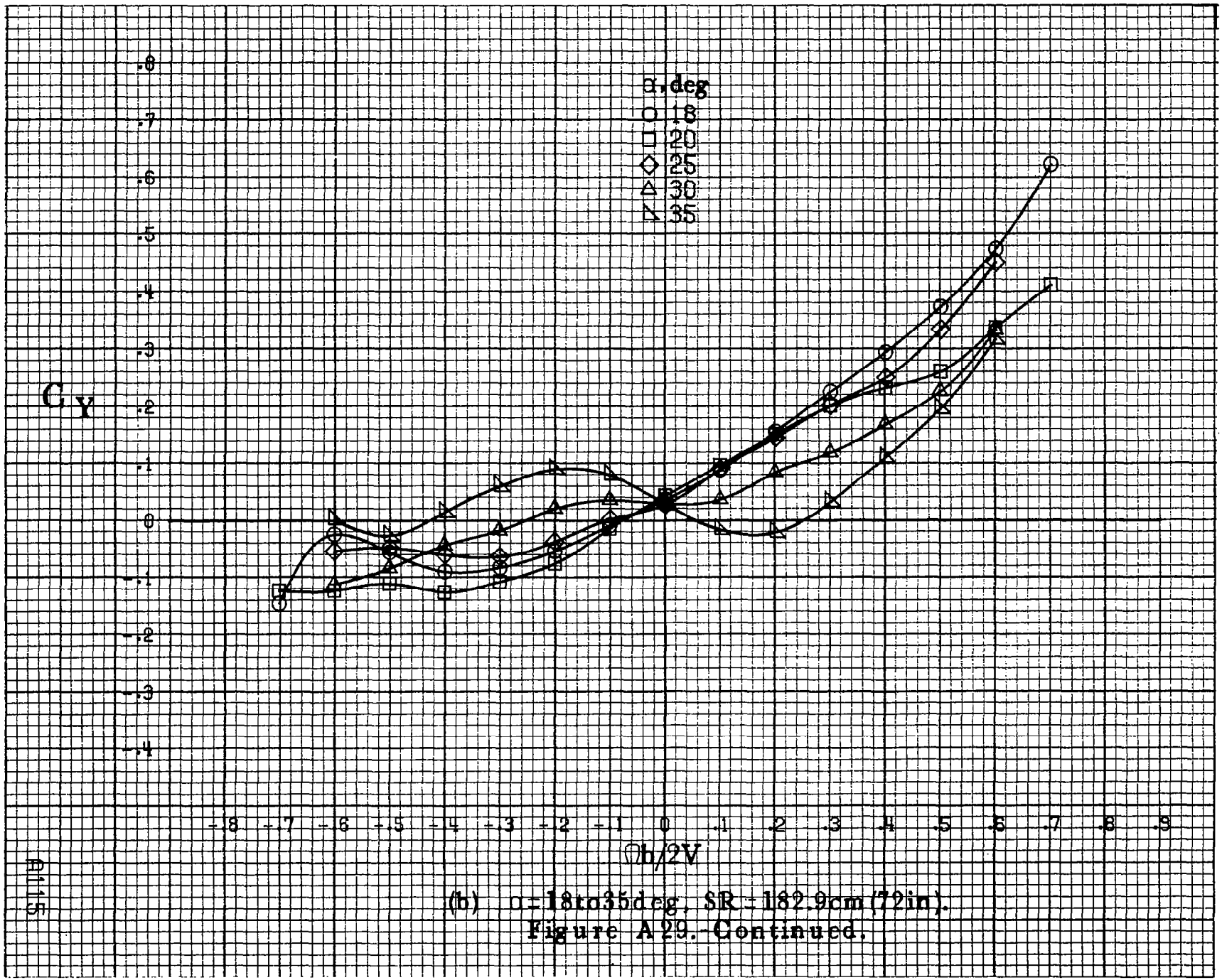

(b) α = 18 to 35 deg, SR = 182.9 cm (72 in).

Figure A29.- Continued.

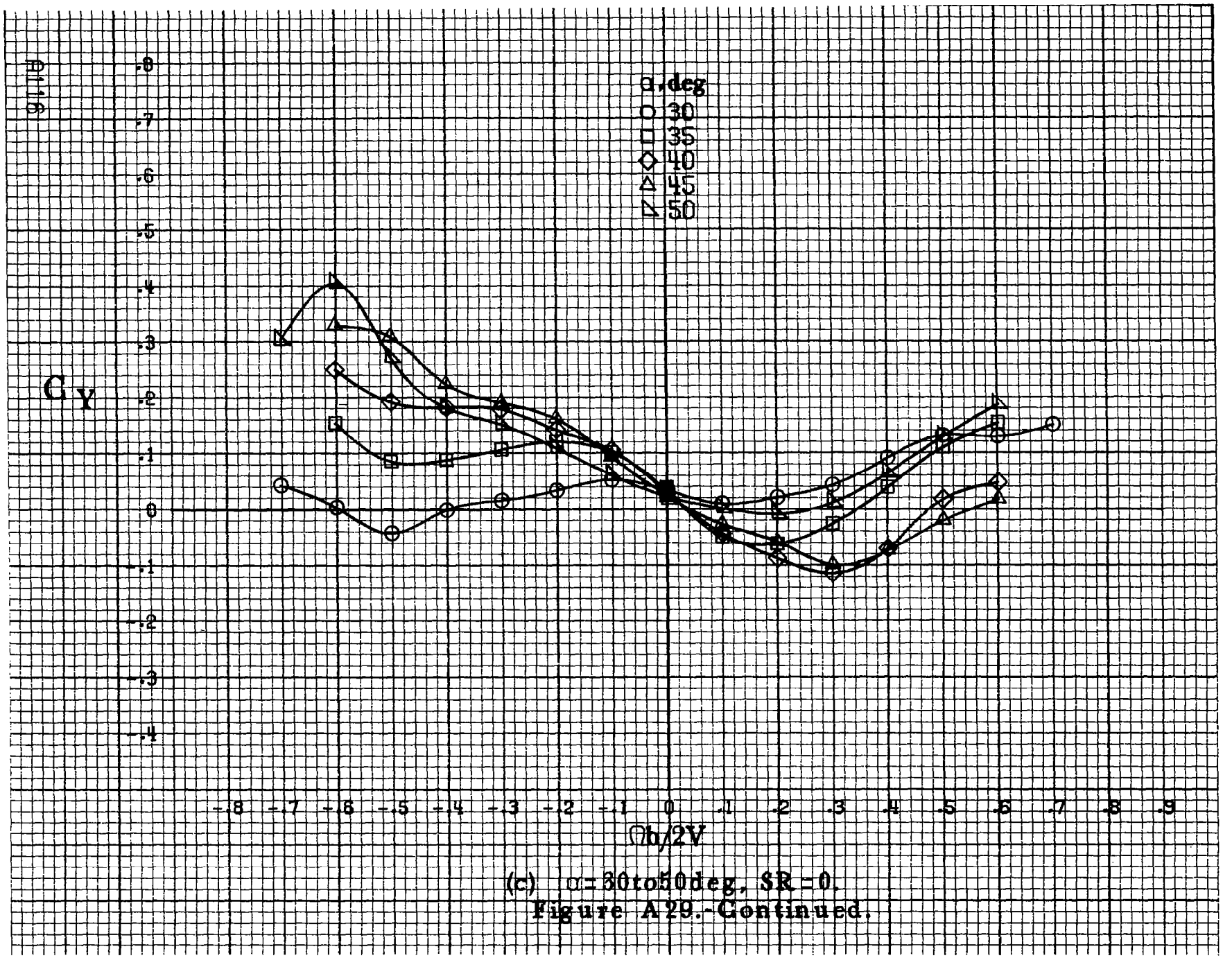

(c) $\alpha = 30$ to 50 deg, SR = 0.

Figure A29.- Continued.

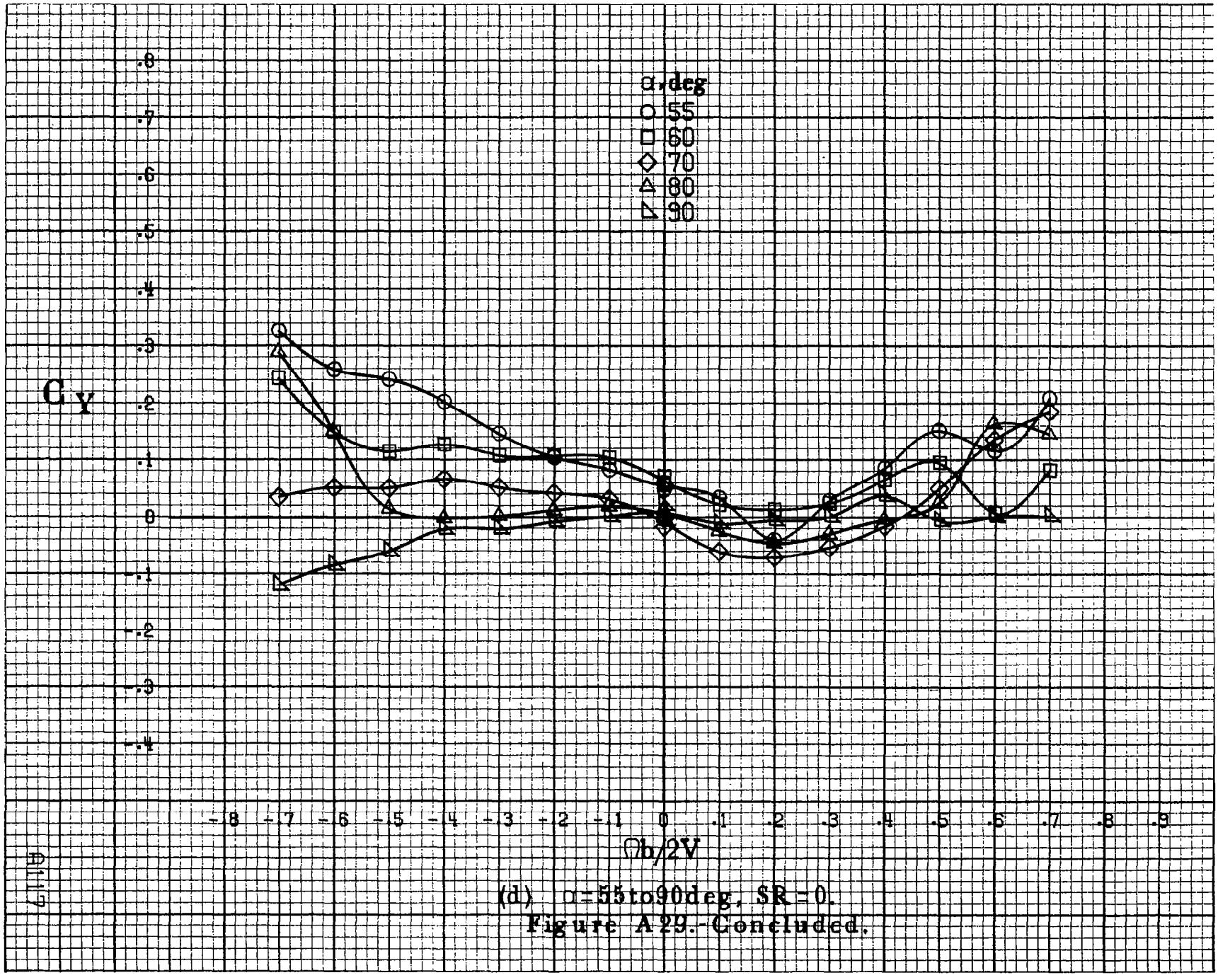

(d) α=55to90deg, SR=0.

Figure A29.-Concluded.

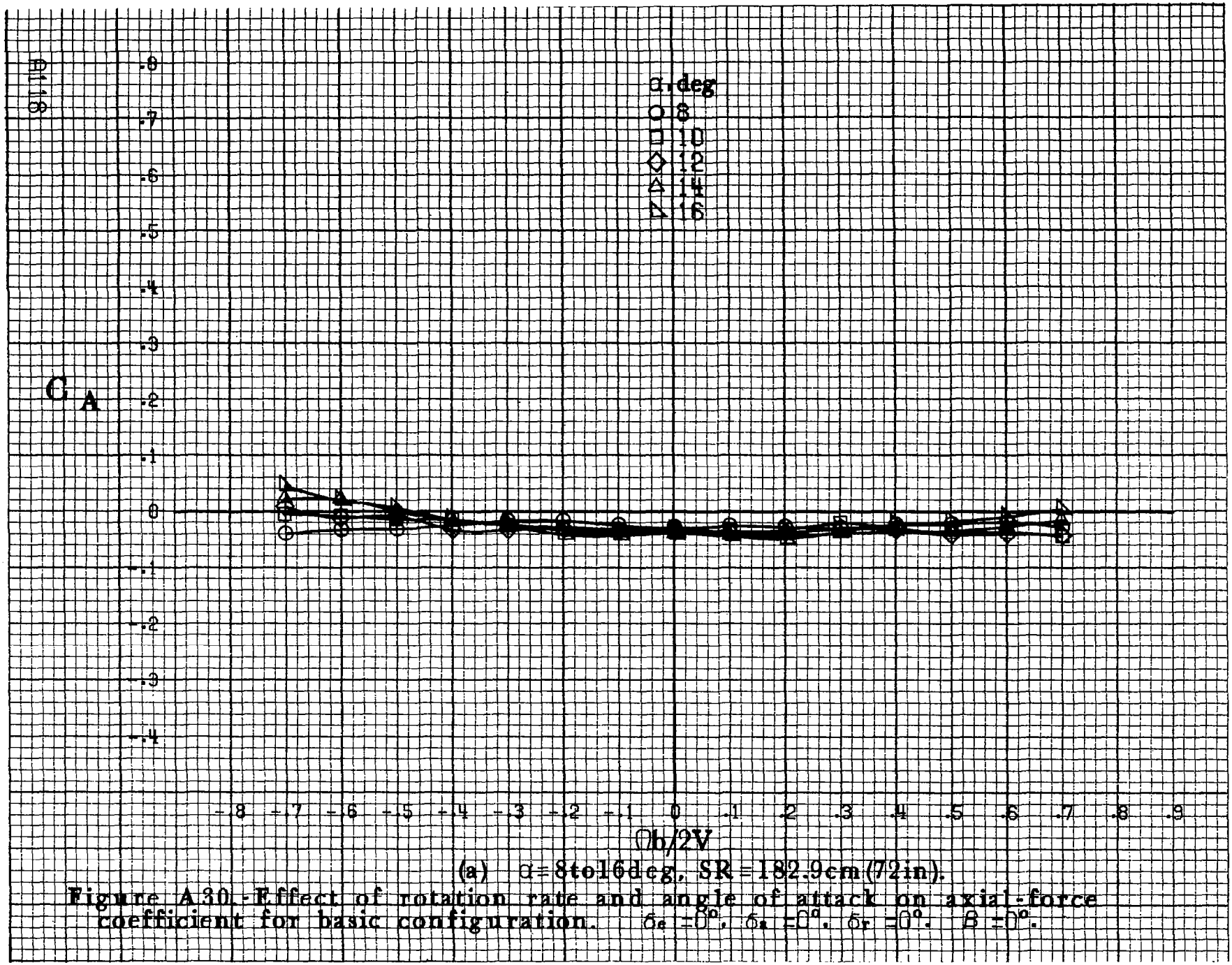

(a) $\alpha = 8$ to 16 deg, SR = 182.9 cm (72 in).

Figure A.30.- Effect of rotation rate and angle of attack on axial-force coefficient for basic configuration. $\delta_e = 0°$, $\delta_a = 0°$, $\delta_r = 0°$, $\beta = 0°$.

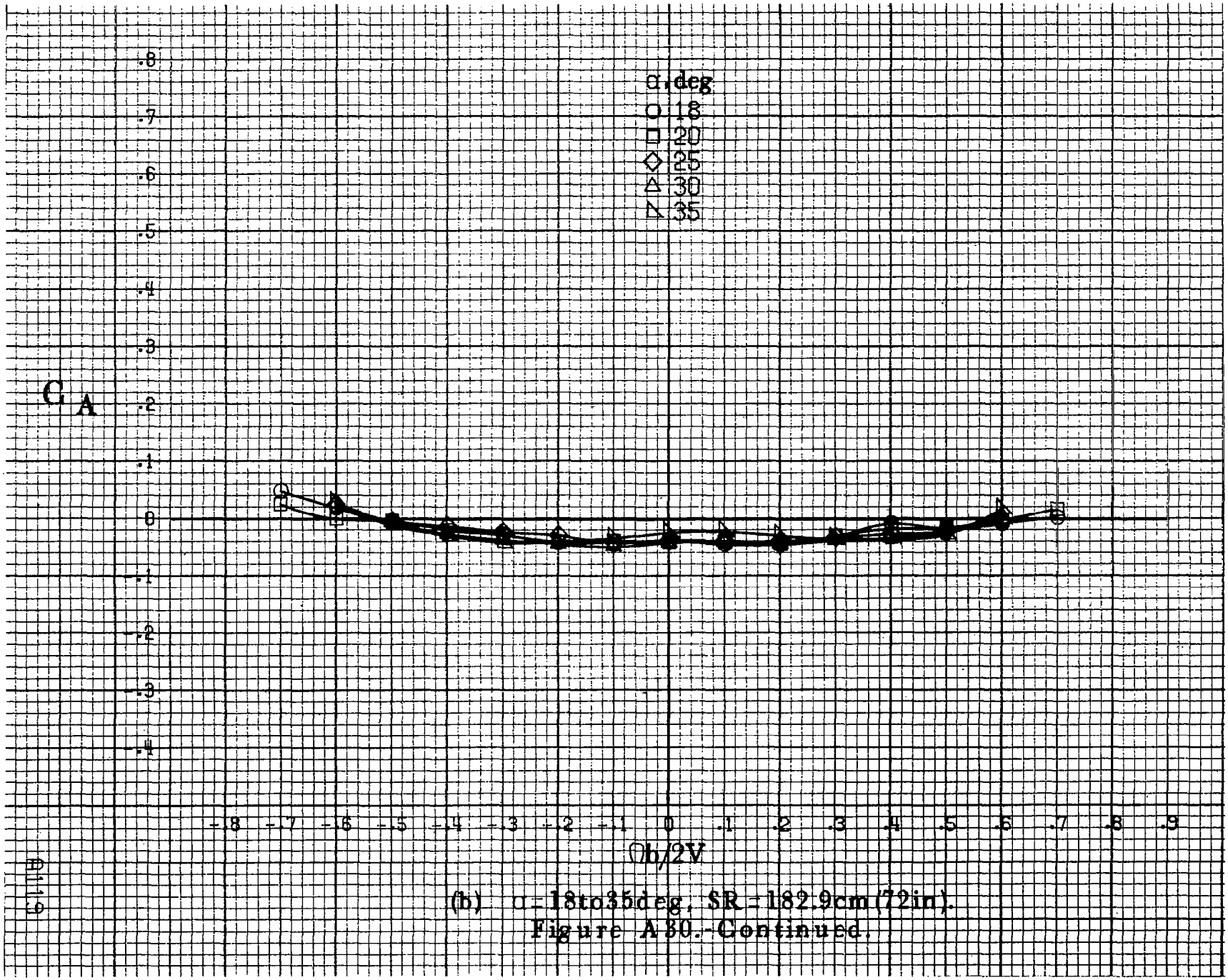

(b) α = 18to35deg, SR = 182.9cm(72in).

Figure A30.-Continued.

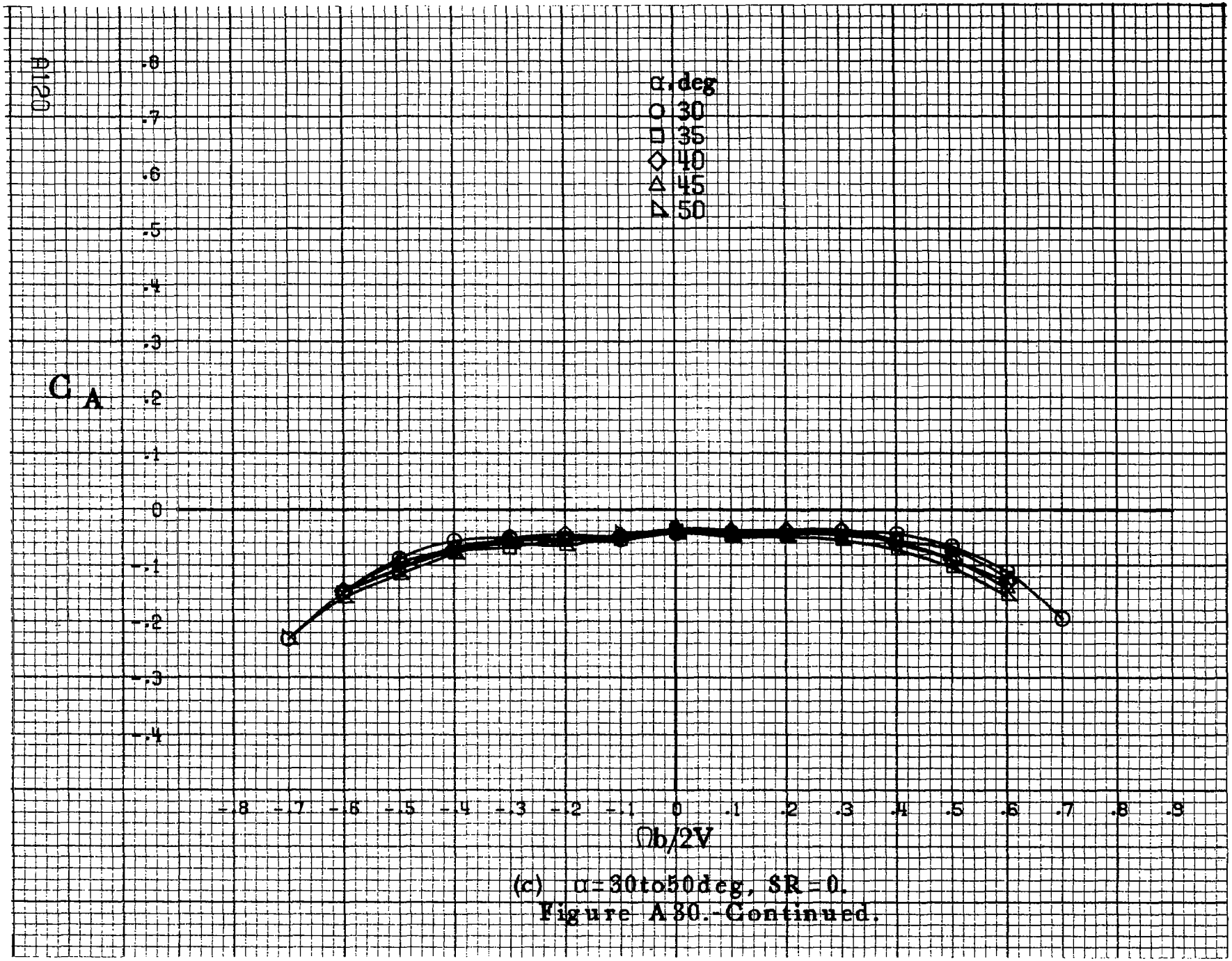

(c) $\alpha = 30$ to 50 deg, SR = 0.

Figure A30.-Continued.

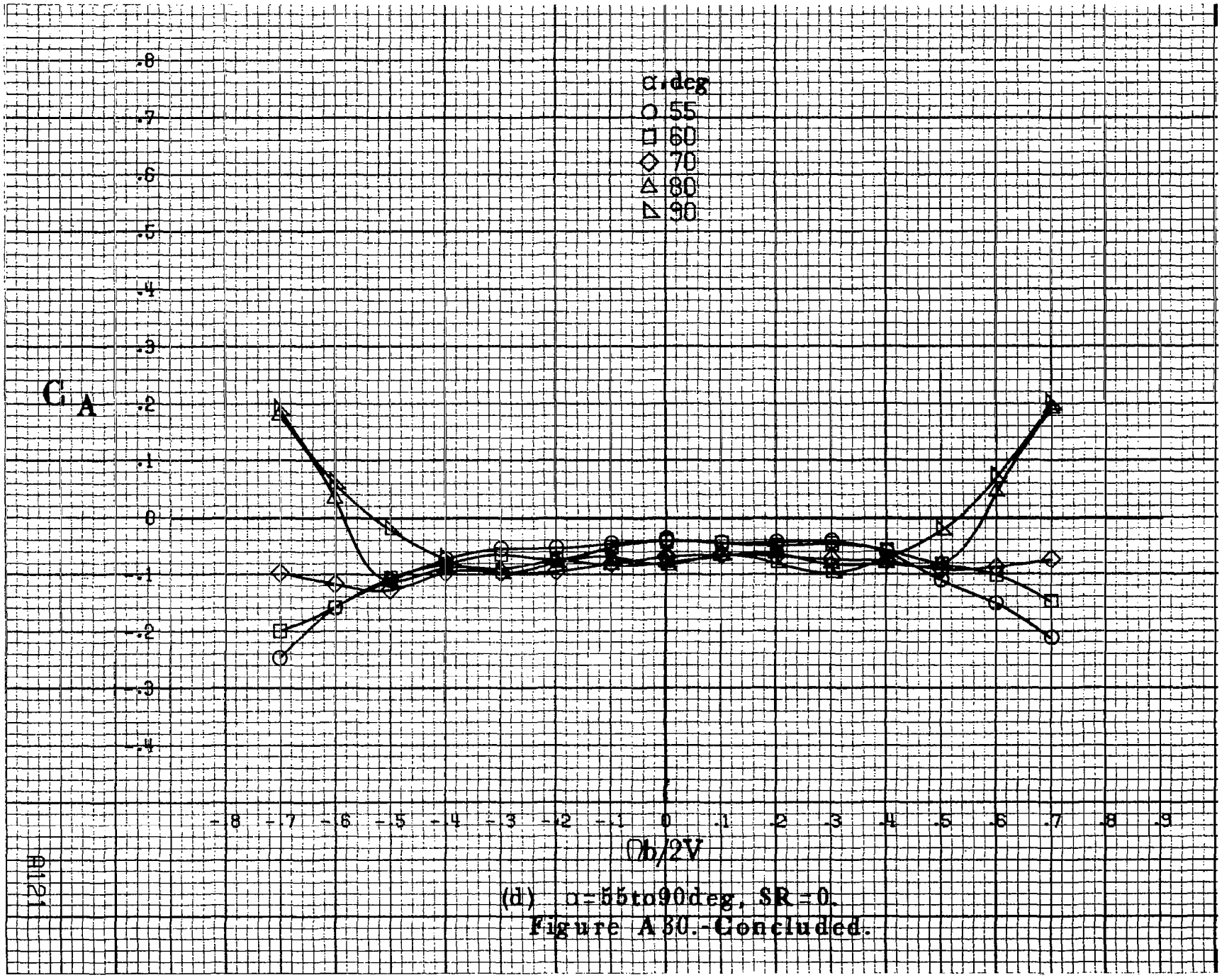

(d) α = 55 to 90 deg, SR = 0.

Figure A30.-Concluded.

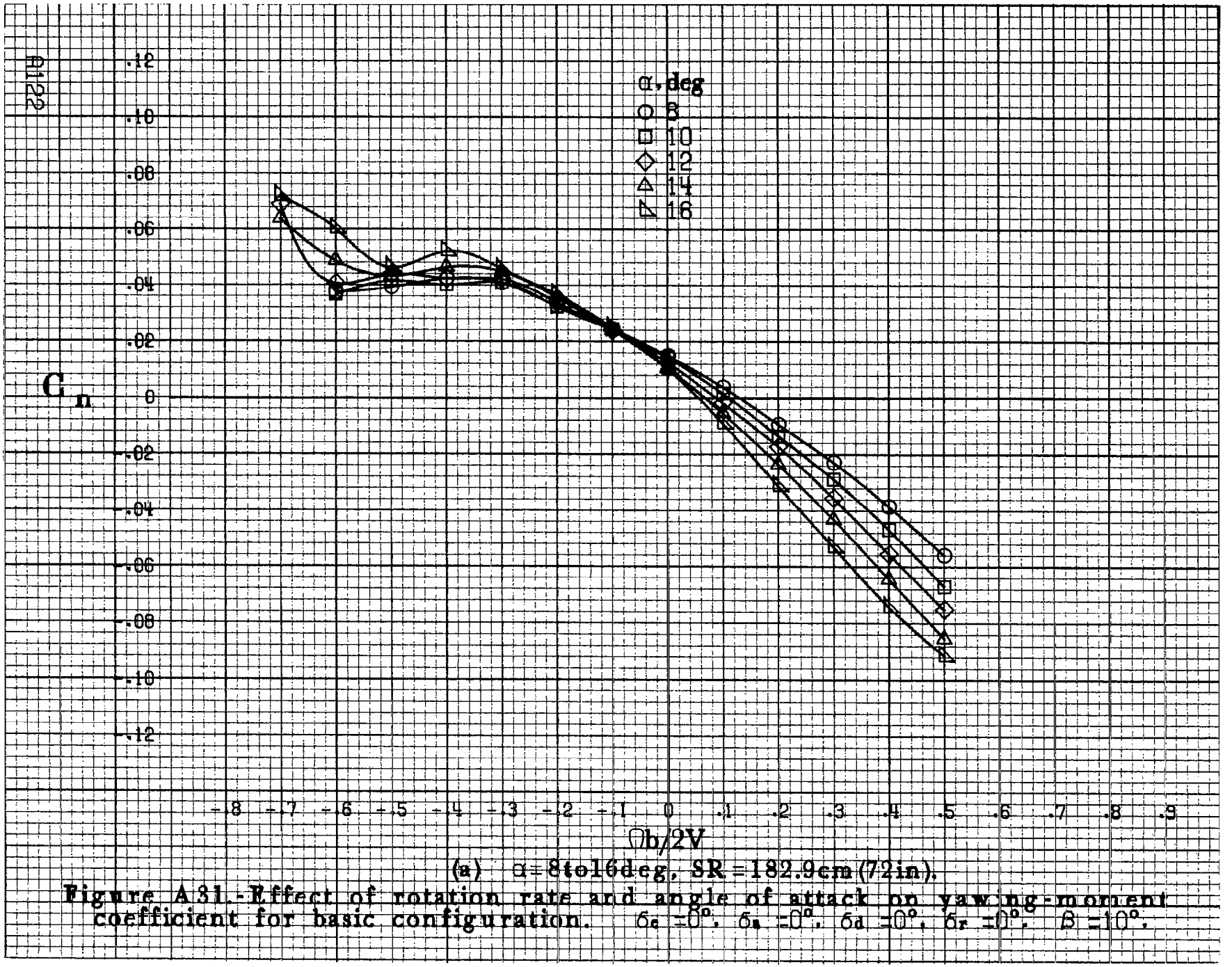

(a) $\alpha = 8$ to 16 deg, SR = 182.9 cm (72 in.).

Figure A31.- Effect of rotation rate and angle of attack on yawing-moment coefficient for basic configuration. $\delta_e = 0°$, $\delta_a = 0°$, $\delta_d = 0°$, $\delta_r = 0°$, $\beta = 10°$.

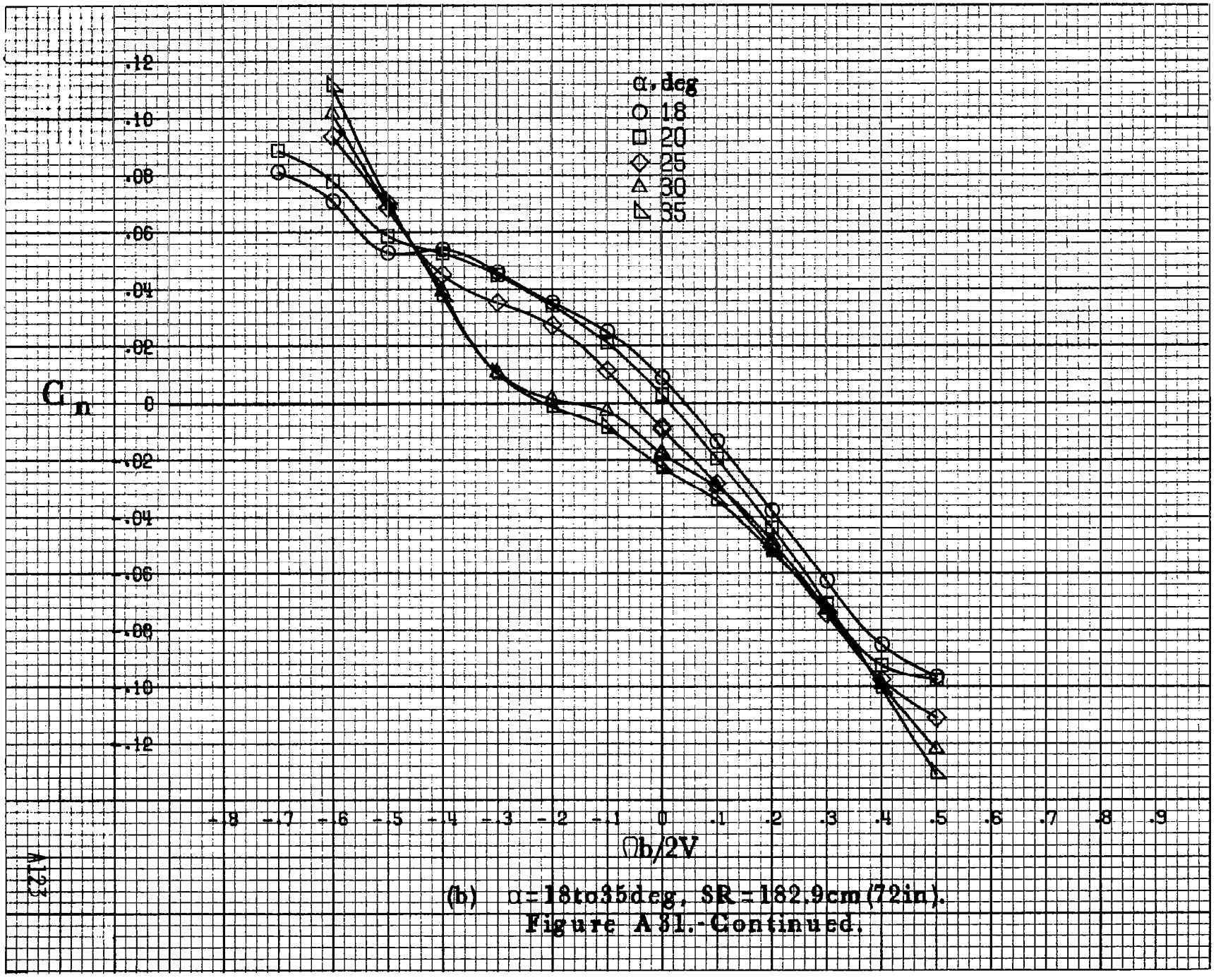

(b) α = 18 to 35 deg, SR = 182.9 cm (72 in).

Figure A31.- Continued.

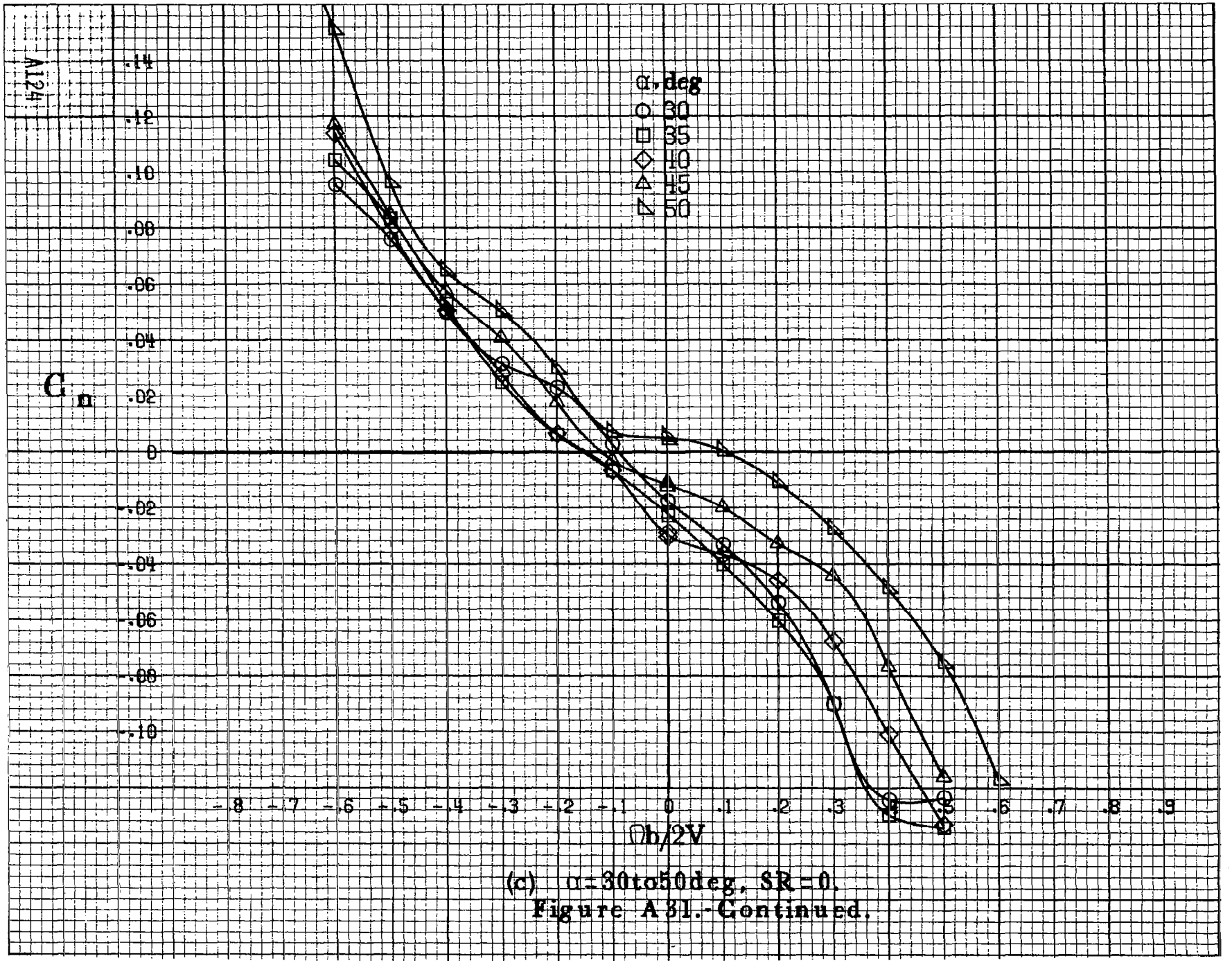

(c) α = 30 to 50 deg, SR = 0.

Figure A31.- Continued.

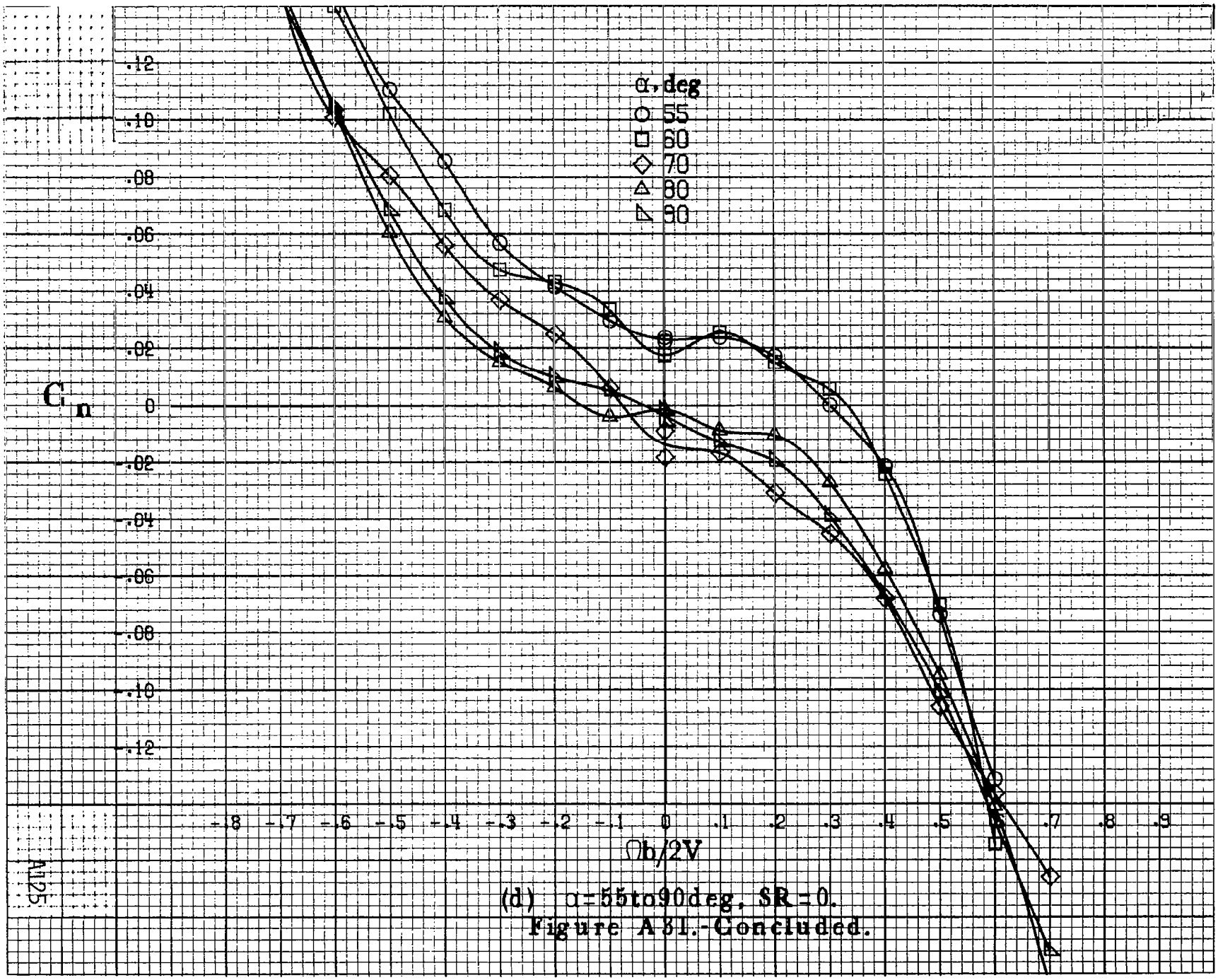

(d) $\alpha = 55$ to 90 deg, $SR = 0$.

Figure A31.- Concluded.

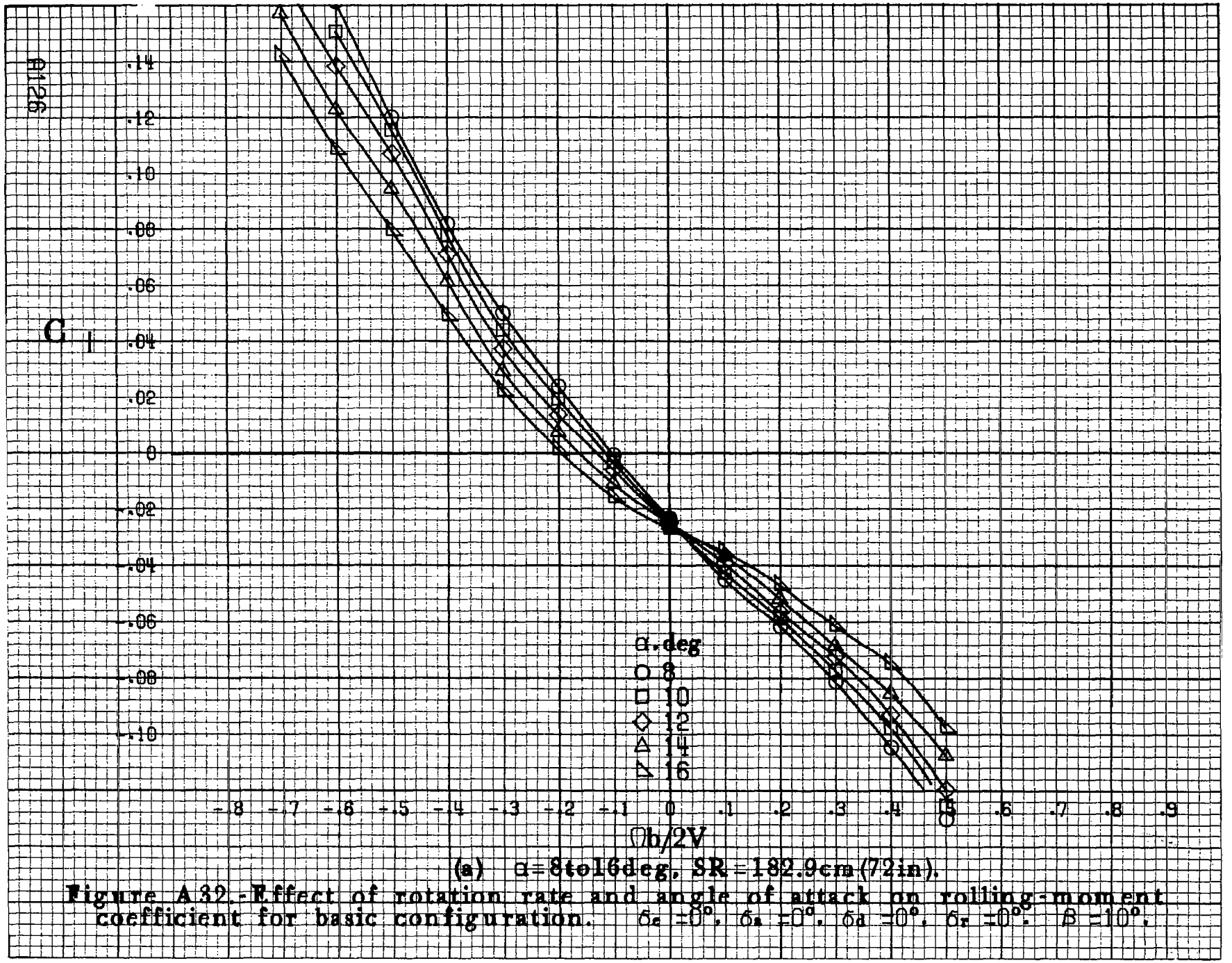

(a) $\alpha = 8$ to 16 deg, SR = 182.9 cm (72 in).

Figure A32.- Effect of rotation rate and angle of attack on rolling-moment coefficient for basic configuration. $\delta_e = 0°$, $\delta_a = 0°$, $\delta_d = 0°$, $\delta_r = 0°$, $\beta = 10°$.

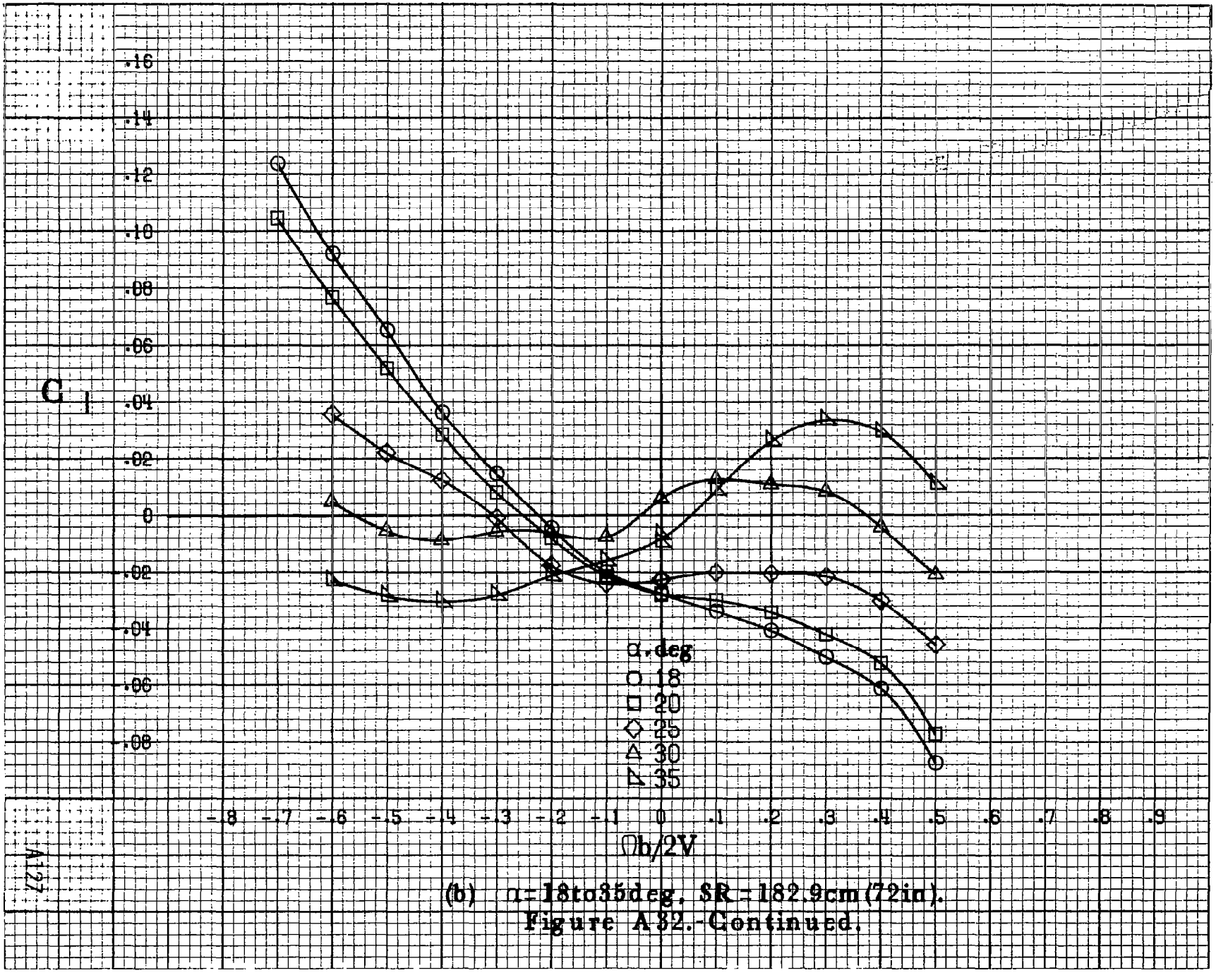

(b) $\alpha = 18$ to 35 deg, $SR = 182.9$ cm (72 in).

Figure A32.- Continued.

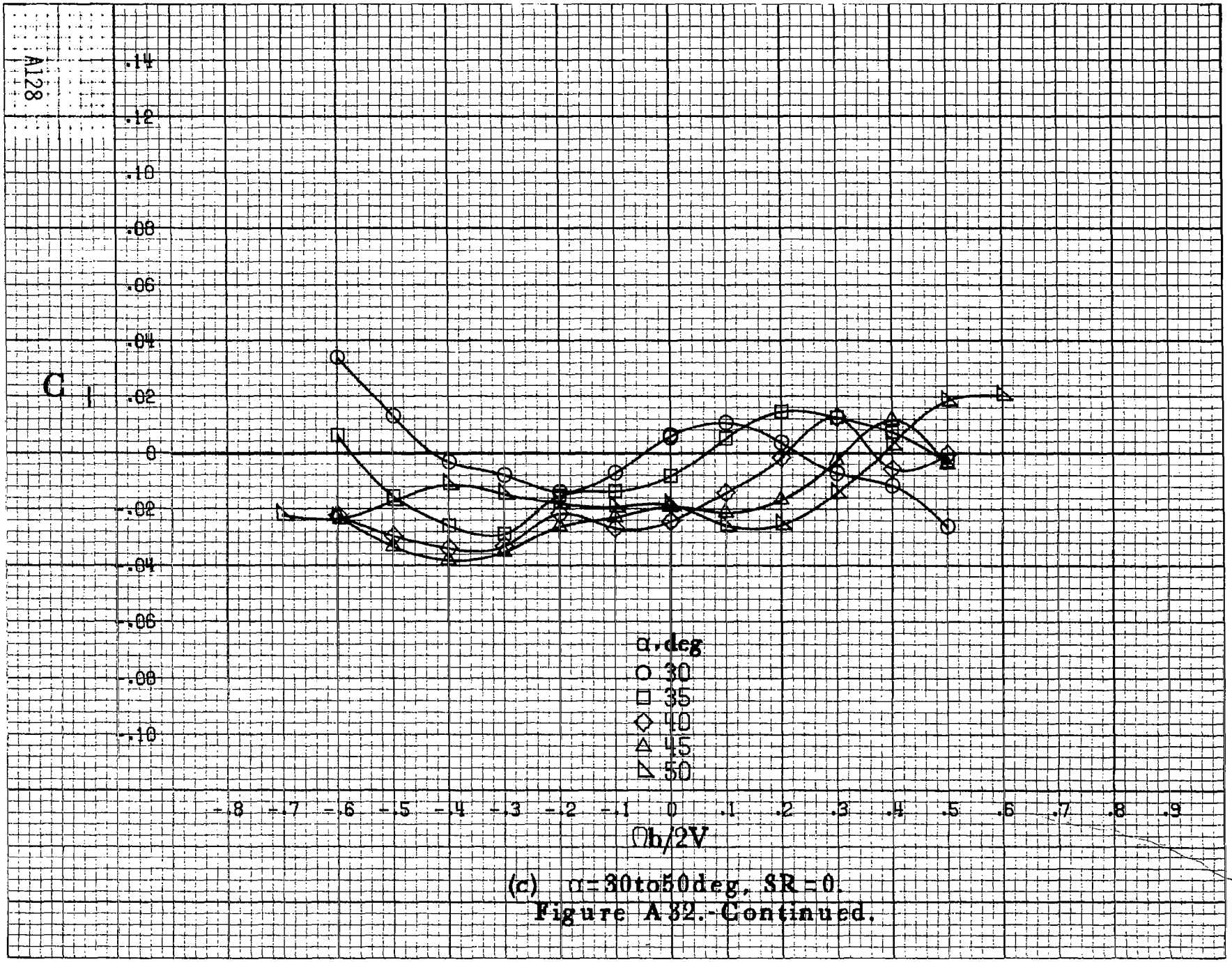

(c) $\alpha = 30$ to 50 deg, SR = 0.

Figure A32.- Continued.

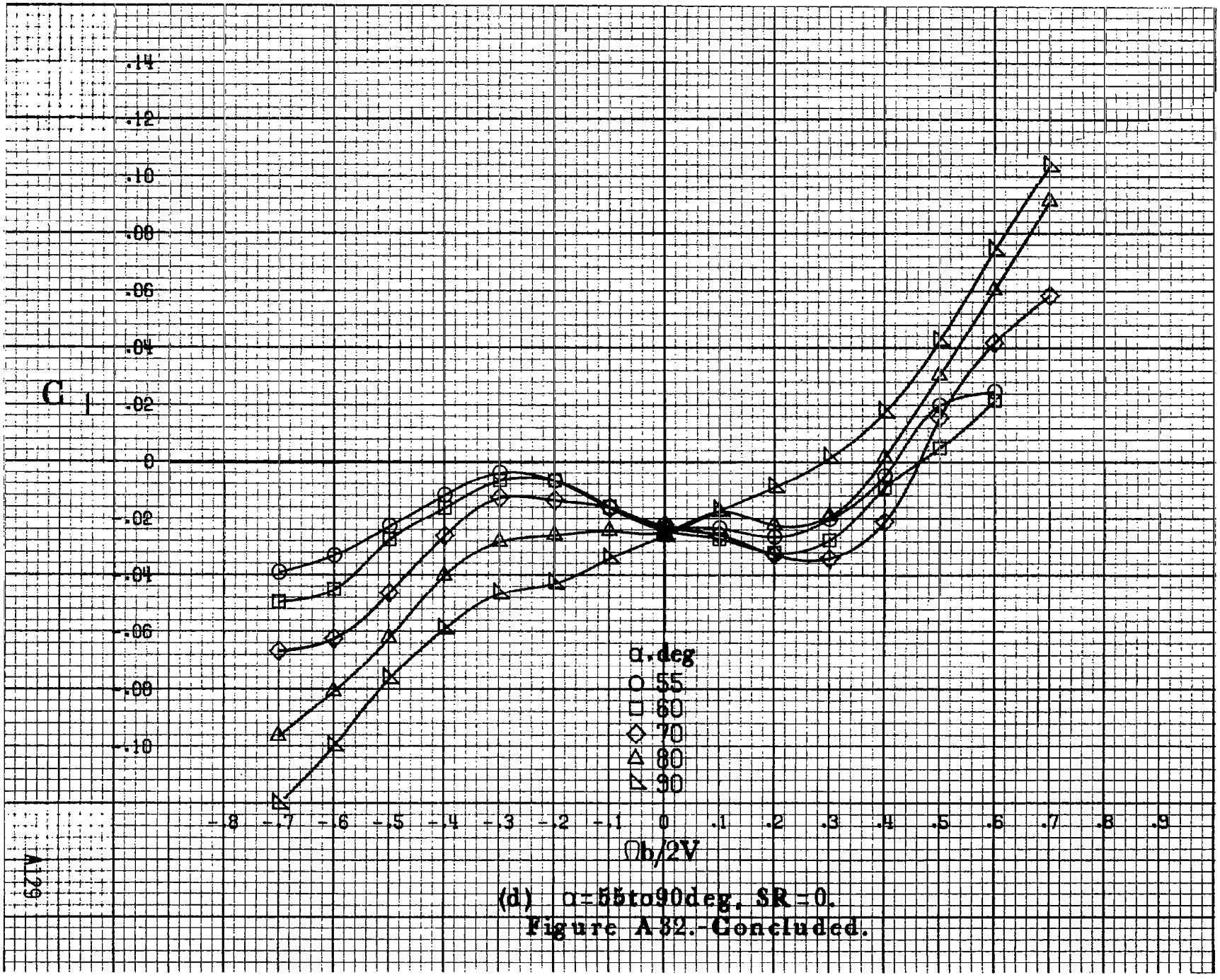

(d) α = 55 to 90 deg, SR = 0.

Figure A32.-Concluded.

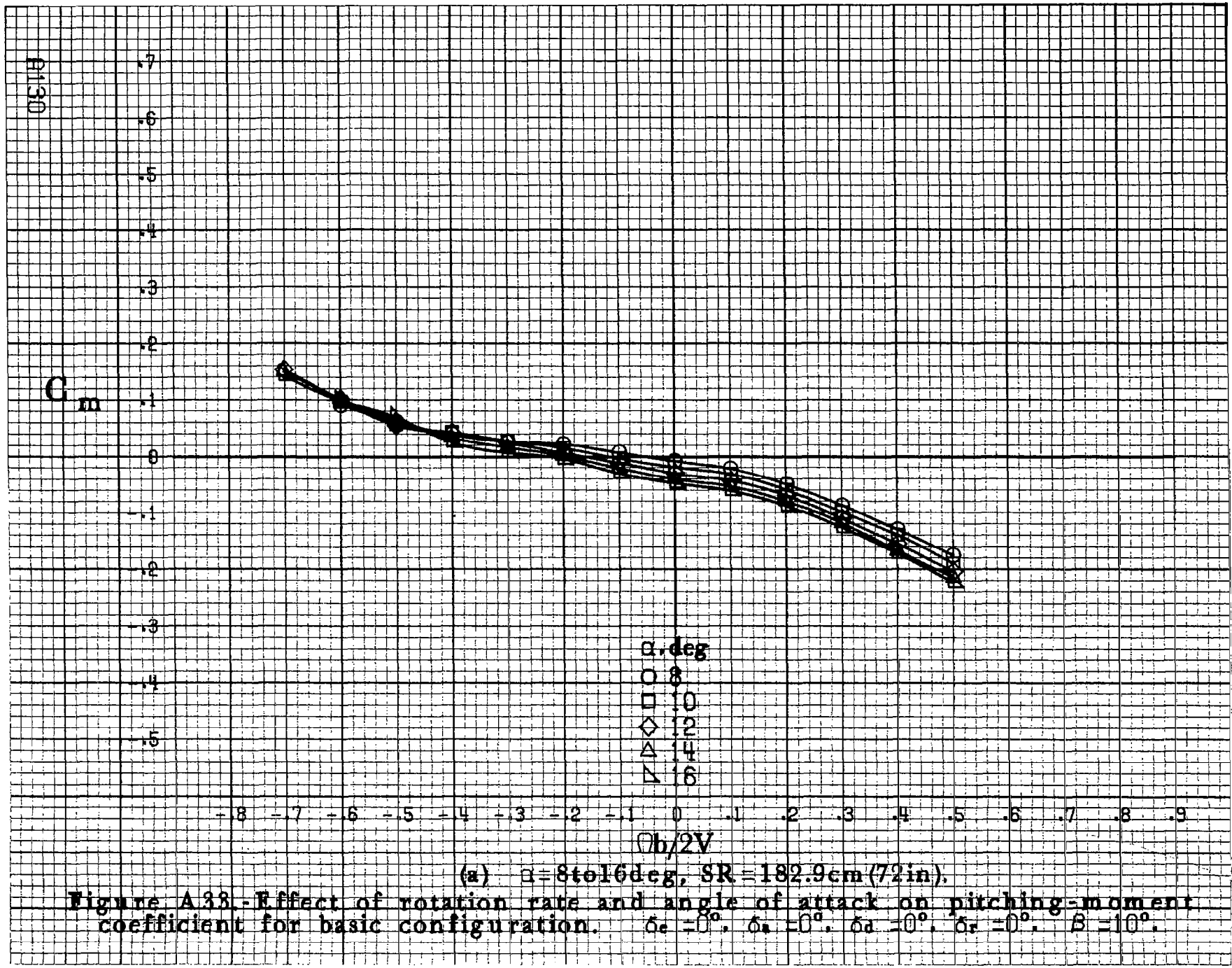

(a) $\alpha = 8$ to 16 deg, SR = 182.9 cm (72 in).

Figure A38.- Effect of rotation rate and angle of attack on pitching-moment coefficient for basic configuration. $\delta_e = 0°$, $\delta_a = 0°$, $\delta_d = 0°$, $\delta_r = 0°$, $\beta = 10°$.

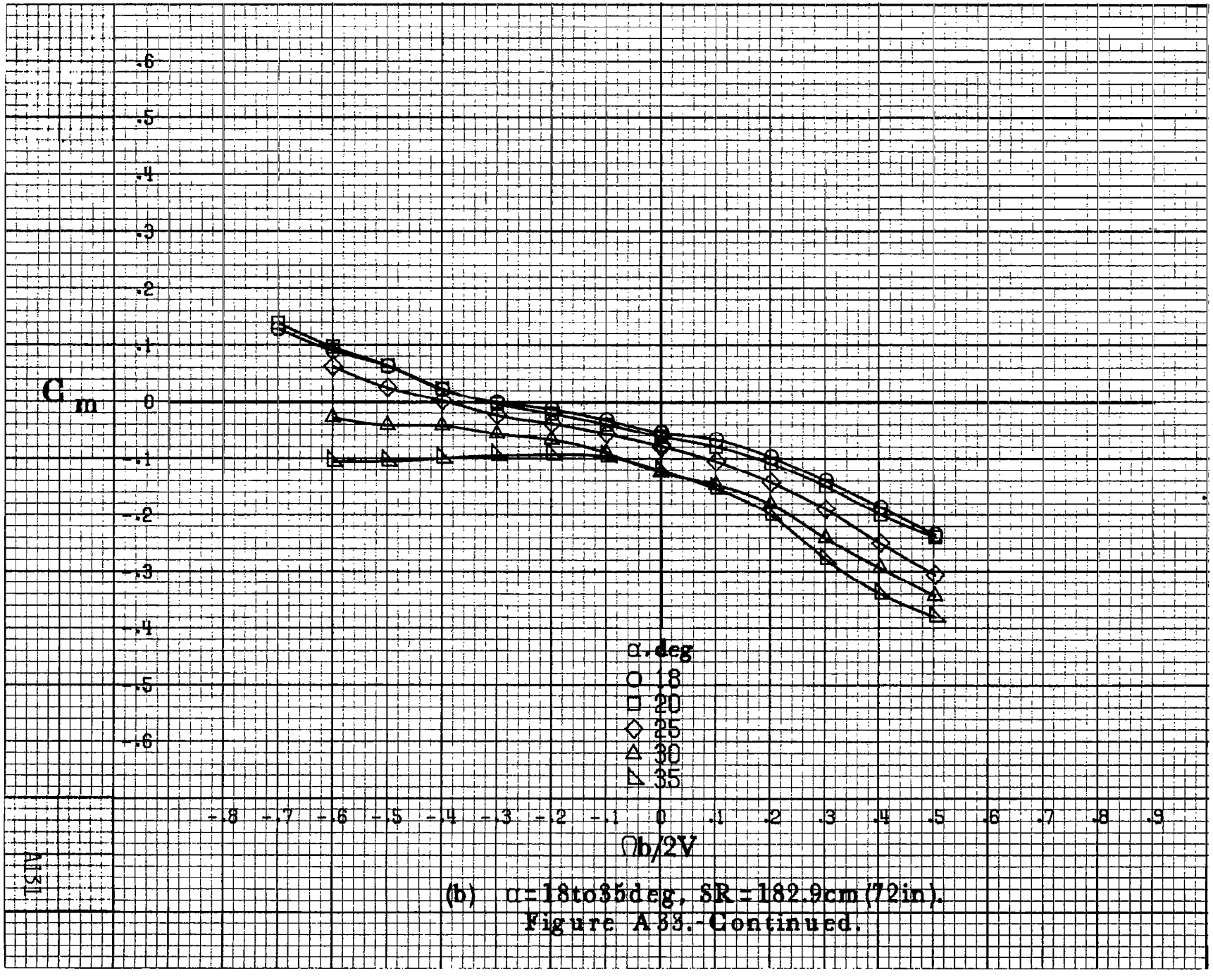

(b) α = 18 to 35 deg, SR = 182.9 cm (72 in).

Figure A33.- Continued.

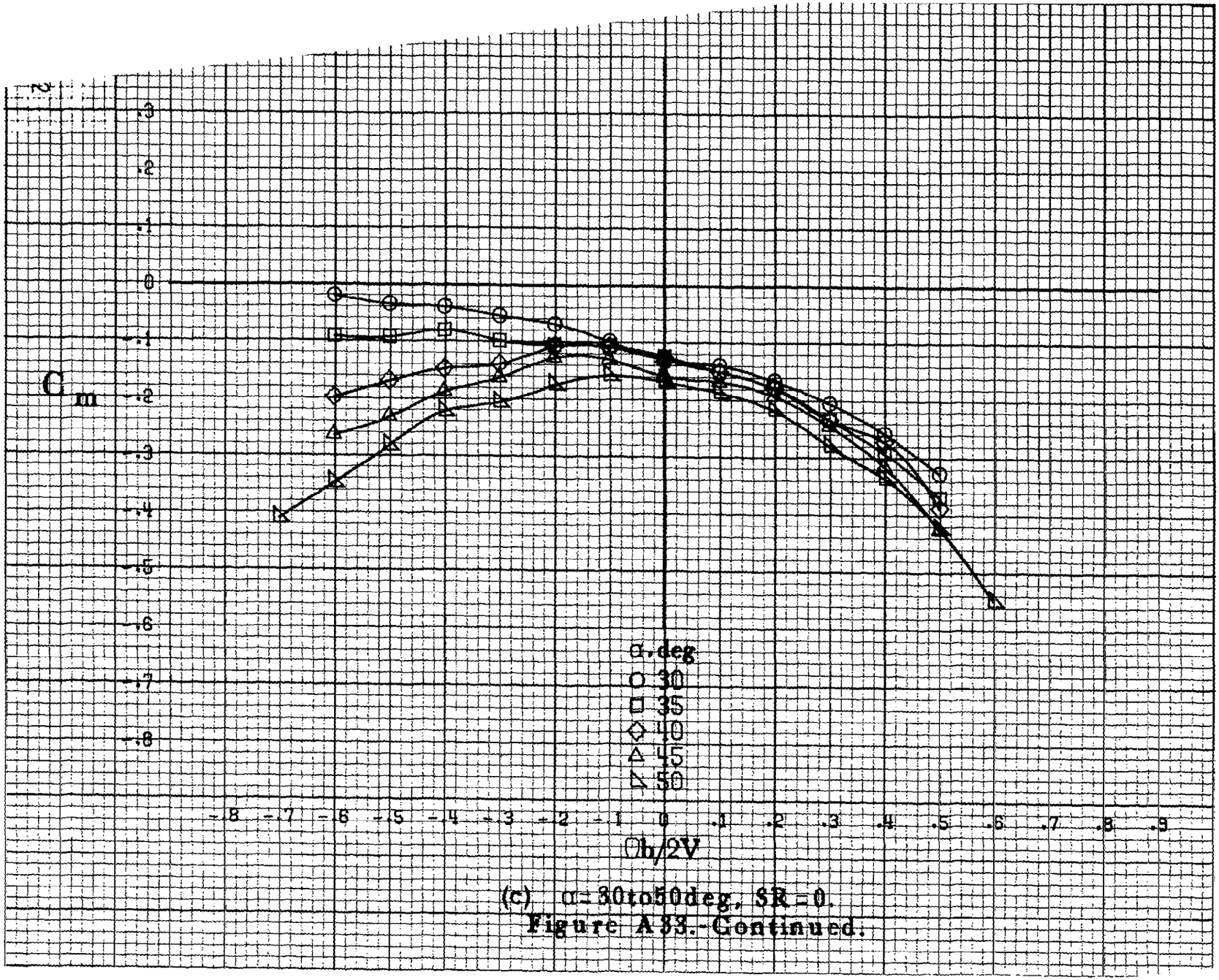

(c) $\alpha = 30$ to 50 deg, $SR = 0$.

Figure A33.- Continued.

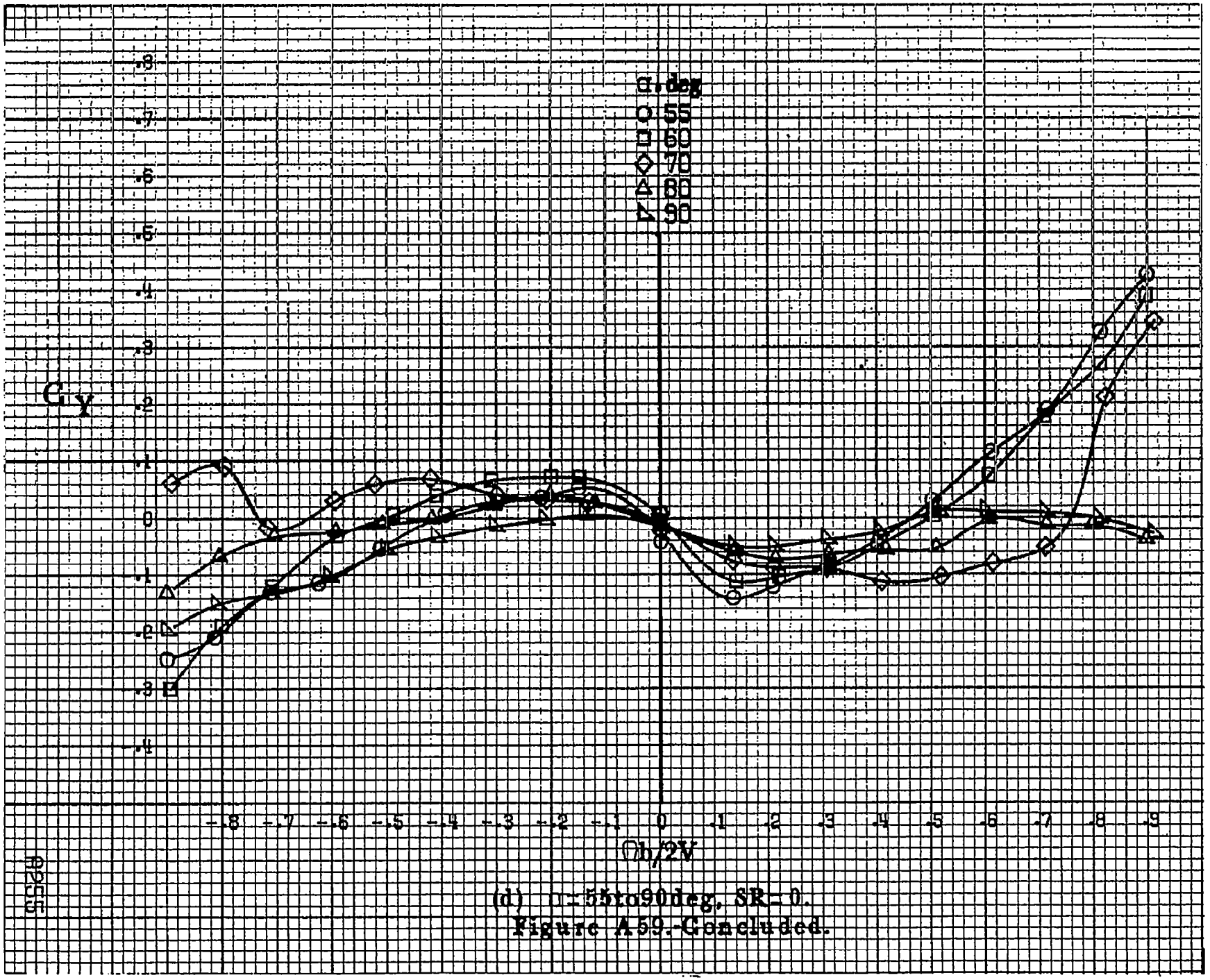

(d) α=55to90deg, δR=0.

Figure A59.-Concluded.

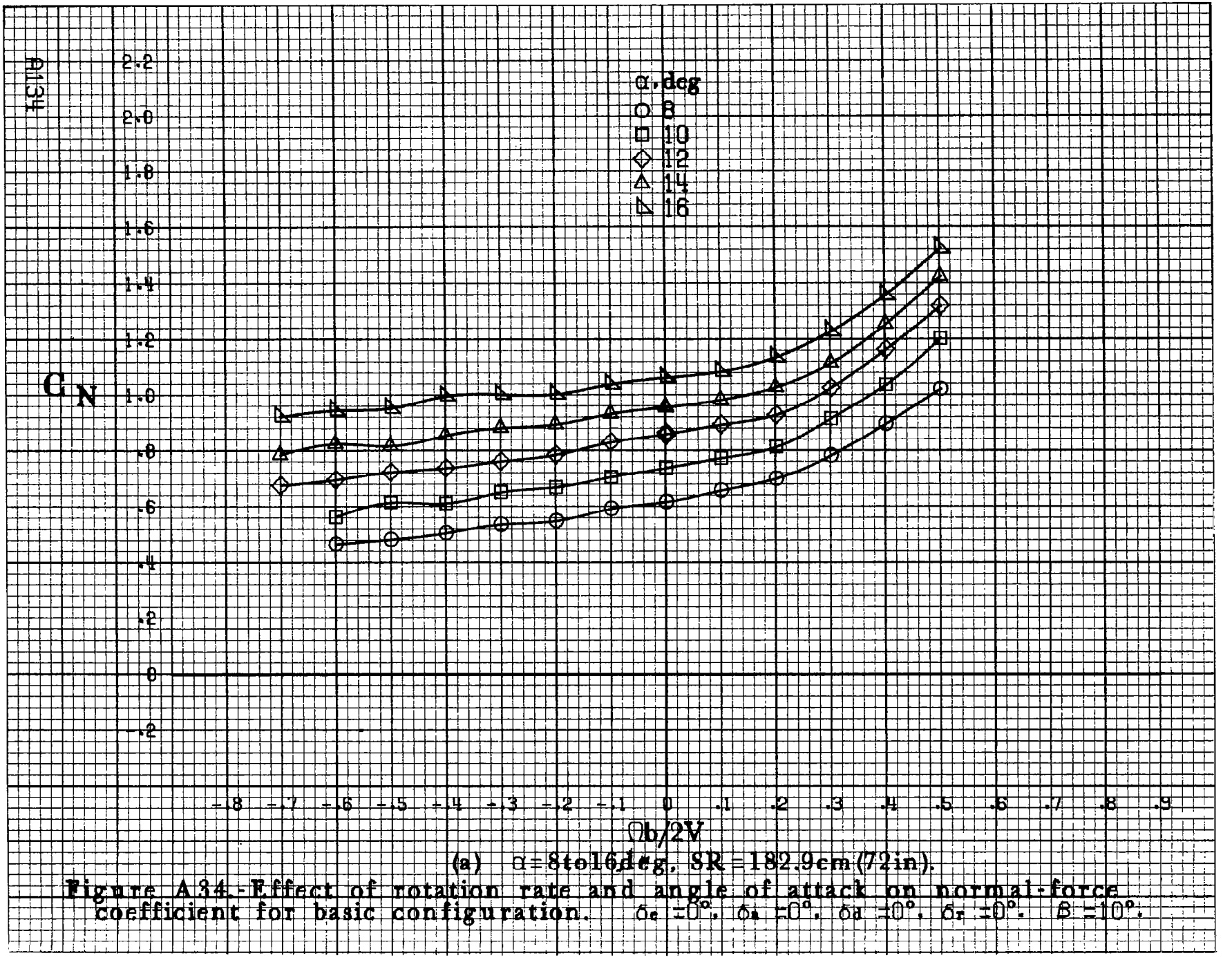

(a) $\alpha = 8$ to 16 deg, SR = 182.9 cm (72 in).

Figure A34.- Effect of rotation rate and angle of attack on normal-force coefficient for basic configuration. δ_e ±0°, δ_a ±0°, δ_d ±0°, δ_r ±0°, β ±10°.

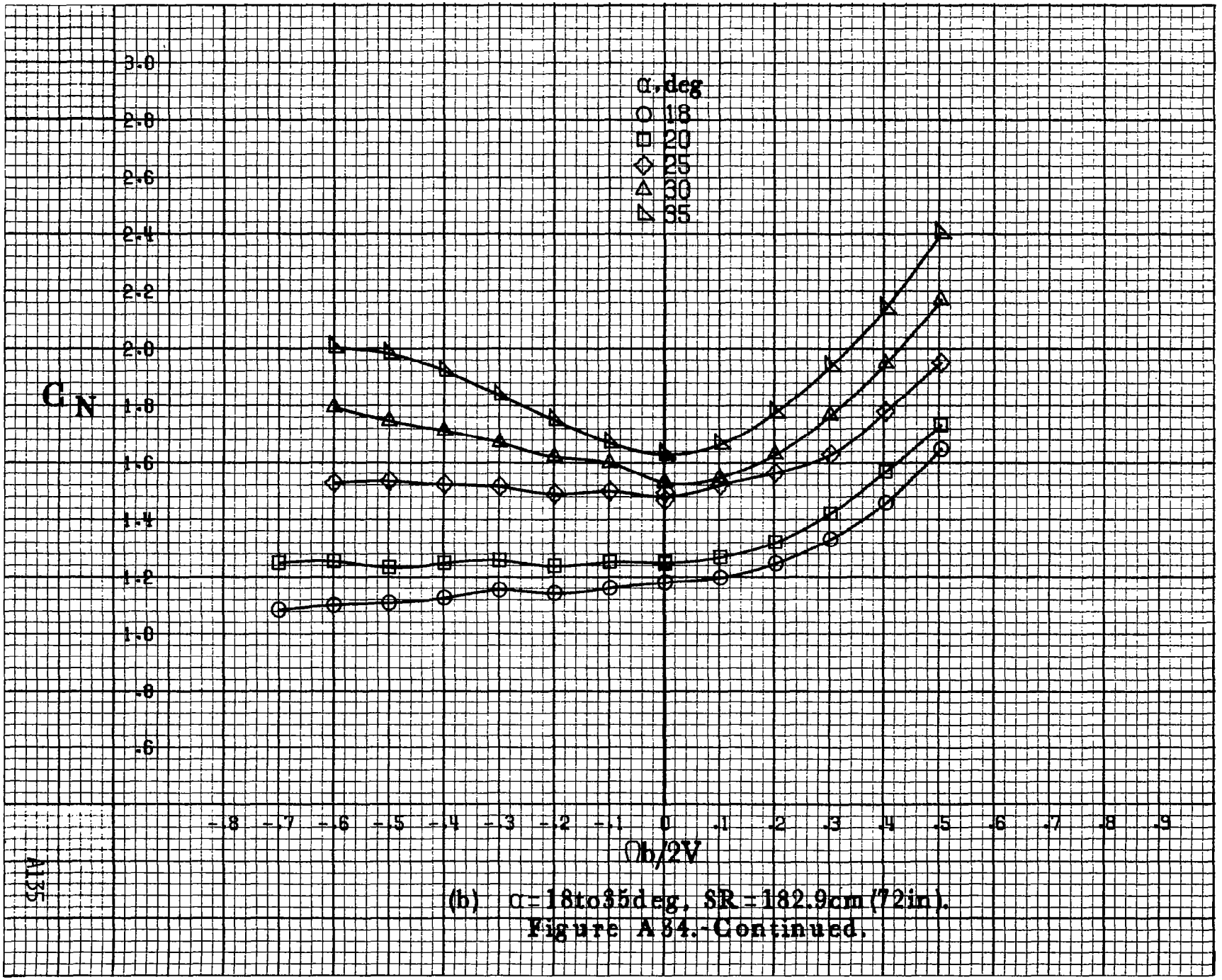

(b) $\alpha = 18$ to 35 deg, SR = 182.9 cm (72 in).

Figure A34.-Continued.

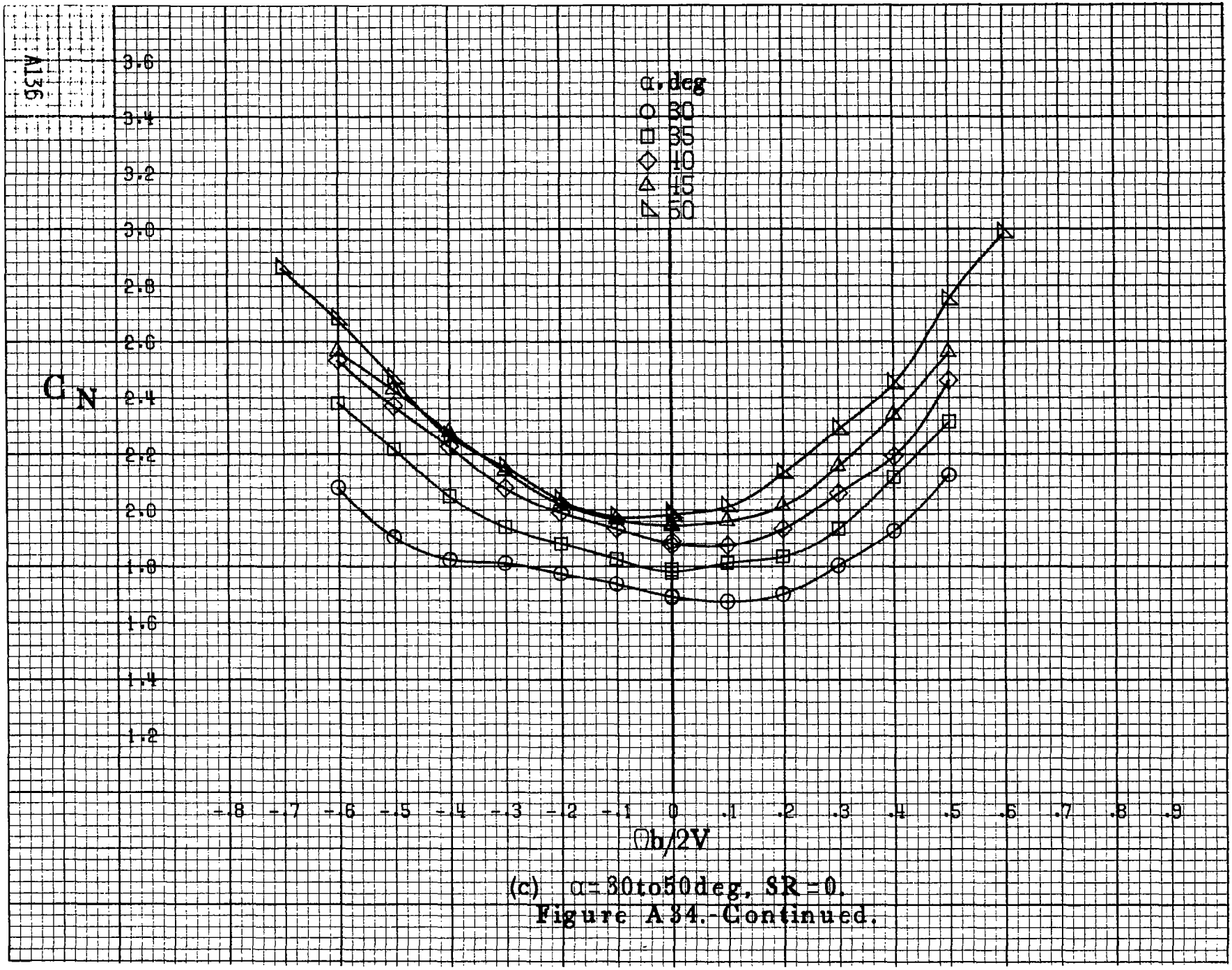

(c) α = 30 to 50 deg, SR = 0.

Figure A34.-Continued.

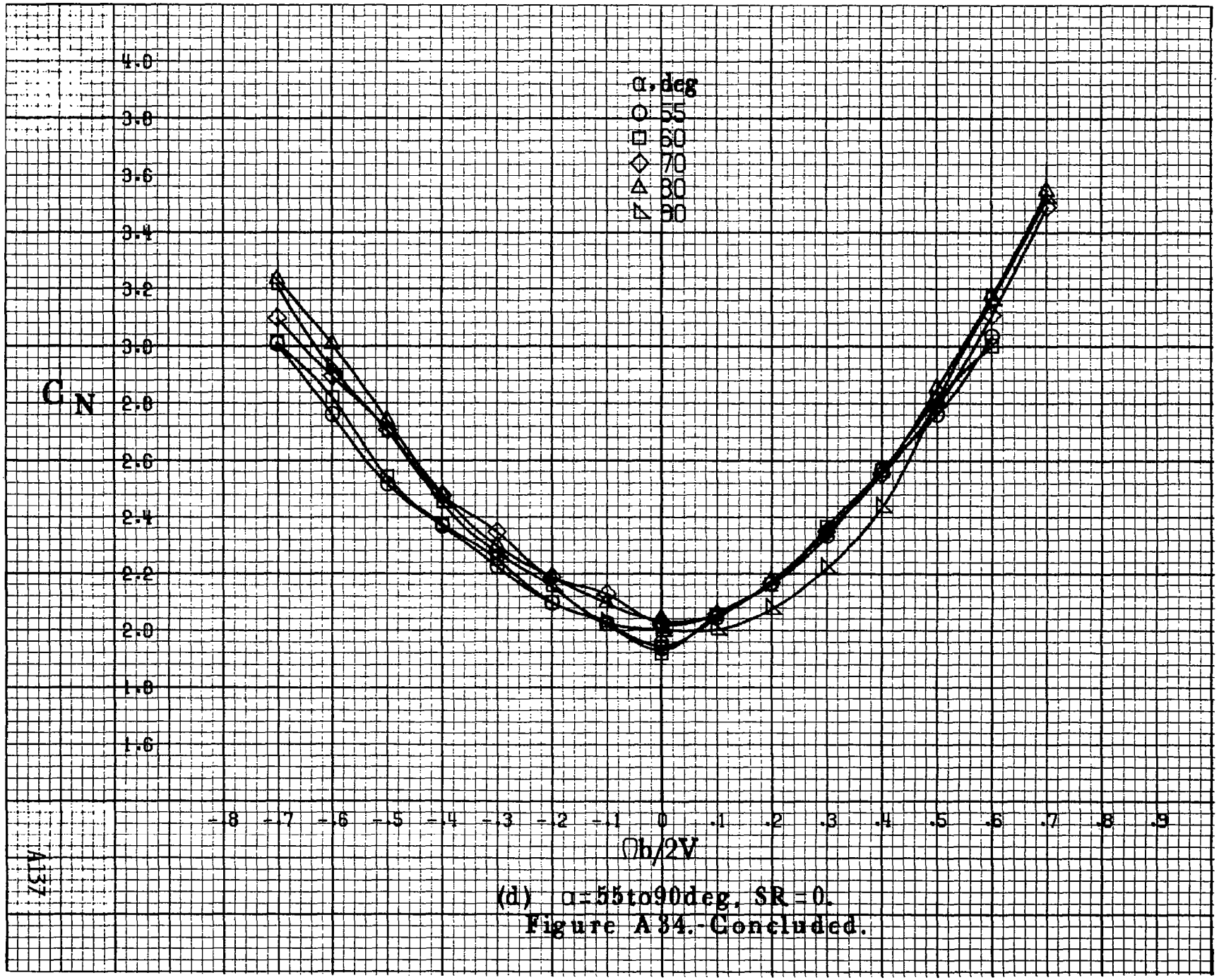

(d) α=55 to 90 deg, SR=0.

Figure A34.-Concluded.

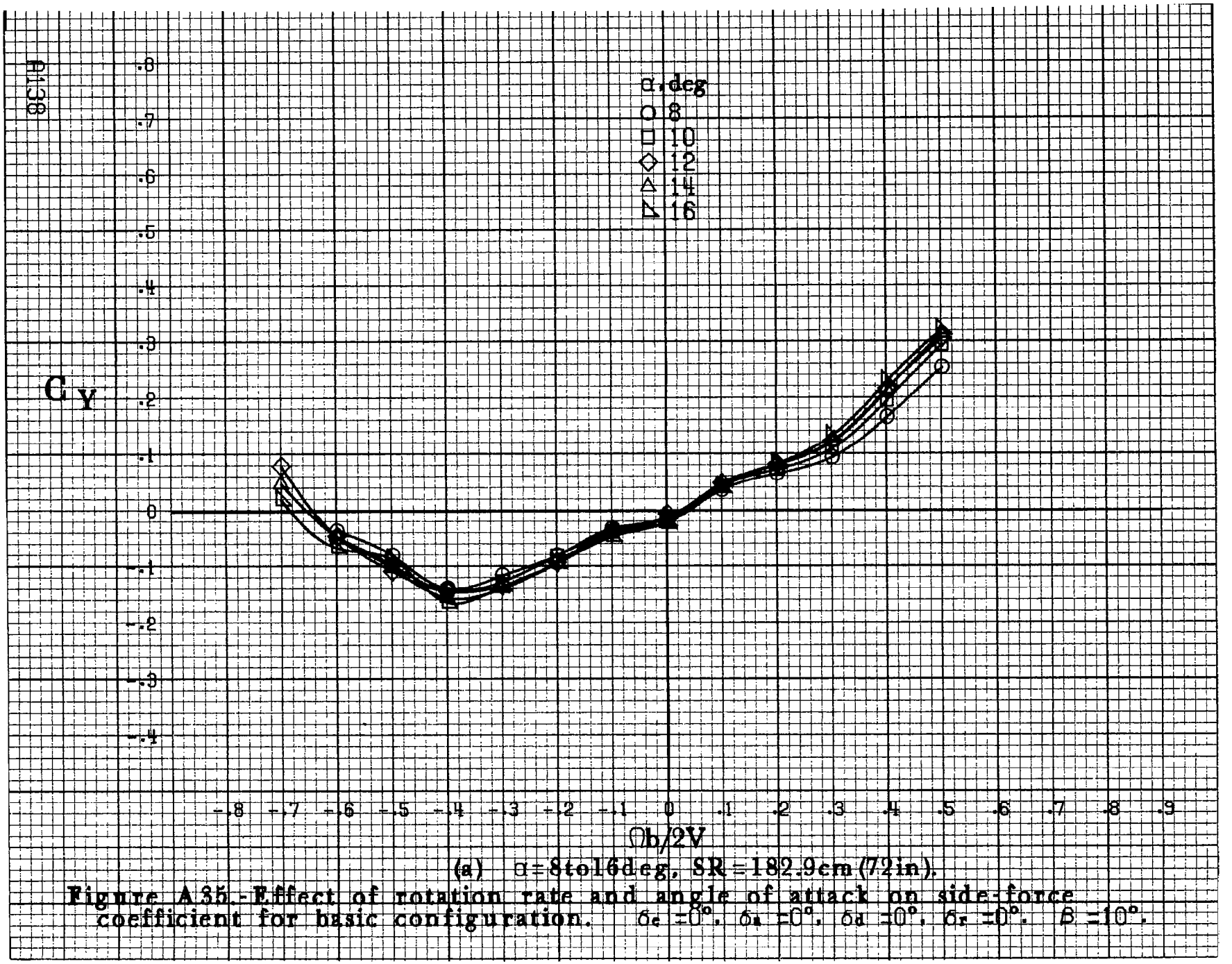

(a) $\alpha = 8$ to 16 deg, SR = 182.9 cm (72 in).

Figure A35.- Effect of rotation rate and angle of attack on side-force coefficient for basic configuration. $\delta_e = 0°$, $\delta_a = 0°$, $\delta_d = 0°$, $\delta_r = 0°$, $\beta = 10°$.

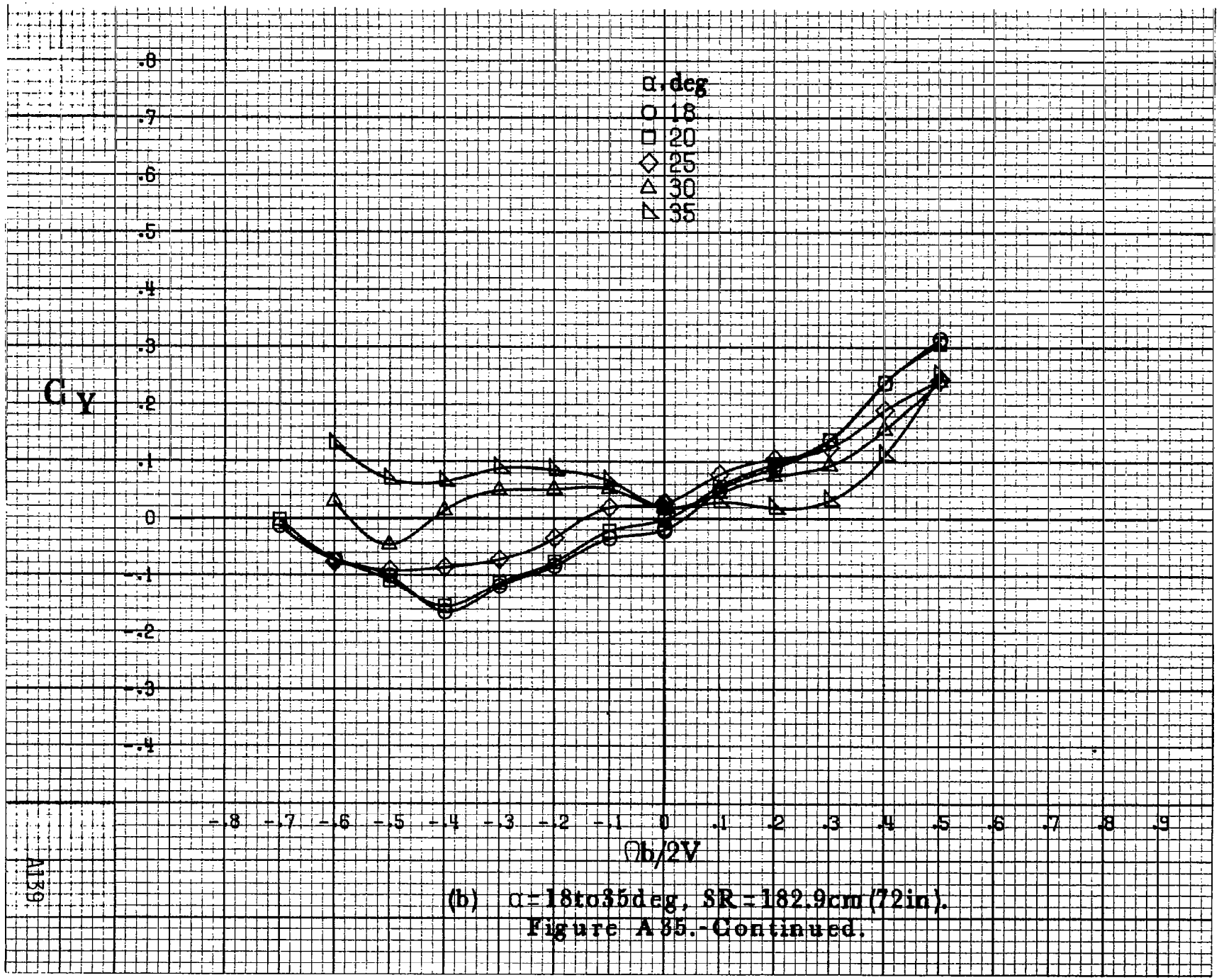

A139

(b) α = 18 to 35 deg, SR = 182.9 cm (72 in).

Figure A35.- Continued.

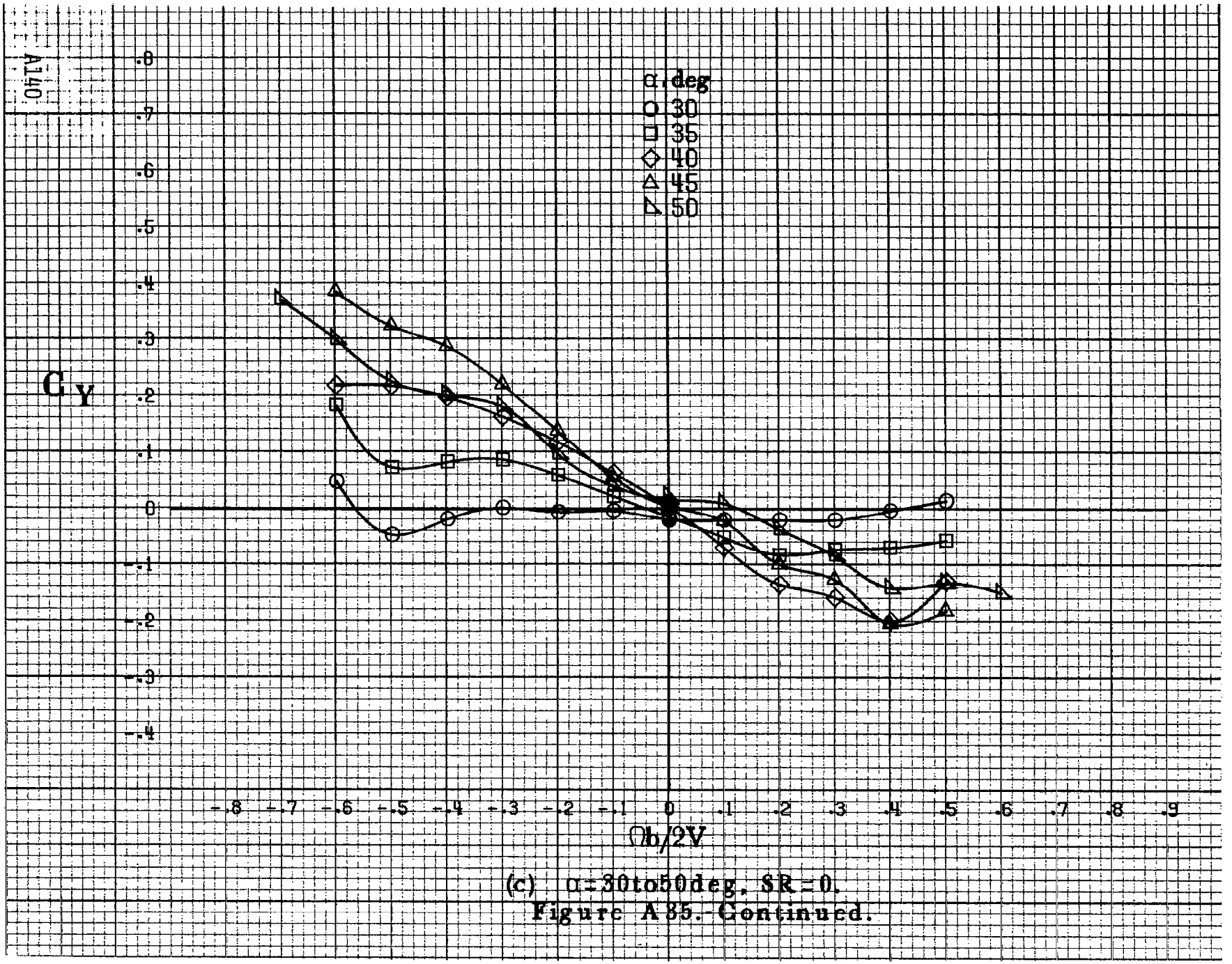

(c) $\alpha = 30$ to 50 deg, SR = 0.

Figure A35.- Continued.

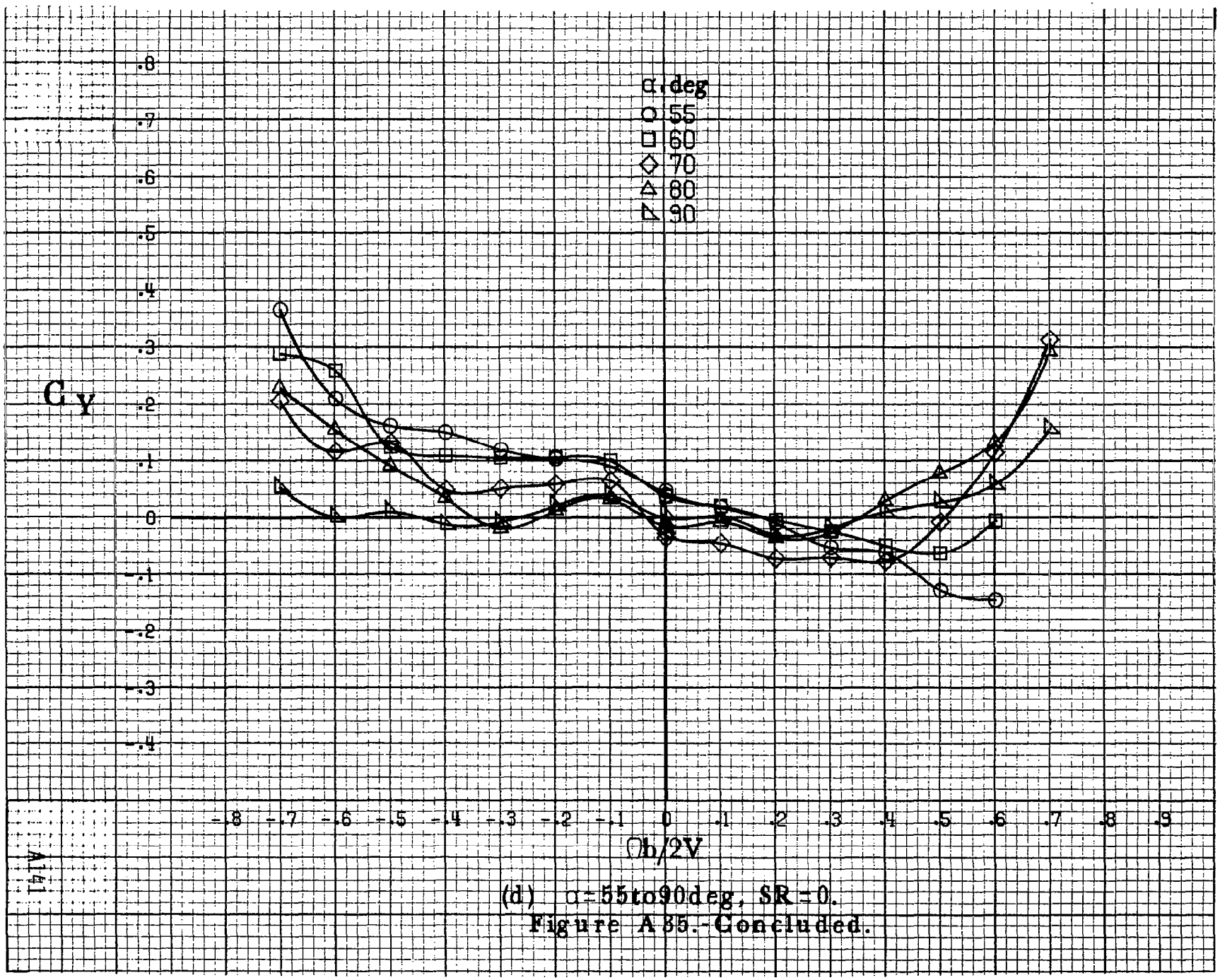

(d) $\alpha = 55$ to 90 deg, SR = 0.

Figure A 35.- Concluded.

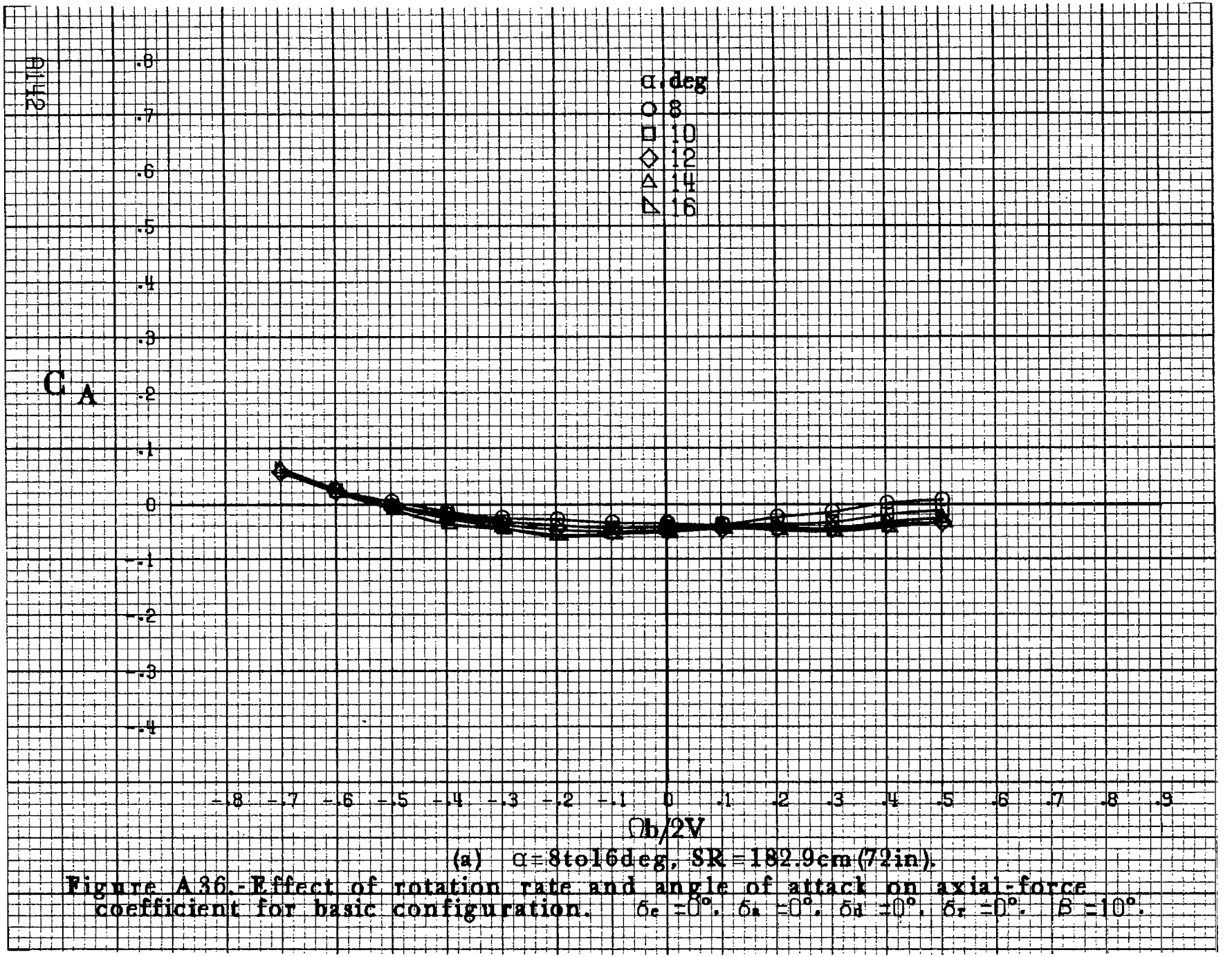

(a) $\alpha = 8$ to 16 deg, SR = 182.9 cm (72 in).

Figure A36.- Effect of rotation rate and angle of attack on axial-force coefficient for basic configuration. $\delta_e = 0°$, $\delta_a = 0°$, $\delta_d = 0°$, $\delta_r = 0°$, $\beta = 10°$.

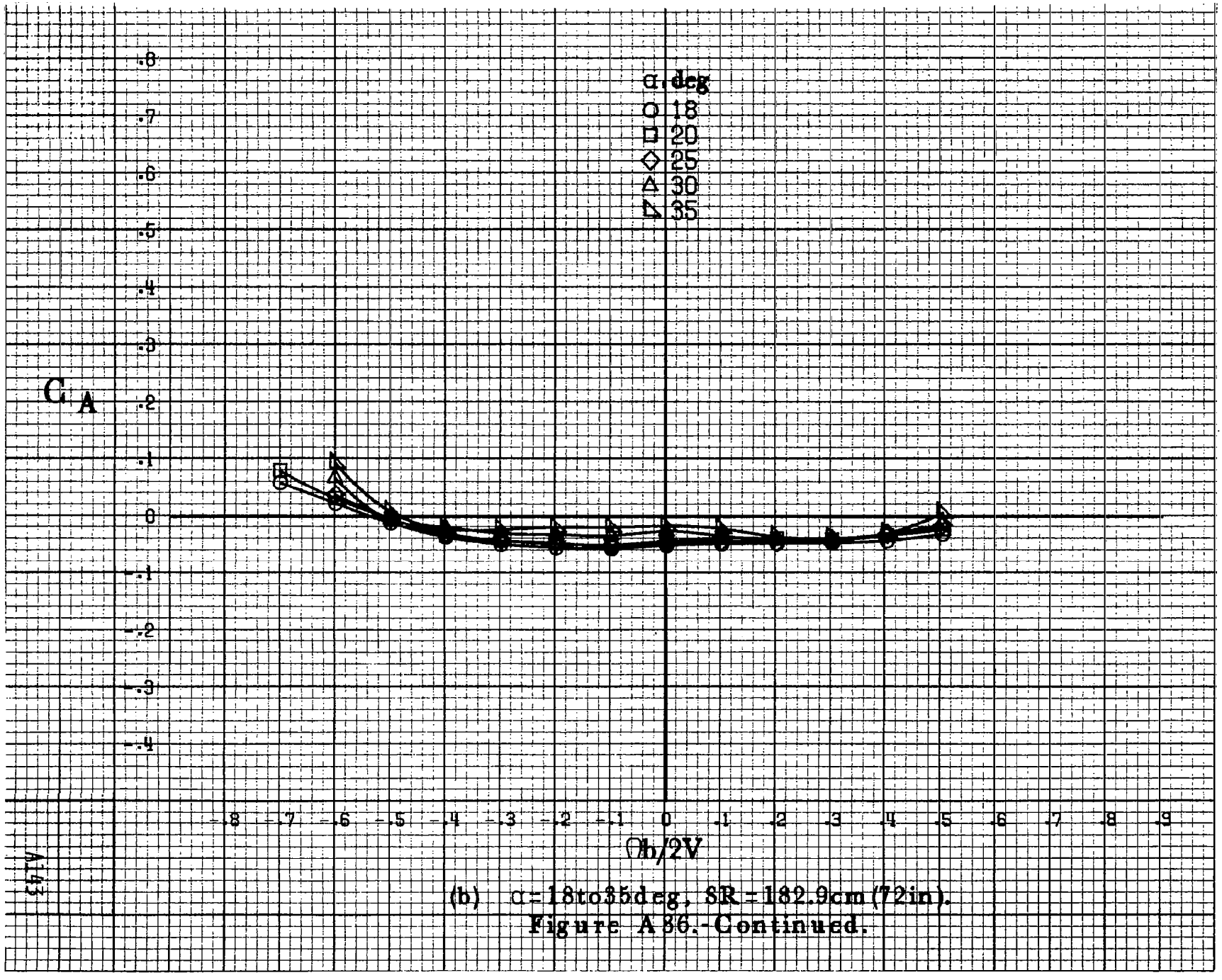

(b) α = 18 to 35 deg, SR = 182.9 cm (72 in).

Figure A36.- Continued.

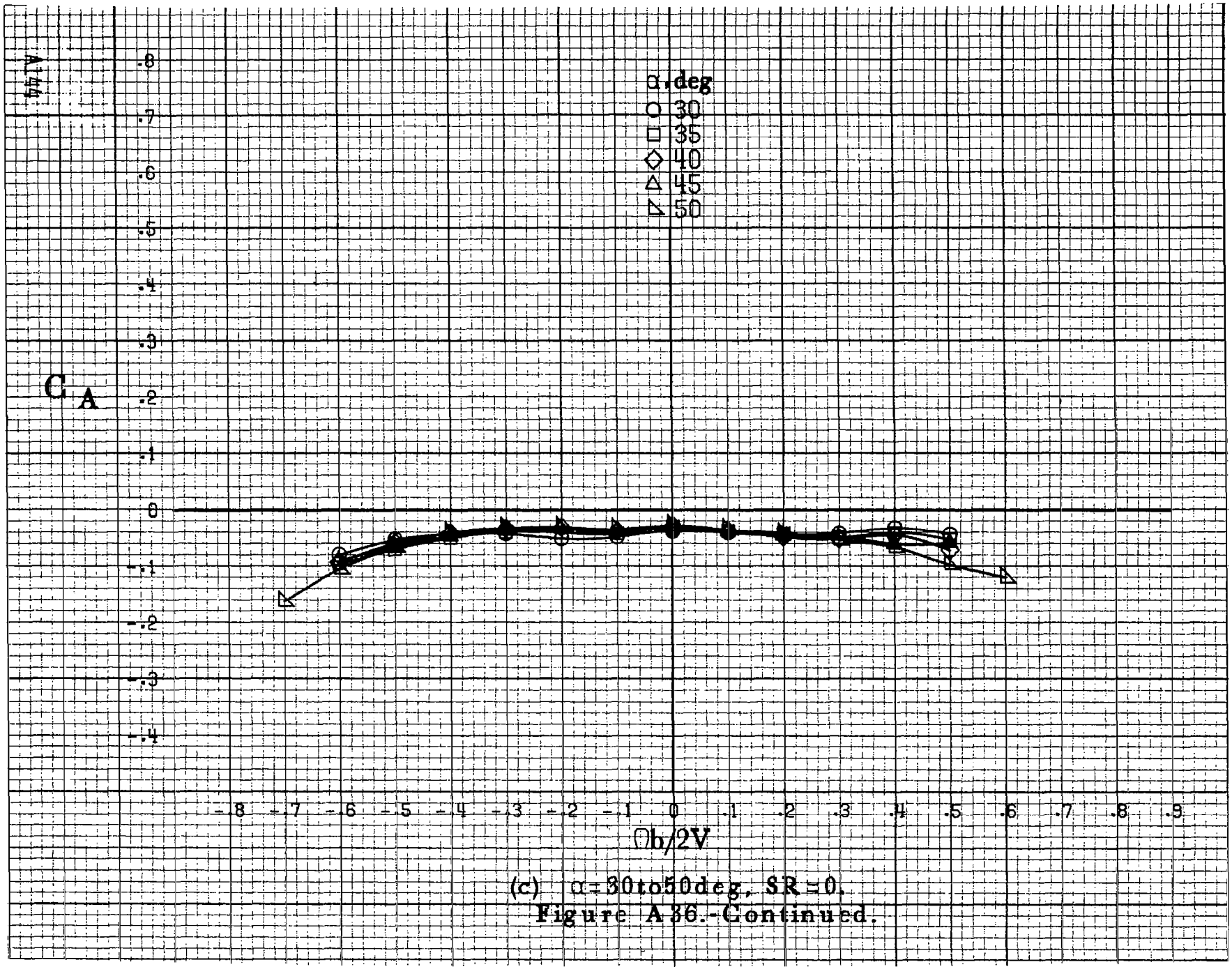

(c) α = 30 to 50 deg, SR = 0.

Figure A36.- Continued.

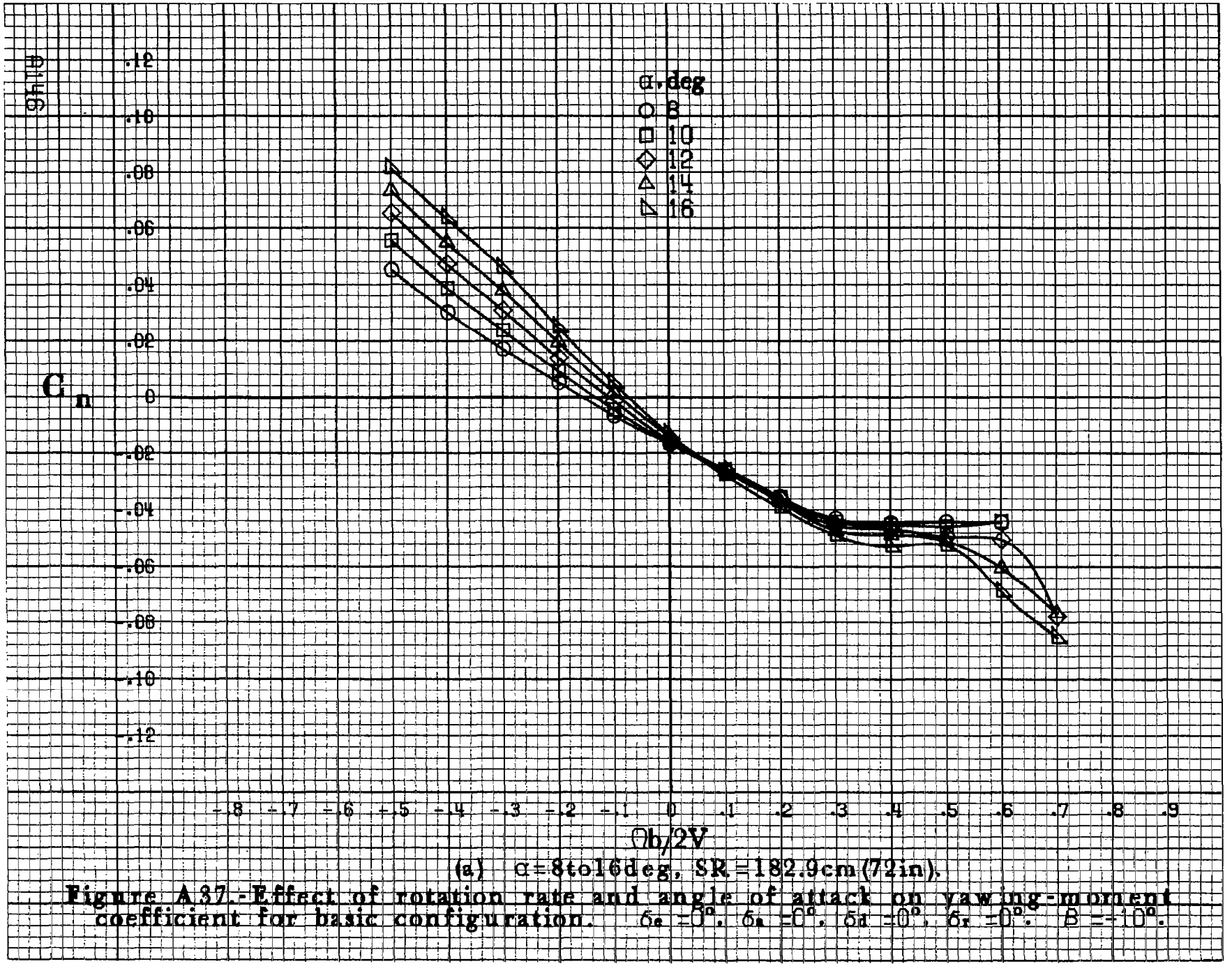

(a) $\alpha = 8$ to 16 deg, SR = 182.9 cm (72 in).

Figure A37.-Effect of rotation rate and angle of attack on yawing-moment coefficient for basic configuration. $\delta_e = 0°$, $\delta_a = 0°$, $\delta_d = 0°$, $\delta_r = 0°$, $\beta = -10°$.

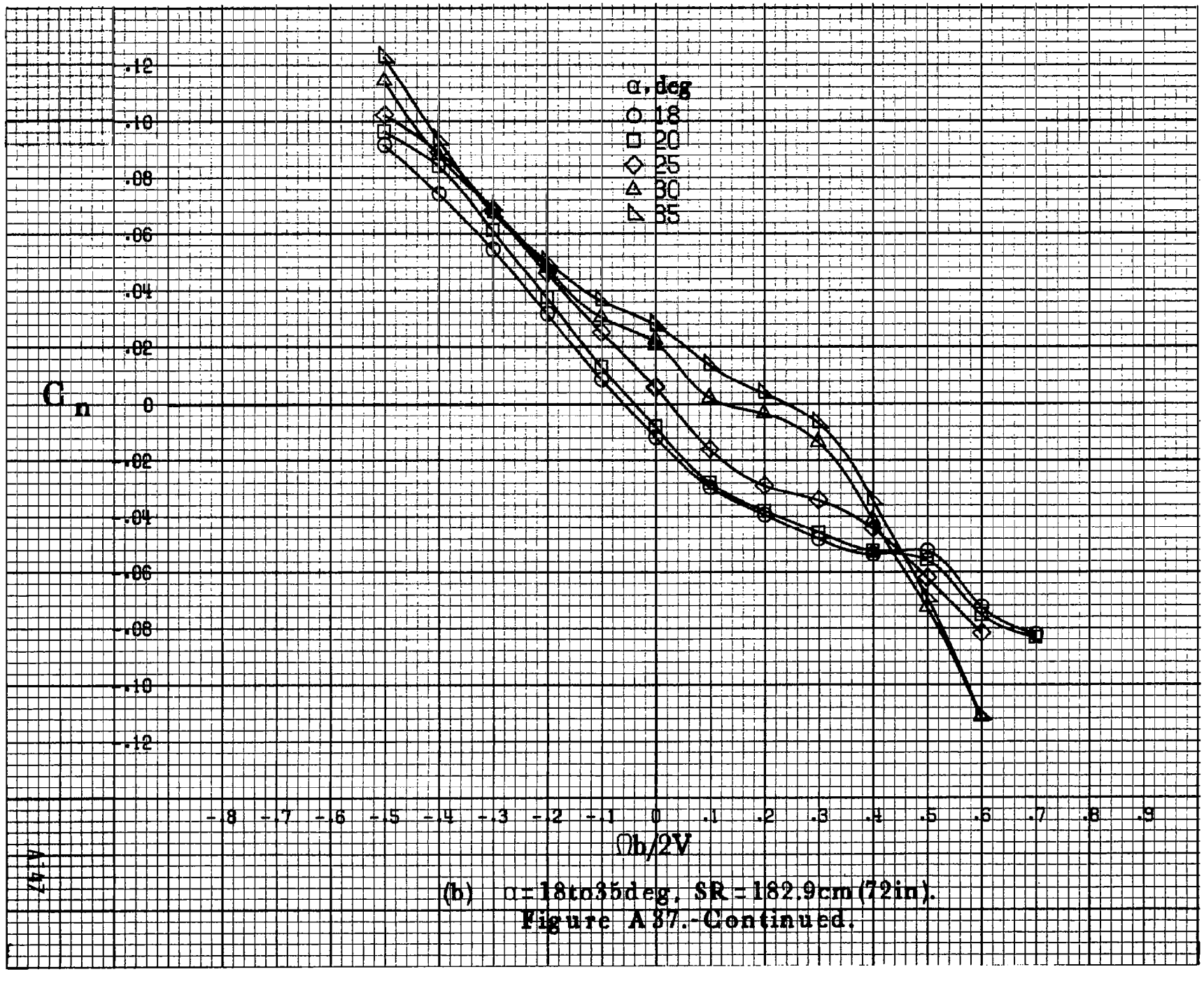

(b) $\alpha = 18$ to 35 deg, SR = 182.9 cm (72 in).

Figure A37.-Continued.

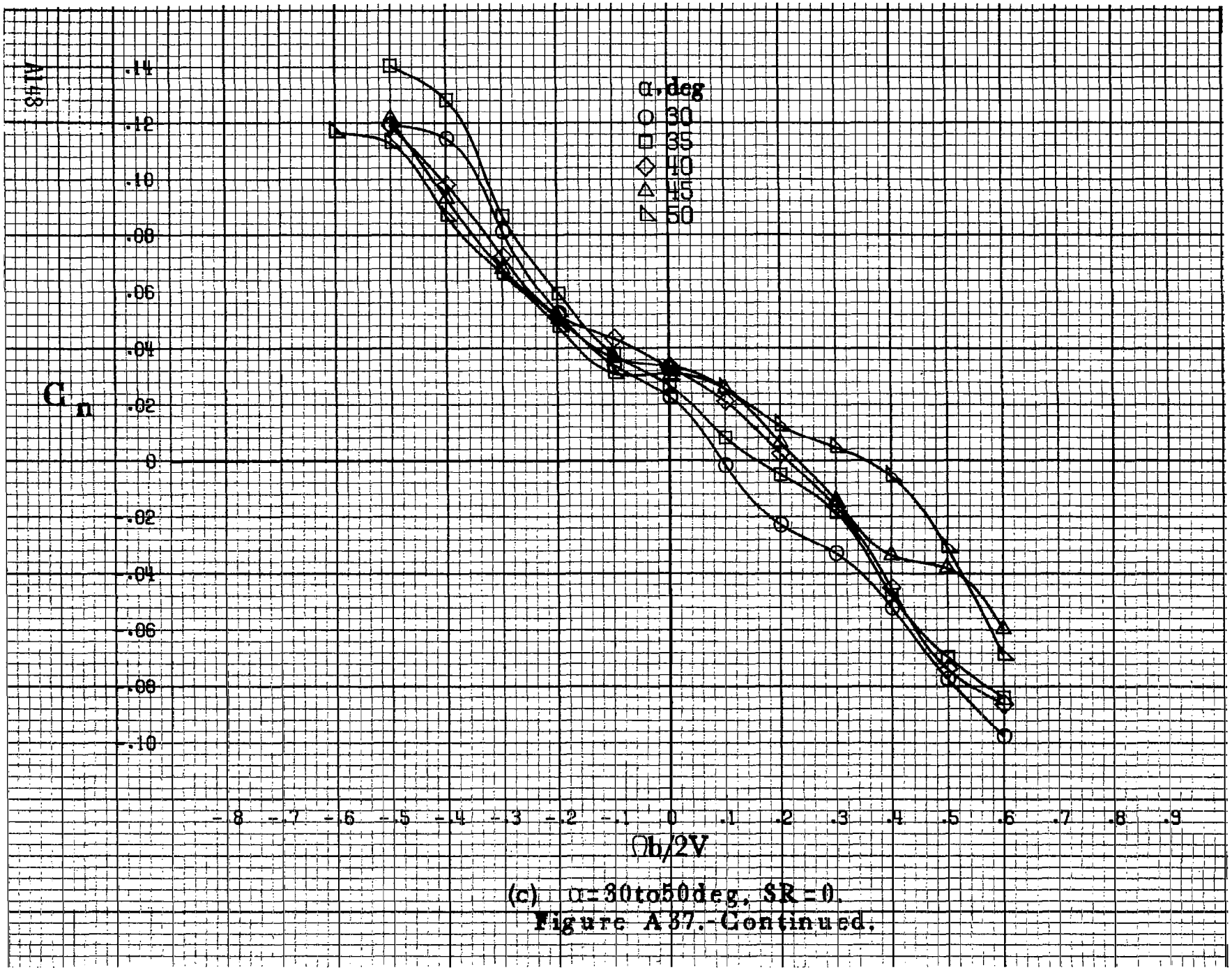

(c) α = 30 to 50 deg, SR = 0.

Figure A37.- Continued.

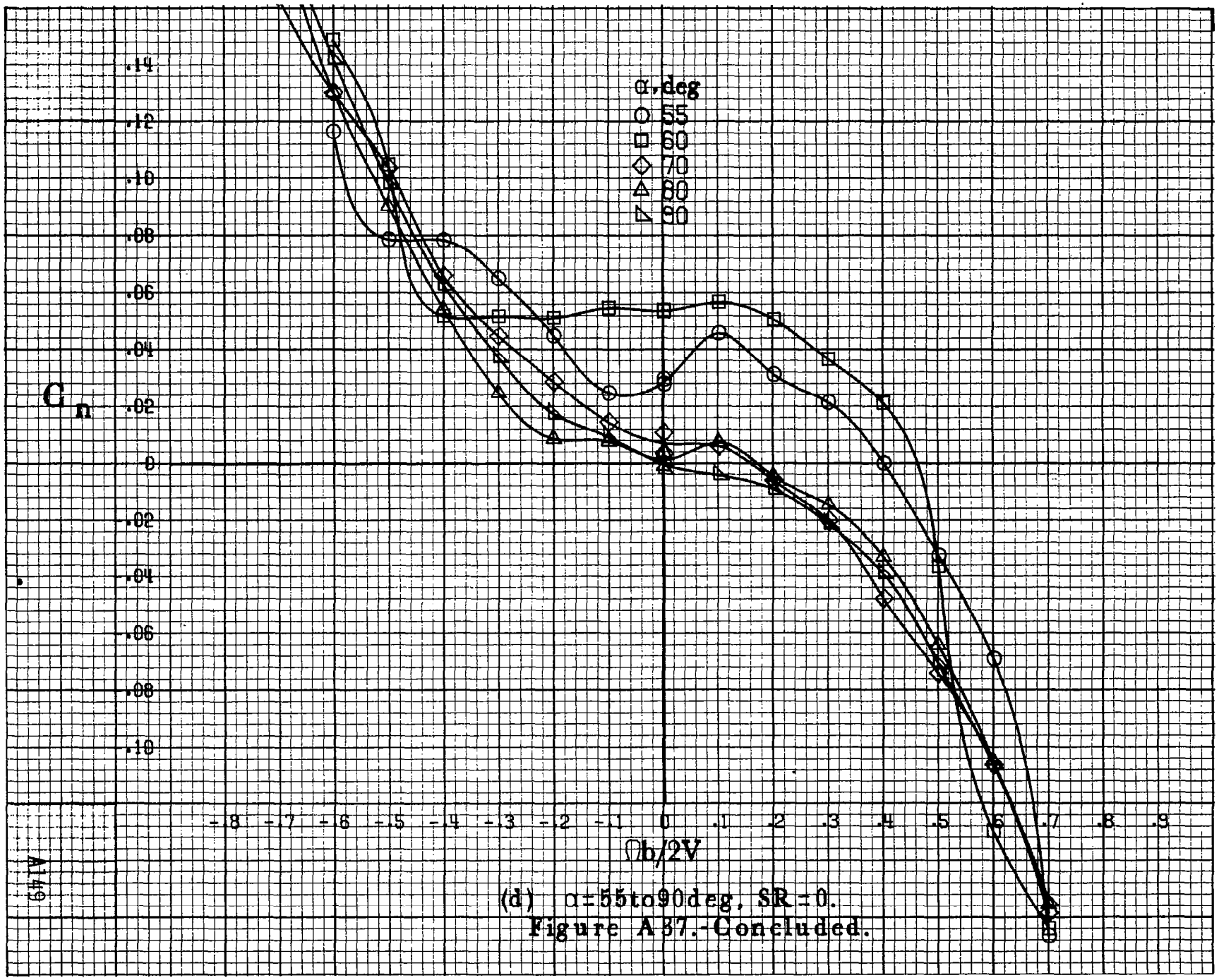

(d) α=55to90deg, SR=0.

Figure A37.-Concluded.

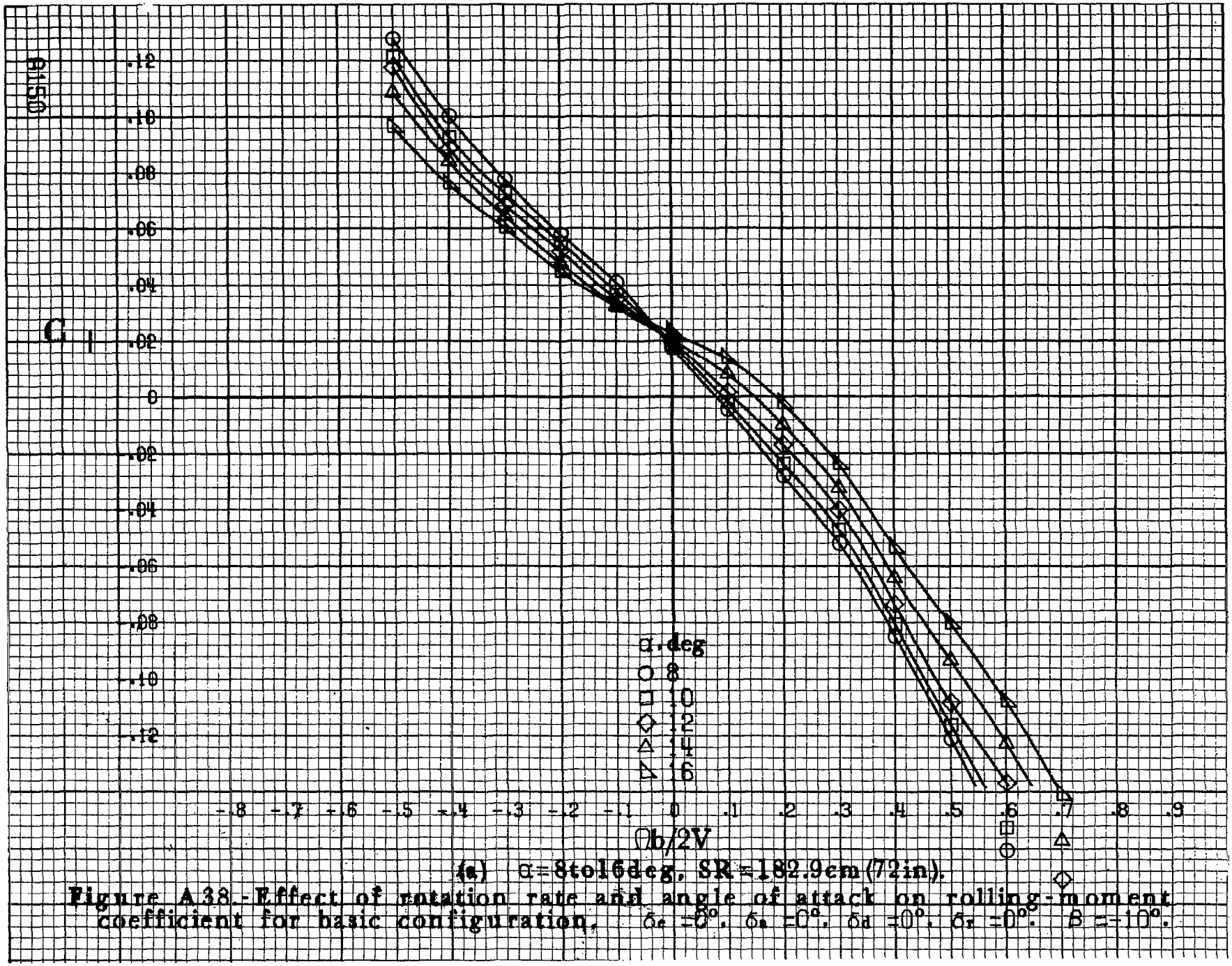

(c) $\alpha = 8$ to 16 deg, SR = 182.9 cm (72 in).

Figure A.38.- Effect of rotation rate and angle of attack on rolling-moment coefficient for basic configuration. $\delta_e = 0°$, $\delta_a = 0°$, $\delta_d = 0°$, $\delta_r = 0°$, $\beta = -10°$.

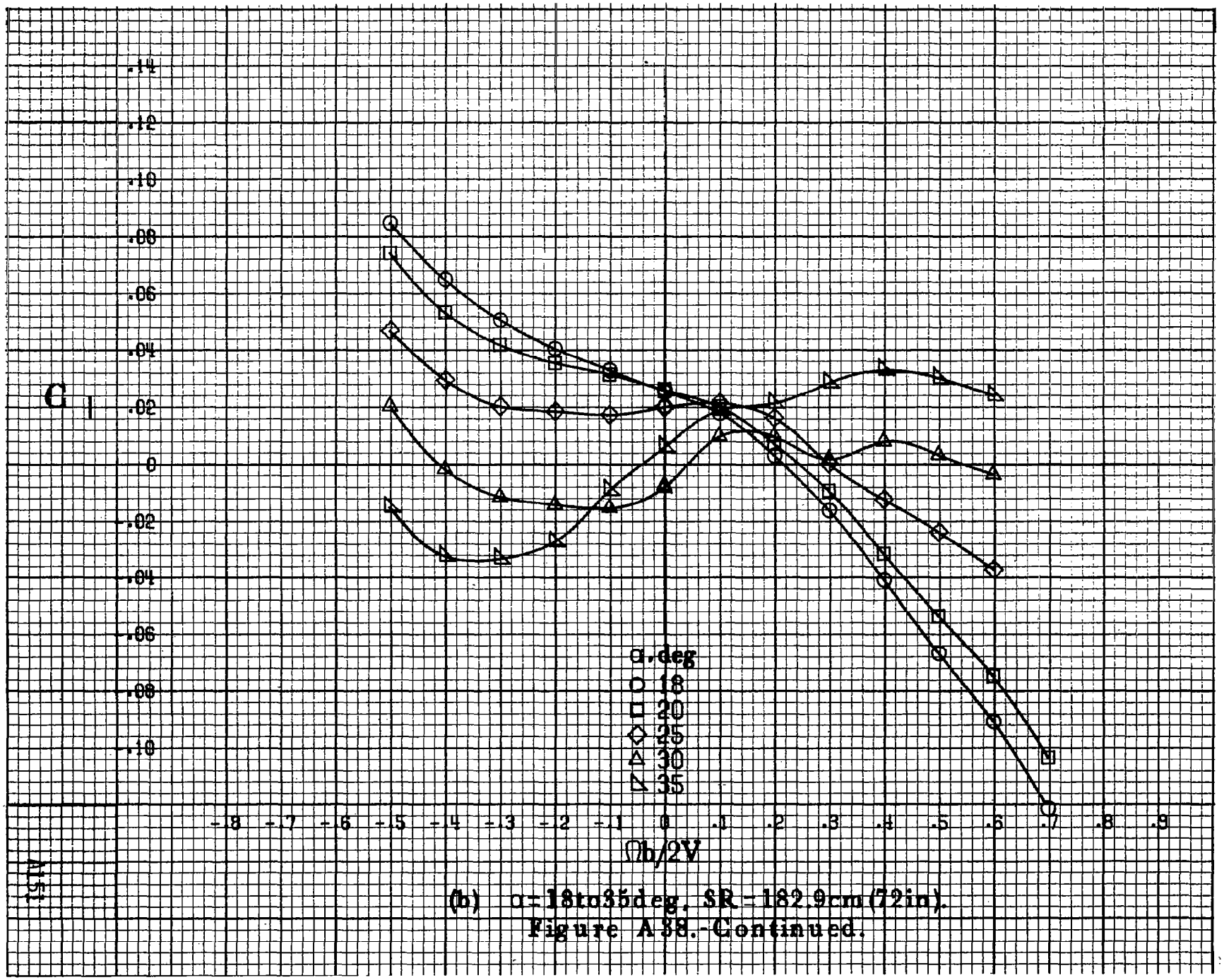

(b) α = 18 to 35 deg. SR = 182.9 cm (72 in).

Figure A38.-Continued.

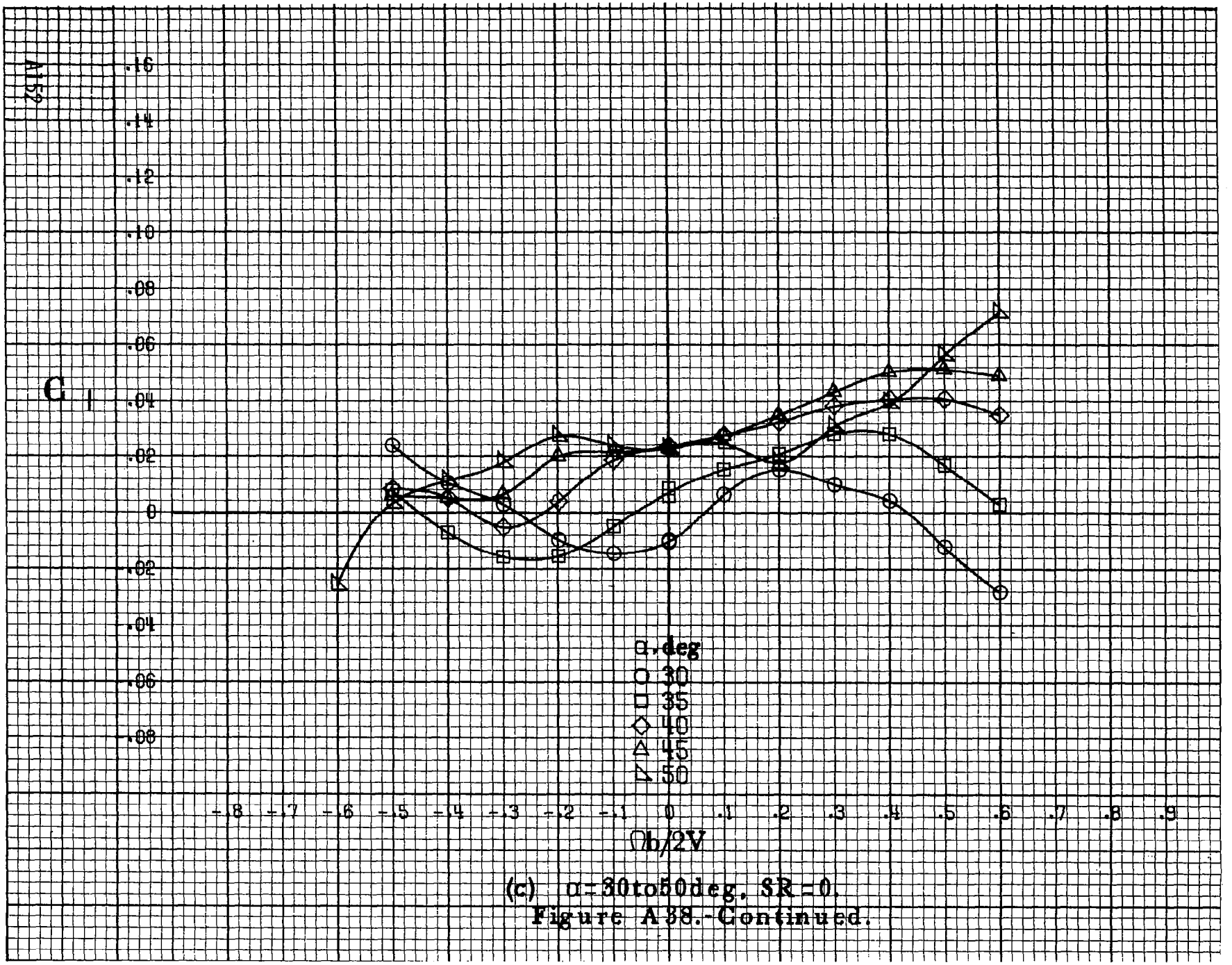

(c) $\alpha = 30$ to 50 deg, SR = 0.

Figure A38.- Continued.

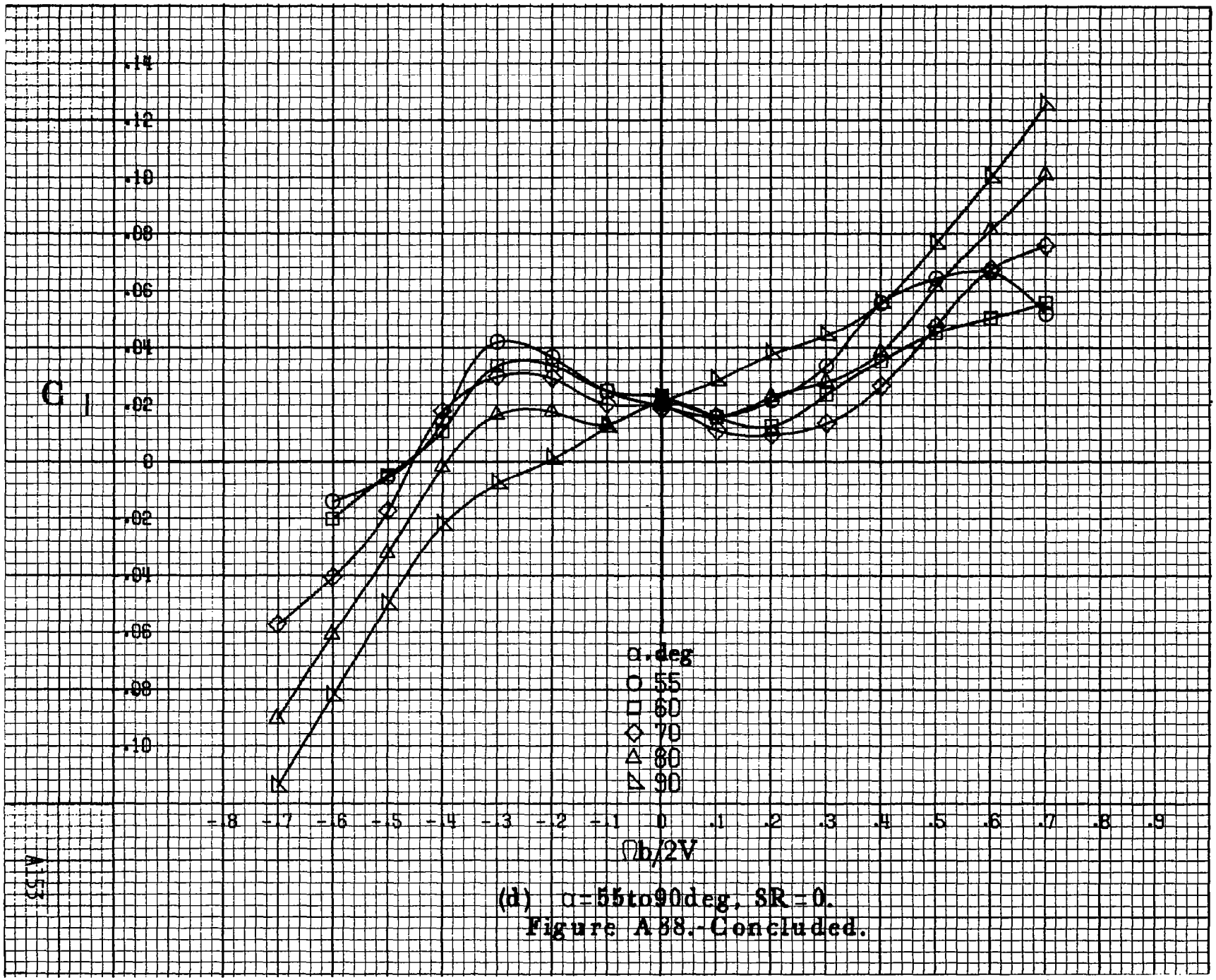

(d) α=55to90deg, SR=0.

Figure A88.-Concluded.

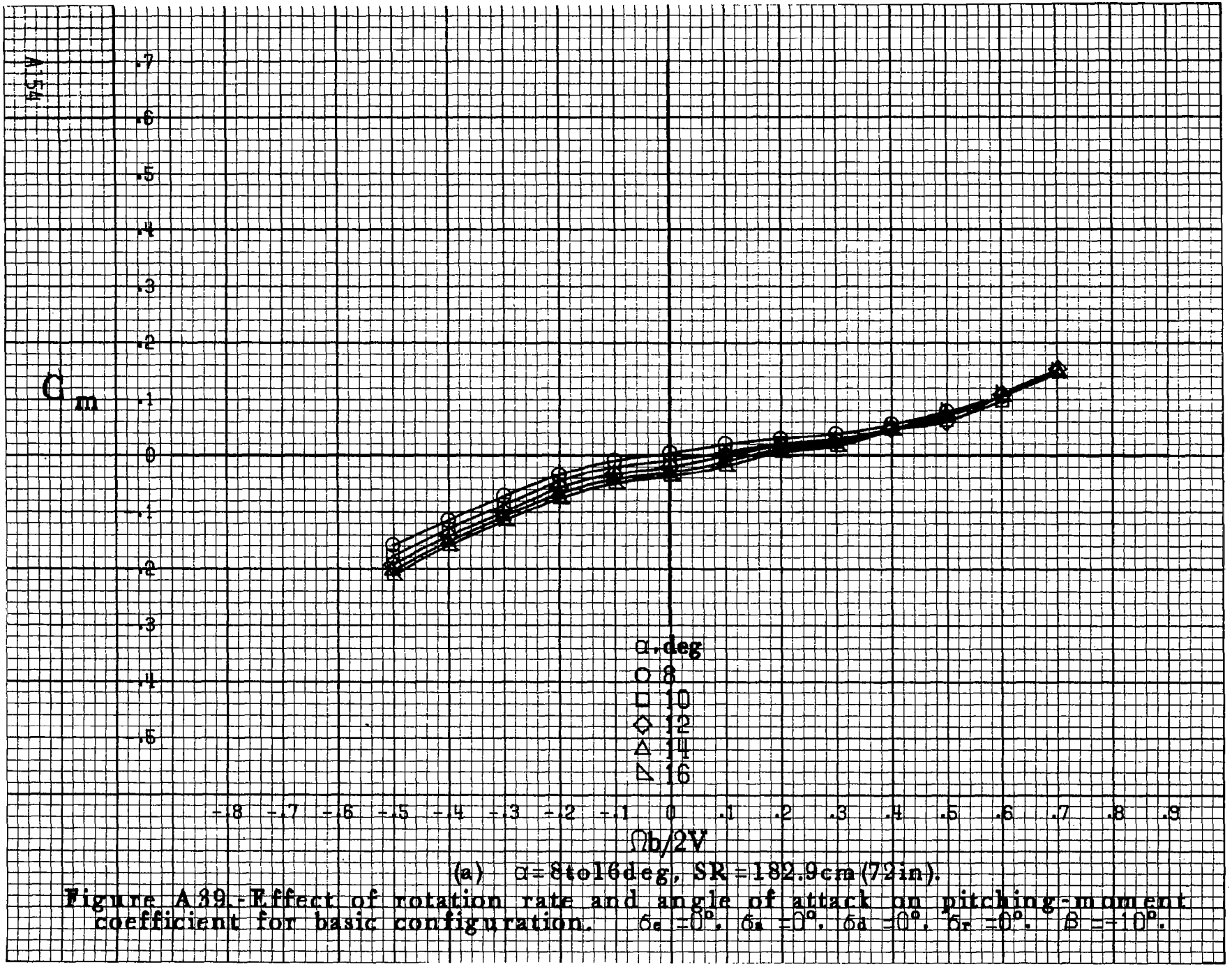

(a) α = 8 to 16 deg, SR = 182.9 cm (72 in).

Figure A39.- Effect of rotation rate and angle of attack on pitching-moment coefficient for basic configuration. $\delta_e = 0°$, $\delta_a = 0°$, $\delta_a = 0°$, $\delta_r = 0°$, $\beta = 10°$.

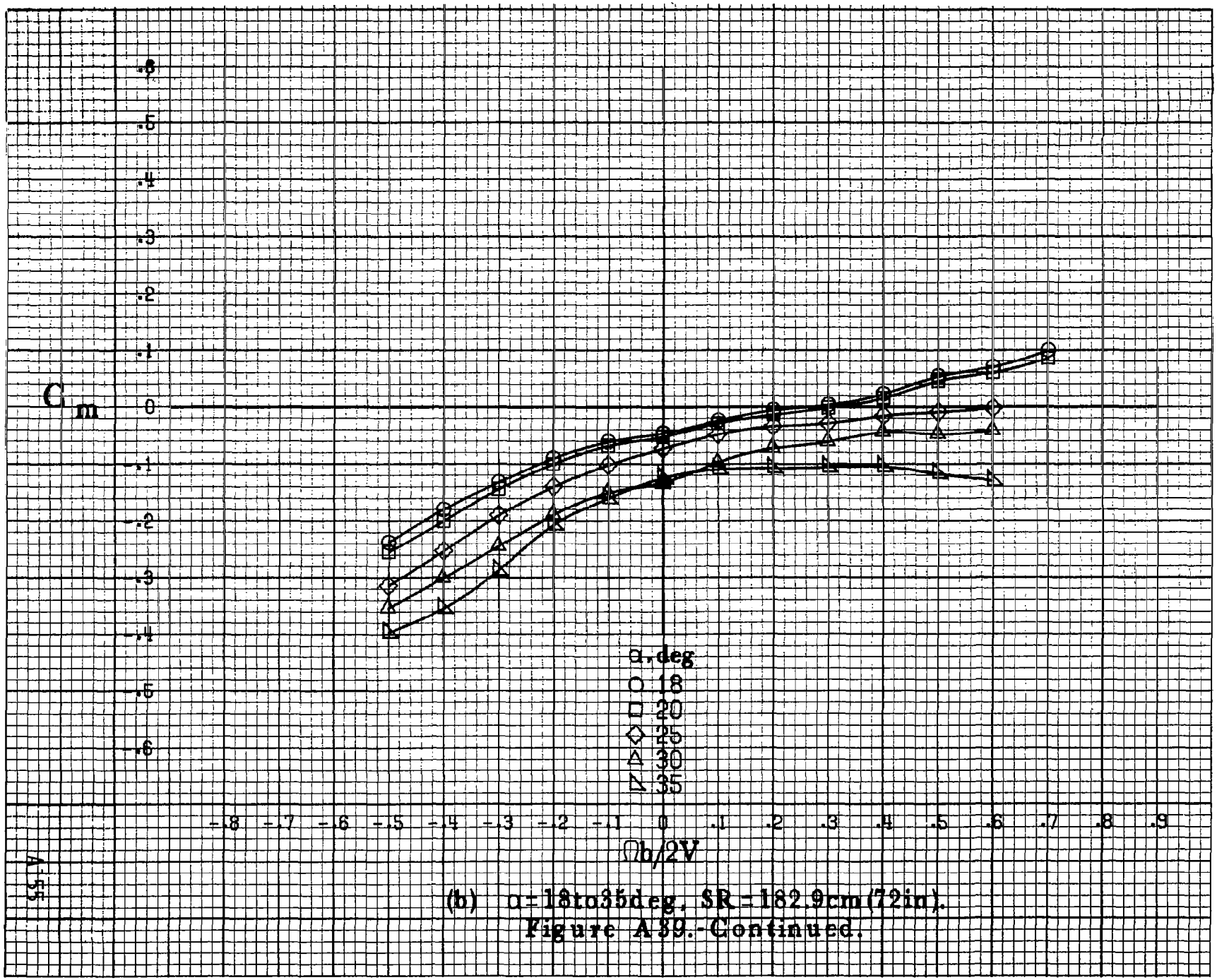

A-55

(b) α = 18 to 35 deg, SR = 182.9 cm (72 in).

Figure A39.- Continued.

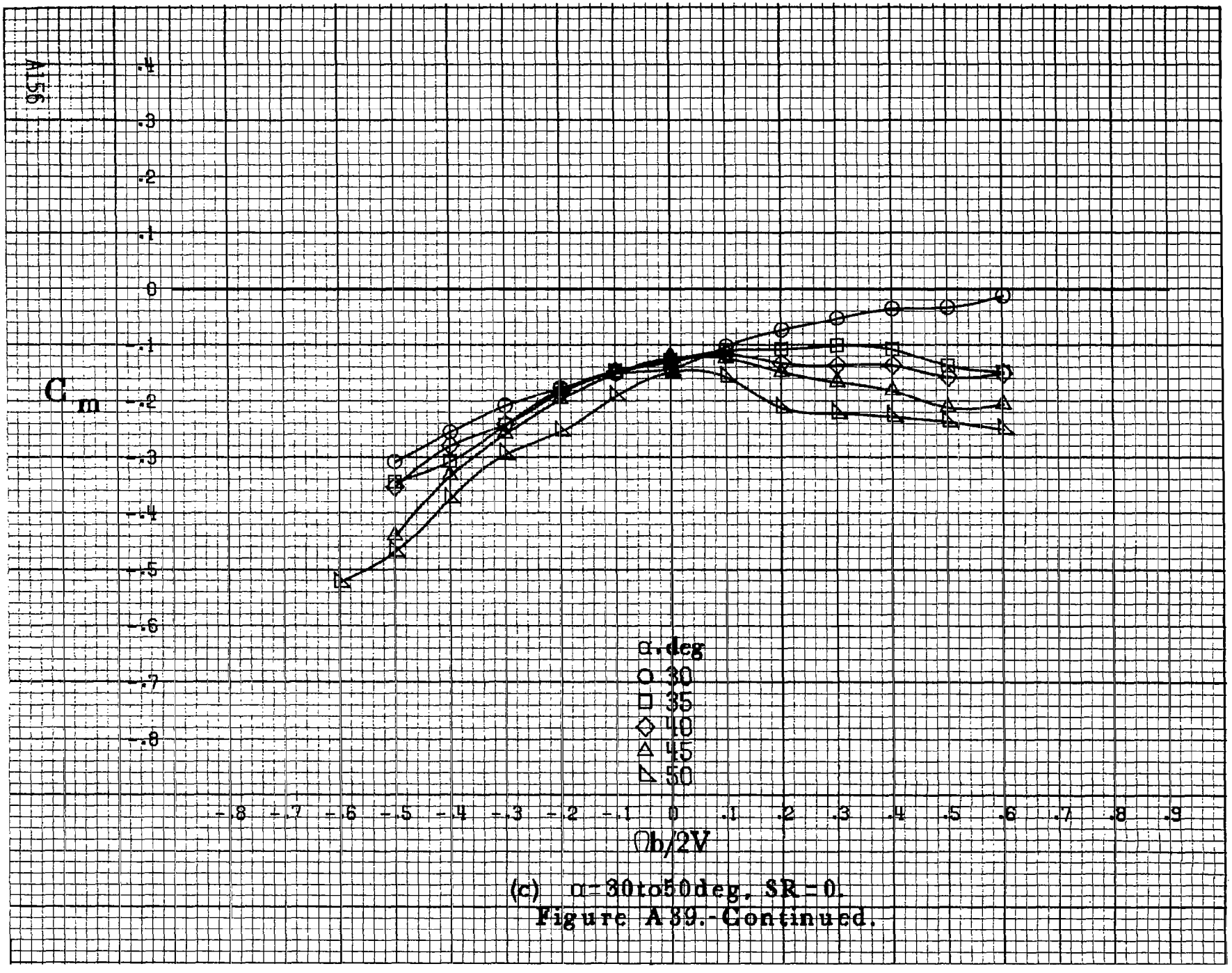

(c) α = 30 to 50 deg, SR = 0.

Figure A39.- Continued.

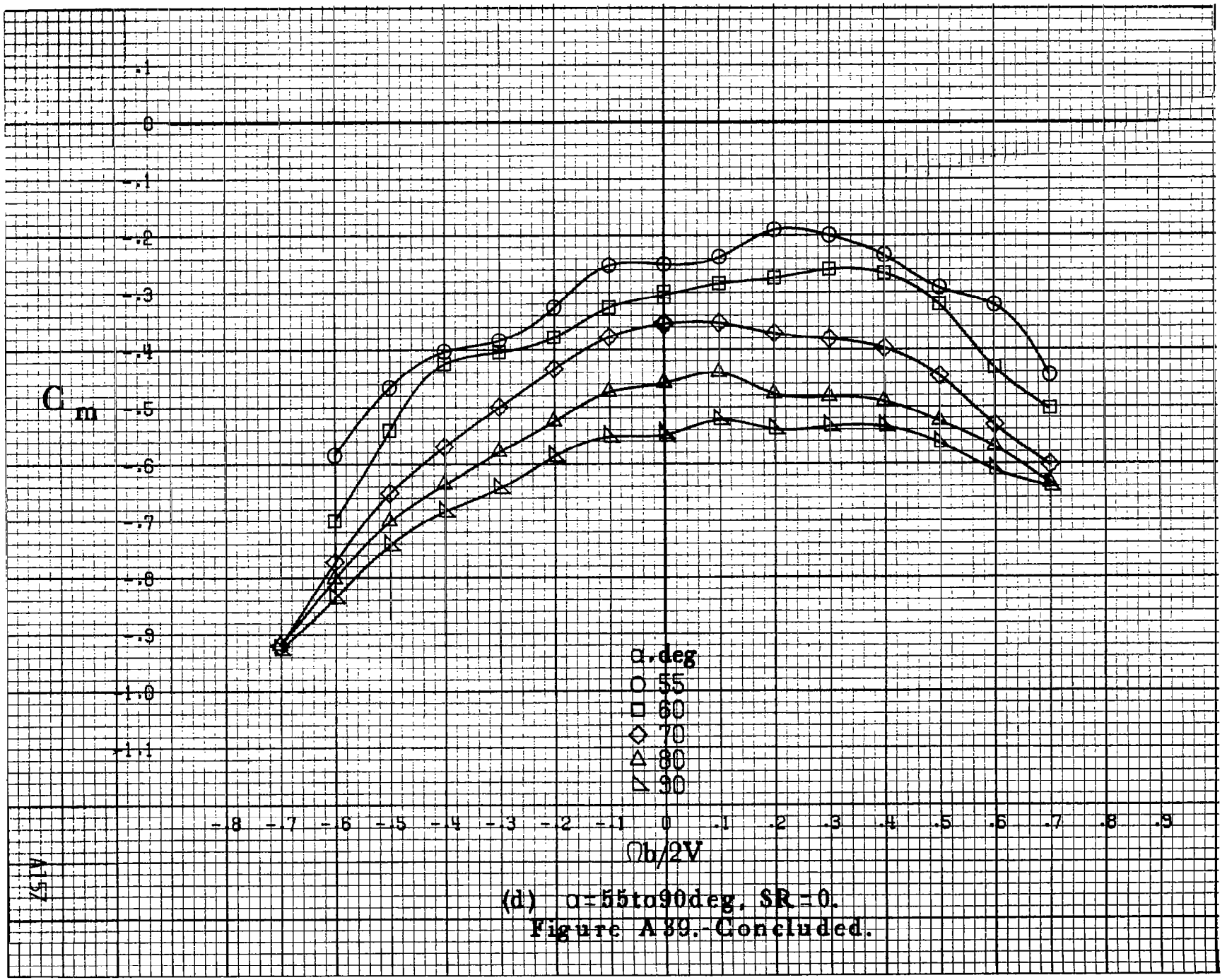

(d) α=55to90deg, SR=0.

Figure A39.- Concluded.

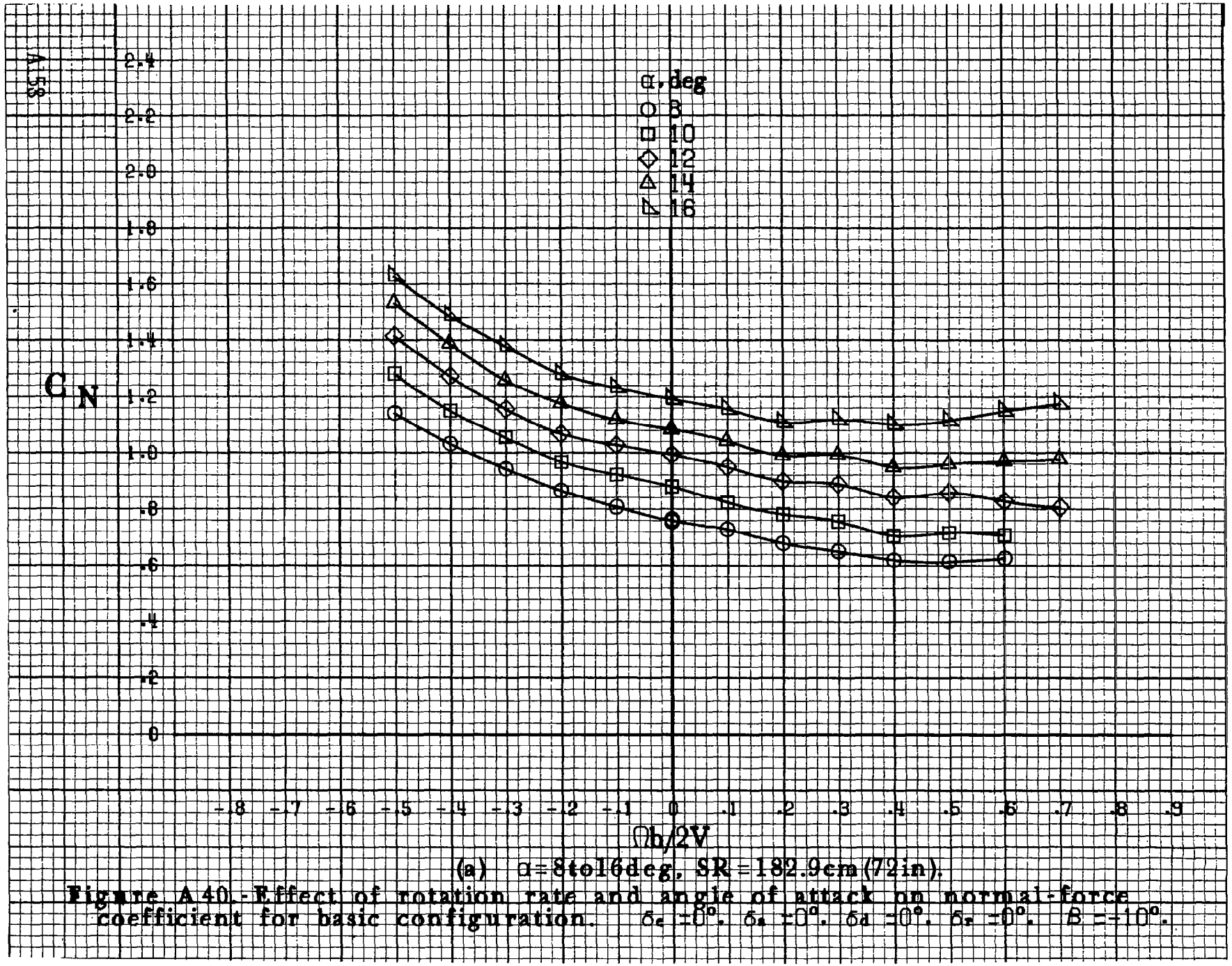

(a) $\alpha = 8$ to 16 deg, SR = 182.9 cm (72 in).

Figure A40.- Effect of rotation rate and angle of attack on normal-force coefficient for basic configuration. $\delta_e = 0°$, $\delta_a = 0°$, $\delta_d = 0°$, $\delta_r = 0°$, $B = +10°$.

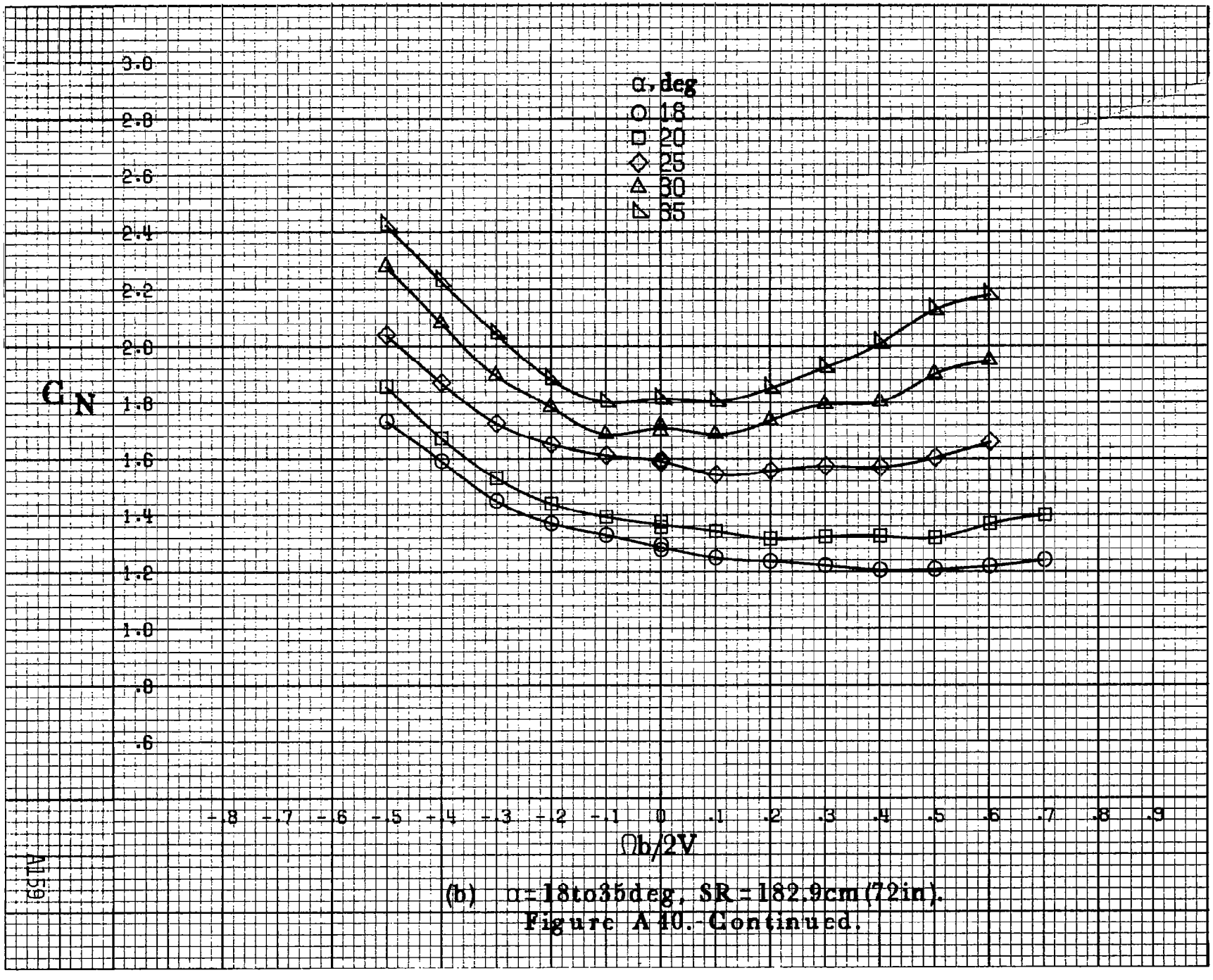

(b) α = 18 to 35 deg, SR = 182.9 cm (72 in).

Figure A40.- Continued.

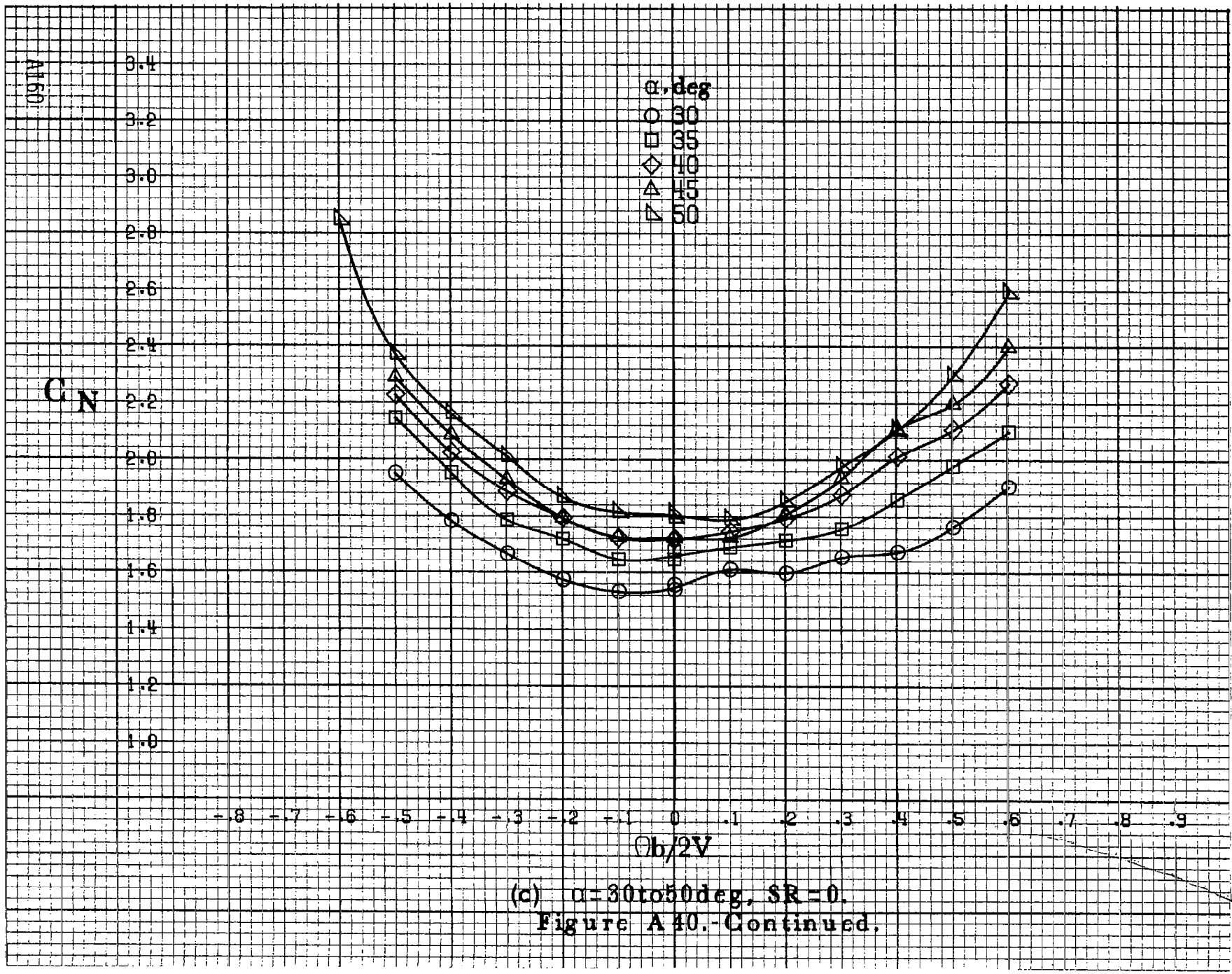

(c) α = 30 to 50 deg, SR = 0.

Figure A 40.- Continued.

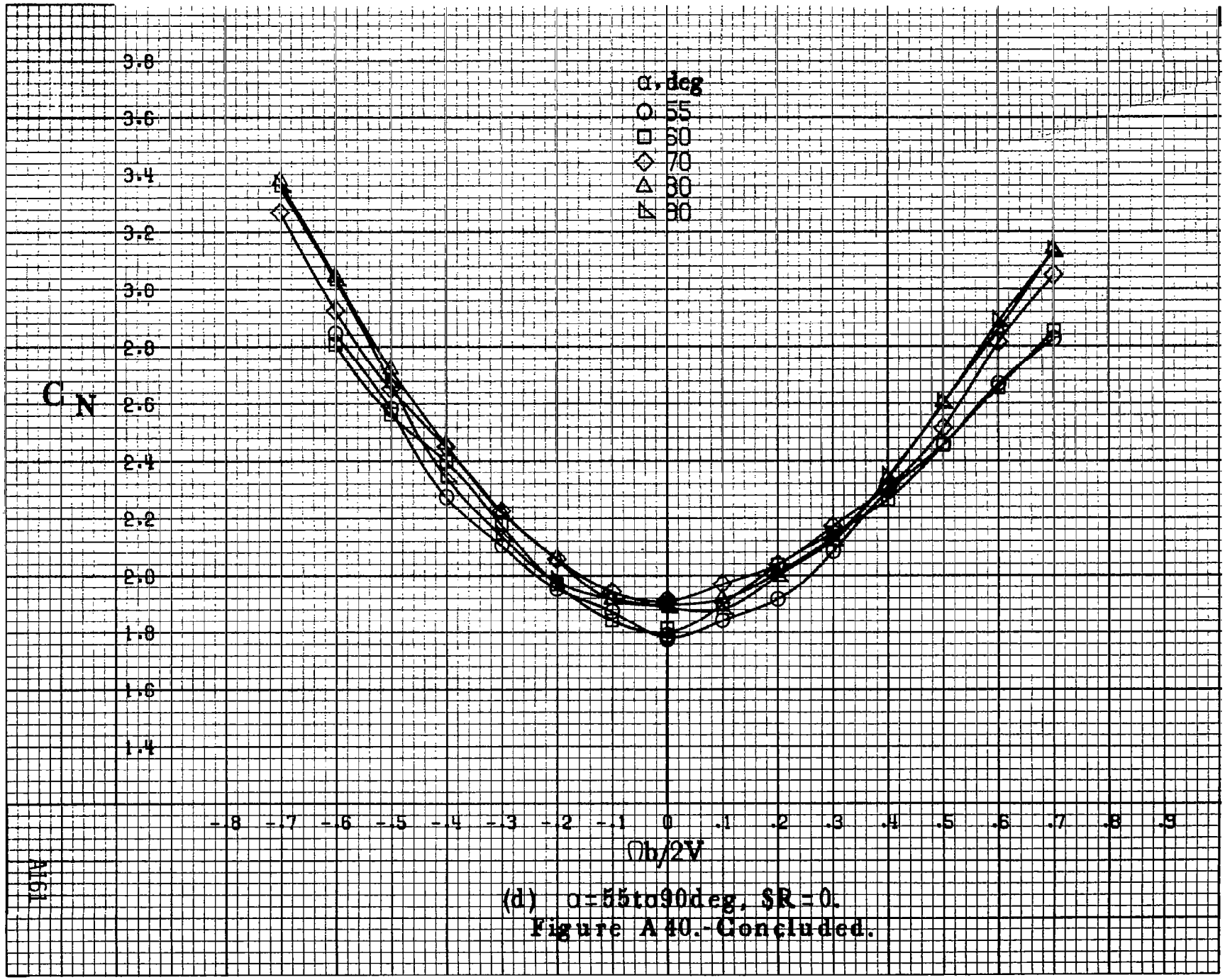

(d) α=55to90deg, $R=0.

Figure A40.-Concluded.

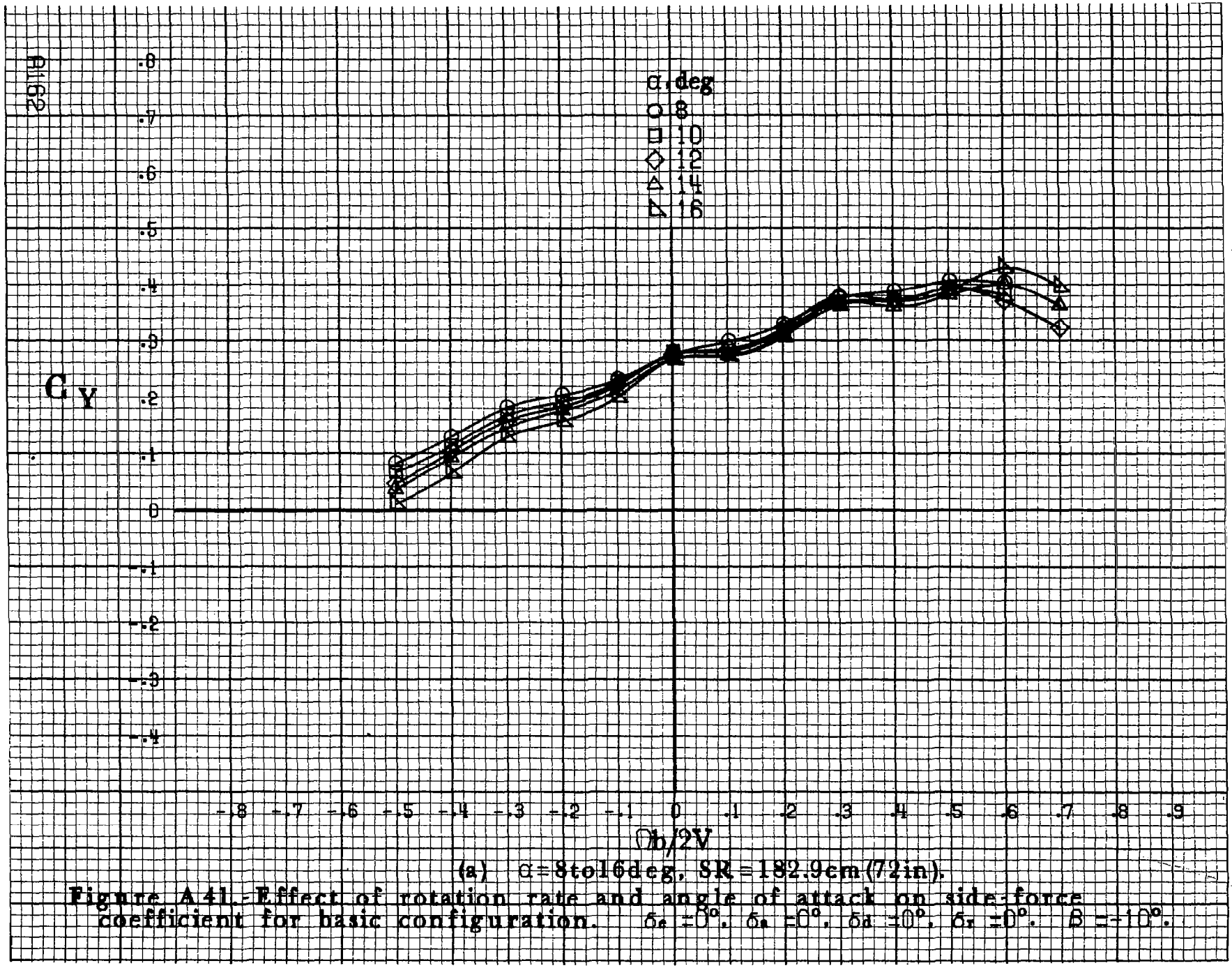

(a) $\alpha = 8$ to 16 deg, SR = 182.9 cm (72 in).

Figure A41.- Effect of rotation rate and angle of attack on side-force coefficient for basic configuration. $\delta_e = 0°$, $\delta_a = 0°$, $\delta_d = 0°$, $\delta_r = 0°$, $\beta = -10°$.

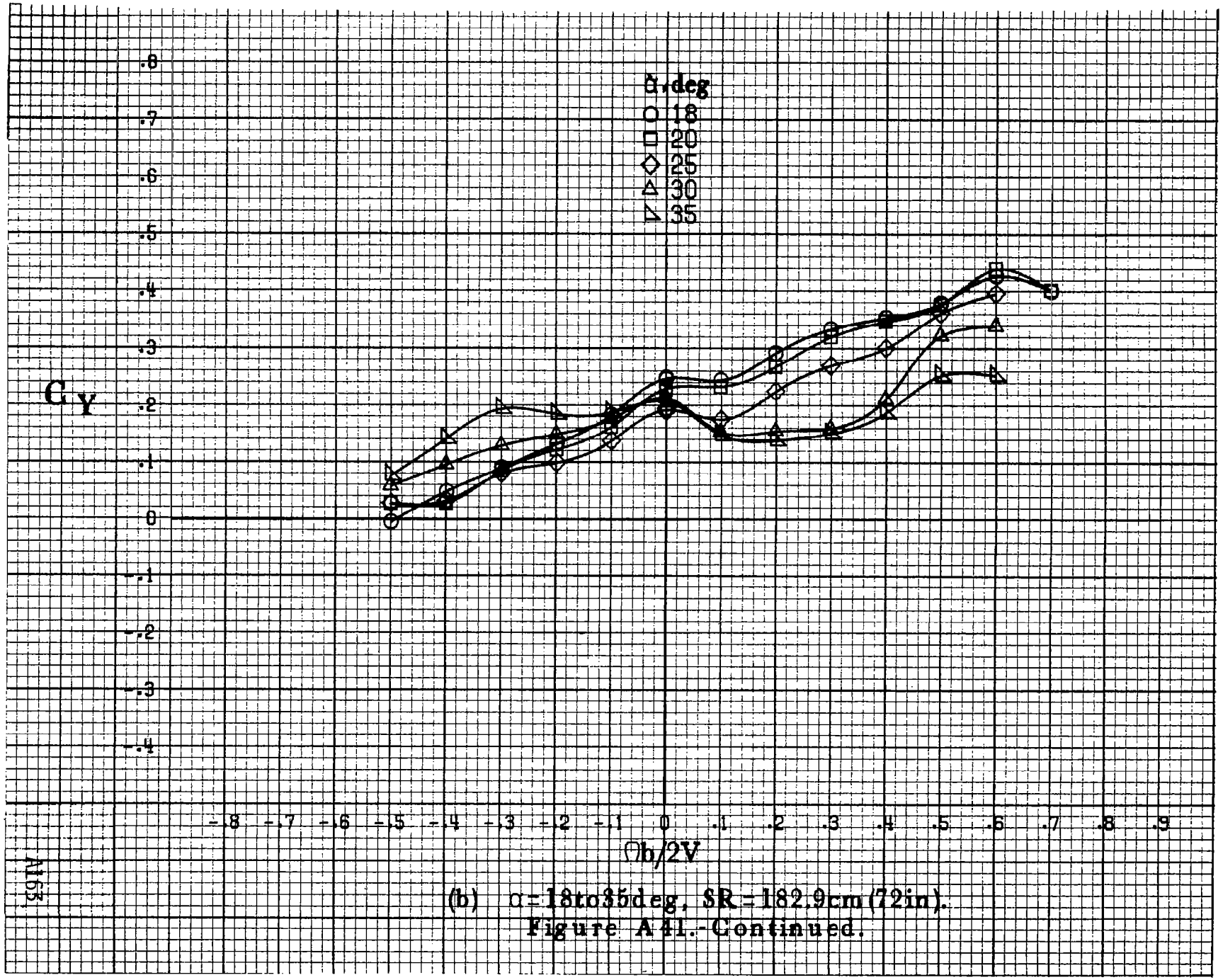

A163

(b) $\alpha = 18$ to 35 deg, SR = 182.9 cm (72 in).

Figure A41.-Continued.

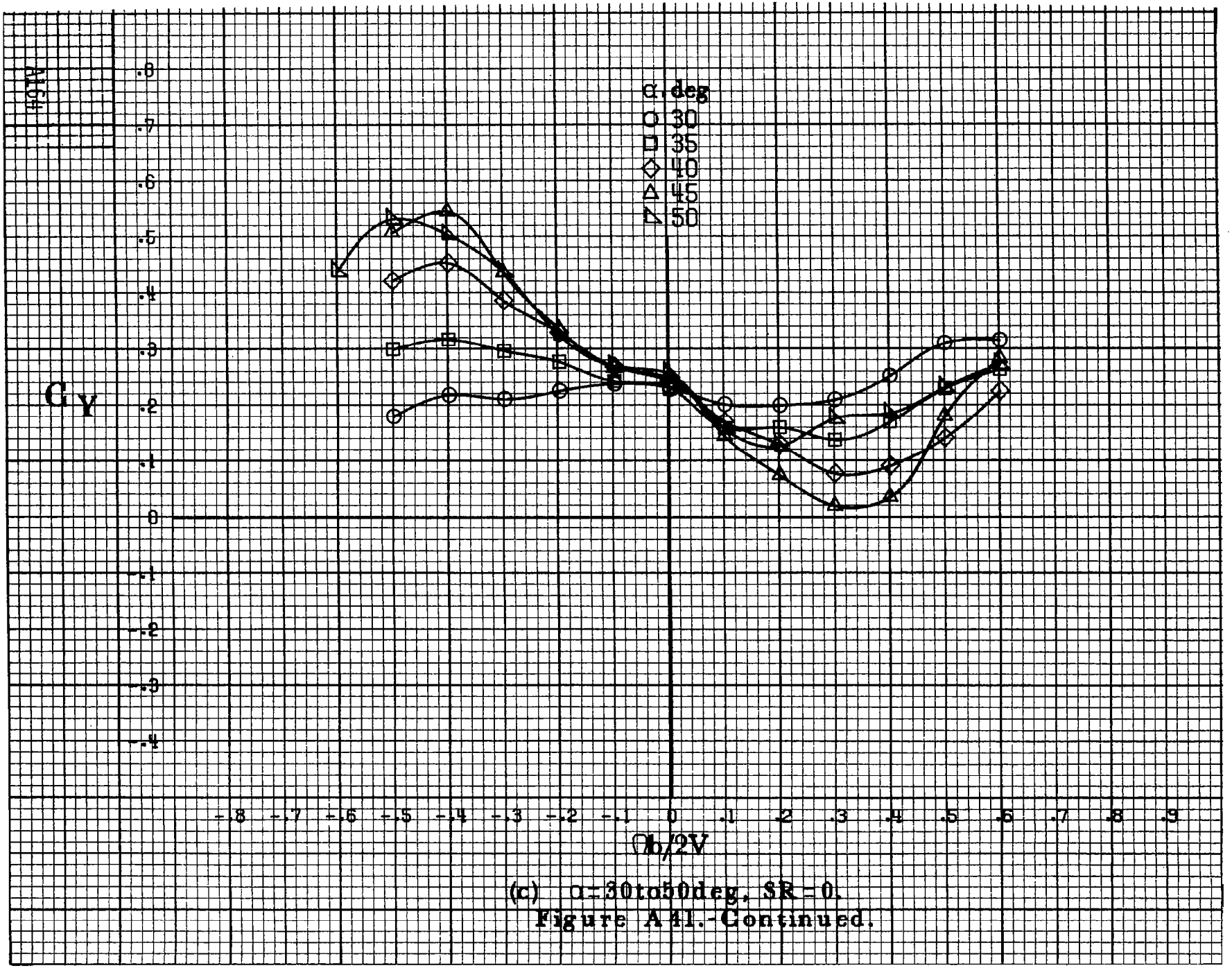

(c) α=30to50deg, SR=0.

Figure A41.-Continued.

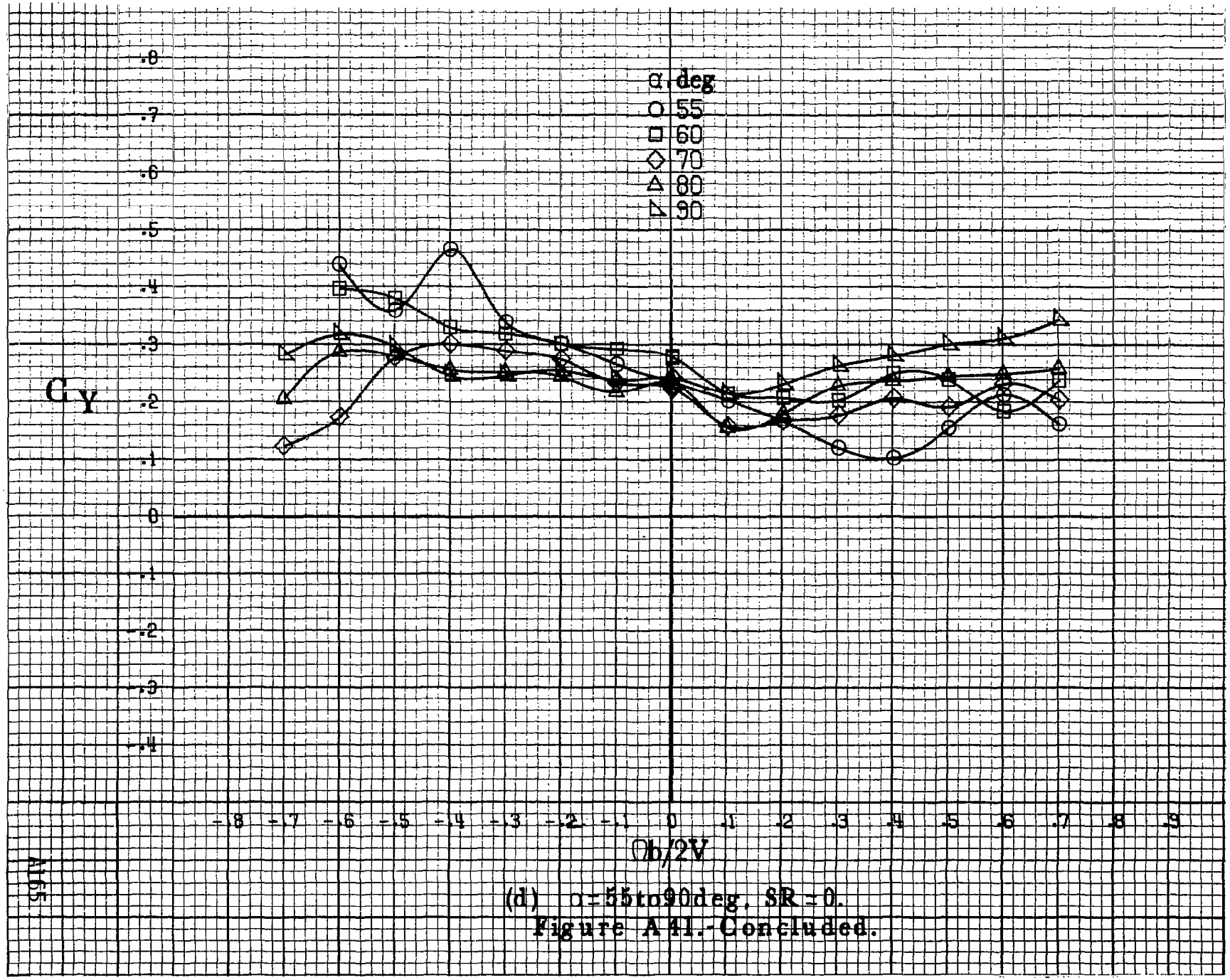

(d) $\alpha = 55$ to 90 deg, SR = 0.

Figure A41.-Concluded.

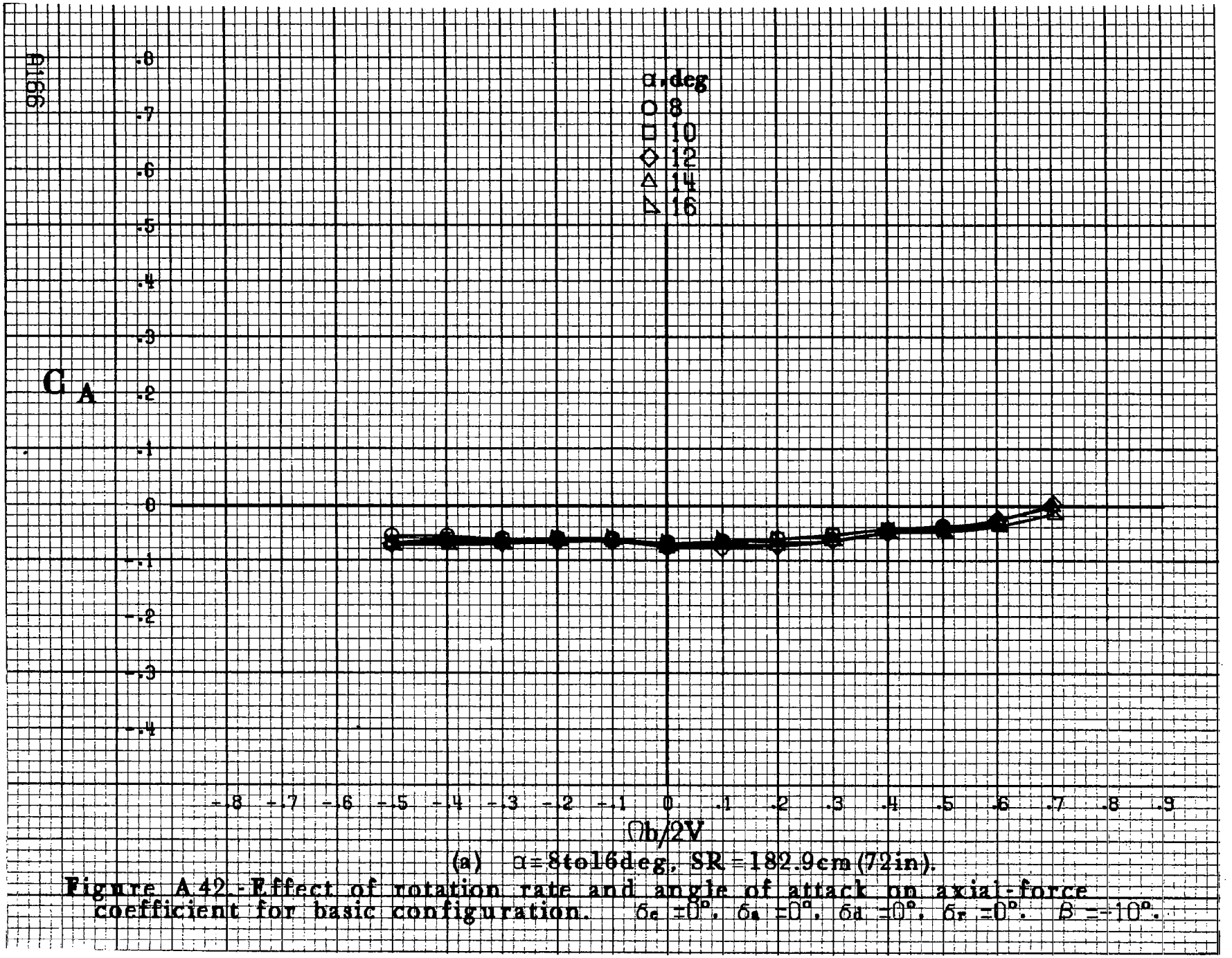

(a) $\alpha = 8$ to 16 deg, SR = 182.9 cm (72 in).

Figure A.42.- Effect of rotation rate and angle of attack on axial-force coefficient for basic configuration. $\delta_e = 0°$, $\delta_a = 0°$, $\delta_d = 0°$, $\delta_r = 0°$, $\beta = -10°$.

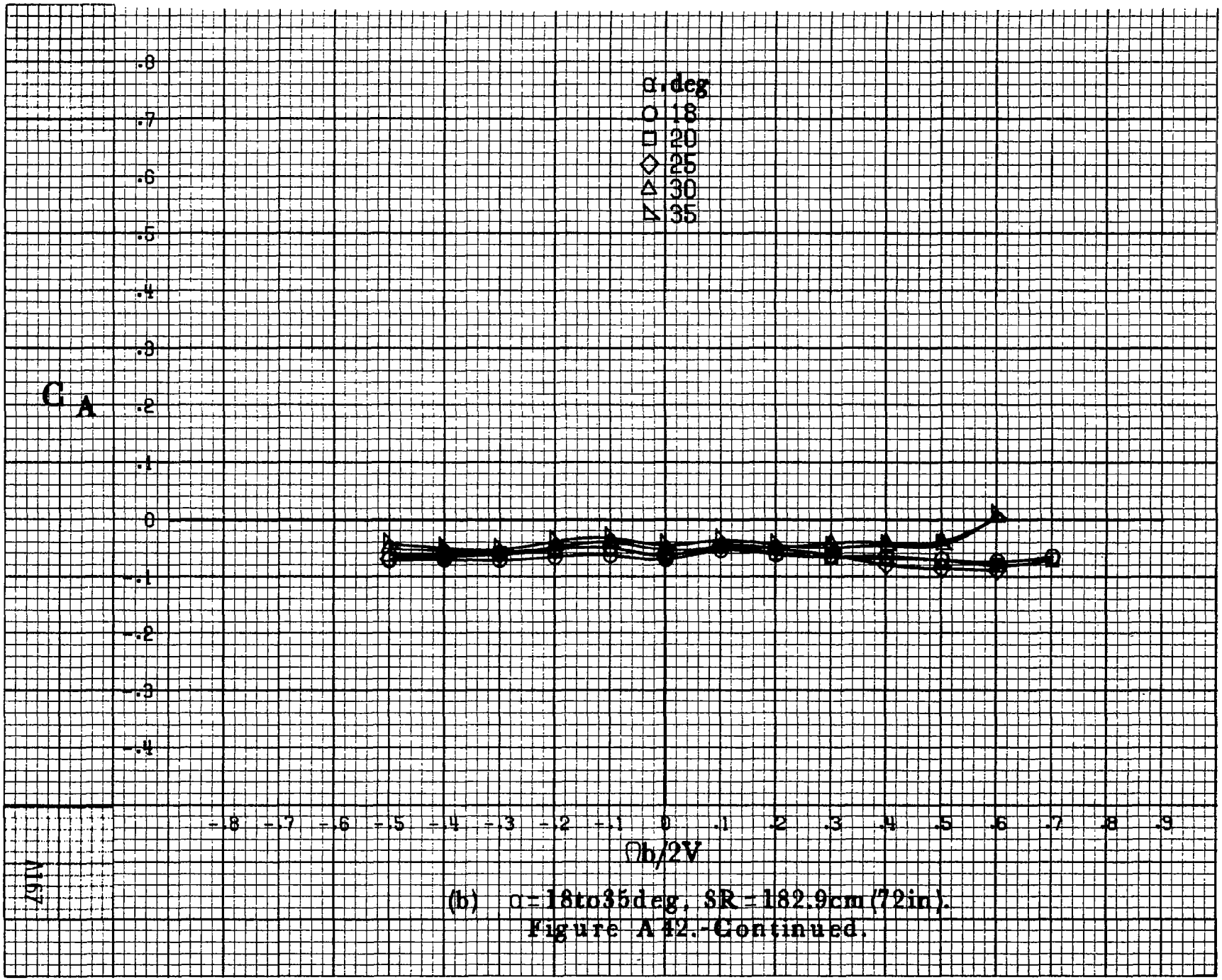

(b) α = 18 to 35 deg, SR = 182.9 cm (72 in).

Figure A42.-Continued.

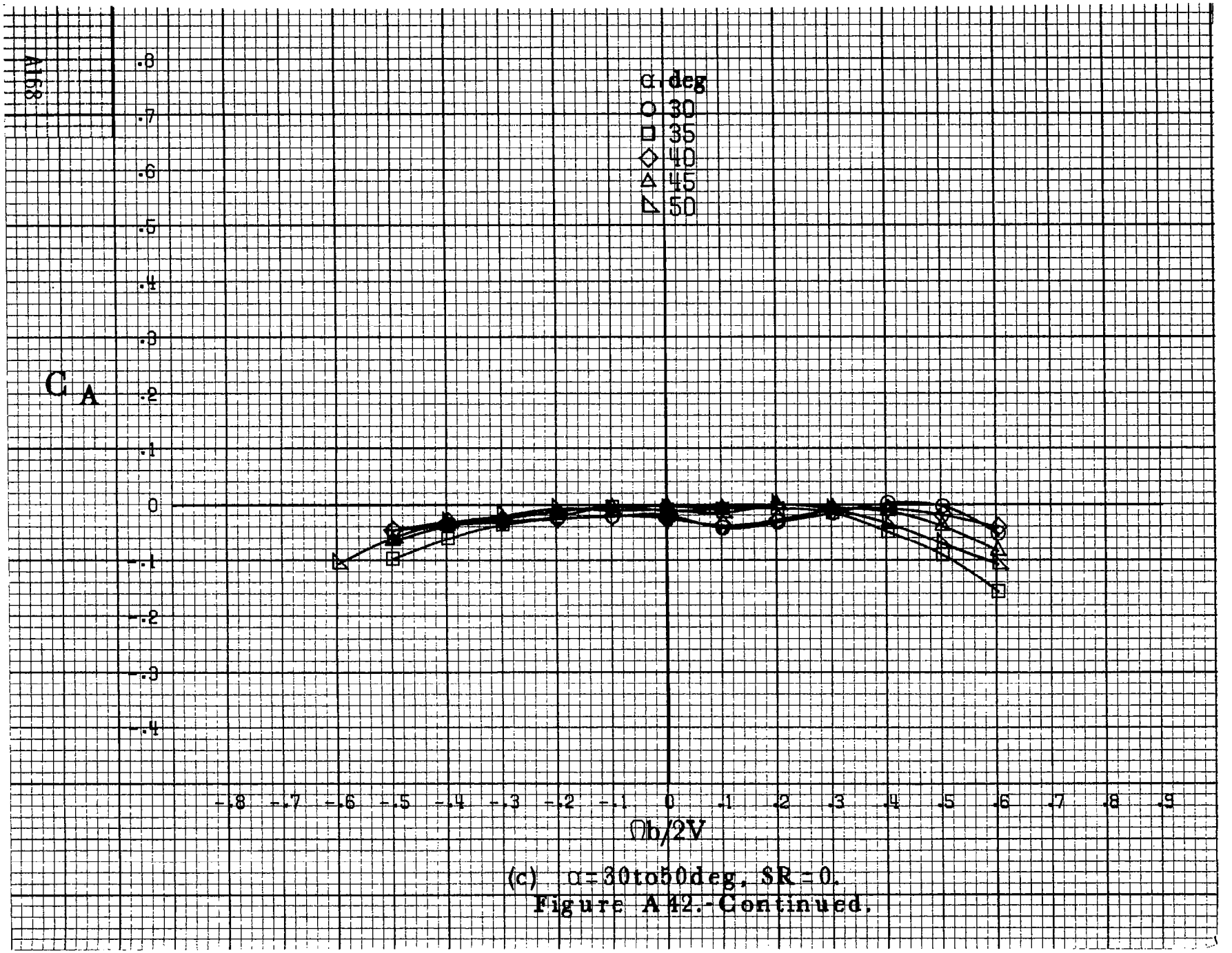

(c) $\alpha = 30$ to 50 deg, $\$R = 0$.

Figure A42.- Continued.

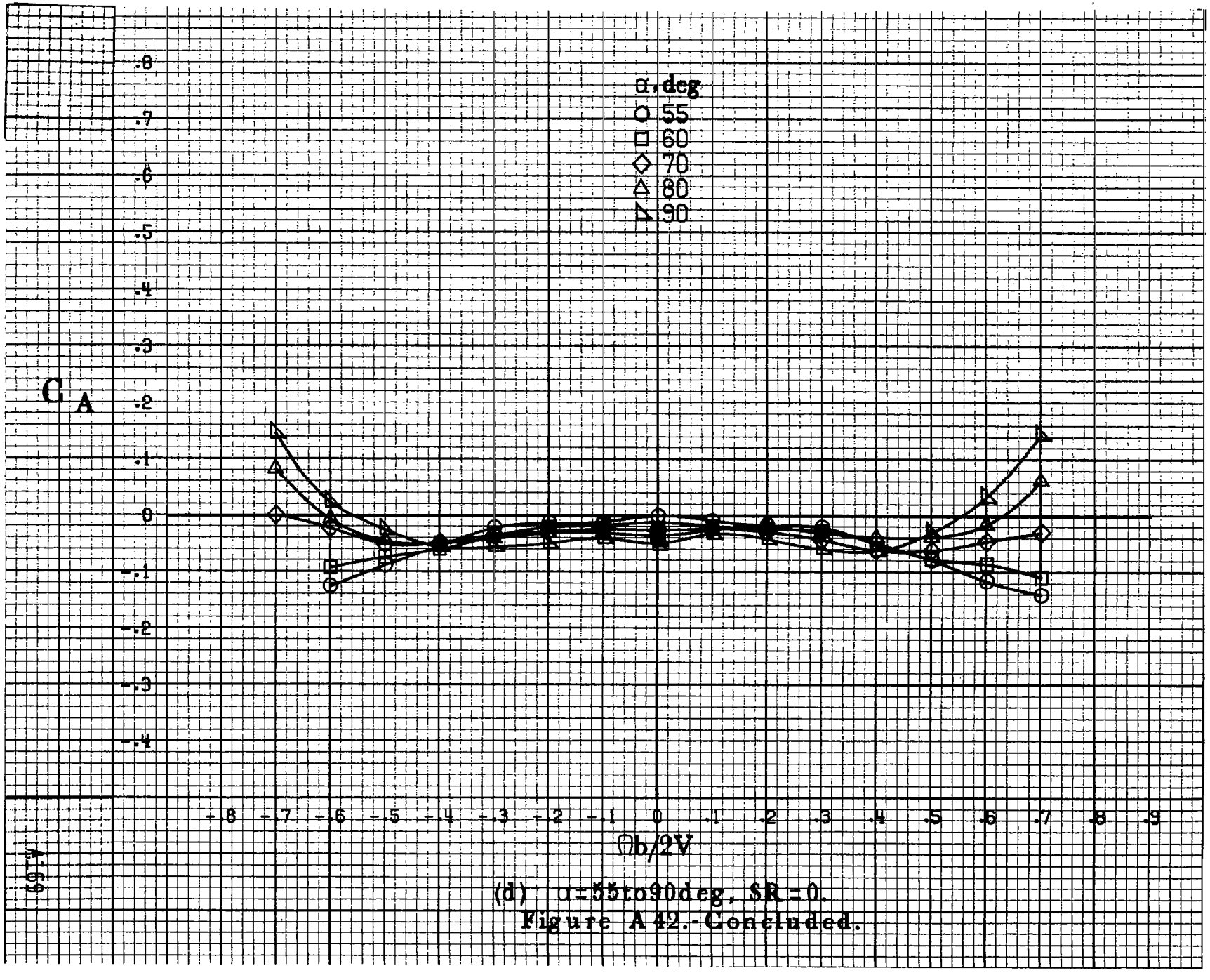

(d) α=55to90deg, $\delta_R = 0$.

Figure A42.-Concluded.

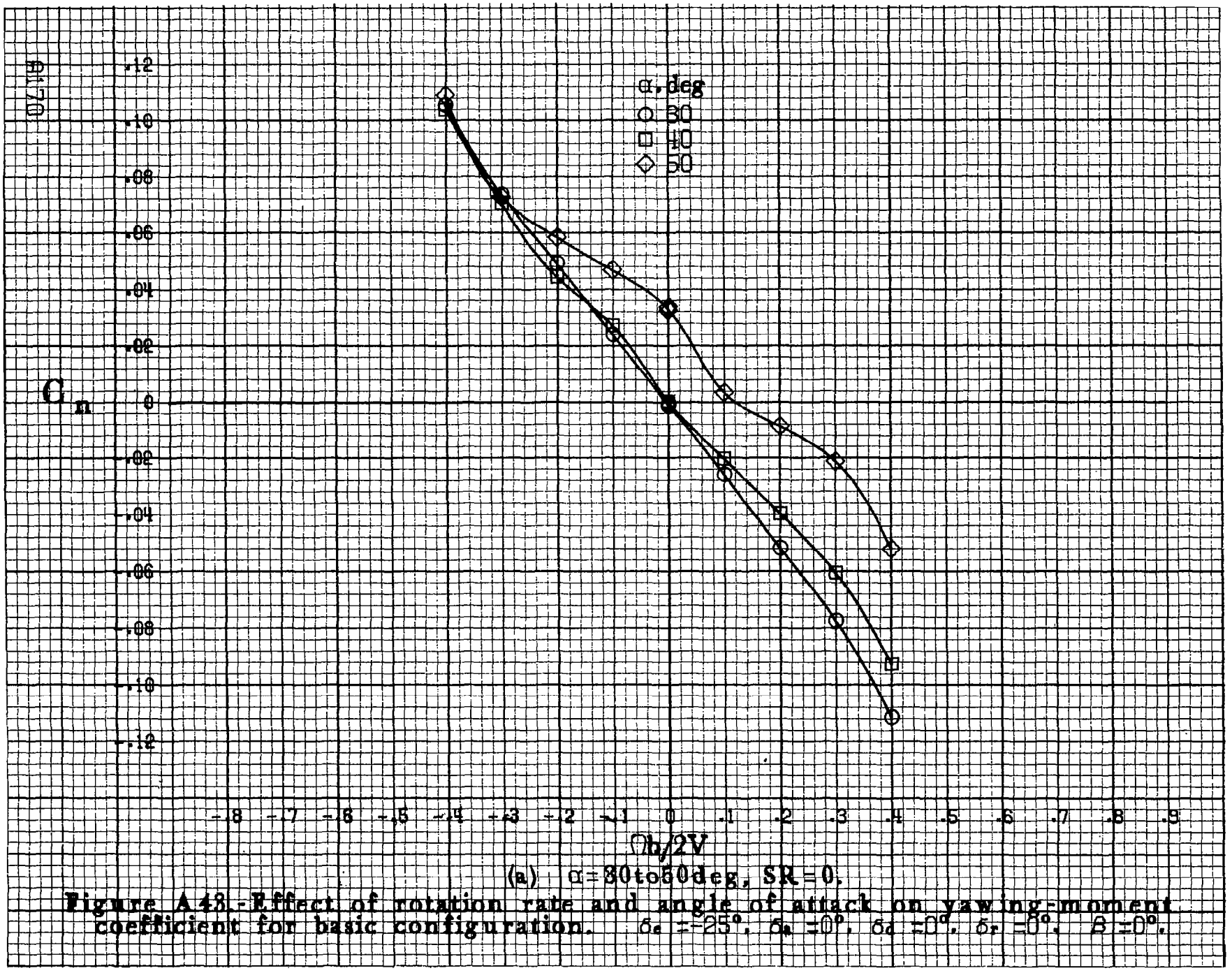

(a) $\alpha = 30$ to 50 deg, SR = 0.

Figure A43.- Effect of rotation rate and angle of attack on yawing-moment coefficient for basic configuration. $\delta_e = -25°$, $\delta_a = 0°$, $\delta_d = 0°$, $\delta_r = 0°$, $\beta = 0°$.

(b) α=55 to 90 deg, δR=0.

Figure A13.- Concluded.

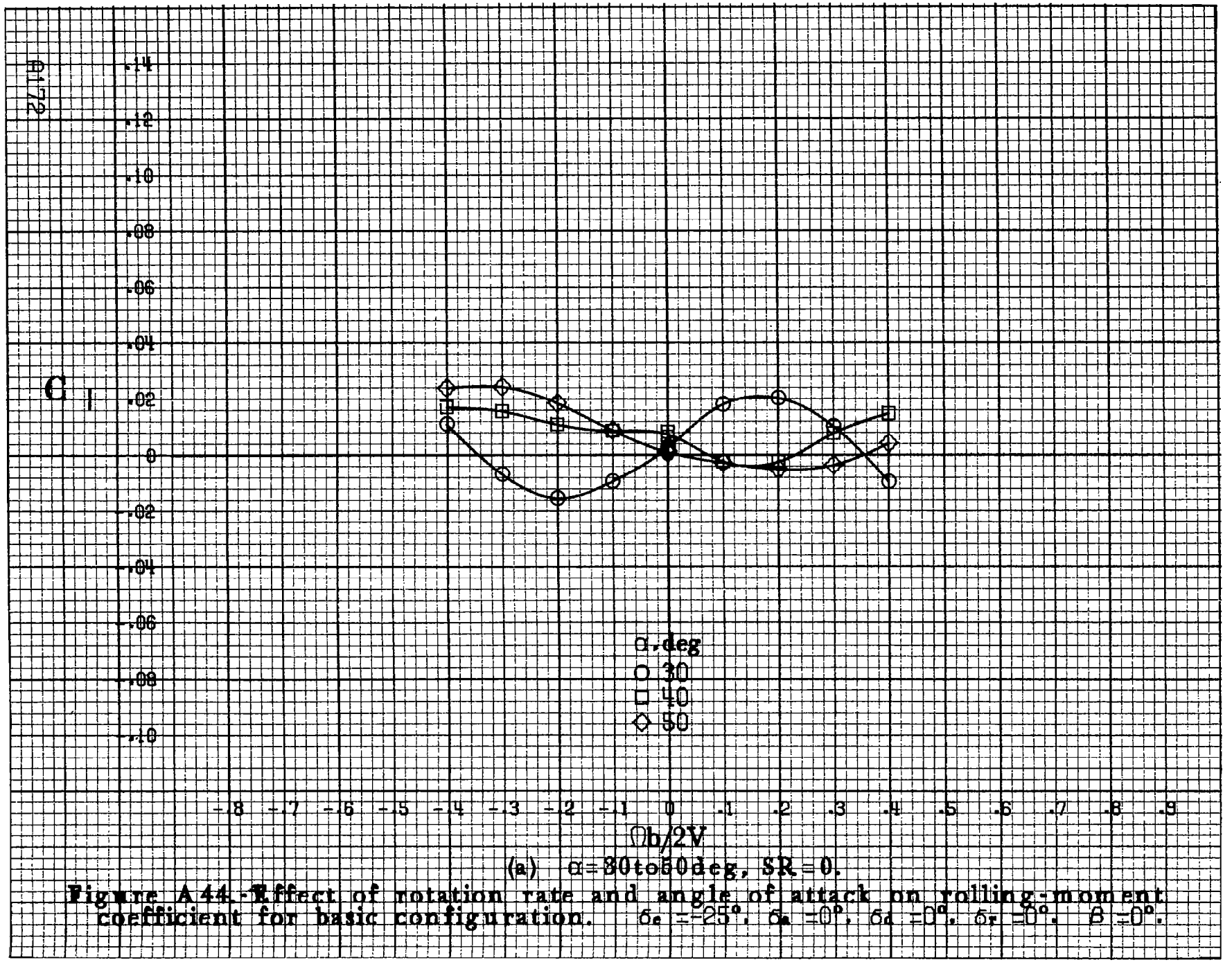

(a) $\alpha = 30$ to 50 deg, $SR = 0$.

Figure A44.- Effect of rotation rate and angle of attack on rolling-moment coefficient for basic configuration. $\delta_e = -25°$, $\delta_a = 0°$, $\delta_d = 0°$, $\delta_r = 0°$, $\beta = 0°$.

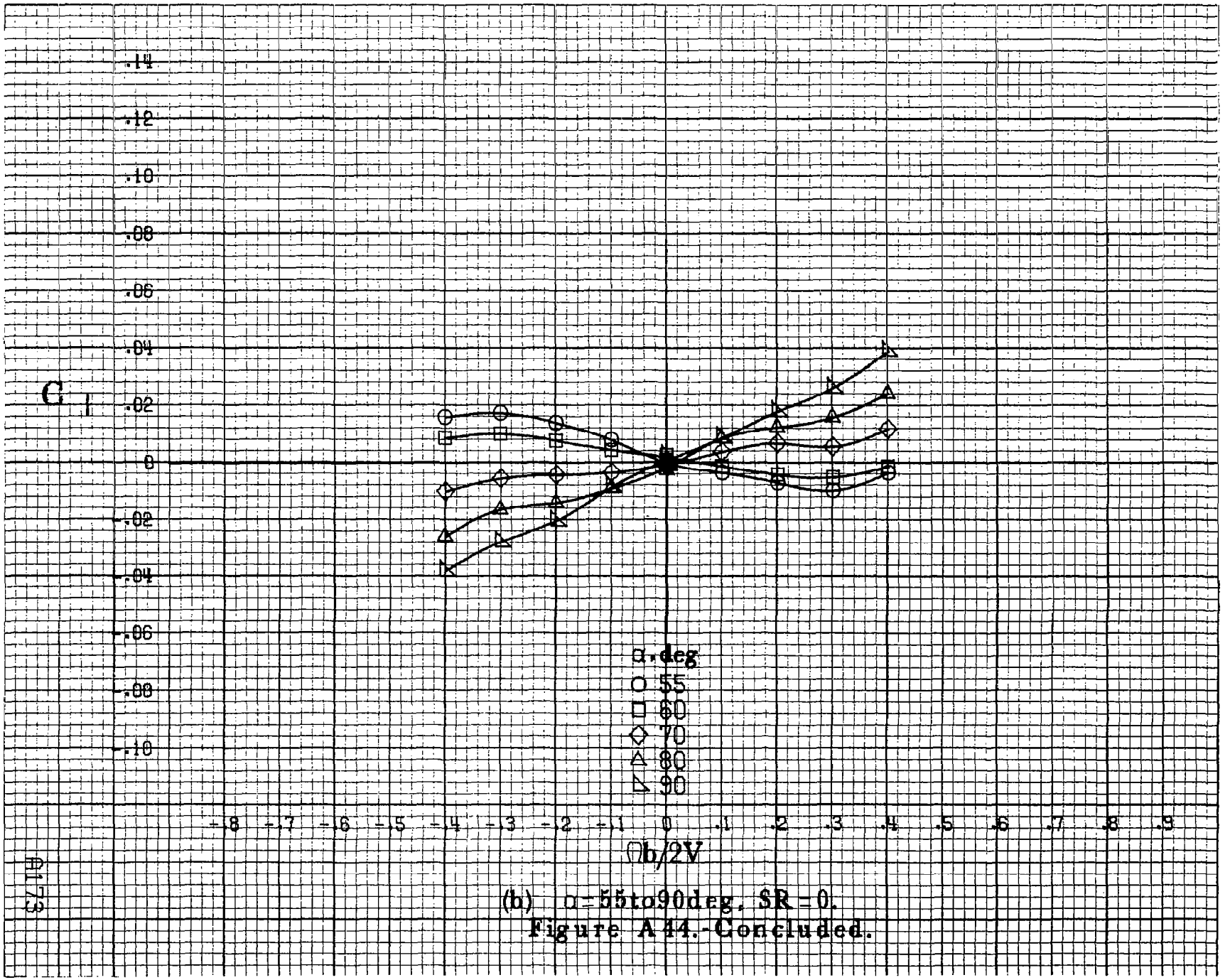

(b) α=55to90deg, SR=0.

Figure A 44.-Concluded.

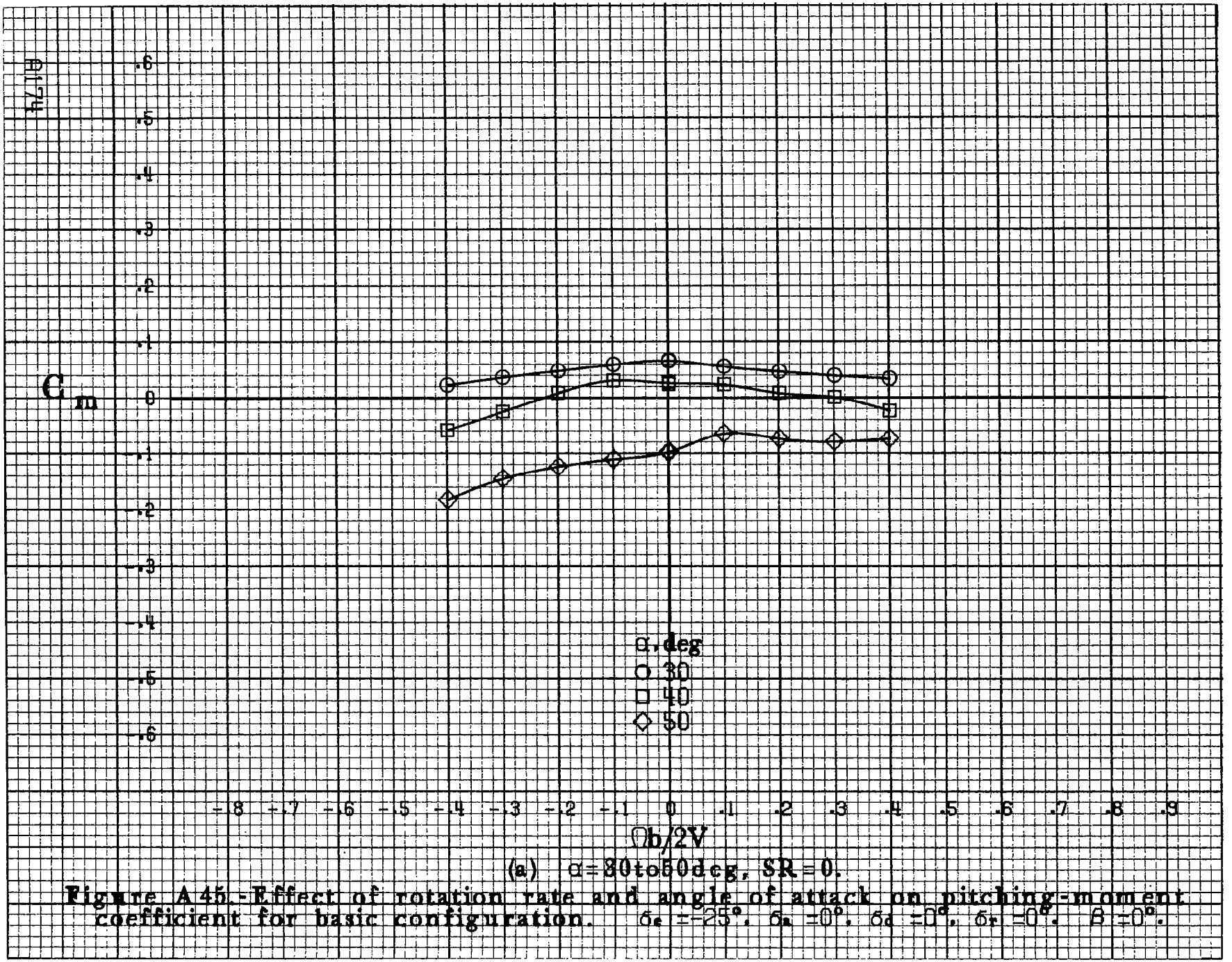

(a) $\alpha = 80$ to 50 deg, $SR = 0$.

Figure A45.-Effect of rotation rate and angle of attack on pitching-moment coefficient for basic configuration. $\delta_e = -25°$, $\delta_a = 0°$, $\delta_d = 0°$, $\delta_r = 0°$, $\beta = 0°$.

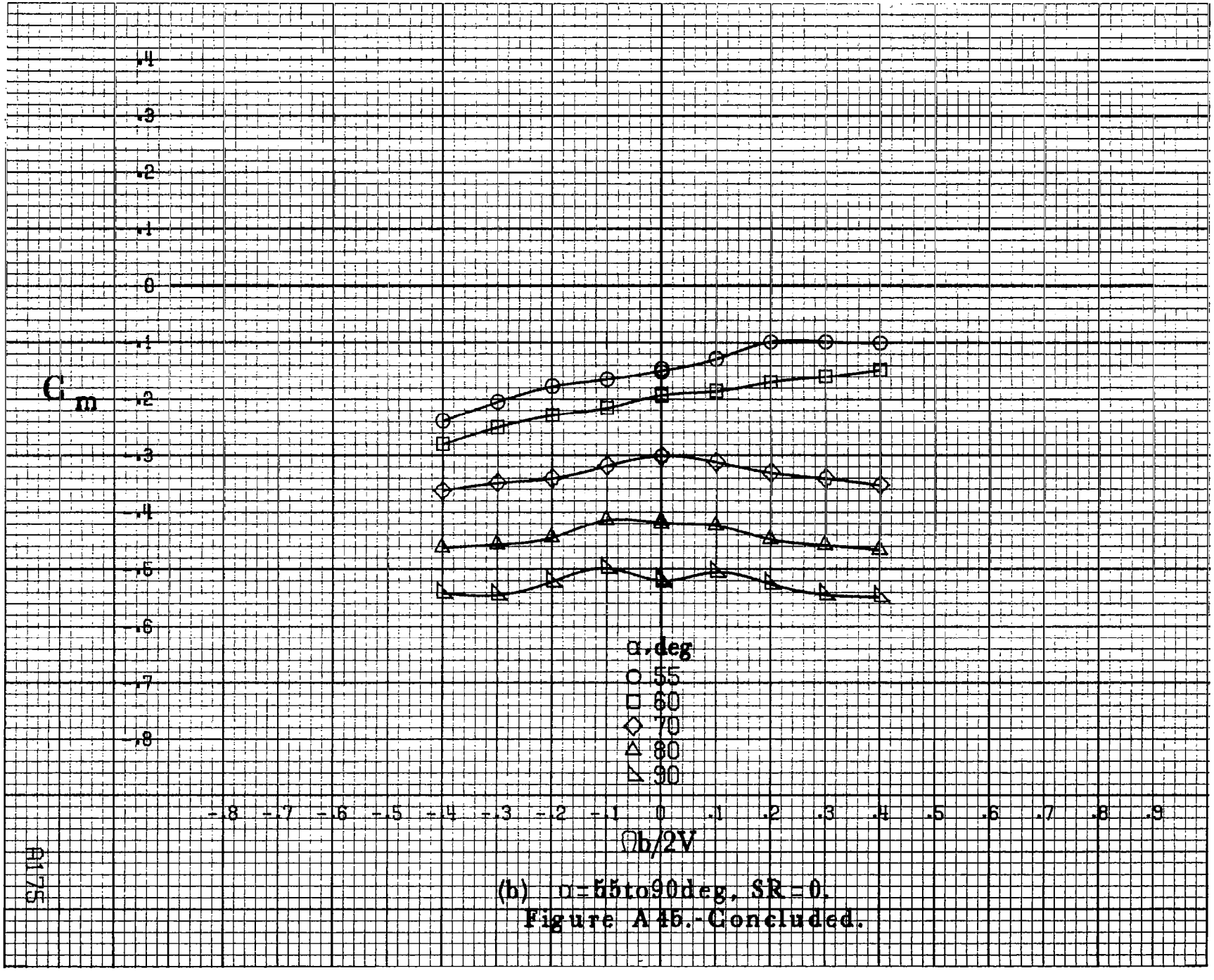

(b) α = 55 to 90 deg, SR = 0.

Figure A 45.- Concluded.

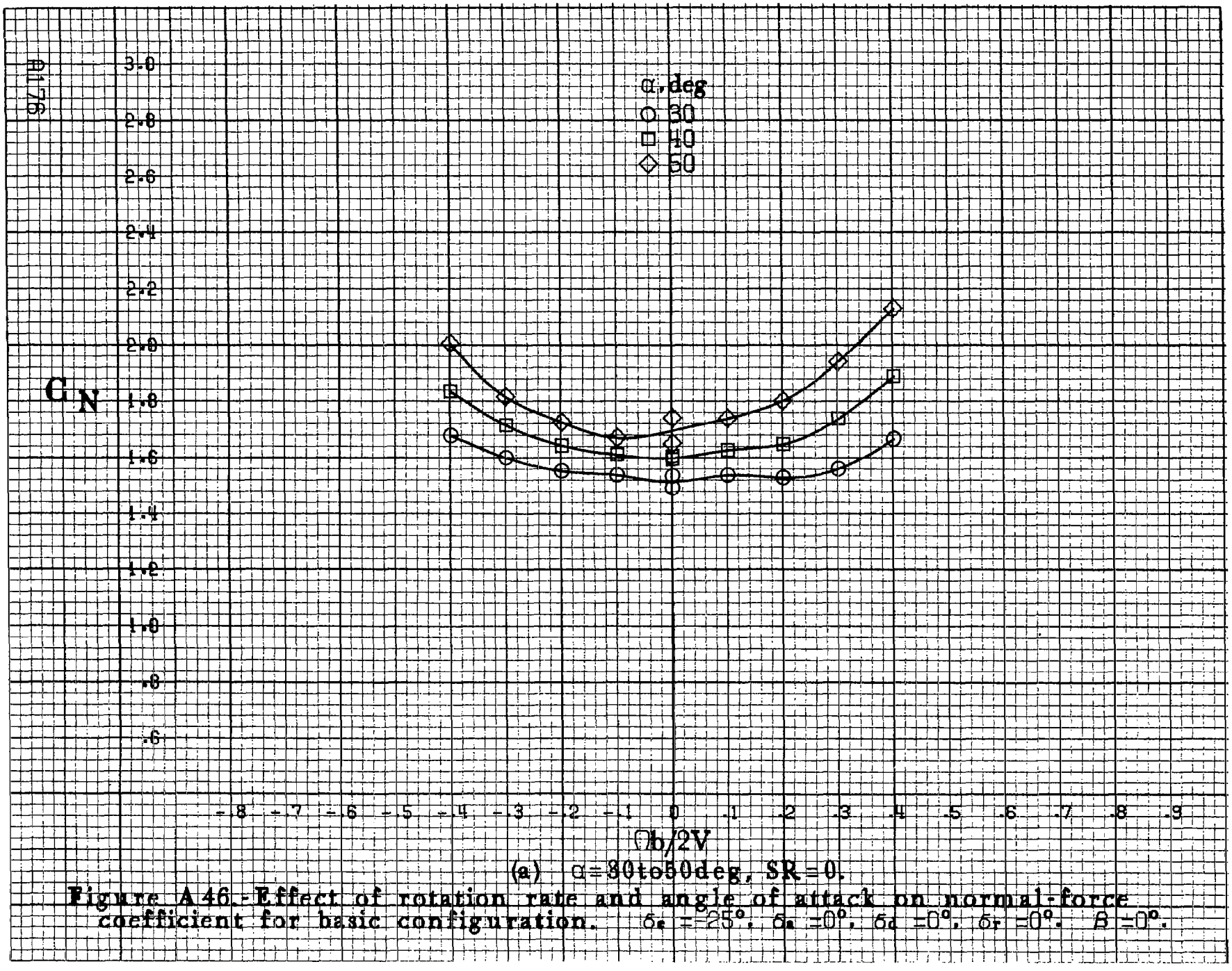

(a) $\alpha = 30$ to 50 deg, SR = 0.

Figure A46.- Effect of rotation rate and angle of attack on normal-force coefficient for basic configuration. $\delta_e = -25°$, $\delta_a = 0°$, $\delta_d = 0°$, $\delta_r = 0°$, $\beta = 0°$.

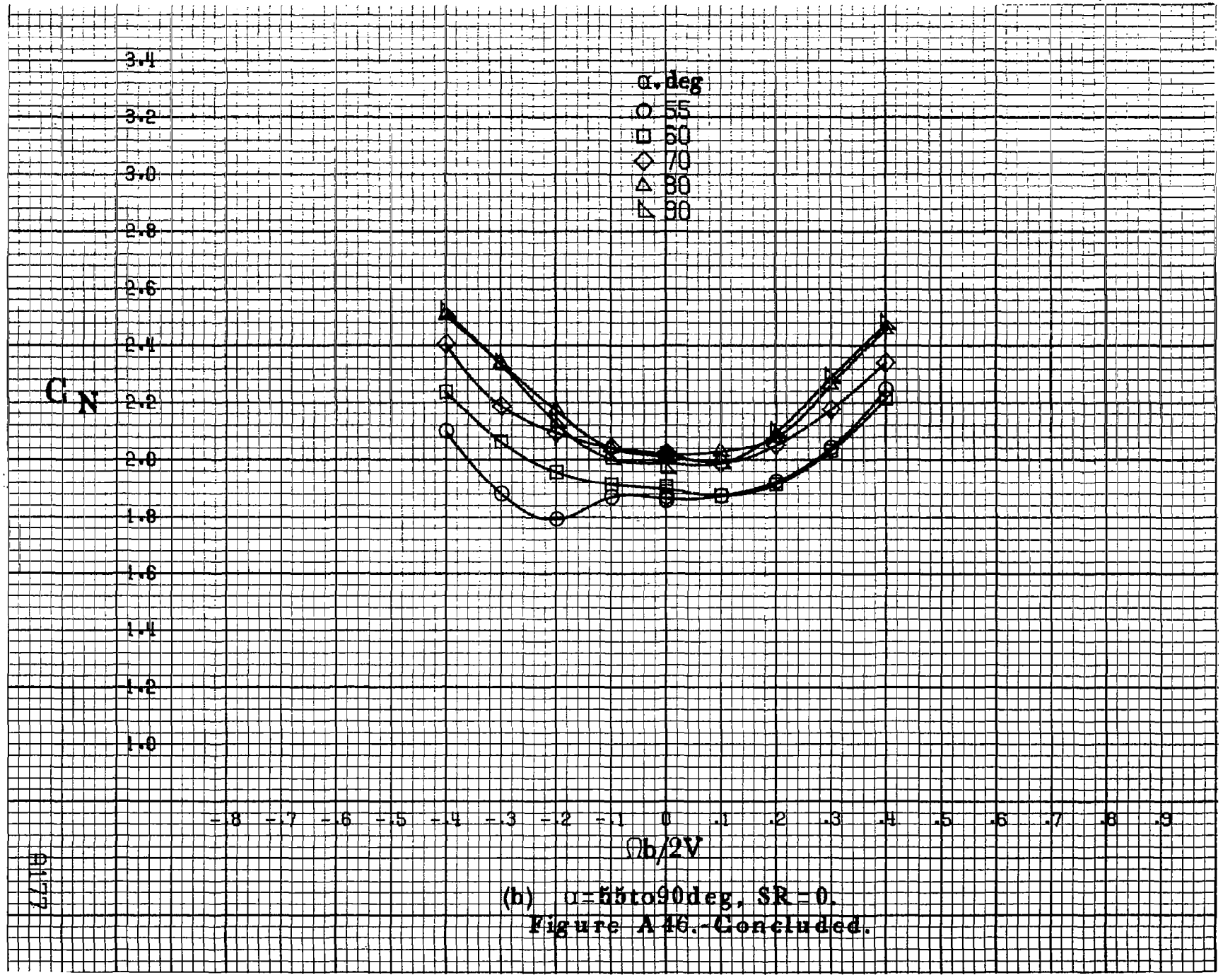

(b) α=55to90deg, SR=0.

Figure A16.-Concluded.

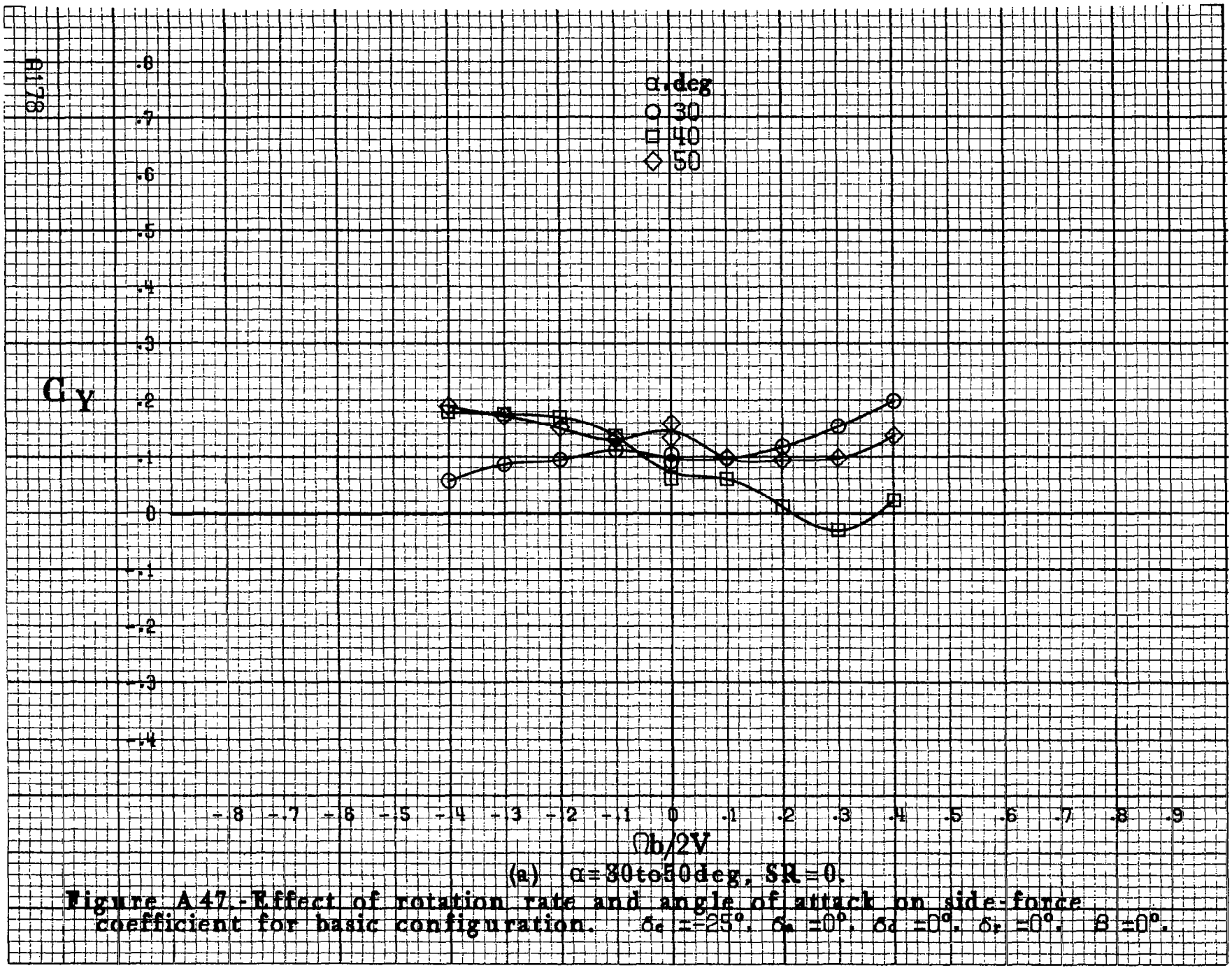

(a) $\alpha = 30$ to 50 deg, SR = 0.

Figure A47.- Effect of rotation rate and angle of attack on side-force coefficient for basic configuration. $\delta_e = -25°$, $\delta_a = 0°$, $\delta_d = 0°$, $\delta_r = 0°$, $\beta = 0°$.

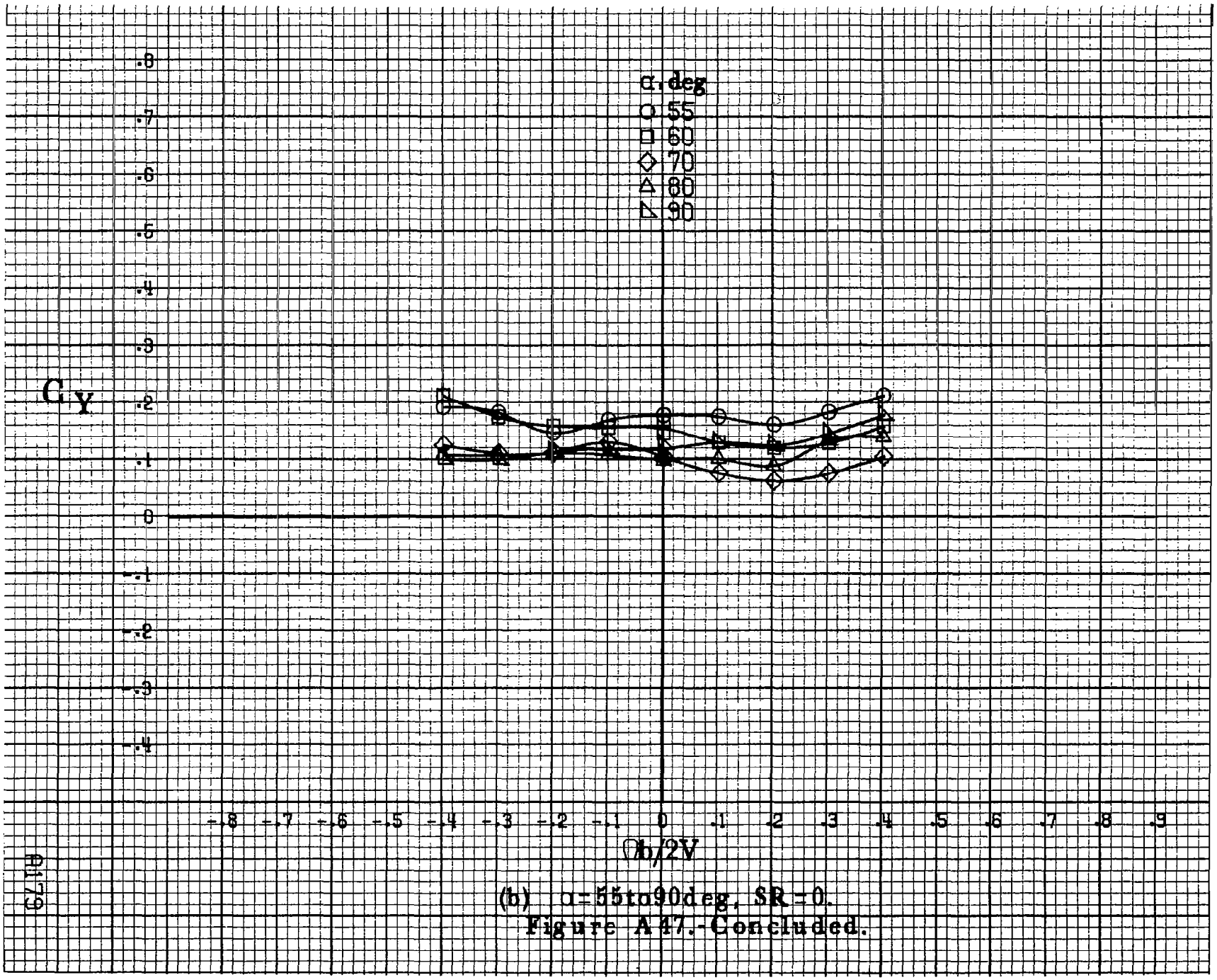

(b) $\alpha = 55$ to 90 deg, SR = 0.

Figure A47.- Concluded.

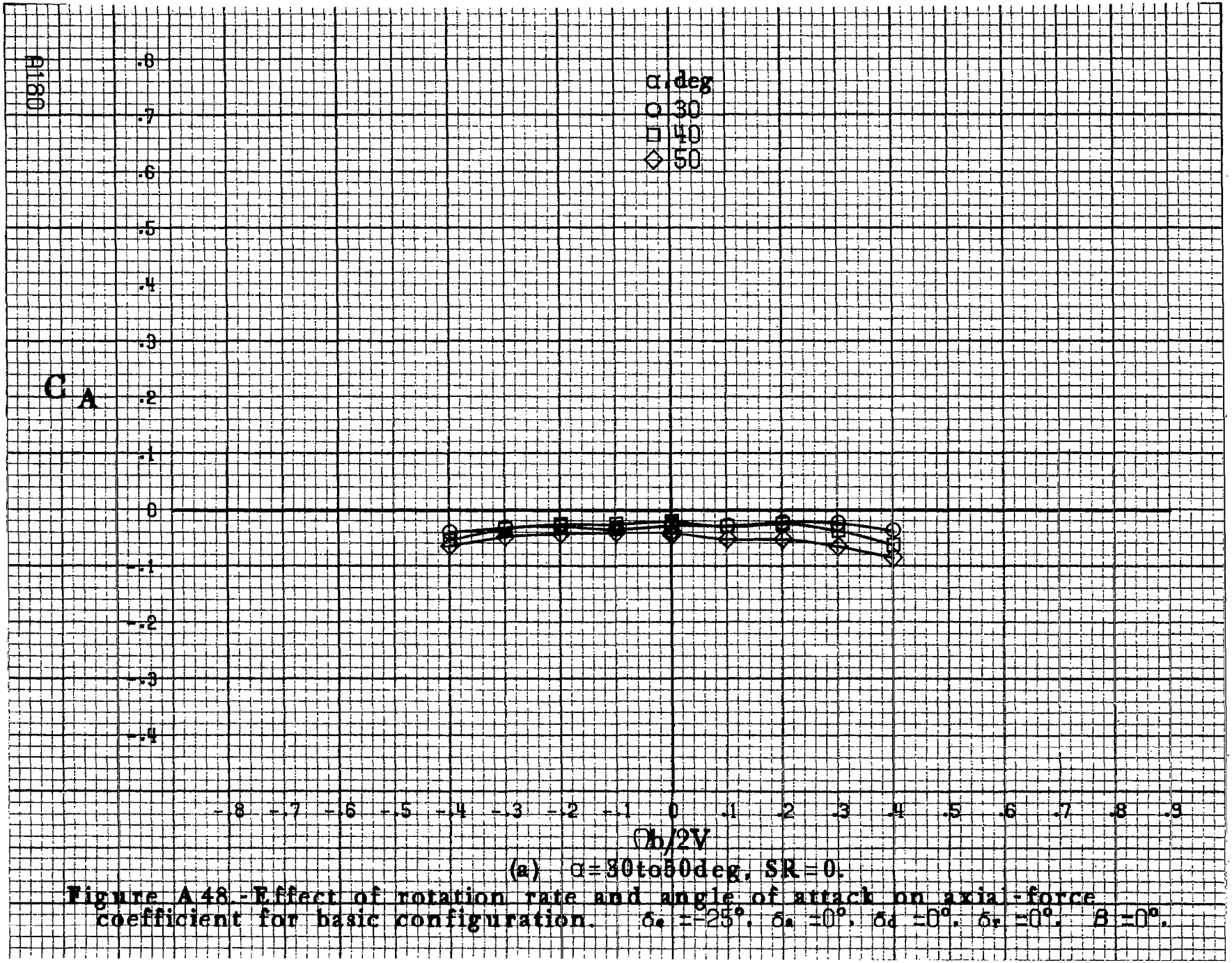

(a) α = 30 to 50 deg, SR = 0.

Figure A48.-Effect of rotation rate and angle of attack on axial-force coefficient for basic configuration. $\delta_e = -25°$, $\delta_a = 0°$, $\delta_d = 0°$, $\delta_r = 0°$, $\beta = 0°$.

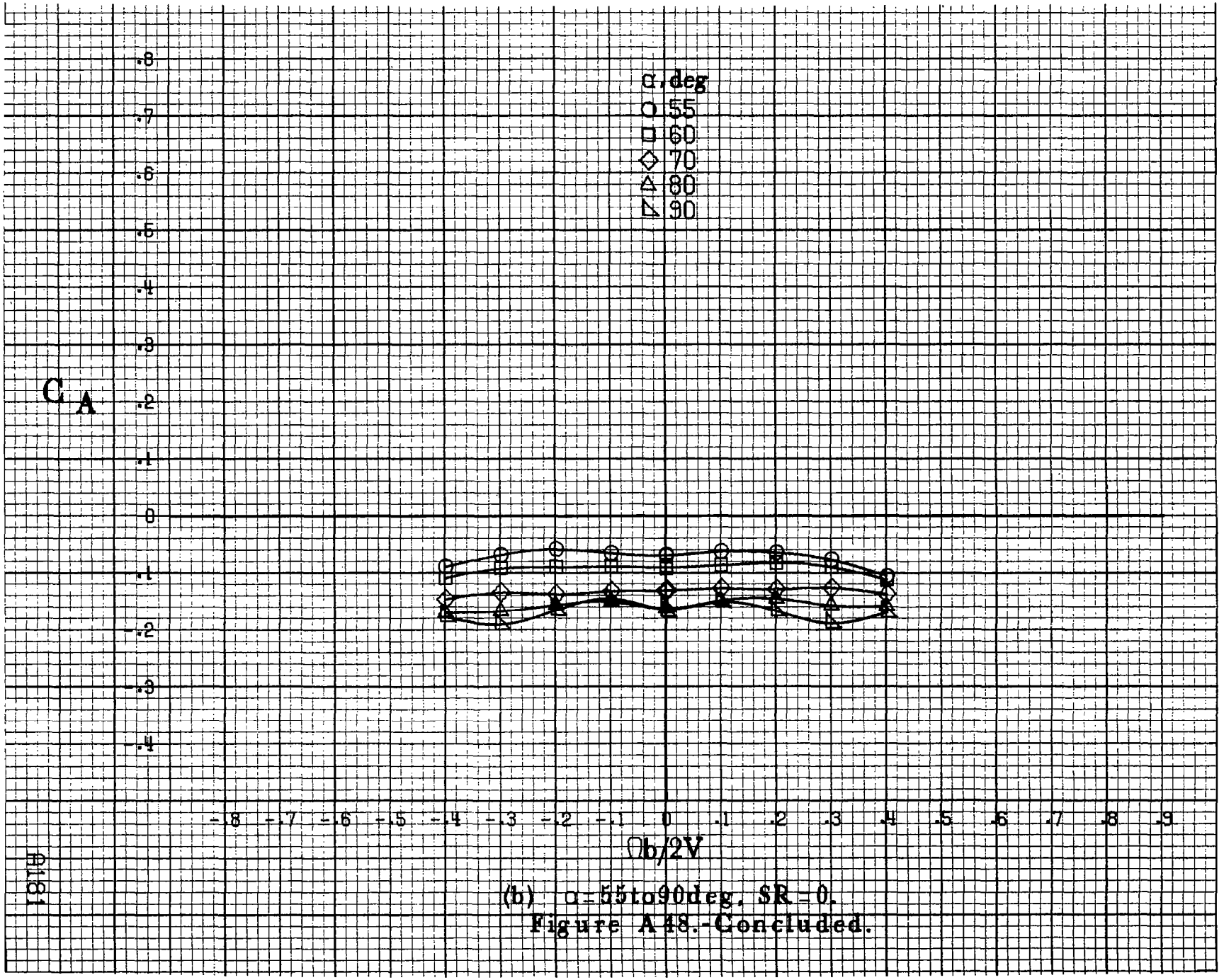

(b) α = 55 to 90 deg, SR = 0.

Figure A48.-Concluded.

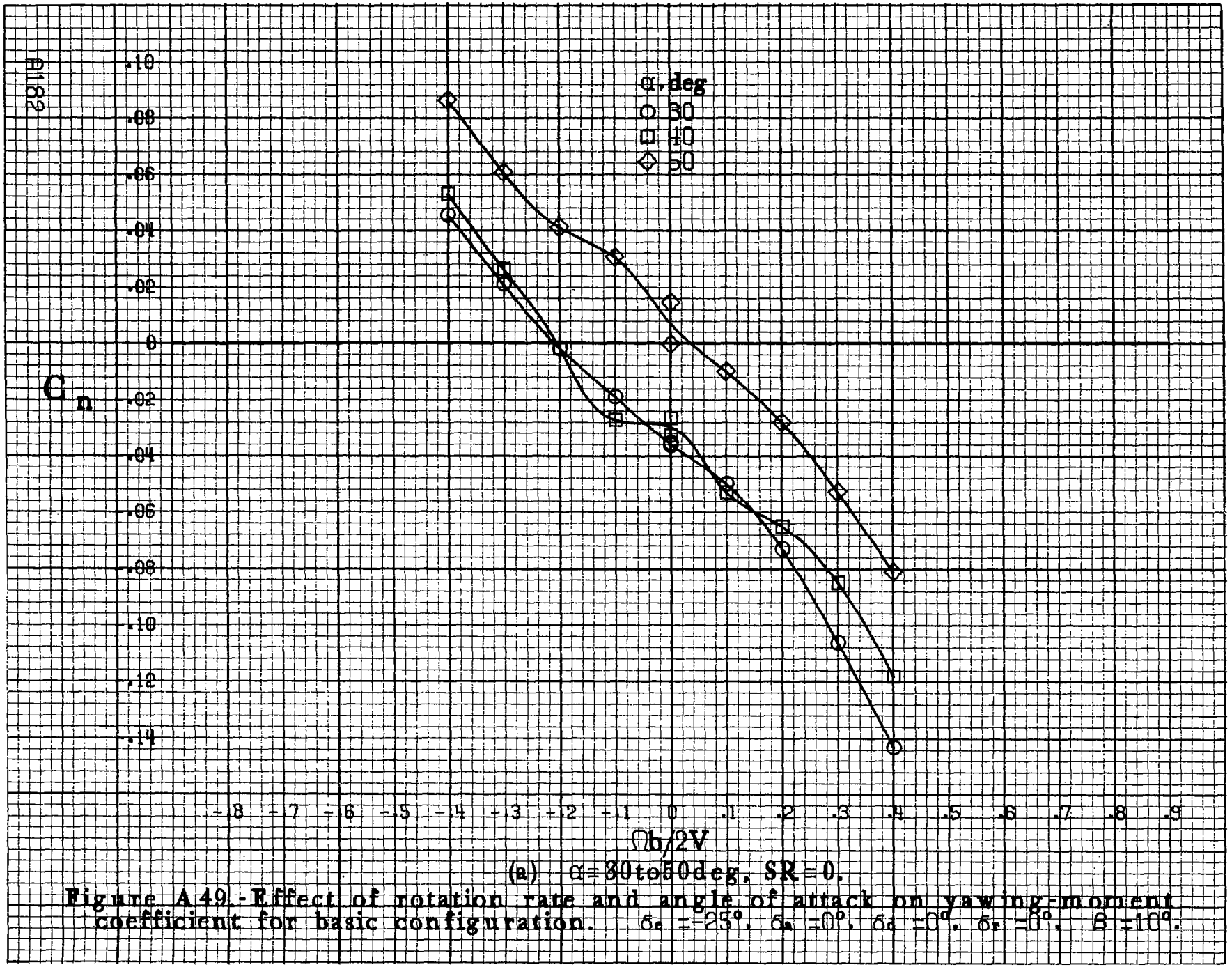

(a) $\alpha = 30$ to 50 deg, SR = 0.

Figure A49.- Effect of rotation rate and angle of attack on yawing-moment coefficient for basic configuration. $\delta_e = -25°$, $\delta_a = 0°$, $\delta_d = 0°$, $\delta_r = 0°$, $\beta = 10°$.

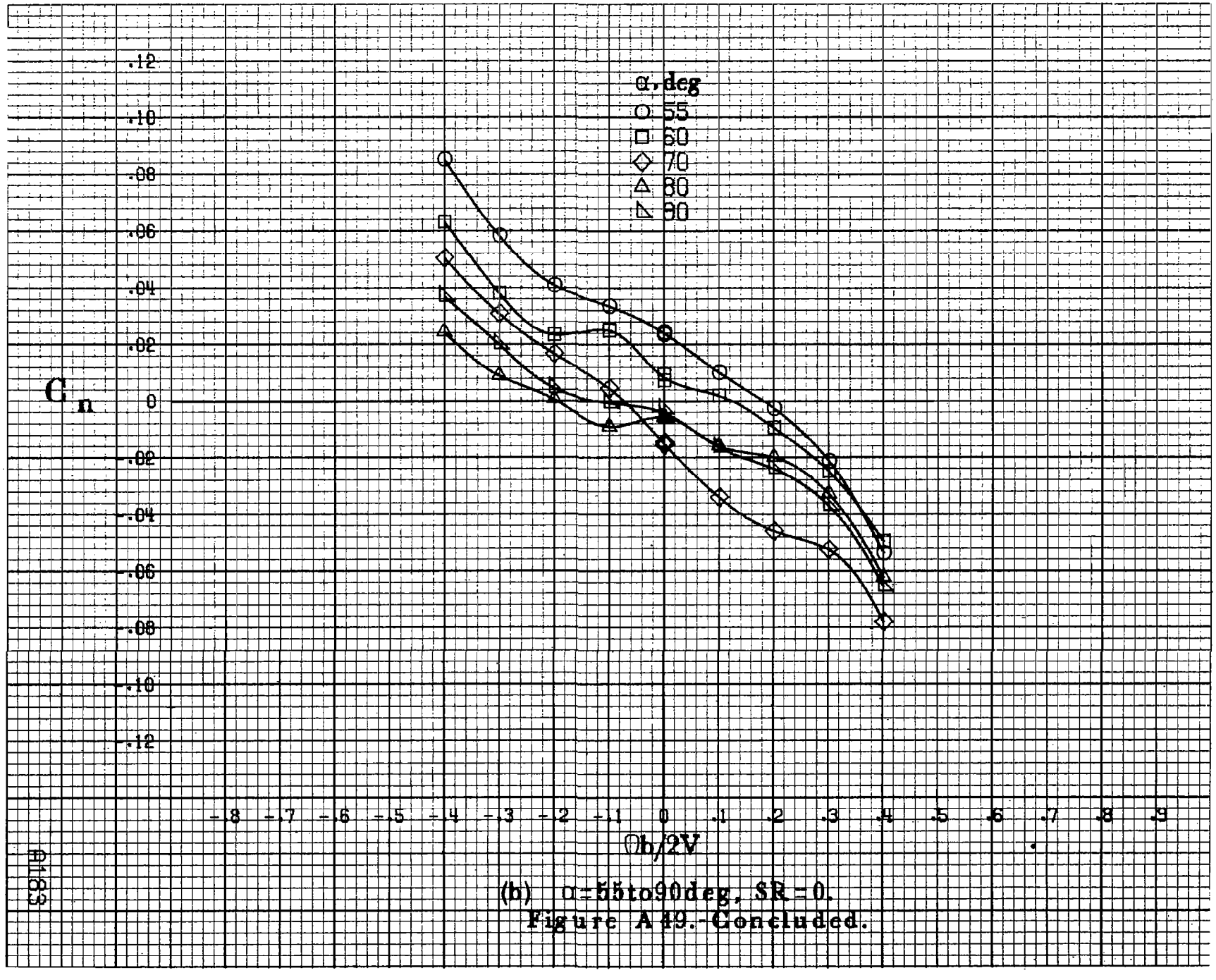

(b) $\alpha = 55$ to 90 deg, SR = 0.

Figure A49.- Concluded.

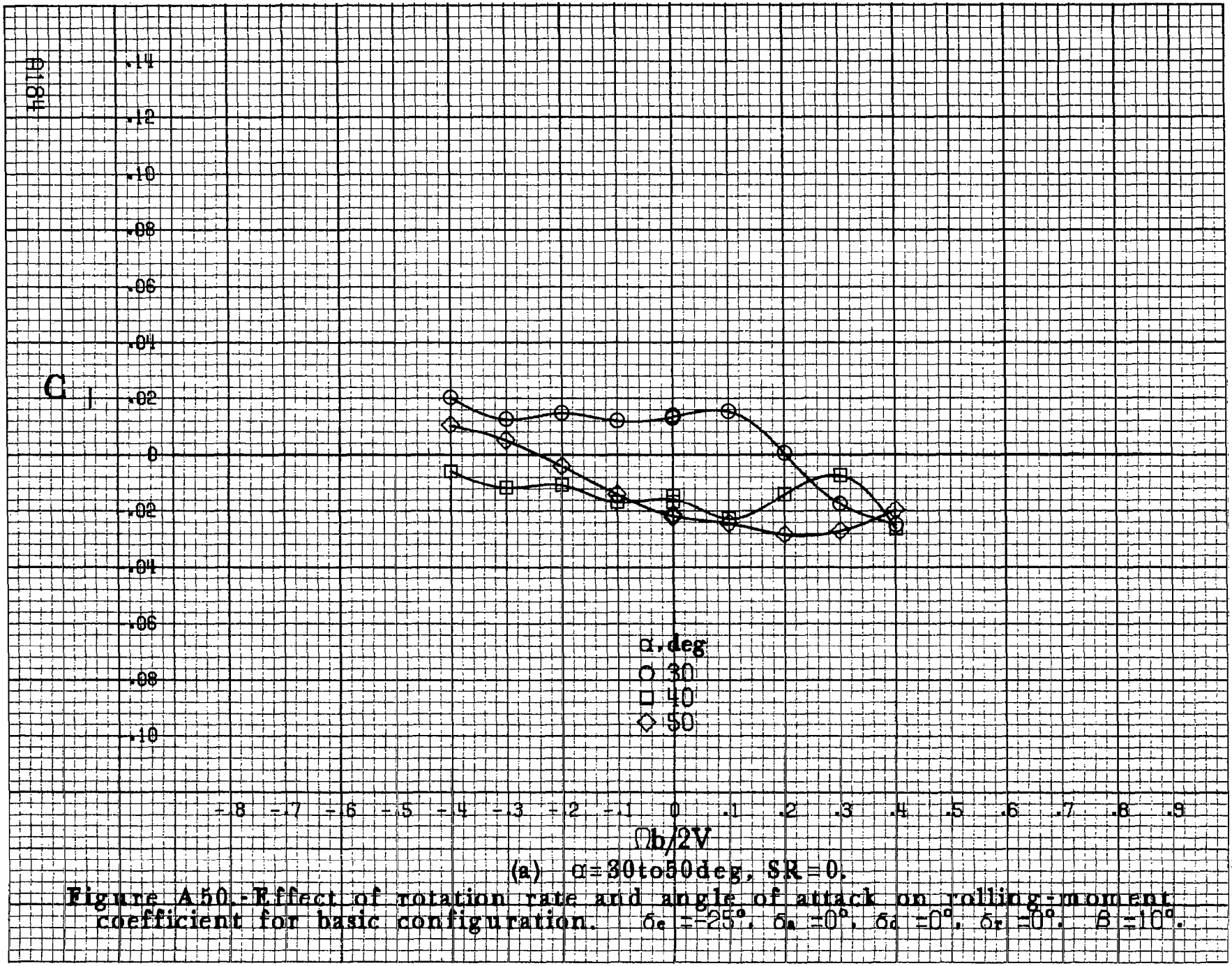

(a) $\alpha = 30$ to 50 deg, $SR = 0$.

Figure A50.- Effect of rotation rate and angle of attack on rolling-moment coefficient for basic configuration. $\delta_e = -25°$, $\delta_a = 0°$, $\delta_d = 0°$, $\delta_r = 0°$, $\beta = 10°$.

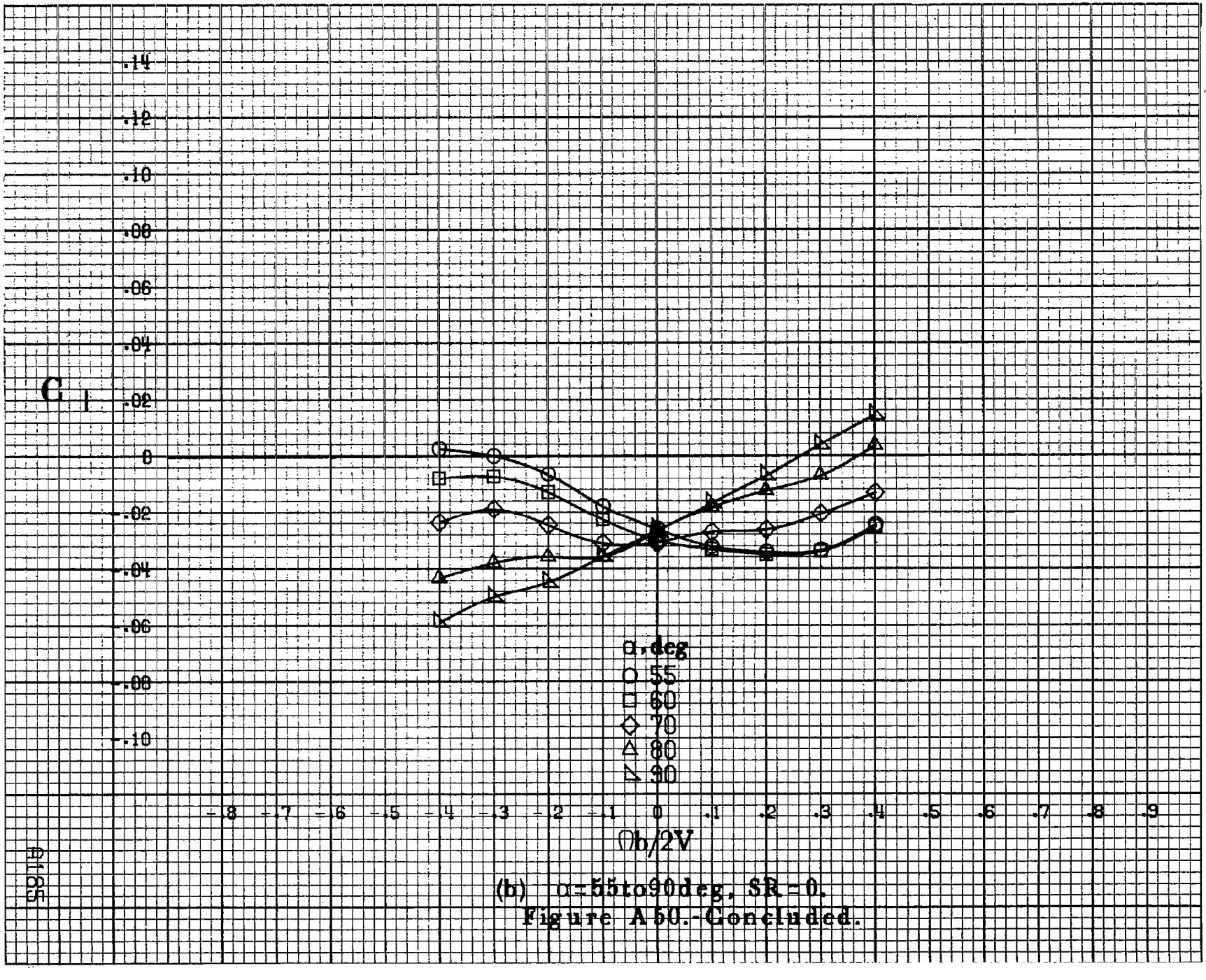

(b) α=55to90deg, SR=0.

Figure A50.-Concluded.

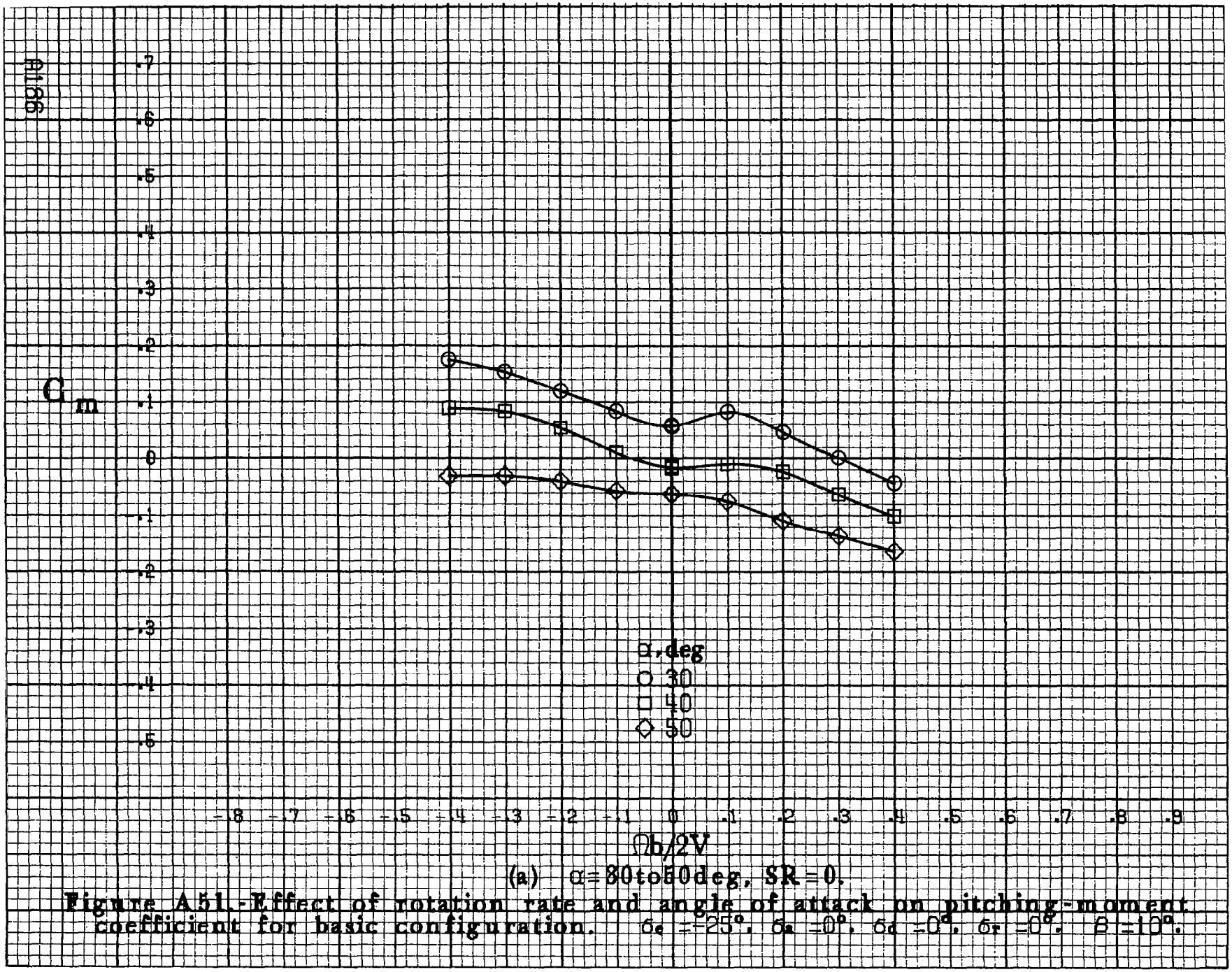

(a) $\alpha = 30$ to 60 deg, SR = 0.

Figure A51.- Effect of rotation rate and angle of attack on pitching-moment coefficient for basic configuration. $\delta_e = -25°$, $\delta_a = 0°$, $\delta_d = 0°$, $\delta_r = 0°$, $\beta = 10°$.

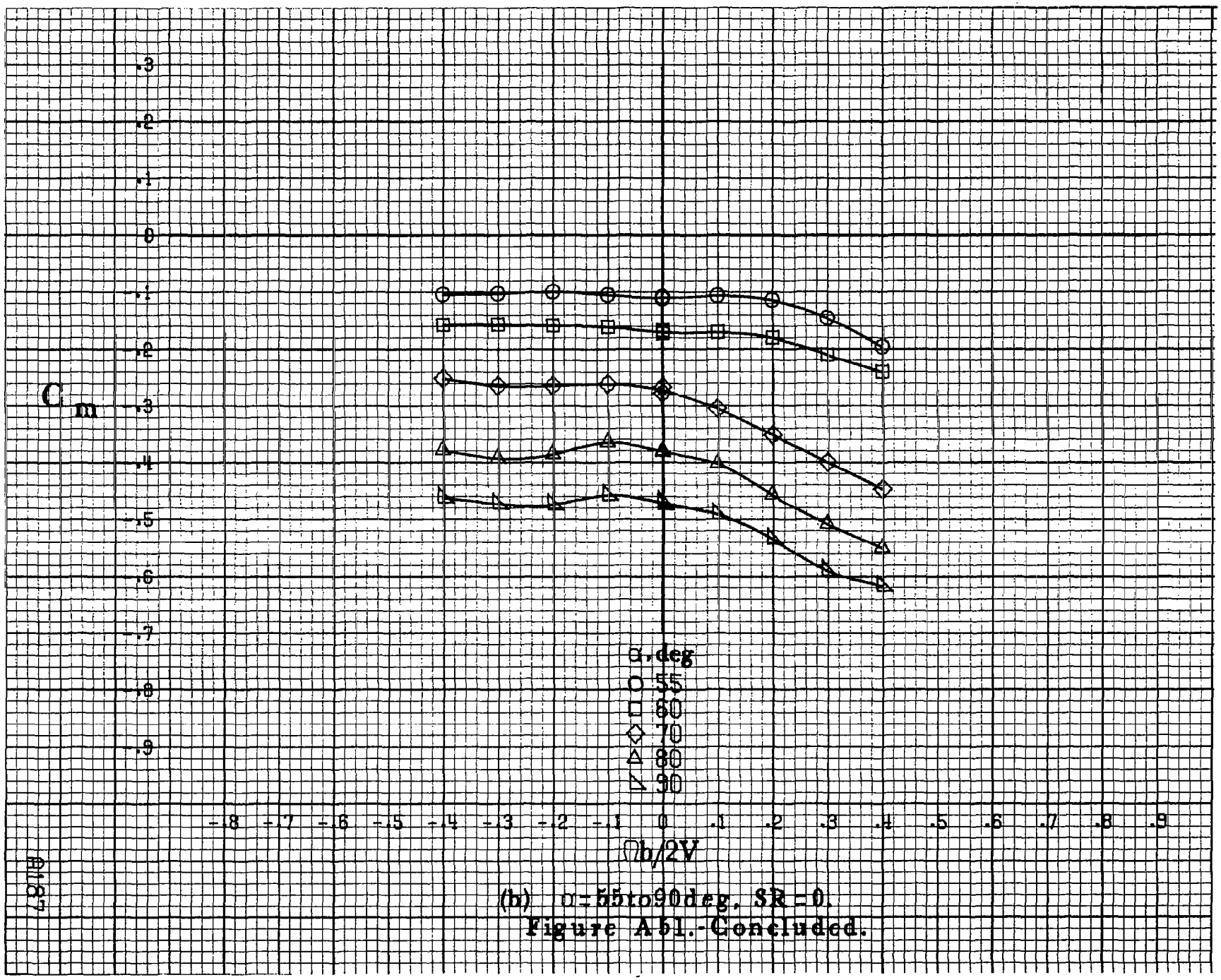

(b) $\alpha = 55$ to 90 deg, $SR = 0$.

Figure A51.-Concluded.

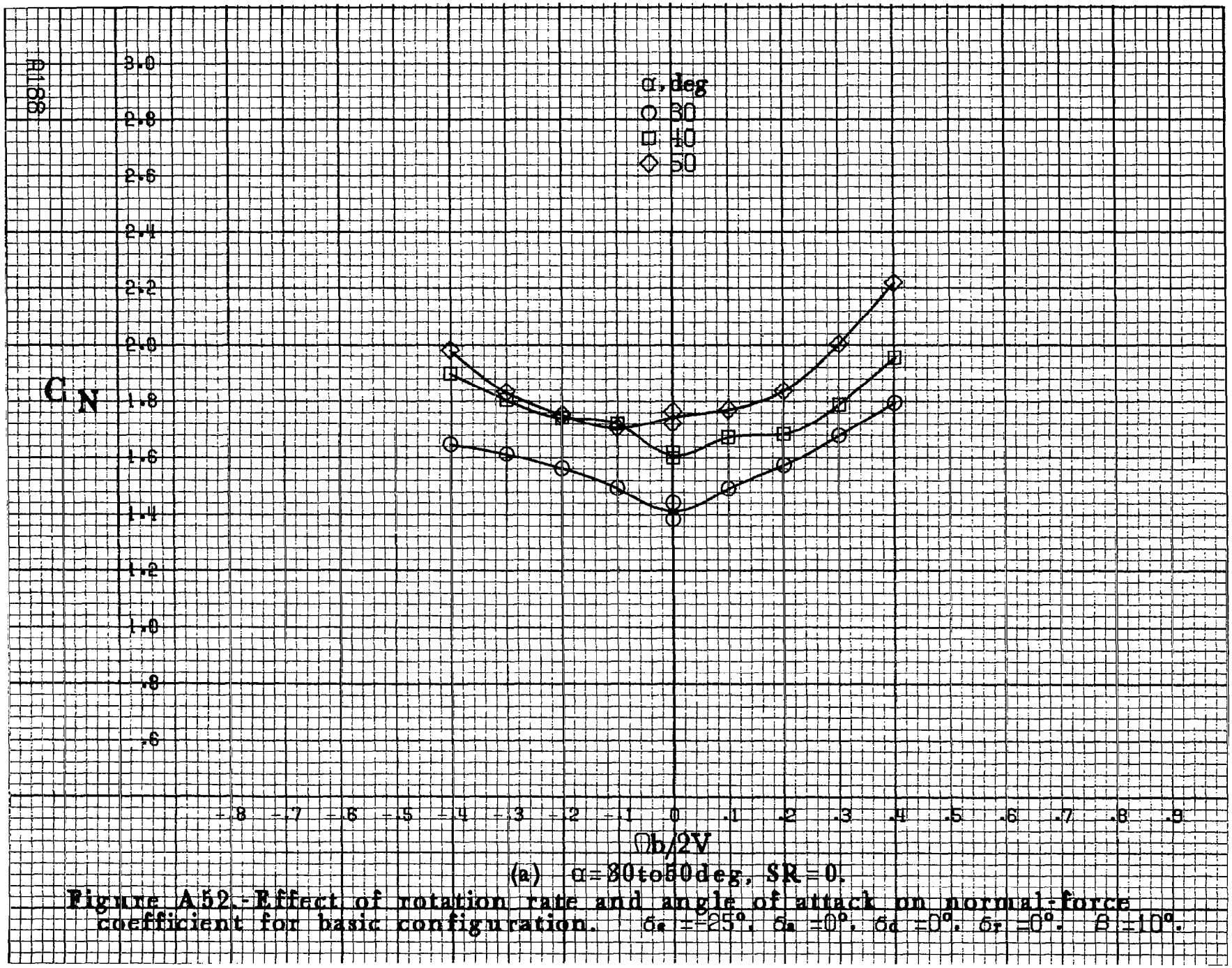

(a) $\alpha = 30$ to 50 deg, SR = 0.

Figure A52.- Effect of rotation rate and angle of attack on normal-force coefficient for basic configuration. $\delta_e = -25°$, $\delta_a = 0°$, $\delta_d = 0°$, $\delta_r = 0°$, $\beta = 10°$.

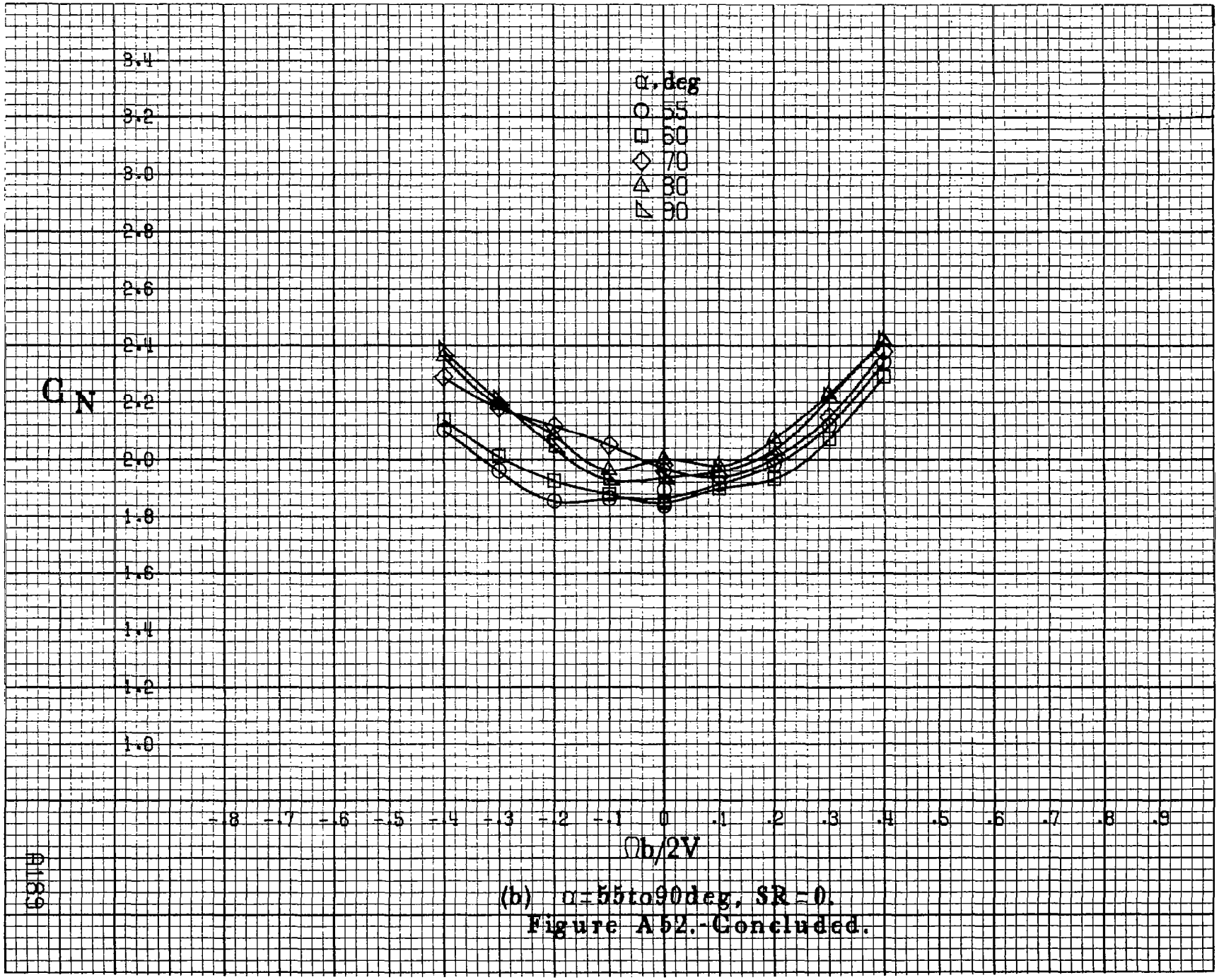

(b) $\alpha = 55$ to 90 deg, SR = 0.

Figure A52.- Concluded.

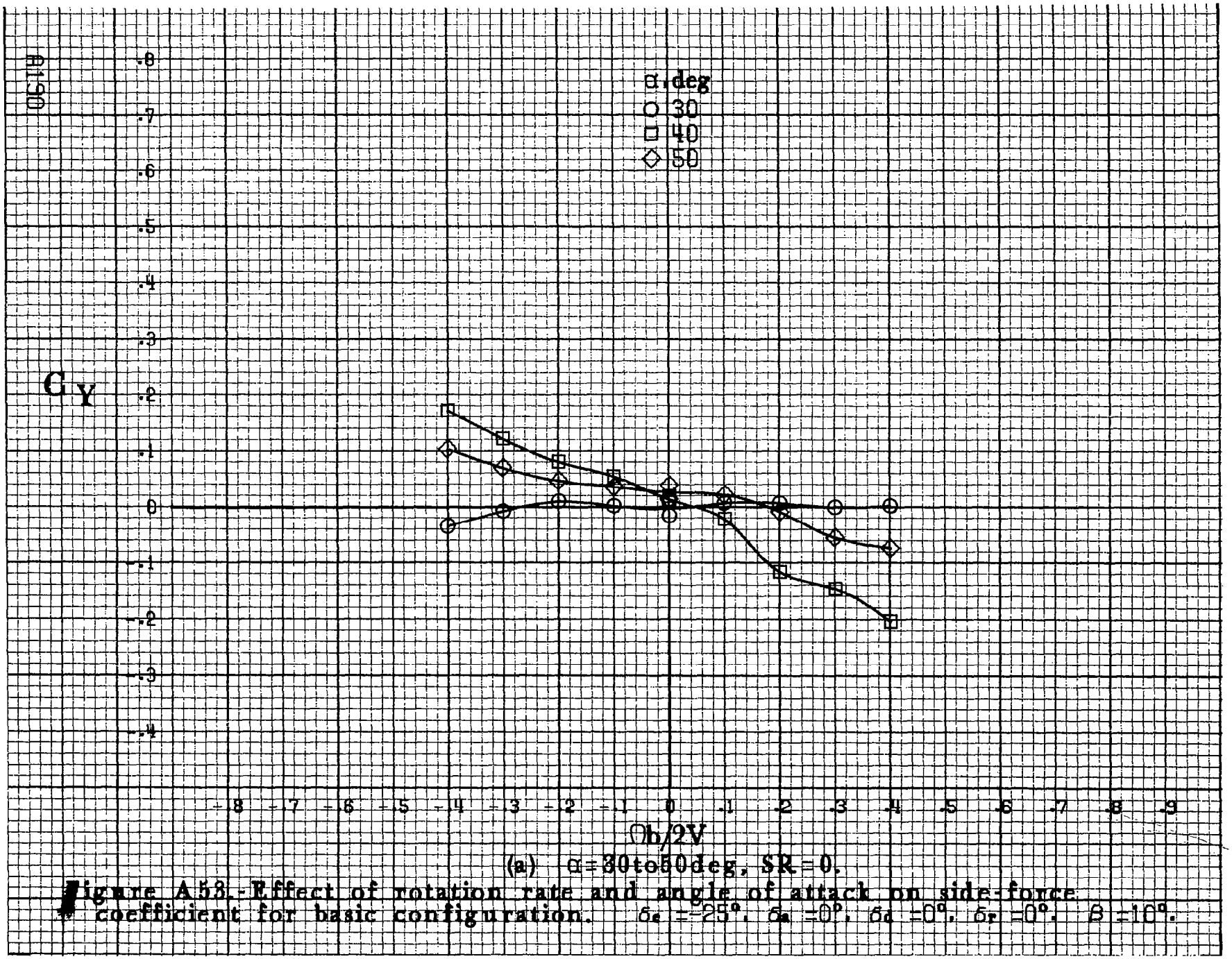

(a) $\alpha = 30$ to 50 deg, SR = 0.

Figure A.53.- Effect of rotation rate and angle of attack on side-force coefficient for basic configuration. $\delta_e = -25°$, $\delta_a = 0°$, $\delta_d = 0°$, $\delta_r = 0°$, $\beta = 10°$.

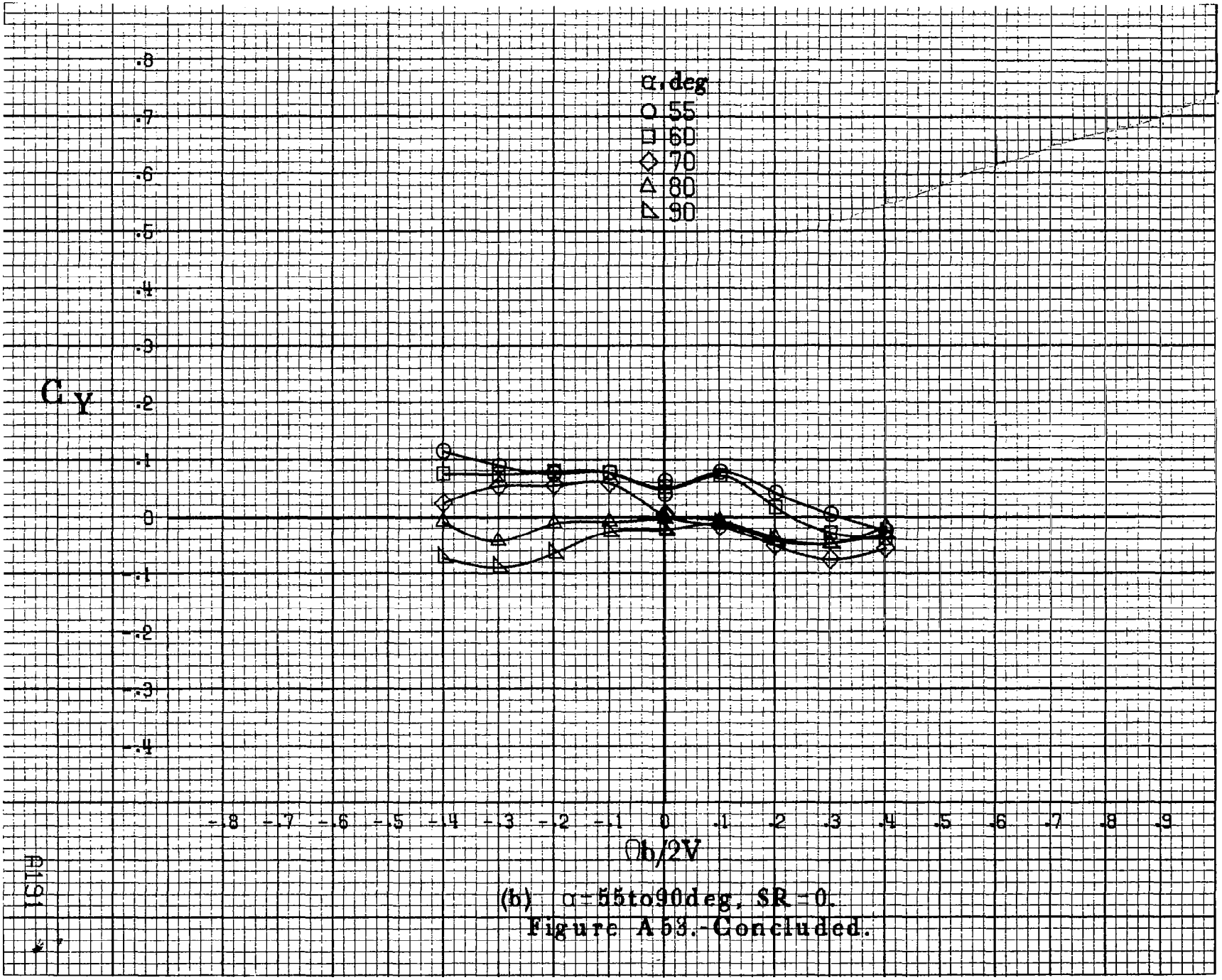

(b) $\alpha = 55$ to 90 deg, $SR = 0$.

Figure A53.-Concluded.

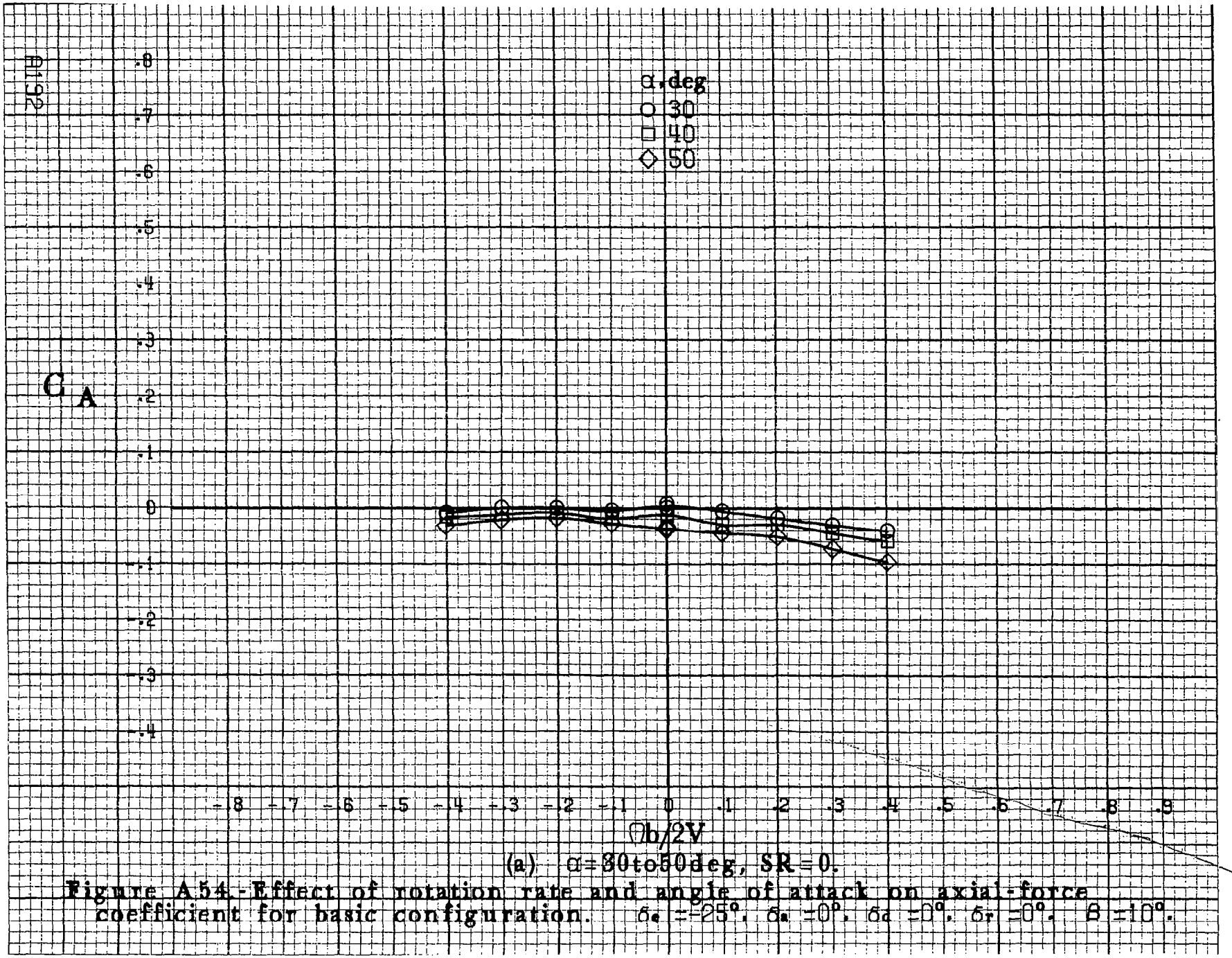

(a) $\alpha = 30$ to 50 deg, SR = 0.

Figure A54.- Effect of rotation rate and angle of attack on axial-force coefficient for basic configuration. $\delta_e = -25°$, $\delta_a = 0°$, $\delta_d = 0°$, $\delta_r = 0°$, $\beta = 10°$.

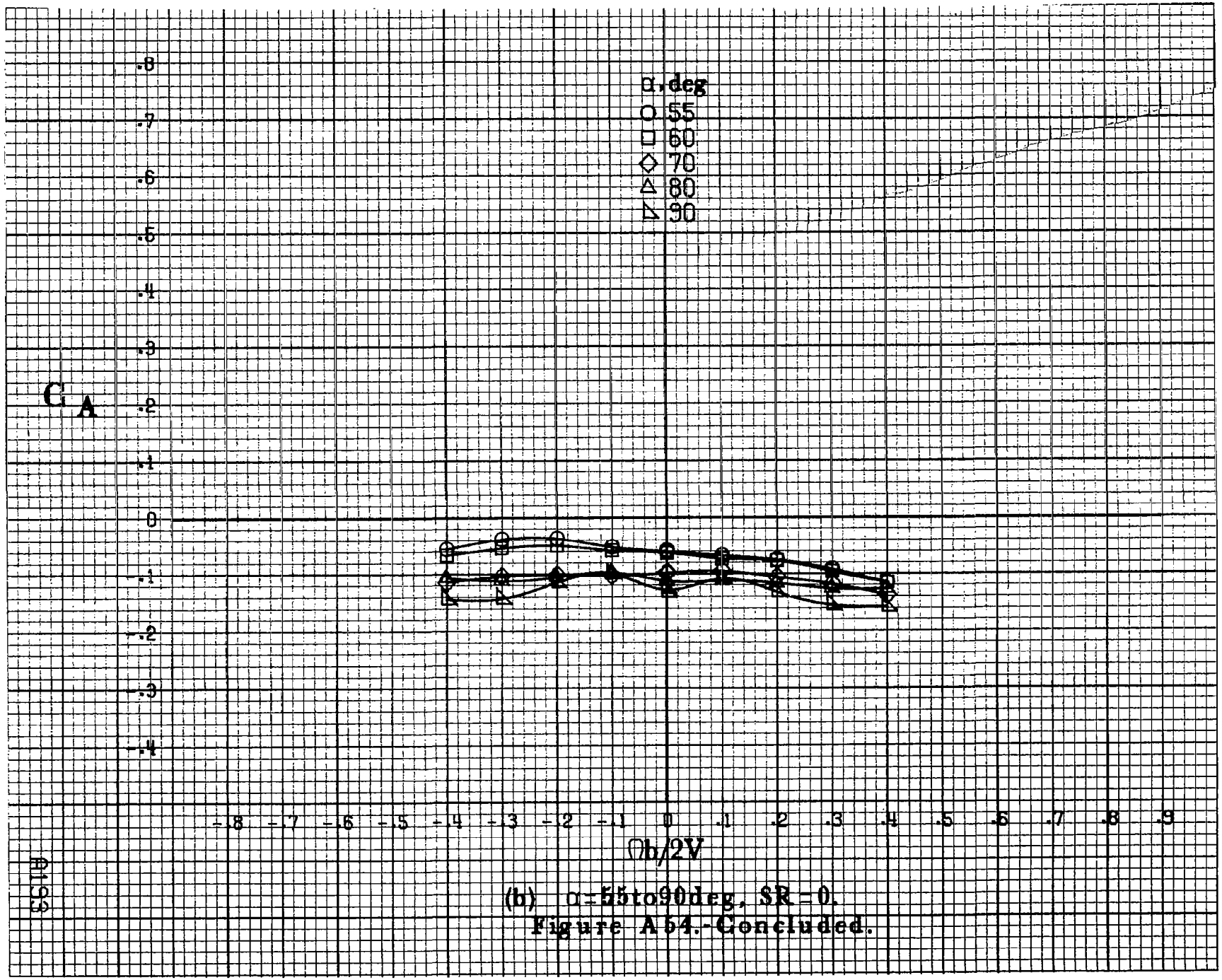

(b) α=55to90deg, S_R=0.

Figure A64.-Concluded.

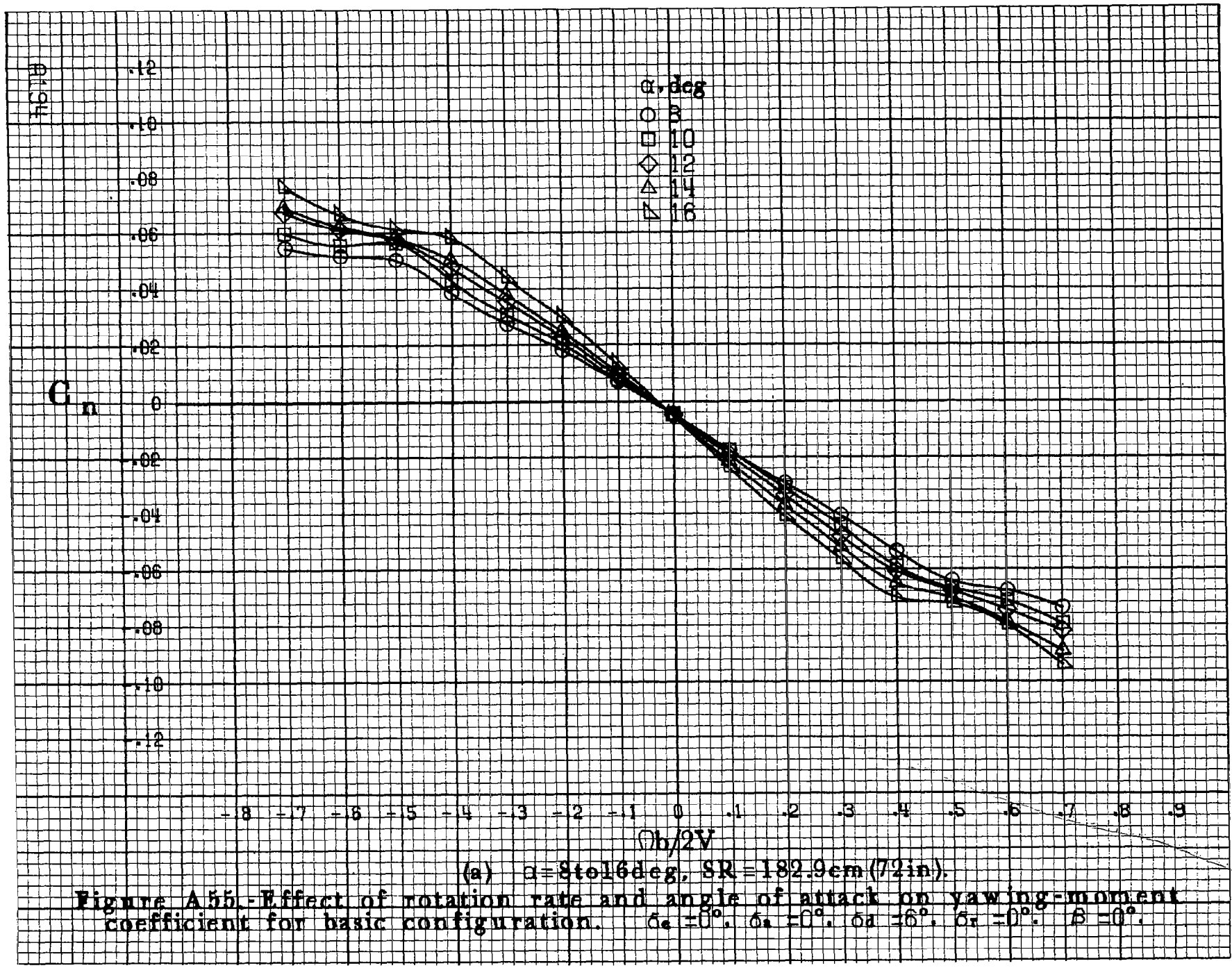

(a) $\alpha = 8$ to 16 deg, SR = 182.9 cm (72 in).

Figure A55.- Effect of rotation rate and angle of attack on yawing-moment coefficient for basic configuration. $\delta_e = 0°$, $\delta_a = 0°$, $\delta_a = 6°$, $\delta_r = 0°$, $\beta = 0°$.

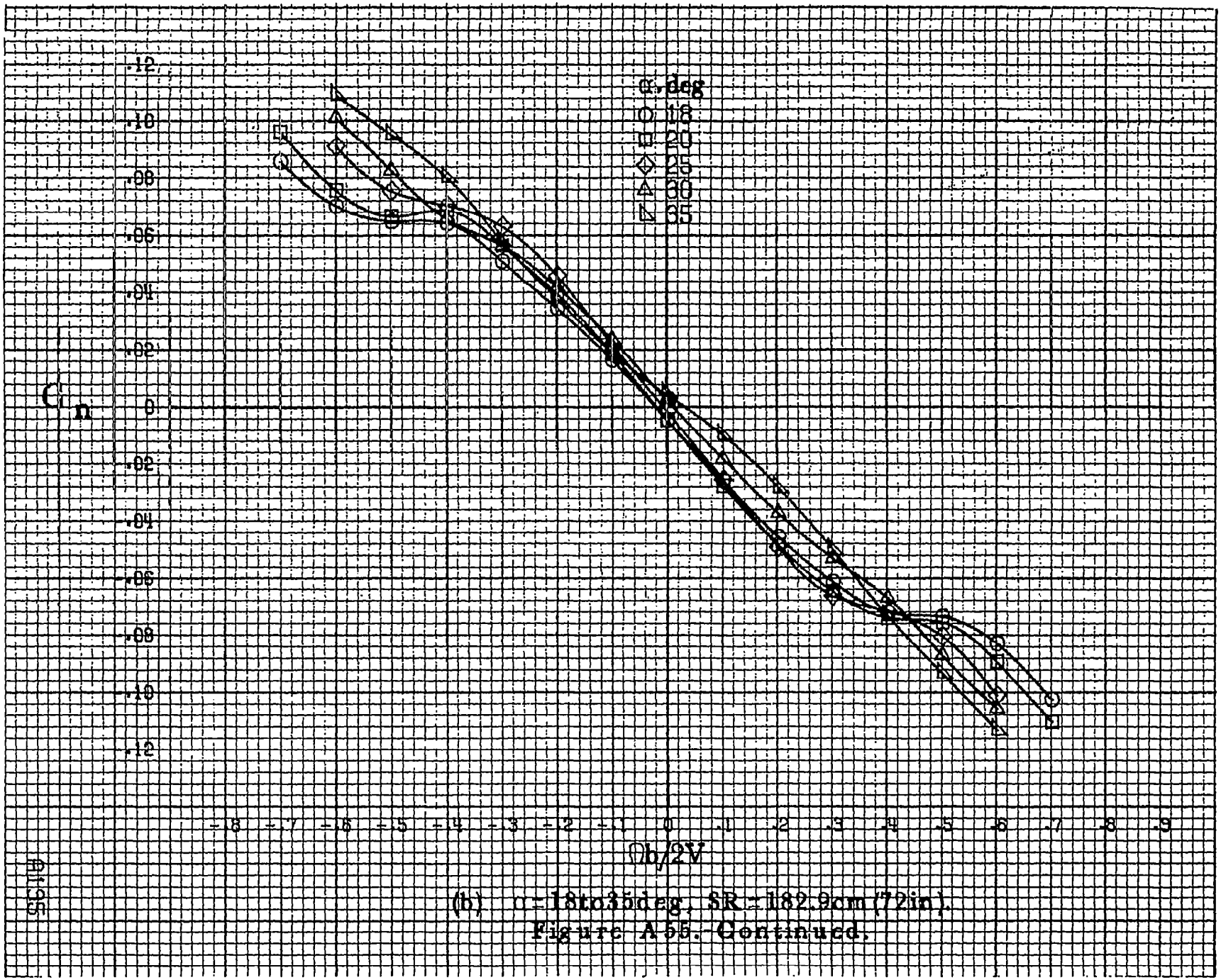

(b) α=18to35deg, SR=182.9cm(72in).

Figure A55.-Continued.

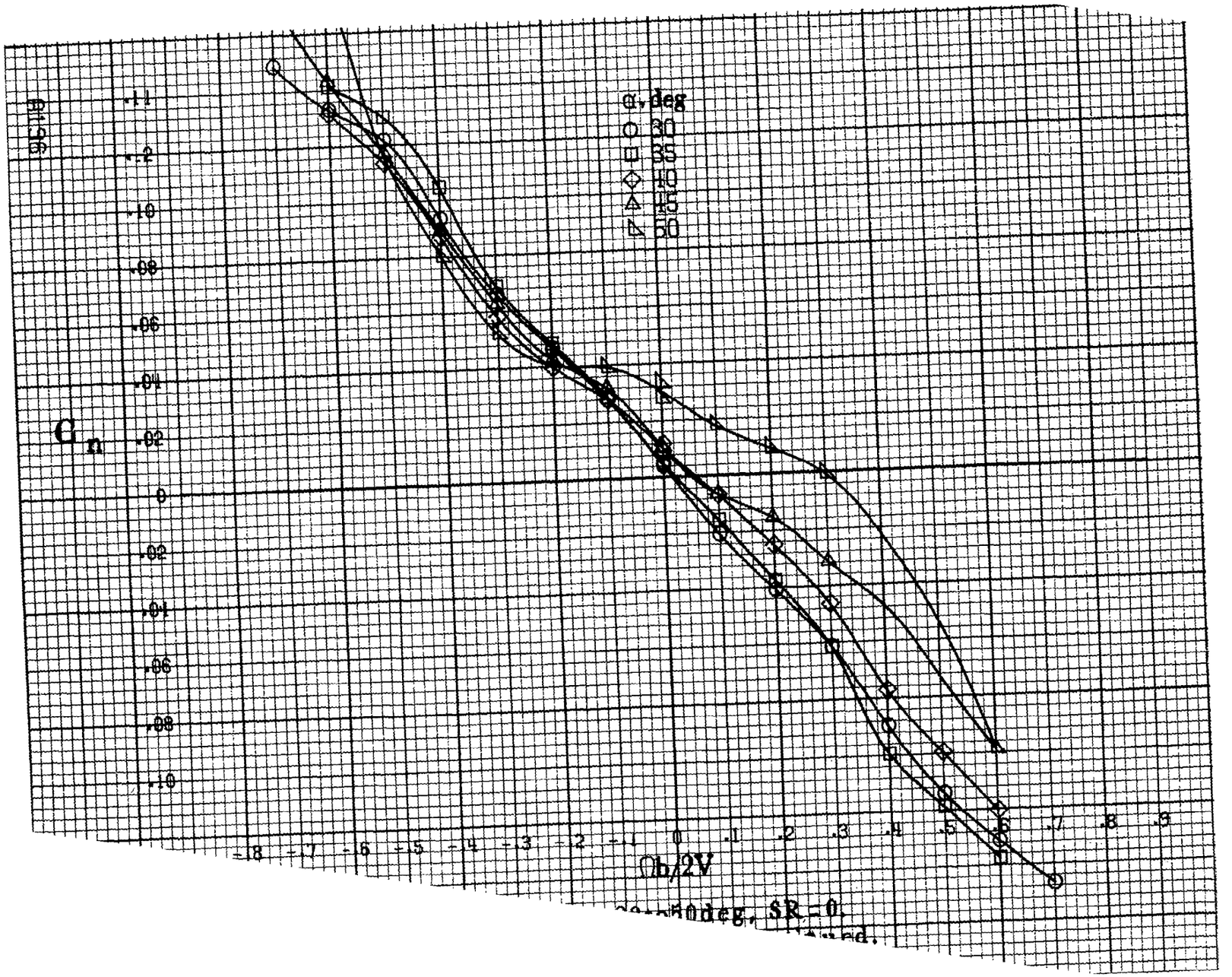
α, deg
30
35
40
45
50
C_n
$\Omega b/2V$
.11
.1
.08
.06
.04
.02
0
.02
.04
.06
.08
.10
-.8
-.7
-.6
-.5
-.4
-.3
-.2
-.1
0
.1
.2
.3
.4
.5
.6
.7
.8
.9

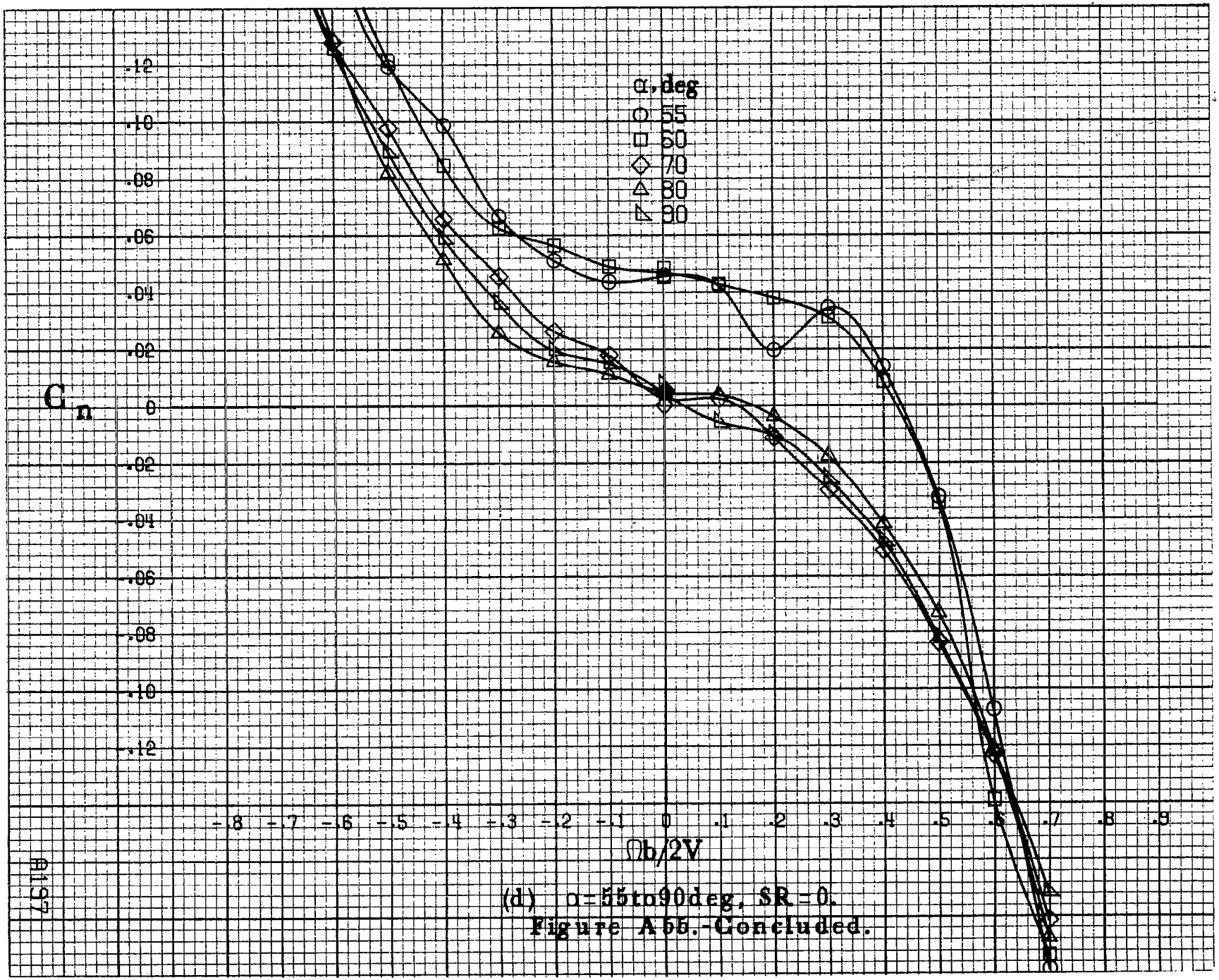

(d) $\alpha = 55$ to 90 deg, $\$R = 0$.

Figure A 66.-Concluded.

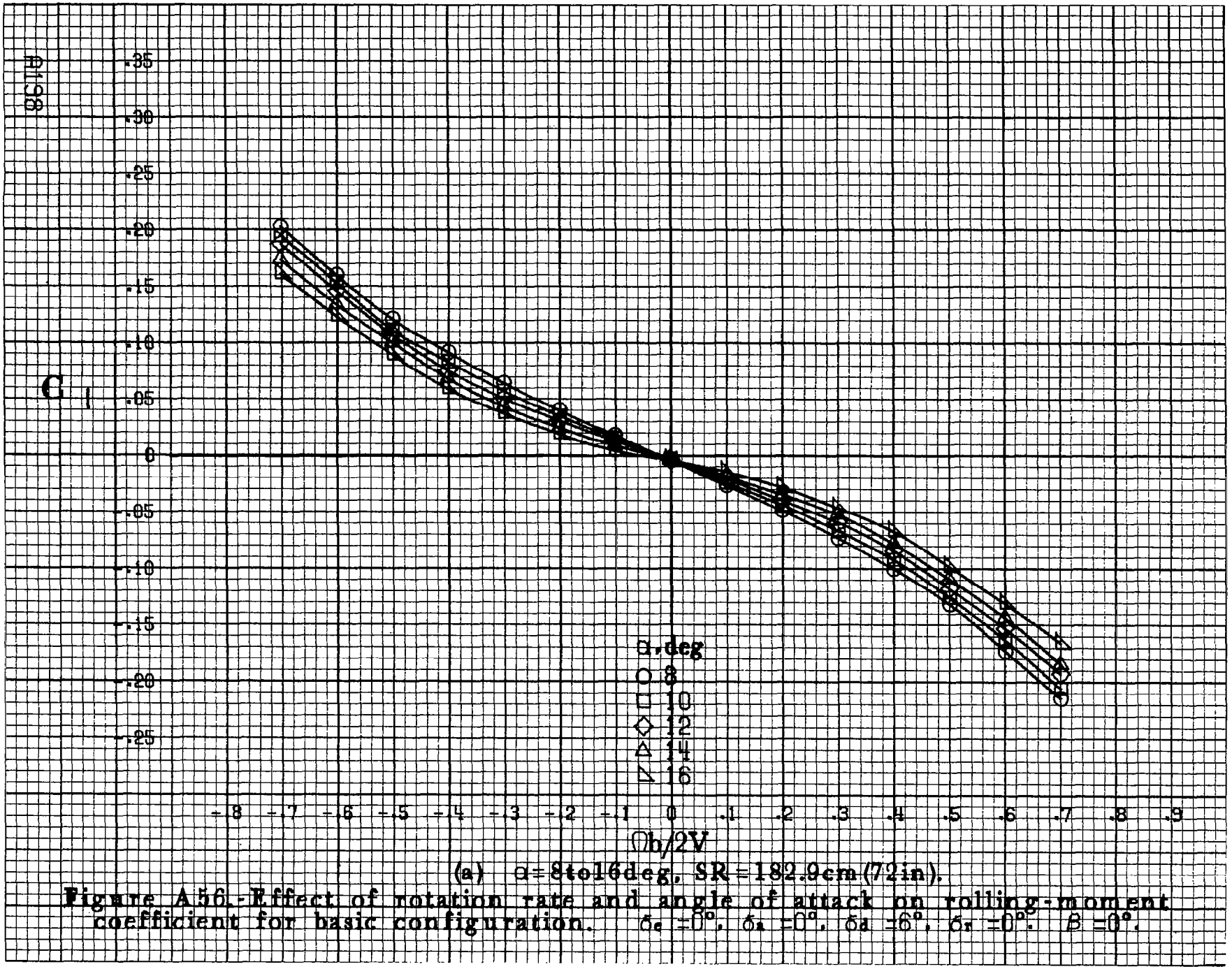

(a) $\alpha = 8$ to 16 deg, SR = 182.9 cm (72 in).

Figure A.56.- Effect of rotation rate and angle of attack on rolling-moment coefficient for basic configuration. $\delta_e = 0°$, $\delta_s = 0°$, $\delta_a = 6°$, $\delta_r = 0°$, $\beta = 0°$.

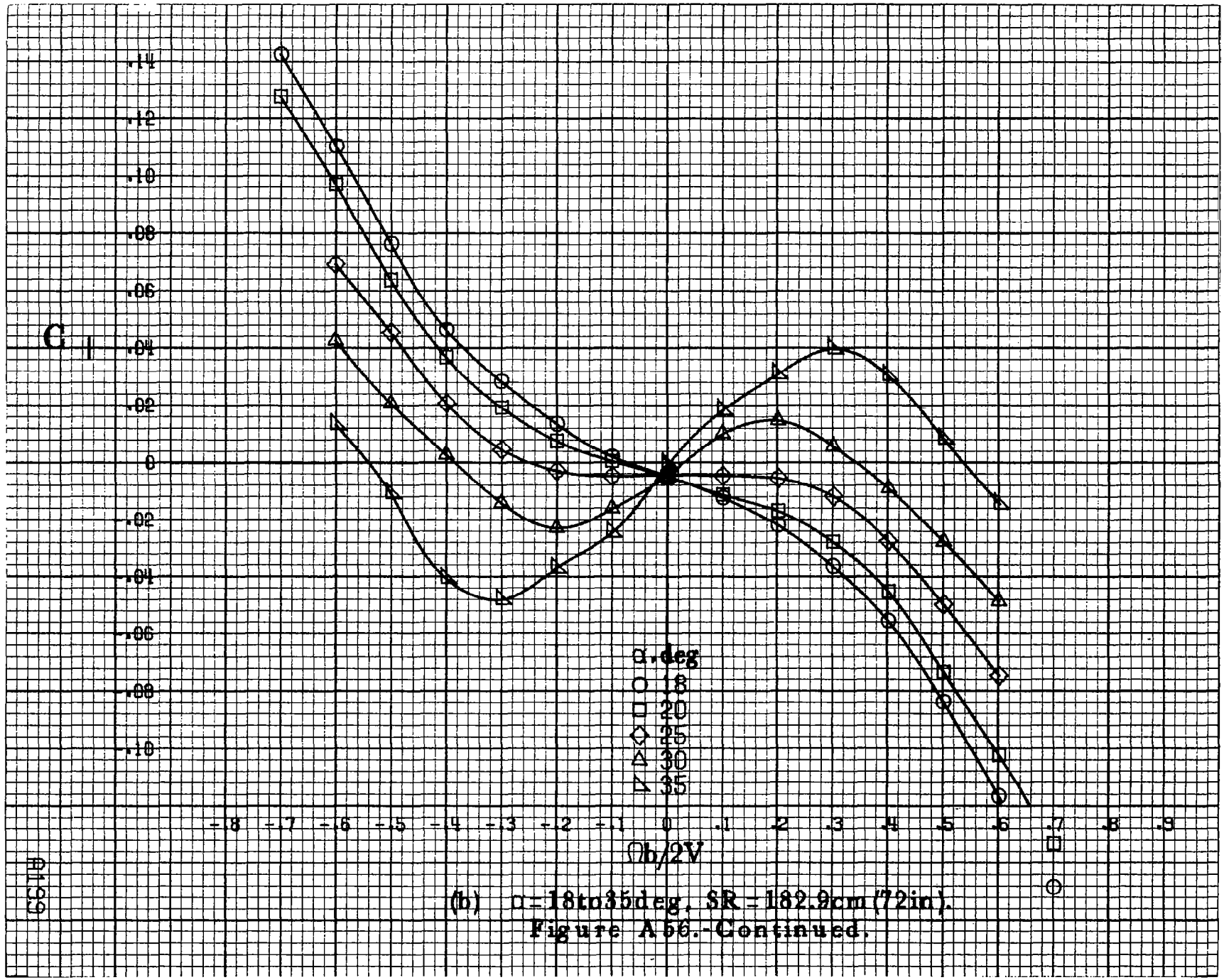

(b) α = 18 to 35 deg, SR = 182.9 cm (72 in.).

Figure A66.- Continued.

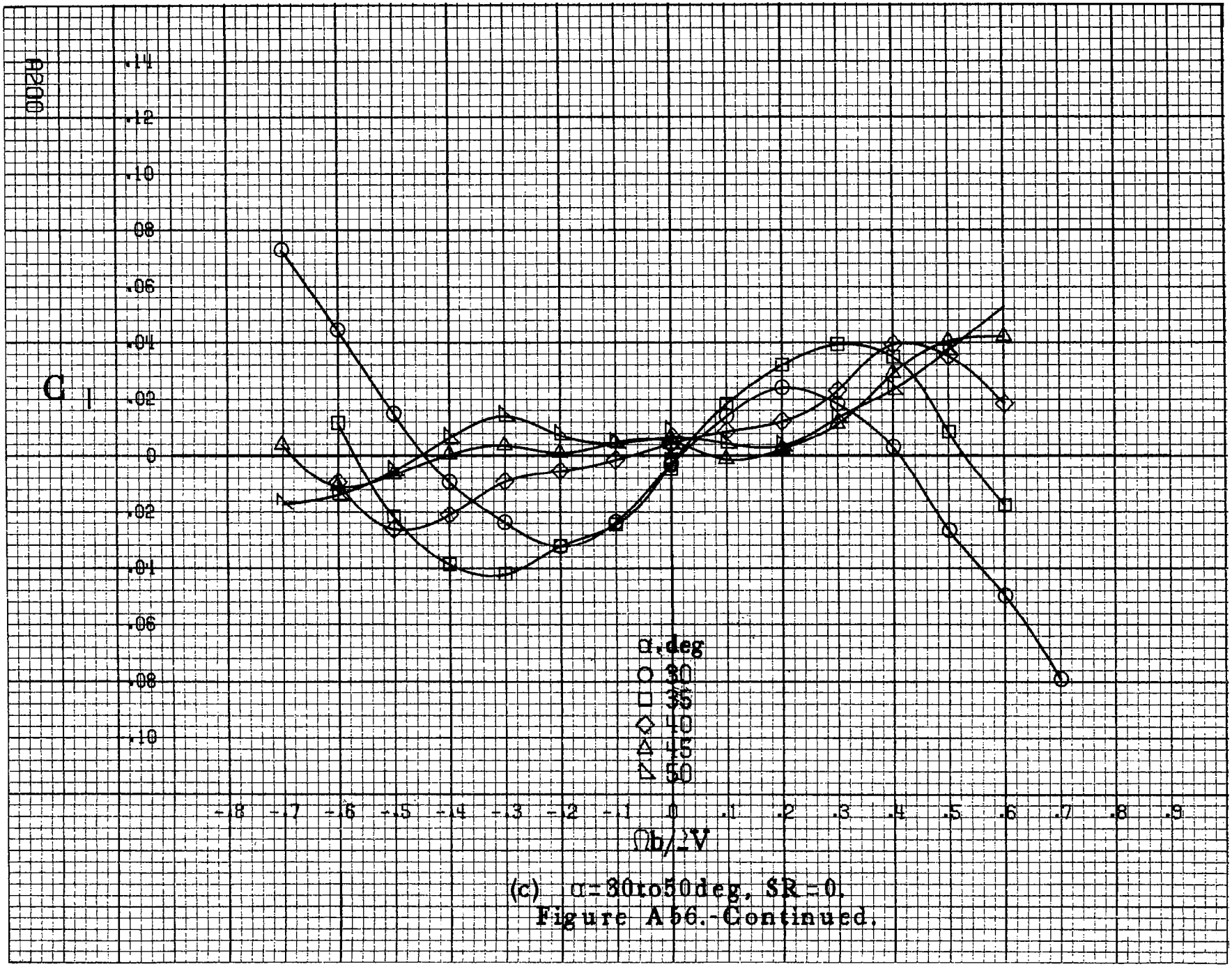

(c) $\alpha = 30$ to 50 deg, $\$R = 0$.

Figure A56.-Continued.

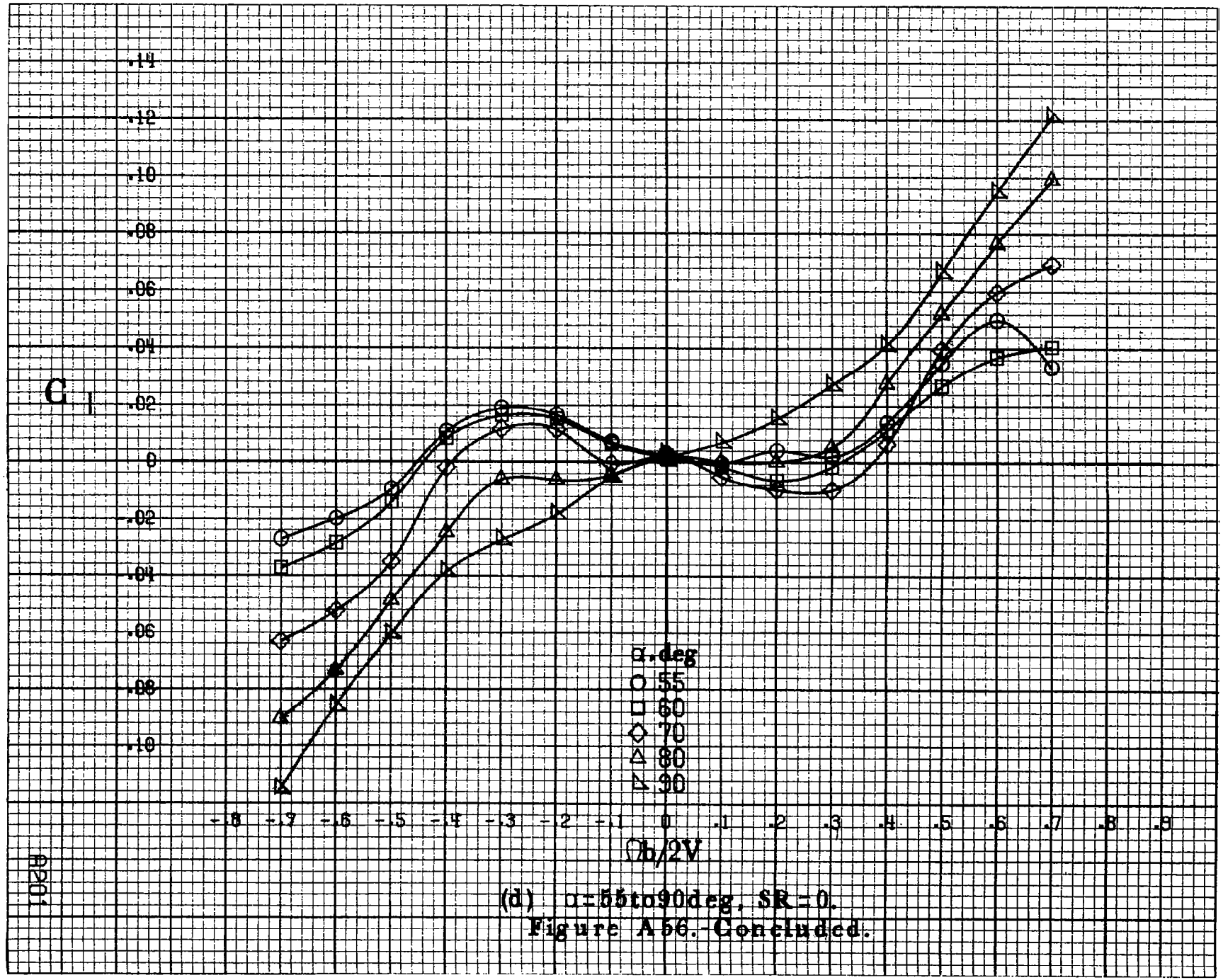

(d) α = 55 to 90 deg, SR = 0.

Figure A56.- Concluded.

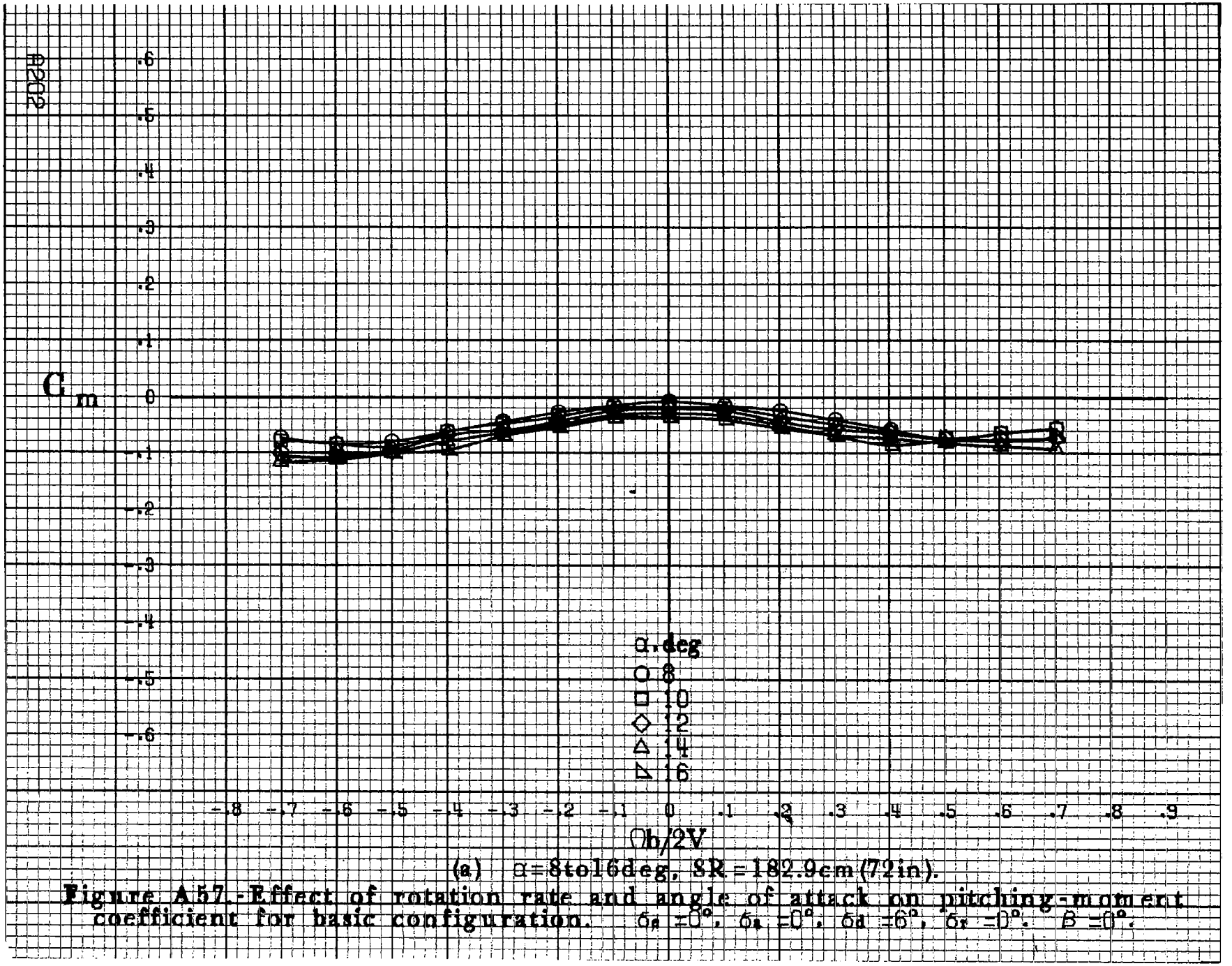

(a) α = 8 to 16 deg, SR = 182.9 cm (72 in).

Figure A57.- Effect of rotation rate and angle of attack on pitching-moment coefficient for basic configuration. $\delta_e = 0°$, $\delta_a = 0°$, $\delta_d = 6°$, $\delta_r = 0°$, $\beta = 0°$.

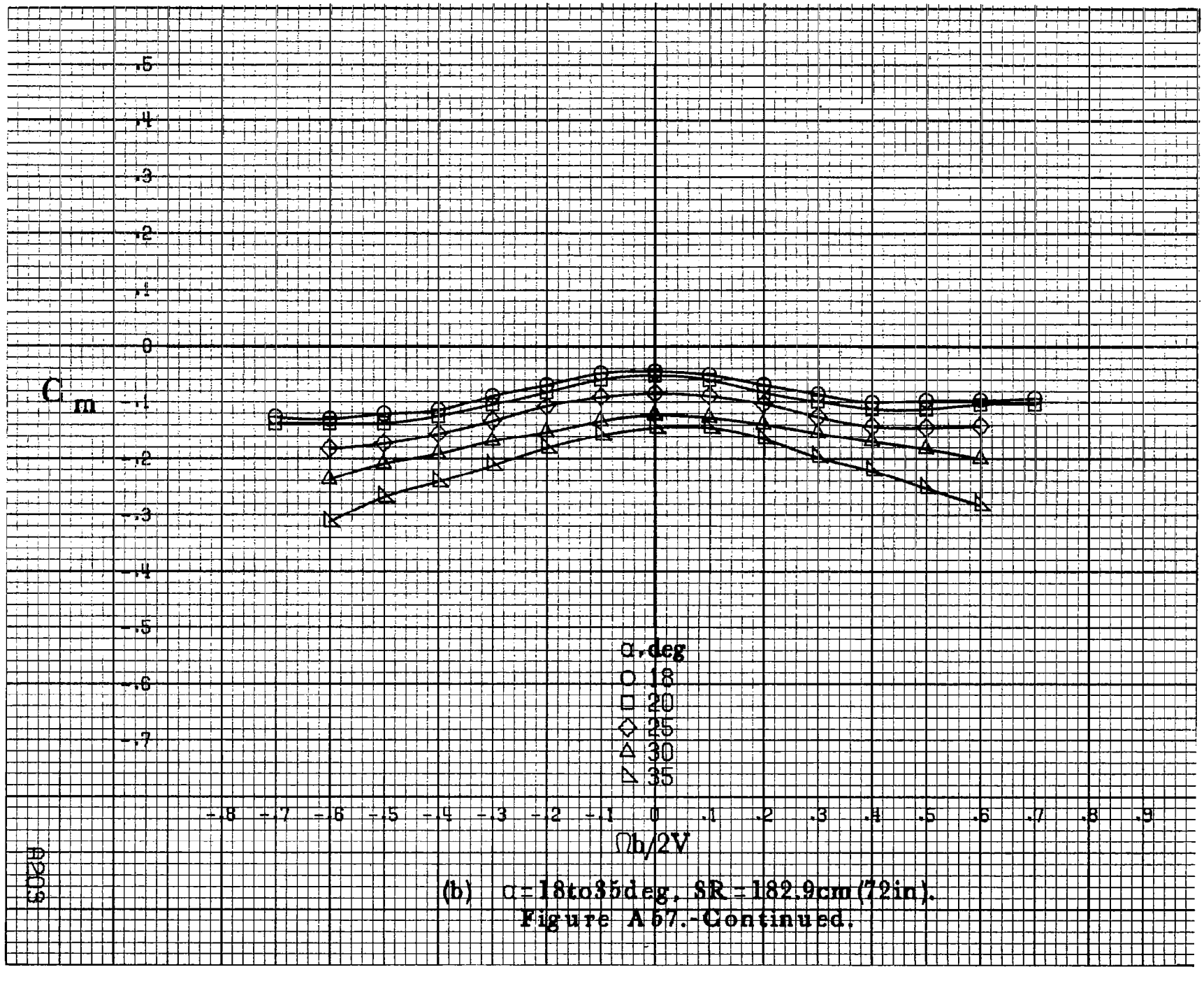

(b) α = 18 to 35 deg, SR = 182.9 cm (72 in).

Figure A 67.- Continued.

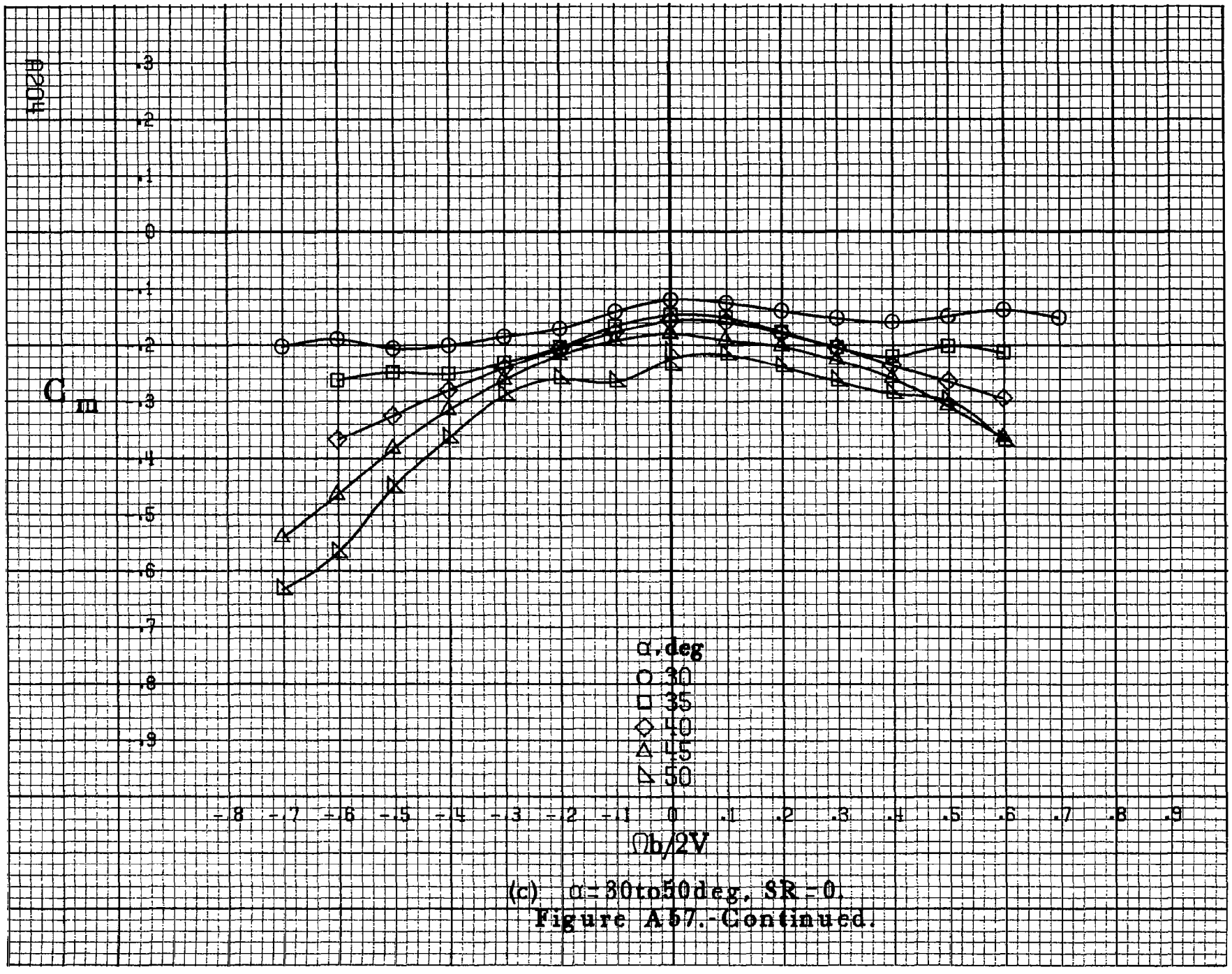

(c) α = 30 to 50 deg, SR = 0.

Figure A57.- Continued.

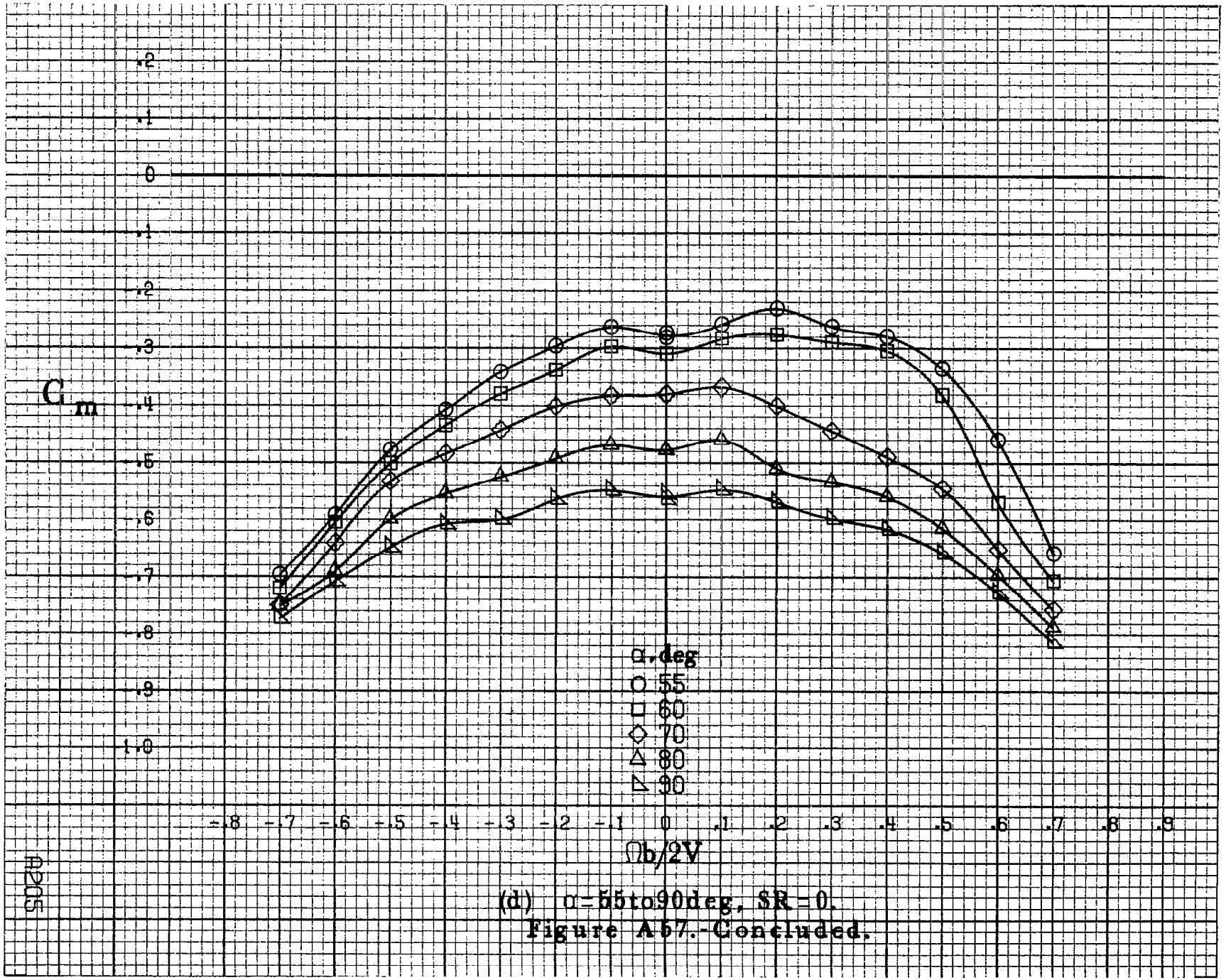

(d) α = 55 to 90 deg, SR = 0.

Figure A57.-Concluded.

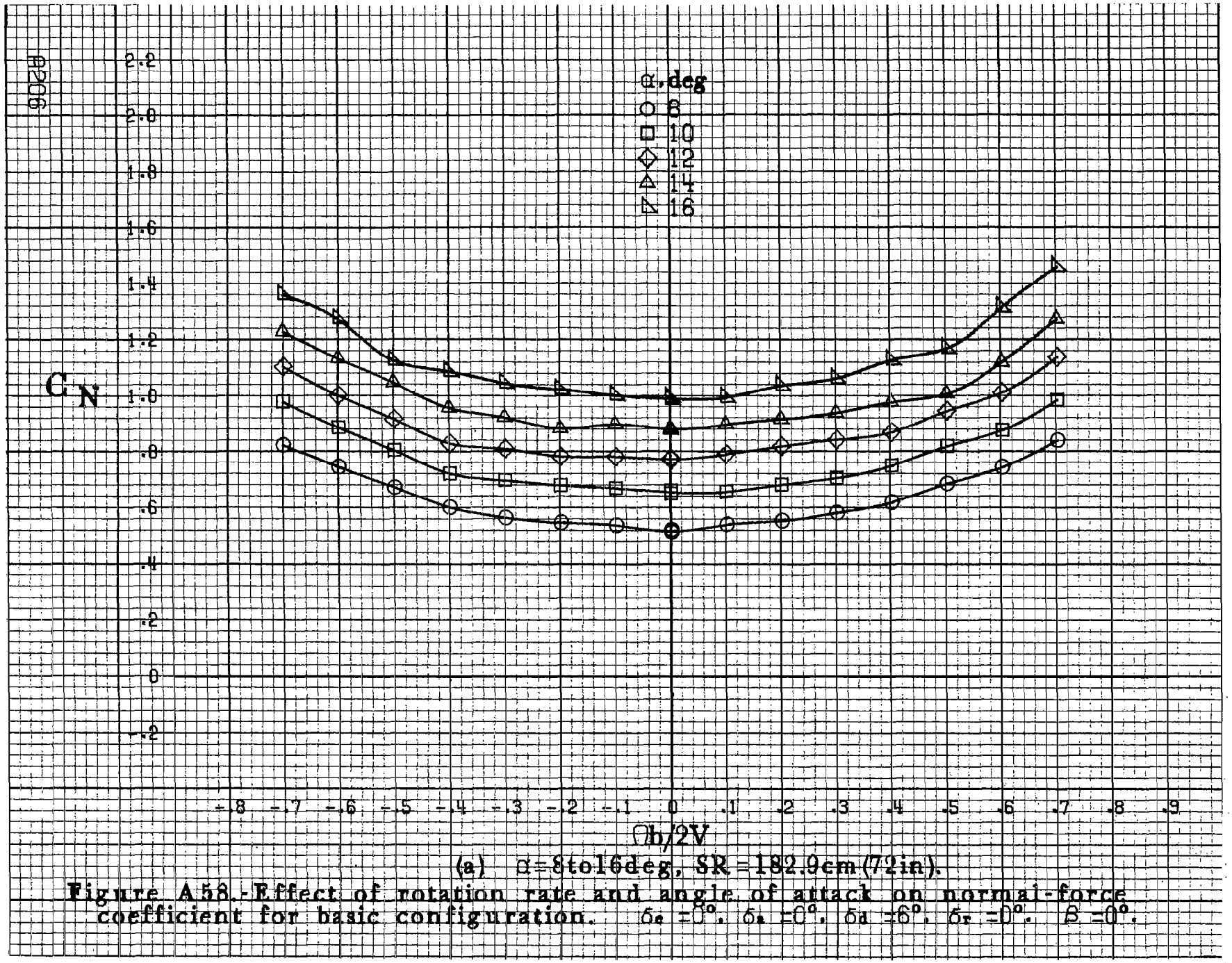

(a) $\alpha = 8$ to 16 deg, SR = 182.9 cm (72 in).

Figure A58.- Effect of rotation rate and angle of attack on normal-force coefficient for basic configuration. $\delta_e = 0°$, $\delta_a = 0°$, $\delta_d = 6°$, $\delta_r = 0°$. $\beta = 0°$.

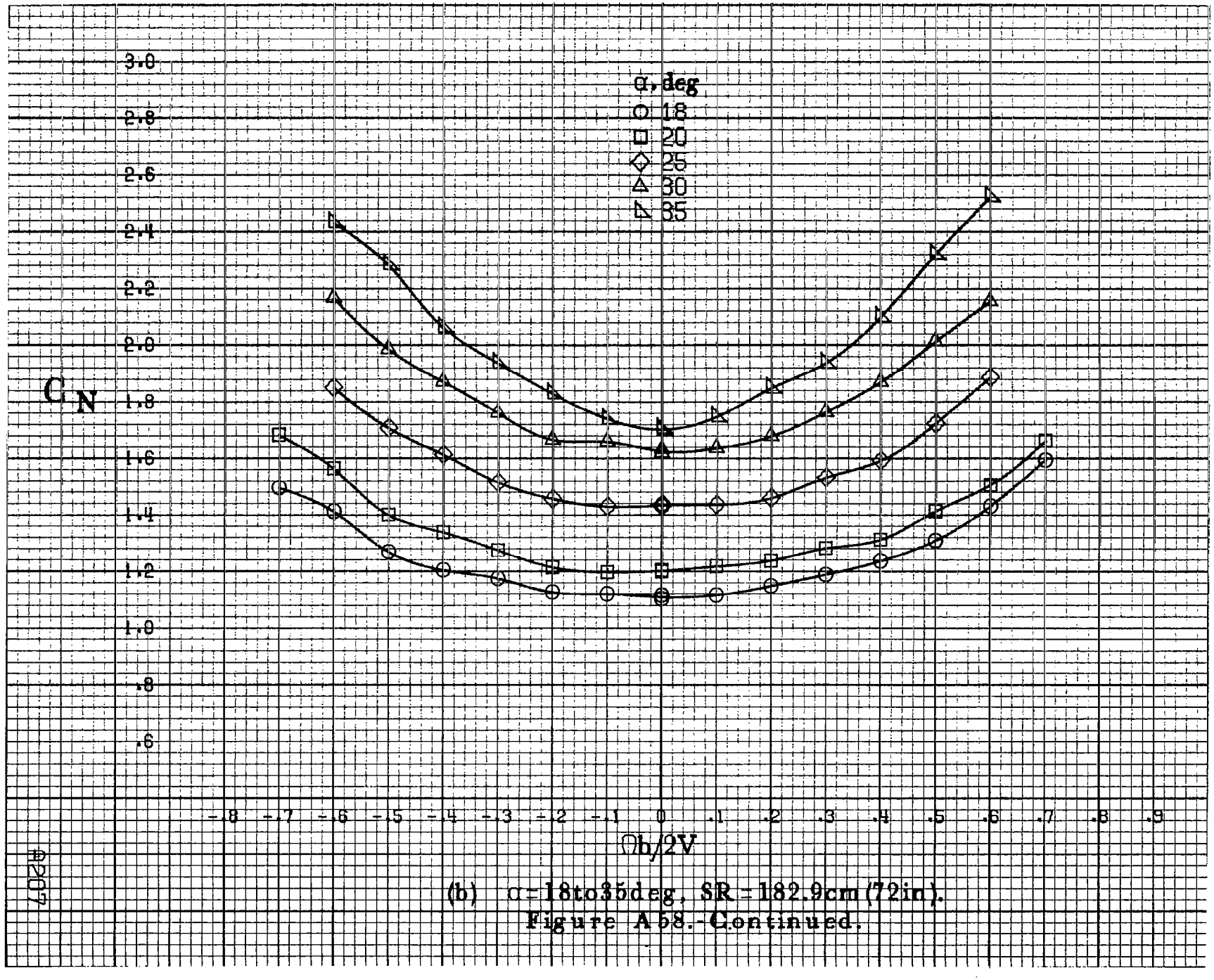

(b) $\alpha = 18$ to 35 deg, SR = 182.9 cm (72 in).

Figure A58.- Continued.

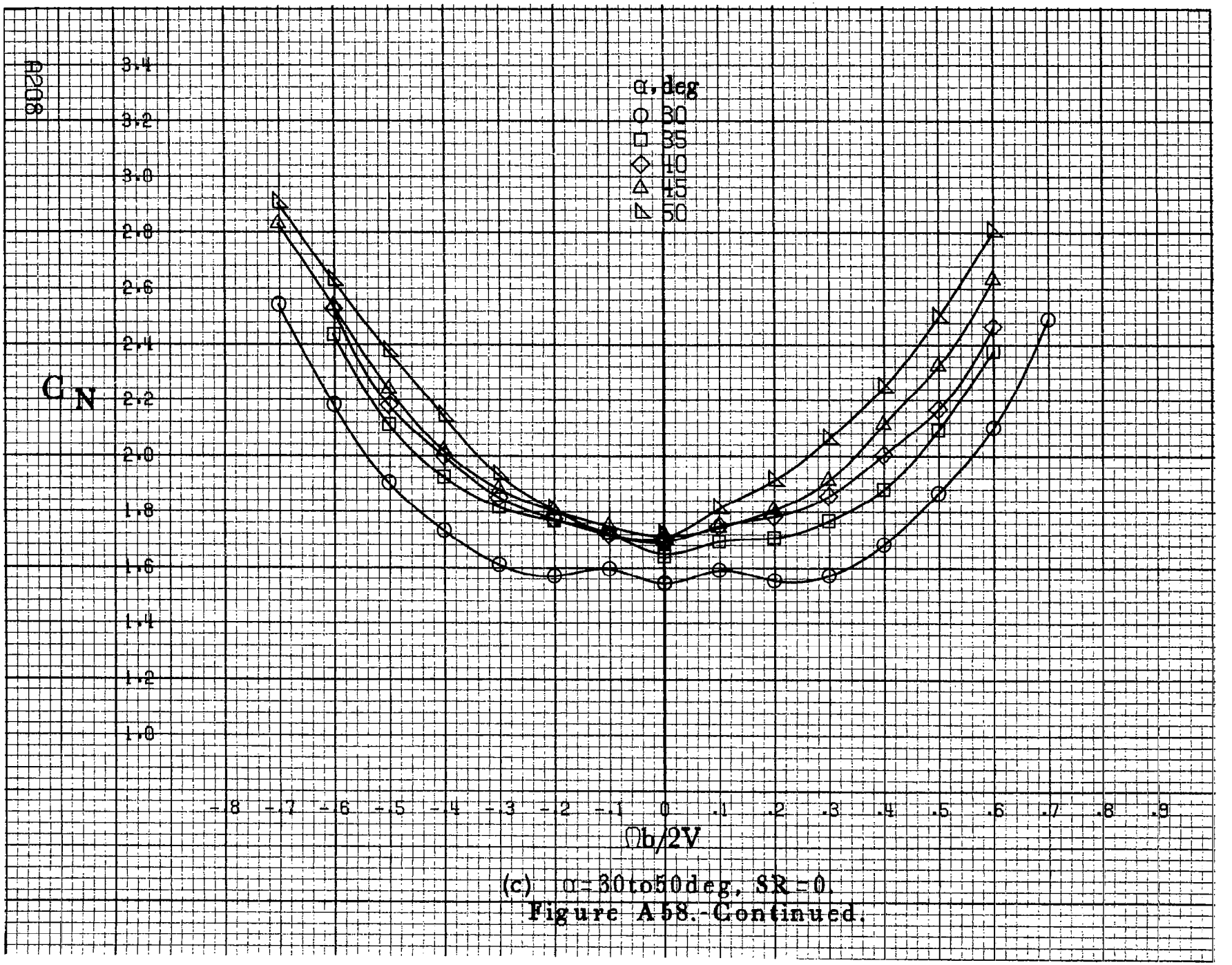

(c) $\alpha = 30$ to 50 deg, SR = 0.

Figure A58.-Continued.

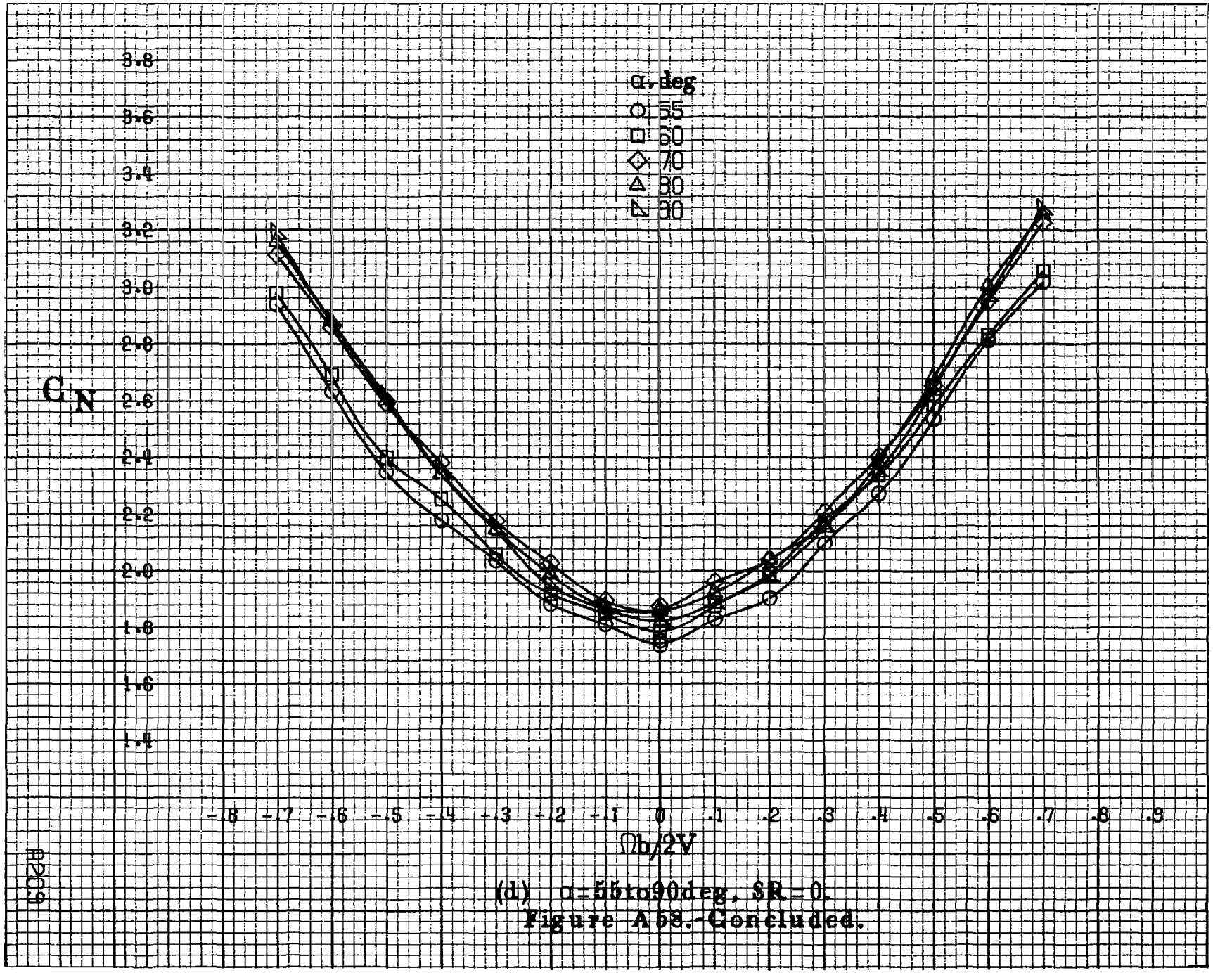

(d) $\alpha = 55$ to 90 deg, $\$R = 0$.

Figure A68.- Concluded.

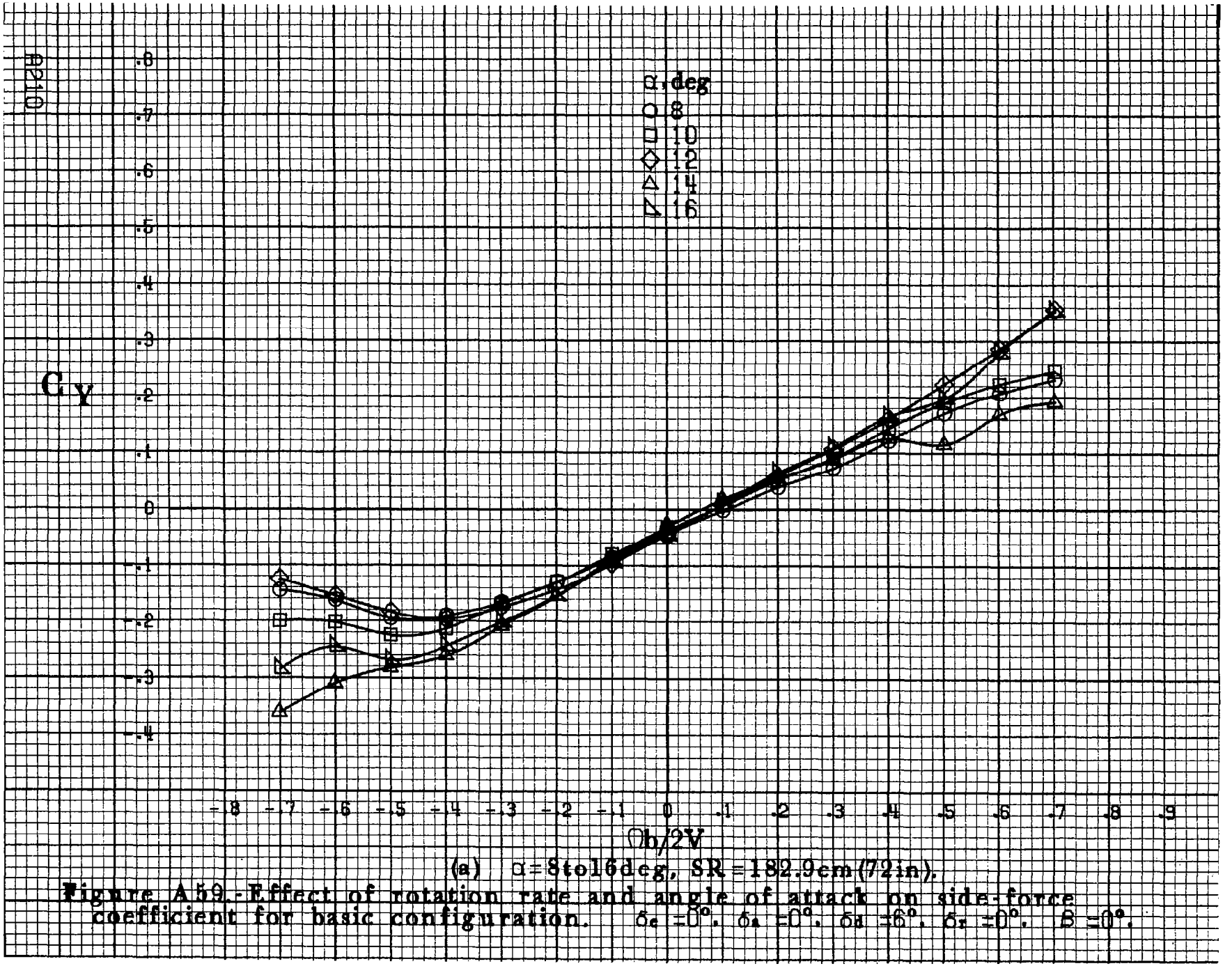

(a) $\alpha = 8$ to 16 deg, SR = 182.9 cm (72 in).

Figure A59.- Effect of rotation rate and angle of attack on side-force coefficient for basic configuration. $\delta_e = 0°$, $\delta_a = 0°$, $\delta_{sl} = 6°$, $\delta_r = 0°$, $\beta = 0°$.

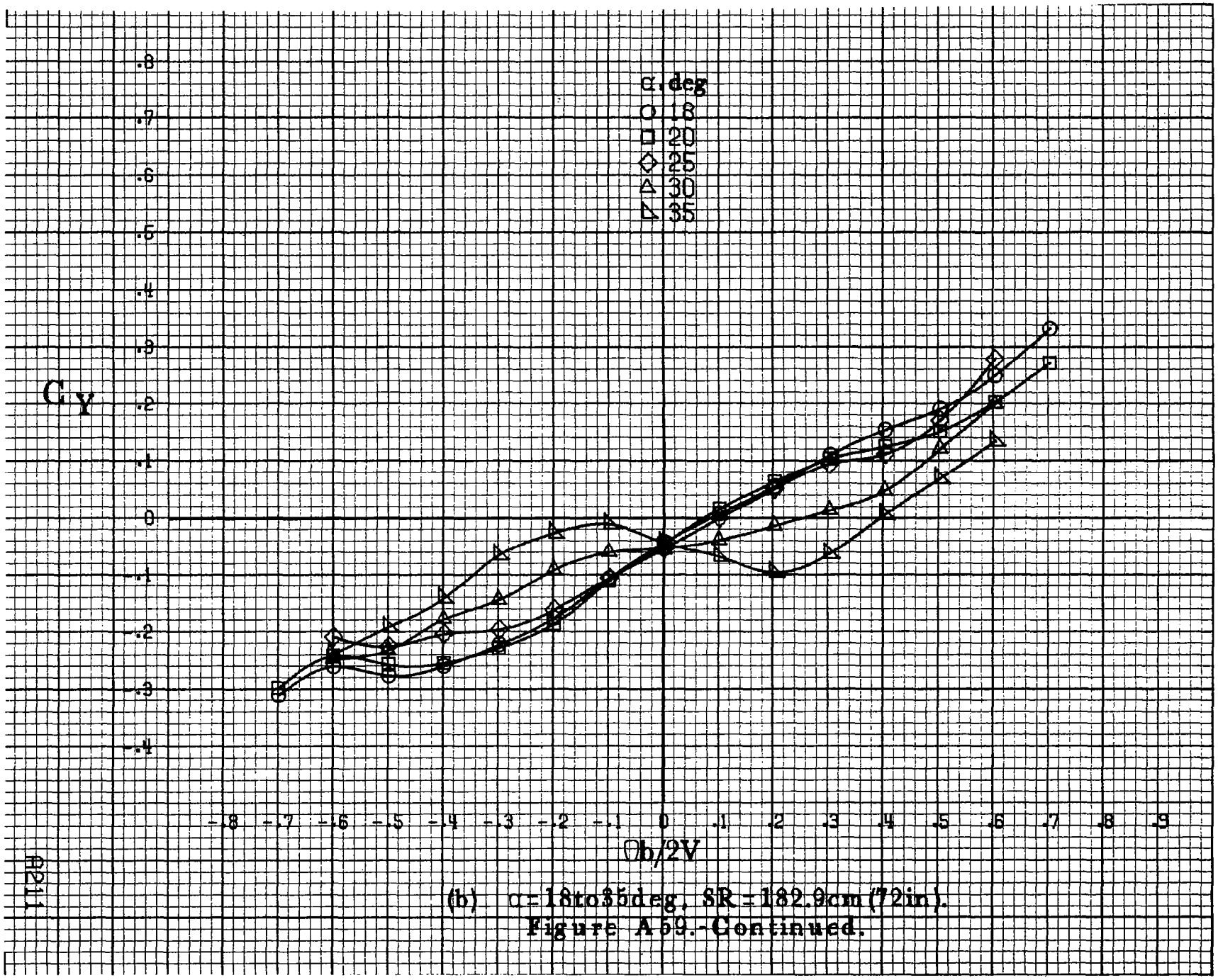

(b) $\alpha = 18$ to 35 deg, SR = 182.9 cm (72 in.).

Figure A69.- Continued.

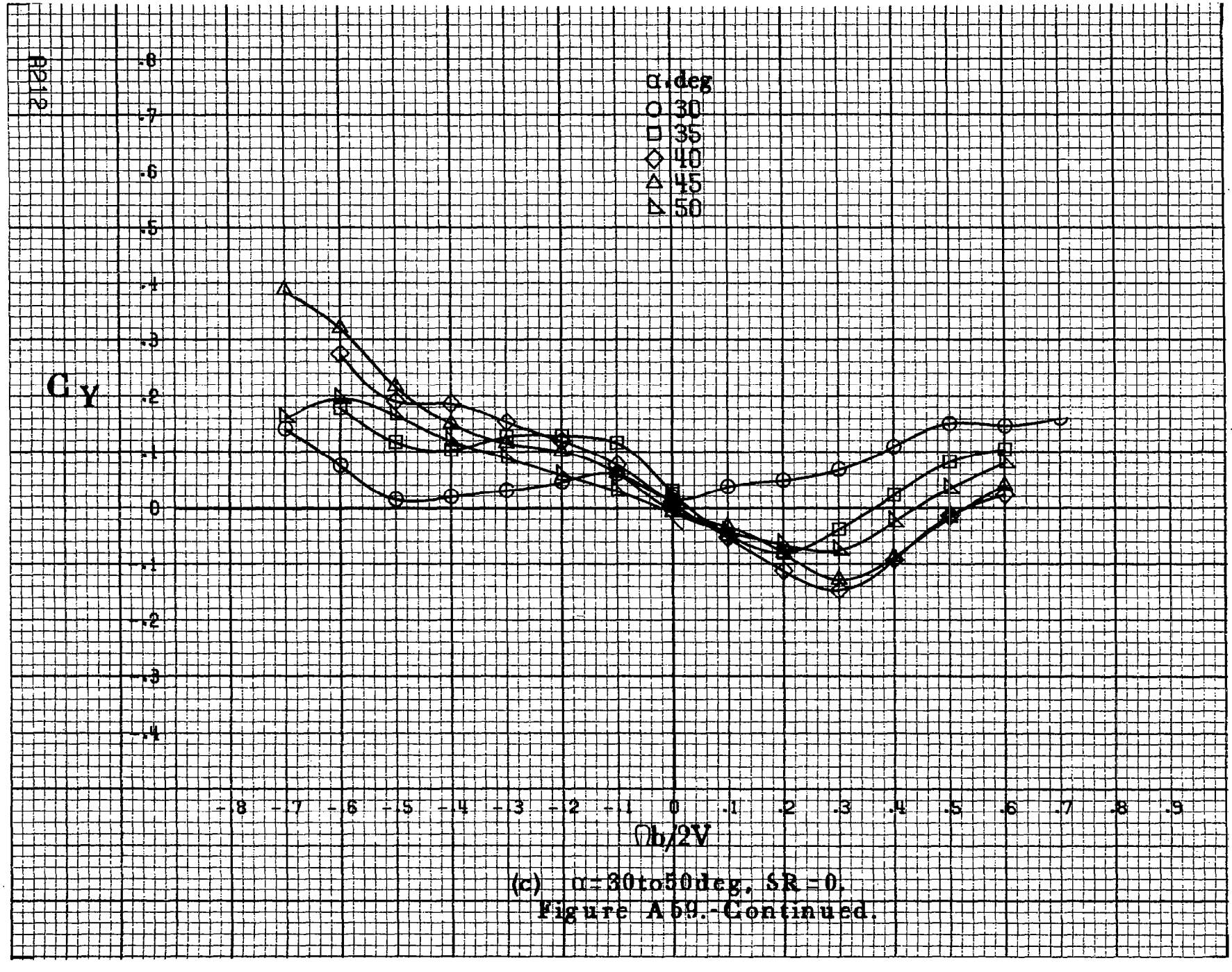

(c) $\alpha = 30$ to 50 deg, SR = 0.

Figure A59.- Continued.

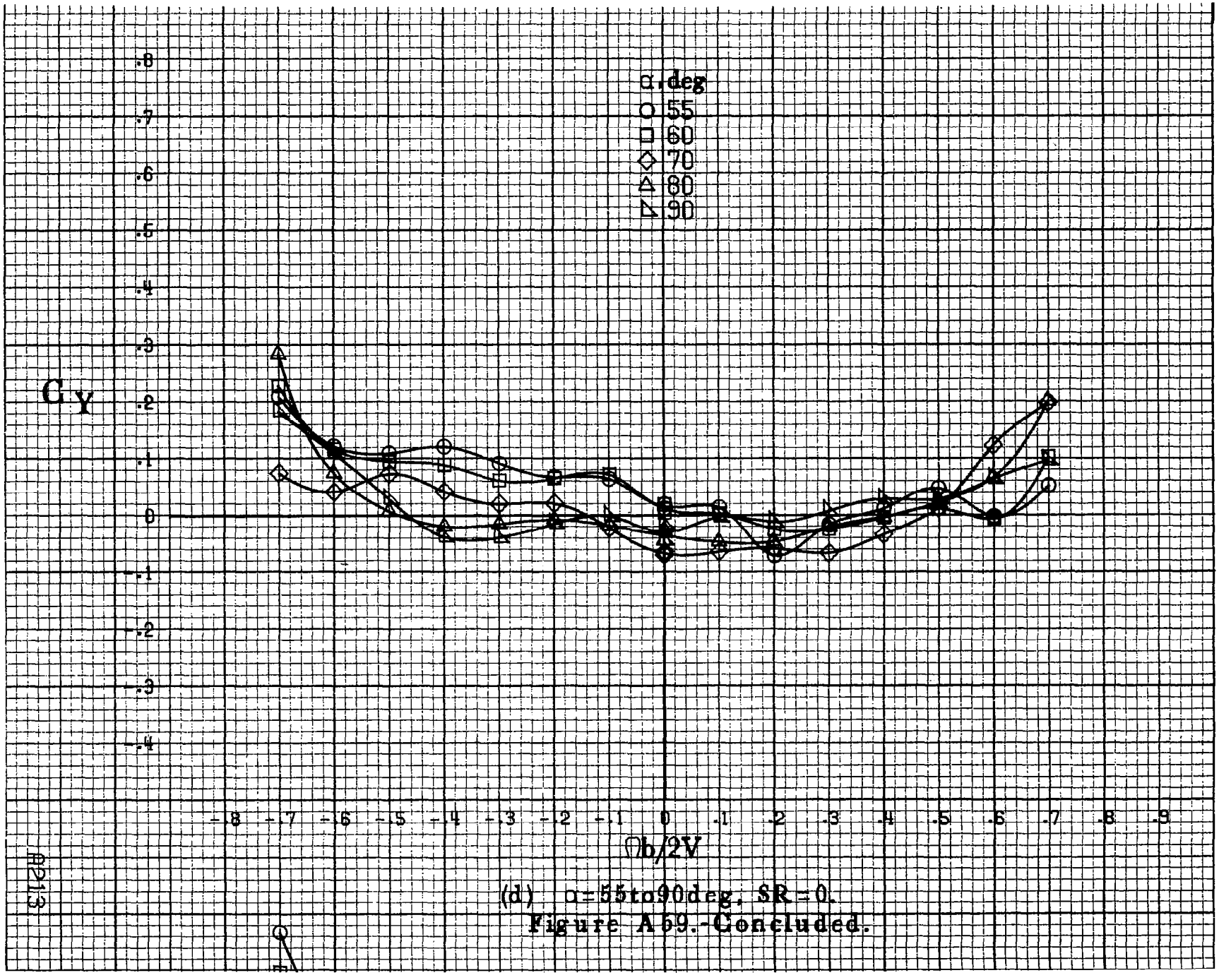

(d) α=55to90deg, SR=0.

Figure A69.-Concluded.

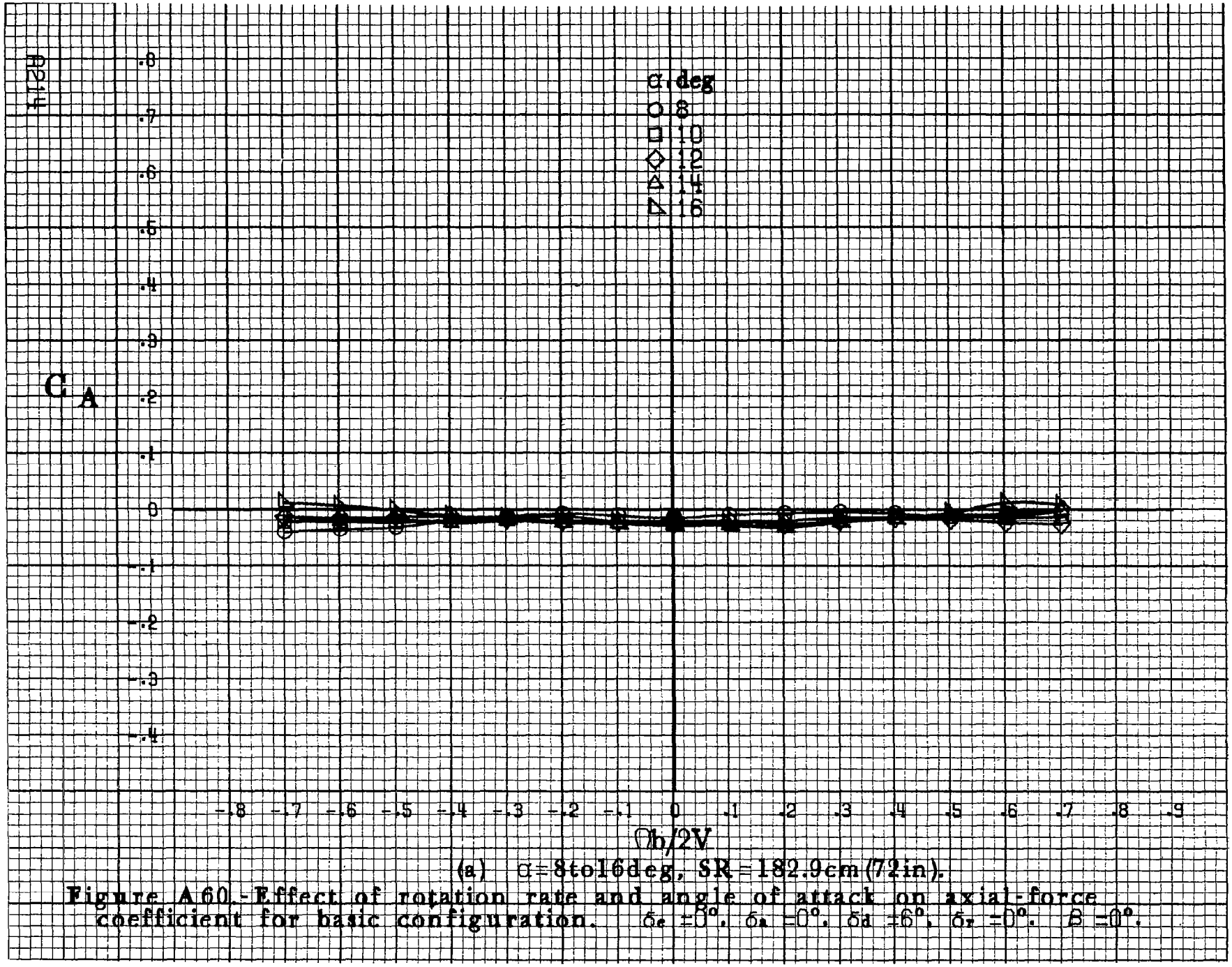

(a) $\alpha = 8$ to 16 deg, SR = 182.9 cm (72 in).

Figure A60.- Effect of rotation rate and angle of attack on axial-force coefficient for basic configuration. $\delta_e = 0°$, $\delta_a = 0°$, $\delta_d = 6°$, $\delta_r = 0°$, $\beta = 0°$.

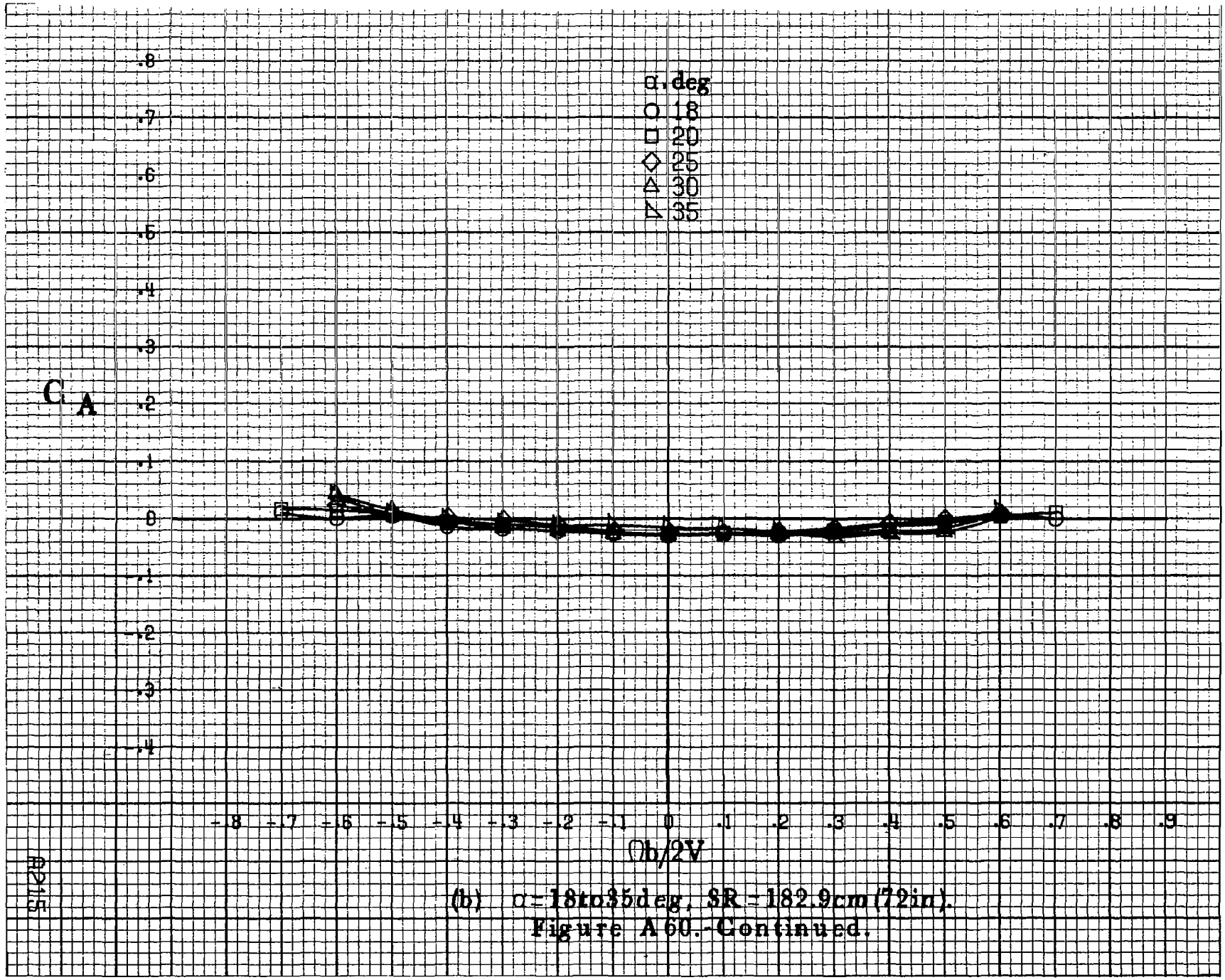

(b) $\alpha = 18$ to 35 deg, SR = 182.9 cm (72 in).

Figure A60.-Continued.

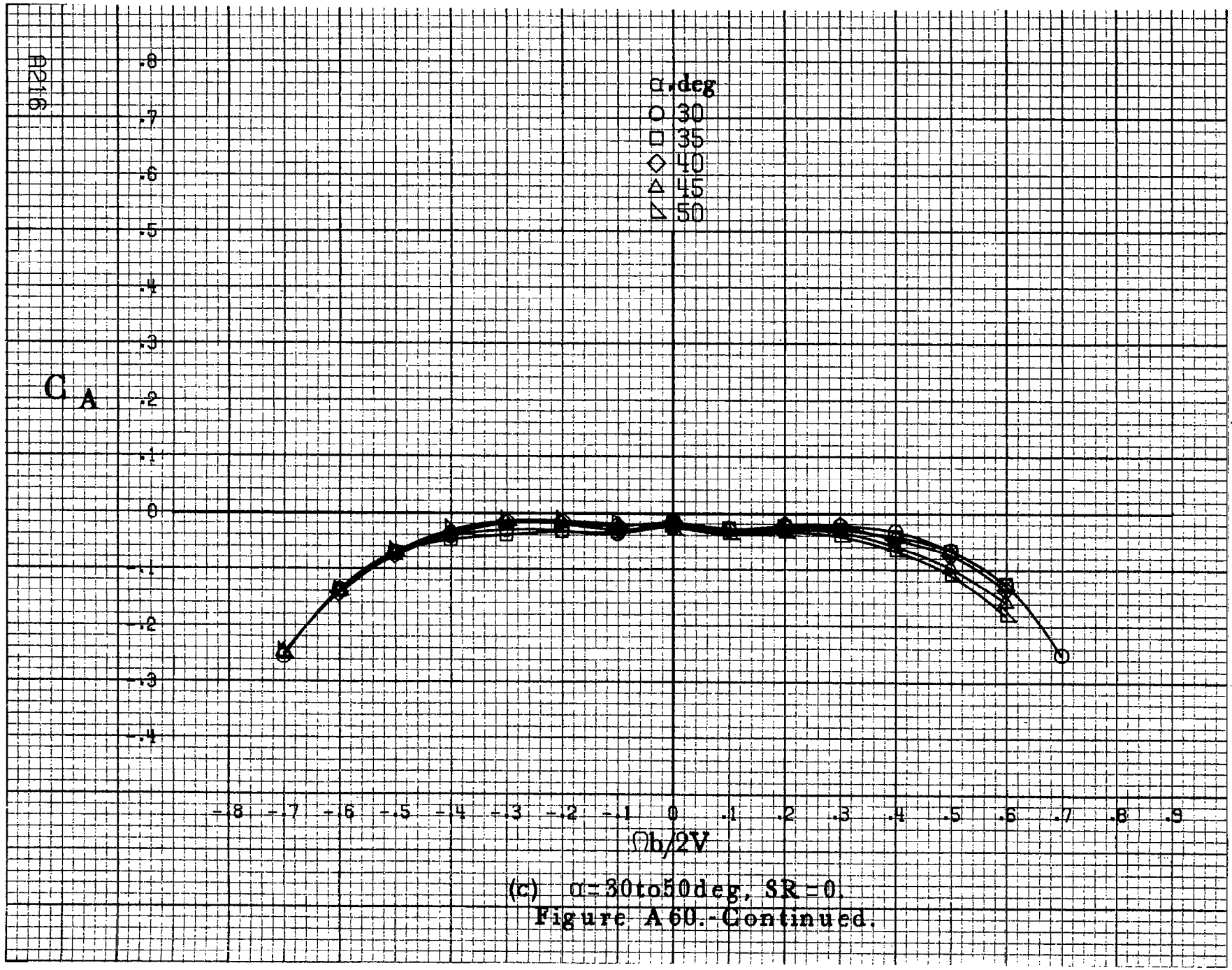

(c) α = 30 to 50 deg, SR = 0.

Figure A60.- Continued.

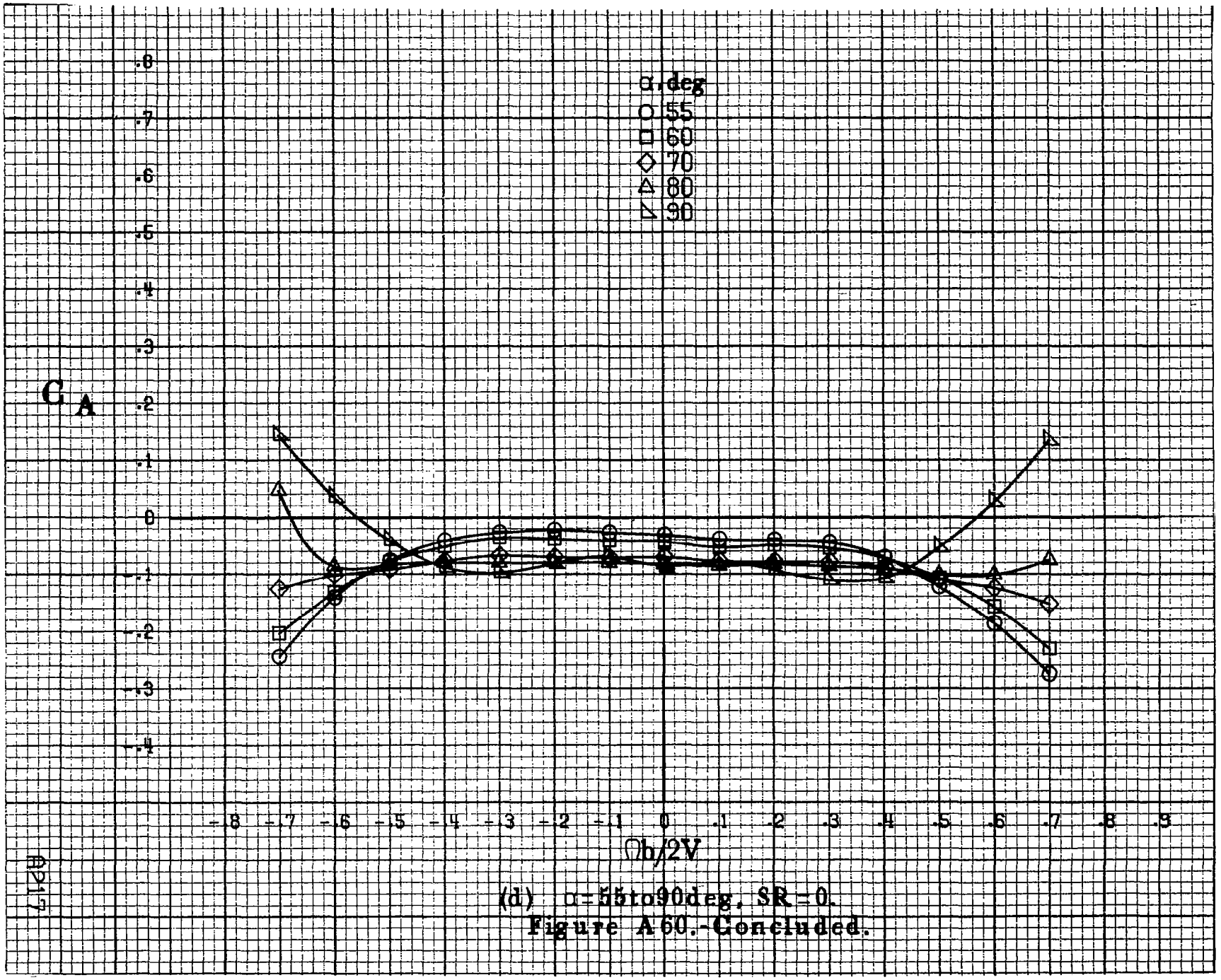

(d) α=55to90deg, SR=0.

Figure A60.-Concluded.

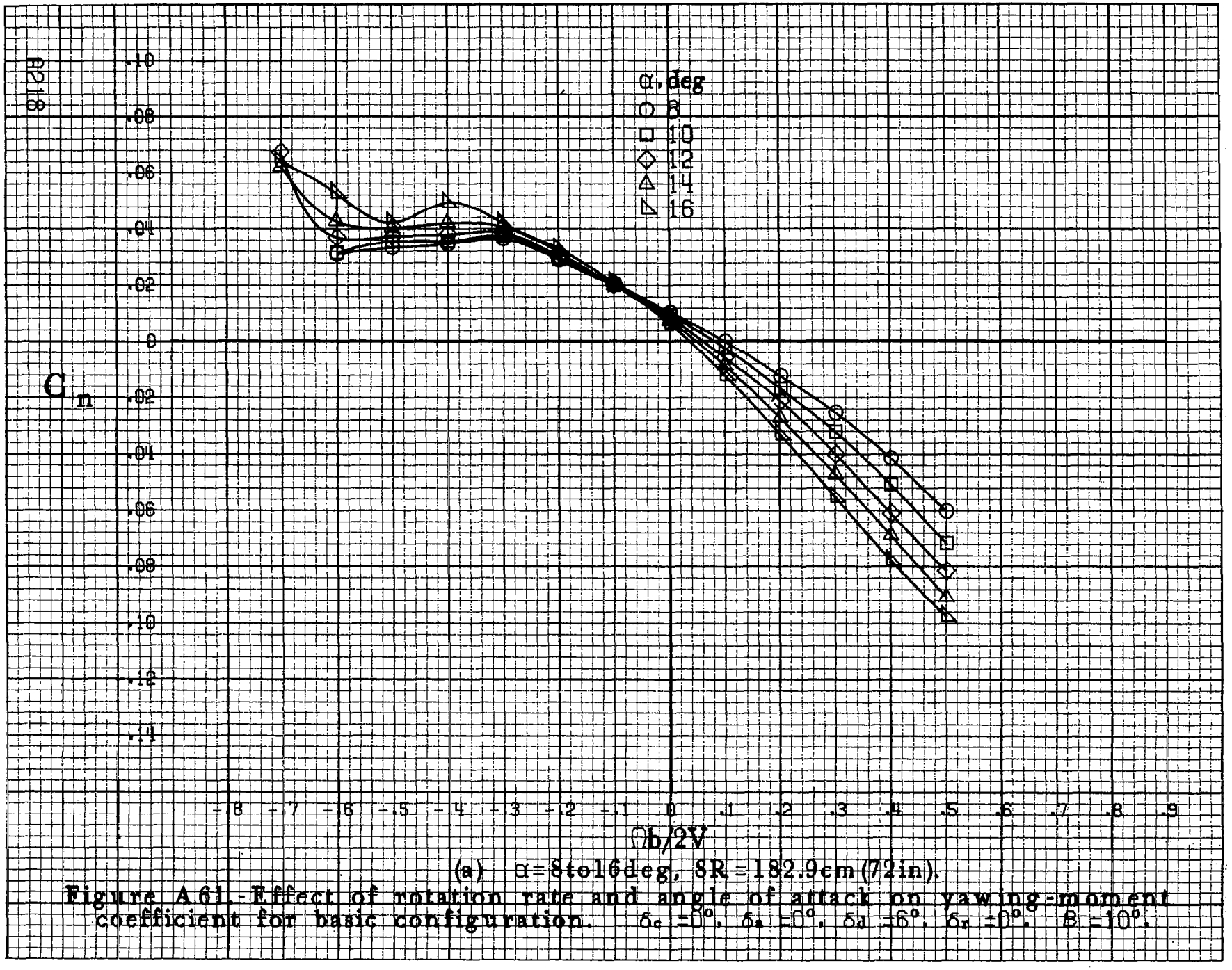

(a) $\alpha = 8$ to 16 deg, SR = 182.9 cm (72 in).

Figure A61.- Effect of rotation rate and angle of attack on yawing-moment coefficient for basic configuration. $\delta_e = 0^\circ$, $\delta_a = 0^\circ$, $\delta_d = 6^\circ$, $\delta_r = 0^\circ$, $\beta = 10^\circ$.

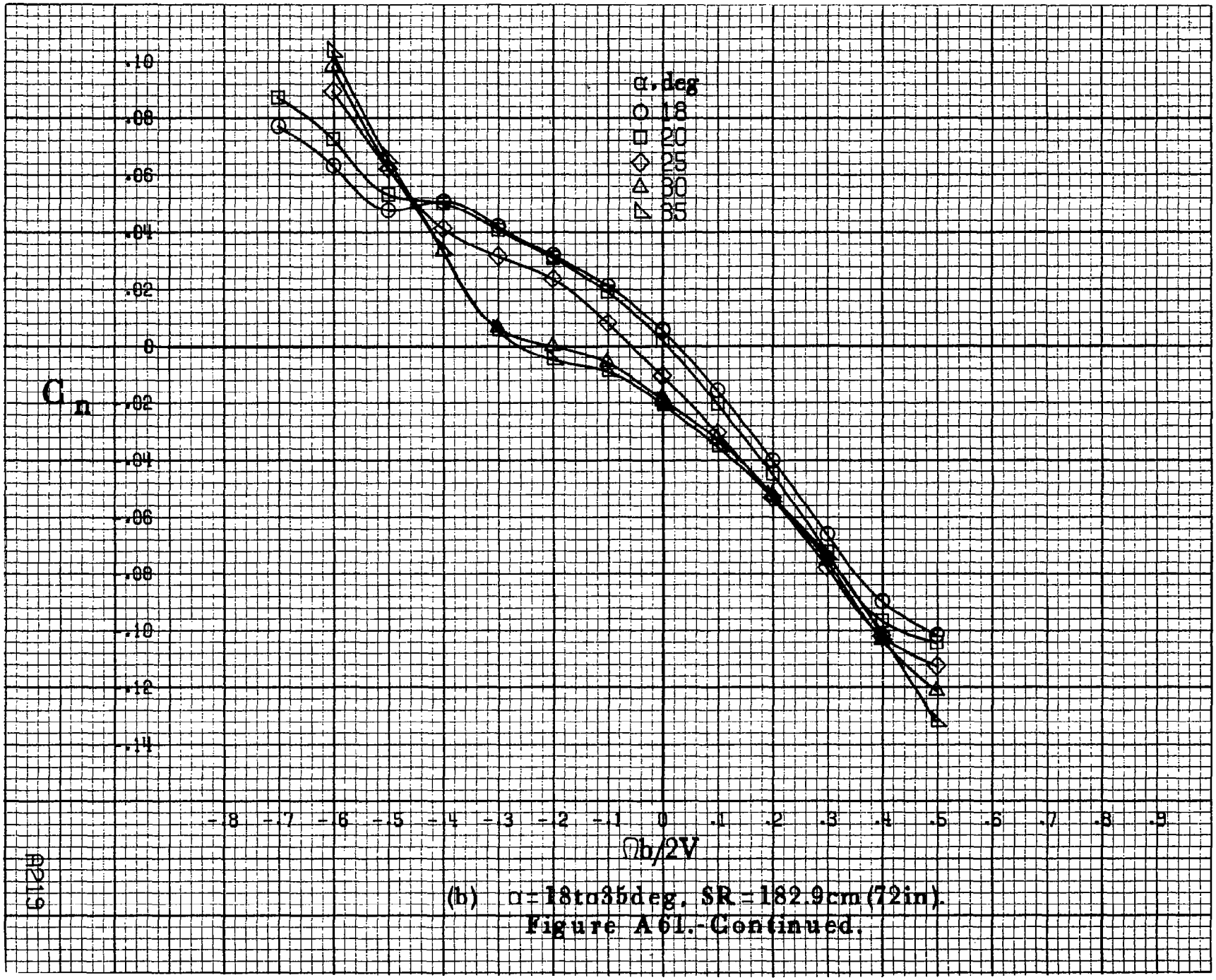

(b) α = 18 to 35 deg, SR = 182.9 cm (72 in).

Figure A61.- Continued.

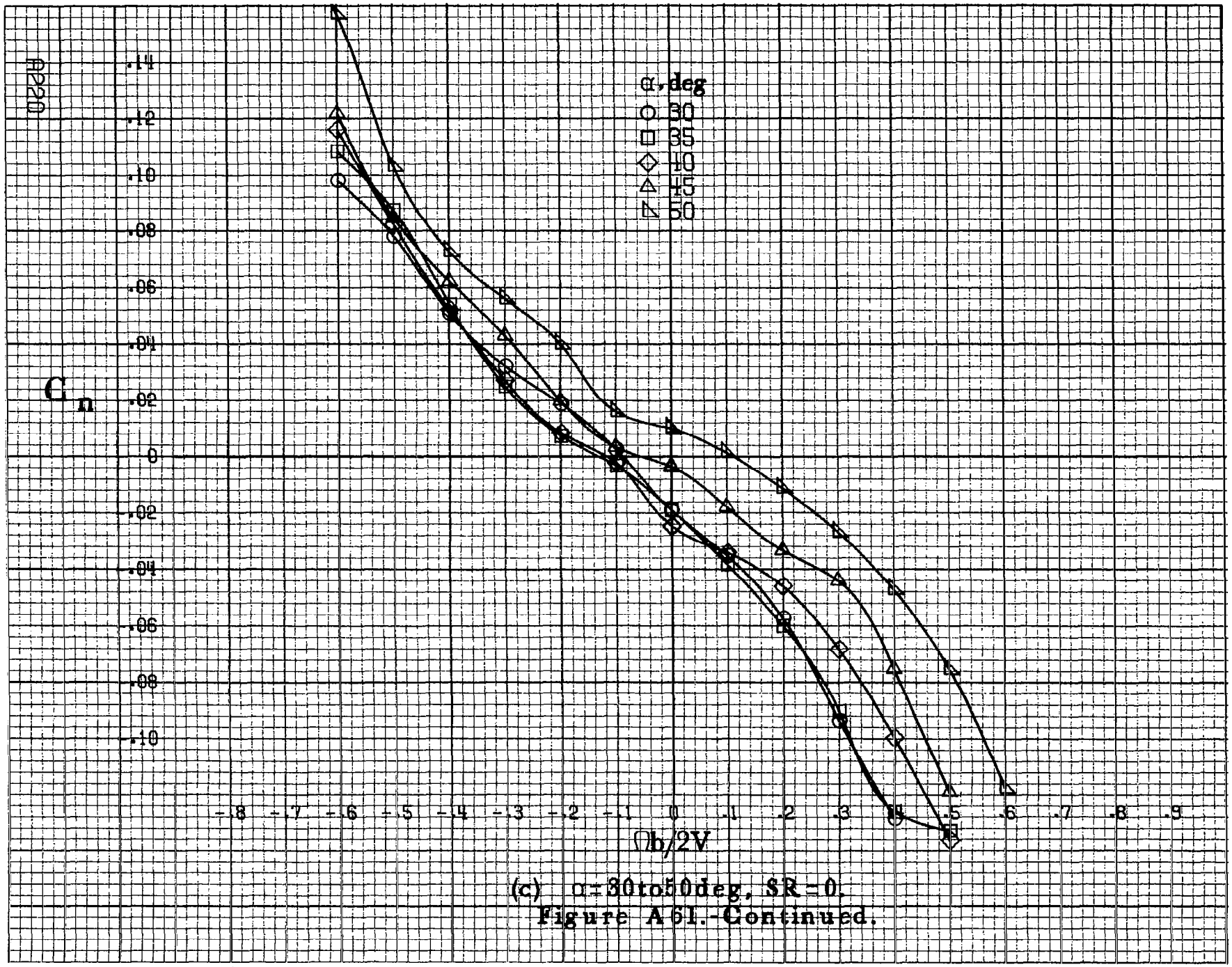

(c) α = 30 to 50 deg, SR = 0.

Figure A61.-Continued.

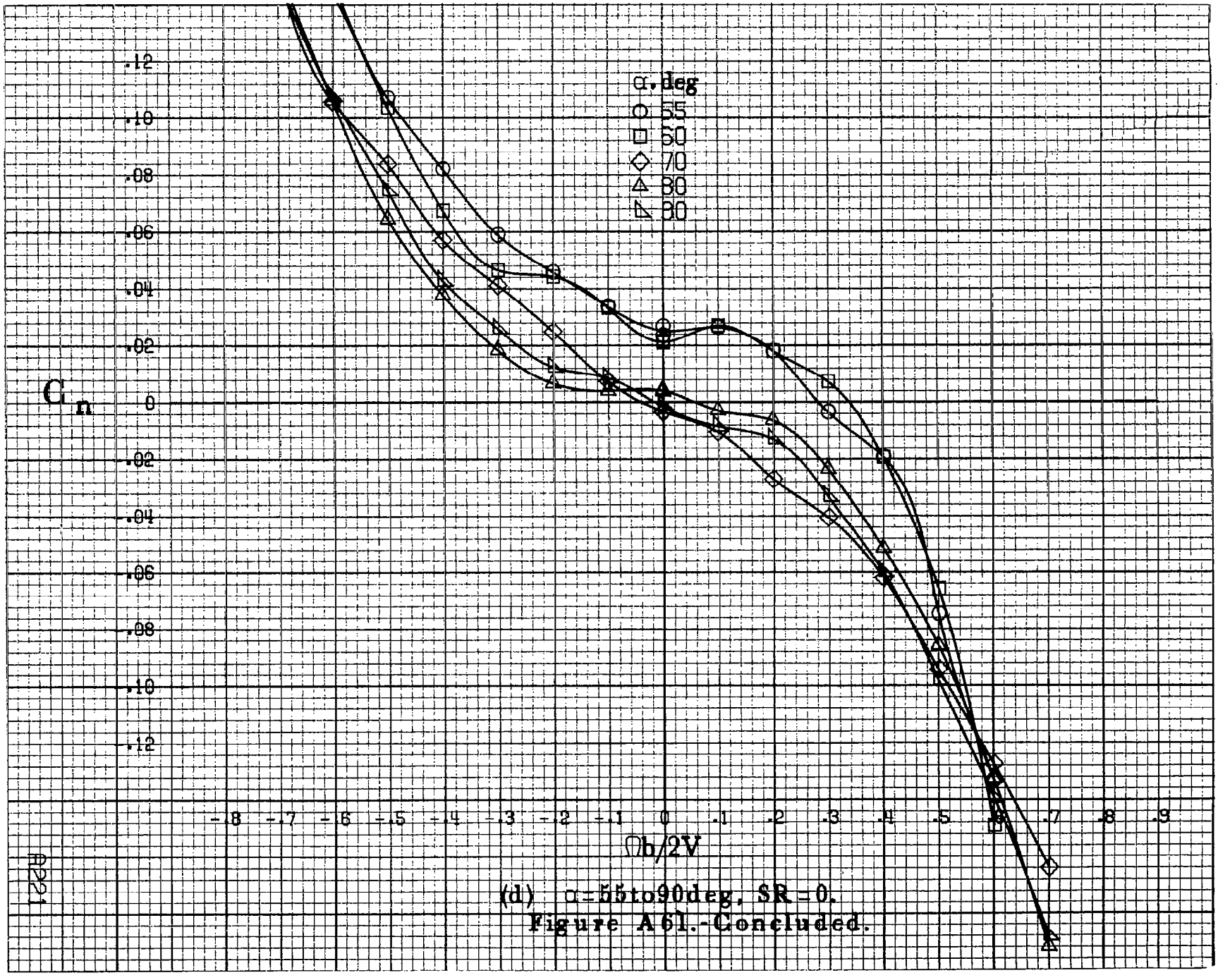

(d) $\alpha = 55$ to 90 deg, $SR = 0$.

Figure A61.- Concluded.

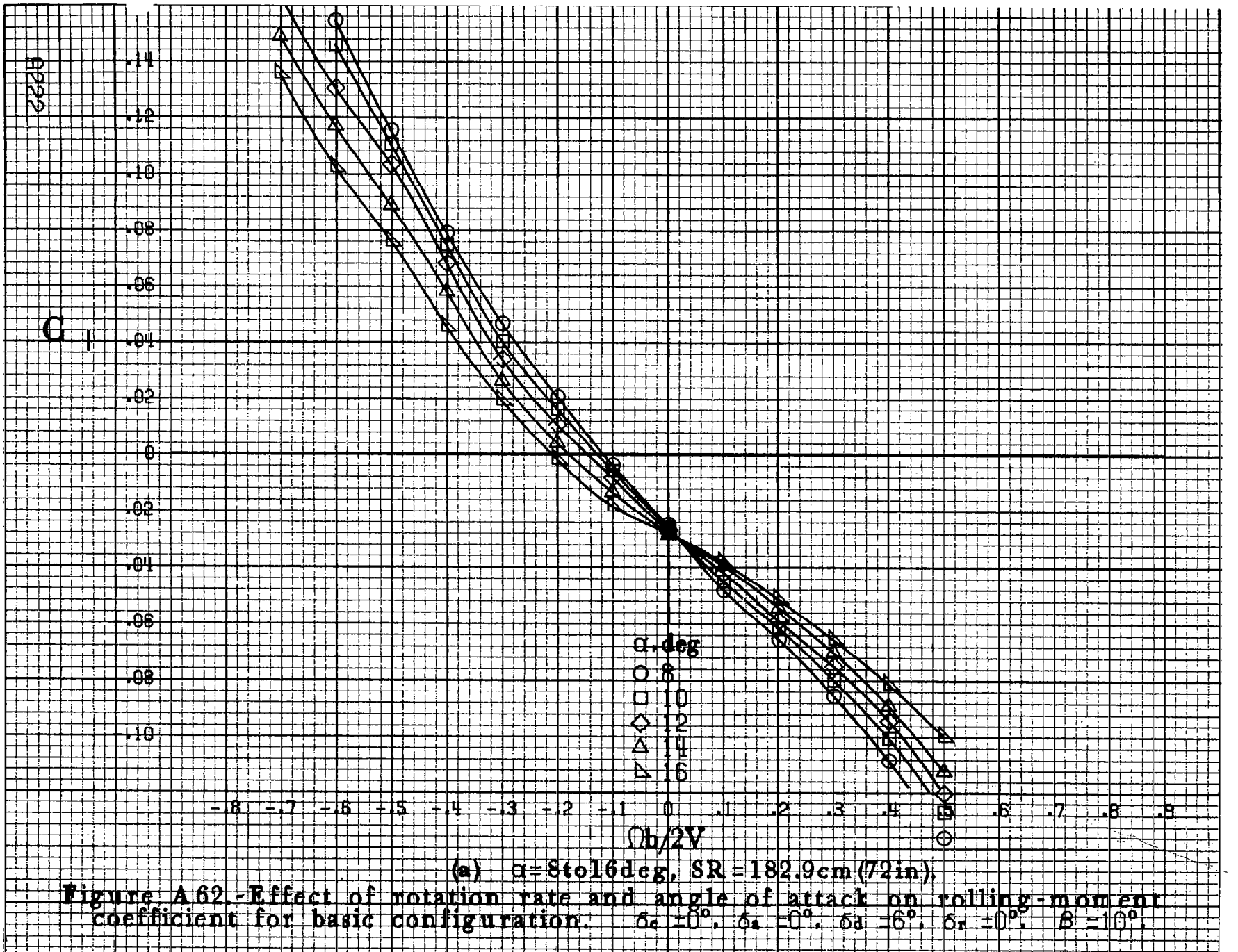

(a) $\alpha = 8$ to 16 deg, SR = 182.9 cm (72 in.).

Figure A62.-Effect of rotation rate and angle of attack on rolling-moment coefficient for basic configuration. $\delta_e = 0°$, $\delta_a = 0°$, $\delta_d = 6°$, $\delta_r = 0°$, $\beta = 10°$.

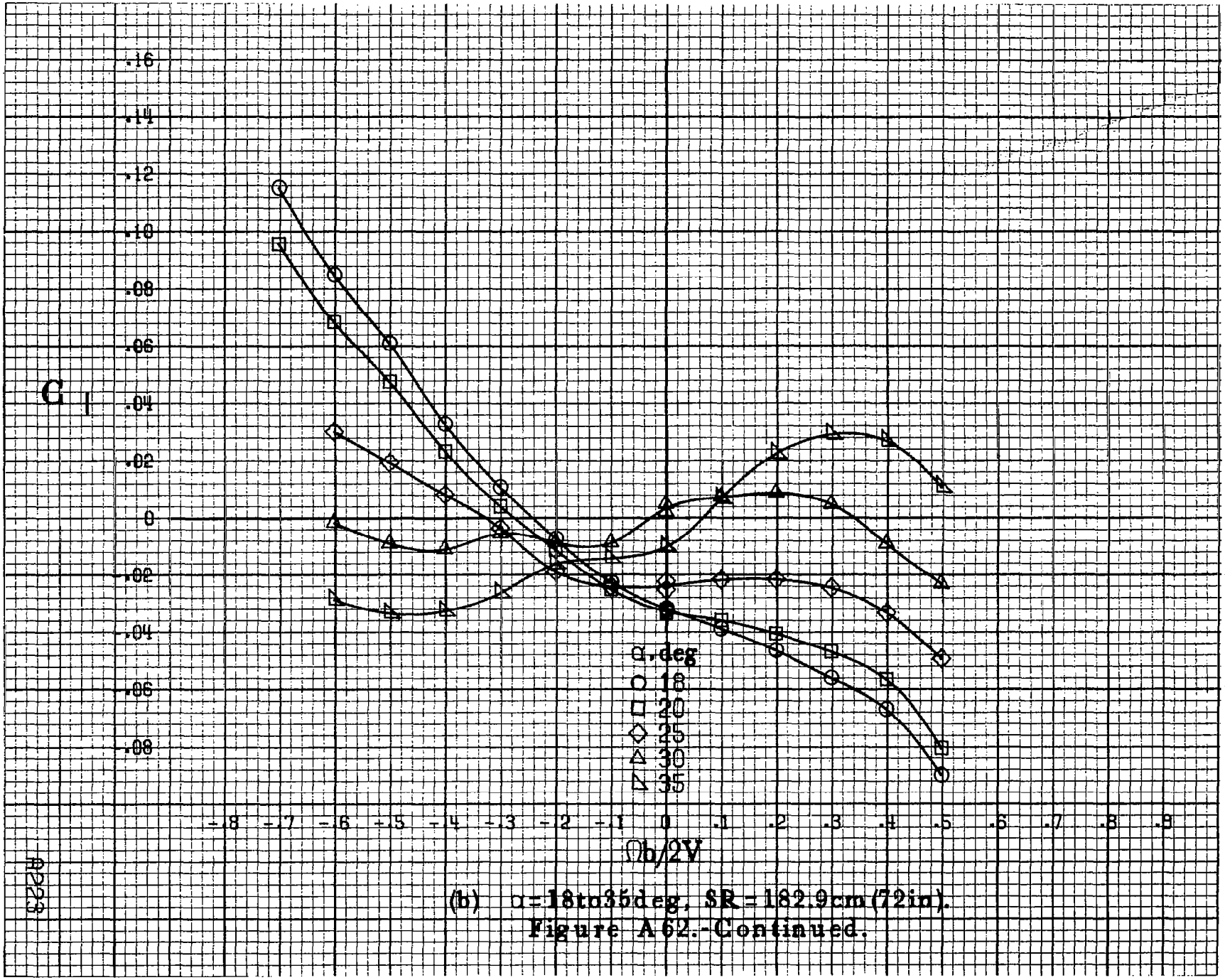

(b) α = 18 to 35 deg, SR = 182.9 cm (72 in).

Figure A62.- Continued.

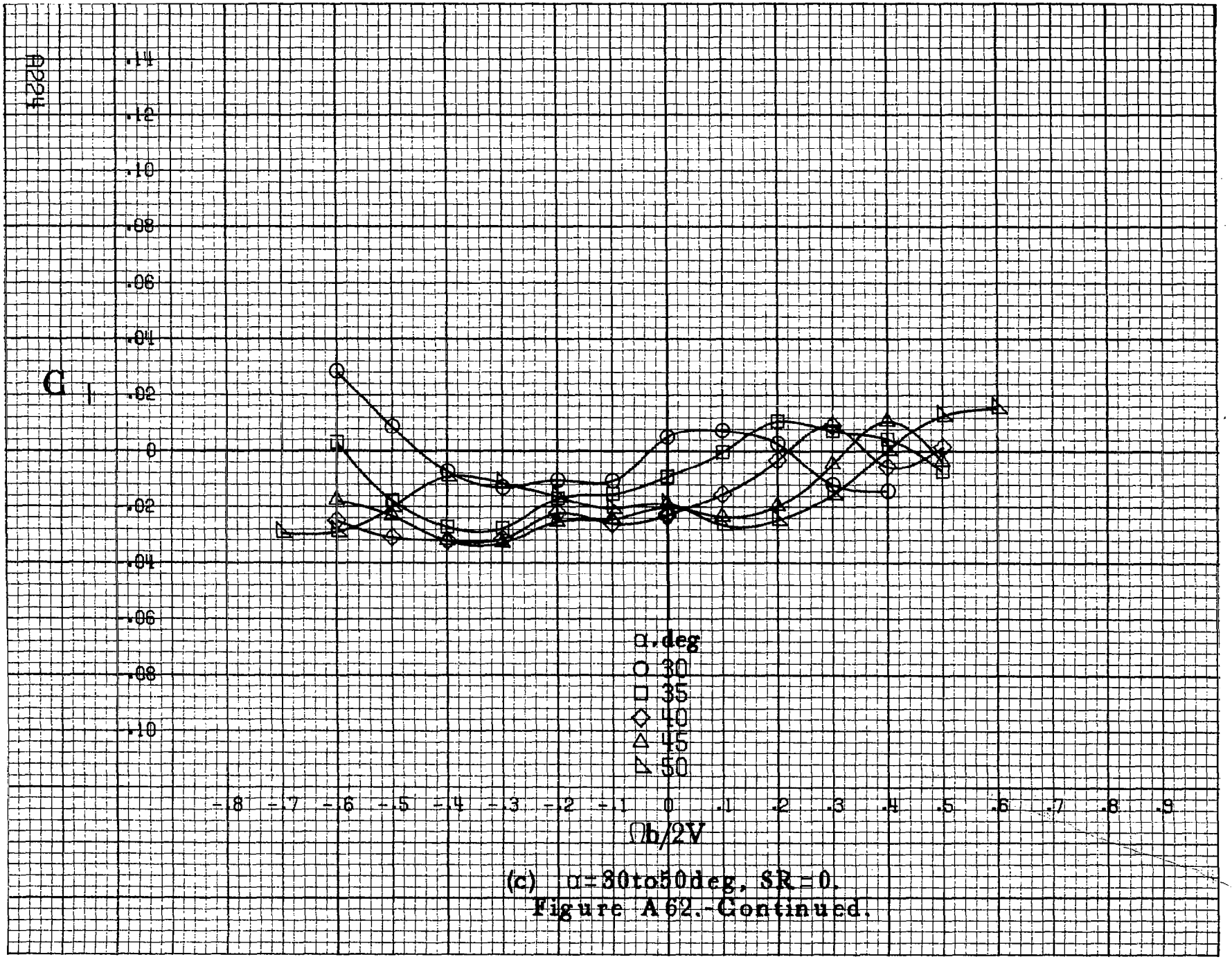

(c) α = 30 to 50 deg, SR = 0.

Figure A62.- Continued.

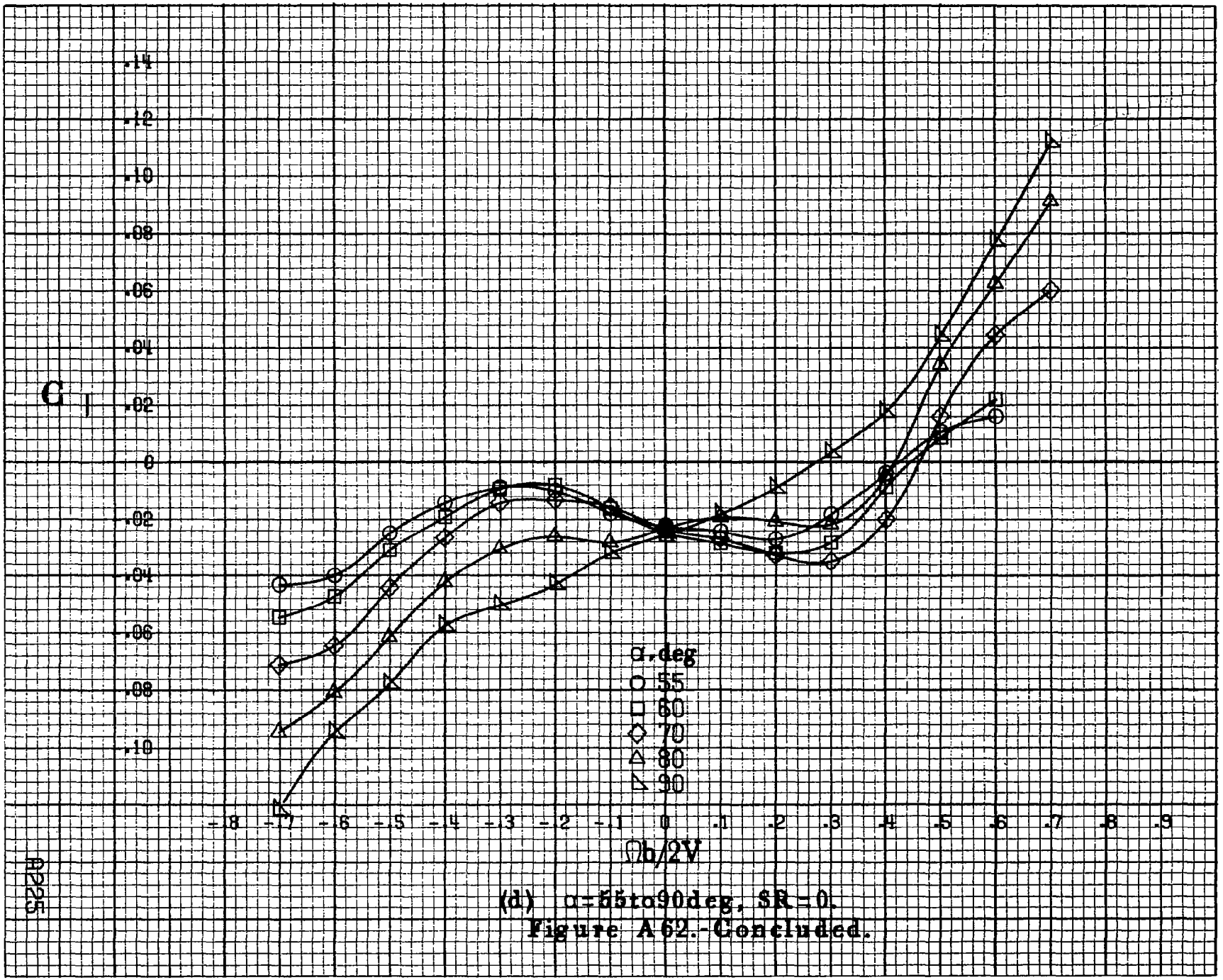

(d) $\alpha = 55$ to 90 deg, $\$R = 0$.

Figure A62.- Concluded.

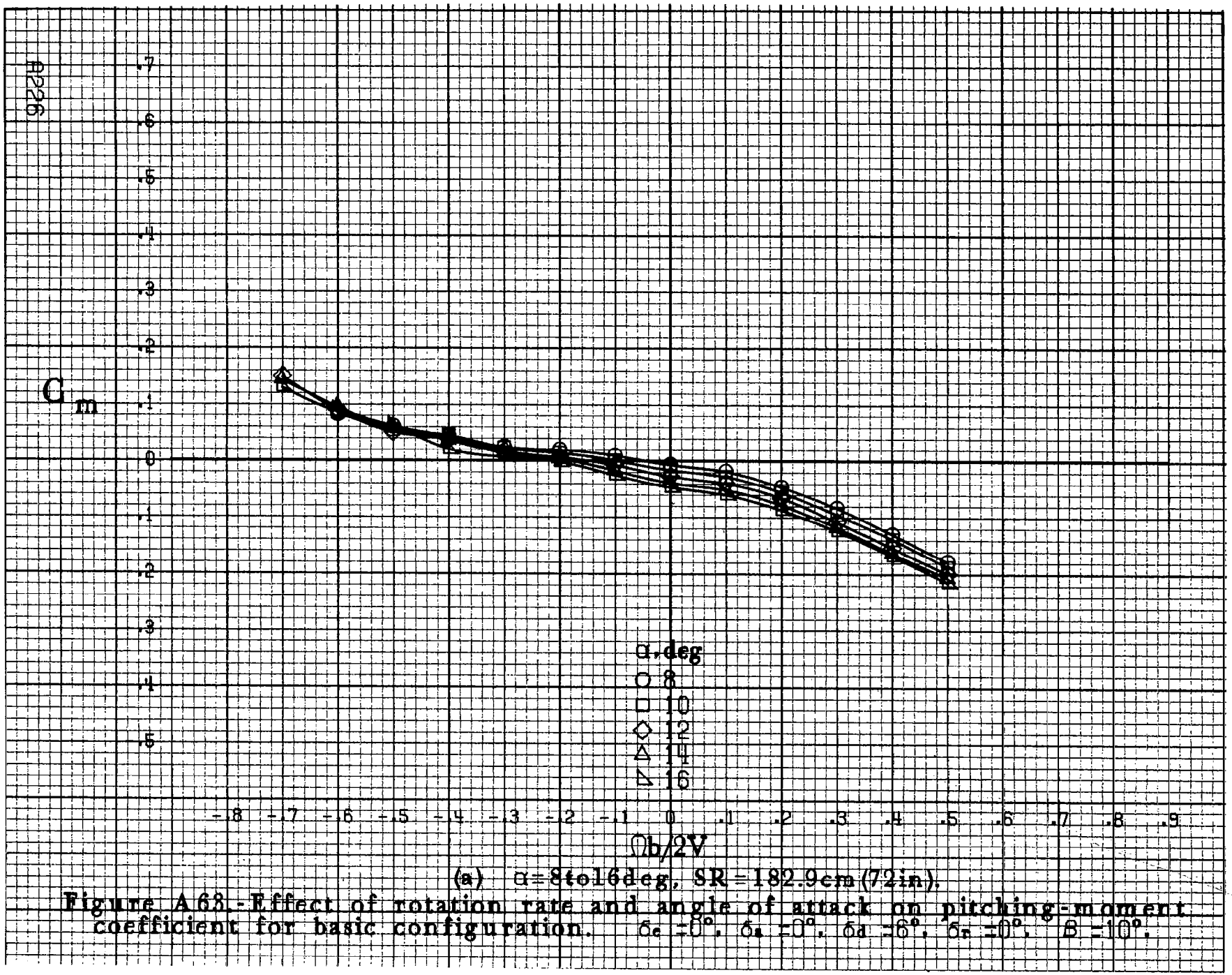

(a) $\alpha = 8$ to 16 deg, SR = 182.9 cm (72 in).

Figure A68.- Effect of rotation rate and angle of attack on pitching-moment coefficient for basic configuration. $\delta_e = 0°$, $\delta_a = 0°$, $\delta_d = 6°$, $\delta_r = 0°$, $\beta = 10°$.

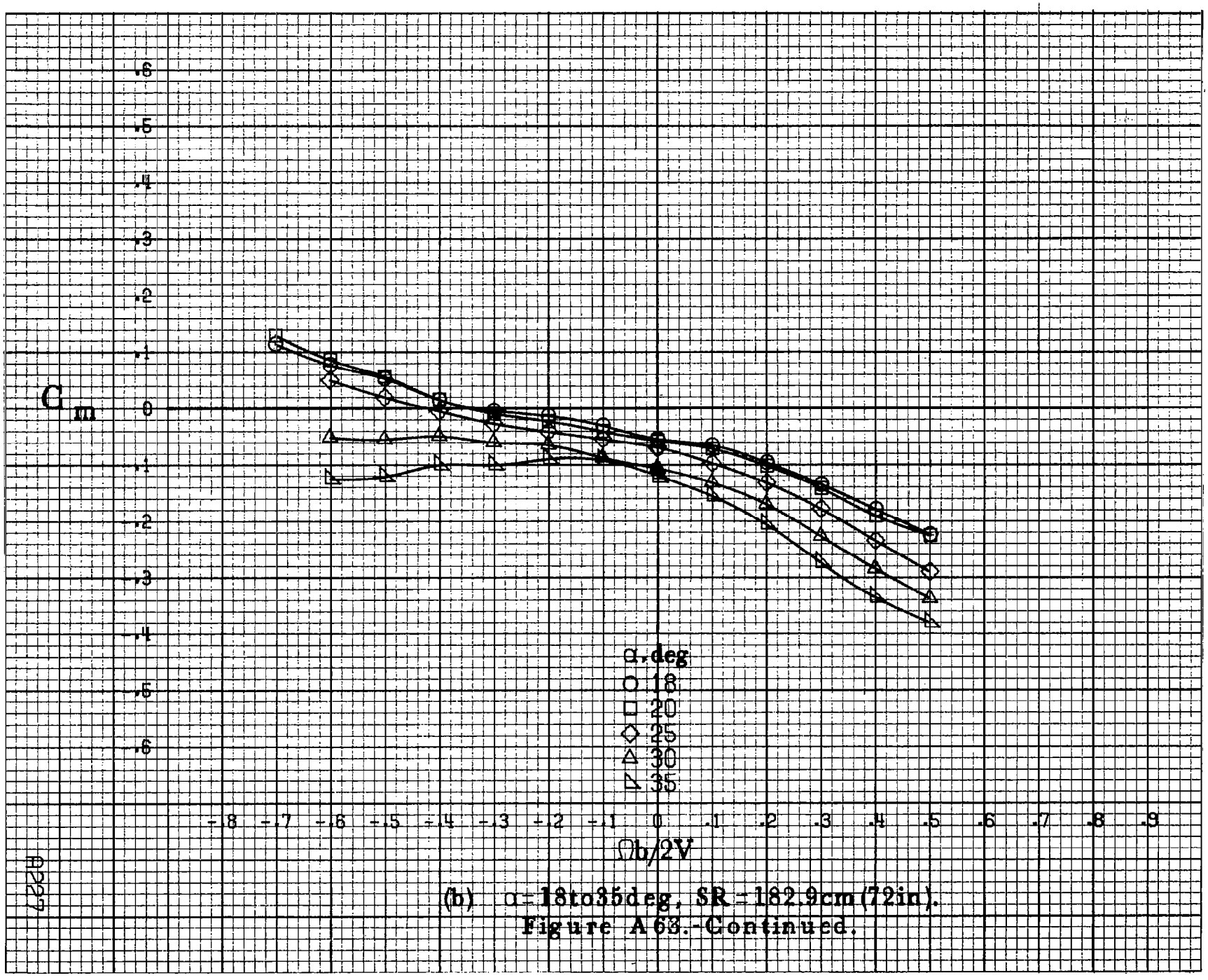

(b) α = 18 to 35 deg, SR = 182.9 cm (72 in).

Figure A63.-Continued.

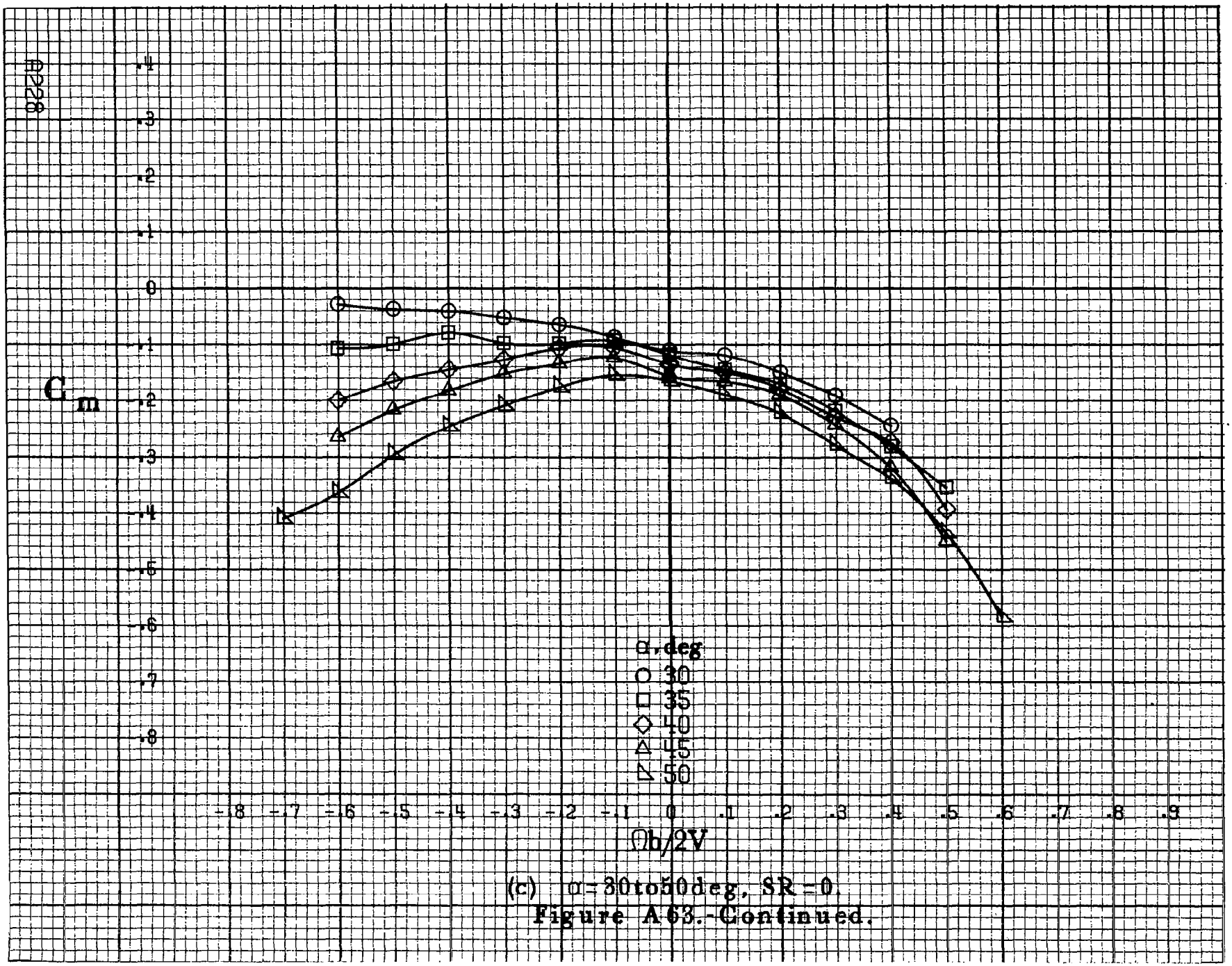

(c) $\alpha = 30$ to 50 deg, SR = 0.

Figure A63.-Continued.

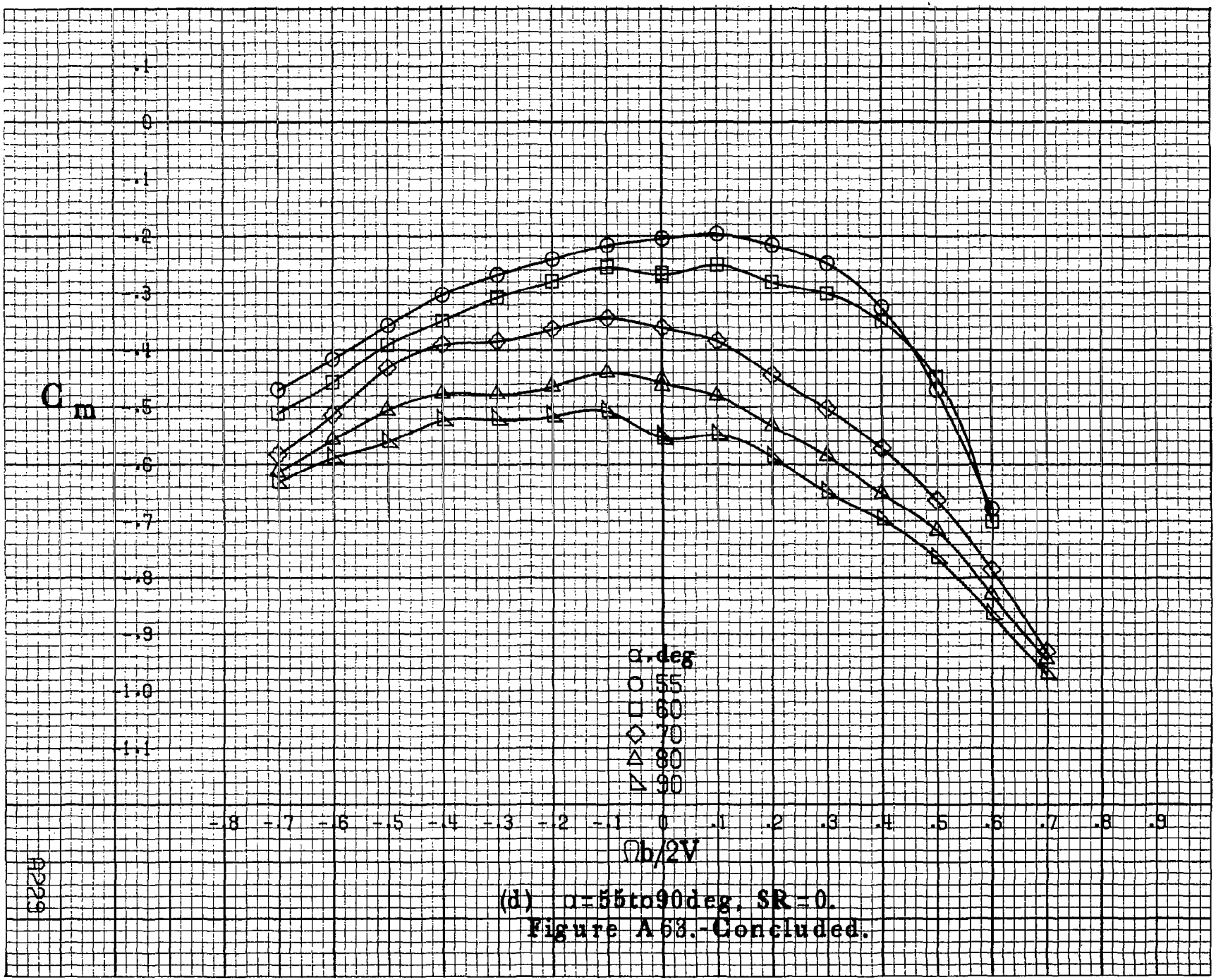

(d) α=55to90deg, SR=0.

Figure A63.-Concluded.

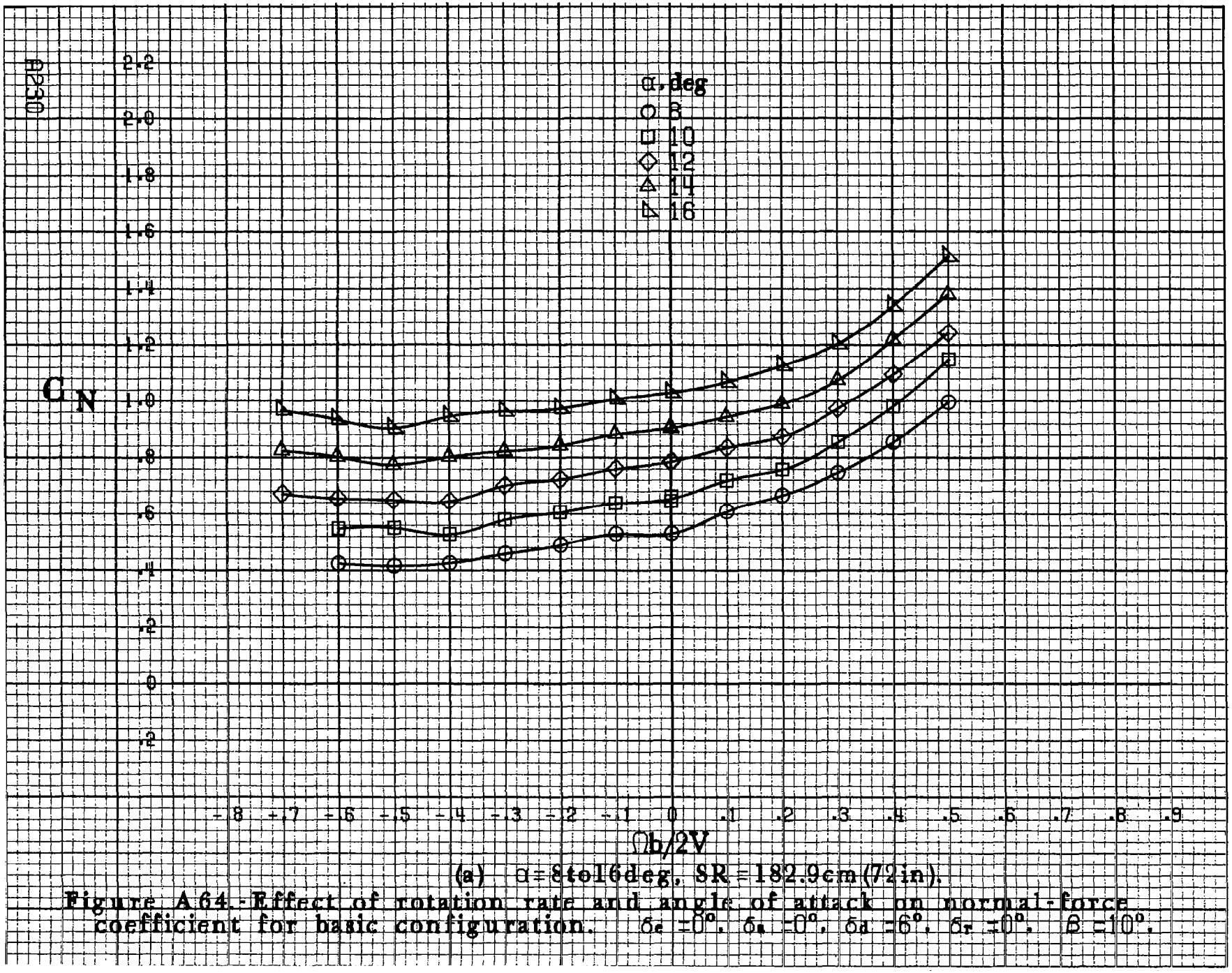

(a) $\alpha = 8$ to 16 deg, SR = 182.9 cm (72 in).

Figure A64.- Effect of rotation rate and angle of attack on normal-force coefficient for basic configuration. $\delta_e = 0°$, $\delta_s = 0°$, $\delta_a = 6°$, $\delta_r = 0°$, $\beta = 10°$.

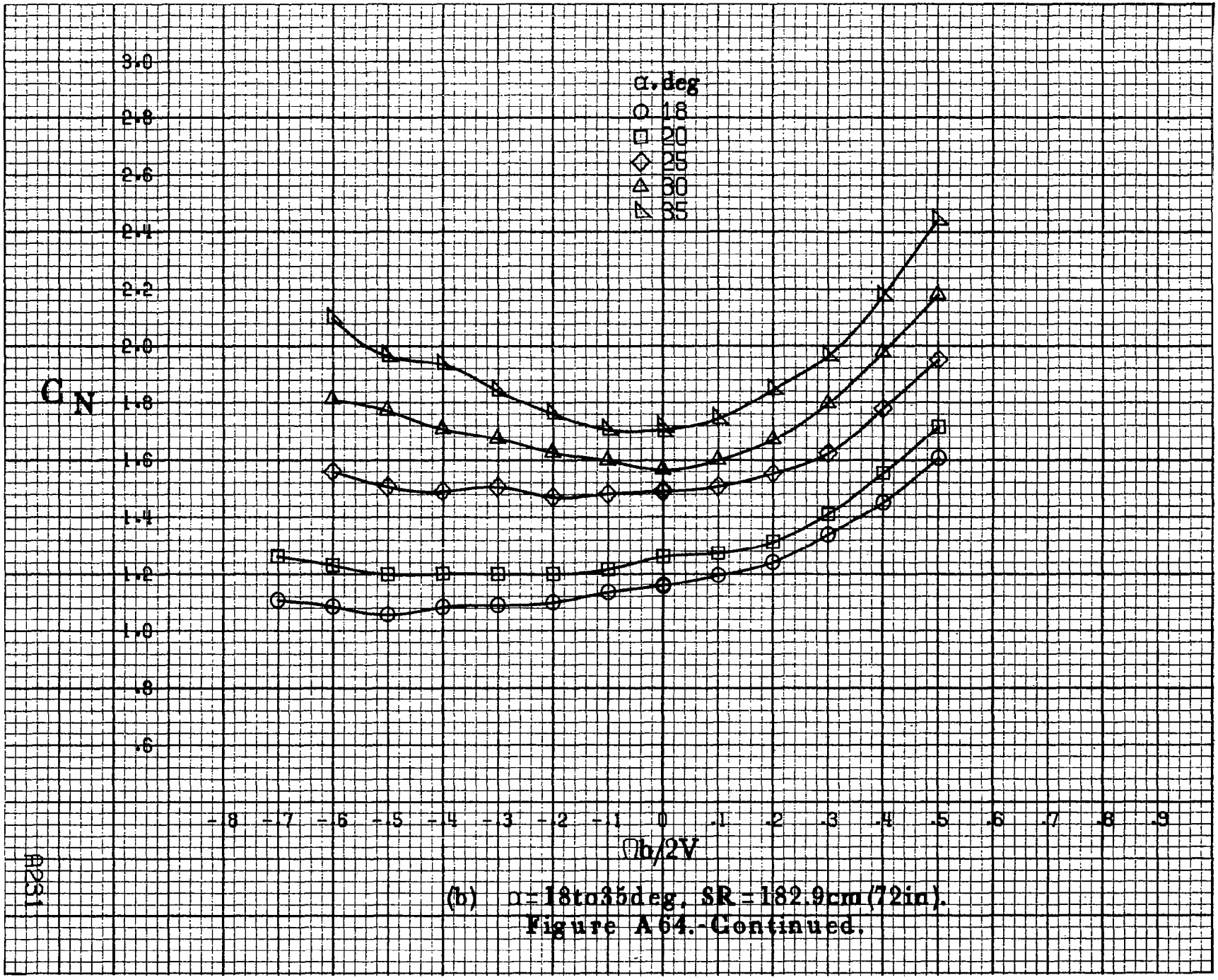

(b) α = 18 to 35 deg, SR = 182.9 cm (72 in).

Figure A 64.- Continued.

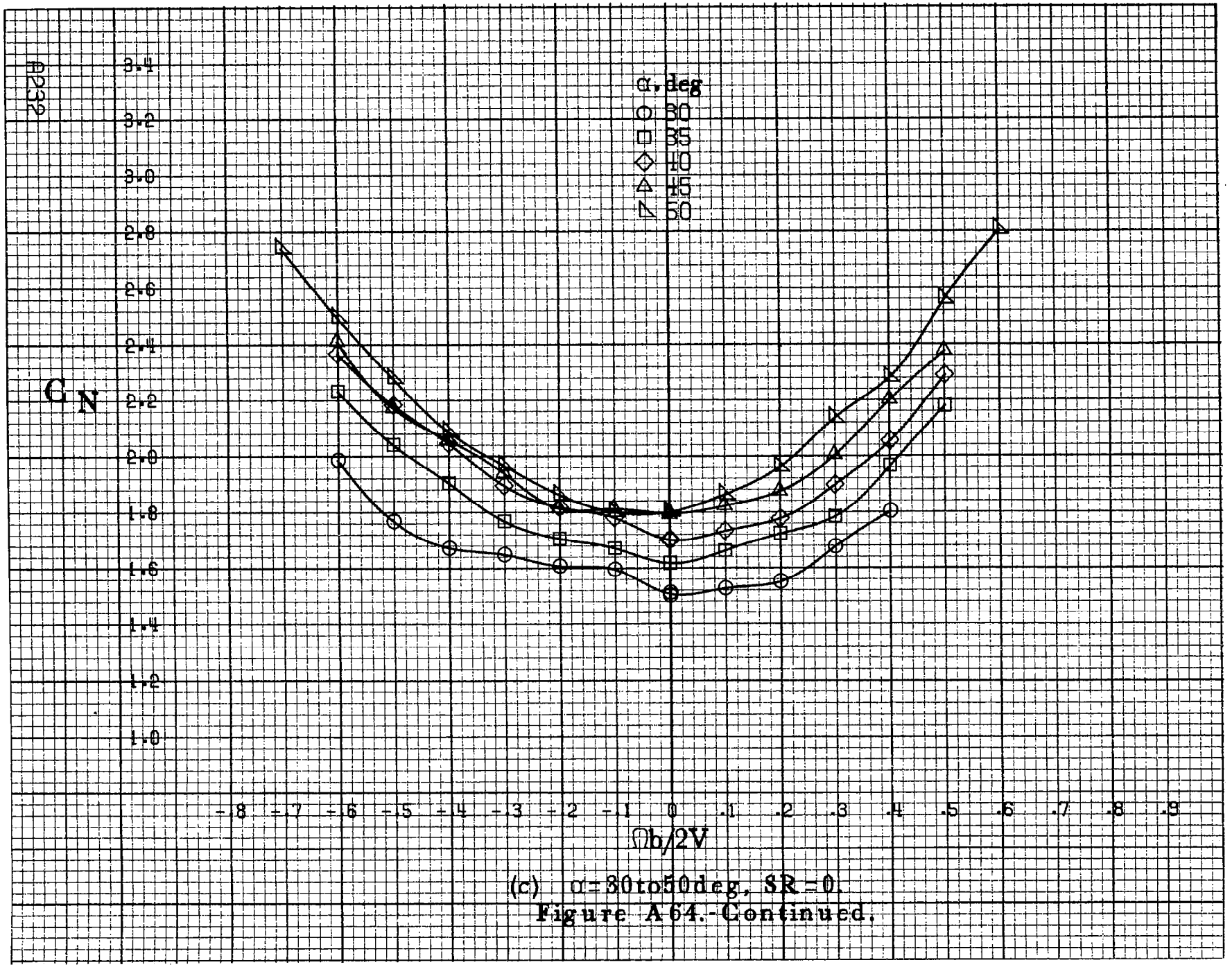

(c) $\alpha = 30$ to 50 deg, SR = 0.

Figure A64.- Continued.

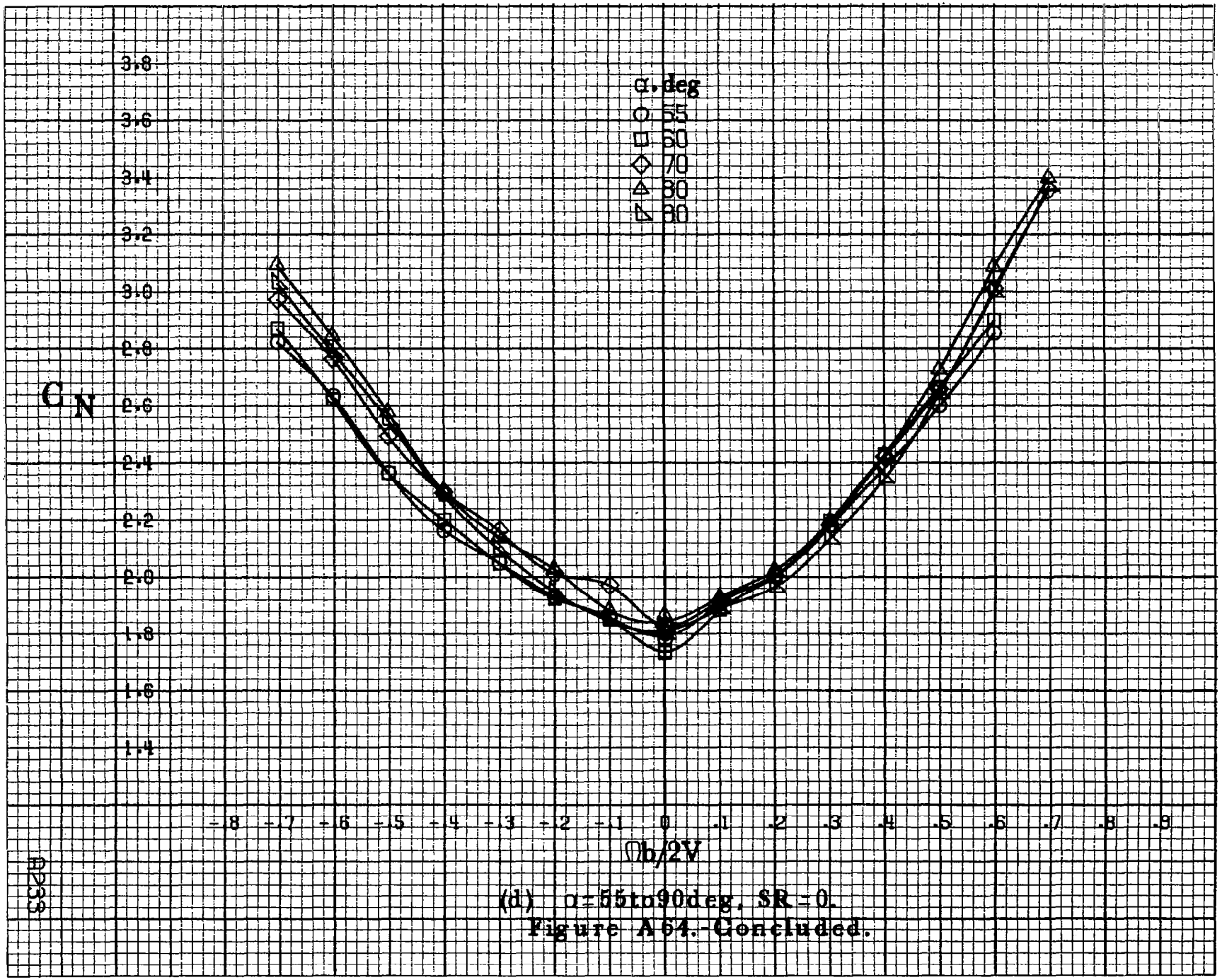

(d) α=55to90deg, SR=0.

Figure A64.-Concluded.

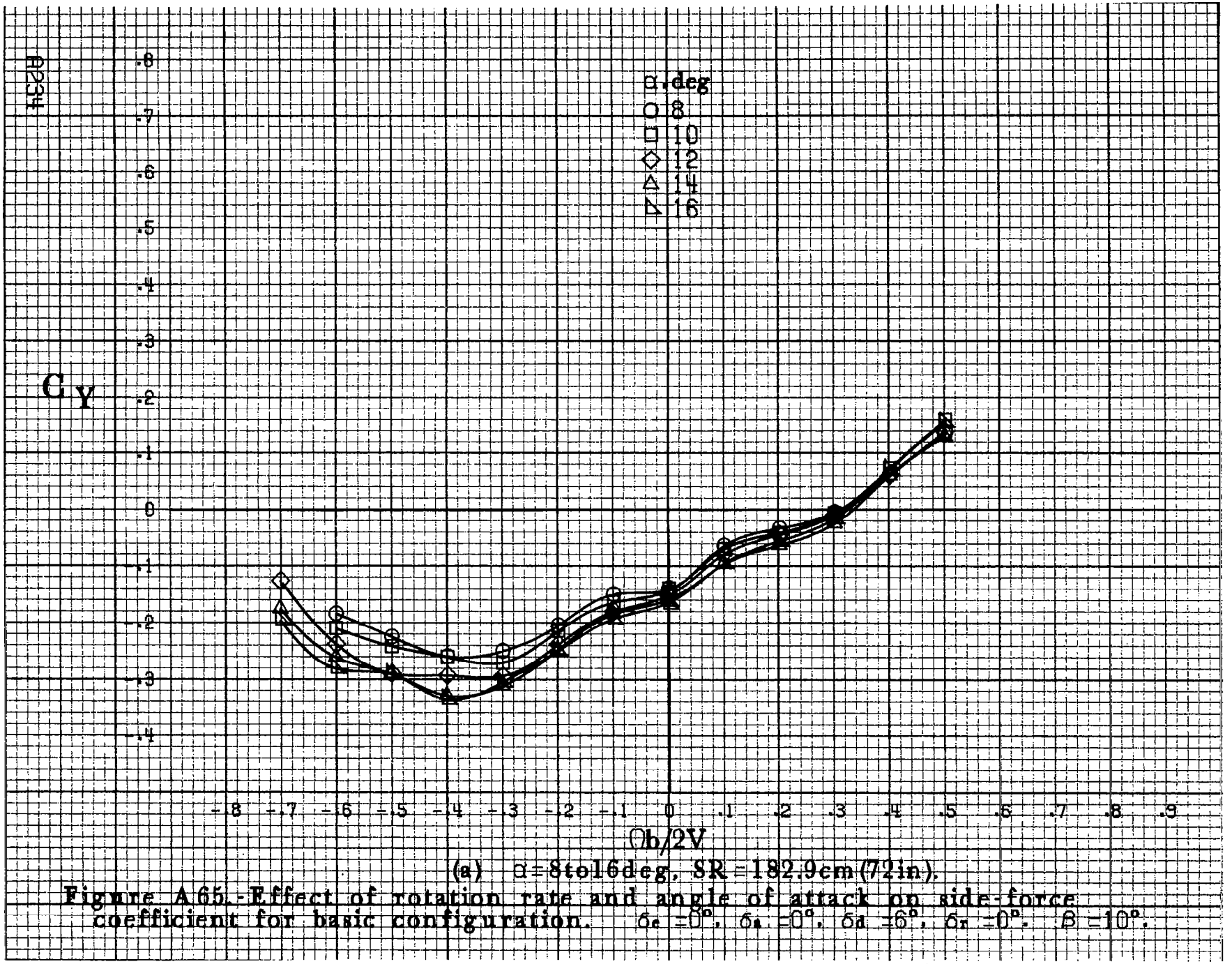

(a) $\alpha = 8$ to 16 deg, SR = 182.9 cm (72 in).

Figure A65.- Effect of rotation rate and angle of attack on side-force coefficient for basic configuration. $\delta_e = 0°$, $\delta_a = 0°$, $\delta_d = 6°$, $\delta_r = 0°$, $\beta = 10°$.

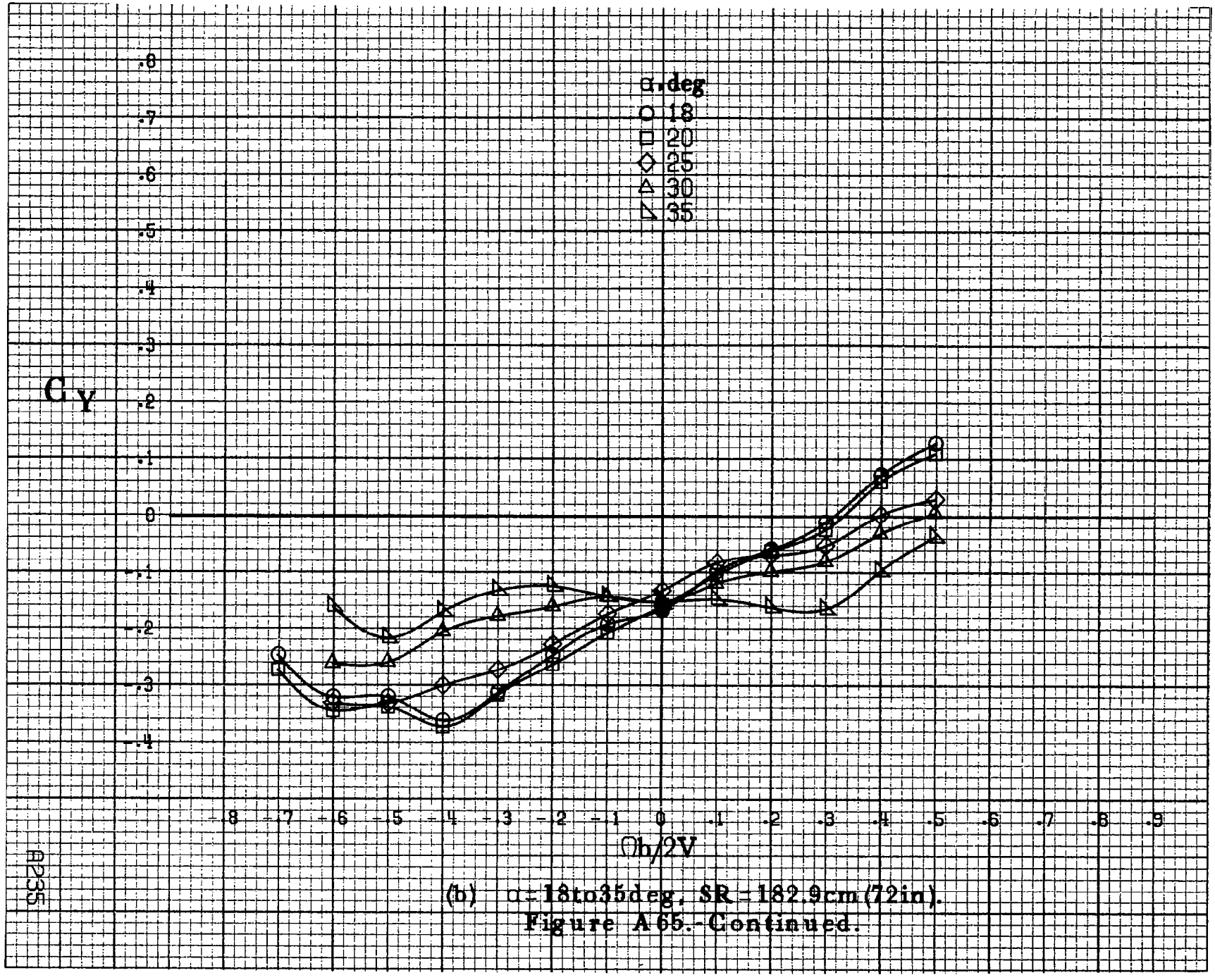

(b) α = 18 to 35 deg, SR = 182.9 cm (72 in).

Figure A65.- Continued.

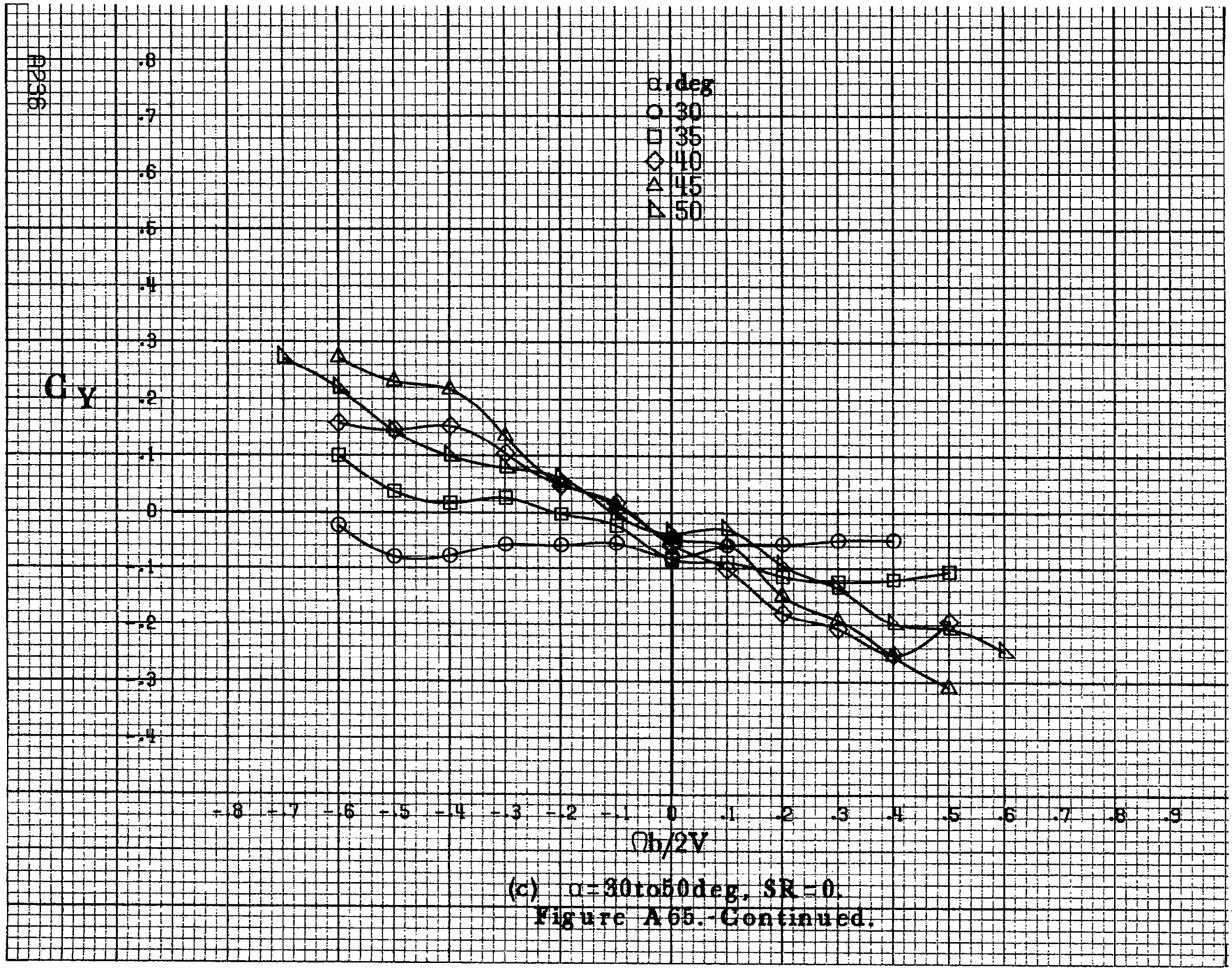

(c) α = 30 to 50 deg, SR = 0.

Figure A65.- Continued.

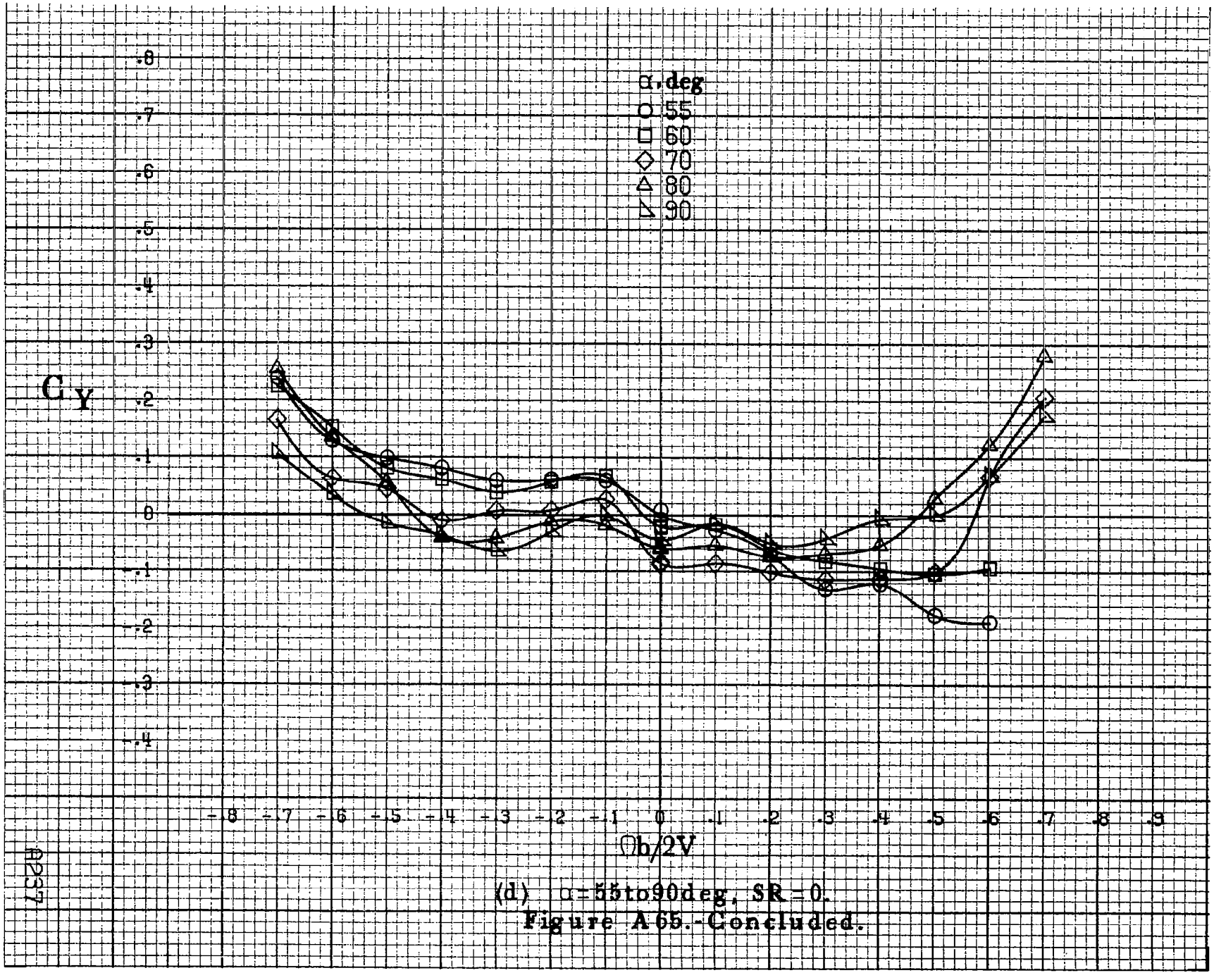

B237

(d) $\alpha = 55$ to 90 deg, $SR = 0$.

Figure A 65.- Concluded.

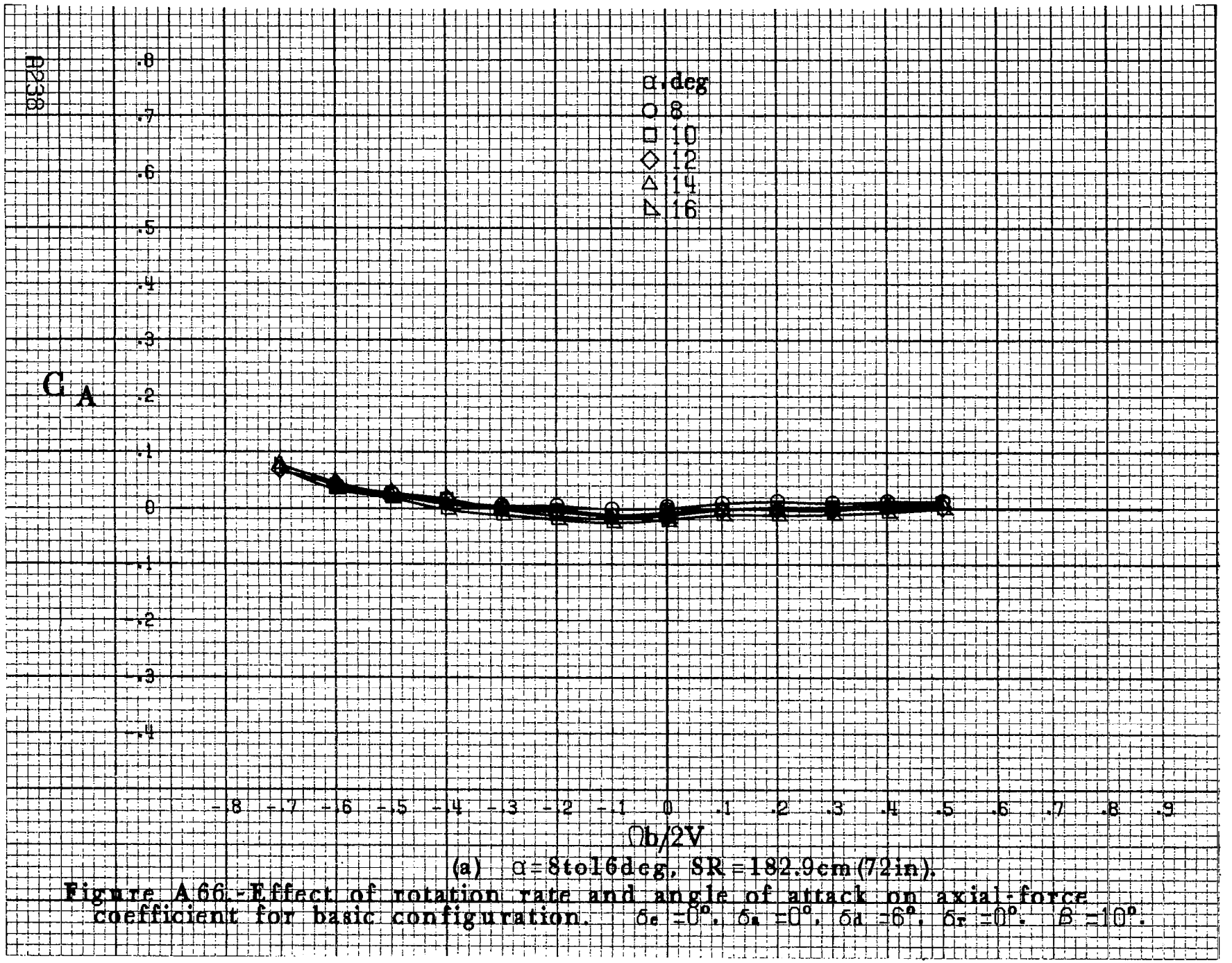

(a) $\alpha = 8$ to 16 deg, SR = 182.9 cm (72 in).

Figure A66.- Effect of rotation rate and angle of attack on axial-force coefficient for basic configuration. $\delta_e = 0°$, $\delta_s = 0°$, $\delta_a = 6°$, $\delta_r = 0°$, $\beta = 10°$.

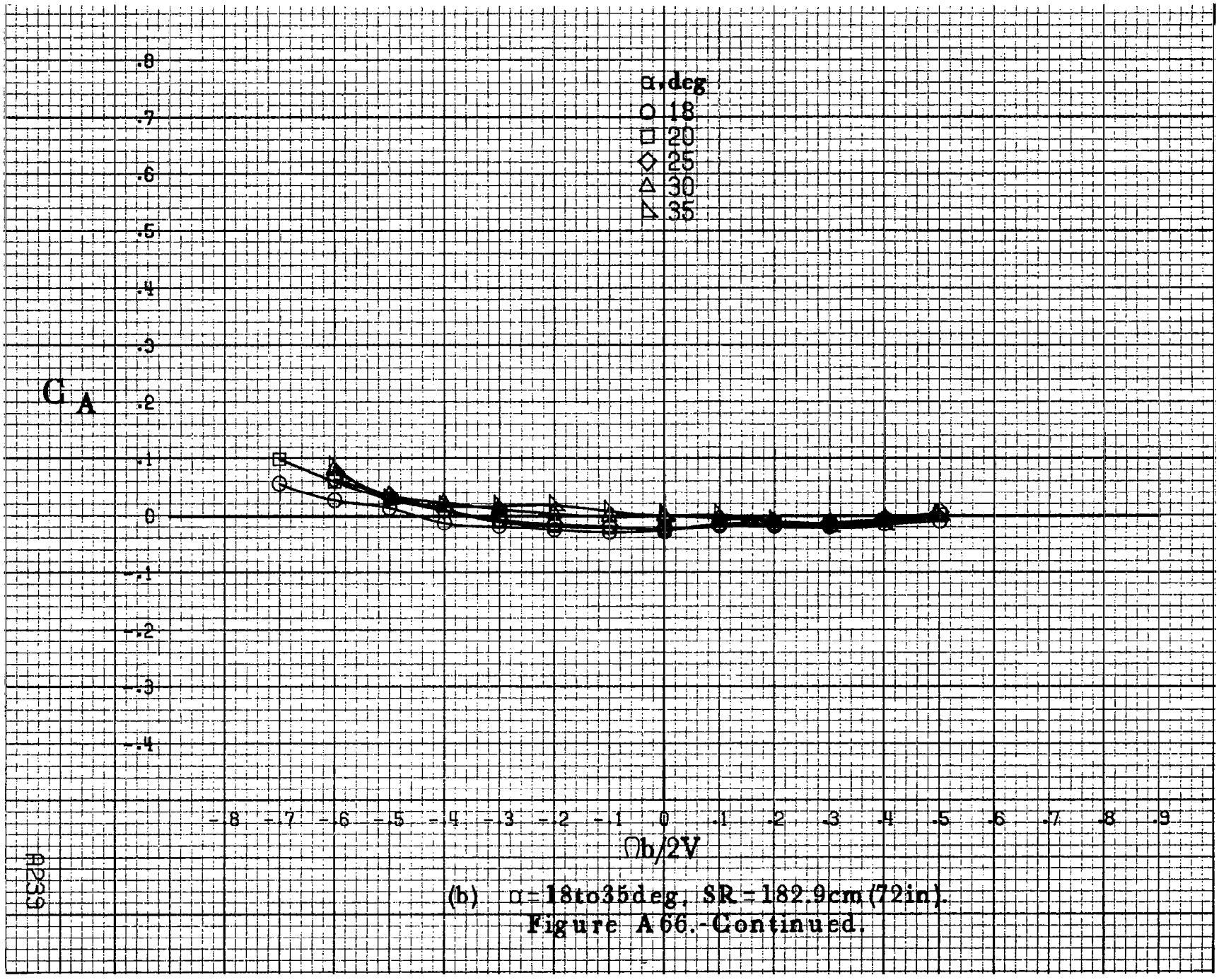

(b) α = 18 to 35 deg, SR = 182.9 cm (72 in).

Figure A66.- Continued.

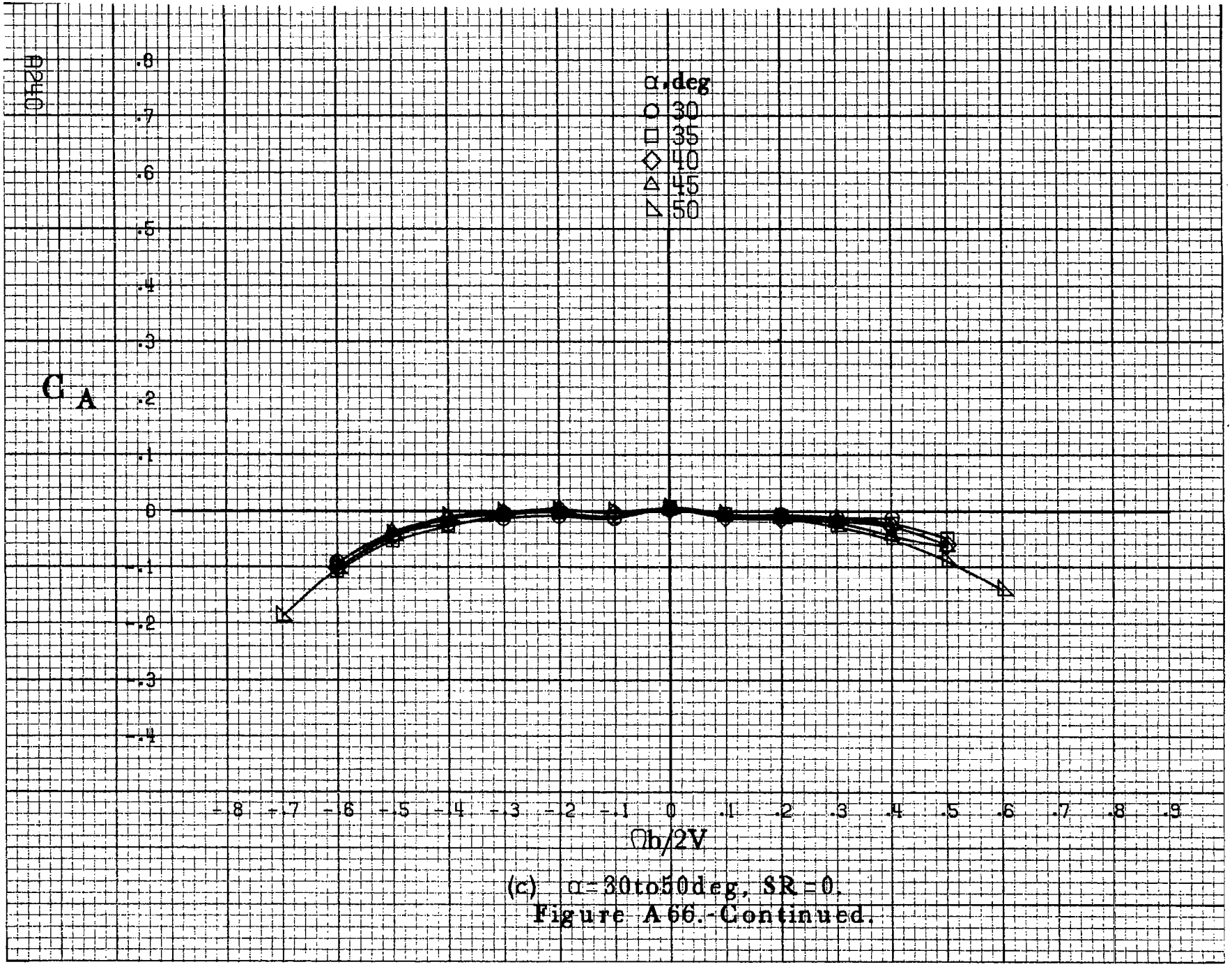

(c) α = 30 to 50 deg, SR = 0.

Figure A66.- Continued.

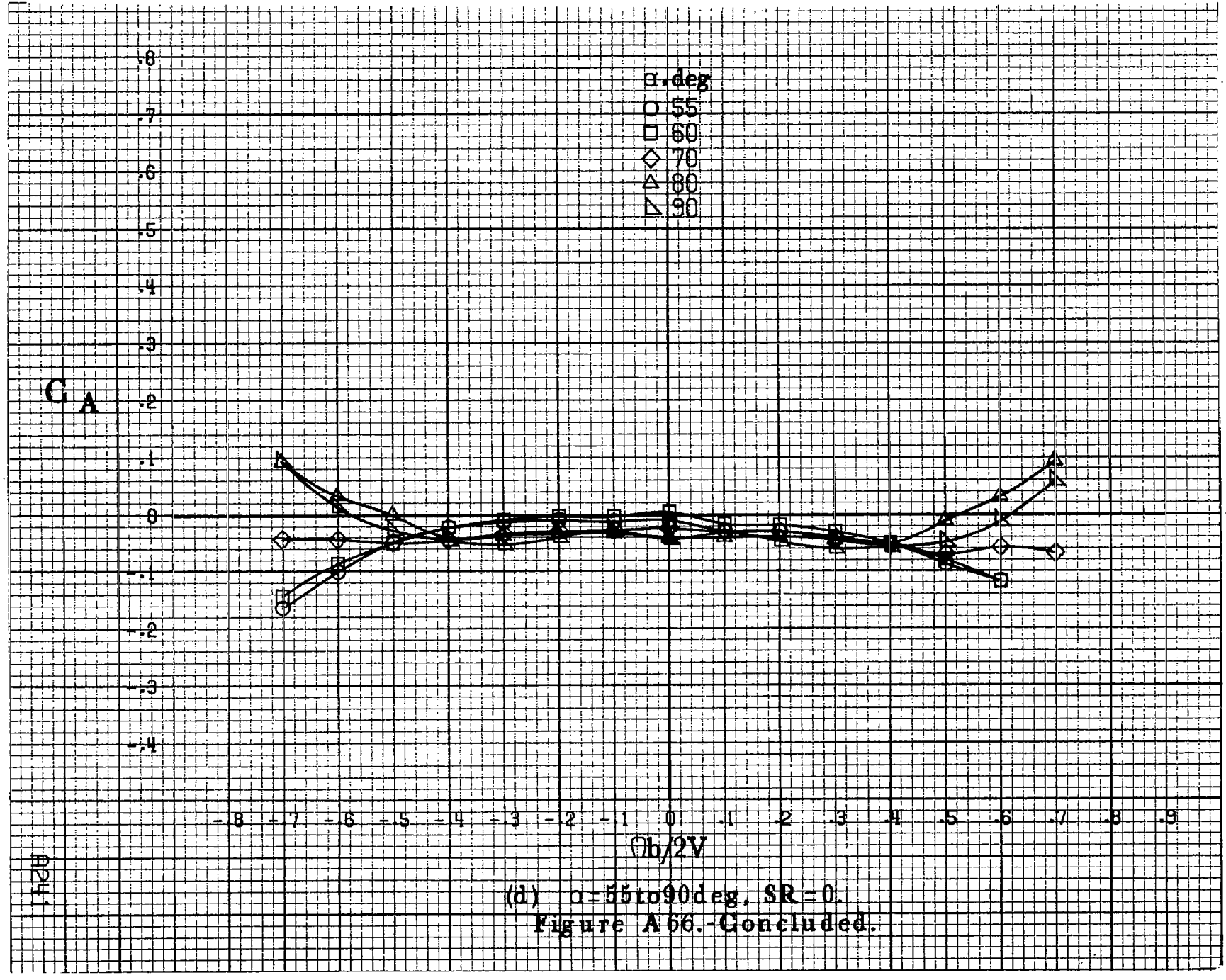

(d) $\alpha = 55$ to 90 deg, SR = 0.

Figure A66.-Concluded.

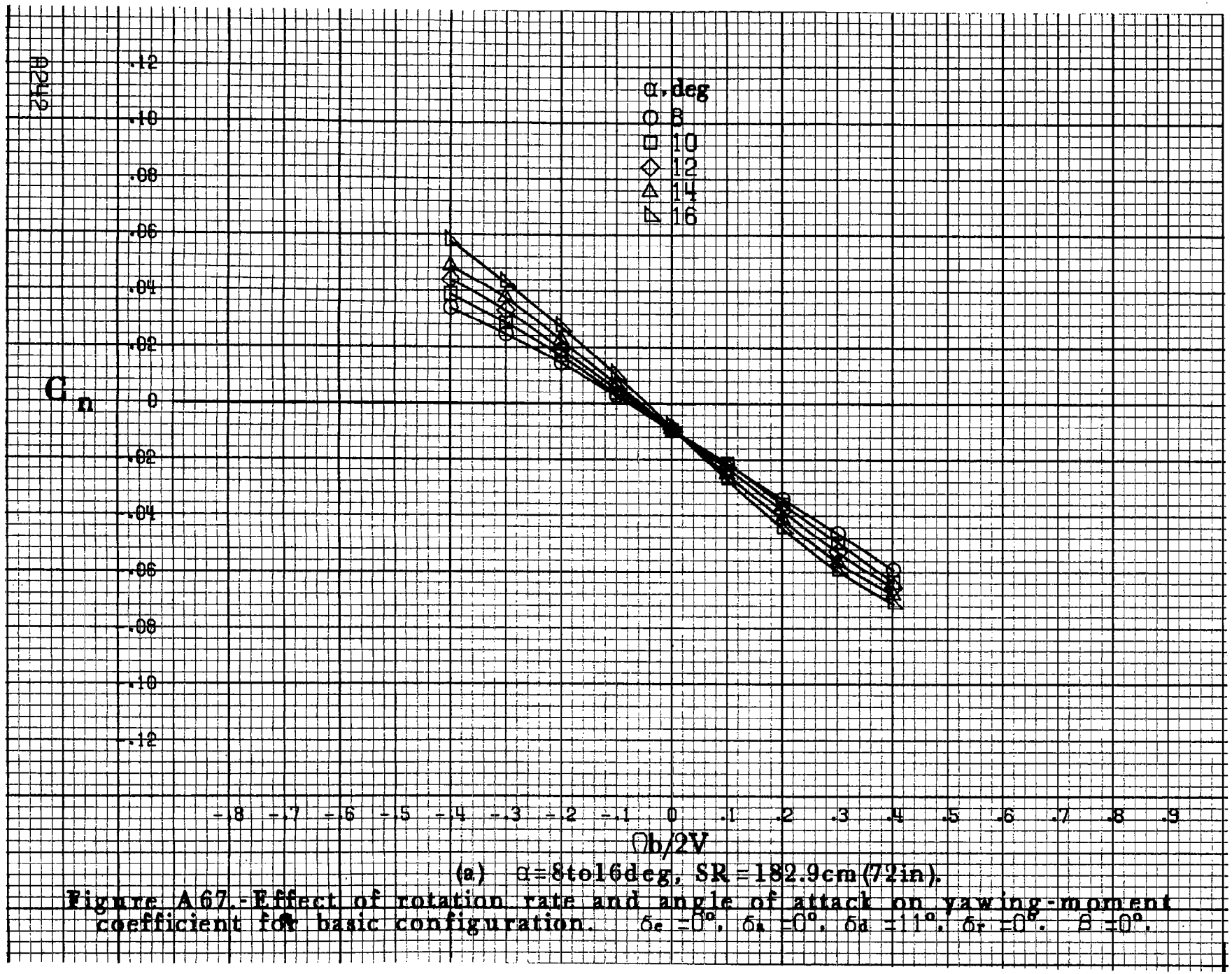

(a) $\alpha = 8$ to 16 deg, SR = 182.9 cm (72 in).

Figure A67.- Effect of rotation rate and angle of attack on yawing-moment coefficient for basic configuration. $\delta_e = 0°$, $\delta_a = 0°$, $\delta_d = 11°$, $\delta_r = 0°$, $\beta = 0°$.

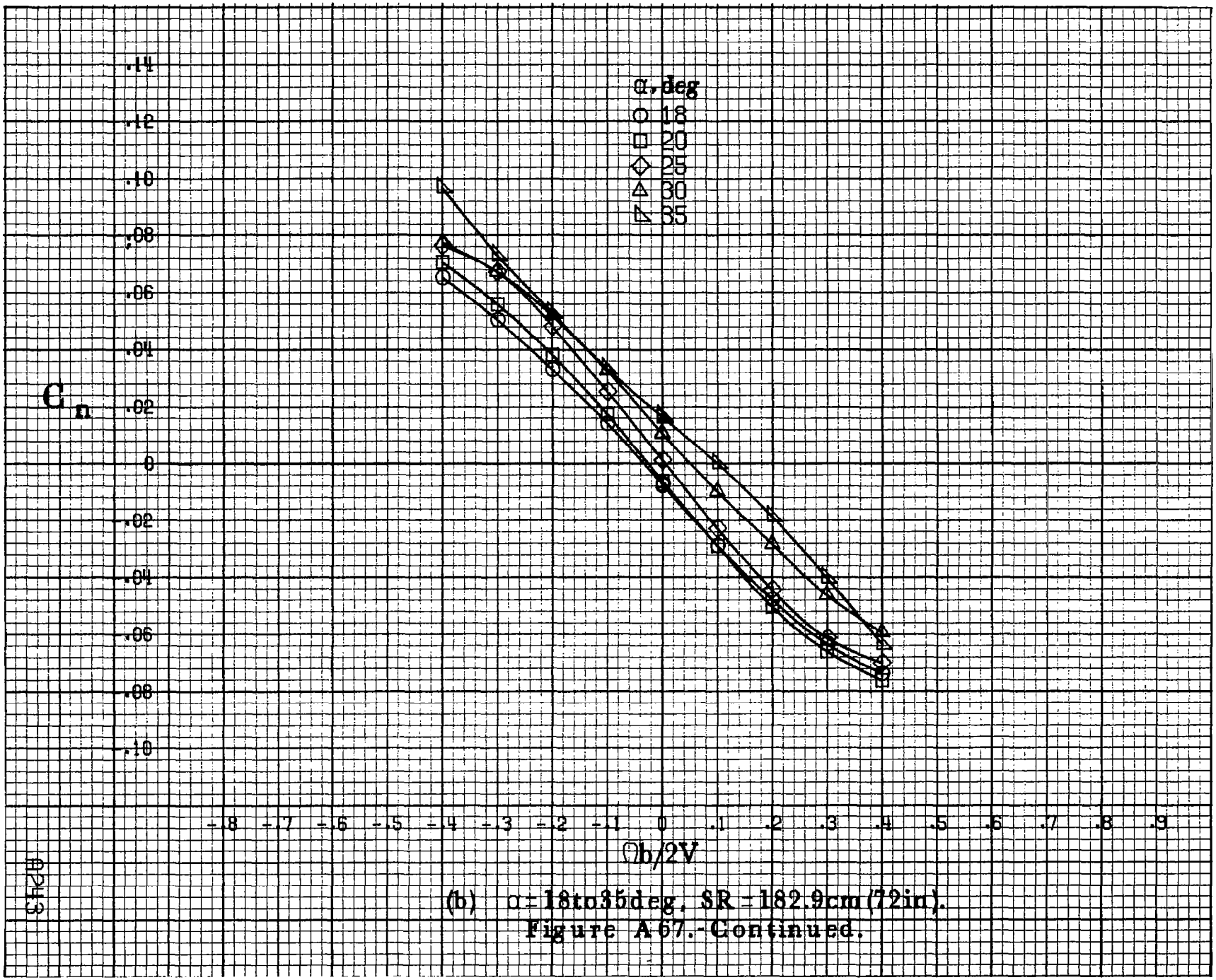

(b) $\alpha = 18$ to 35 deg, SR = 182.9 cm (72 in).

Figure A67.- Continued.

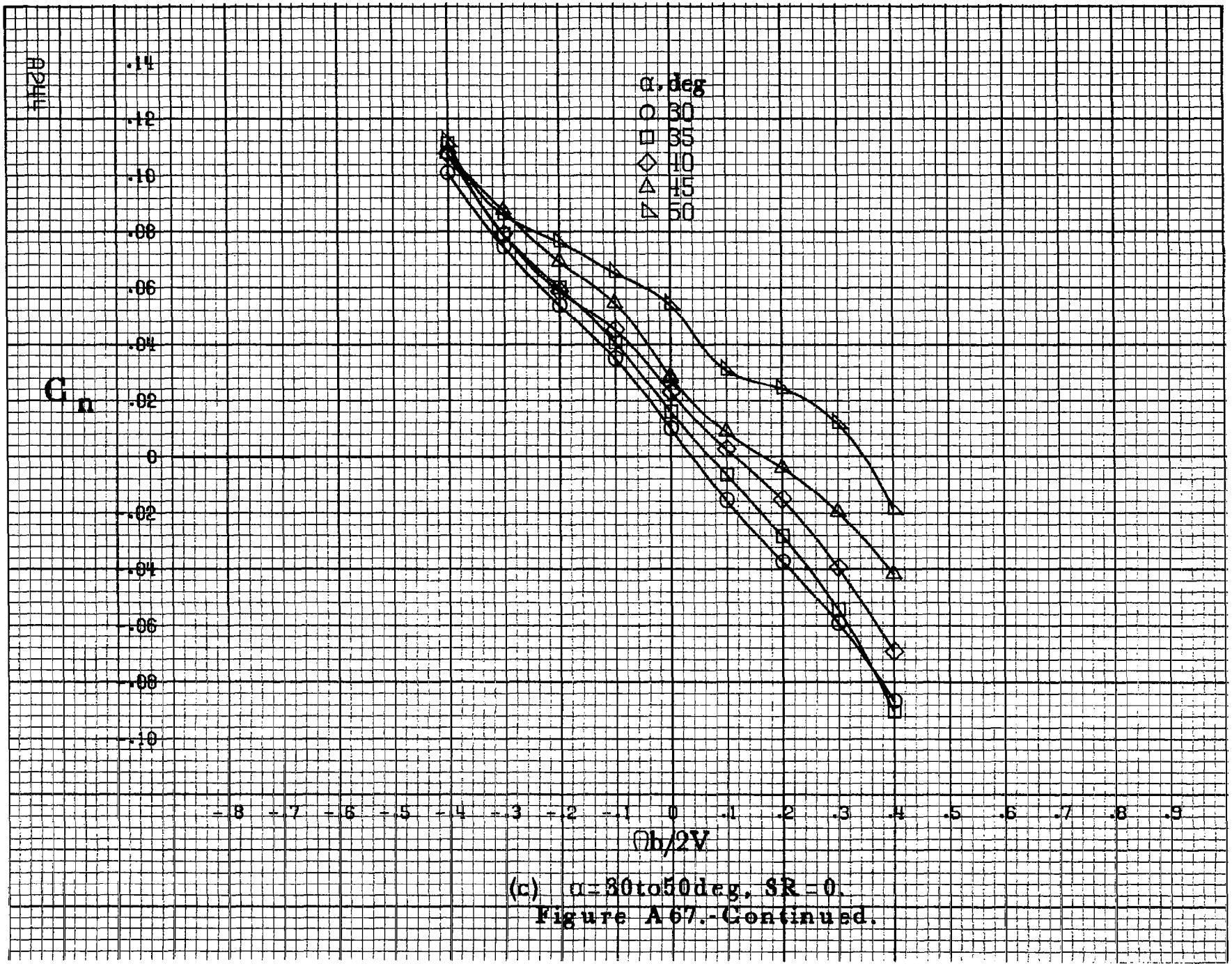

(c) $\alpha = 30$ to 50 deg, SR = 0.

Figure A67.- Continued.

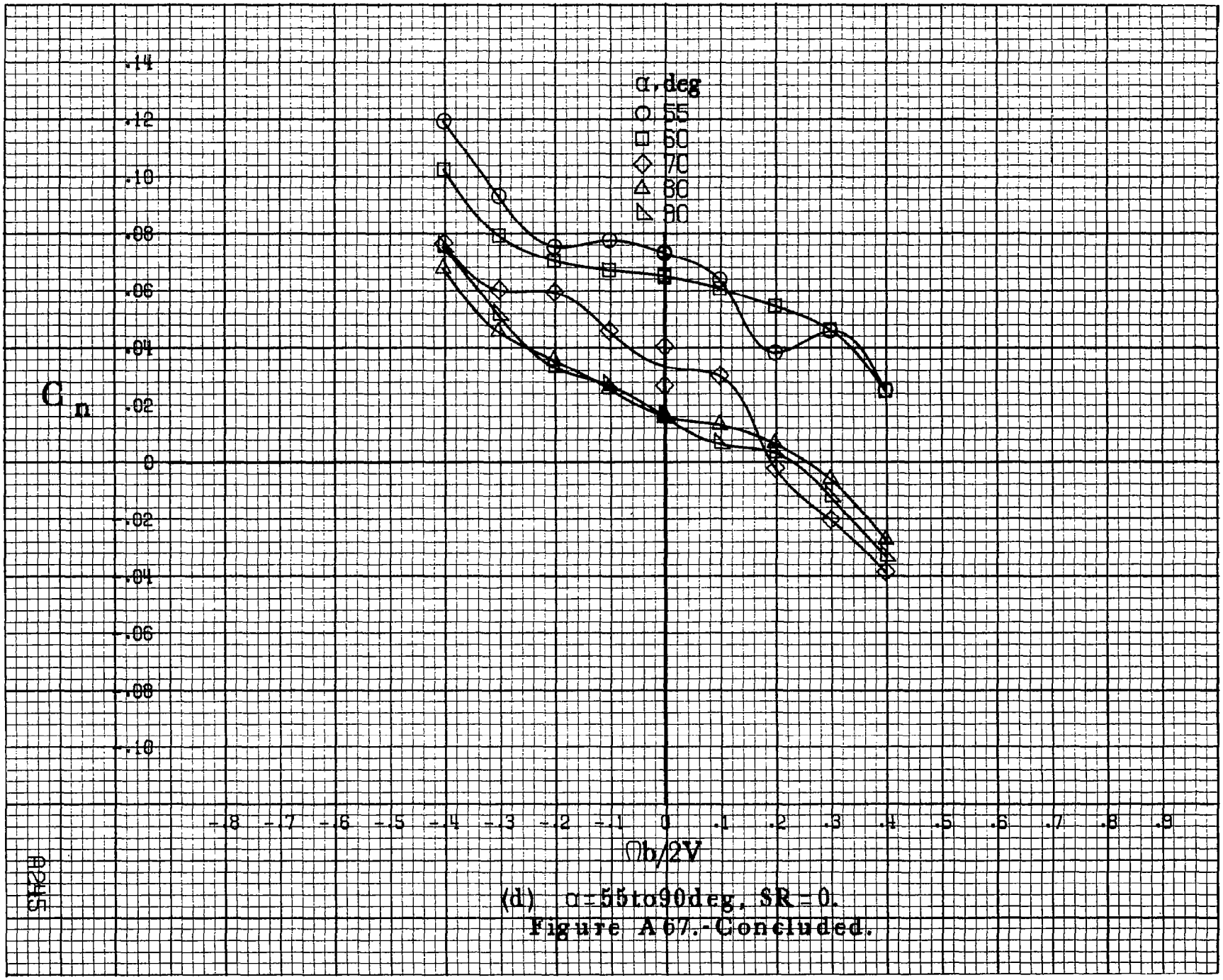

(d) $\alpha = 55$ to 90 deg, $\$R = 0$.

Figure A67.- Concluded.

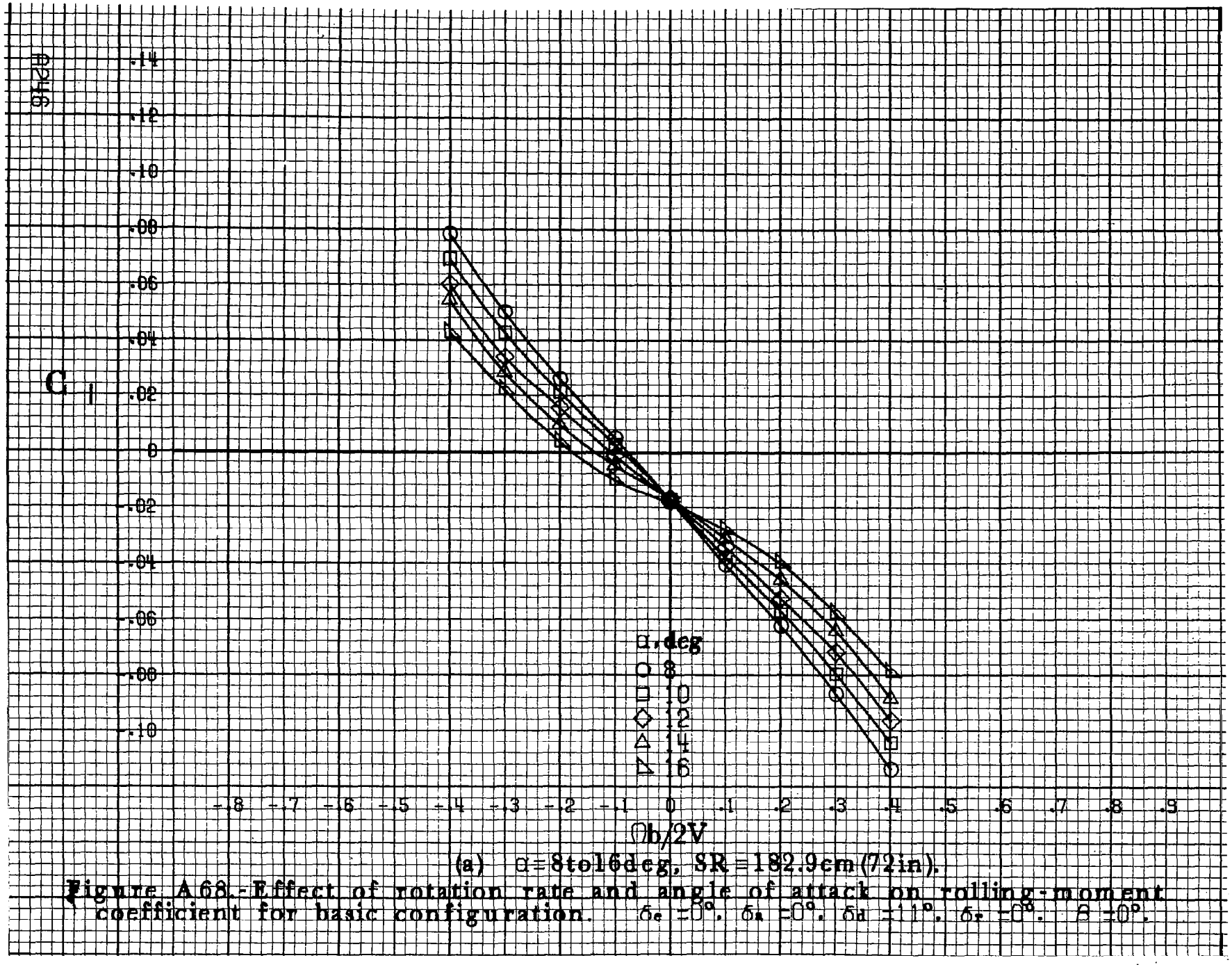

(a) α = 8 to 16 deg, SR = 182.9 cm (72 in).

Figure A68.- Effect of rotation rate and angle of attack on rolling-moment coefficient for basic configuration. $\delta_e = 0°$, $\delta_a = 0°$, $\delta_d = 11°$, $\delta_r = 0°$, $\beta = 0°$.

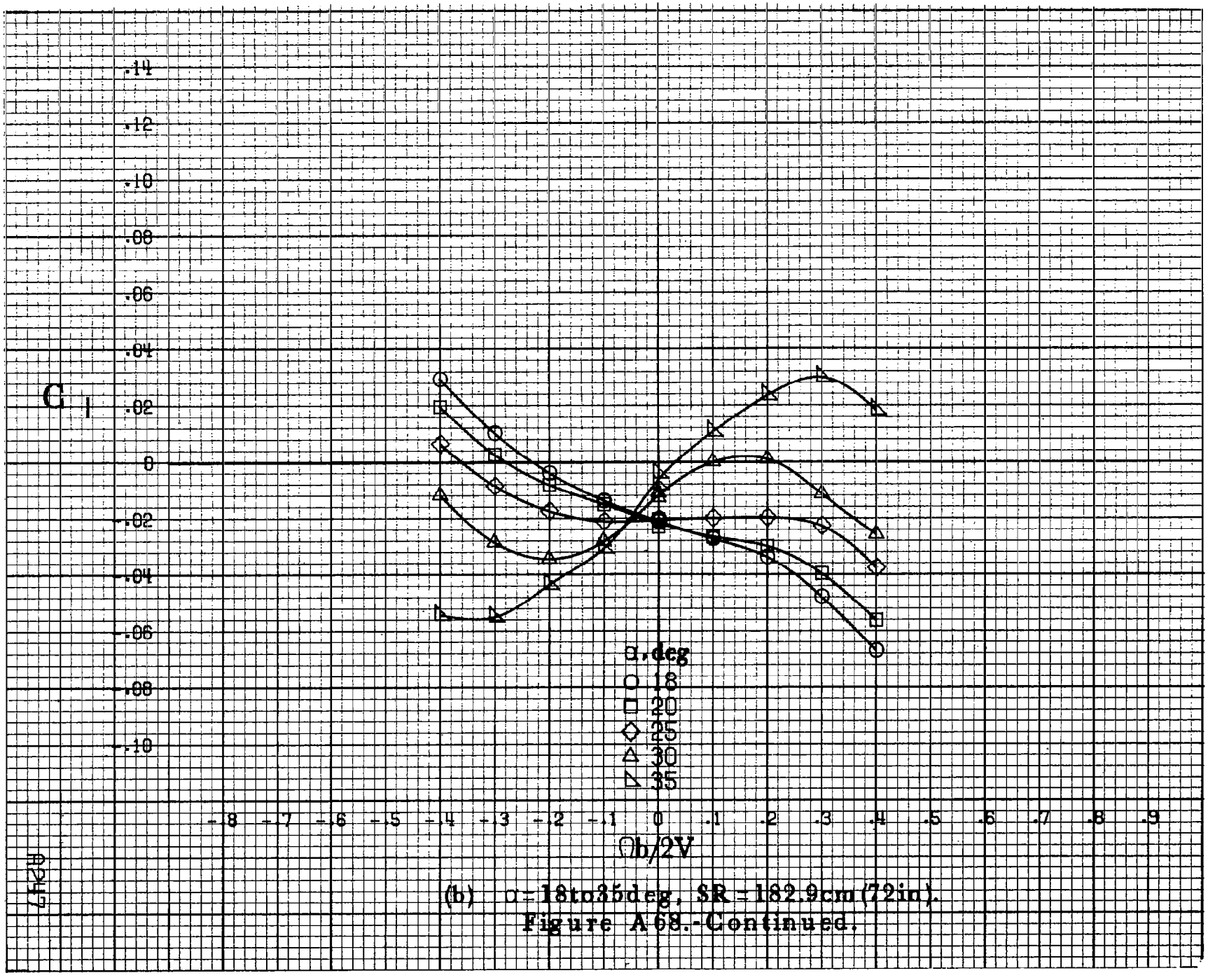

(b) $\alpha = 18$ to 35 deg, SR = 182.9 cm (72 in).

Figure A68.- Continued.

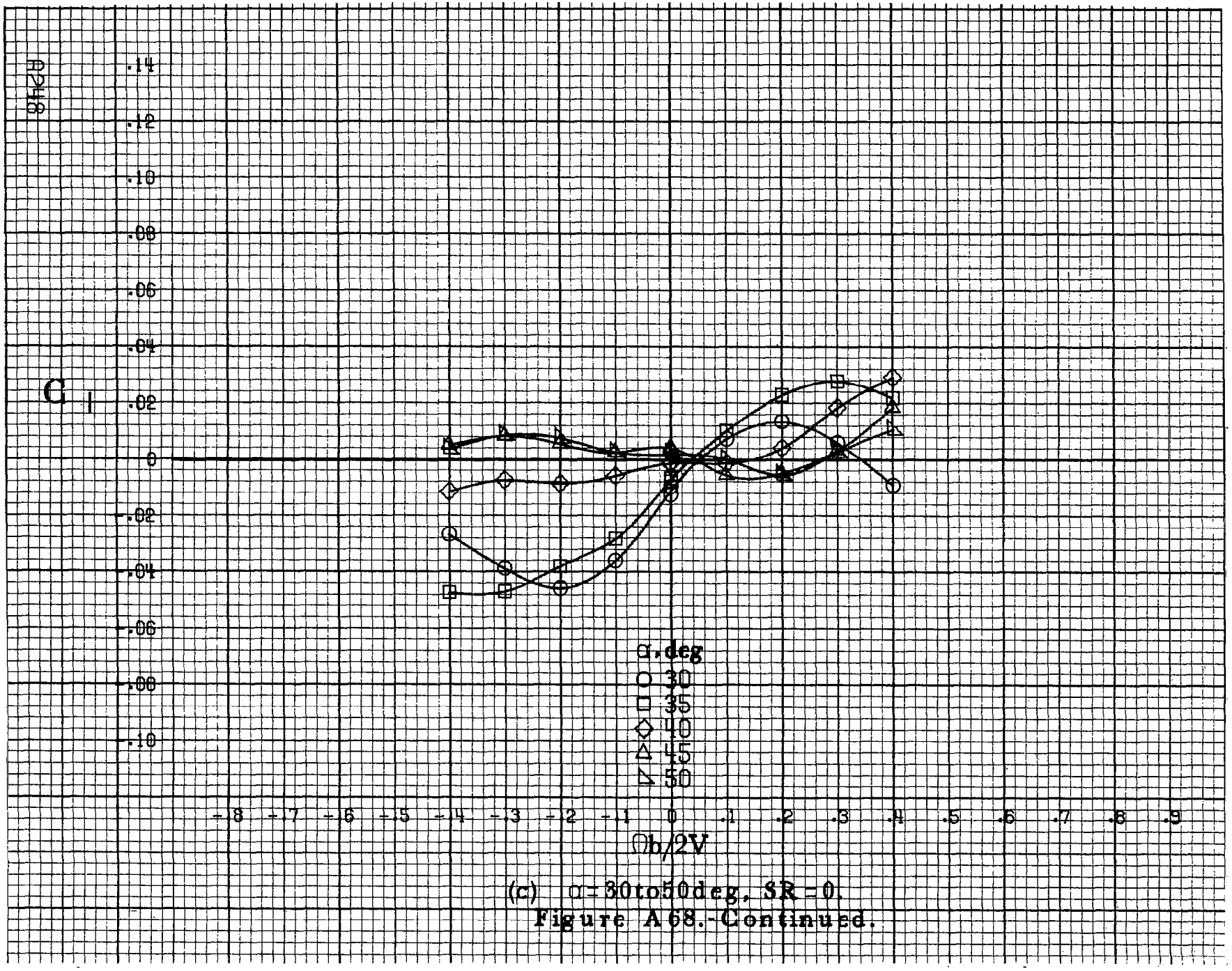

(c) $\alpha = 30$ to 50 deg, SR = 0.

Figure A68.- Continued.

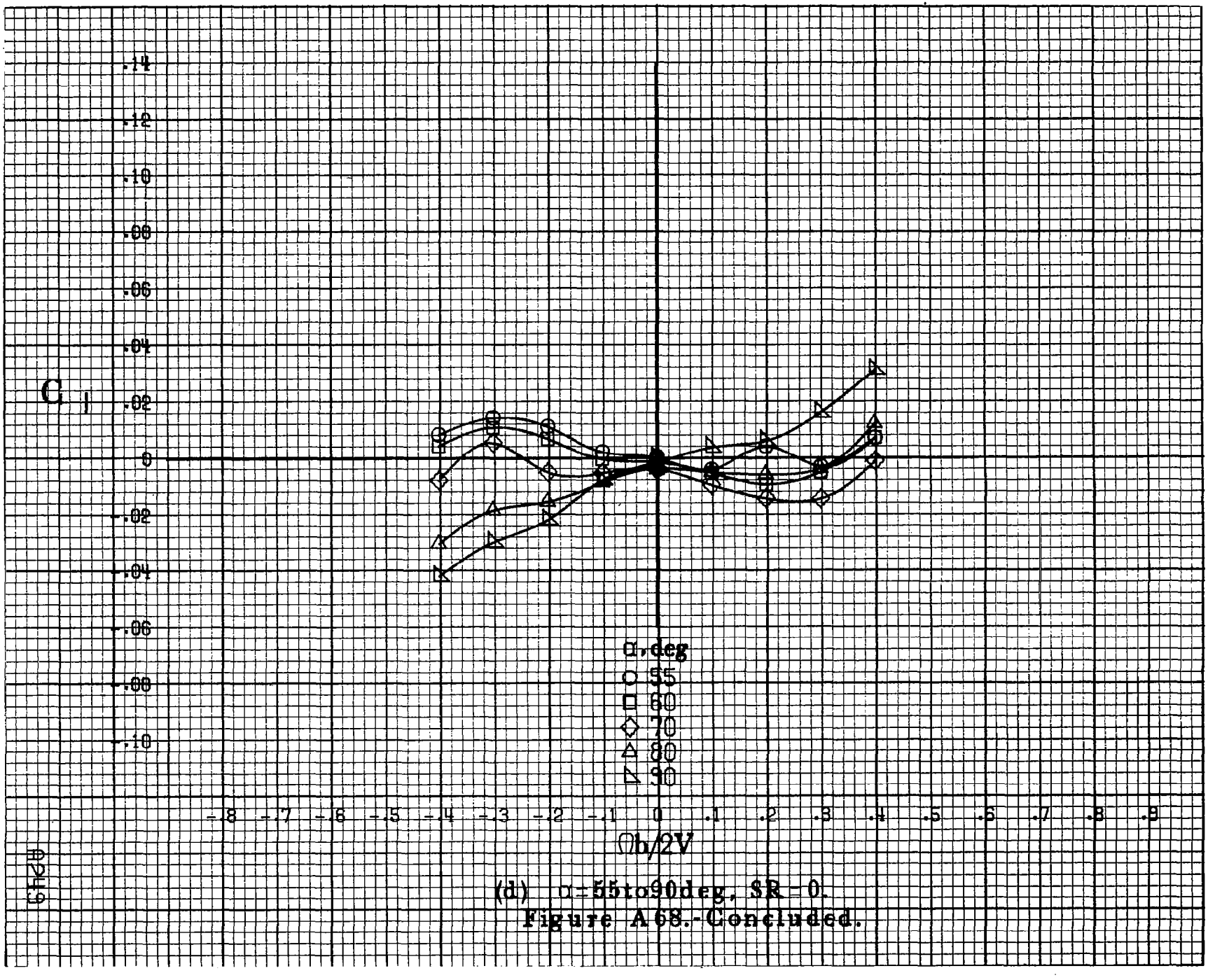

(d) α=55to90deg, SR=0.

Figure A68.-Concluded.

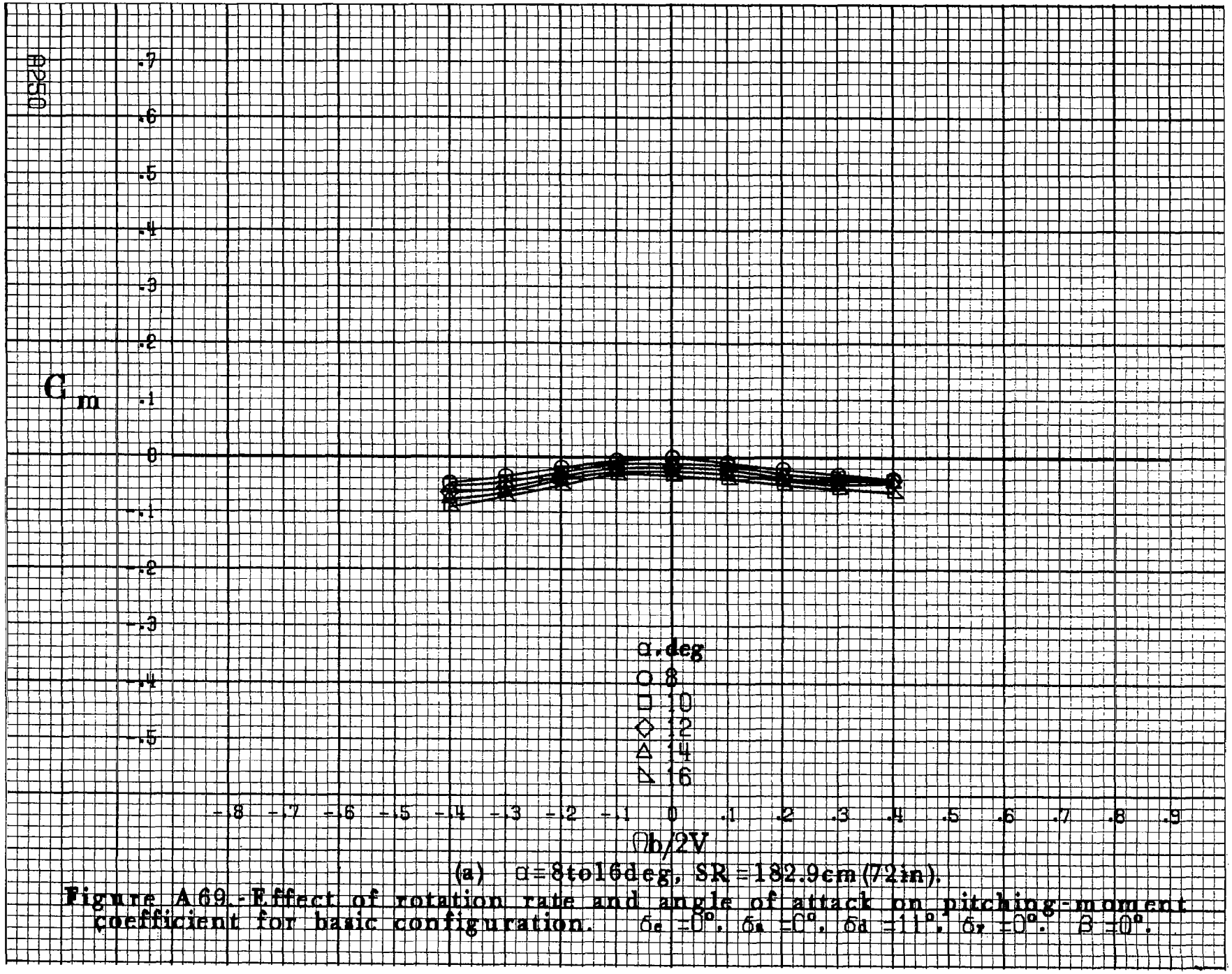

(a) $\alpha = 8$ to 16 deg, SR = 182.9 cm (72 in).

Figure A69.- Effect of rotation rate and angle of attack on pitching-moment coefficient for basic configuration. $\delta_e = 0°$, $\delta_a = 0°$, $\delta_d = 11°$, $\delta_r = 0°$, $\beta = 0°$.

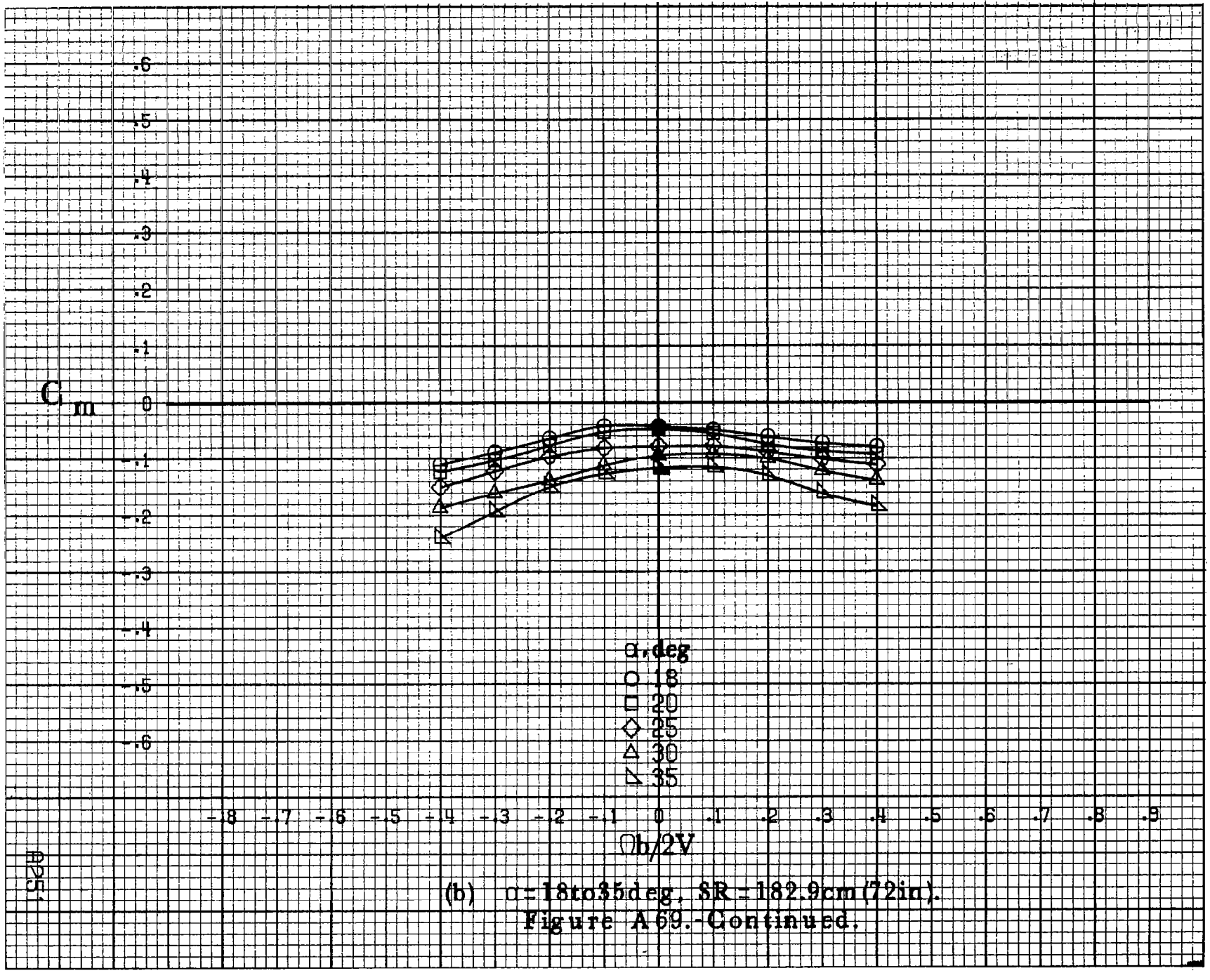

(b) $\alpha = 18$ to 35 deg, SR = 182.9 cm (72 in).

Figure A69.- Continued.

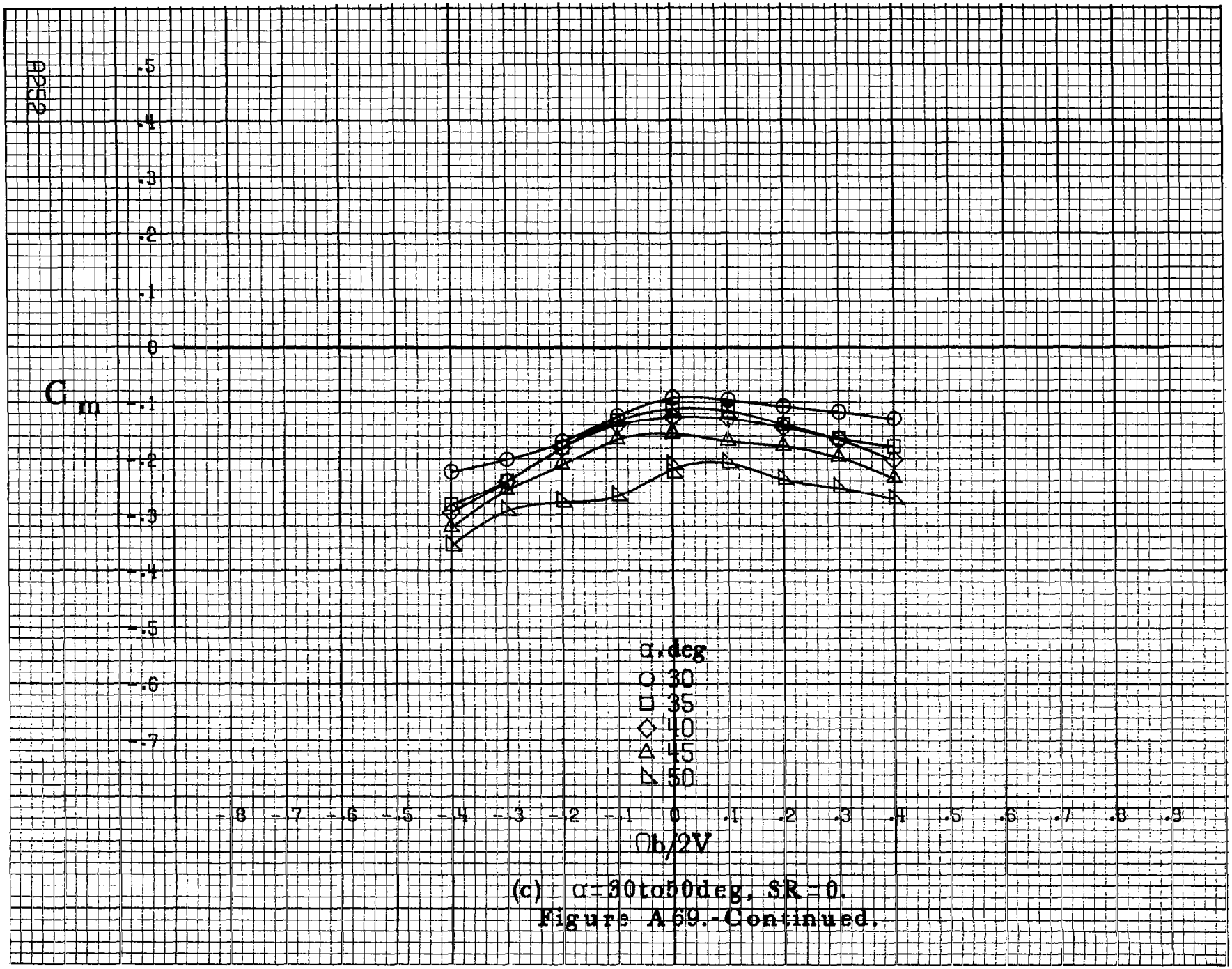

(c) $\alpha = 30$ to 50 deg, $SR = 0$.

Figure A69.-Continued.

(d) $\alpha = 55$ to 90 deg, $SR = 0$.

Figure A69.-Concluded.

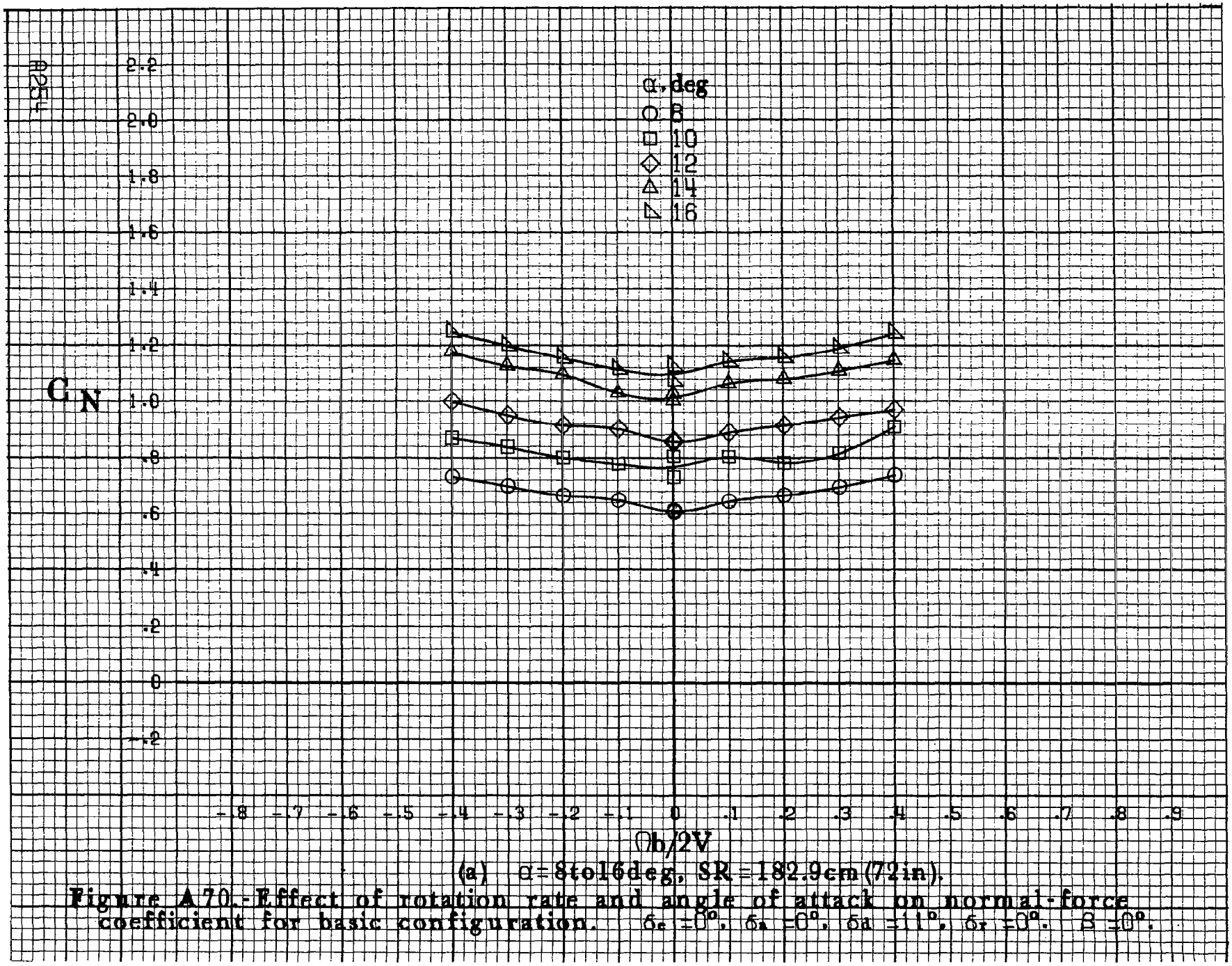

(a) $\alpha = 8$ to 16 deg, SR = 182.9 cm (72 in).

Figure A70.- Effect of rotation rate and angle of attack on normal-force coefficient for basic configuration. $\delta_e = 0°$, $\delta_a = 0°$, $\delta_a = 11°$, $\delta_r = 0°$, $\beta = 0°$.

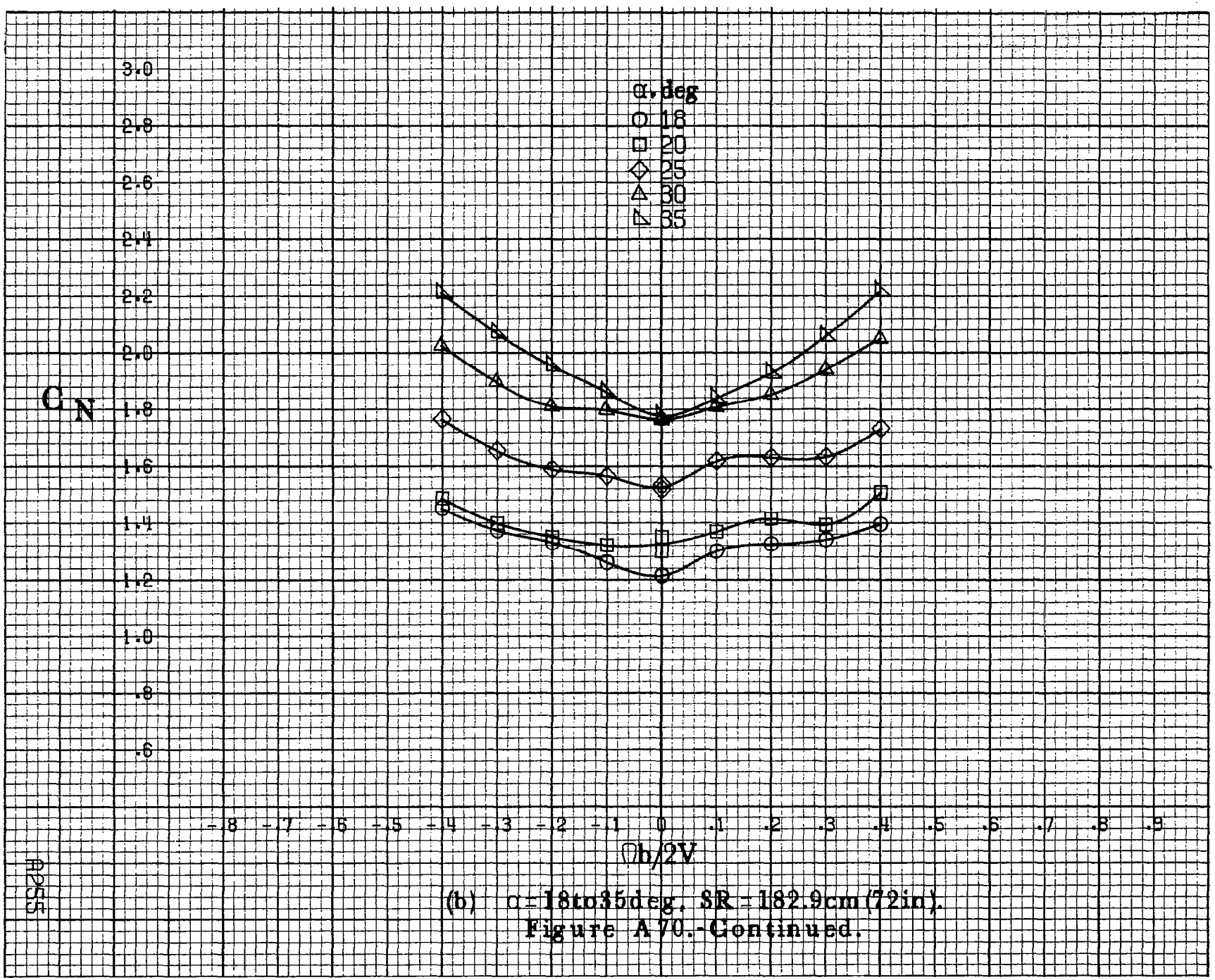

(b) α = 18 to 35 deg, SR = 182.9 cm (72 in).

Figure A70.- Continued.

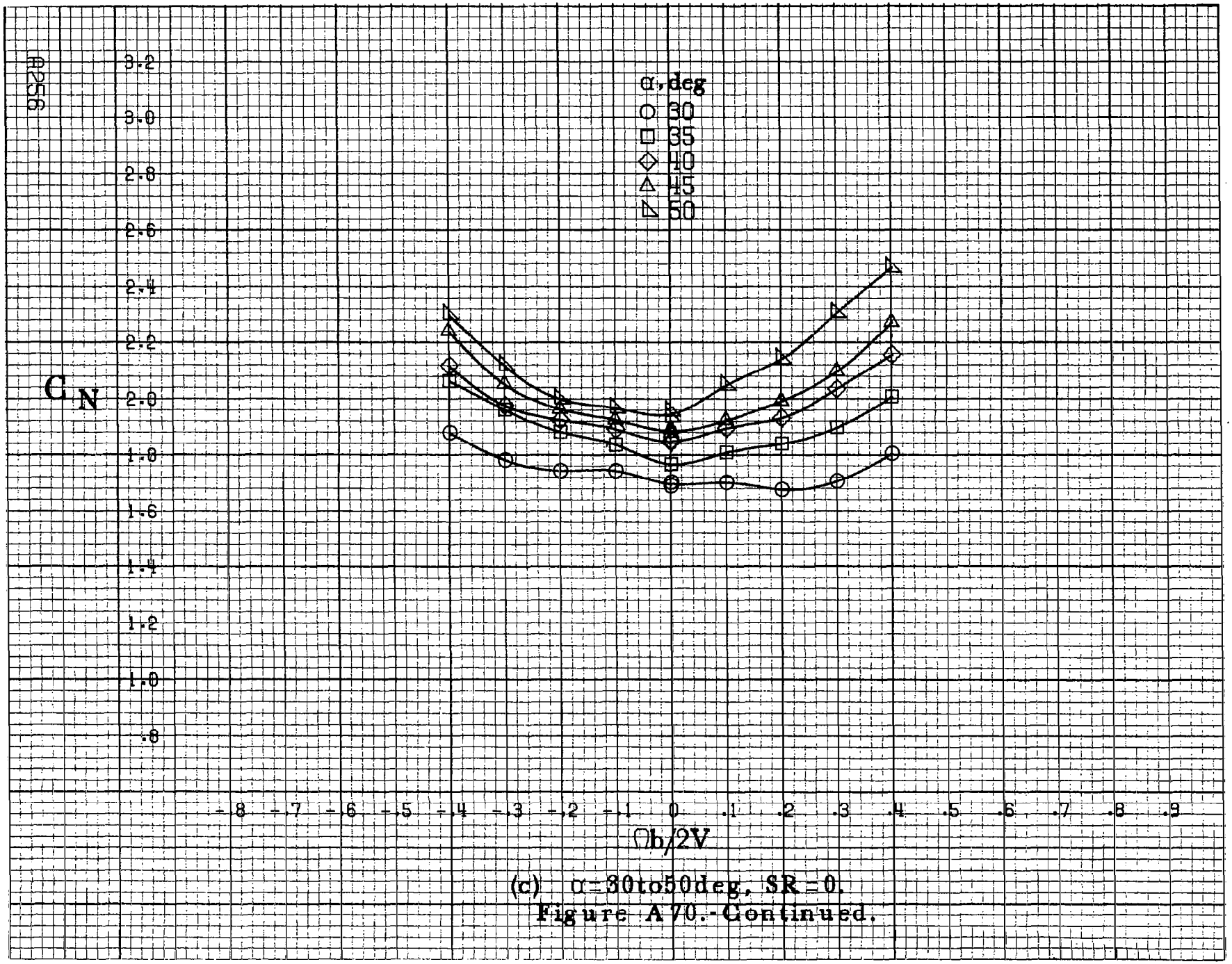

(c) $\alpha = 30$ to 50 deg, SR = 0.

Figure A70.- Continued.

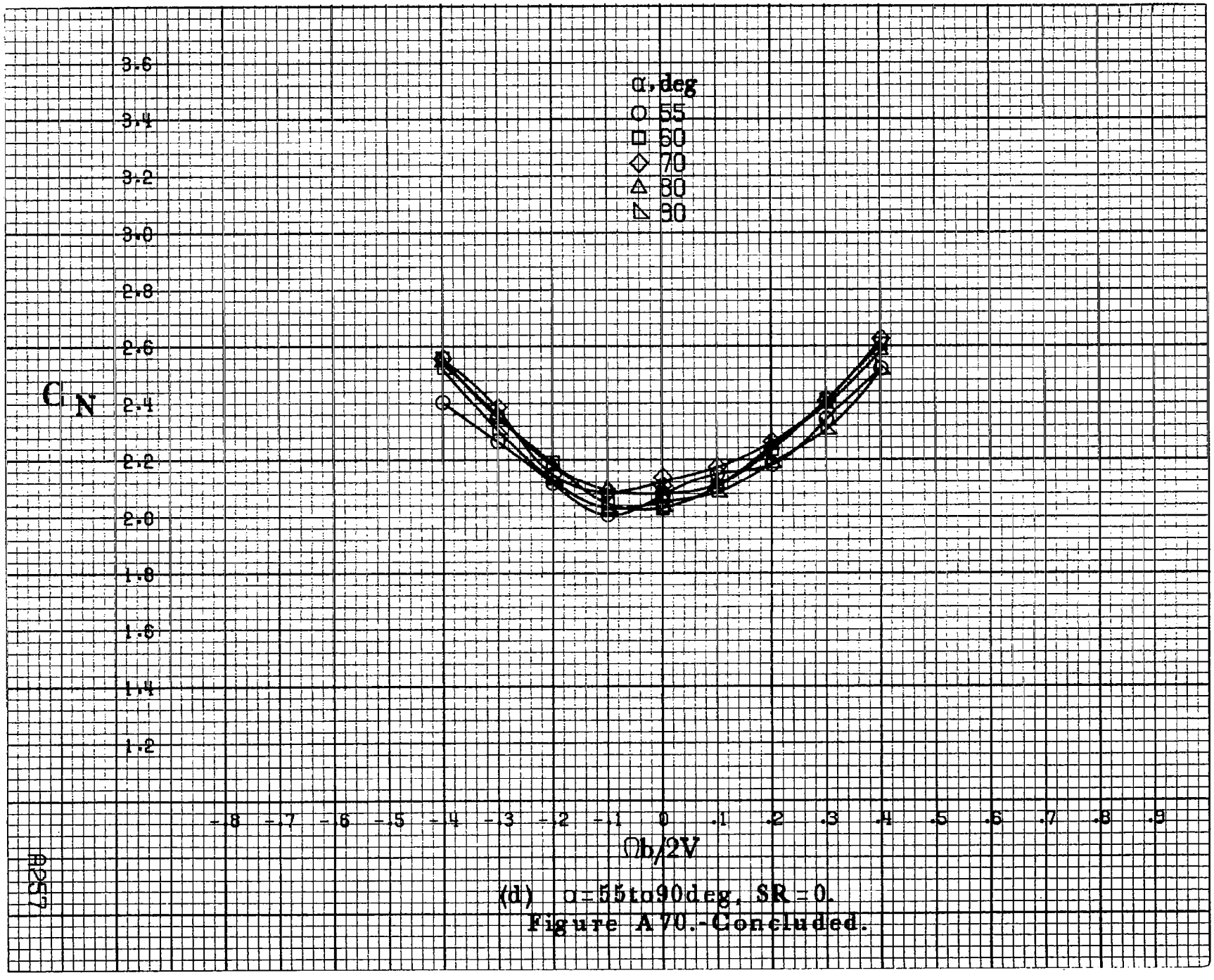

(d) $\alpha = 55$ to 90 deg, SR = 0.

Figure A70.-Concluded.

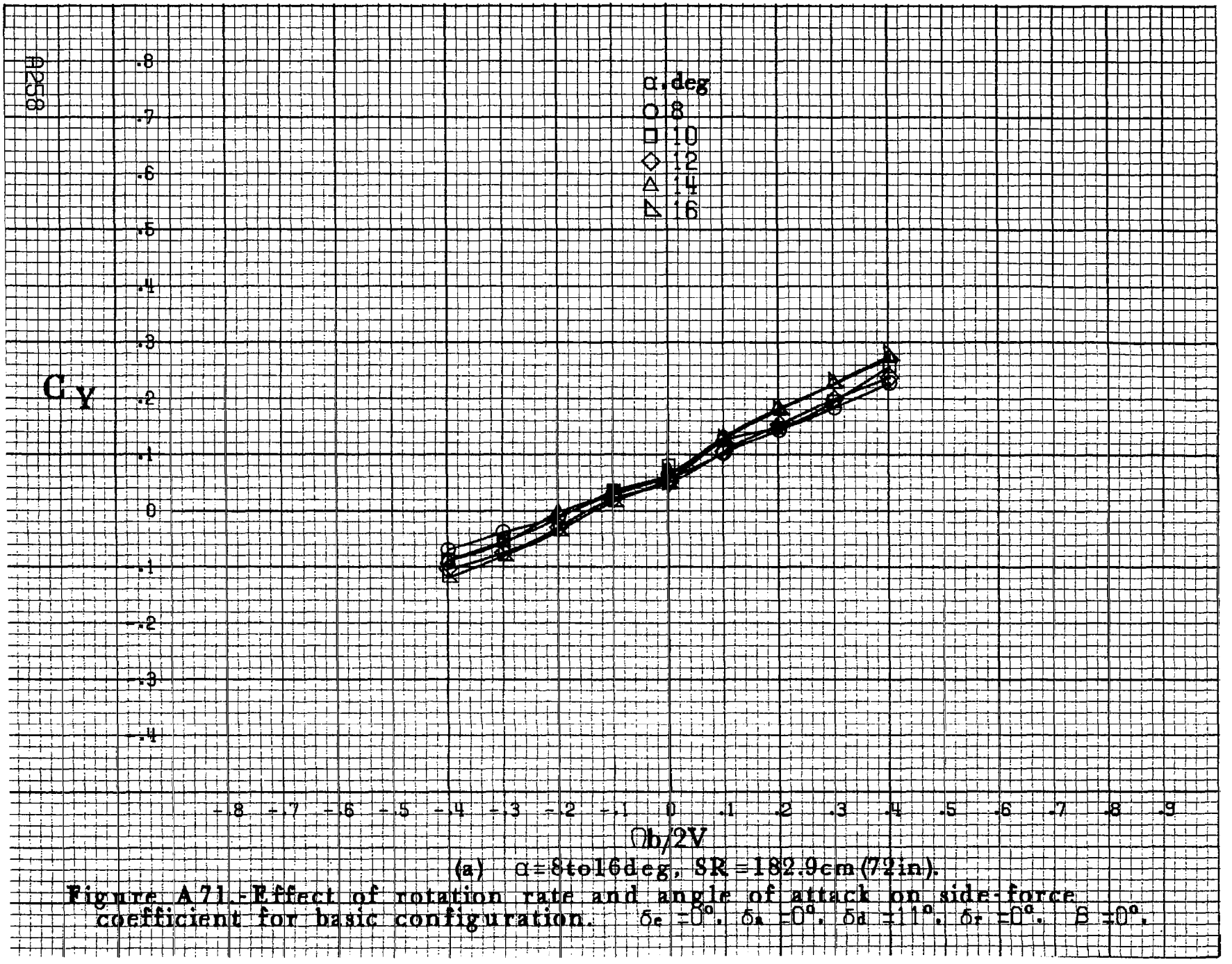

(a) $\alpha = 8$ to 16 deg, SR = 182.9 cm (72 in).

Figure A71.- Effect of rotation rate and angle of attack on side-force coefficient for basic configuration. $\delta_e = 0°$, $\delta_a = 0°$, $\delta_d = 11°$, $\delta_r = 0°$, $\beta = 0°$.

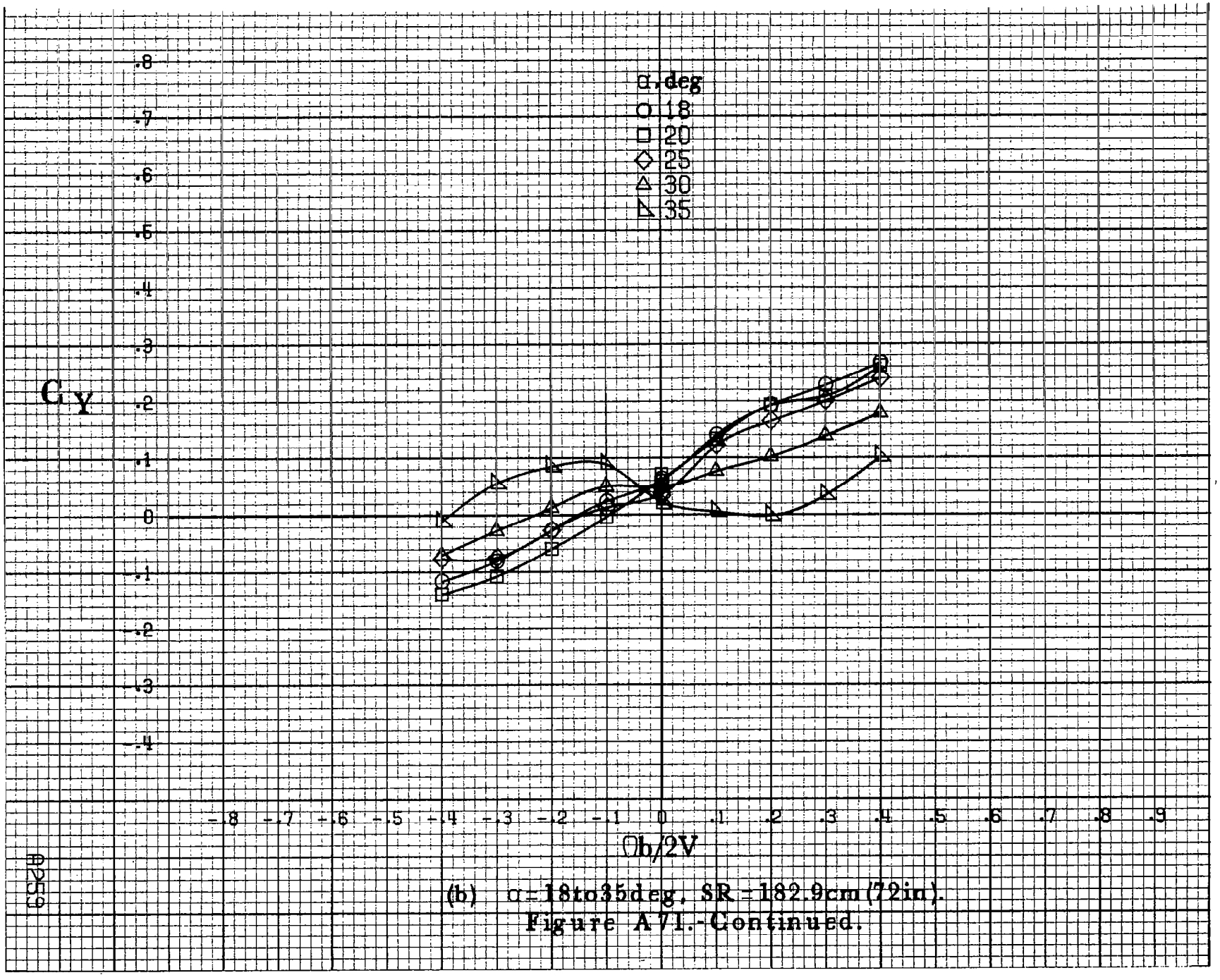

(b) $\alpha = 18$ to 35 deg, SR = 182.9 cm (72 in).

Figure A71.- Continued.

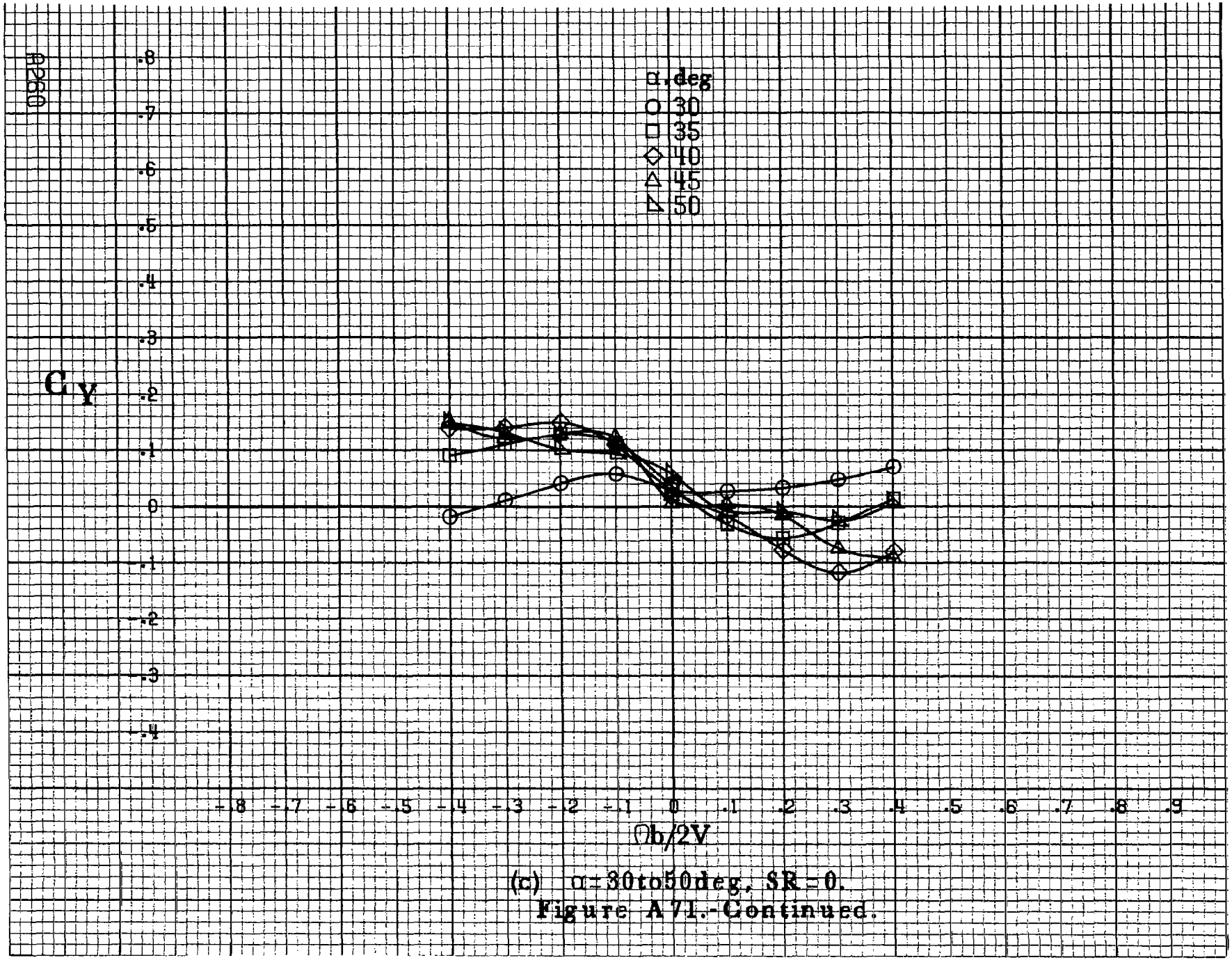

(c) α = 30 to 50 deg, SR = 0.

Figure A71.- Continued.

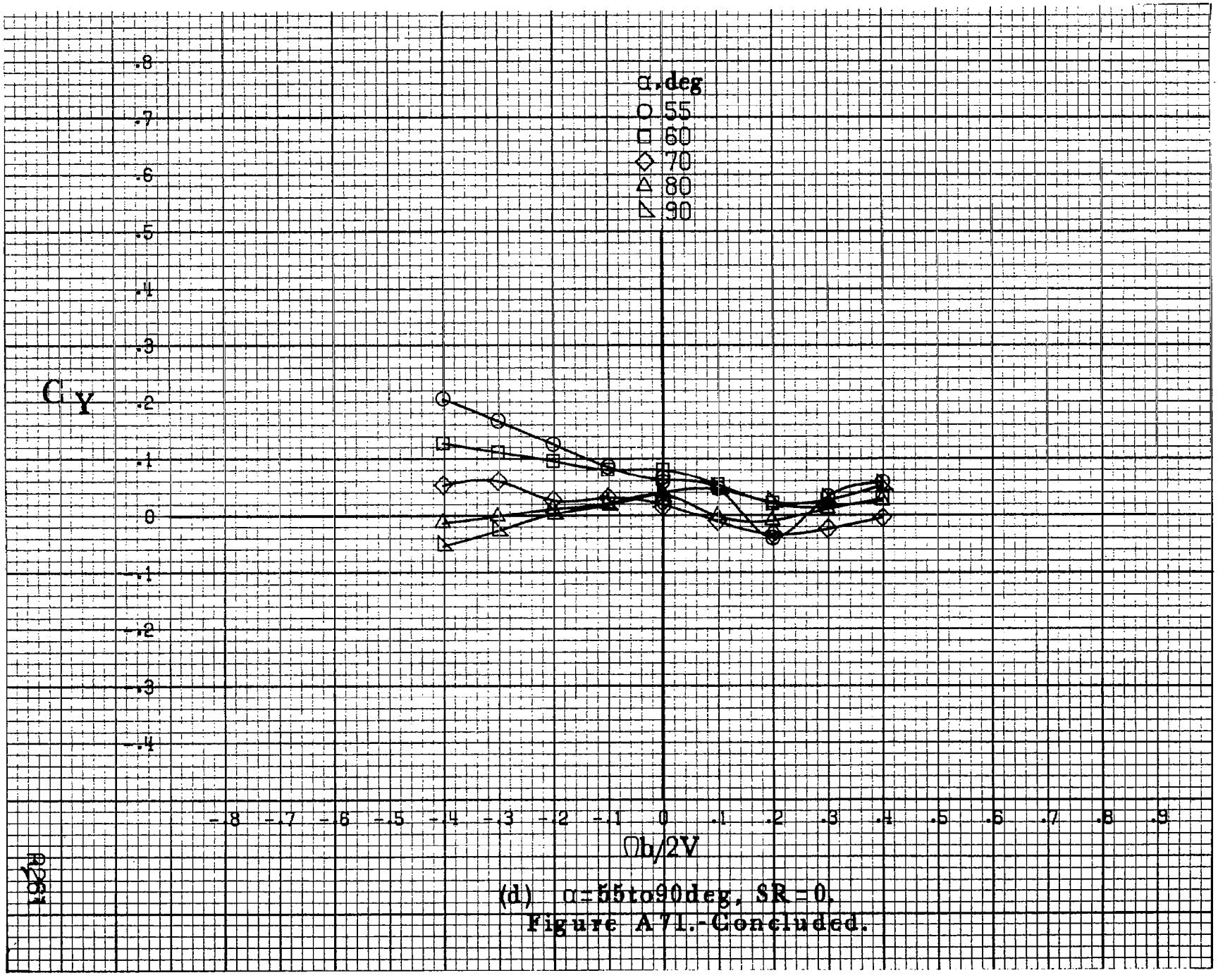

(d) $\alpha = 55$ to 90 deg, $SR = 0$.

Figure A71.-Concluded.

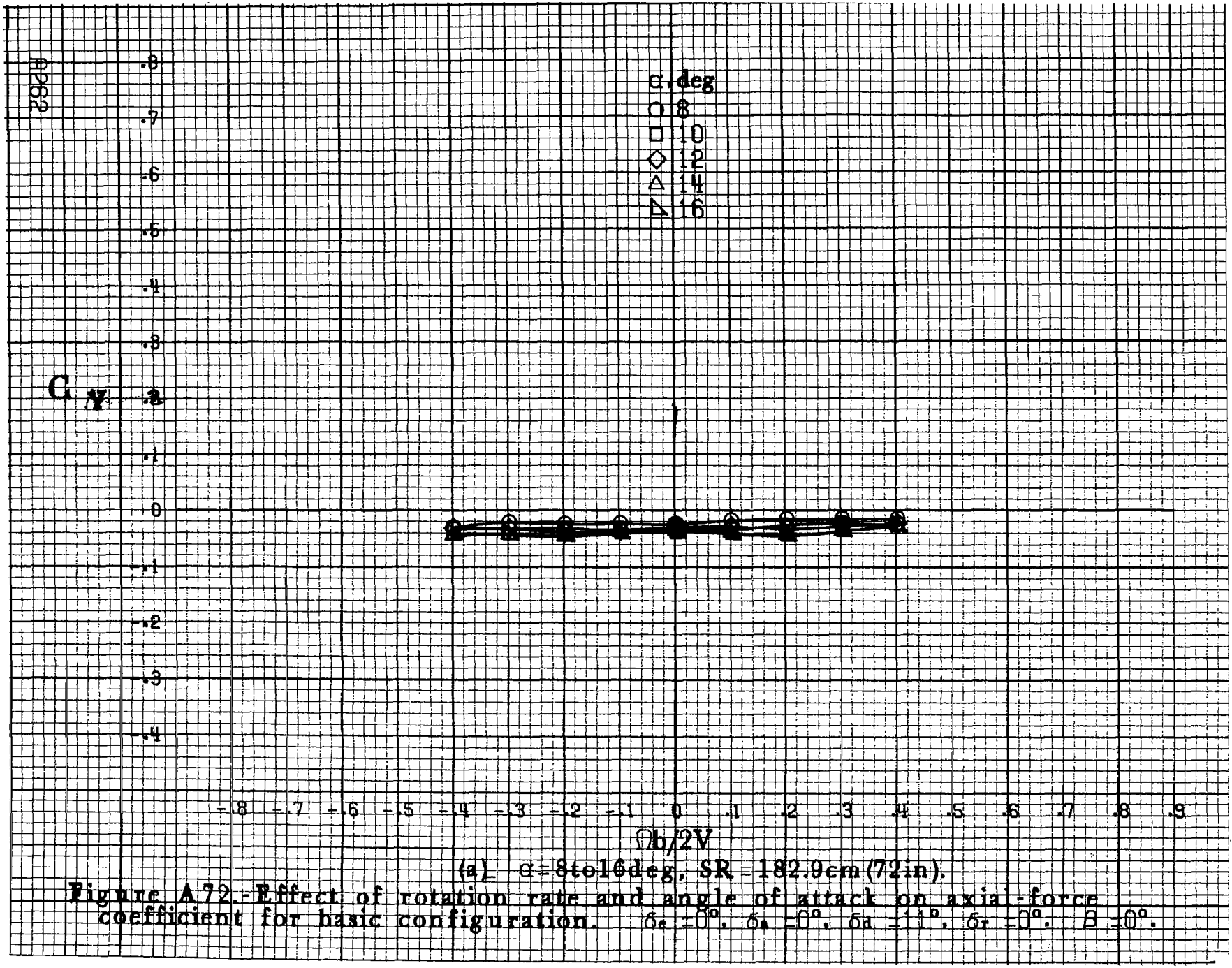

(a) $\alpha = 8$ to 16 deg, SR = 182.9 cm (72 in).

Figure A72.- Effect of rotation rate and angle of attack on axial-force coefficient for basic configuration. $\delta_e = 0°$, $\delta_a = 0°$, $\delta_d = 11°$, $\delta_r = 0°$. $\beta = 0°$.

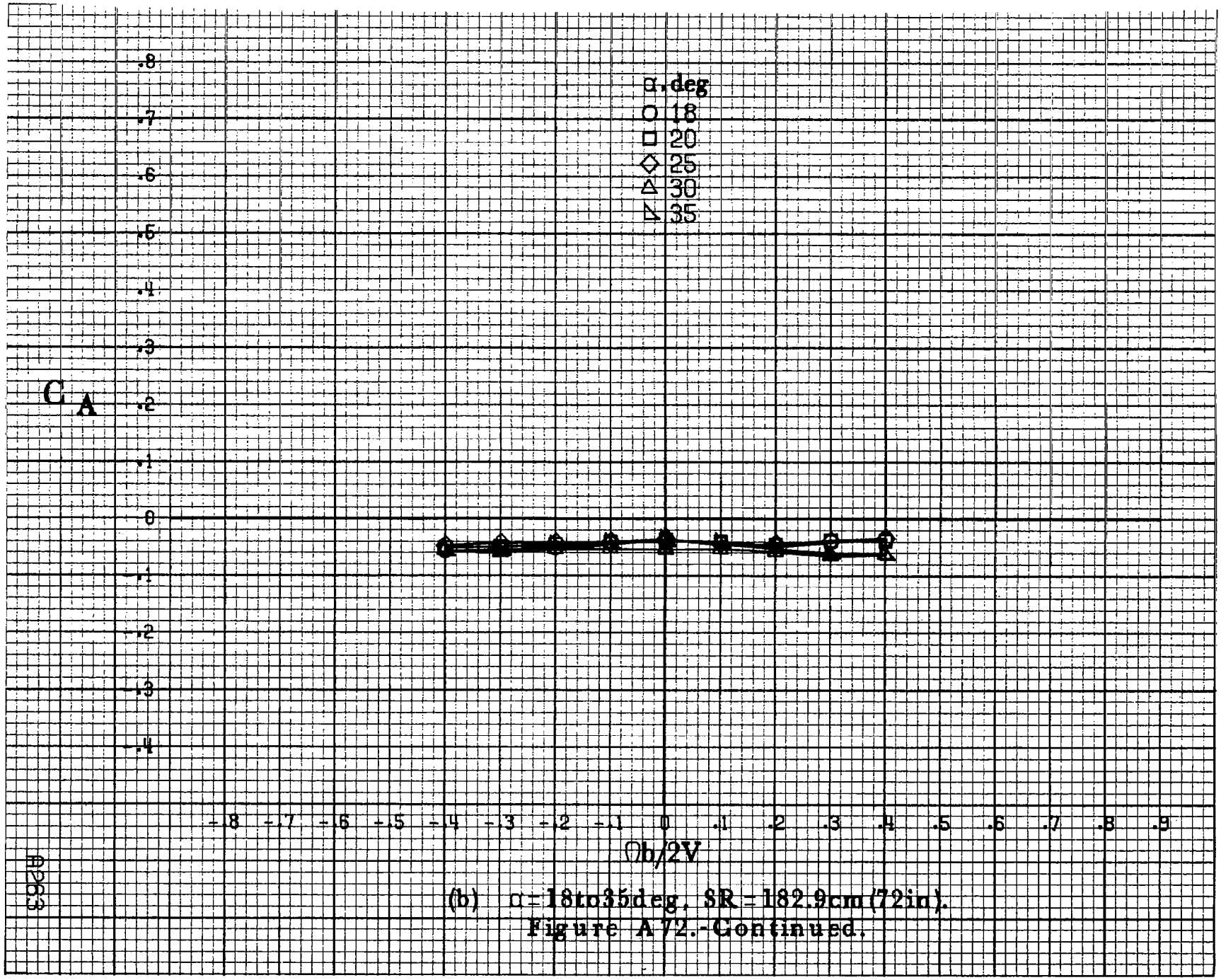

(b) α = 18 to 35 deg, SR = 182.9 cm (72 in).

Figure A72.- Continued.

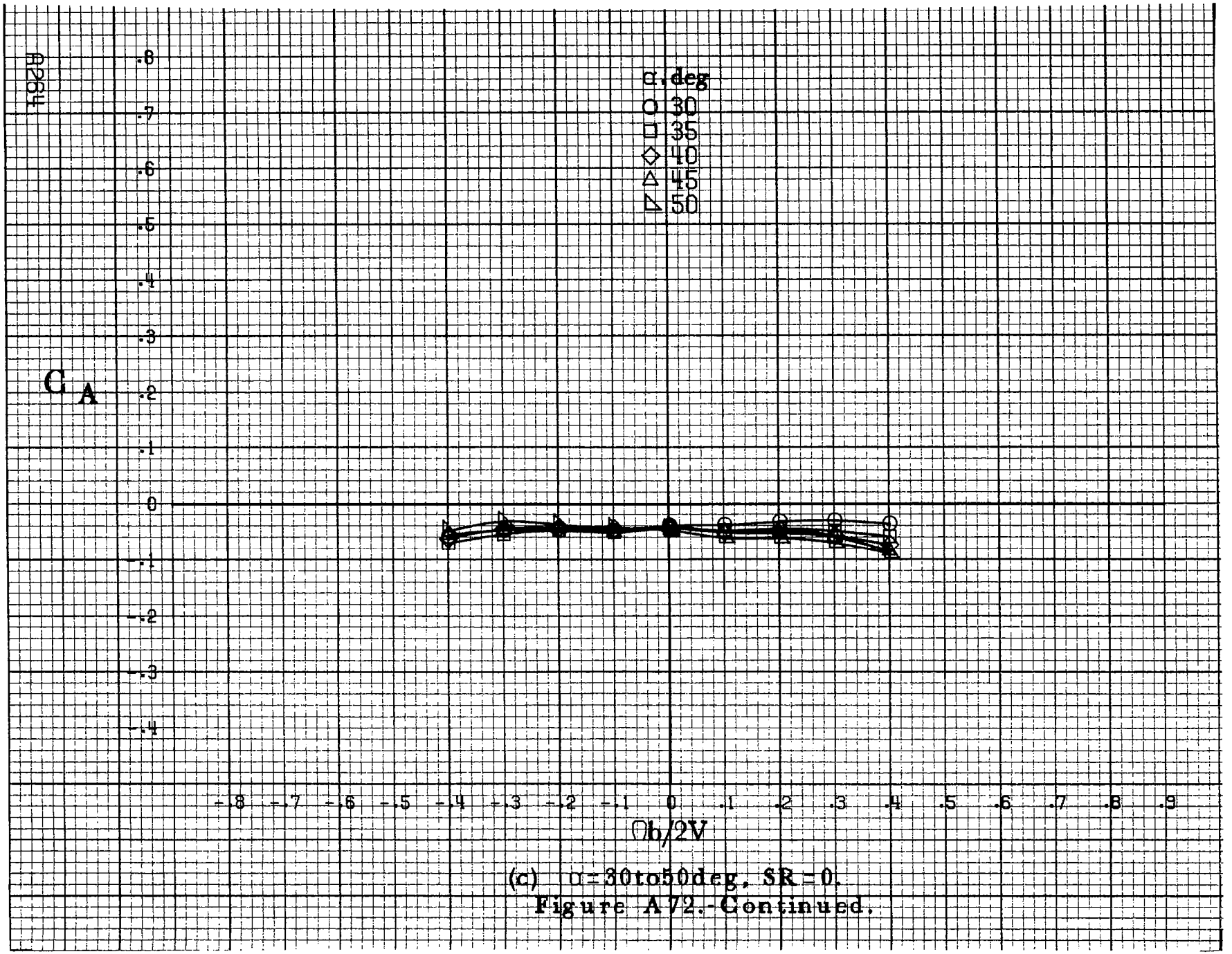

(c) $\alpha = 30$ to 50 deg, SR = 0.

Figure A72.- Continued.

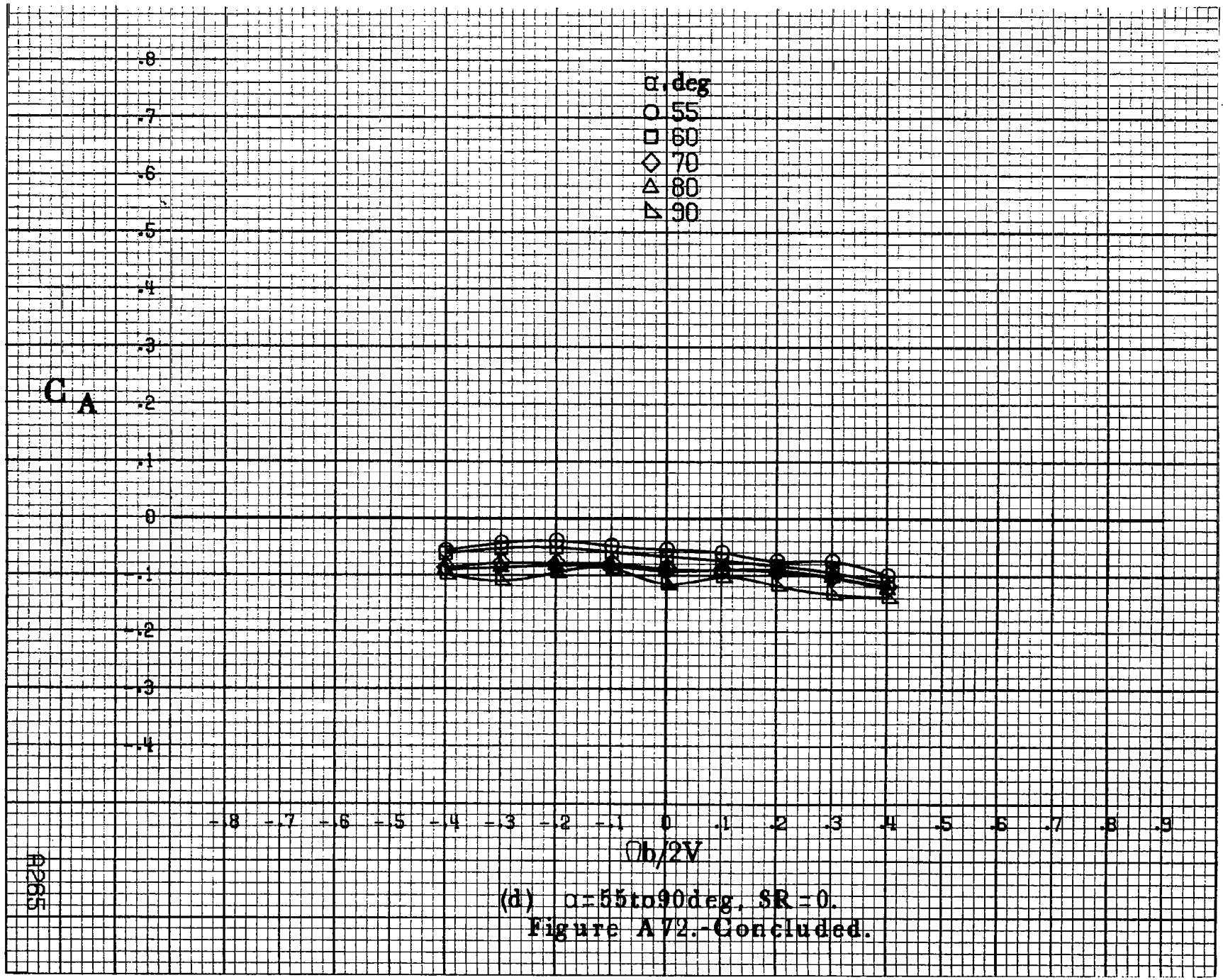

(d) α = 55 to 90 deg, SR = 0.

Figure A72.- Concluded.

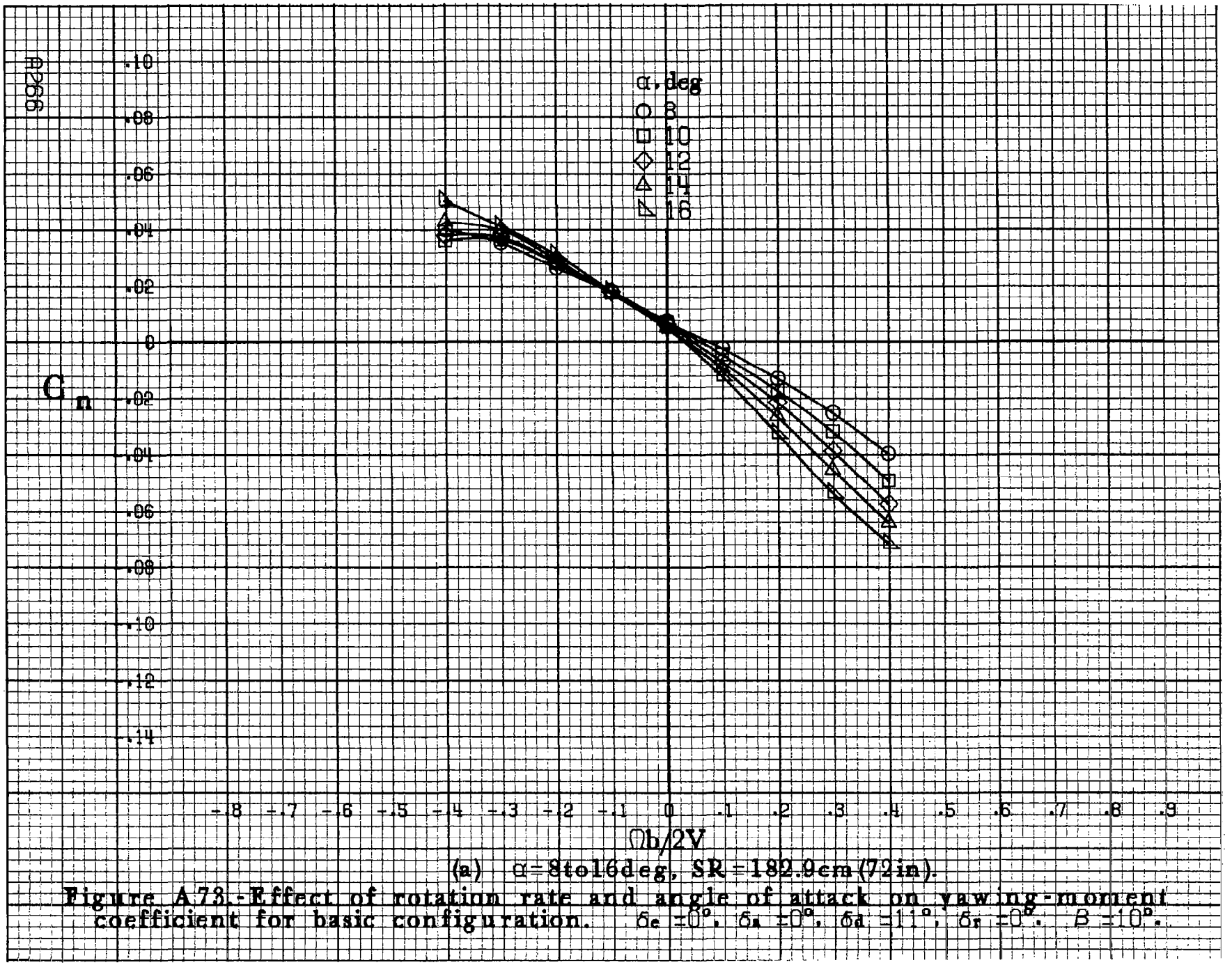

(a) $\alpha = 8$ to 16 deg, SR = 182.9 cm (72 in).

Figure A.73.- Effect of rotation rate and angle of attack on yawing-moment coefficient for basic configuration. $\delta_e = 0°$, $\delta_A = 0°$, $\delta_d = 11°$, $\delta_r = 0°$, $\beta = 10°$.

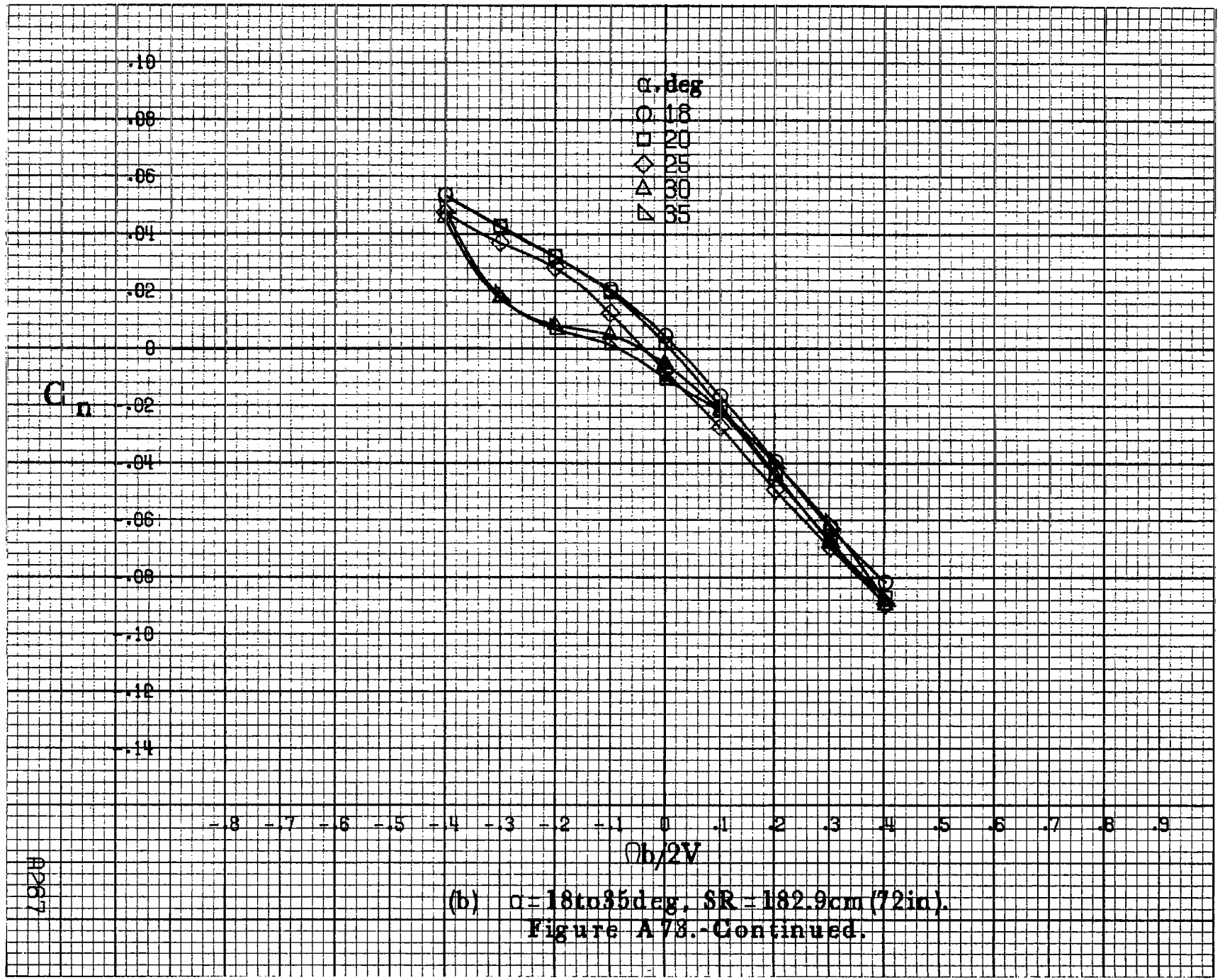

(b) α = 18 to 35 deg, SR = 182.9 cm (72 in.).

Figure A78.- Continued.

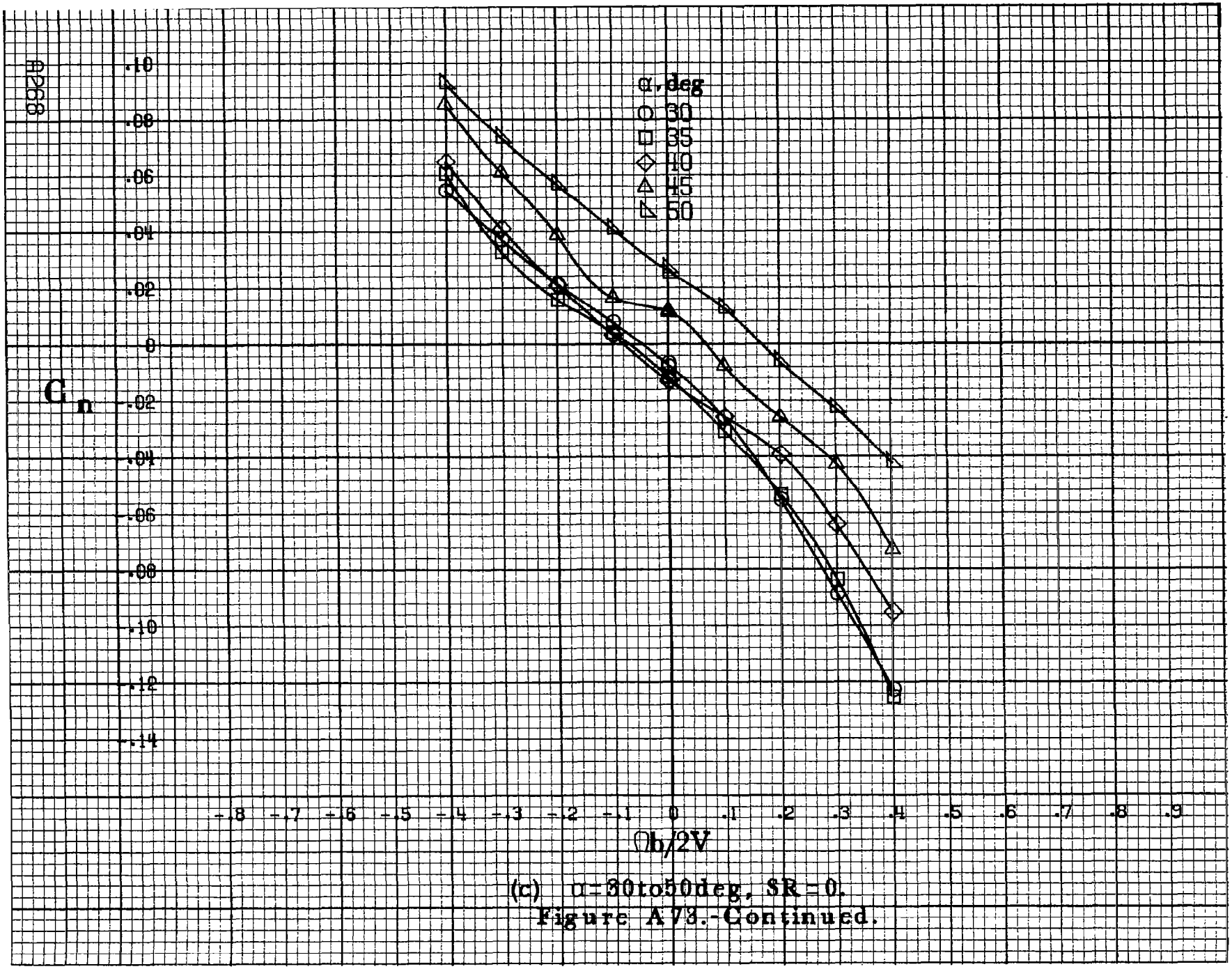

(c) α=30to50deg, SR = 0.

Figure A78.-Continued.

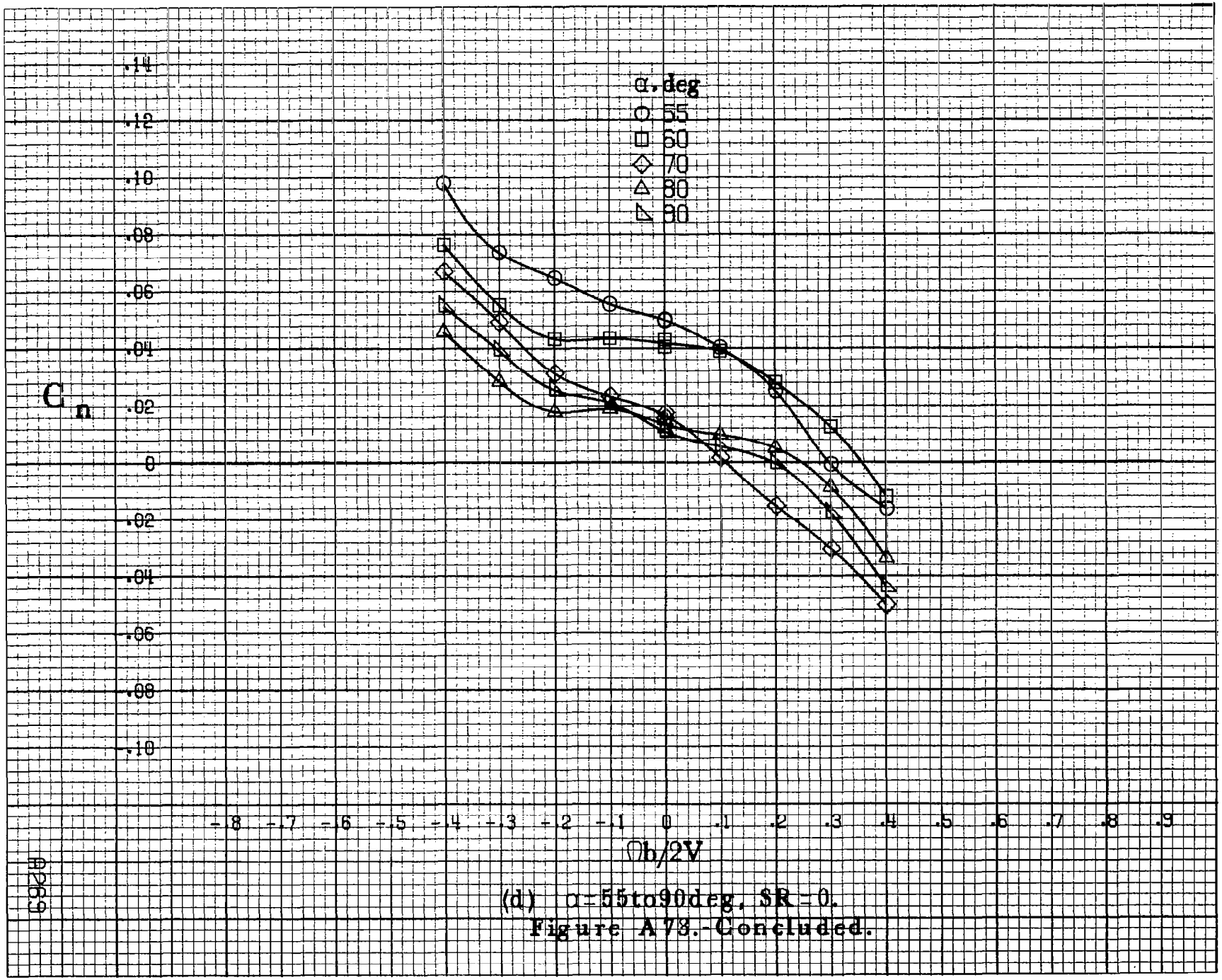

(d) $\alpha = 55$ to 90 deg. $SR = 0$.

Figure A73.- Concluded.

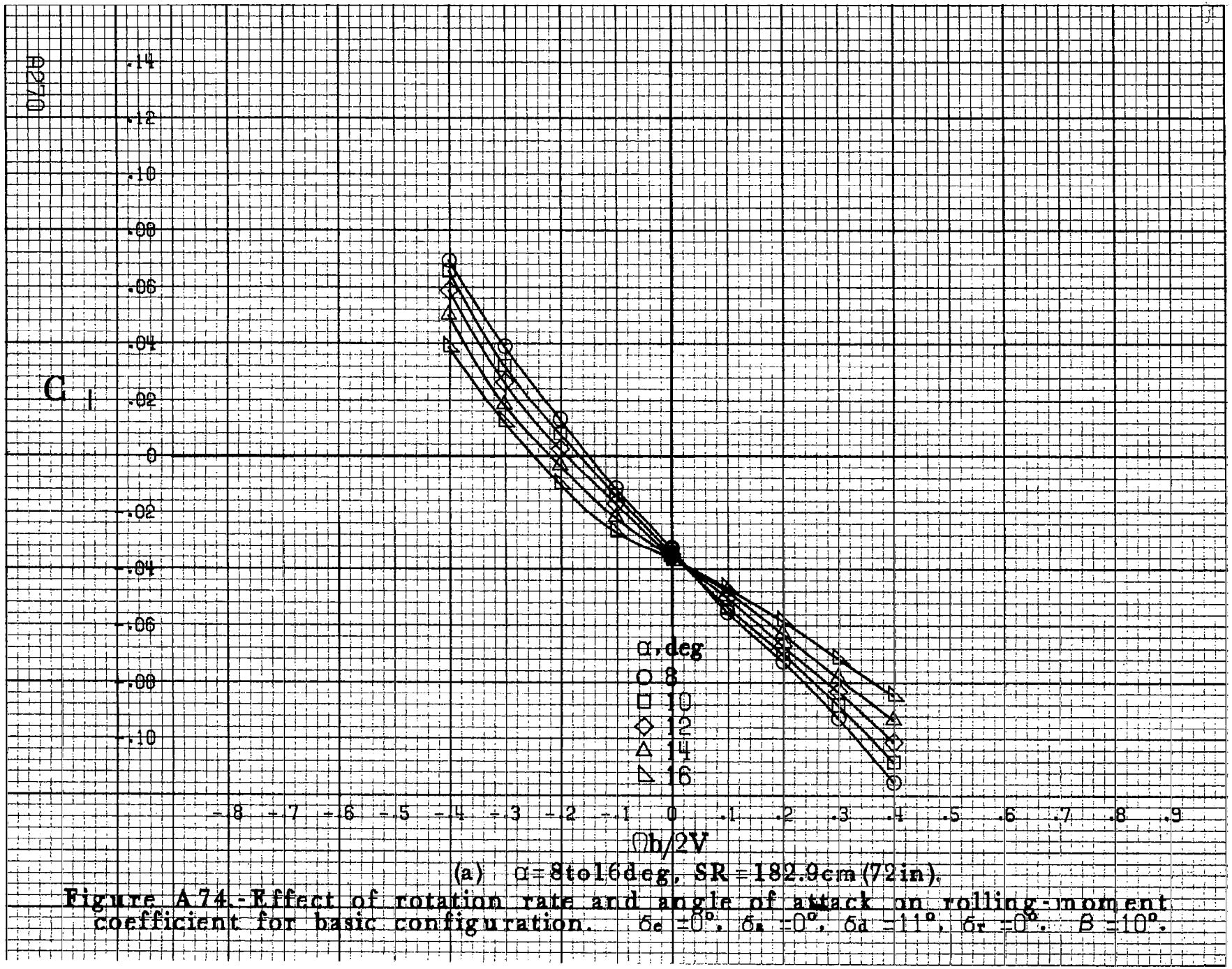

(a) $\alpha = 8$ to 16 deg, SR = 182.9 cm (72 in).

Figure A74.- Effect of rotation rate and angle of attack on rolling-moment coefficient for basic configuration. $\delta_e = 0°$, $\delta_s = 0°$, $\delta_a = 11°$, $\delta_r = 0°$, $\beta = 10°$.

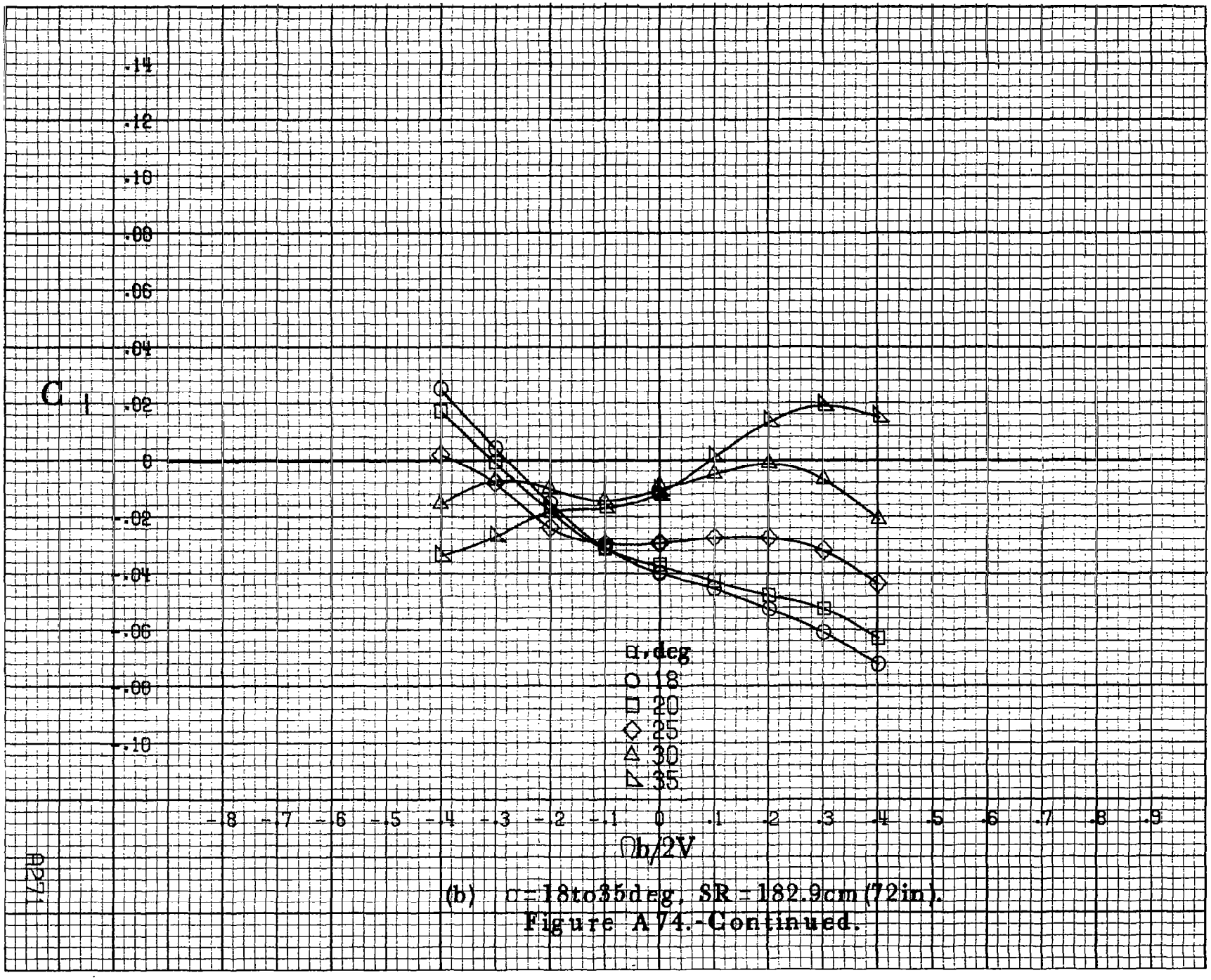

(b) $\alpha = 18$ to 35 deg, SR = 182.9 cm (72 in).

Figure A74.-Continued.

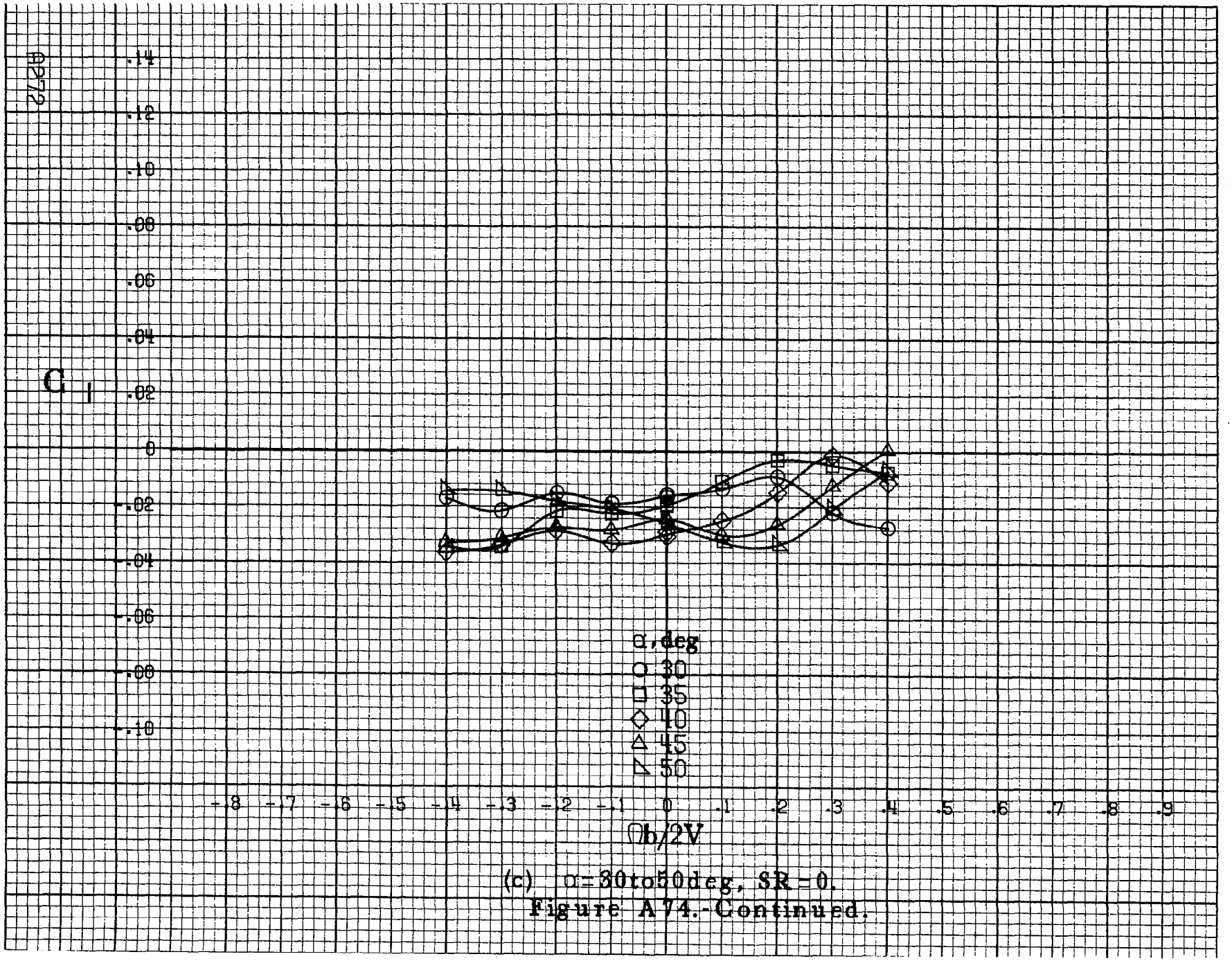

(c) α = 30 to 50 deg, SR = 0.

Figure A74.-Continued.

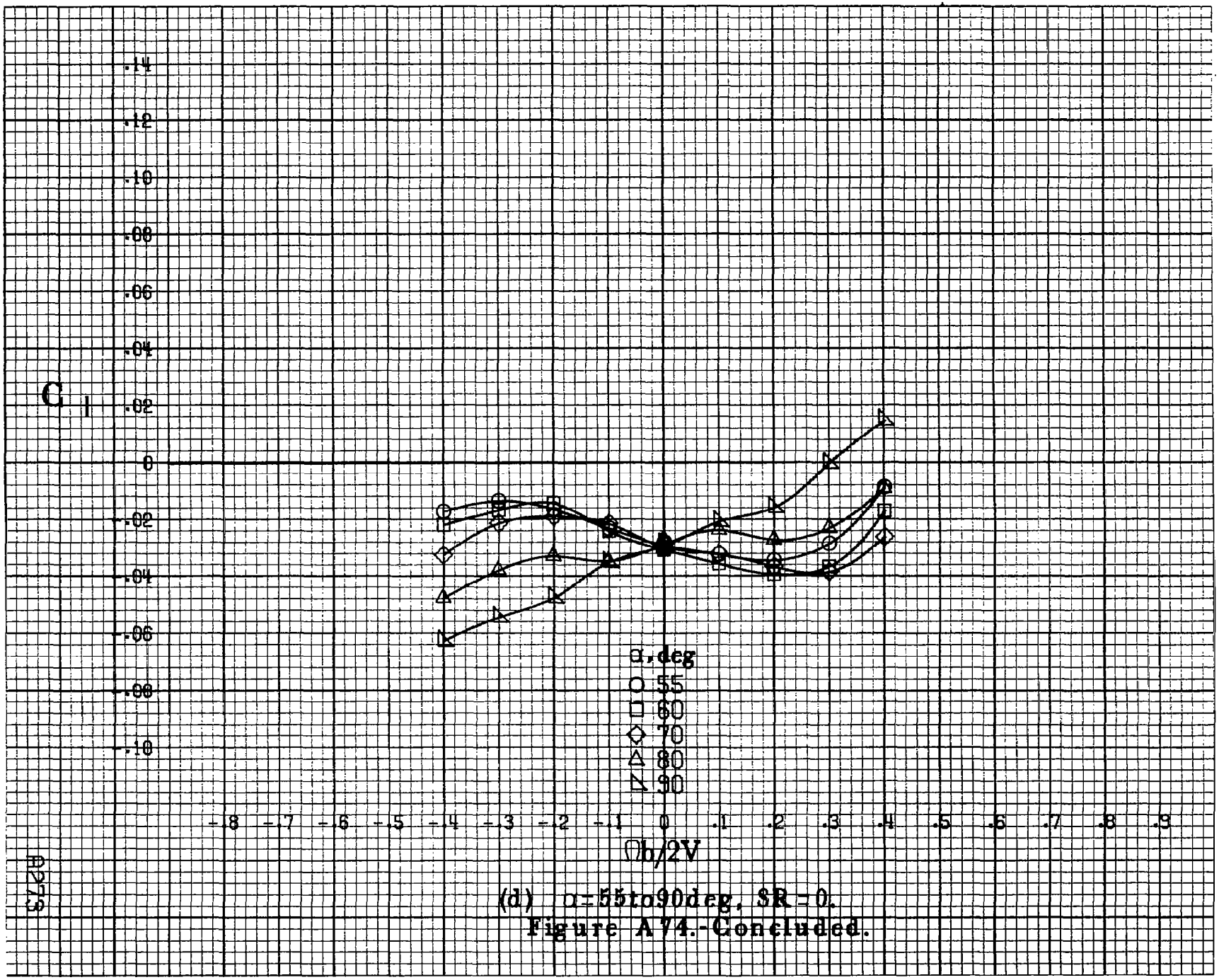

(d) $\alpha = 55$ to 90 deg, $SR = 0$.

Figure A74.- Concluded.

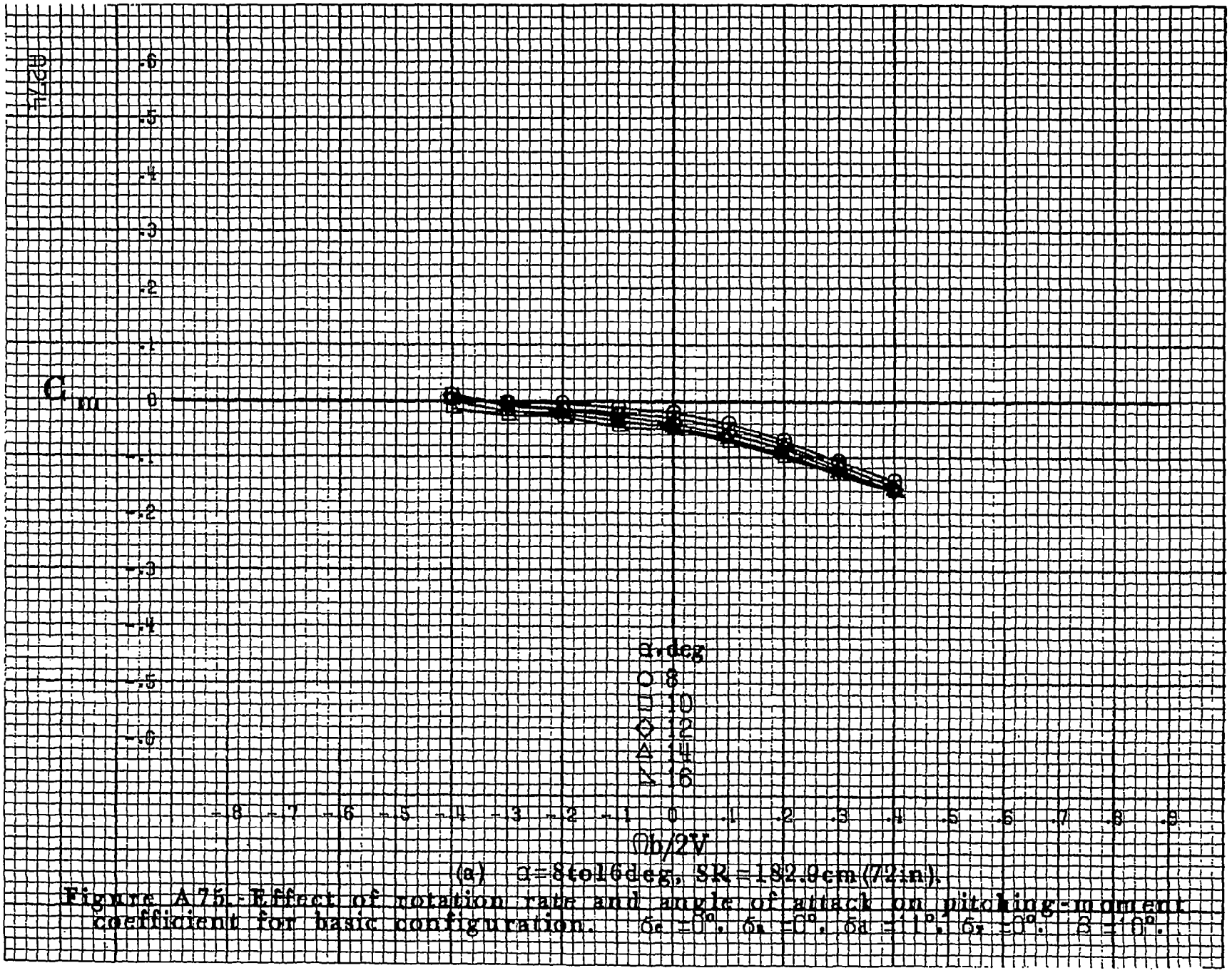

(a) α=8to16deg, SR = 182.9cm(72in).

Figure A75.- Effect of rotation rate and angle of attack on pitching-moment coefficient for basic configuration. $\delta_e = 0°$, $\delta_a = 0°$, $\delta_d = 11°$, $\delta_r = 0°$, $\beta = 0°$.

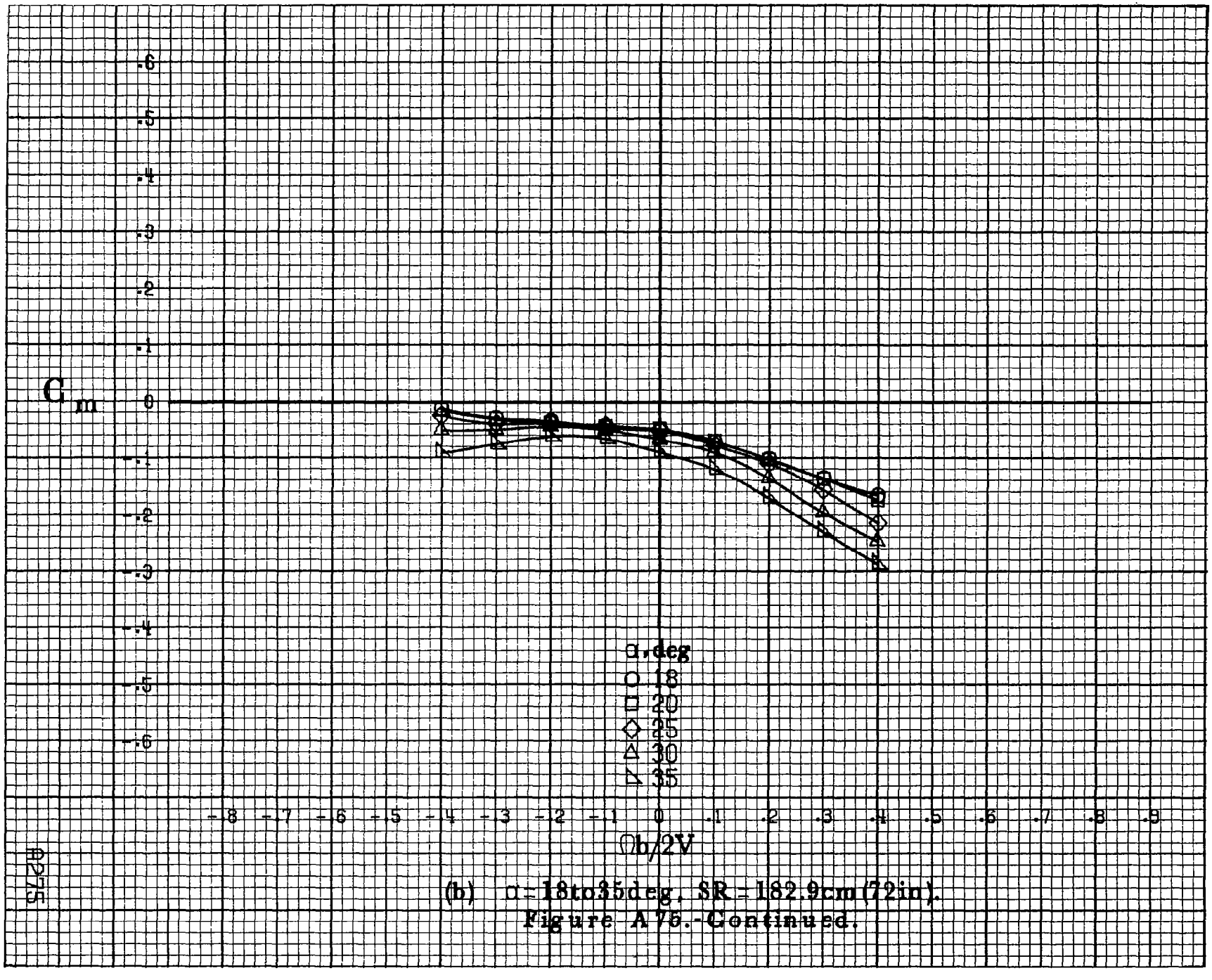

(b) α = 18 to 35 deg, SR = 182.9 cm (72 in).

Figure A76.-Continued.

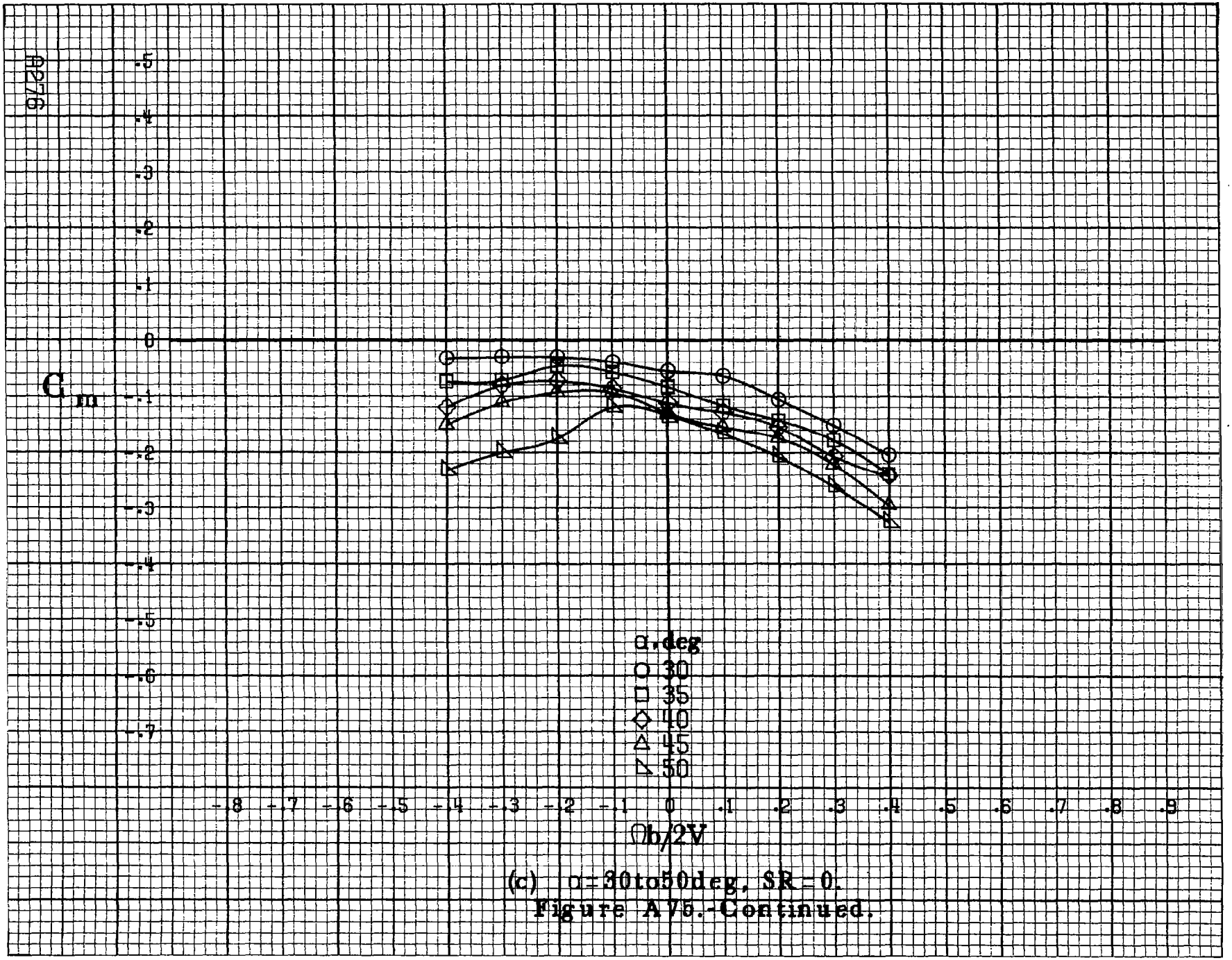

(c) α = 30 to 50 deg, SR = 0.

Figure A76.-Continued.

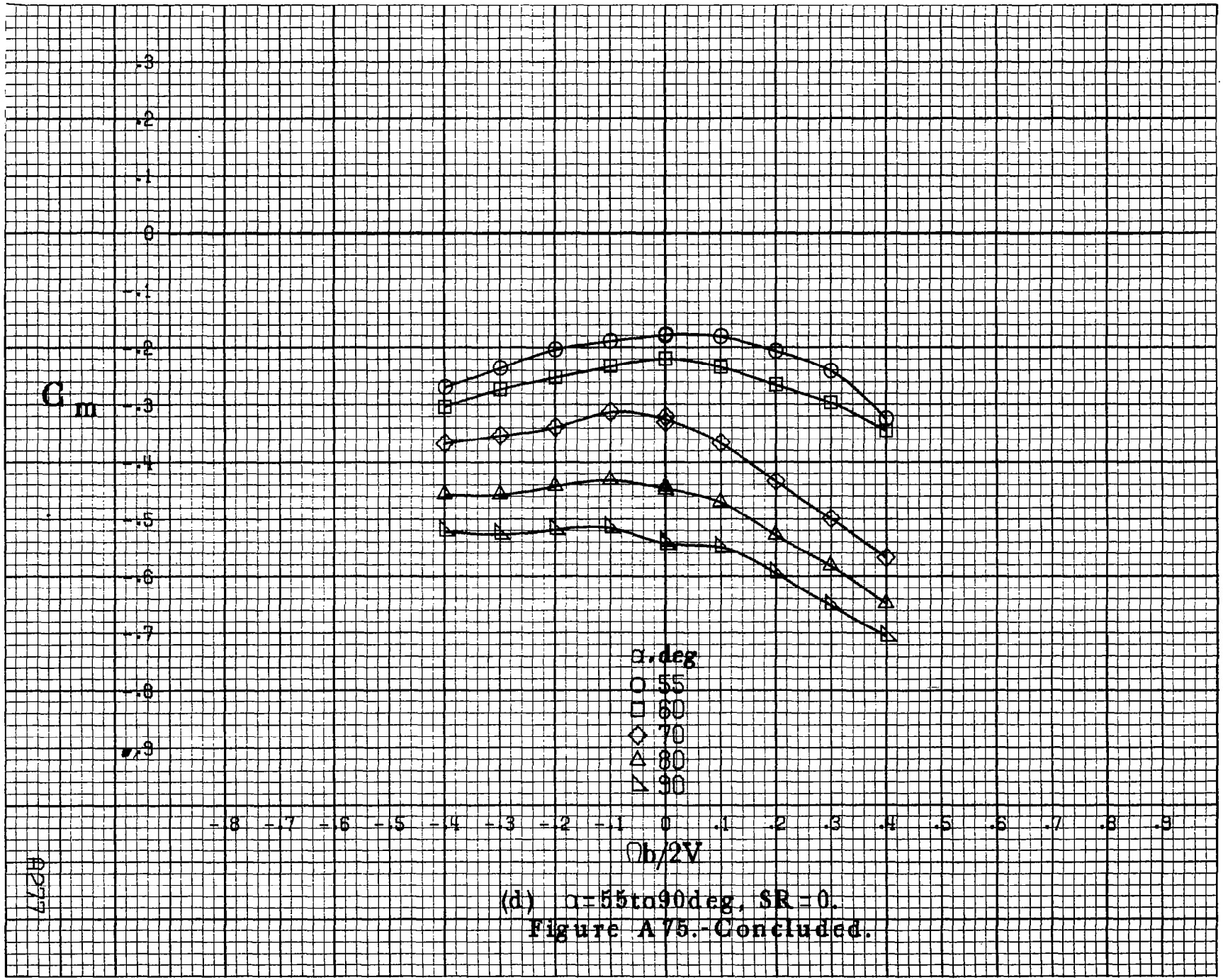

(d) $\alpha = 55$ to 90 deg, $\$R = 0$.

Figure A75.-Concluded.

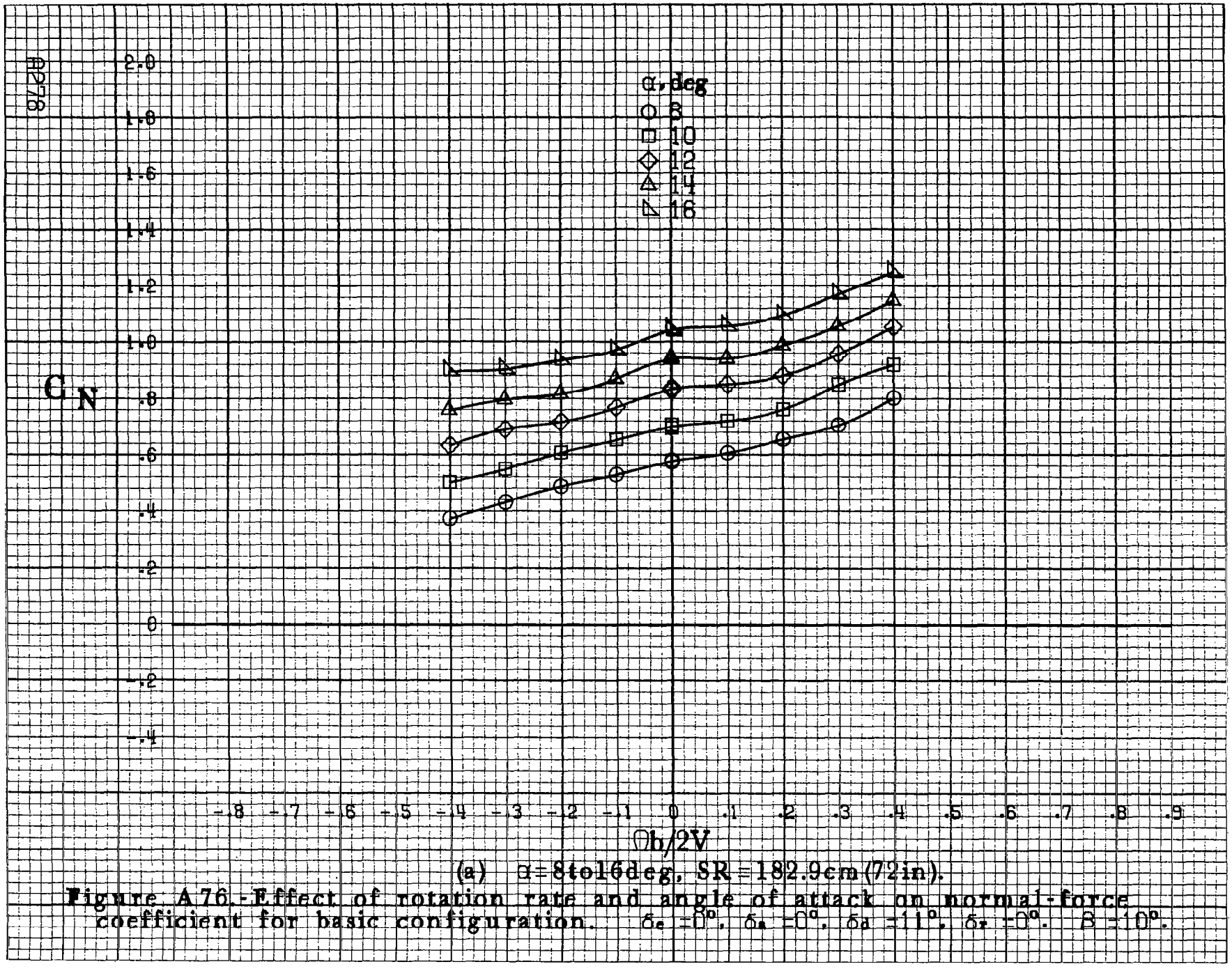

(a) α = 8 to 16 deg, SR = 182.9 cm (72 in).

Figure A 76.- Effect of rotation rate and angle of attack on normal-force coefficient for basic configuration. $\delta_e = 0°$, $\delta_s = 0°$, $\delta_a = 11°$, $\delta_r = 0°$. $\beta = 10°$.

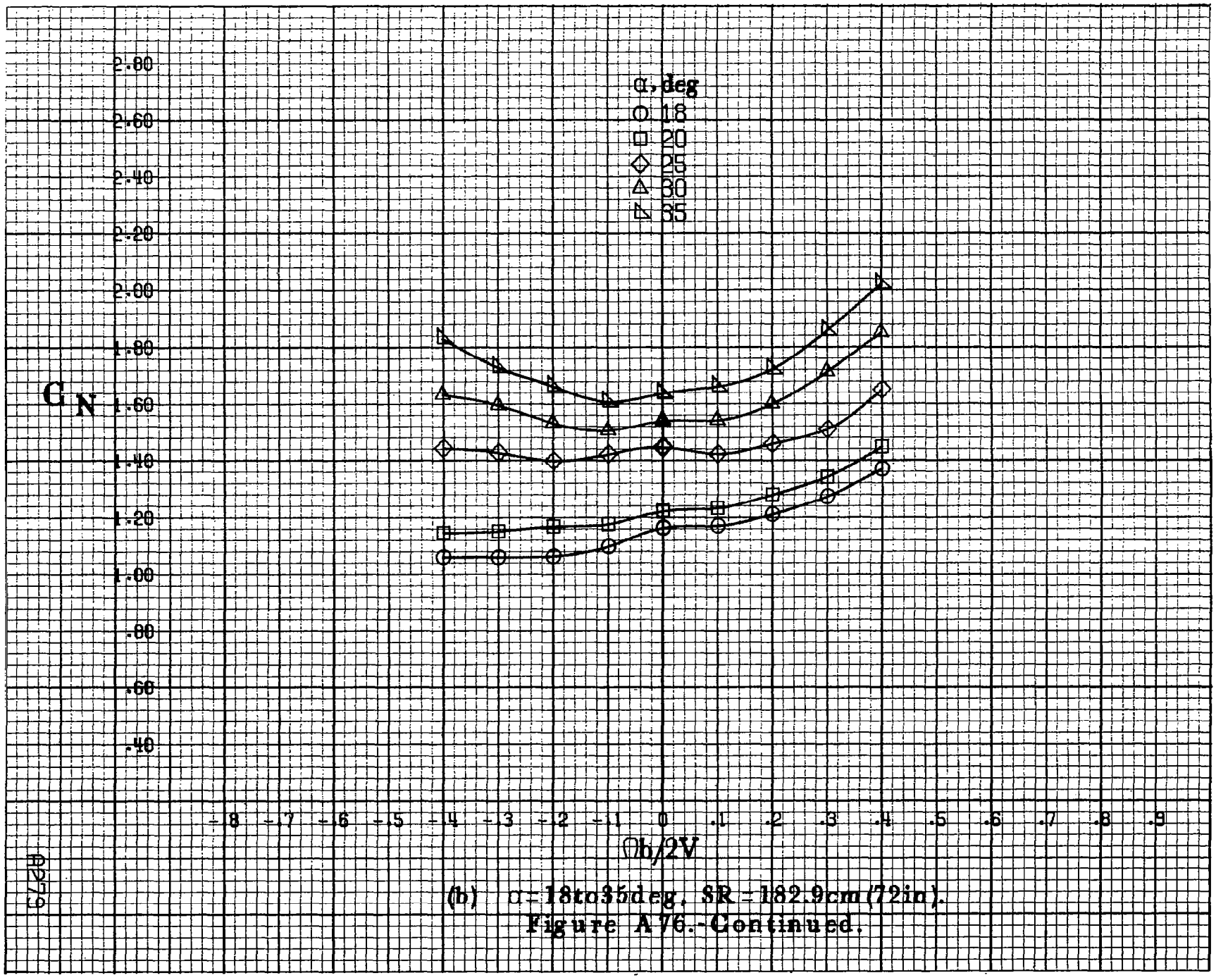

(b) α = 18 to 35 deg, SR = 182.9 cm (72 in).

Figure A76.- Continued.

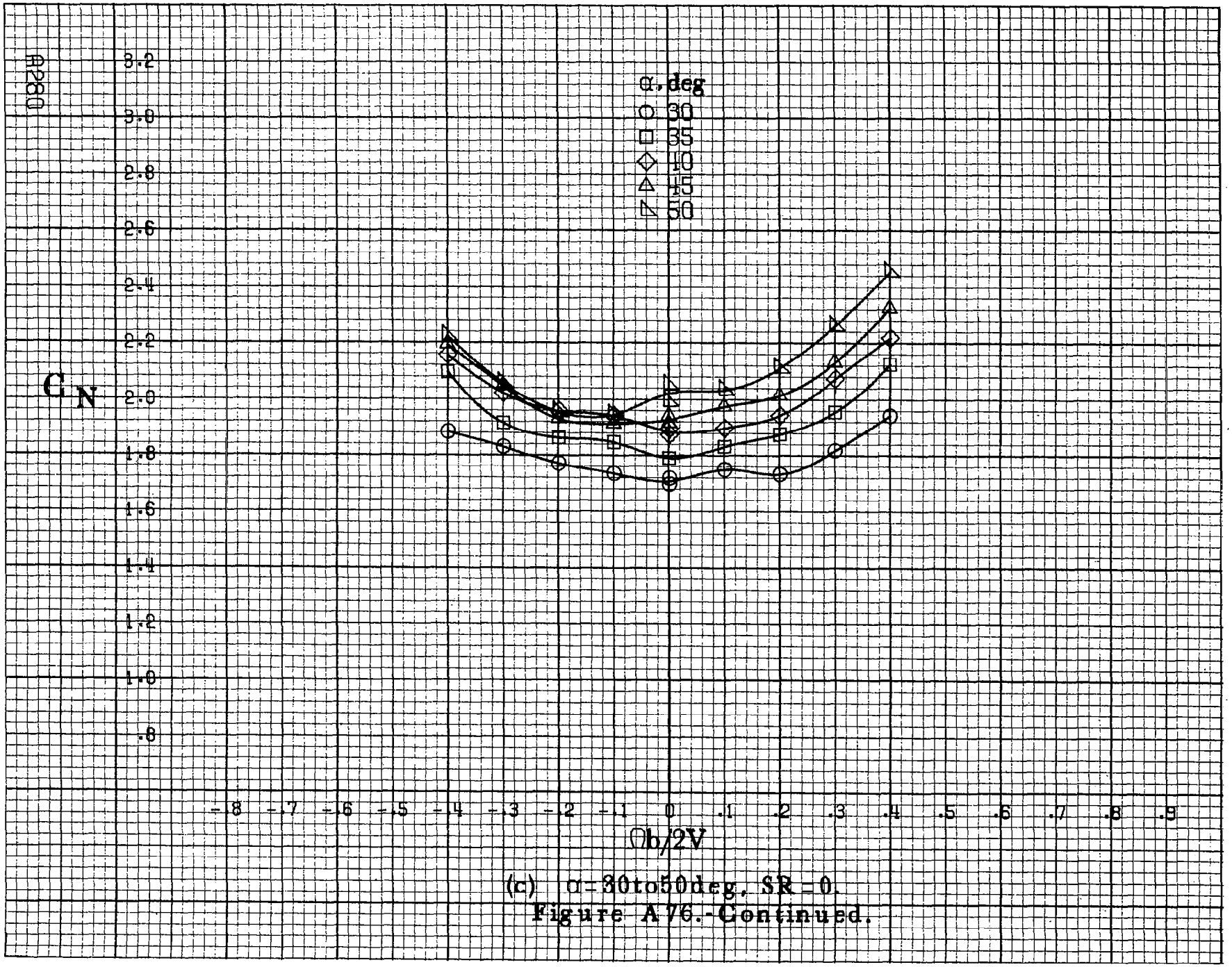

(c) $\alpha = 30$ to 50 deg, SR = 0.

Figure A76.- Continued.

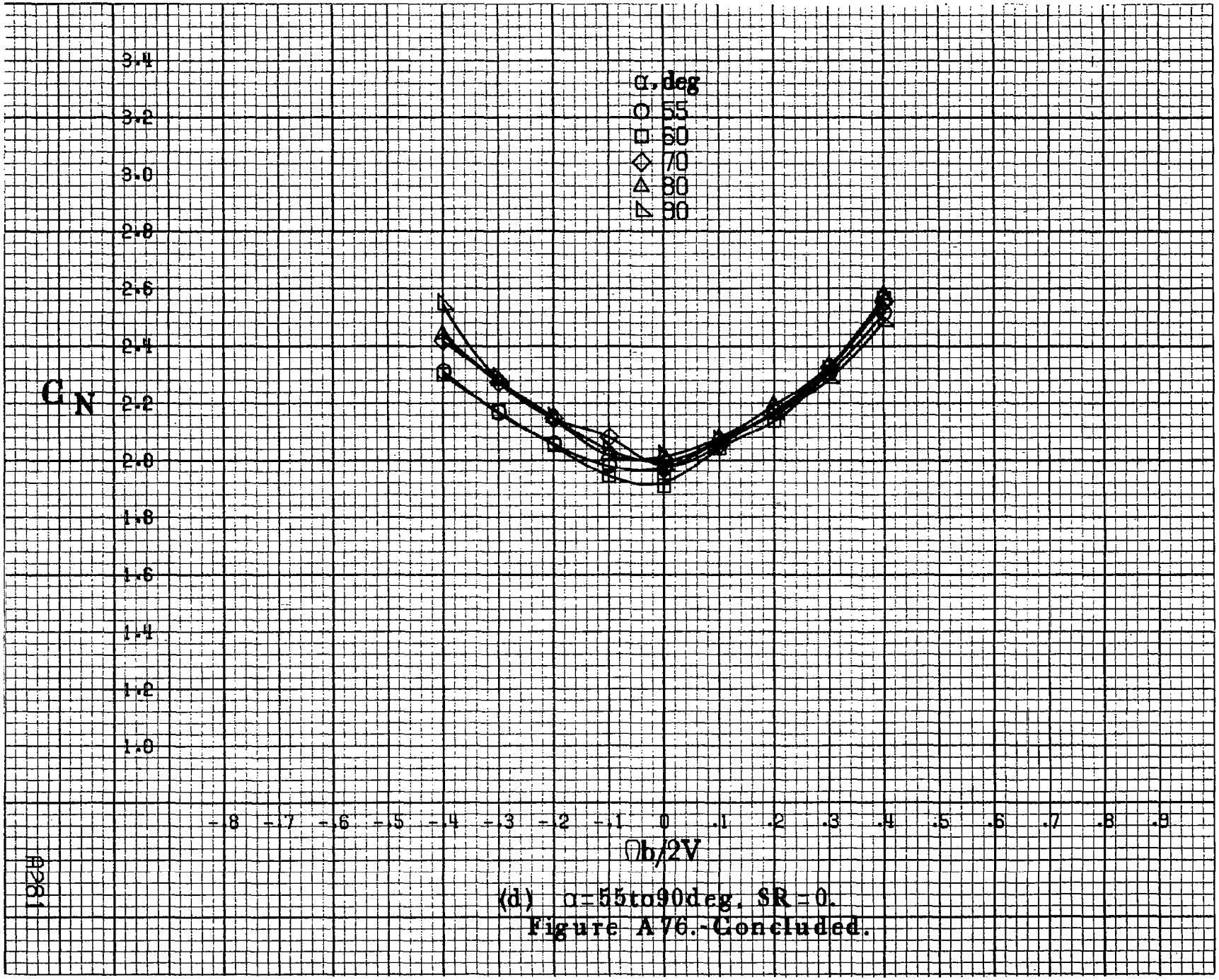

(d) α=55to90deg, SR=0.

Figure A76.-Concluded.

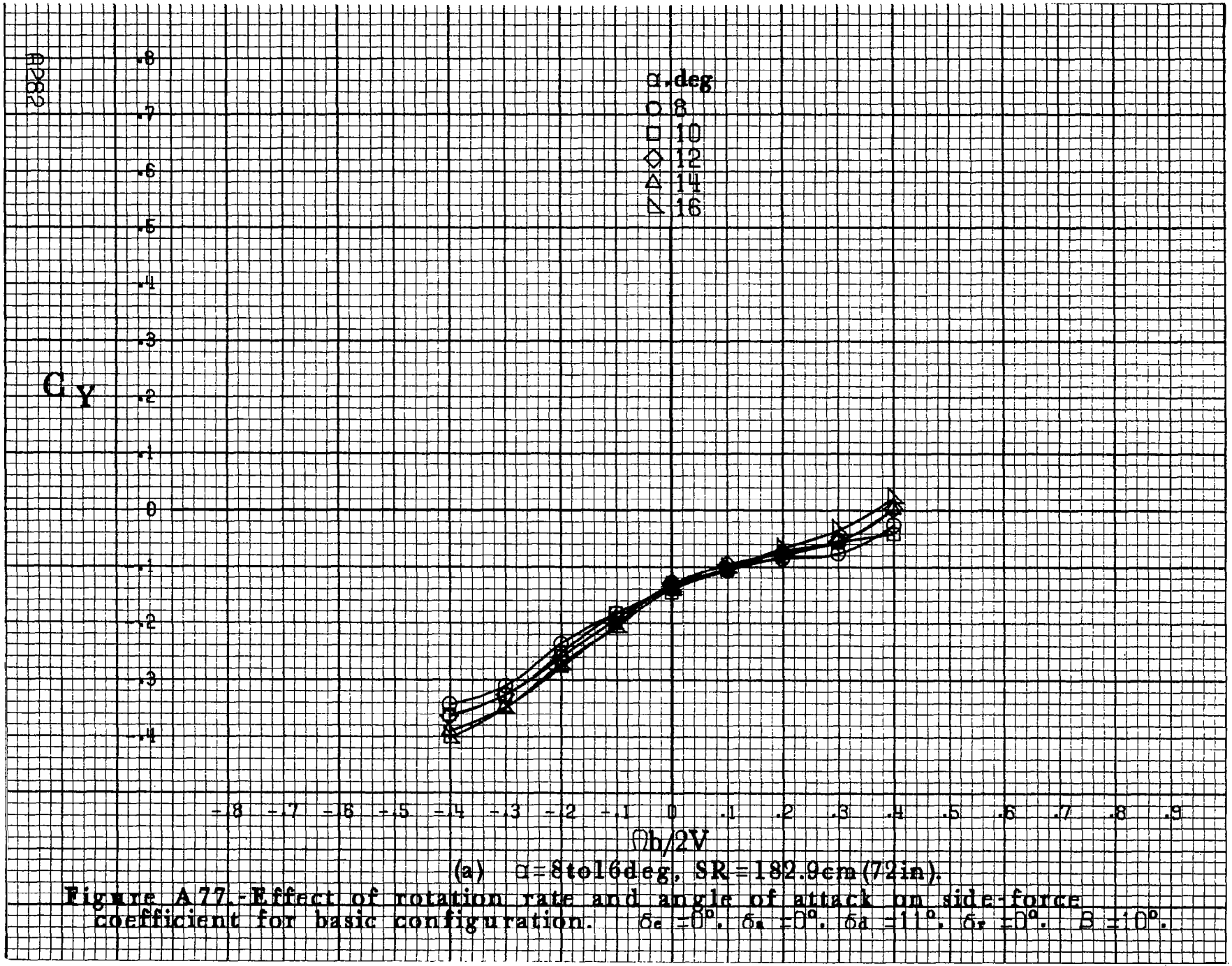

(a) $\alpha = 8$ to 16 deg, SR = 182.9 cm (72 in).

Figure A77.-Effect of rotation rate and angle of attack on side-force coefficient for basic configuration. $\delta_e = 0°$, $\delta_s = 0°$, $\delta_a = 11°$, $\delta_r = 0°$, $\beta = 0°$.

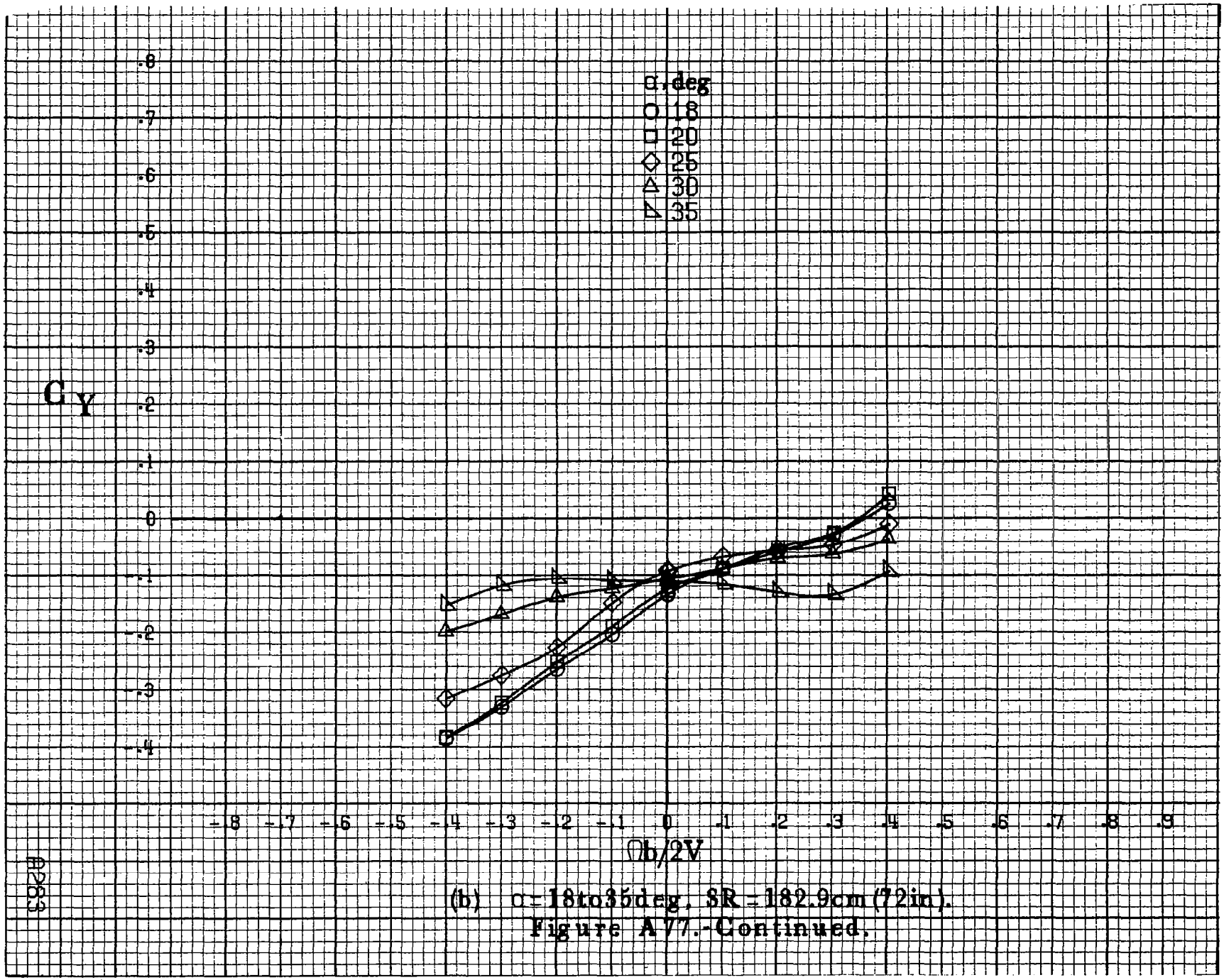

(b) $\alpha = 18$ to 35 deg, SR = 182.9 cm (72 in.).

Figure A77.-Continued.

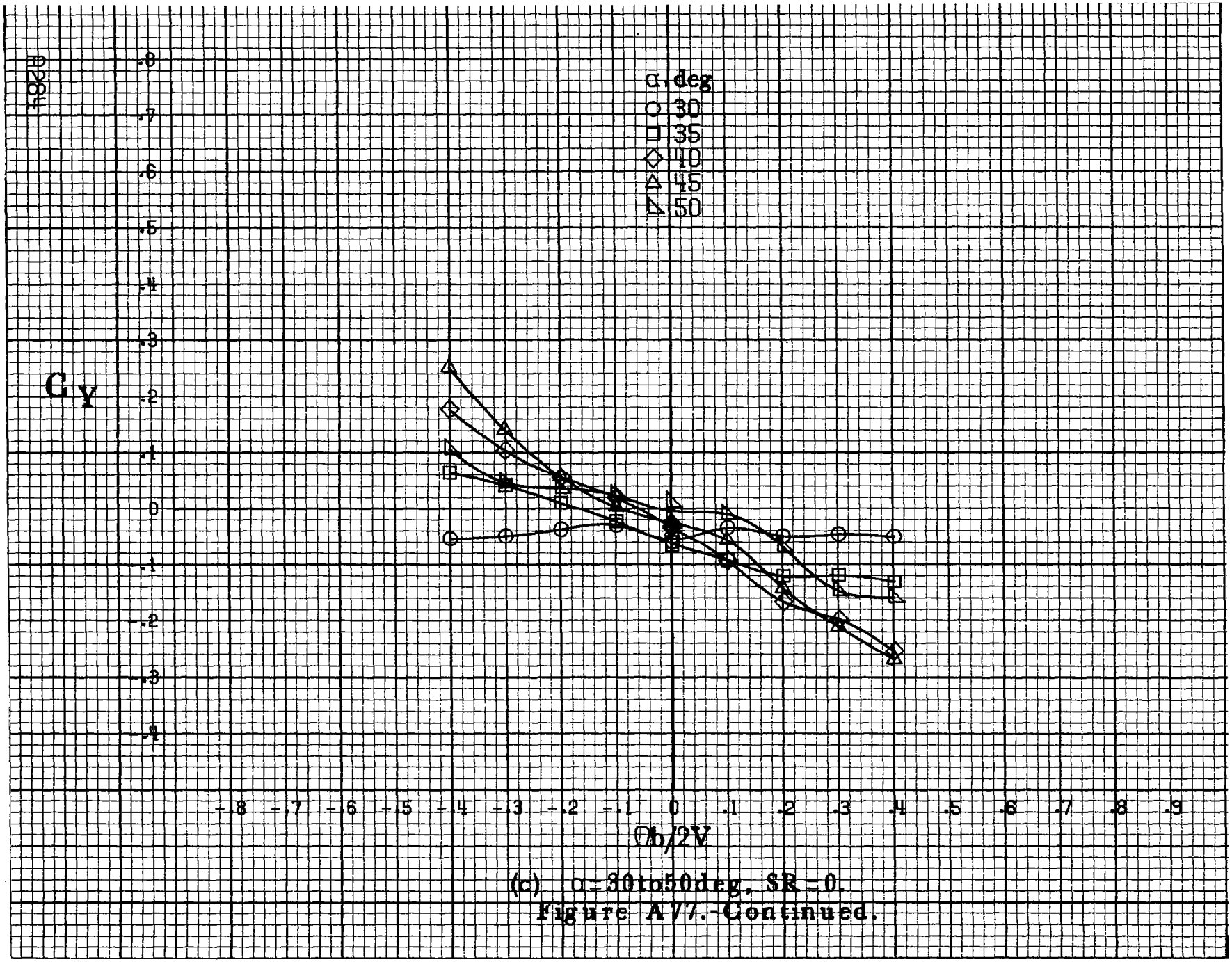

(c) $\alpha = 30$ to 50 deg, $SR = 0$.

Figure A77.-Continued.

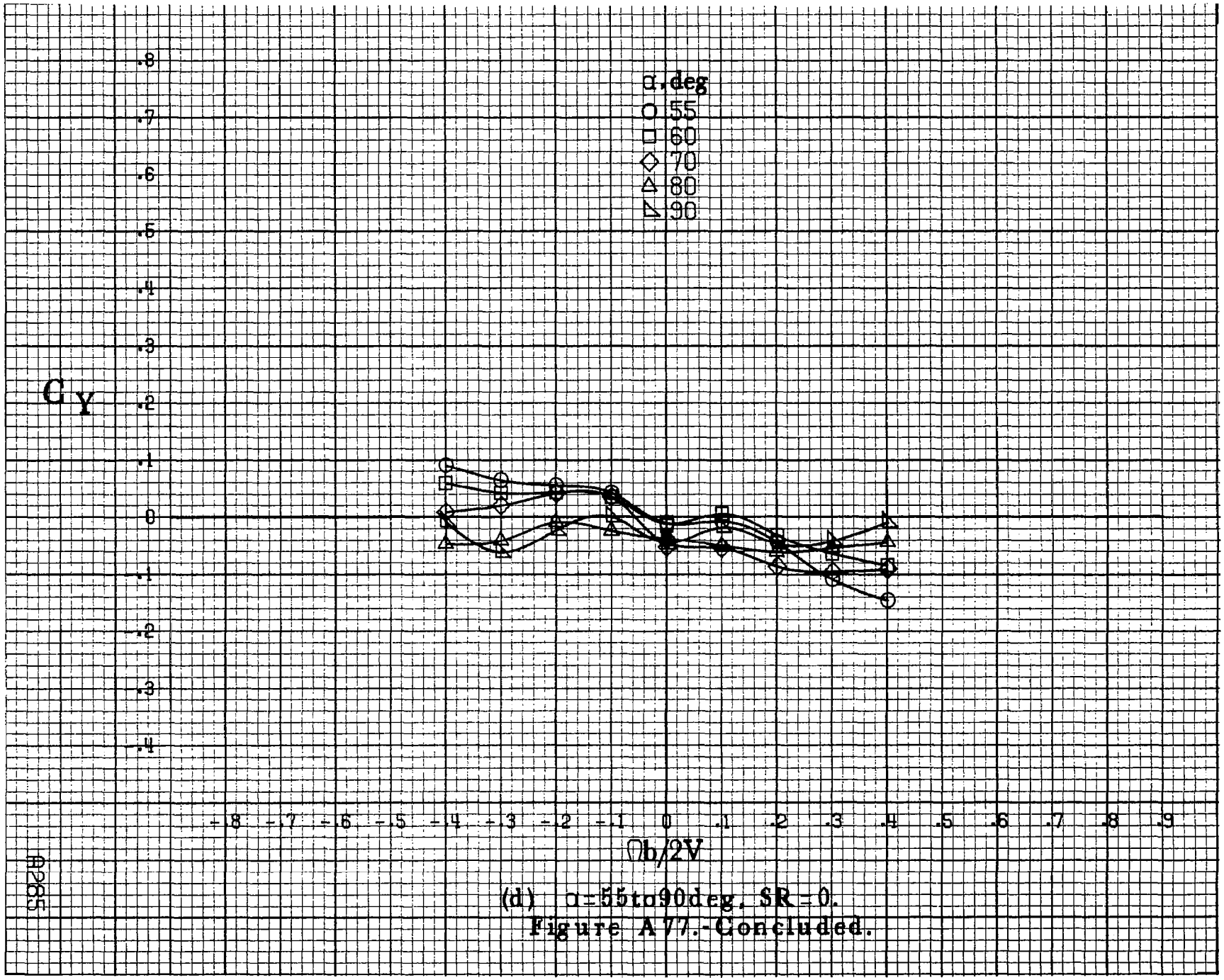

(d) $\alpha = 55$ to 90 deg, $SR = 0$.

Figure A77.-Concluded.

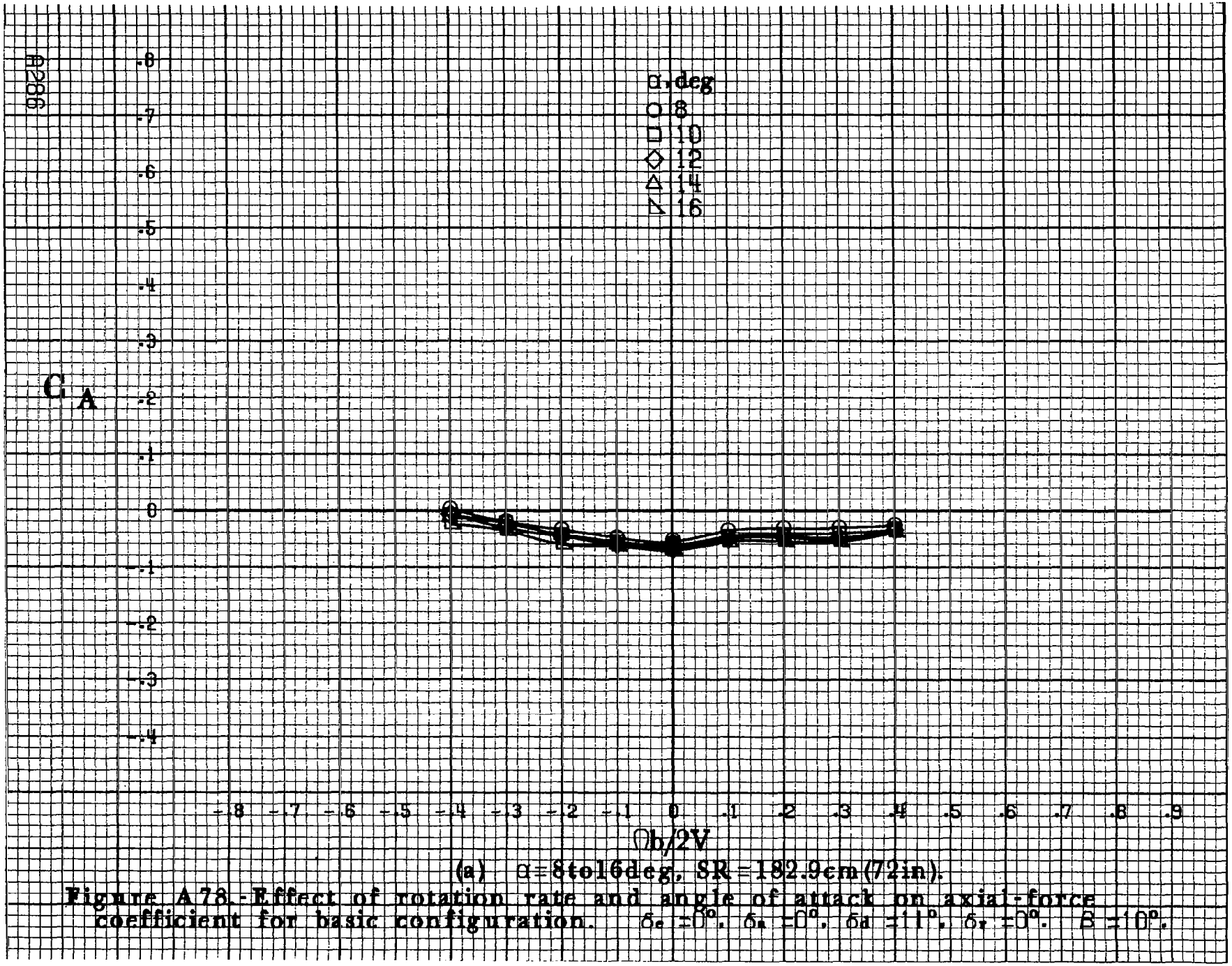

(a) α = 8 to 16 deg, SR = 182.9 cm (72 in).

Figure A 78.- Effect of rotation rate and angle of attack on axial-force coefficient for basic configuration. $\delta_e = 0°$, $\delta_a = 0°$, $\delta_d = 11°$, $\delta_r = 0°$, $\beta = 10°$.

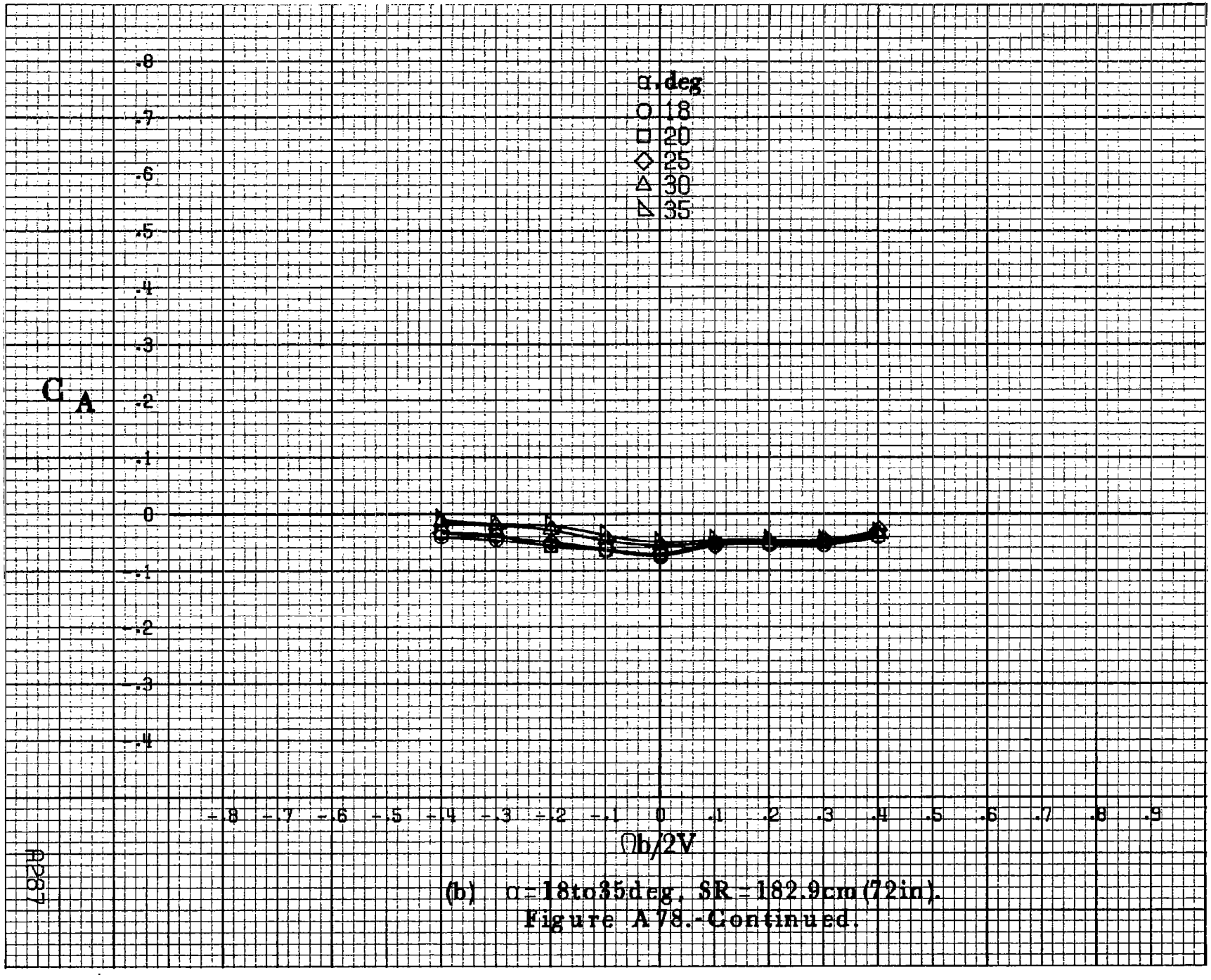

(b) α = 18 to 35 deg, SR = 182.9 cm (72 in).

Figure A78.- Continued.

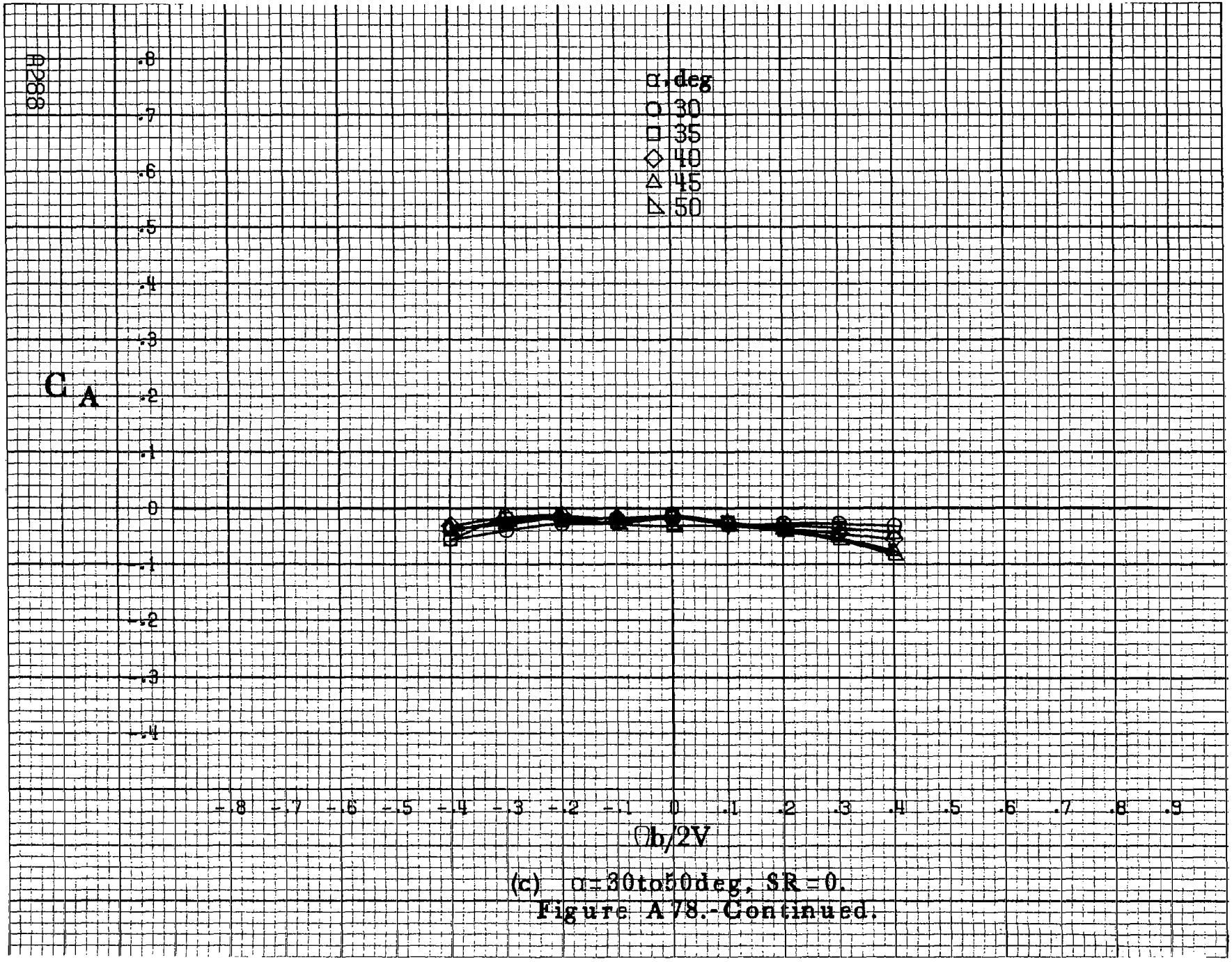

(c) α = 30 to 50 deg, $\delta_R = 0$.

Figure A78.- Continued.

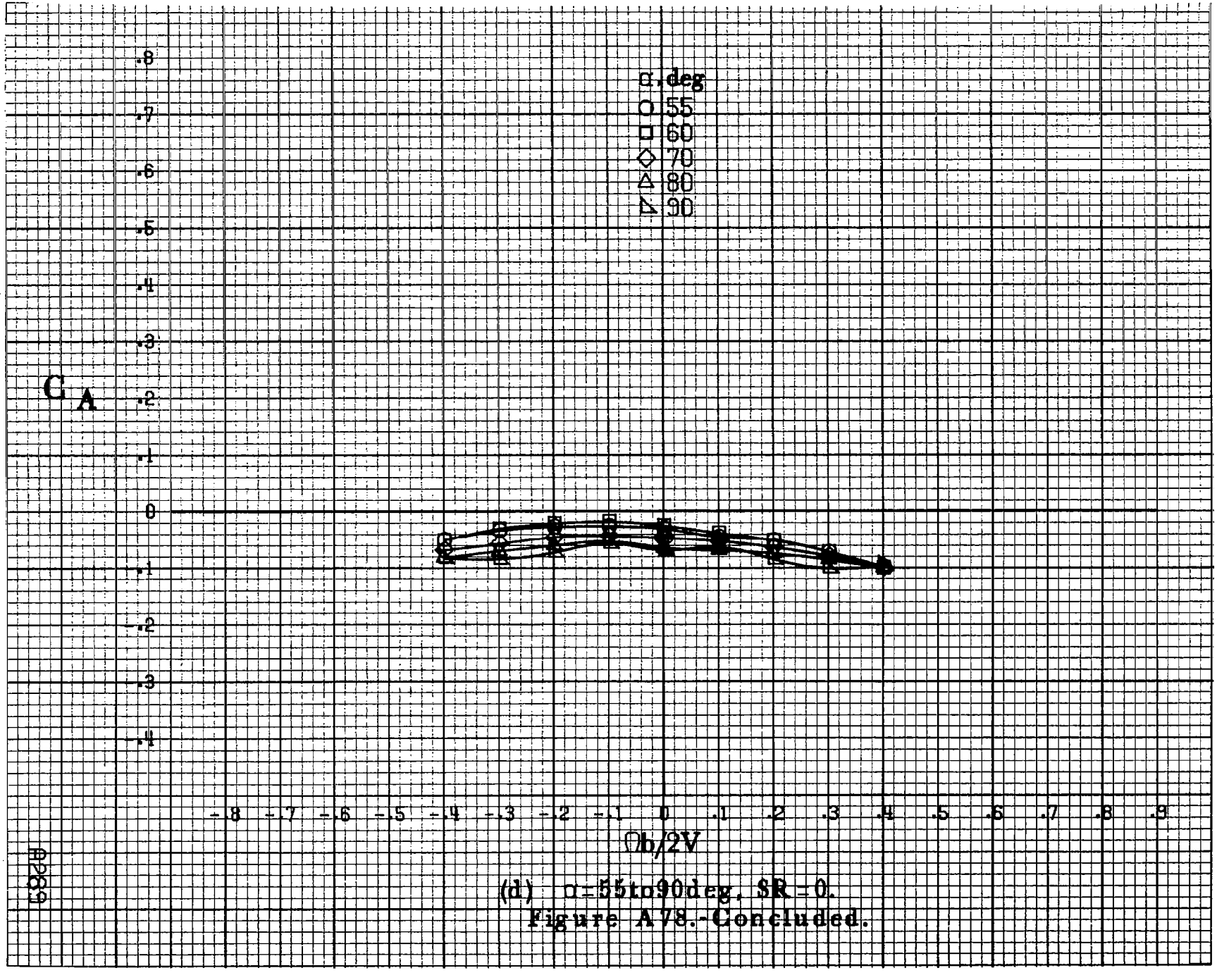

(d) α=55to90deg, $R=0.

Figure A78.-Concluded.

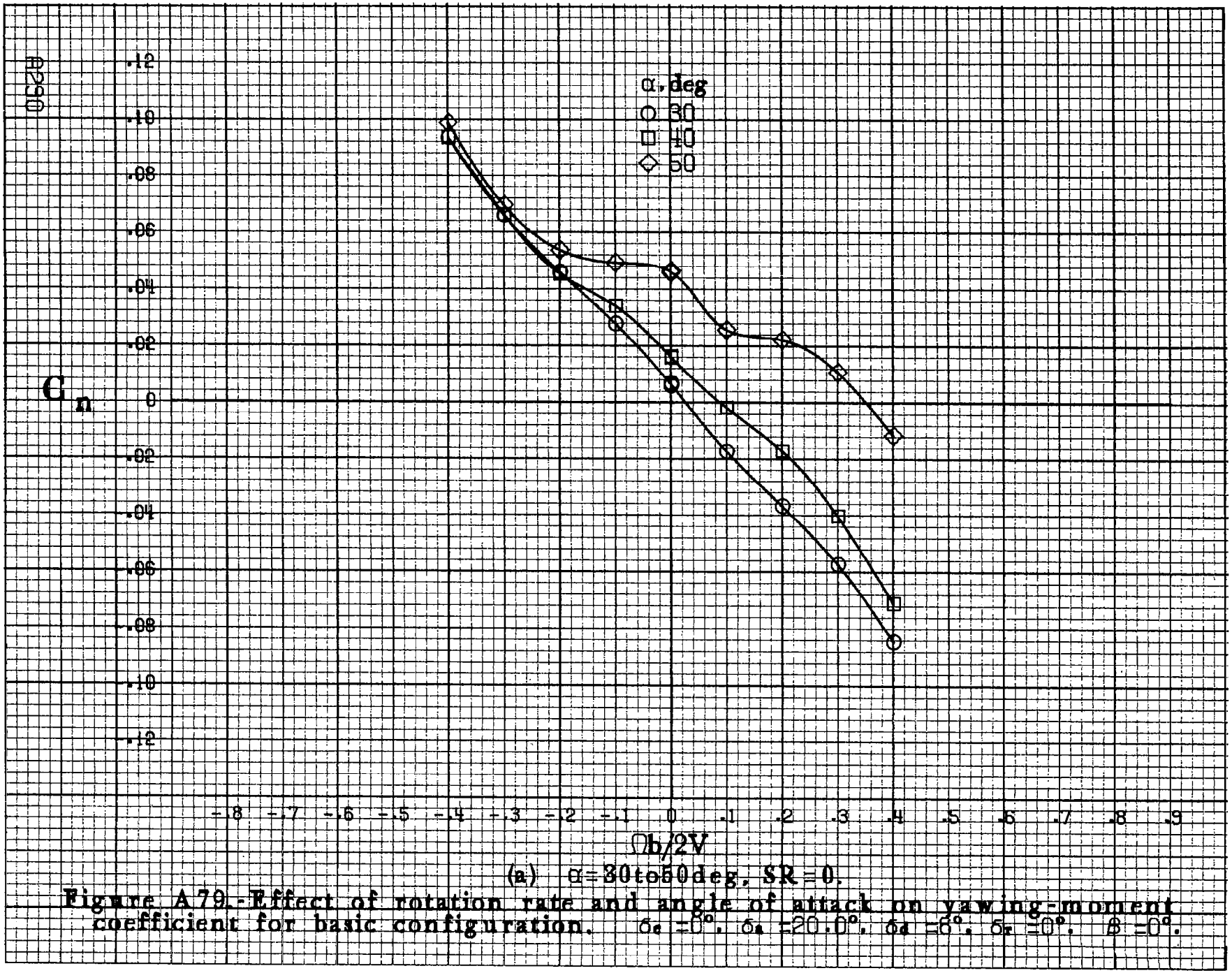

(a) $\alpha = 30$ to 50 deg, SR = 0.

Figure A79.- Effect of rotation rate and angle of attack on yawing-moment coefficient for basic configuration. $\delta_e = 0°$, $\delta_a = 20.0°$, $\delta_d = 6°$, $\delta_r = 0°$, $\beta = 0°$.

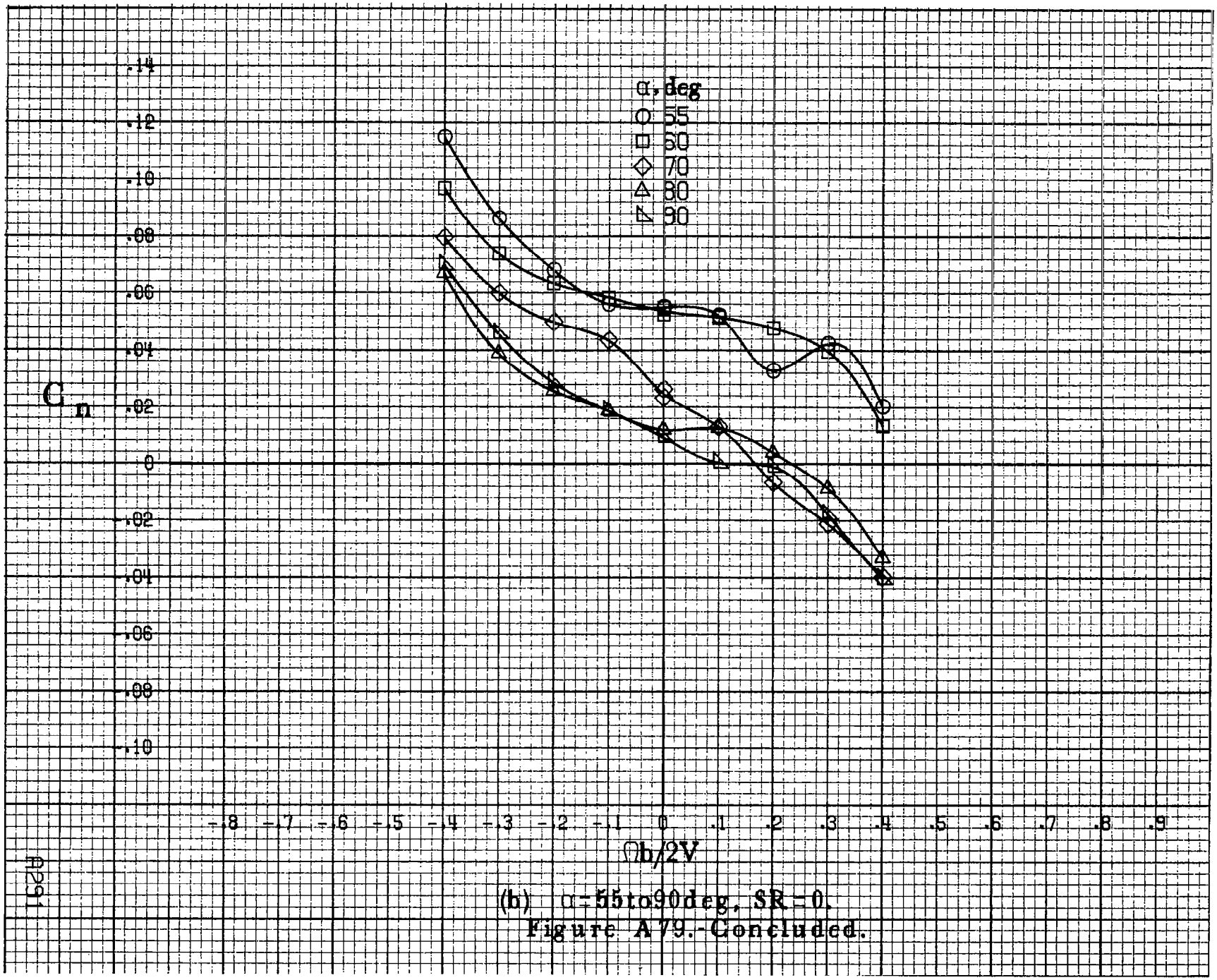

(b) α=55to90deg, SR=0.

Figure A79.-Concluded.

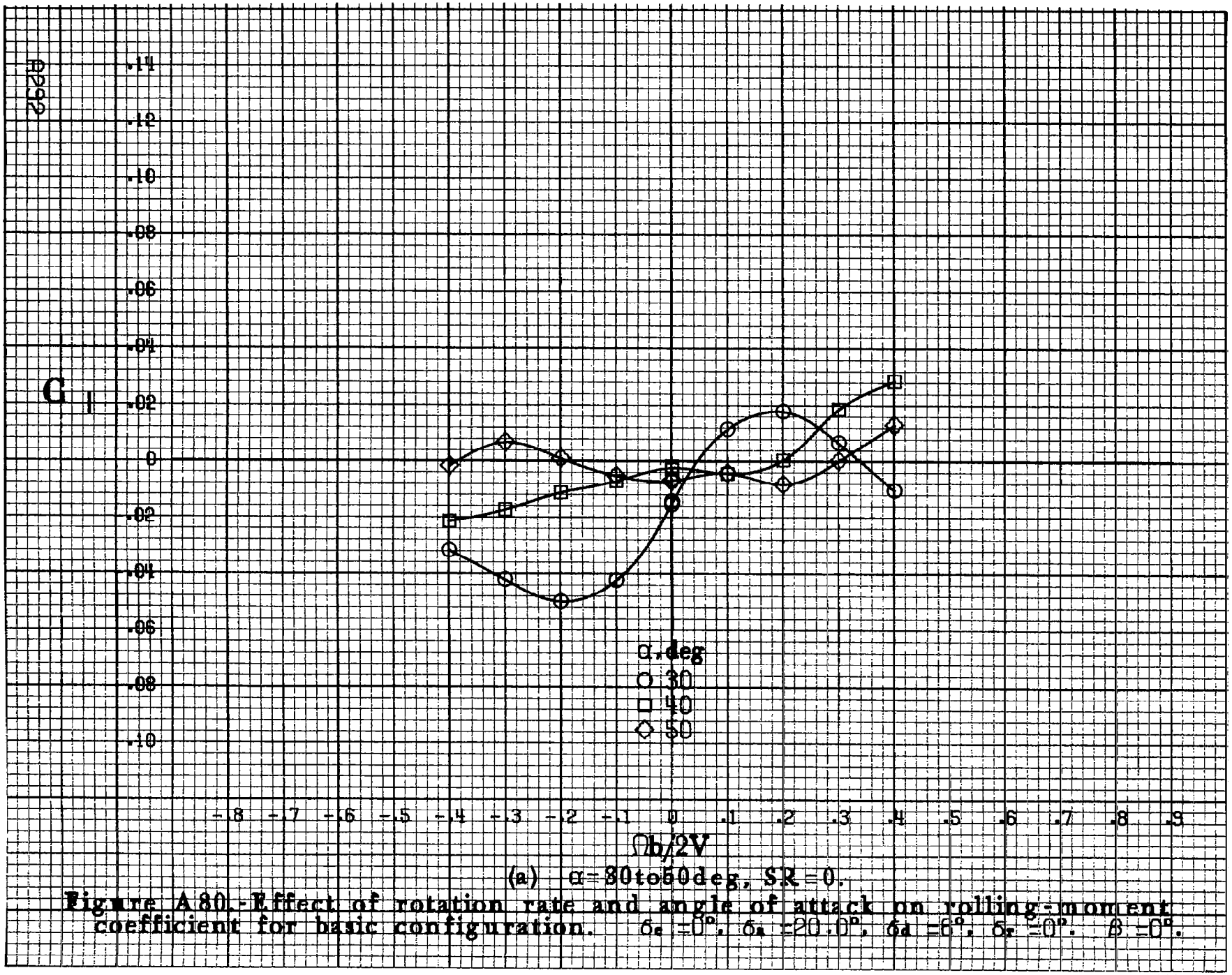

(a) $\alpha = 30$ to 60 deg, SR = 0.

Figure A80.- Effect of rotation rate and angle of attack on rolling-moment coefficient for basic configuration. $\delta_e = 0°$, $\delta_s = 20.0°$, $\delta_a = 6°$, $\delta_r = 0°$, $\beta = 0°$.

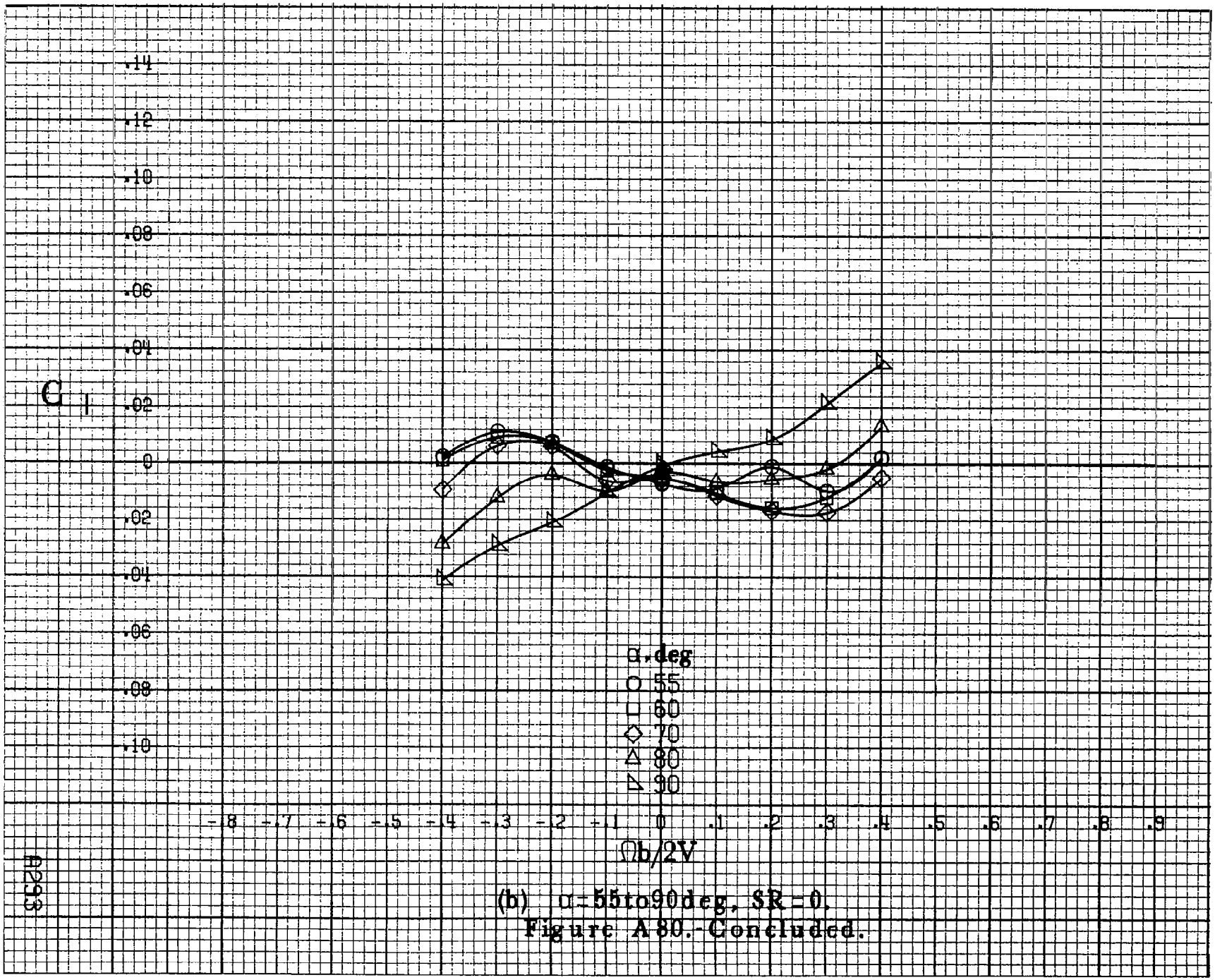

(b) α=55to90deg, SR=0.

Figure A80.-Concluded.

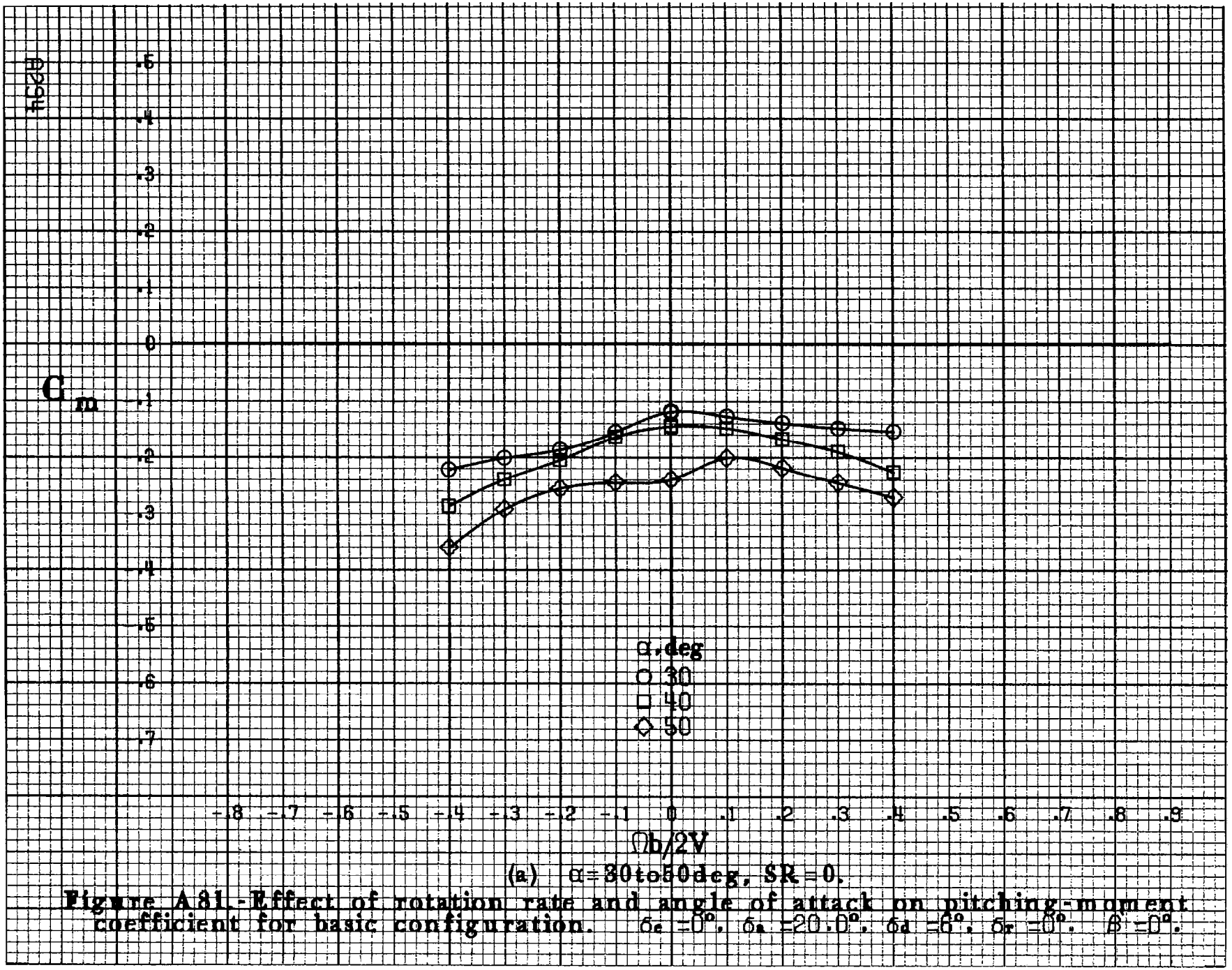

(a) $\alpha = 30$ to 50 deg, $SR = 0$.

Figure A81.- Effect of rotation rate and angle of attack on pitching-moment coefficient for basic configuration. $\delta_e = 0°$, $\delta_a = 20.0°$, $\delta_d = 0°$, $\delta_r = 0°$, $\beta = 0°$.

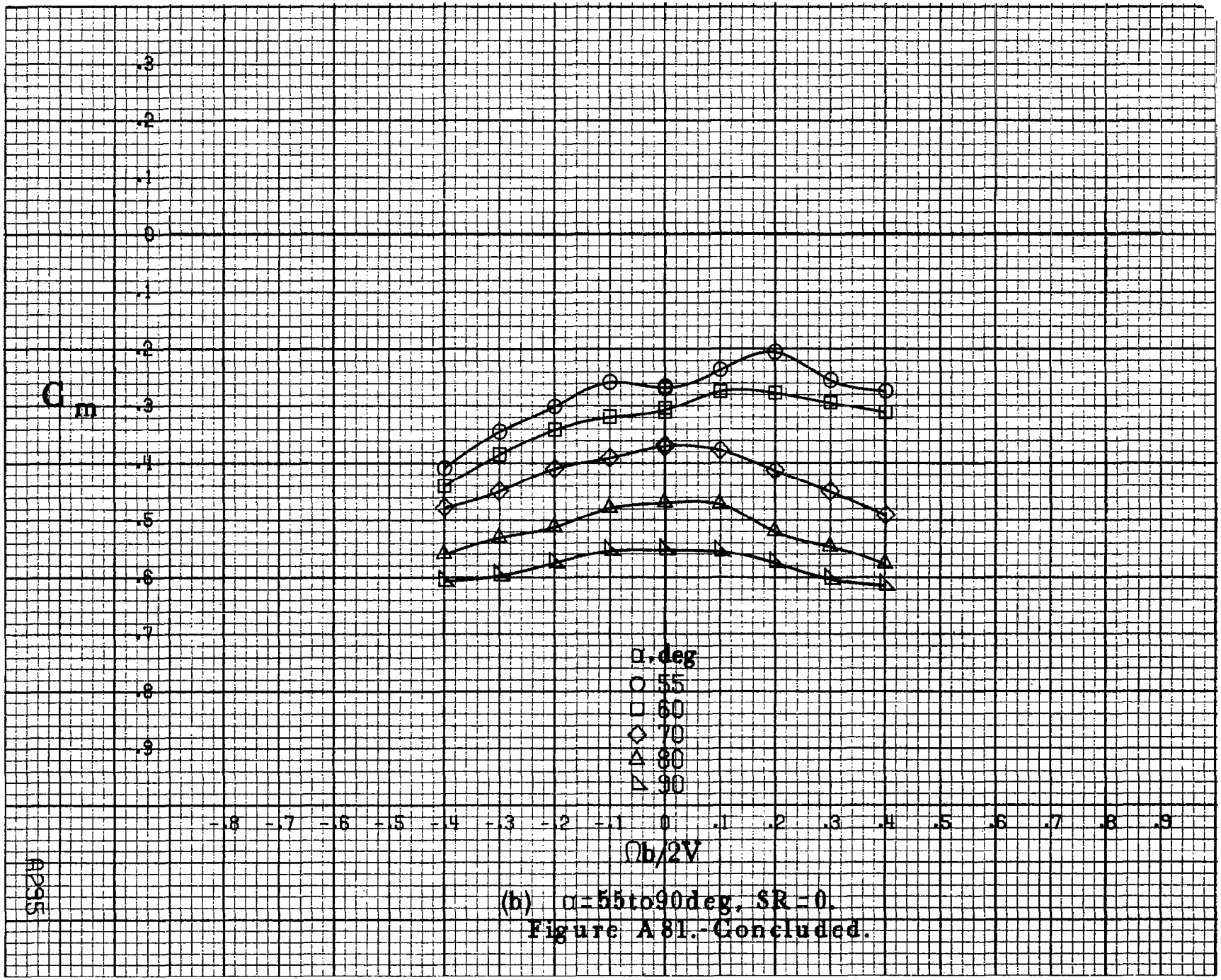

(b) $\alpha = 55$ to 90 deg, SR = 0.

Figure A 81.- Concluded.

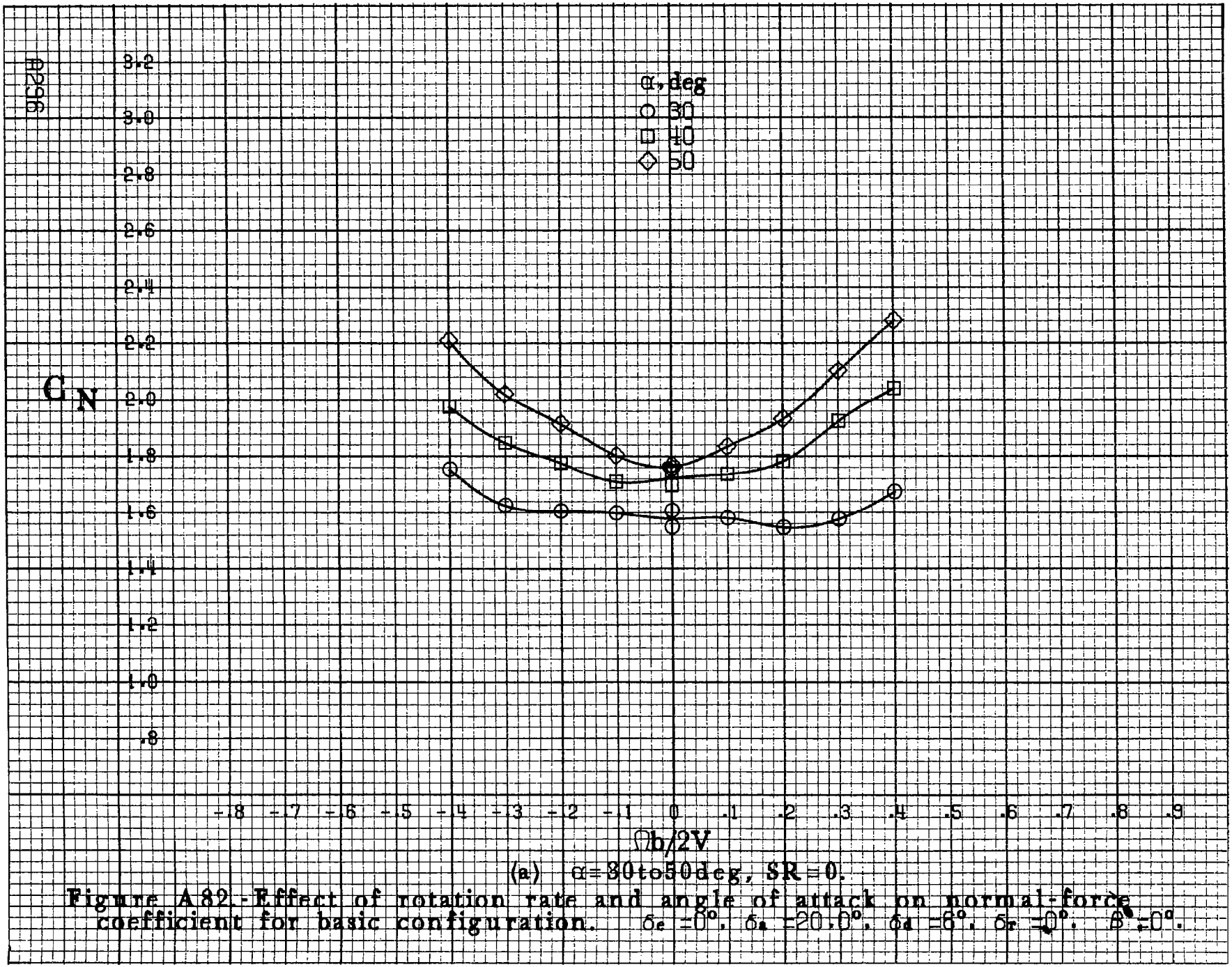

(a) $\alpha = 30$ to 50 deg, $SR = 0$.

Figure A82.- Effect of rotation rate and angle of attack on normal-force coefficient for basic configuration. $\delta_e = 0^\circ$, $\delta_a = 20.0^\circ$, $\delta_d = 6^\circ$, $\delta_r = 0^\circ$, $\beta = 0^\circ$.

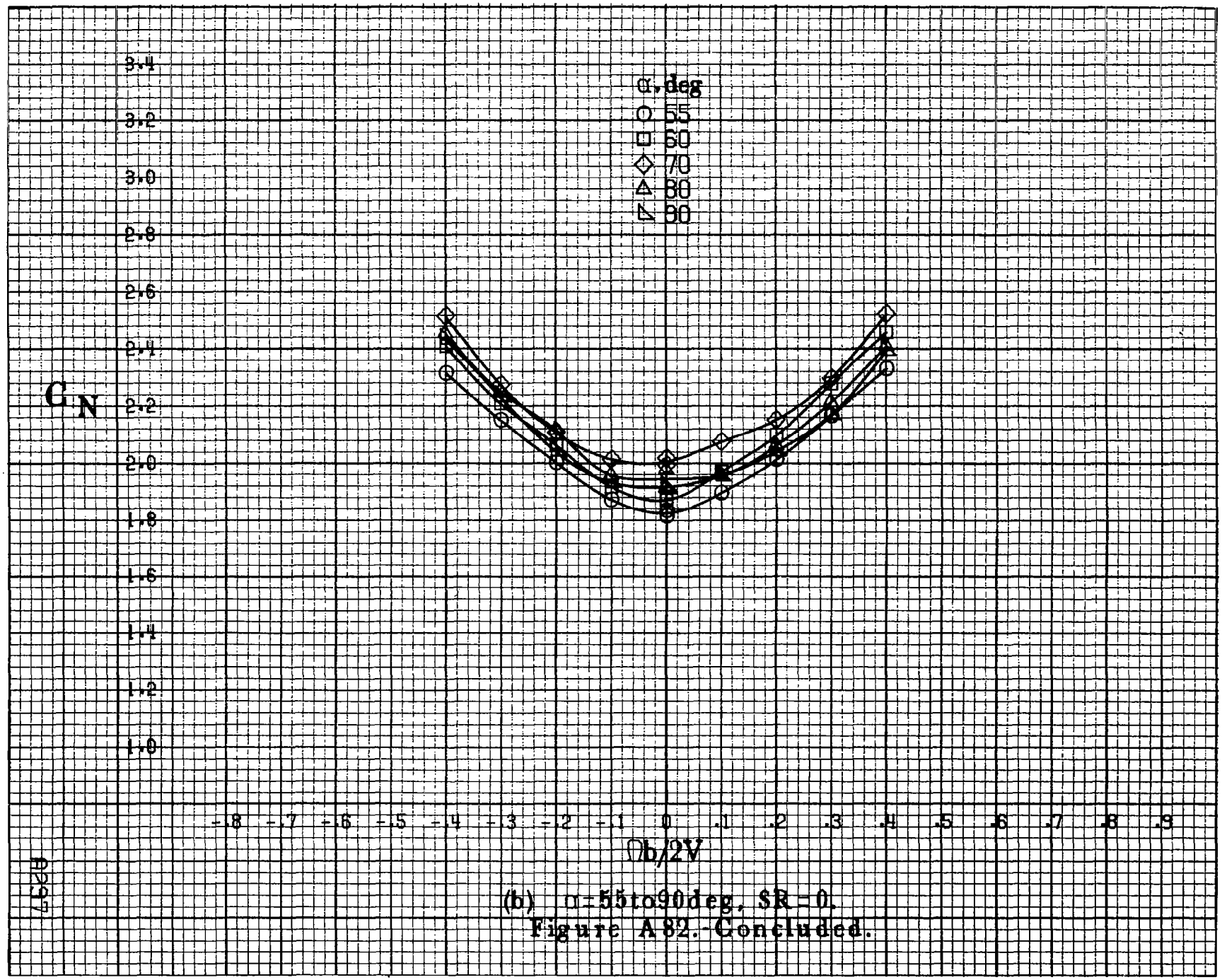

(b) α = 55 to 90 deg, $R = 0.

Figure A82.- Concluded.

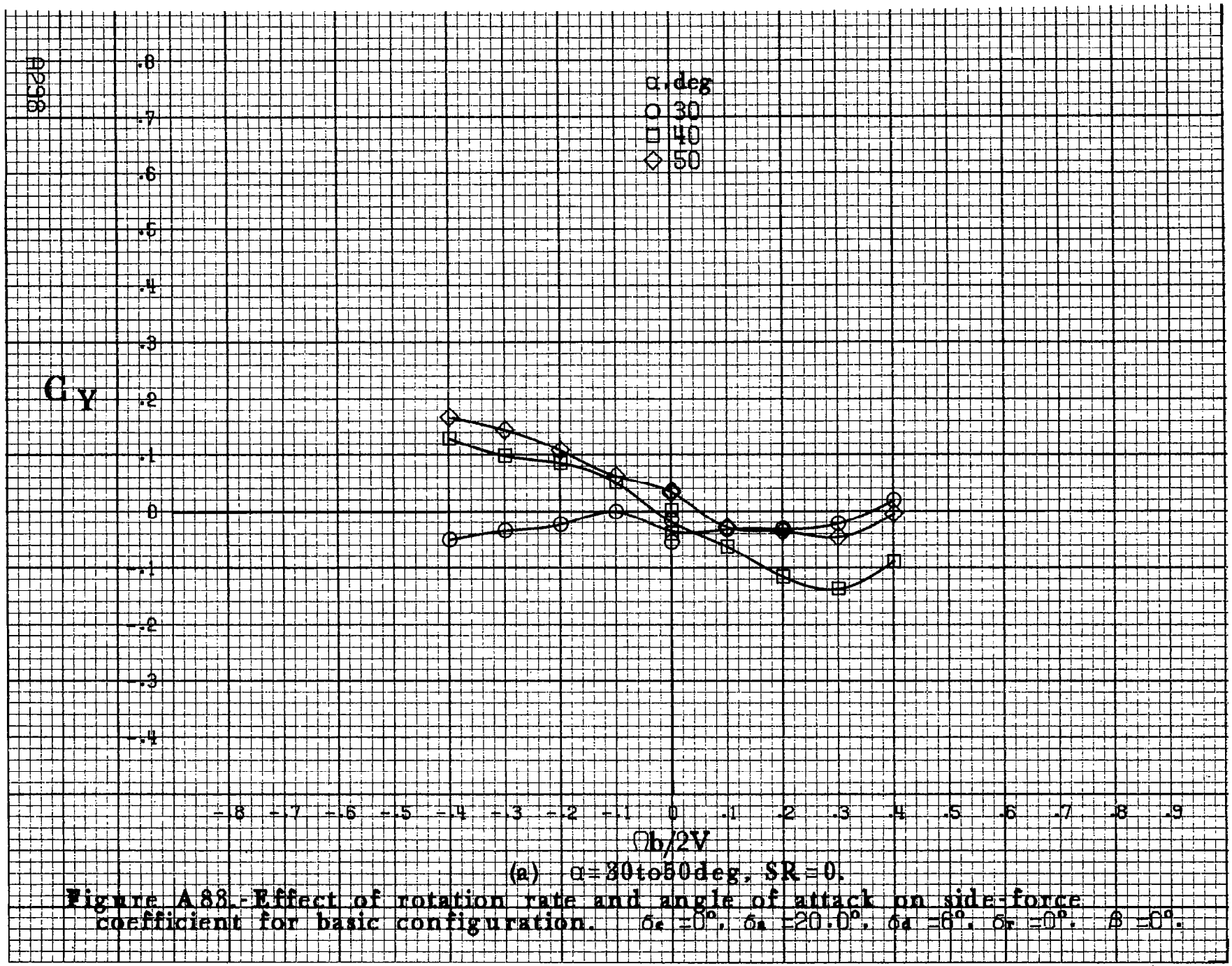

(a) $\alpha = 30$ to 50 deg, SR = 0.

Figure A88.- Effect of rotation rate and angle of attack on side-force coefficient for basic configuration. $\delta_e = 0°$, $\delta_{a_1} = 20.0°$, $\delta_{a_2} = 6°$, $\delta_r = 0°$, $\beta = 6°$.

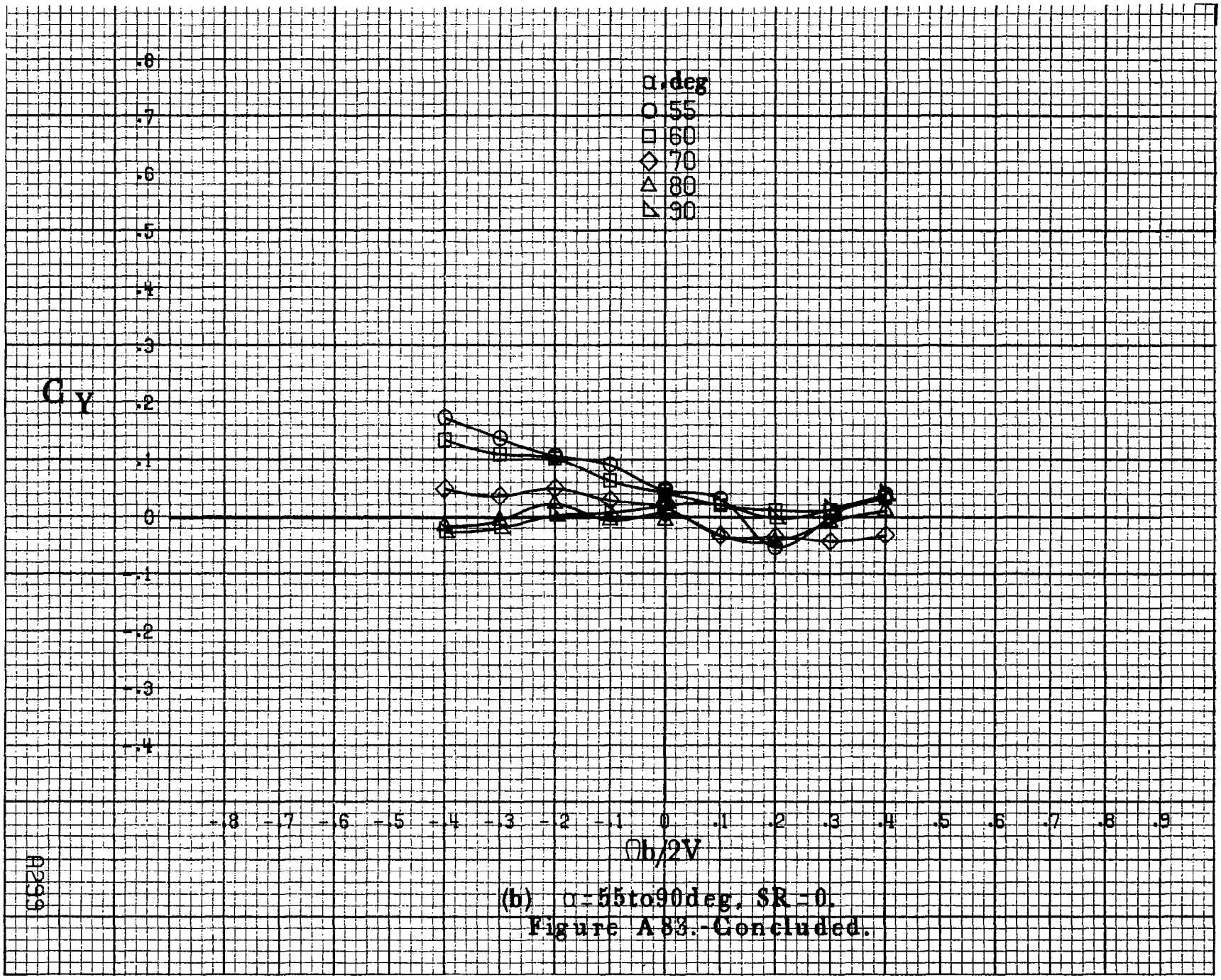

(b) α = 55 to 90 deg, SR = 0.

Figure A83.- Concluded.

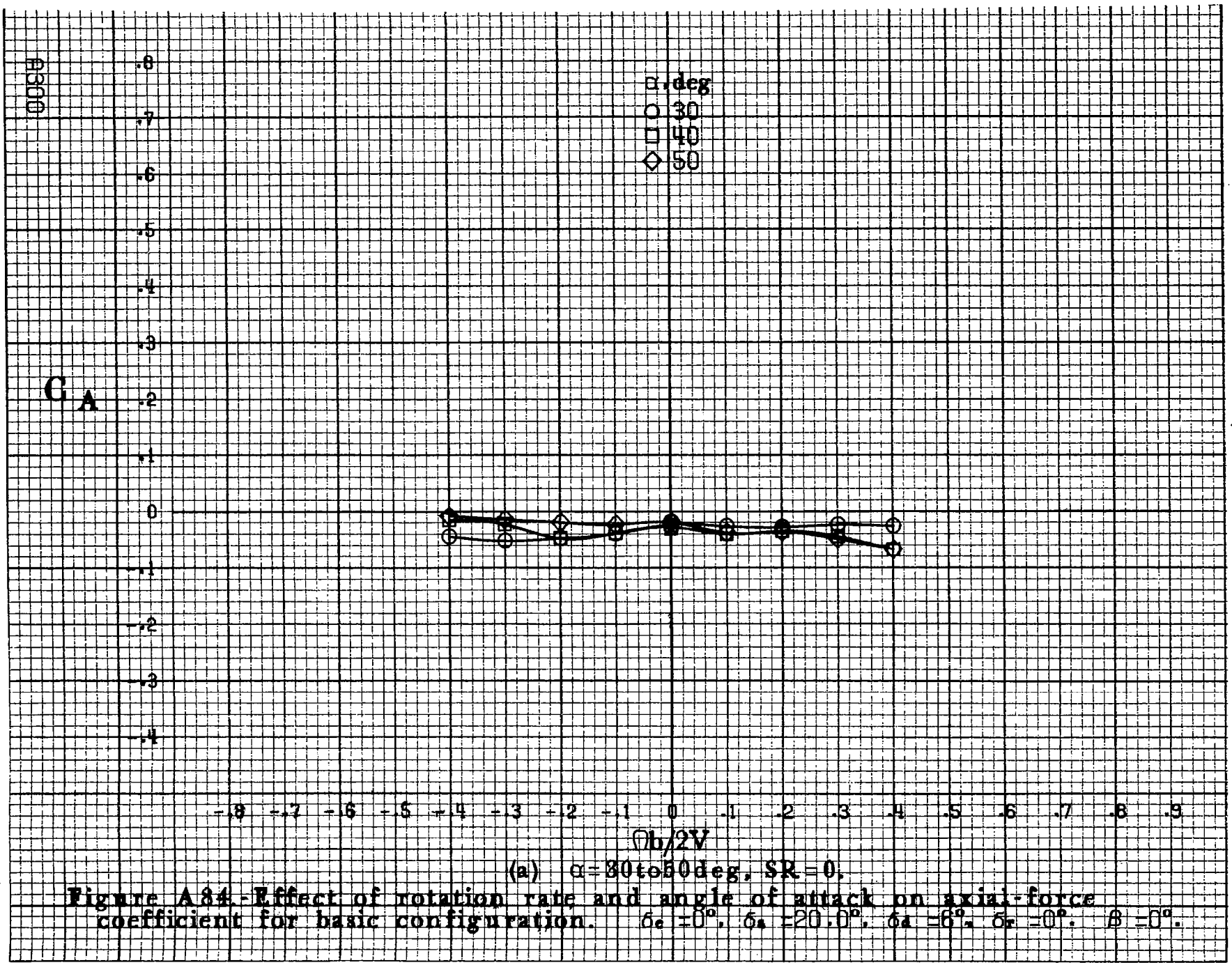

(a) $\alpha = 30$ to 50 deg, $SR = 0$.

Figure A84.-Effect of rotation rate and angle of attack on axial-force coefficient for basic configuration. $\delta_e = 0°$, $\delta_a = 20.0°$, $\delta_d = 6°$, $\delta_r = 0°$, $\beta = 0°$.

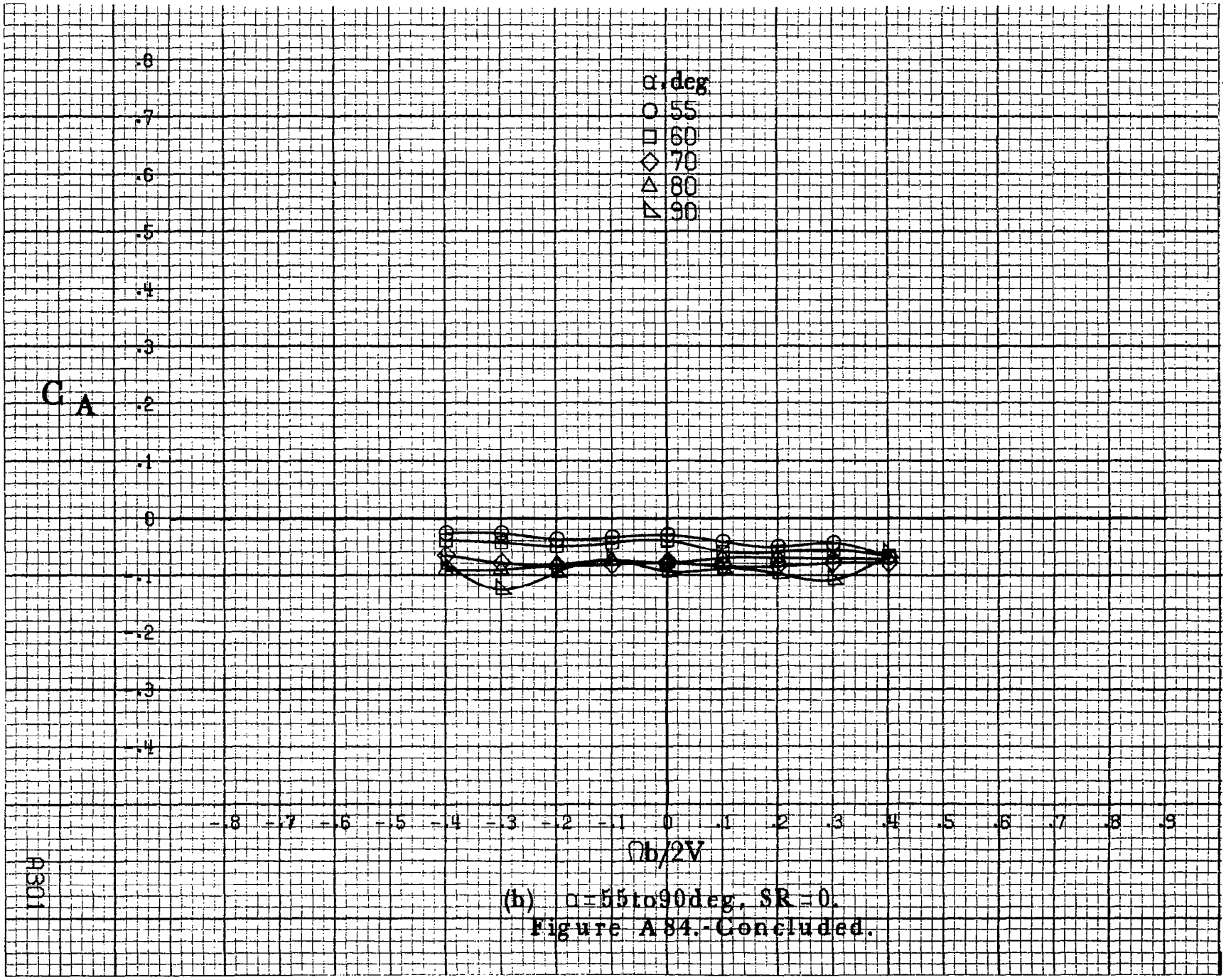

(b) α = 55 to 90 deg, SR = 0.

Figure A84.- Concluded.

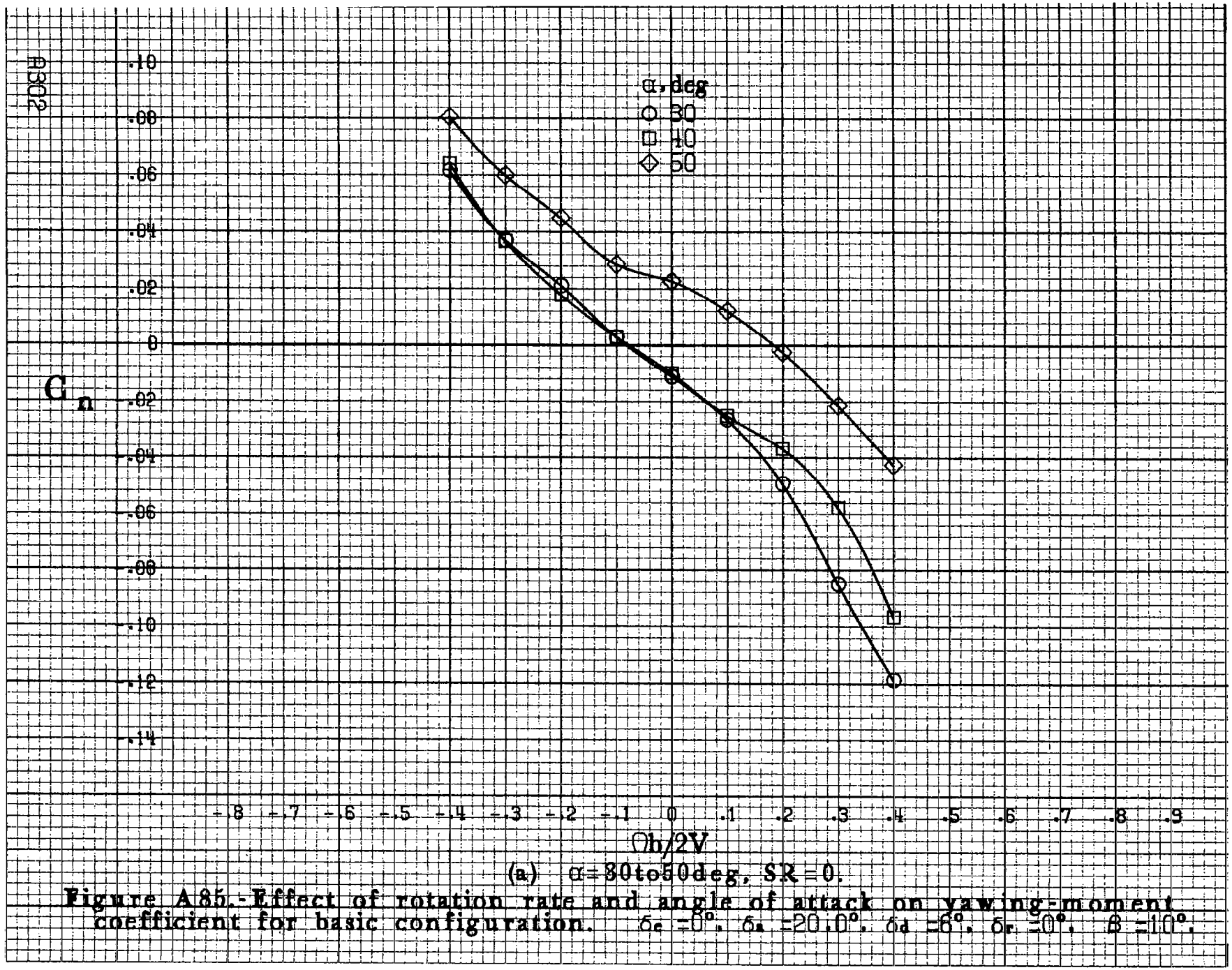

(a) $\alpha = 30$ to 50 deg, $SR = 0$.

Figure A85.- Effect of rotation rate and angle of attack on yawing-moment coefficient for basic configuration. $\delta_e = 0°$, $\delta_a = 20.0°$, $\delta_d = 6°$, $\delta_r = 0°$, $\beta = 10°$.

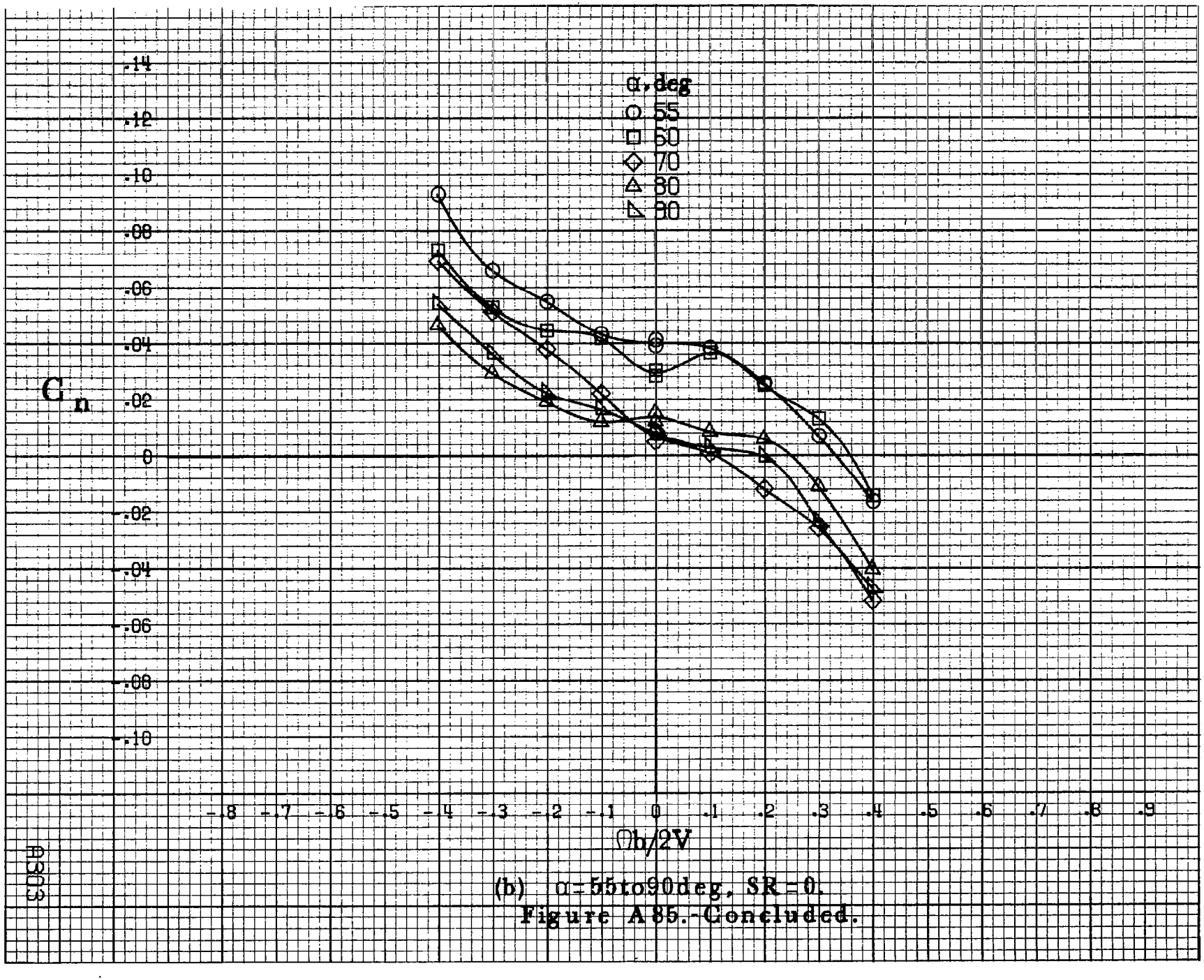

(b) α=55to90deg, SR=0.

Figure A85.-Concluded.

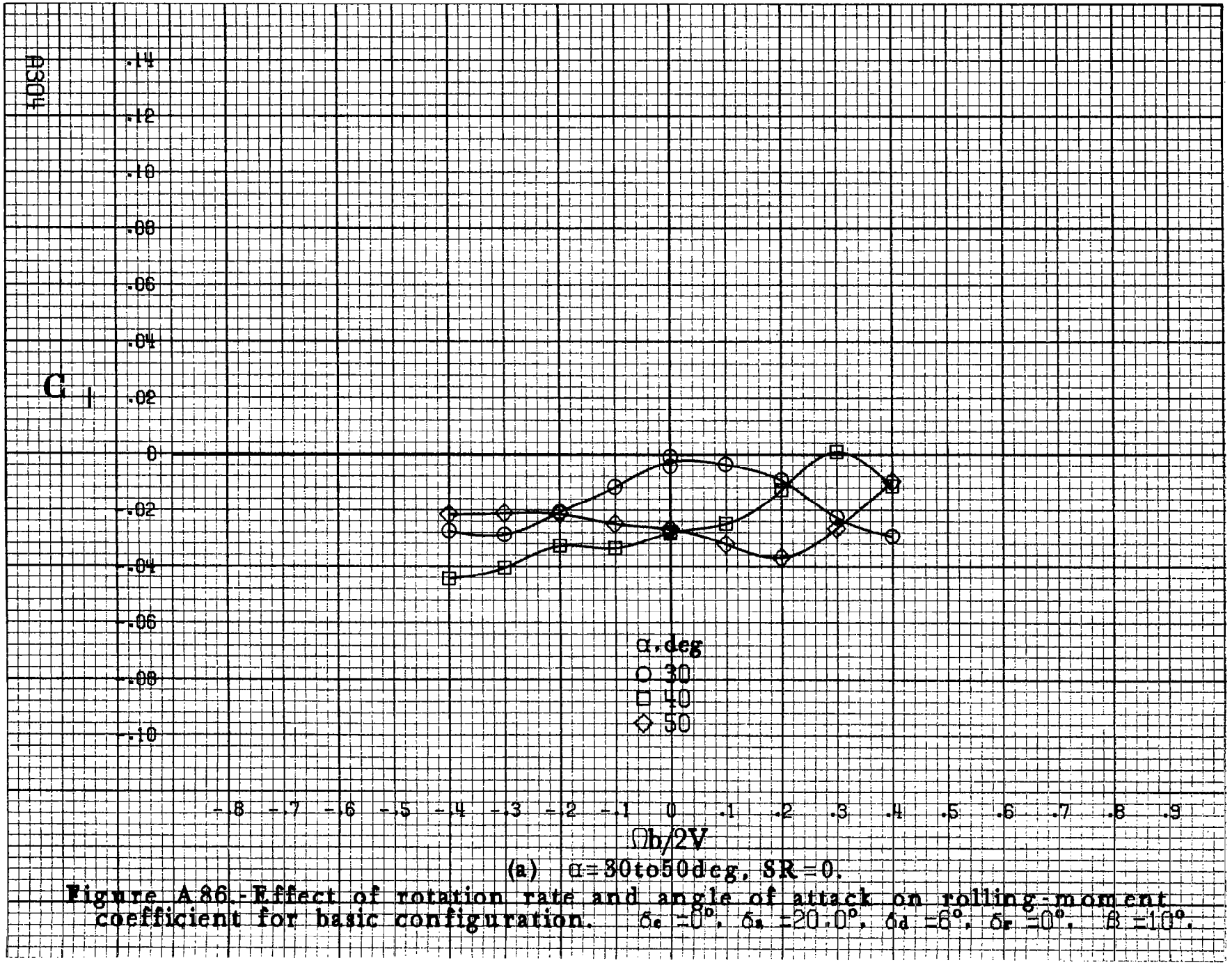

(a) $\alpha = 30$ to 50 deg, $SR = 0$.

Figure A.86.- Effect of rotation rate and angle of attack on rolling-moment coefficient for basic configuration. $\delta_e = 0°$, $\delta_a = 20.0°$, $\delta_d = 6°$, $\delta_r = 0°$, $\beta = 10°$.

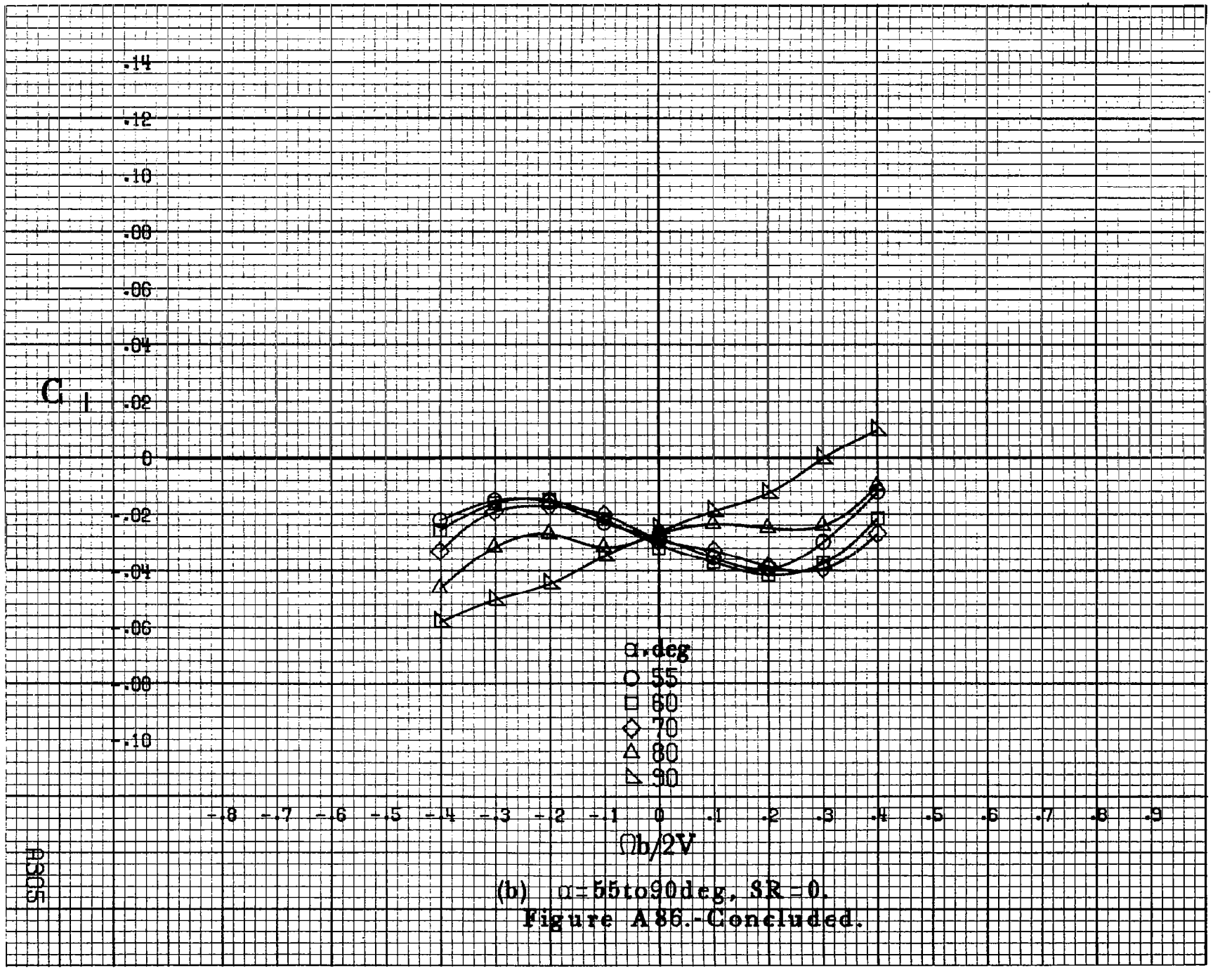

(b) $\alpha = 55$ to 90 deg, $SR = 0$.

Figure A86.-Concluded.

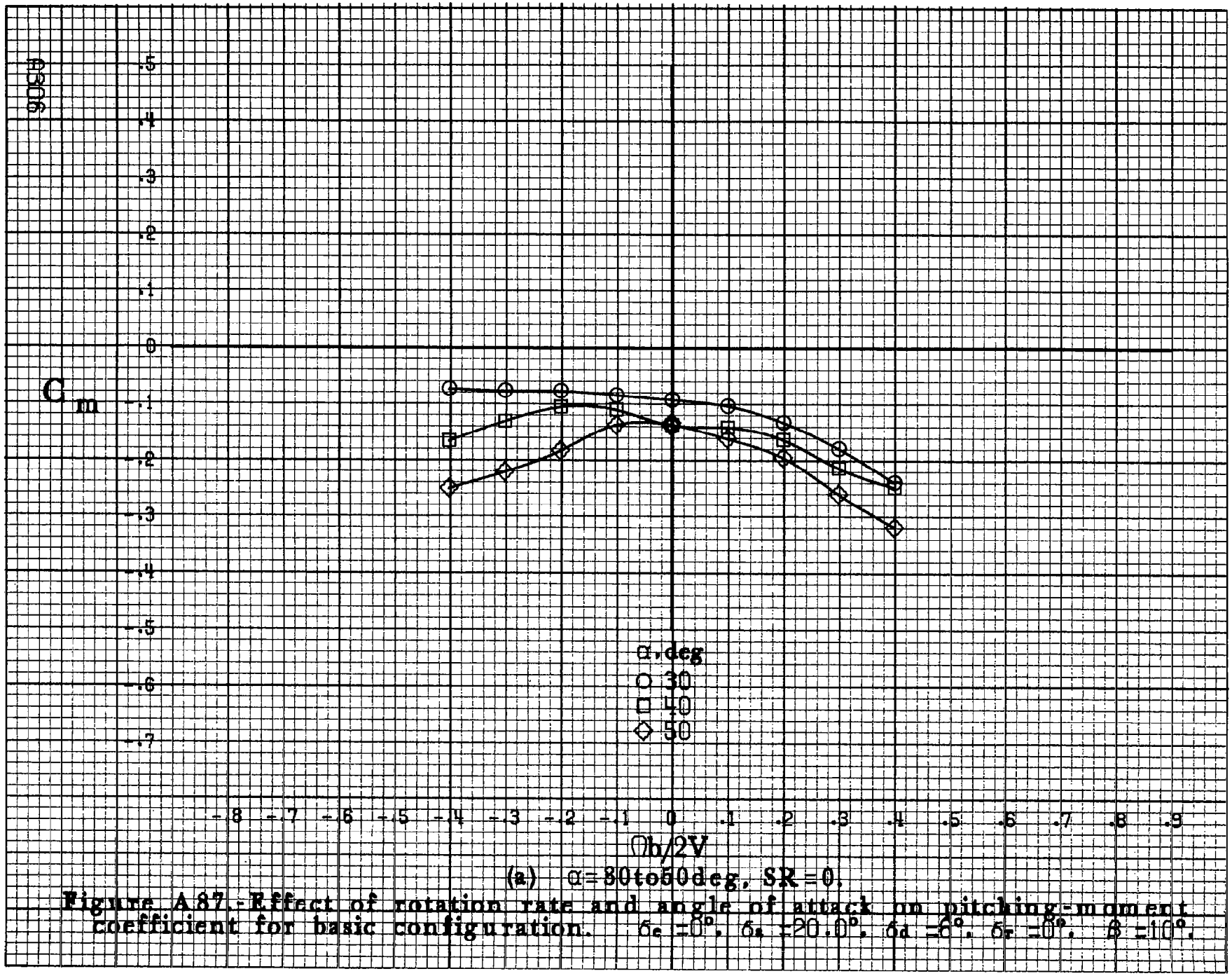

(a) $\alpha = 30$ to 60 deg, SR = 0.

Figure A.87.- Effect of rotation rate and angle of attack on pitching-moment coefficient for basic configuration. $\delta_e = 0°$, $\delta_a = 20.0°$, $\delta_d = 6°$, $\delta_r = 0°$, $\beta = 10°$.

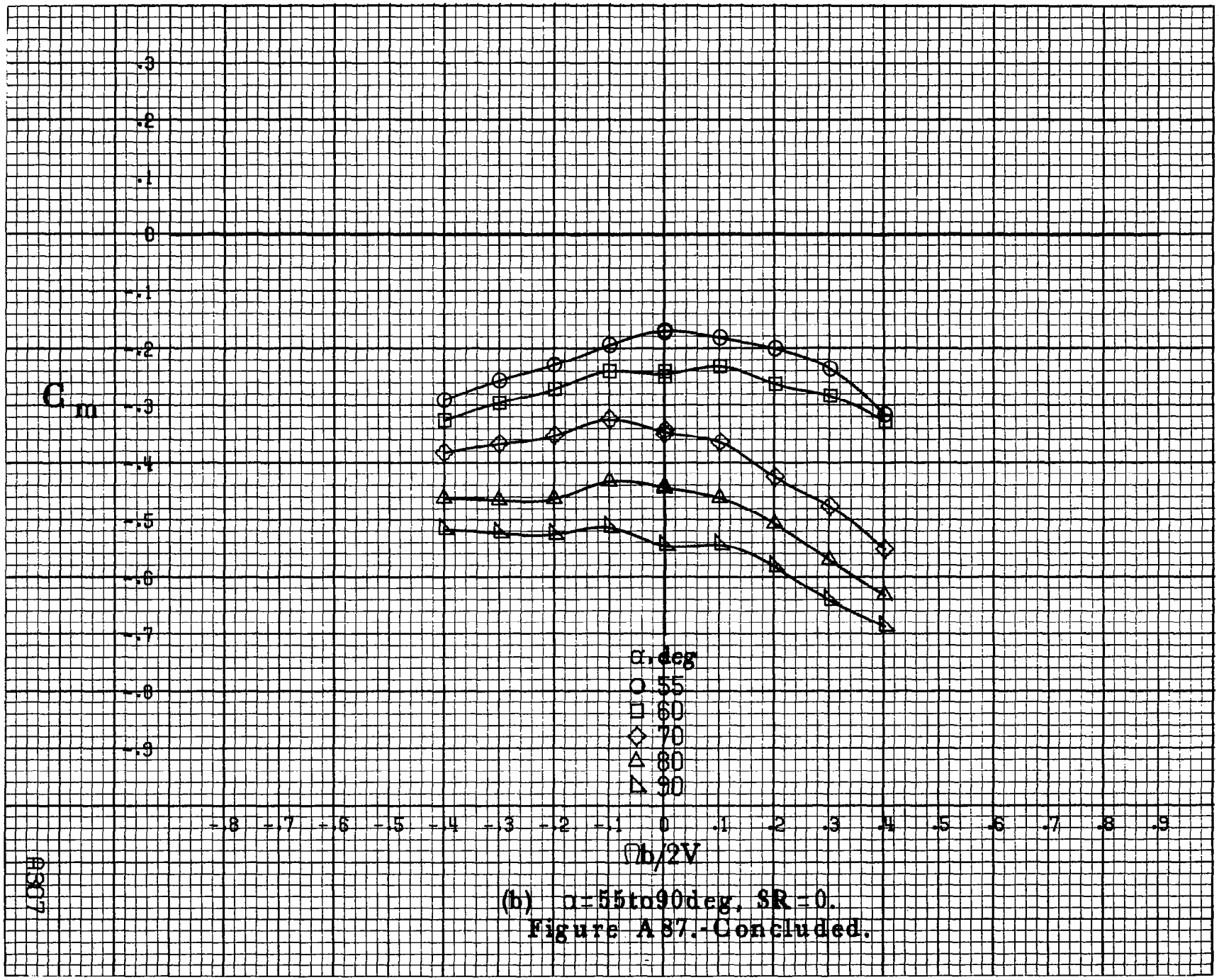

(b) α=55to90deg. SR=0.

Figure A87.-Concluded.

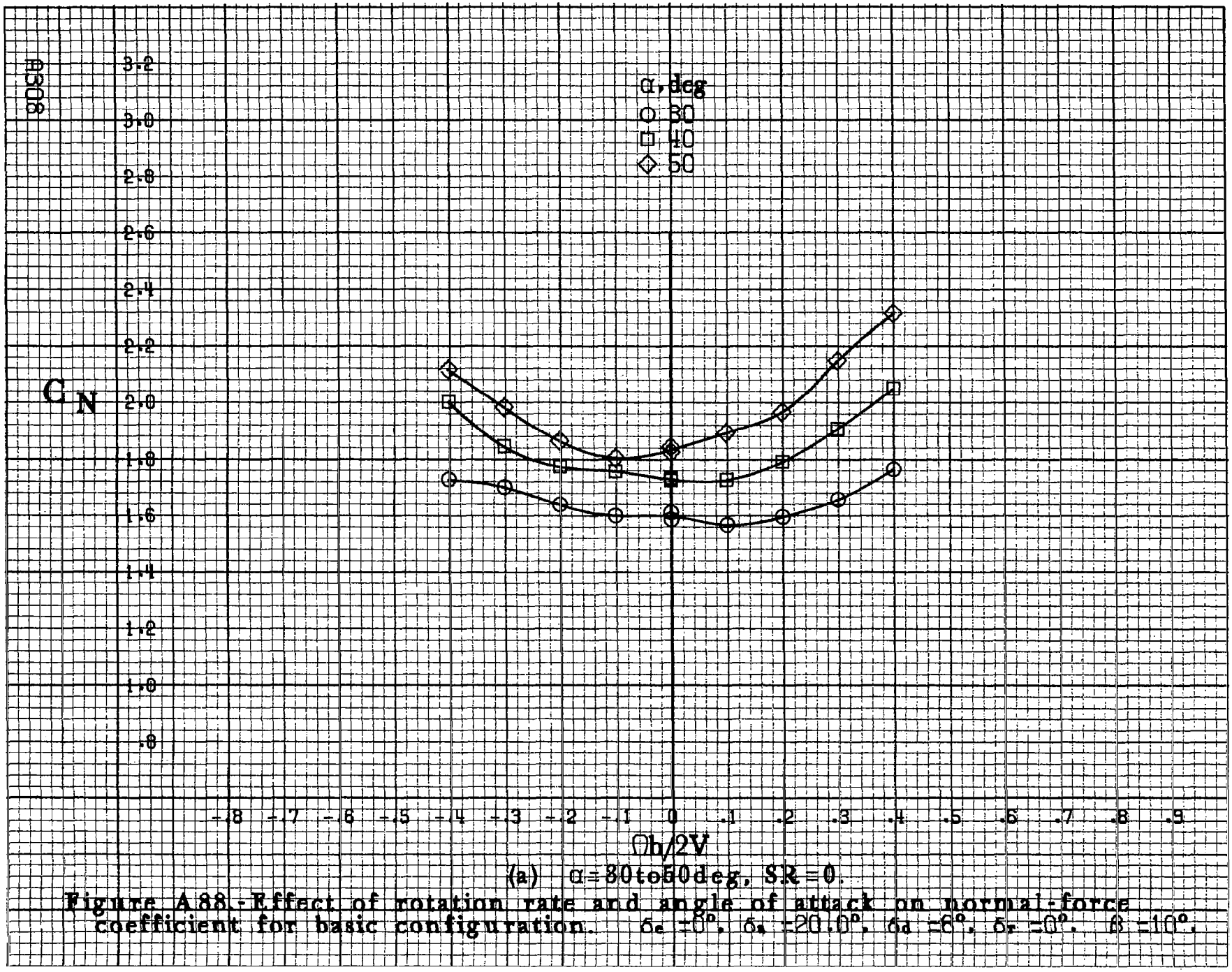

(a) $\alpha = 30$ to 50 deg, $SR = 0$.

Figure A88.- Effect of rotation rate and angle of attack on normal-force coefficient for basic configuration. $\delta_e = 0°$, $\delta_a = 20.0°$, $\delta_d = 6°$, $\delta_r = 0°$, $\beta = 10°$.

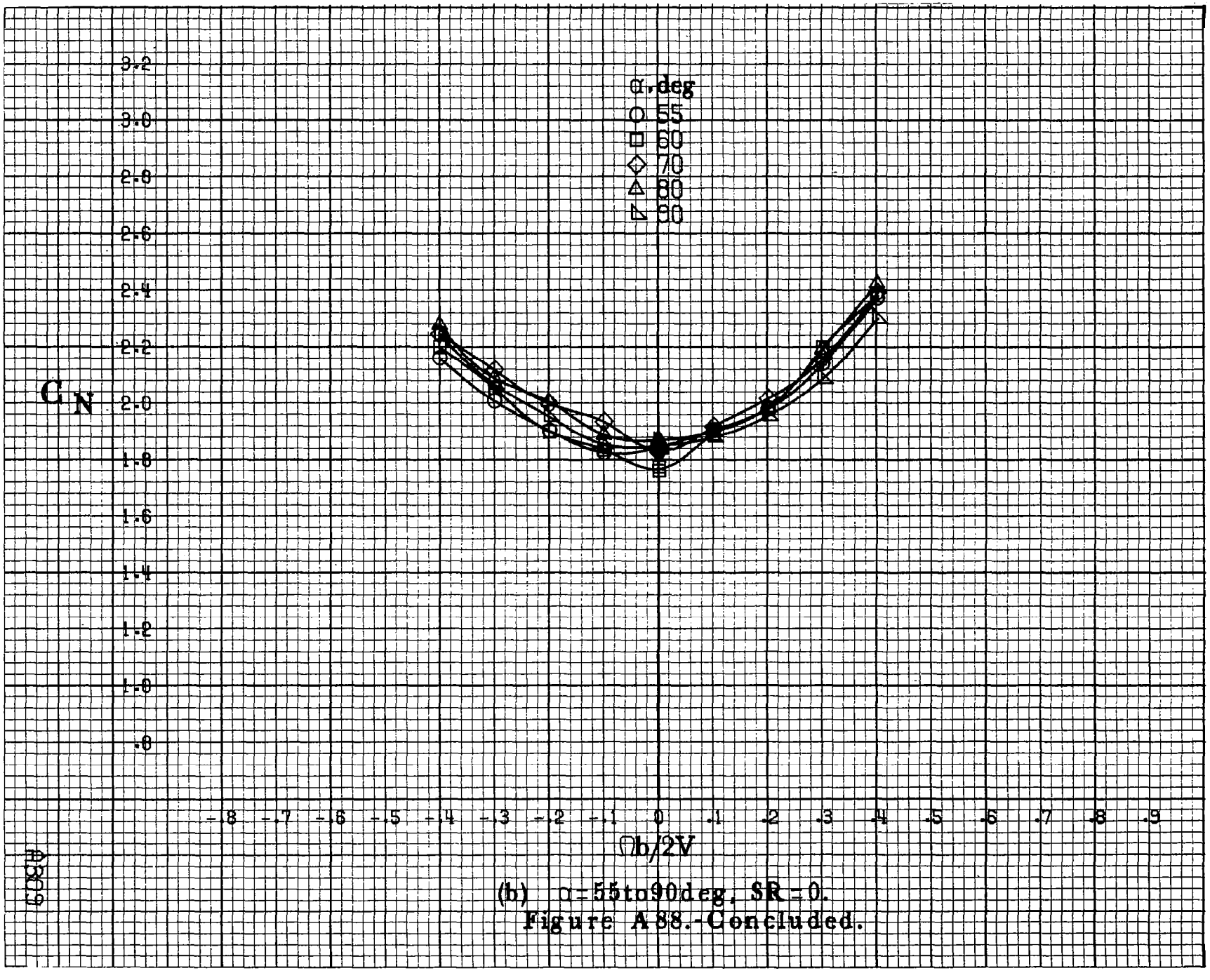

(b) α=55to90deg, SR=0.

Figure A88.-Concluded.

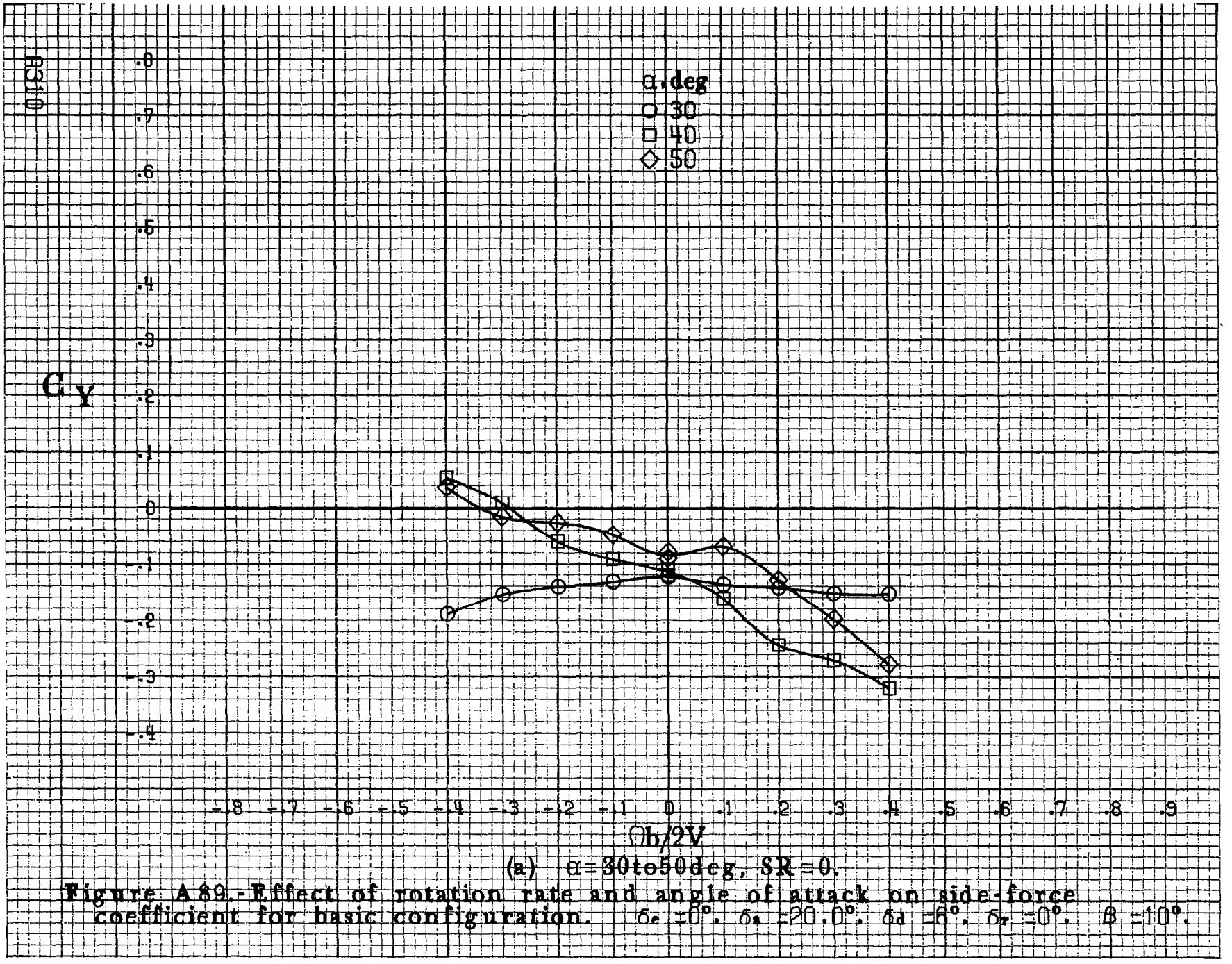

(a) $\alpha = 30$ to 50 deg, SR = 0.

Figure A89.-Effect of rotation rate and angle of attack on side-force coefficient for basic configuration. $\delta_e = 0°$, $\delta_a = 20.0°$, $\delta_d = 6°$, $\delta_r = 0°$, $\beta = 10°$.

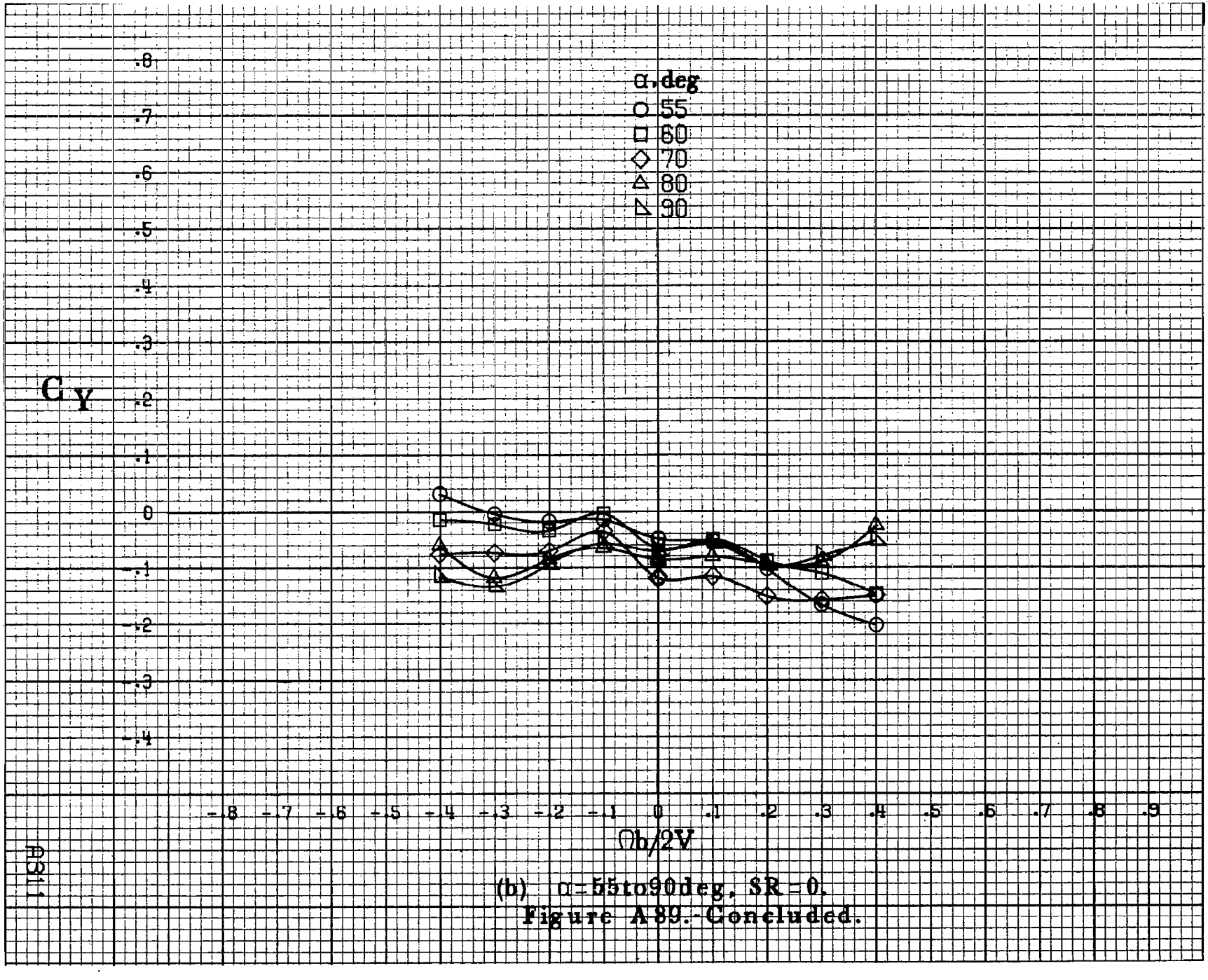

(b) $\alpha = 55$ to 90 deg, SR = 0.

Figure A89.- Concluded.

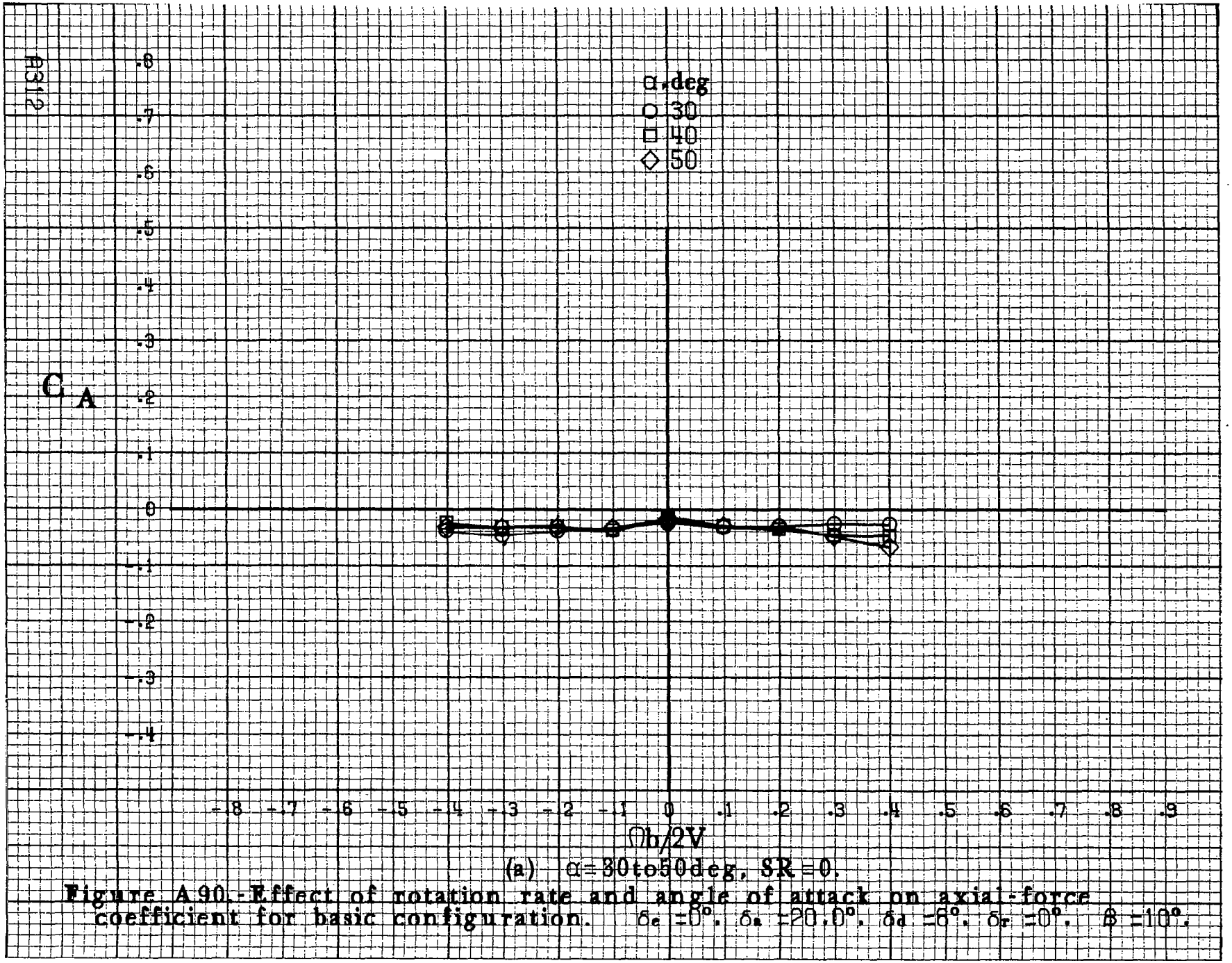

(a) $\alpha = 30$ to 50 deg, $SR = 0$.

Figure A90.- Effect of rotation rate and angle of attack on axial-force coefficient for basic configuration. $\delta_e = 0°$, $\delta_a = 20.0°$, $\delta_d = 8°$, $\delta_r = 0°$, $\beta = 10°$.

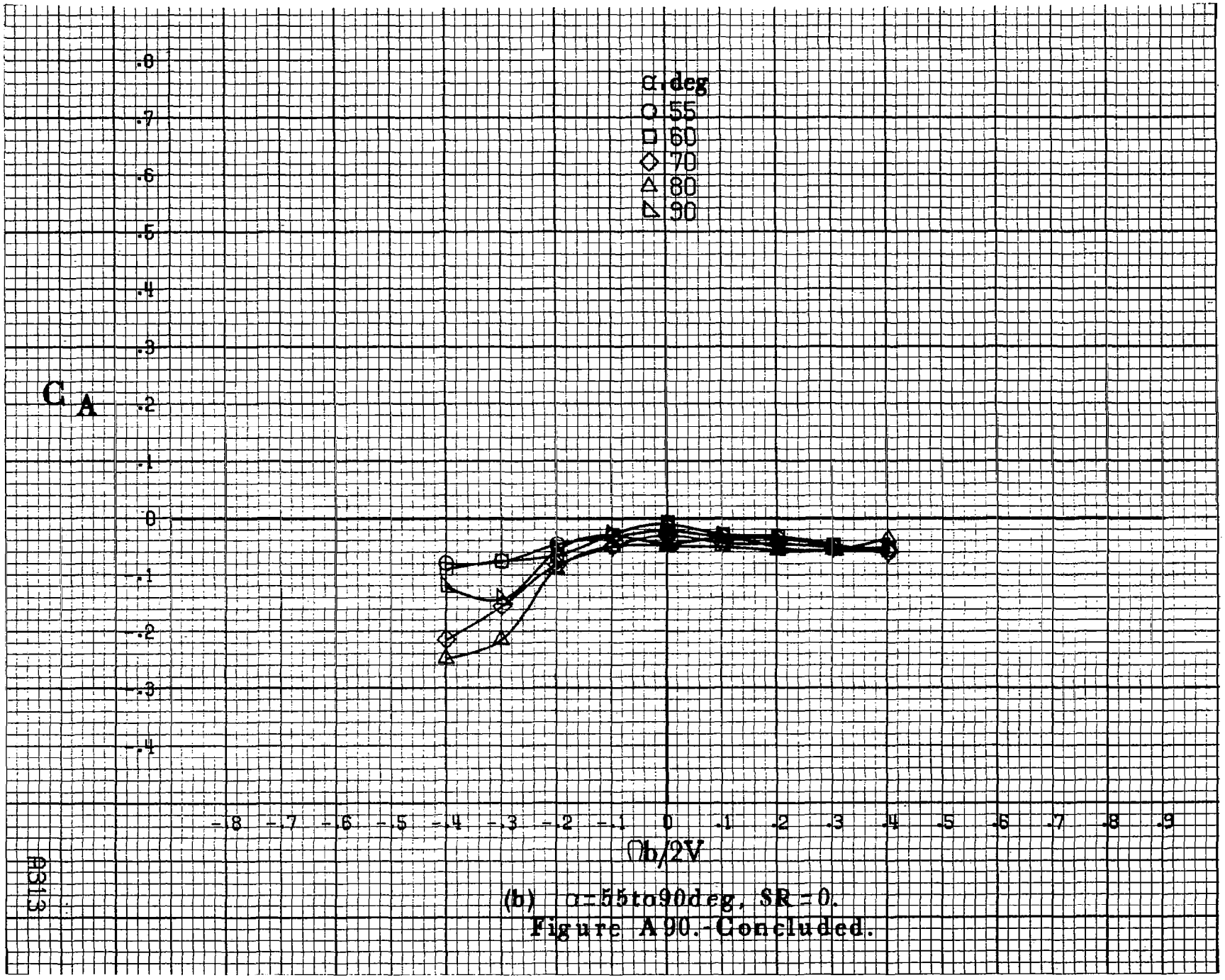

(b) $\alpha = 55$ to 90 deg, $SR = 0$.

Figure A90.- Concluded.

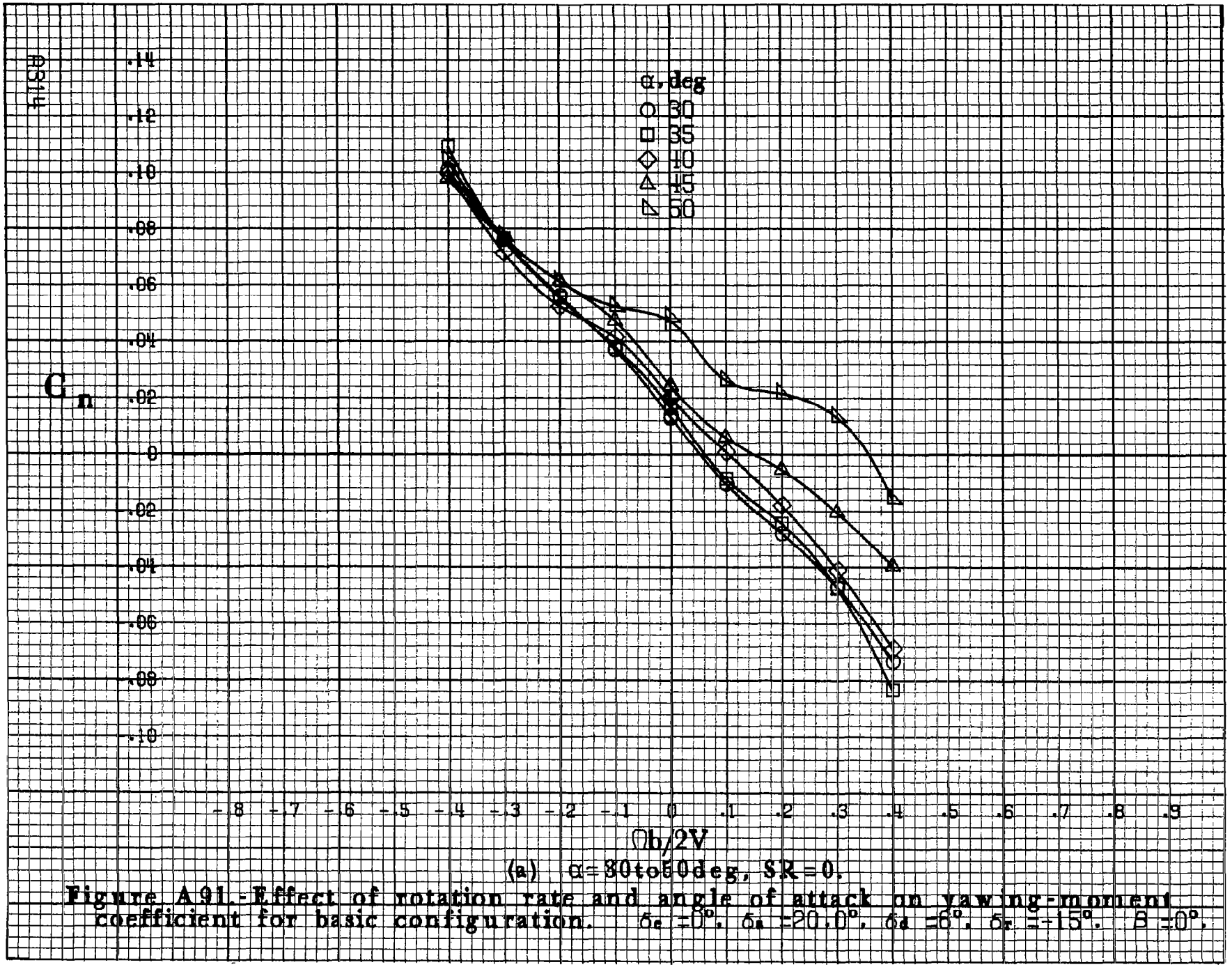

(a) $\alpha = 30$ to 50 deg, $SR = 0$.

Figure A.91.- Effect of rotation rate and angle of attack on yawing-moment coefficient for basic configuration. $\delta_e = 0°$, $\delta_a = -20.0°$, $\delta_d = 6°$, $\delta_r = -15°$, $\beta = 0°$.

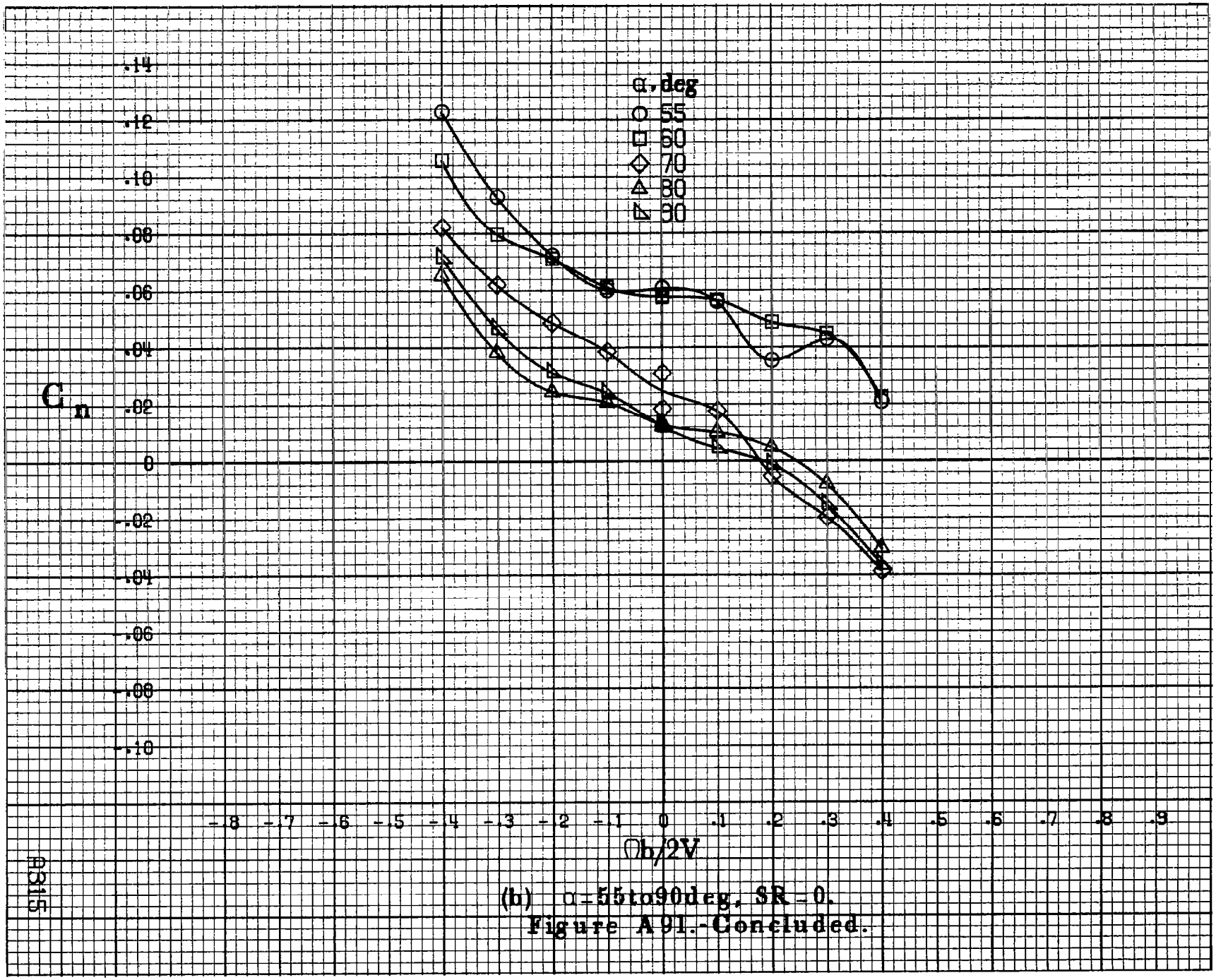

(b) $\alpha = 55$ to 90 deg, SR = 0.

Figure A91.- Concluded.

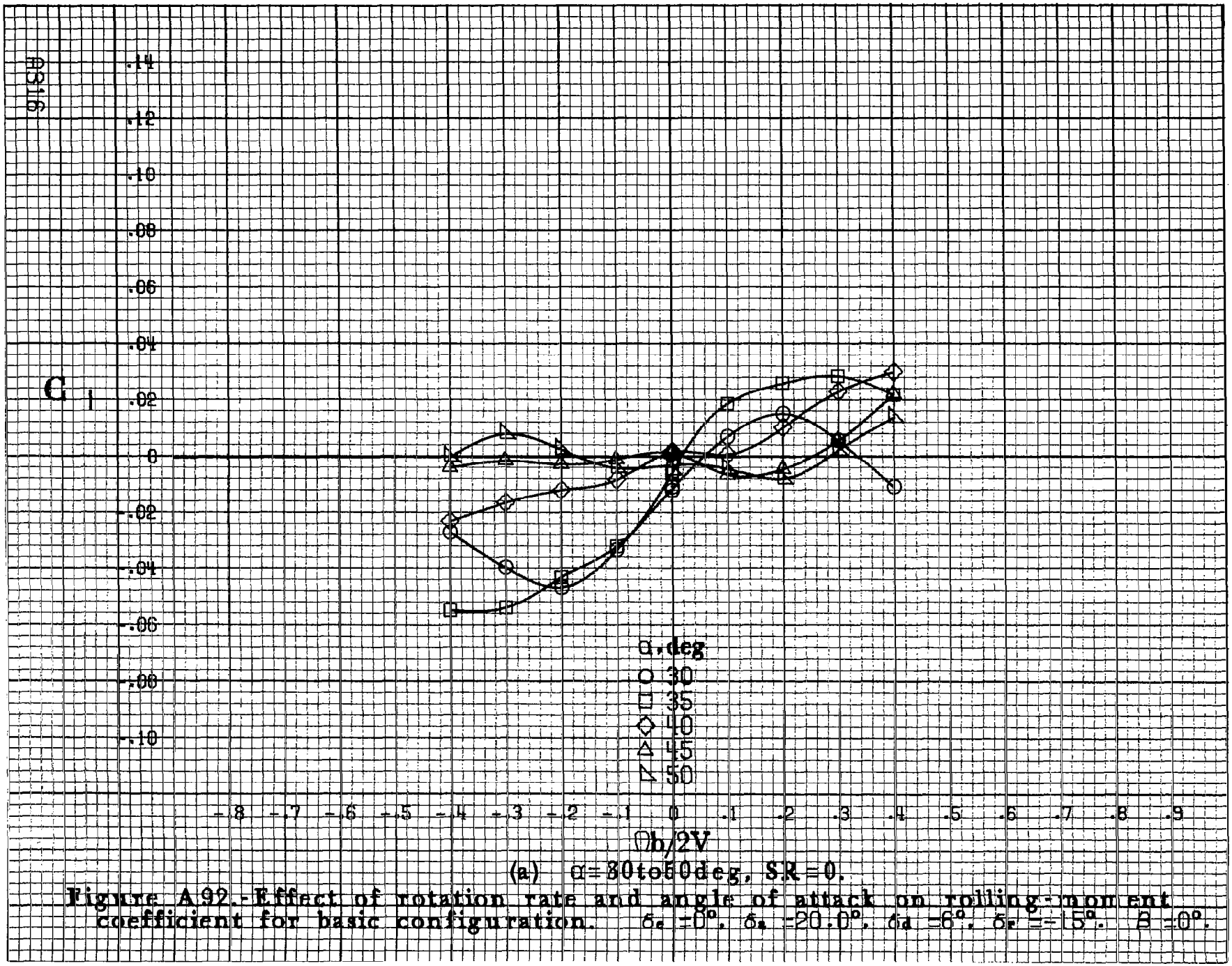

(a) $\alpha = 30$ to 60 deg, S.R. $= 0$.

Figure A.92.- Effect of rotation rate and angle of attack on rolling-moment coefficient for basic configuration. $\delta_e = 0°$, $\delta_a = -20.0°$, $\delta_d = 6°$, $\delta_r = -15°$, $\beta = 0°$.

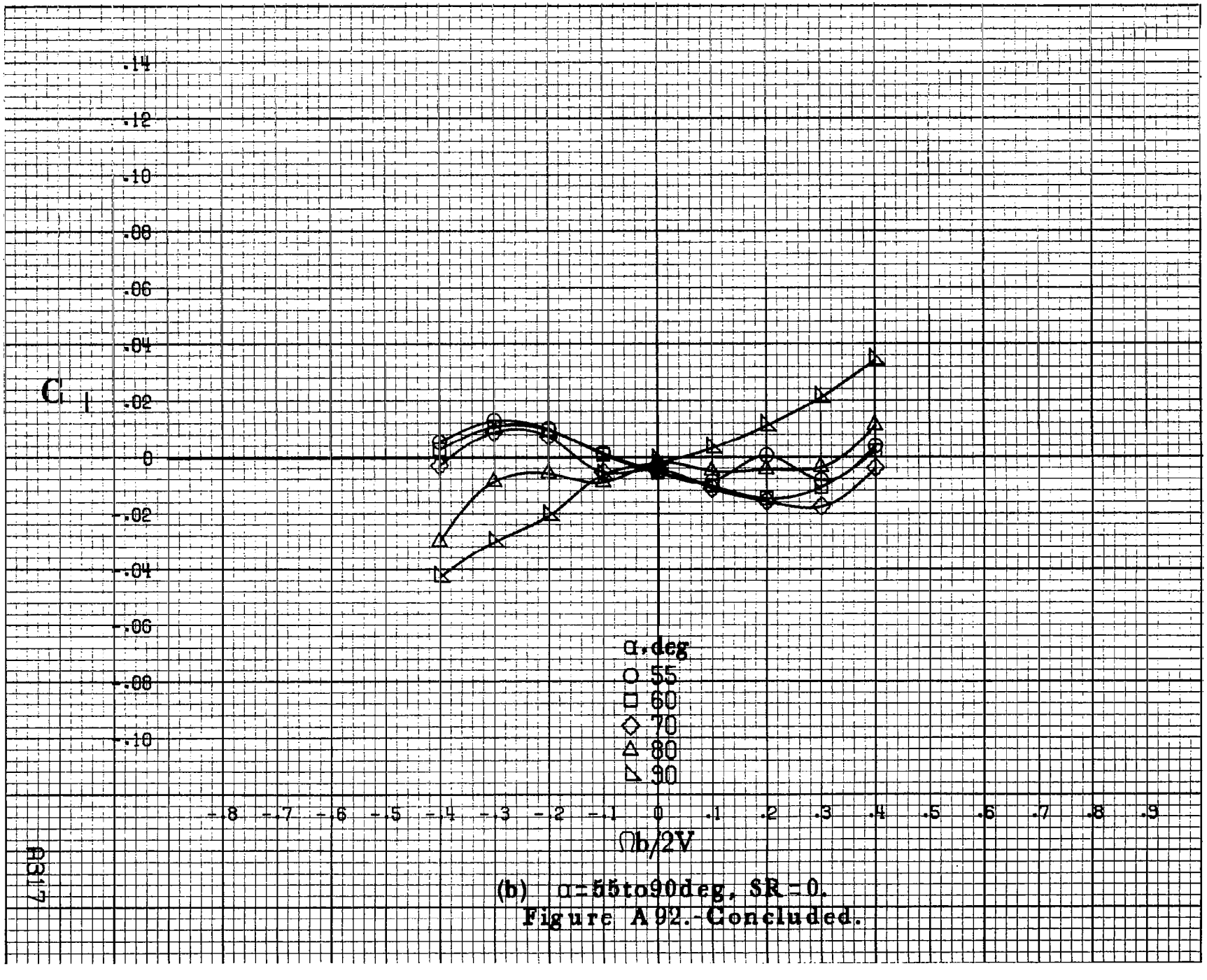

(b) $\alpha = 55$ to 90 deg, $SR = 0$.

Figure A92.- Concluded.

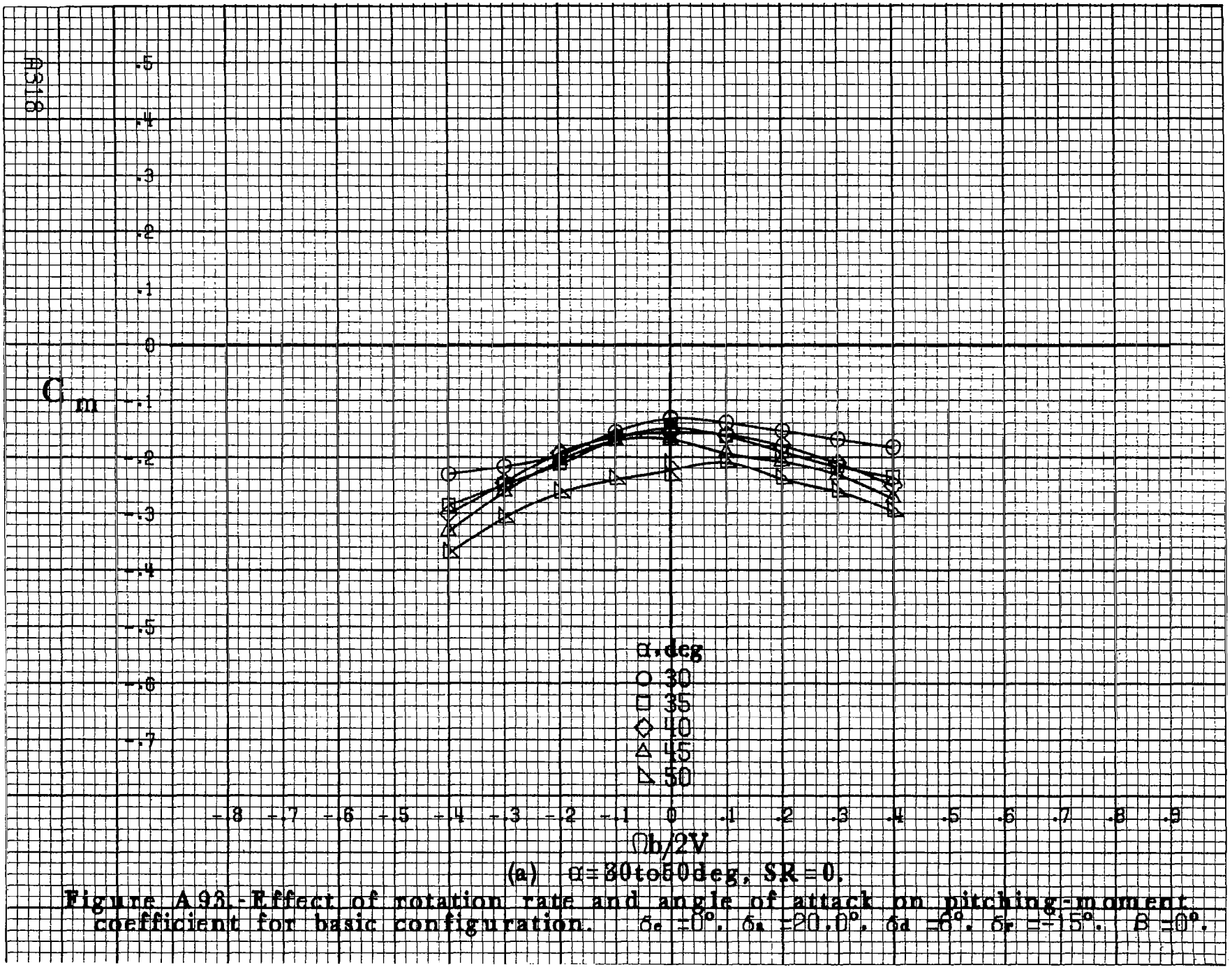

(a) $\alpha = 30$ to 60 deg, SR = 0.

Figure A-98.- Effect of rotation rate and angle of attack on pitching-moment coefficient for basic configuration. $\delta_e = 0°$, $\delta_{a_1} = 20.0°$, $\delta_a = 6°$, $\delta_r = -15°$, $\beta = 0°$.

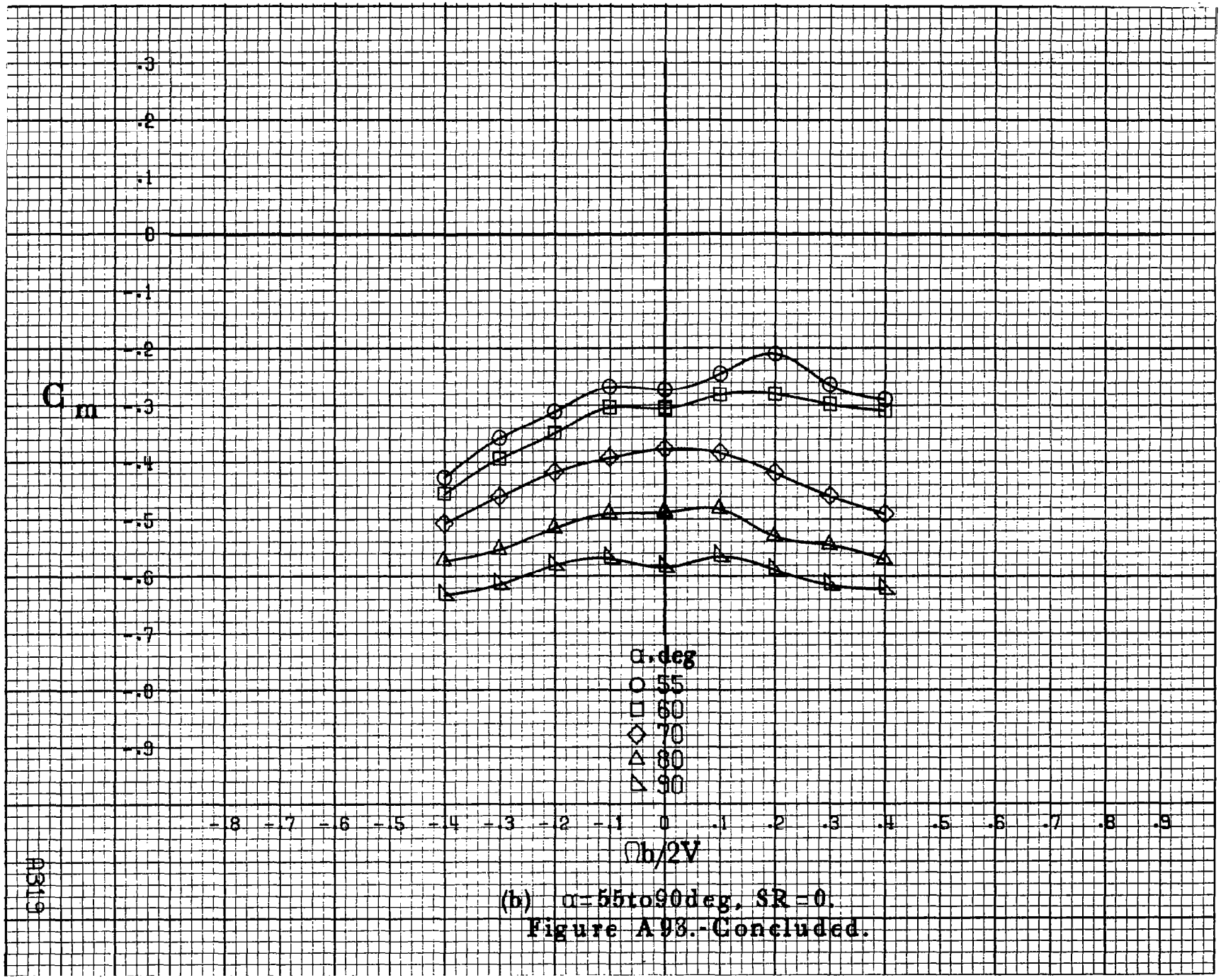

(b) $\alpha = 55$ to 90 deg, $SR = 0$.

Figure A98.- Concluded.

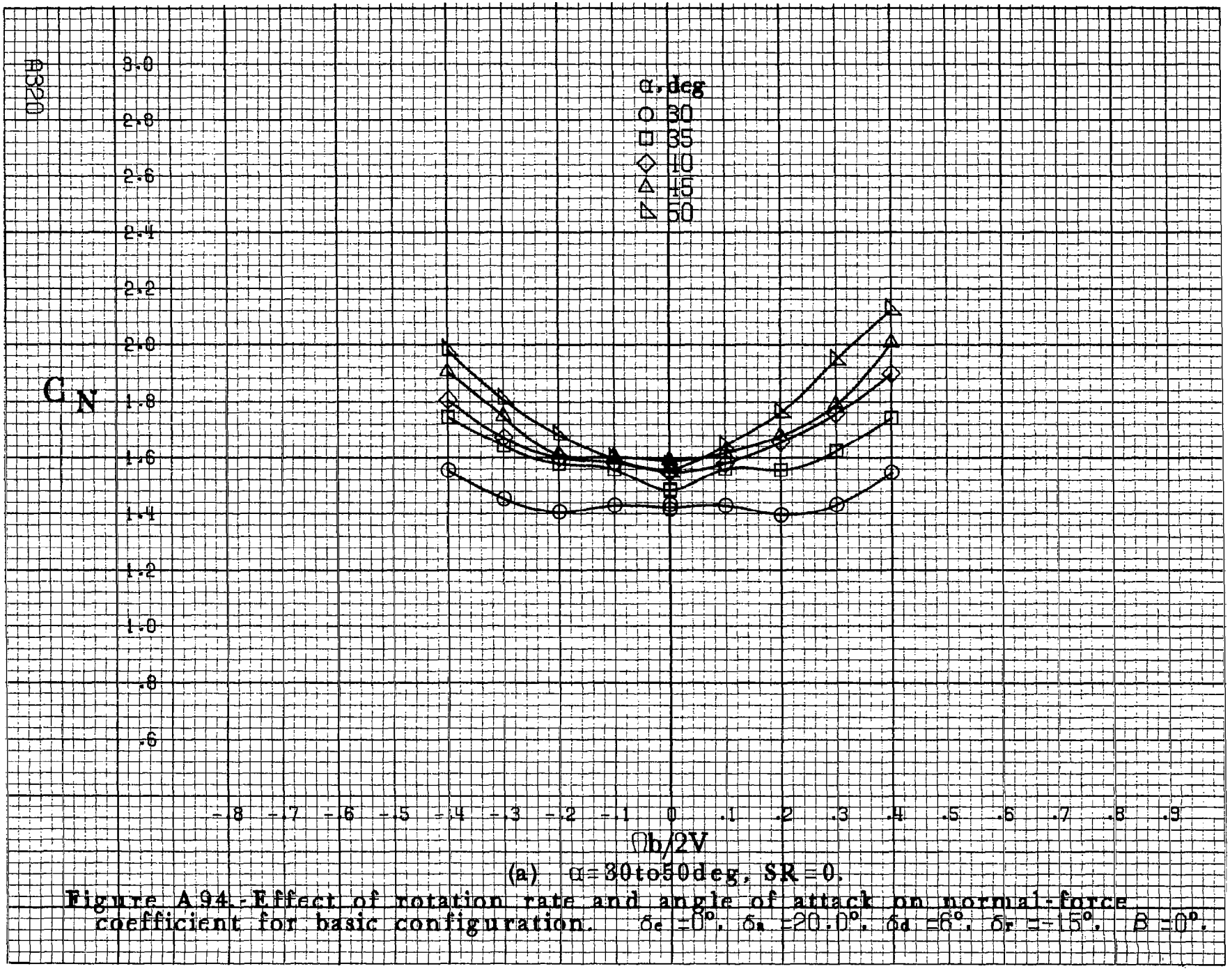

(a) $\alpha = 30$ to 50 deg, SR = 0.

Figure A.94.- Effect of rotation rate and angle of attack on normal-force coefficient for basic configuration. $\delta_e = 0°$, $\delta_a = 20.0°$, $\delta_d = 6°$, $\delta_r = -15°$, $\beta = 0°$.

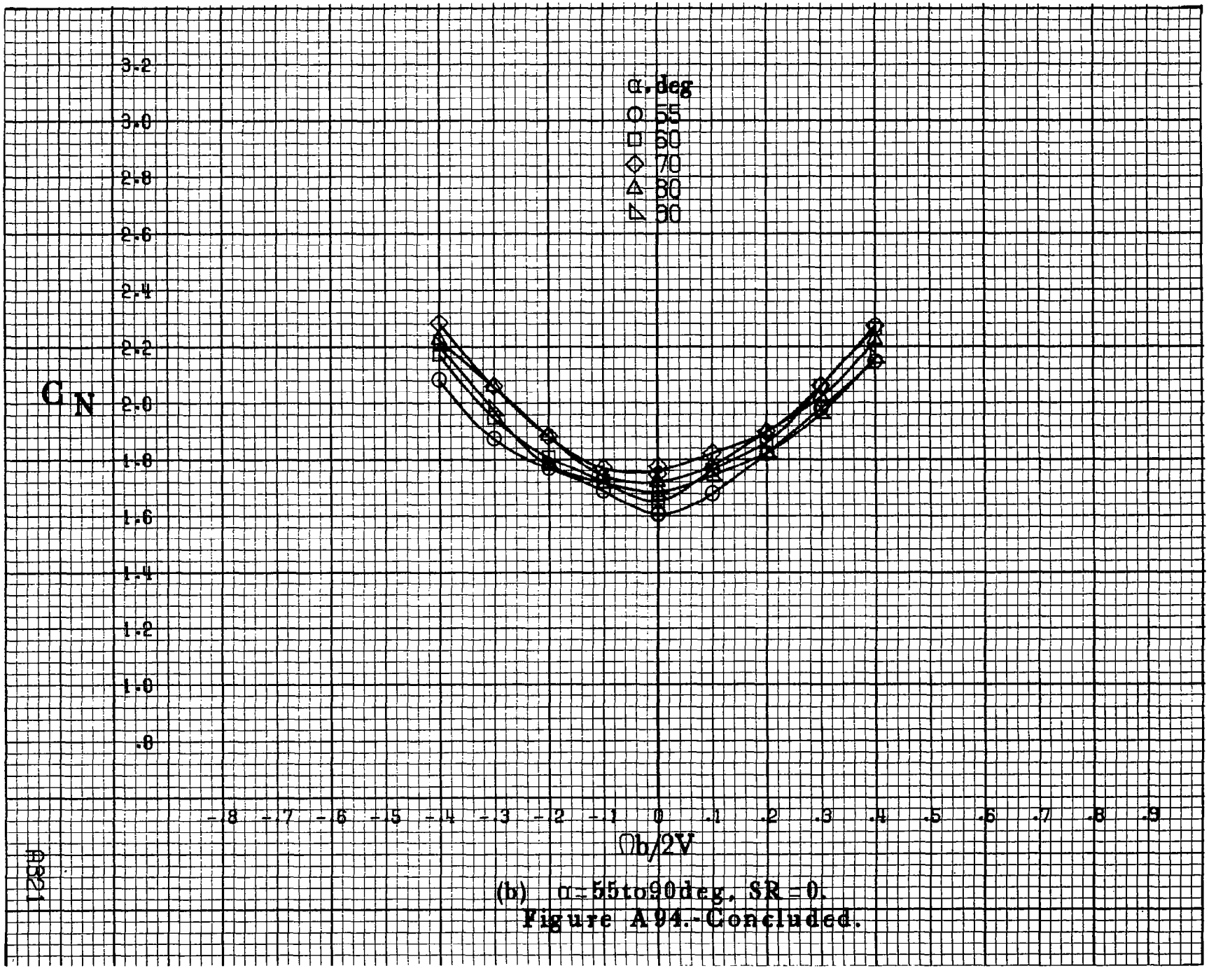

(b) α = 55 to 90 deg, SR = 0.

Figure A94.- Concluded.

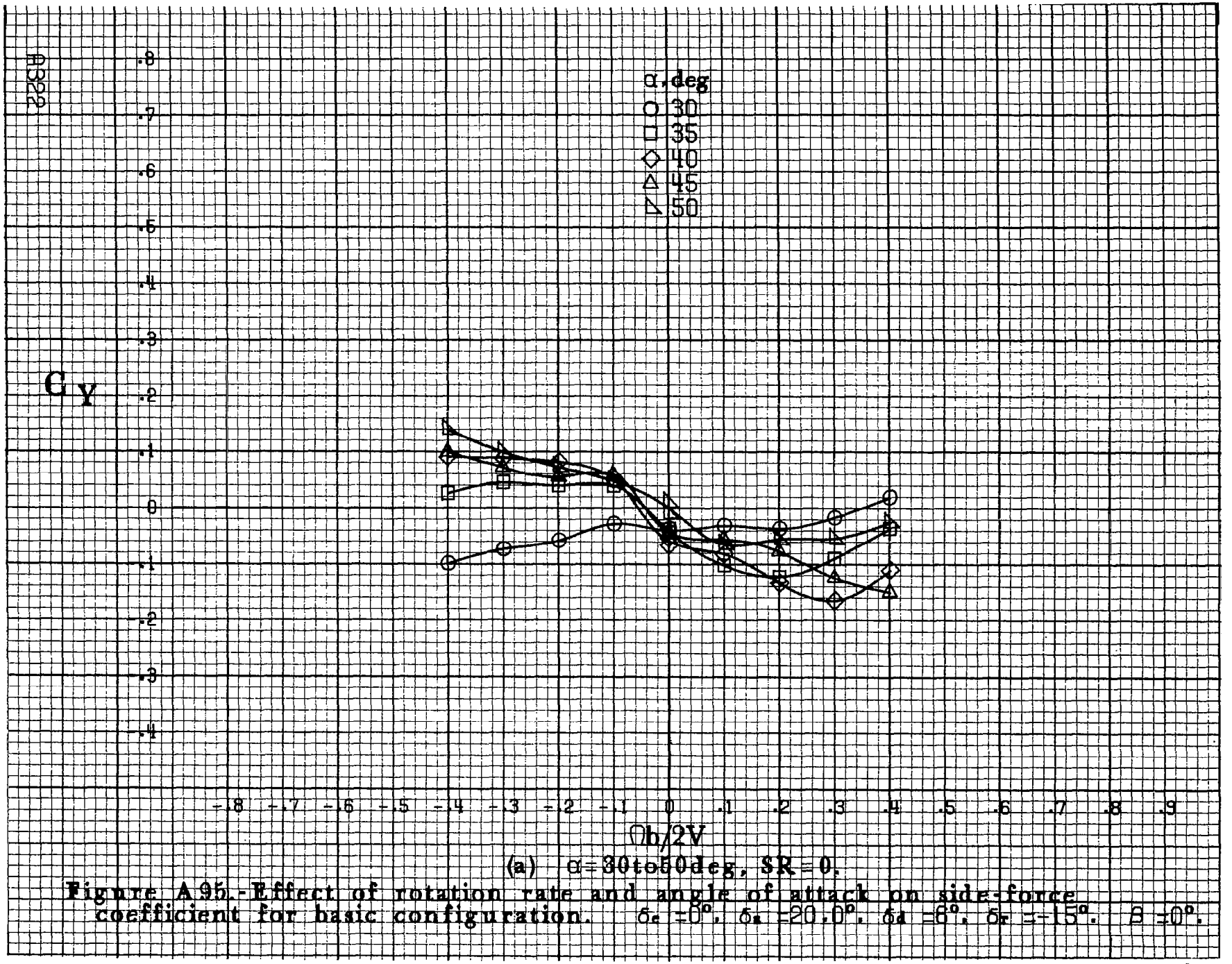

(a) $\alpha = 30$ to 50 deg, $SR = 0$.

Figure A95.- Effect of rotation rate and angle of attack on side-force coefficient for basic configuration. $\delta_e = 0°$, $\delta_{a_1} = 20.0°$, $\delta_{a_2} = 6°$, $\delta_r = +15°$, $\beta = 0°$.

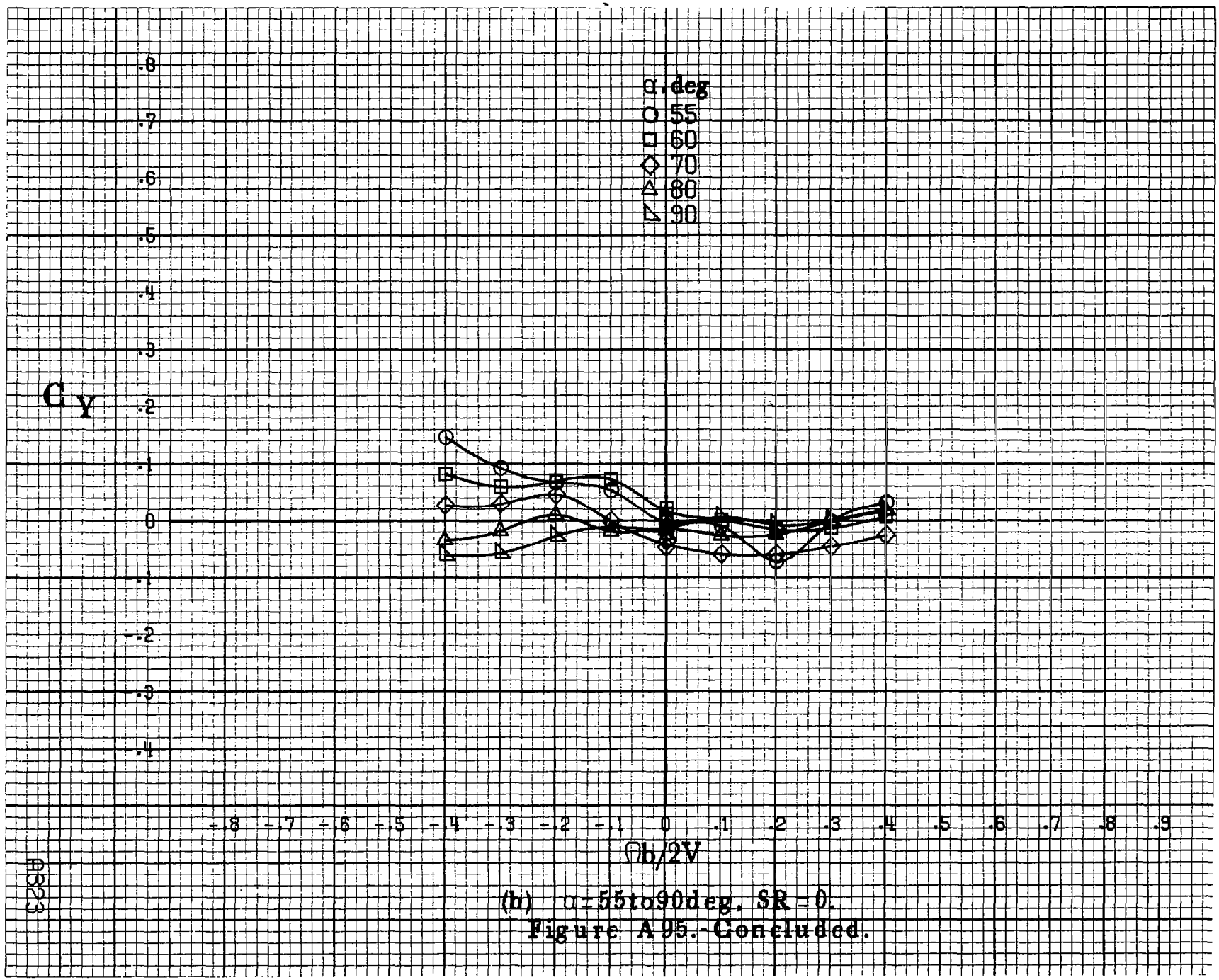

(b) $\alpha = 55$ to 90 deg, SR = 0.

Figure A95.- Concluded.

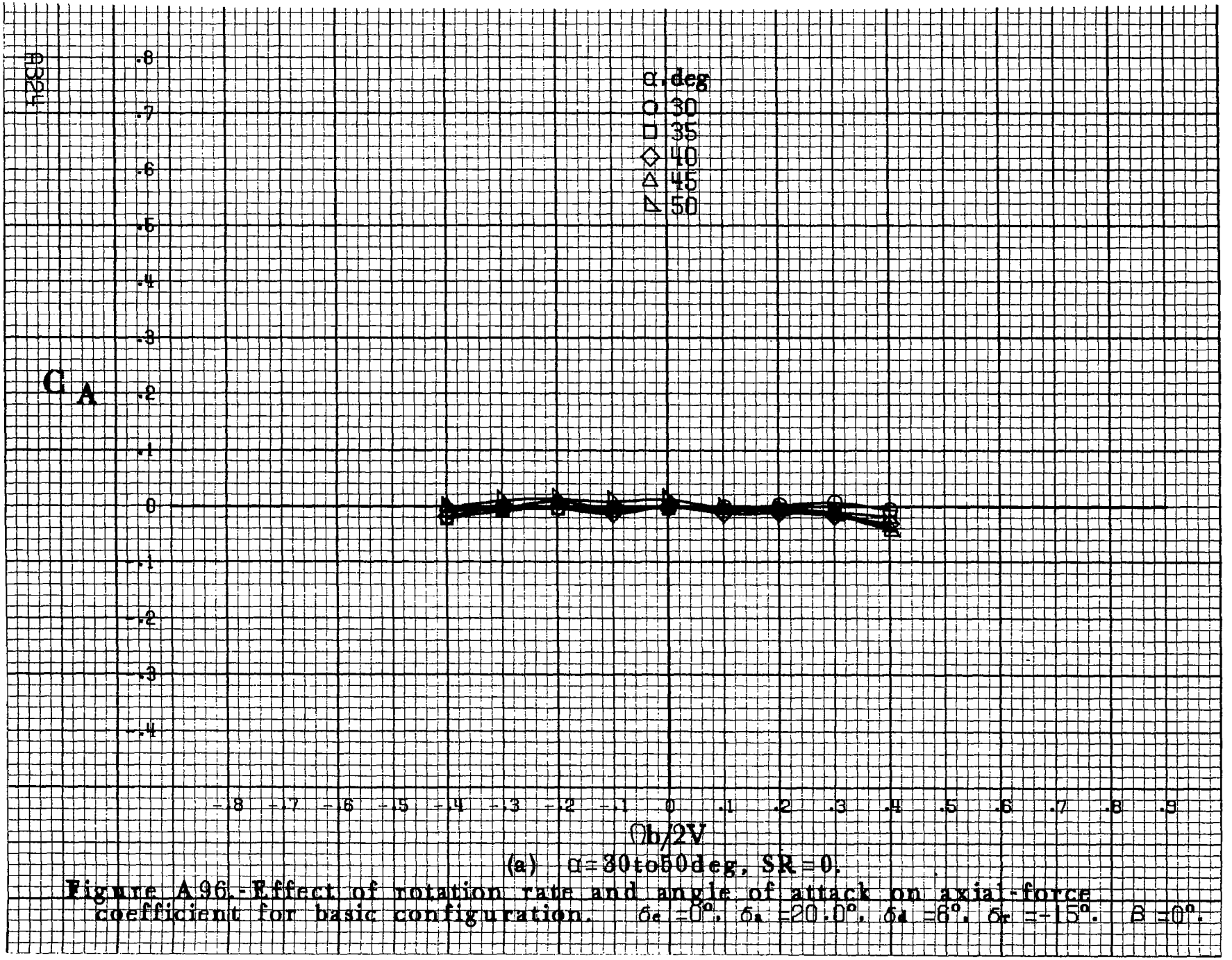

(a) $\alpha = 30$ to 60 deg, $SR = 0$.

Figure A96.- Effect of rotation rate and angle of attack on axial-force coefficient for basic configuration. $\delta_e = 0^\circ$, $\delta_{a_1} = 20.0^\circ$, $\delta_{a_4} = 6^\circ$, $\delta_r = -15^\circ$, $\beta = 0^\circ$.

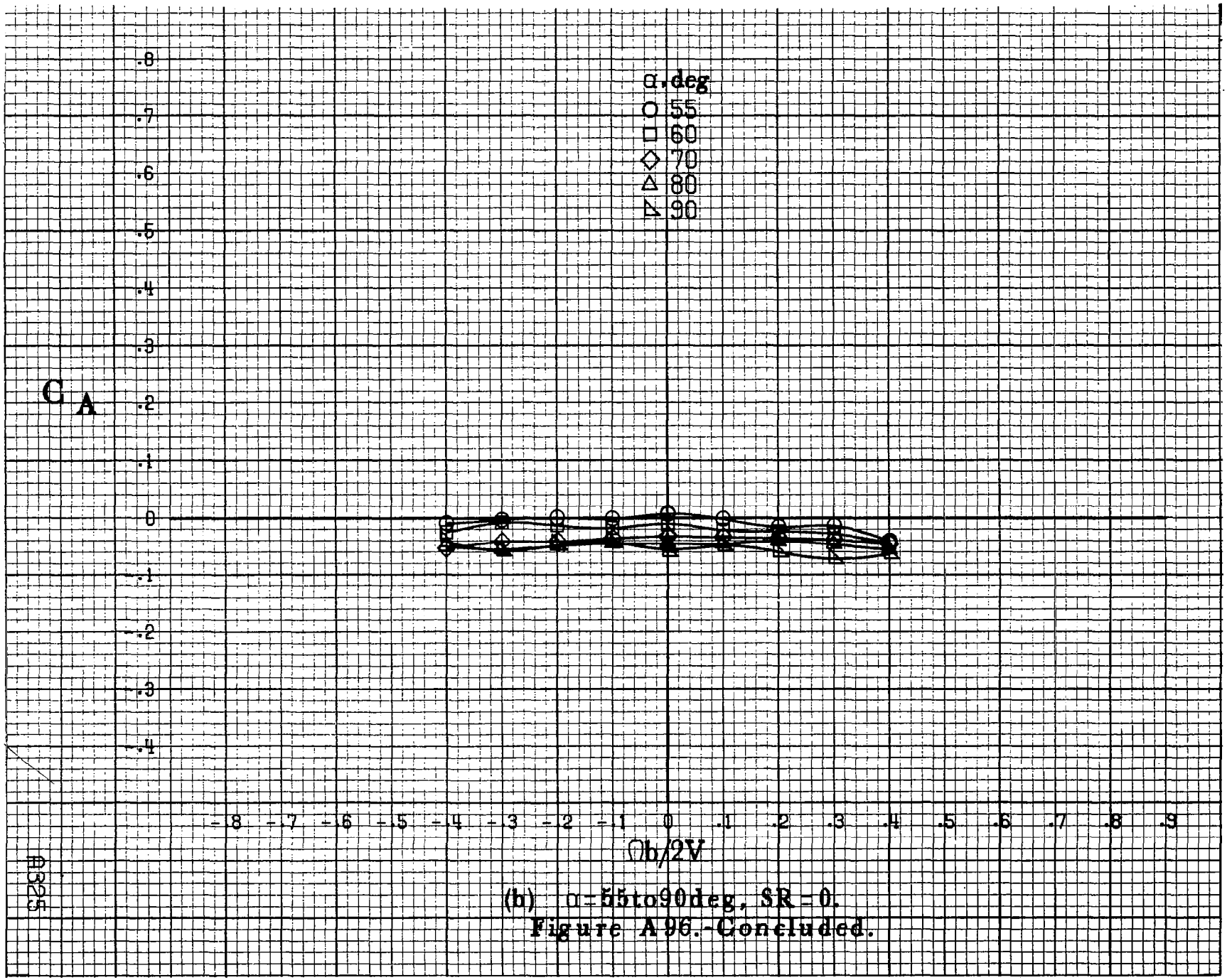

(b) $\alpha = 55$ to 90 deg, SR = 0.

Figure A96.-Concluded.

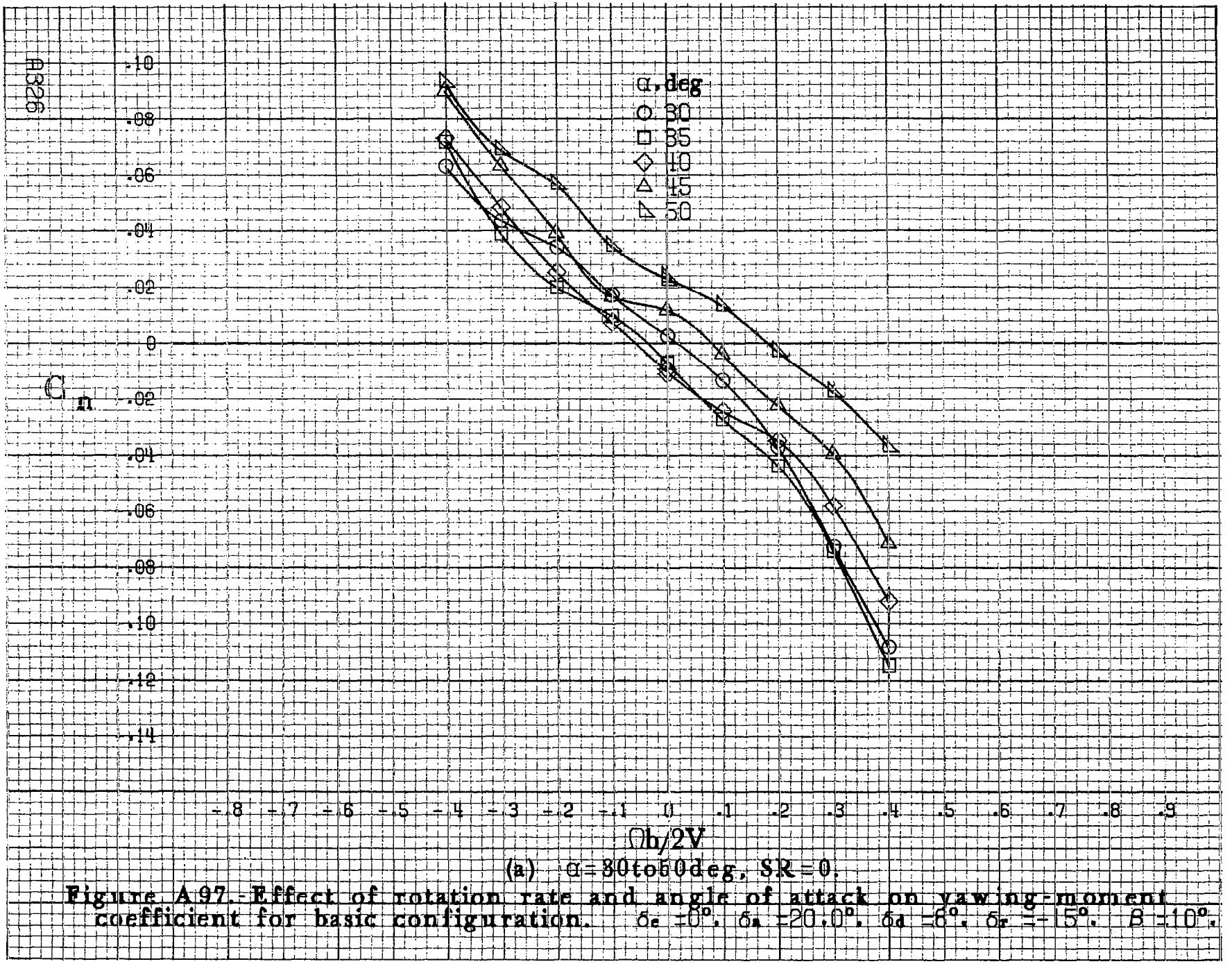

(a) $\alpha = 30$ to 60 deg, SR = 0.

Figure A97.- Effect of rotation rate and angle of attack on yawing-moment coefficient for basic configuration. $\delta_e = 0°$, $\delta_a = 20.0°$, $\delta_d = 6°$, $\delta_r = -15°$, $\beta = 10°$.

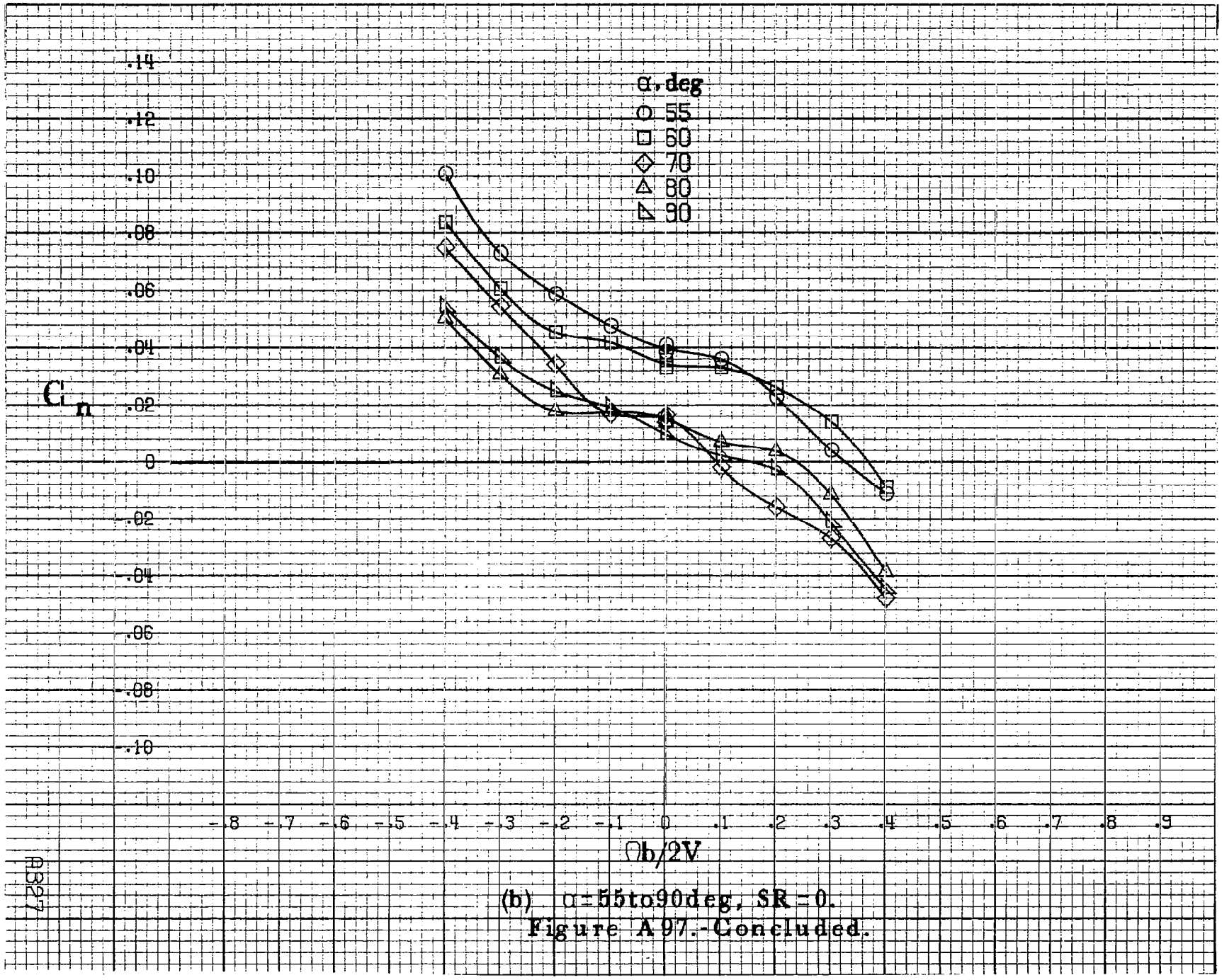

(b) $\alpha = 55$ to 90 deg, SR = 0.

Figure A97.- Concluded.

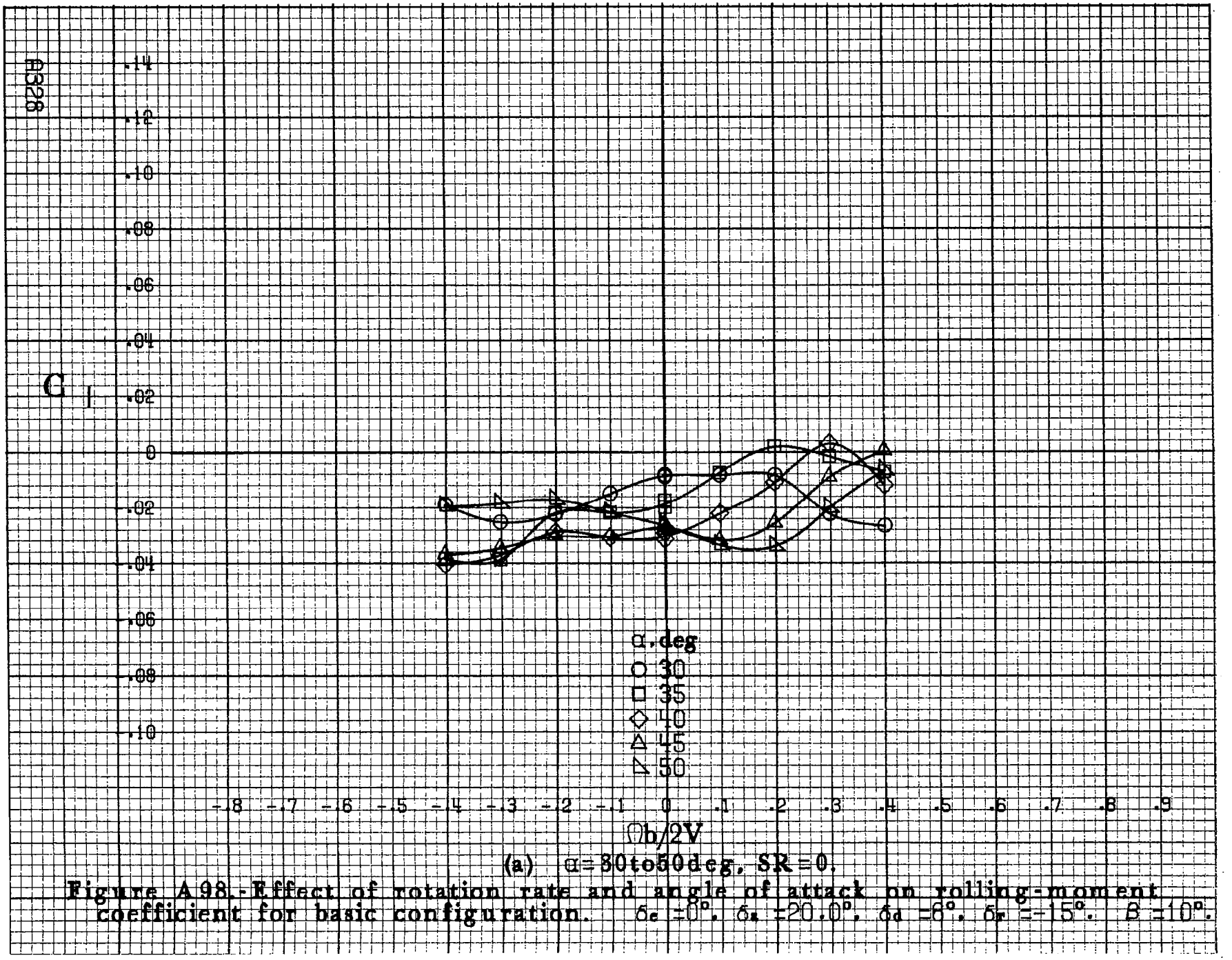

(a) $\alpha = 30$ to 50 deg, SR = 0.

Figure A98.- Effect of rotation rate and angle of attack on rolling-moment coefficient for basic configuration. $\delta_e = 0°$, $\delta_a = 20.0°$, $\delta_d = 6°$, $\delta_r = -15°$, $\beta = 10°$.

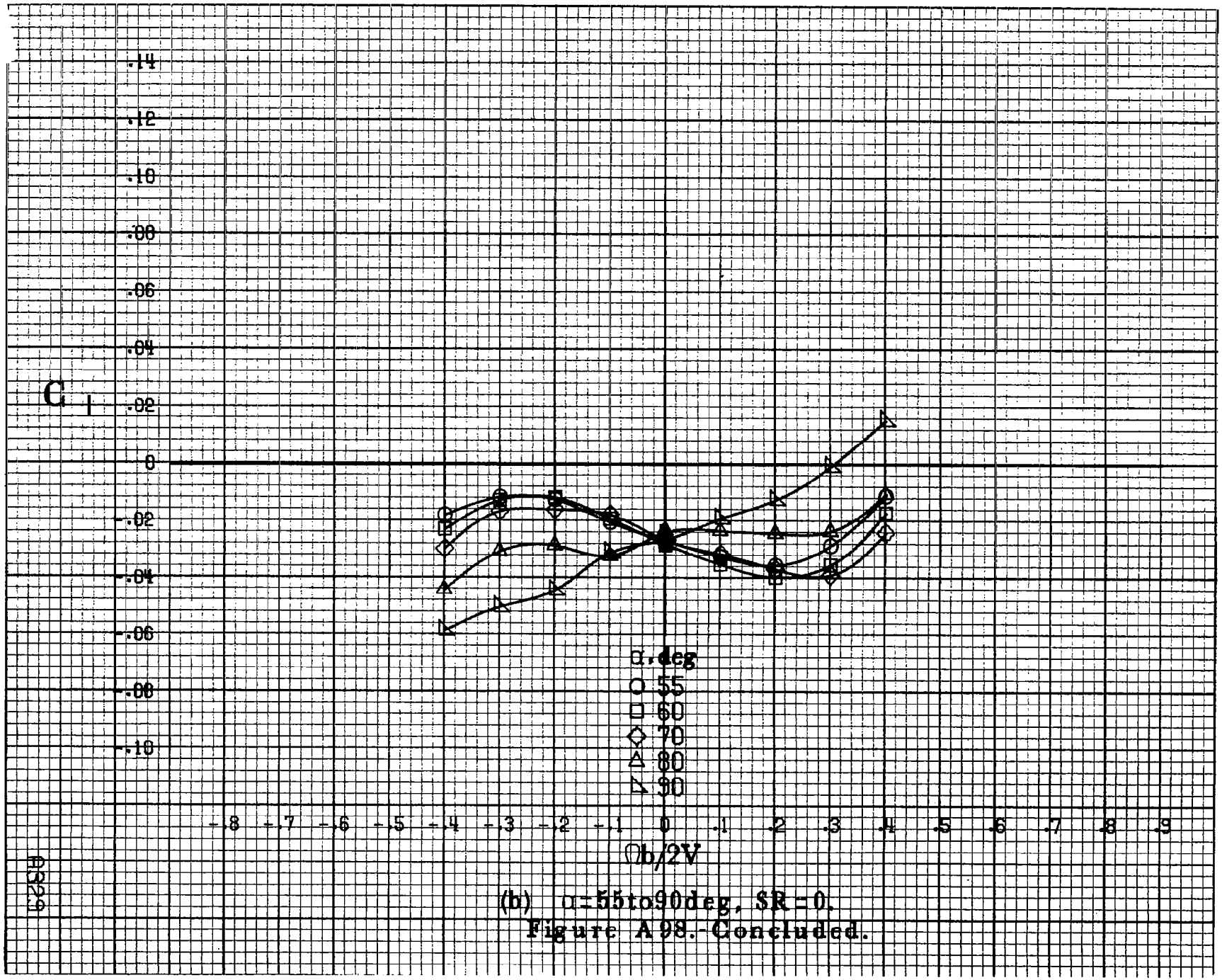

(b) $\alpha = 55$ to 90 deg, $SR = 0$.

Figure A98.- Concluded.

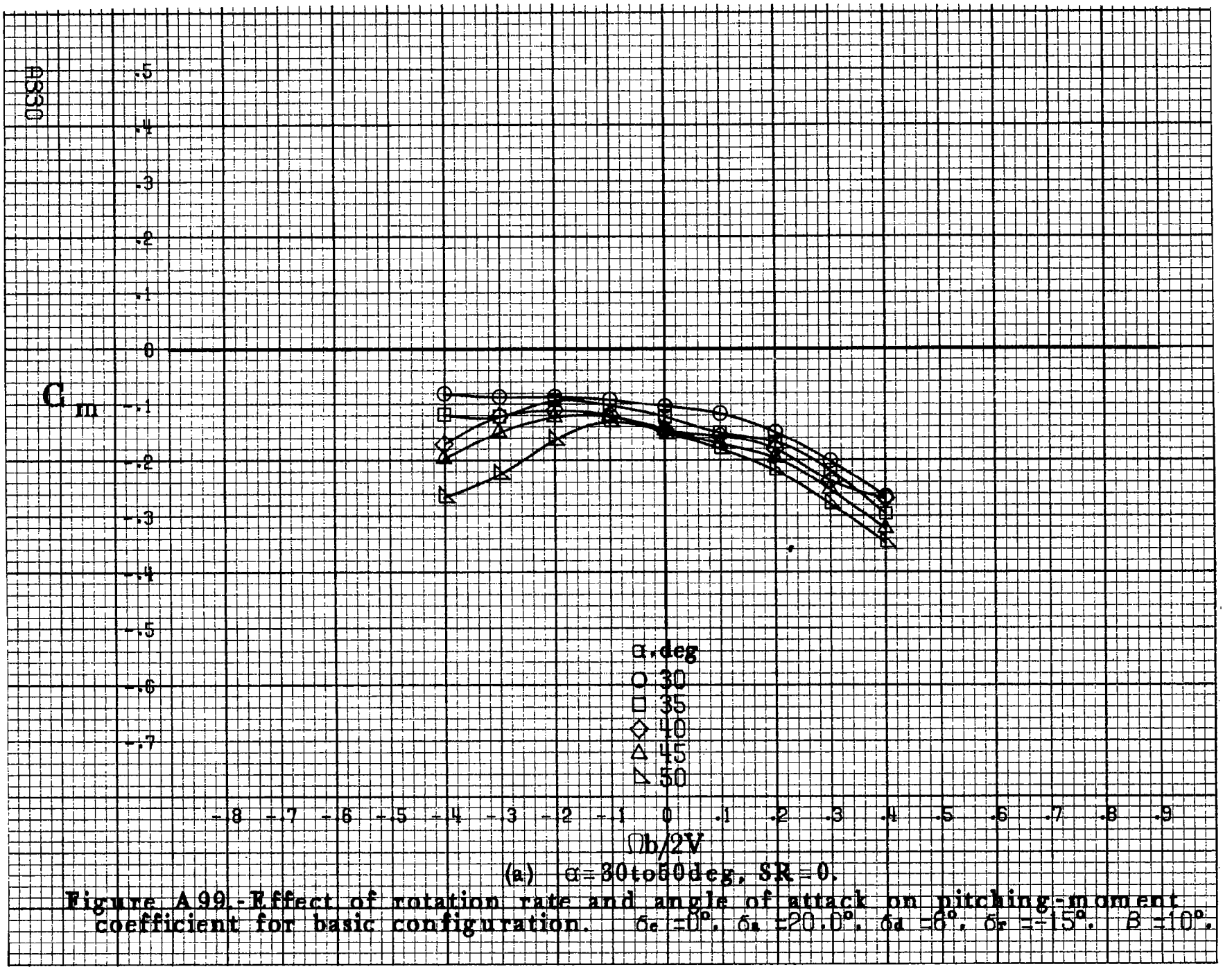

(a) $\alpha = 30$ to 50 deg, $SR = 0$.

Figure A.99.- Effect of rotation rate and angle of attack on pitching-moment coefficient for basic configuration. $\delta_e = 0°$, $\delta_a = 20.0°$, $\delta_d = 6°$, $\delta_r = 15°$, $\beta = 10°$.

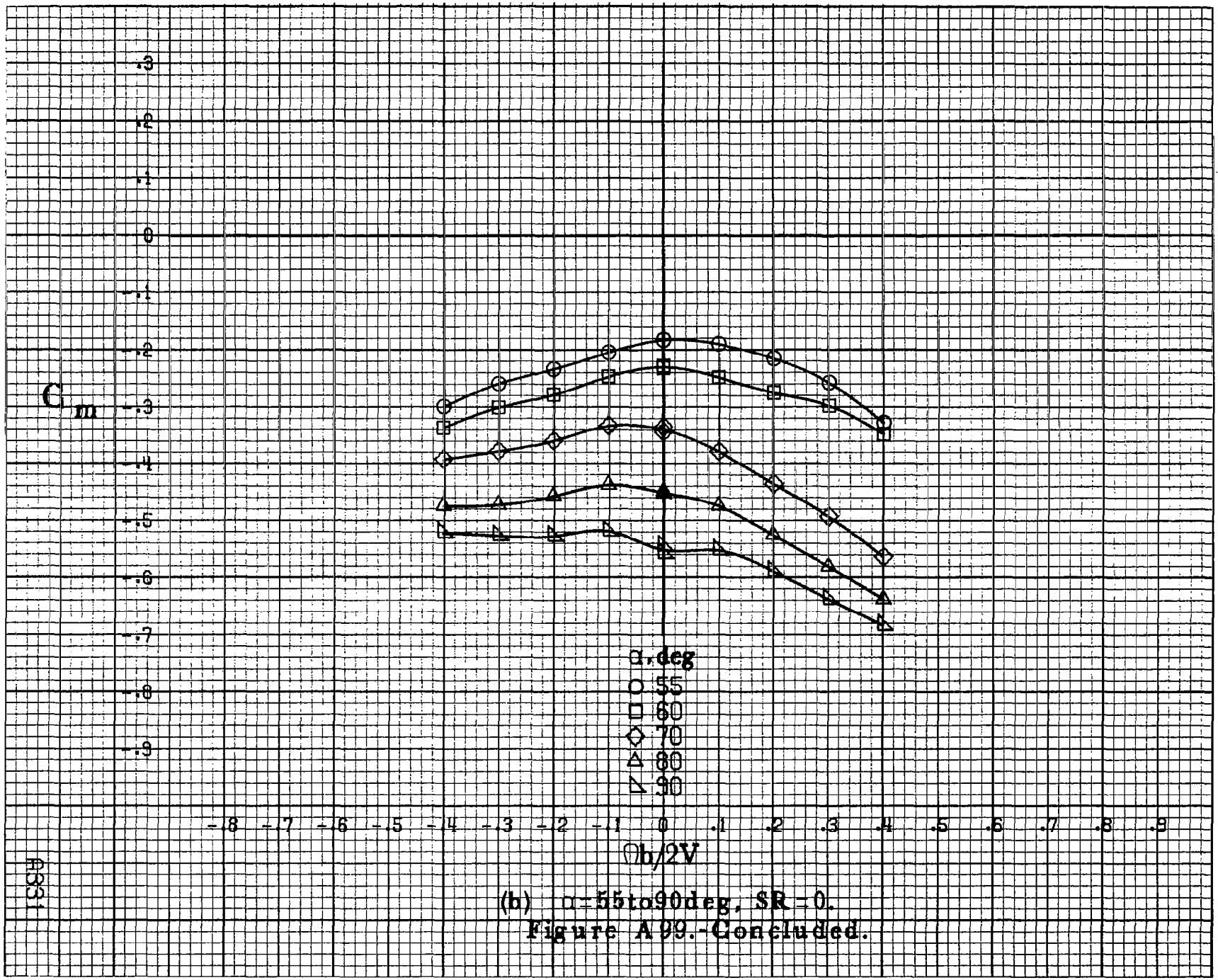

(b) α=55 to 90 deg, SR=0.

Figure A99.-Concluded.

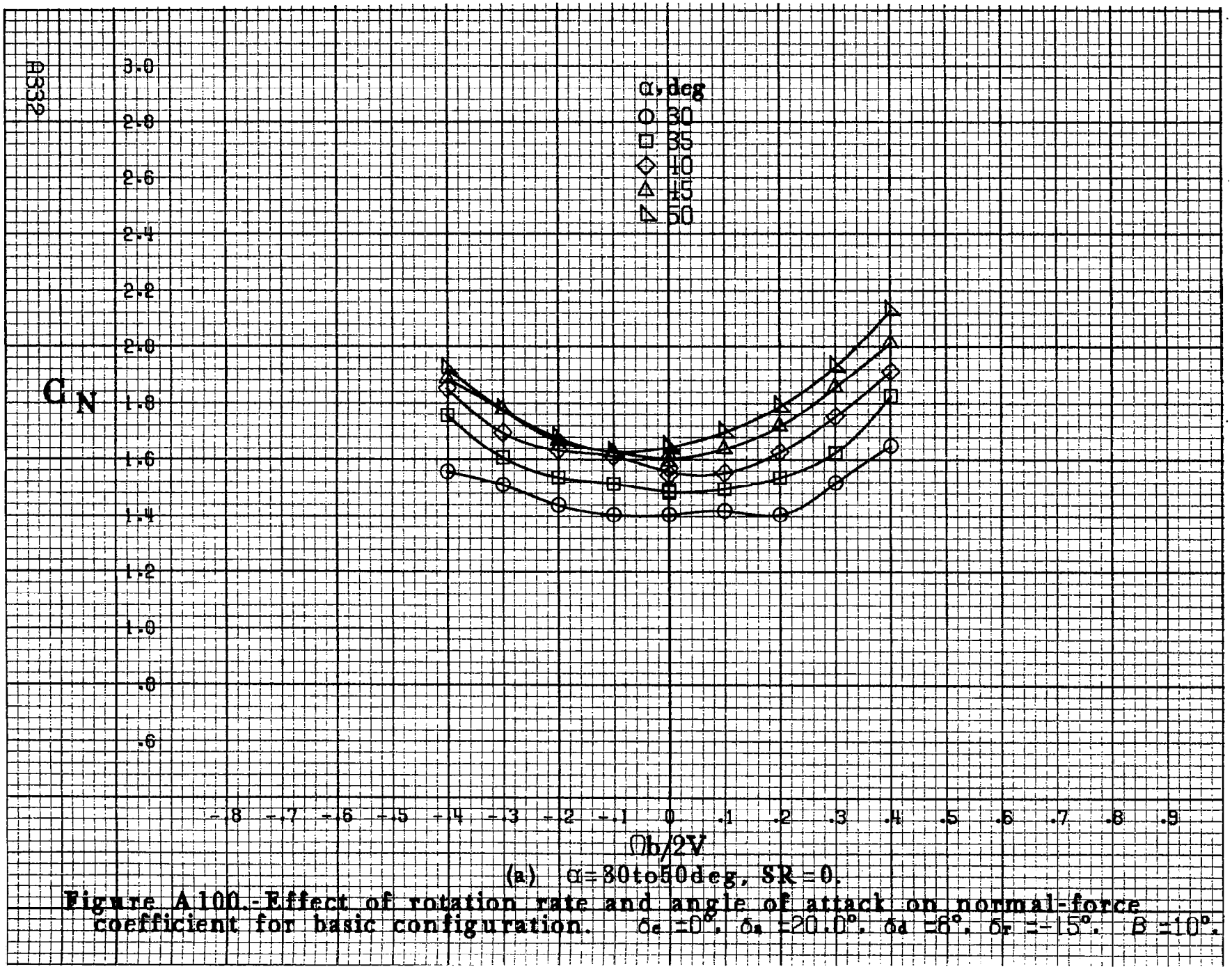

(a) $\alpha = 30$ to 50 deg, SR = 0.

Figure A100.- Effect of rotation rate and angle of attack on normal-force coefficient for basic configuration. $\delta_e = 0°$, $\delta_a = 20.0°$, $\delta_d = 8°$, $\delta_r = -15°$, $\beta = 10°$.

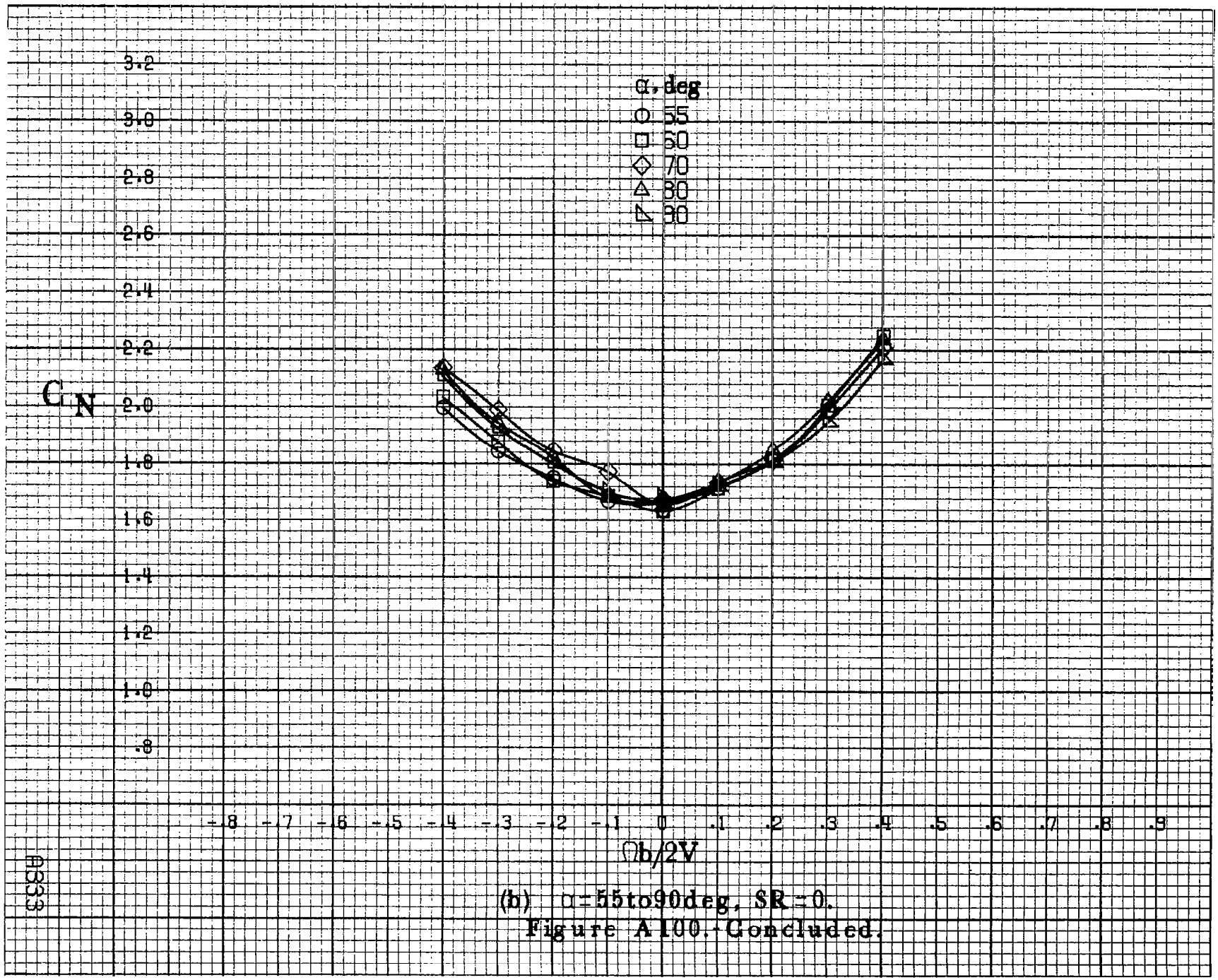

(b) α = 55 to 90 deg, SR = 0.

Figure A100.- Concluded.

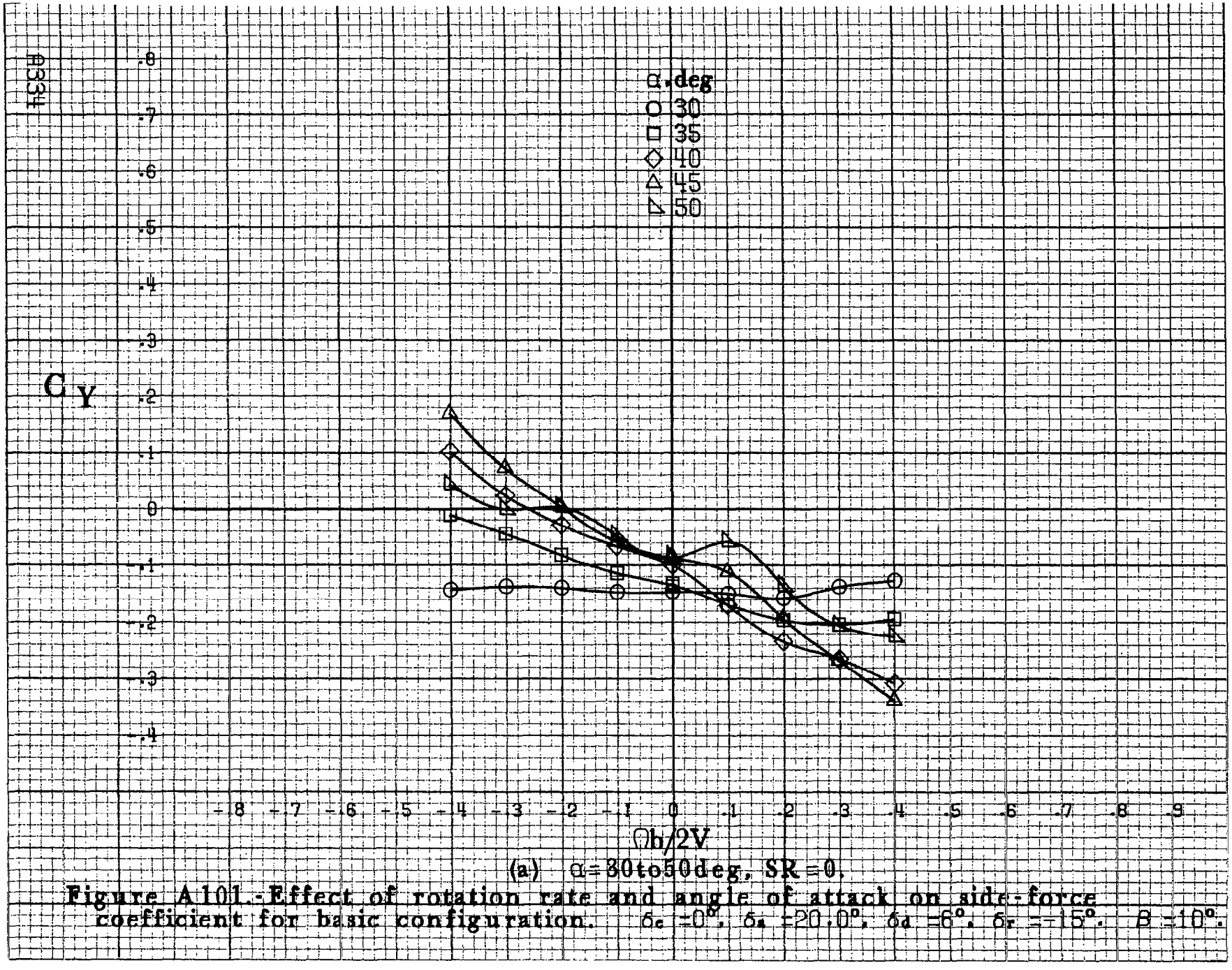

(a) $\alpha = 30$ to 50 deg, SR = 0.

Figure A101.-Effect of rotation rate and angle of attack on side-force coefficient for basic configuration. $\delta_e = 0°$, $\delta_a = 20.0°$, $\delta_d = 6°$, $\delta_r = -15°$, $\beta = 10°$.

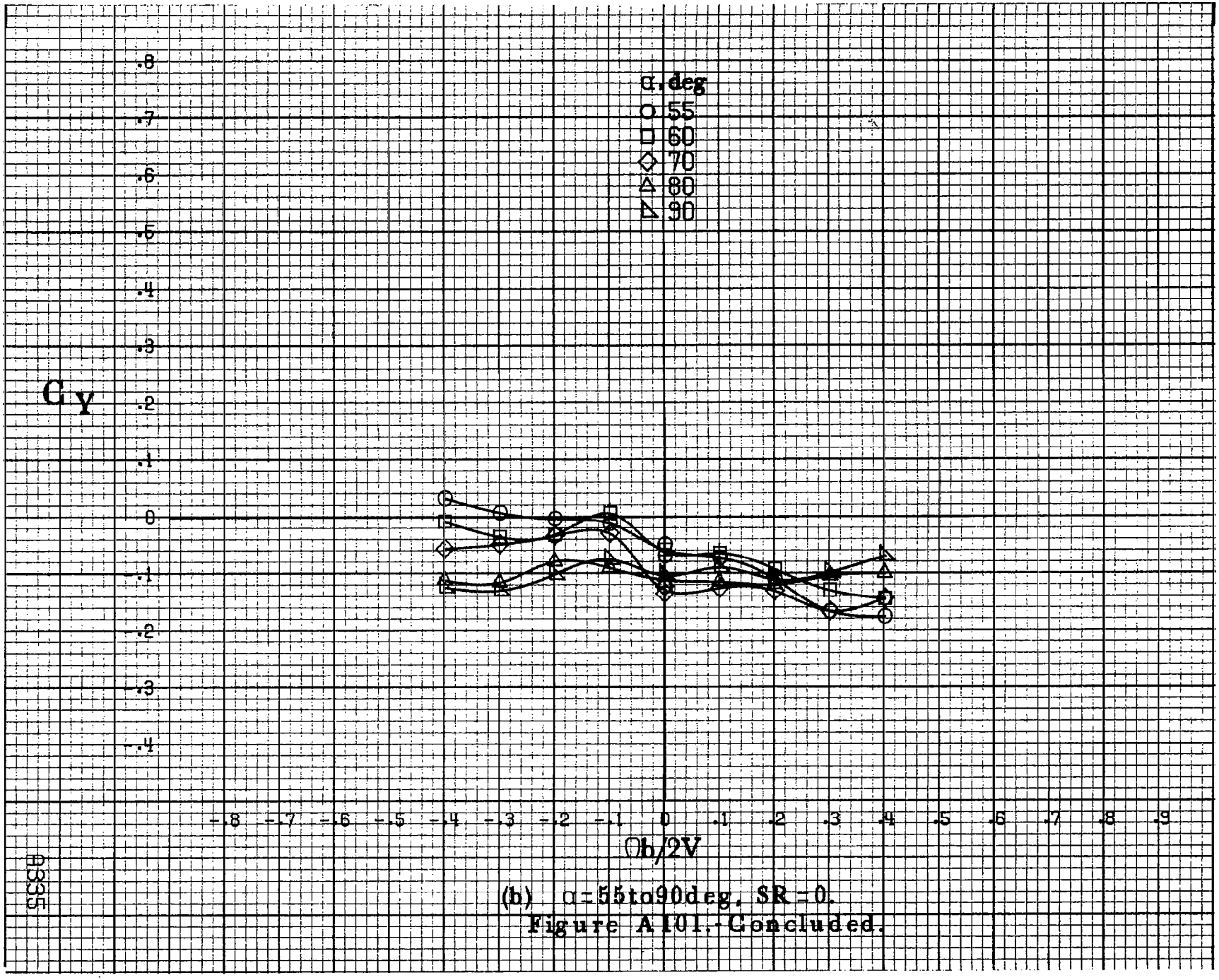

(b) $\alpha = 55$ to 90 deg, $SR = 0$.

Figure A101.- Concluded.

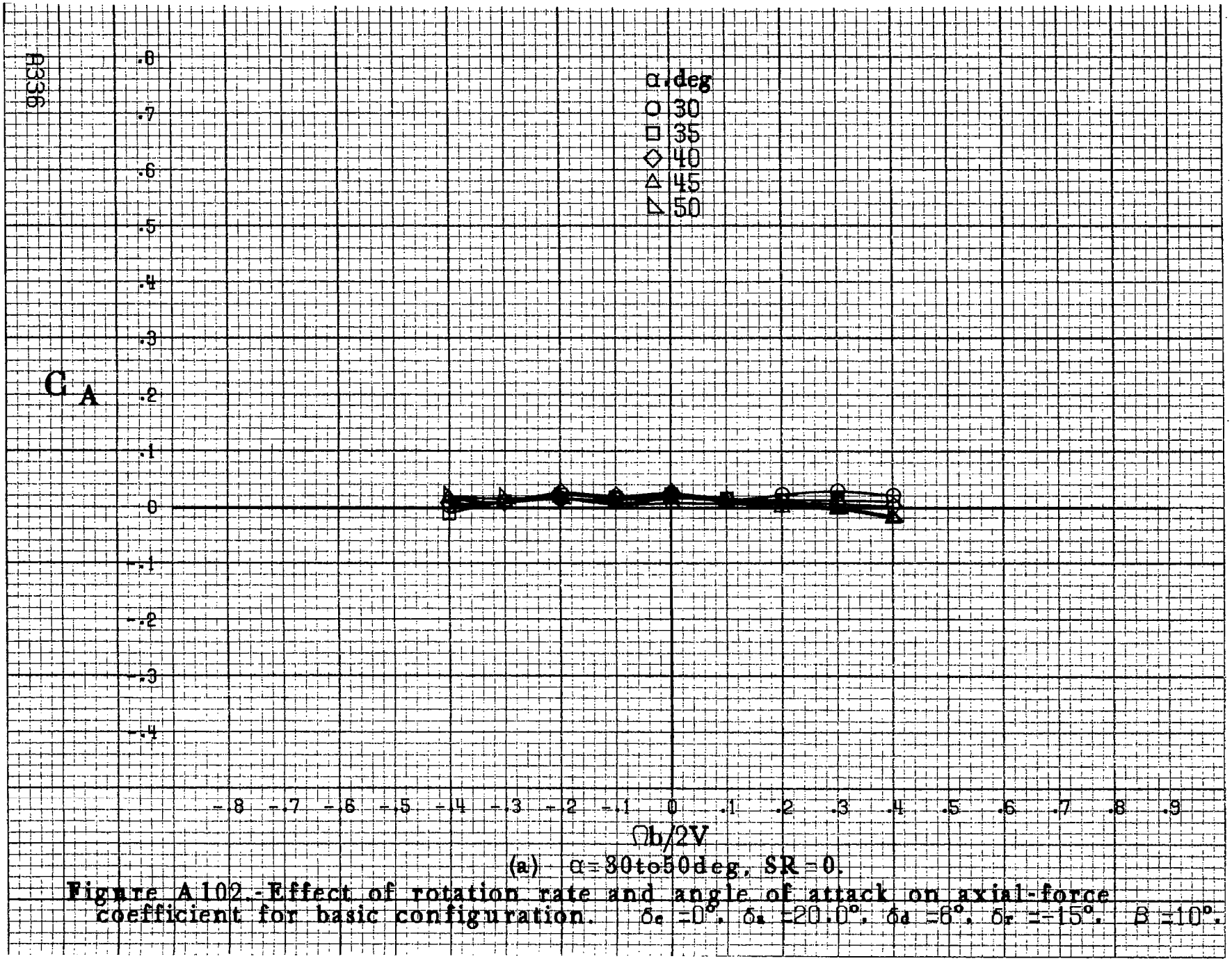

(a) $\alpha = 30$ to 50 deg, SR = 0.

Figure A102.-Effect of rotation rate and angle of attack on axial-force coefficient for basic configuration. $\delta_e = 0°$, $\delta_a = 20.0°$, $\delta_d = 6°$, $\delta_r = -15°$, $\beta = 10°$.

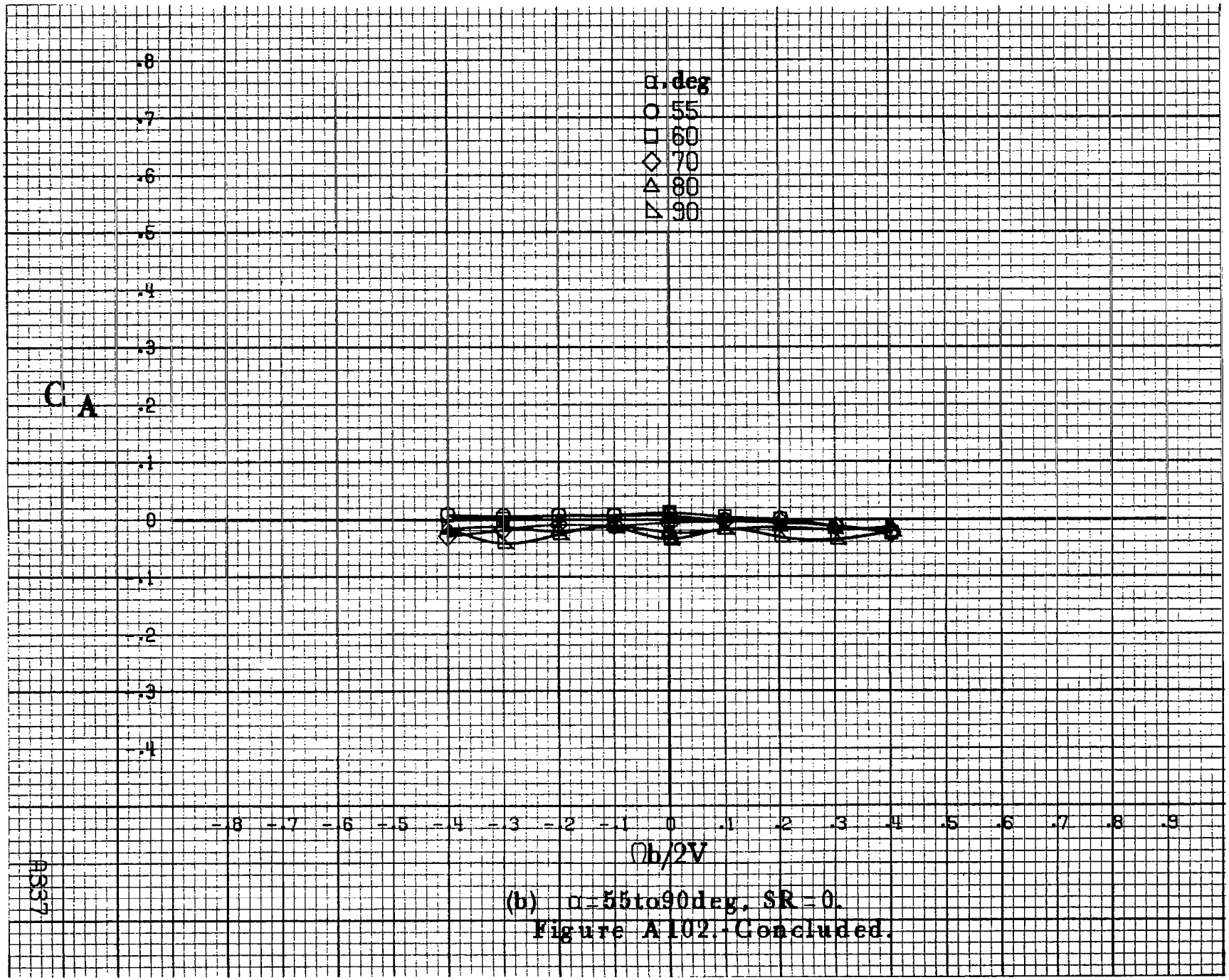

(b) $\alpha = 55$ to 90 deg, $SR = 0$.

Figure A102.- Concluded.

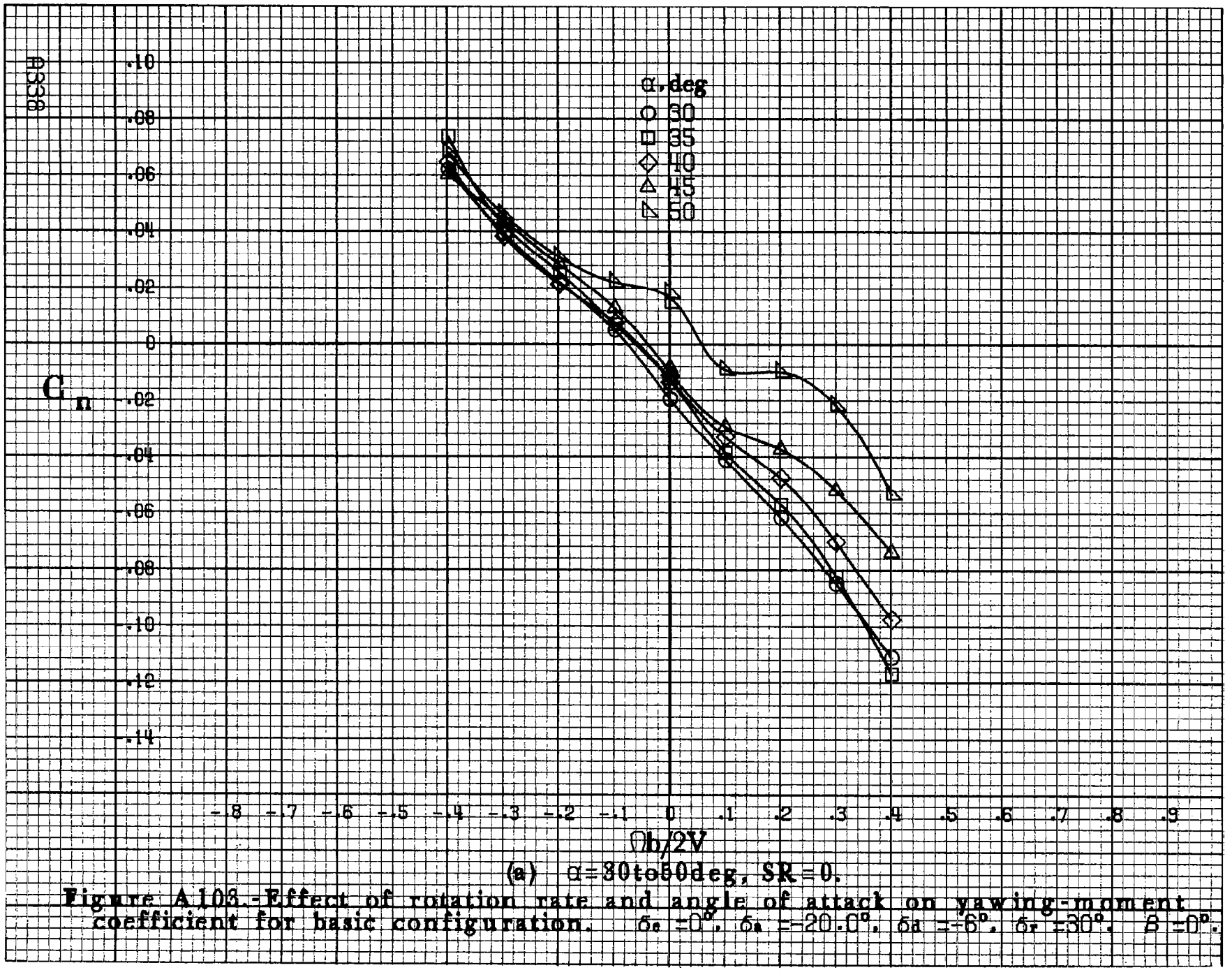

(a) $\alpha = 30$ to 60 deg, SR = 0.

Figure A103.-Effect of rotation rate and angle of attack on yawing-moment coefficient for basic configuration. $\delta_e = 0°$, $\delta_{sb} = -20.0°$, $\delta_a = -6°$, $\delta_r = 30°$, $\beta = 0°$.

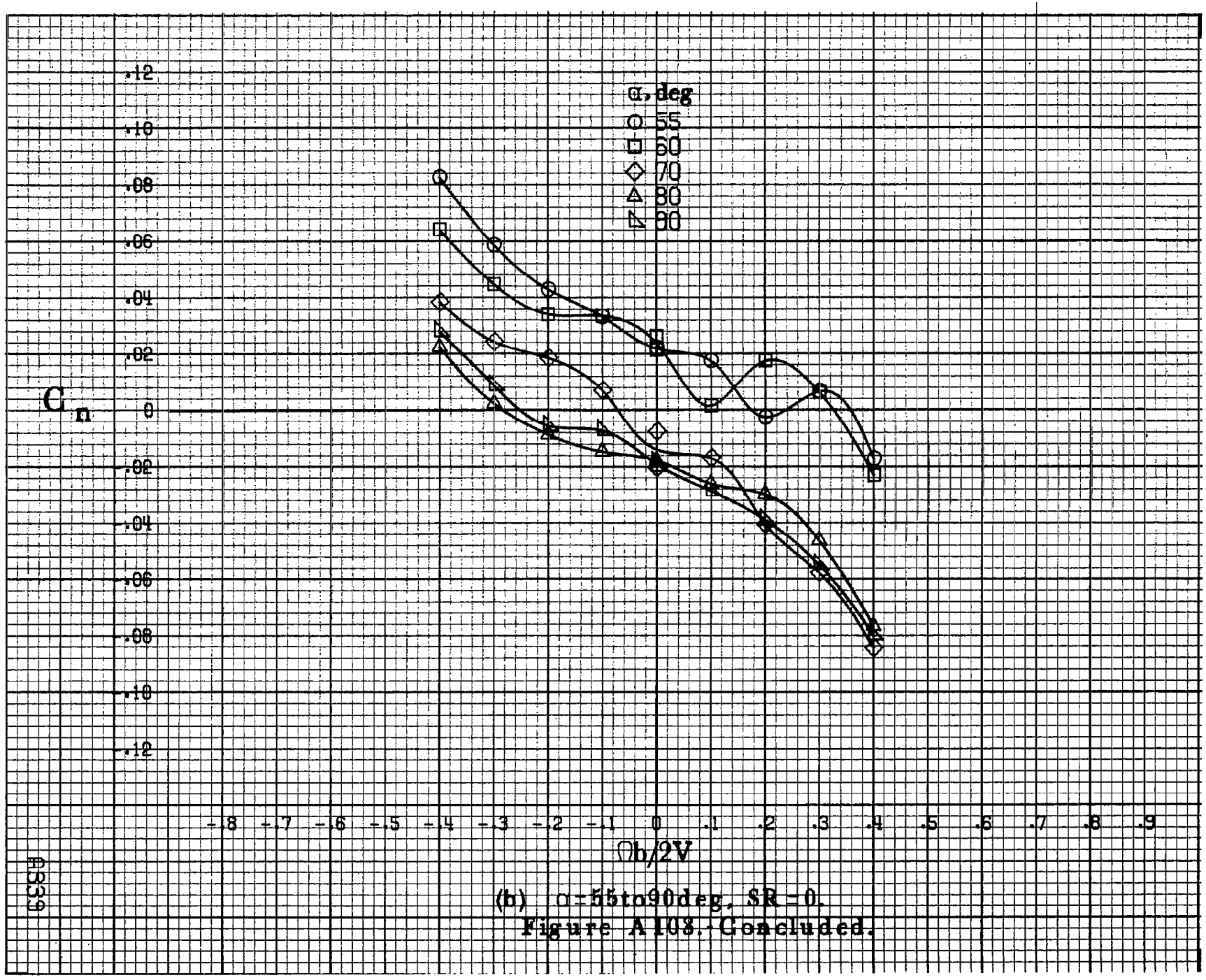

(b) $\alpha = 55$ to 90 deg, SR = 0.

Figure A103.- Concluded.

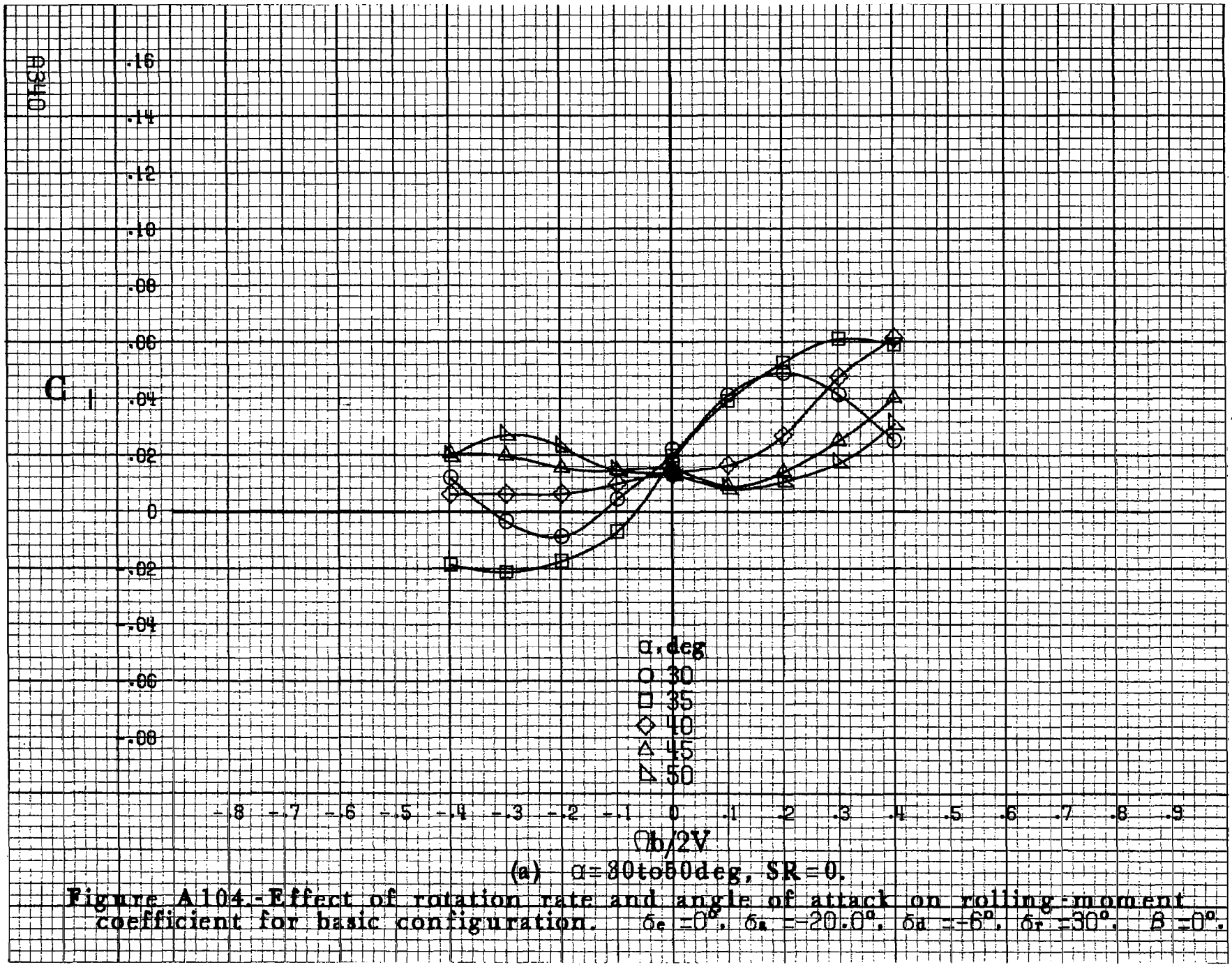

(a) $\alpha = 30$ to 50 deg, $SR = 0$.

Figure A104.- Effect of rotation rate and angle of attack on rolling-moment coefficient for basic configuration. $\delta_e = 0°$, $\delta_s = -20.0°$, $\delta_a = +6°$, $\delta_r = 30°$, $\beta = 0°$.

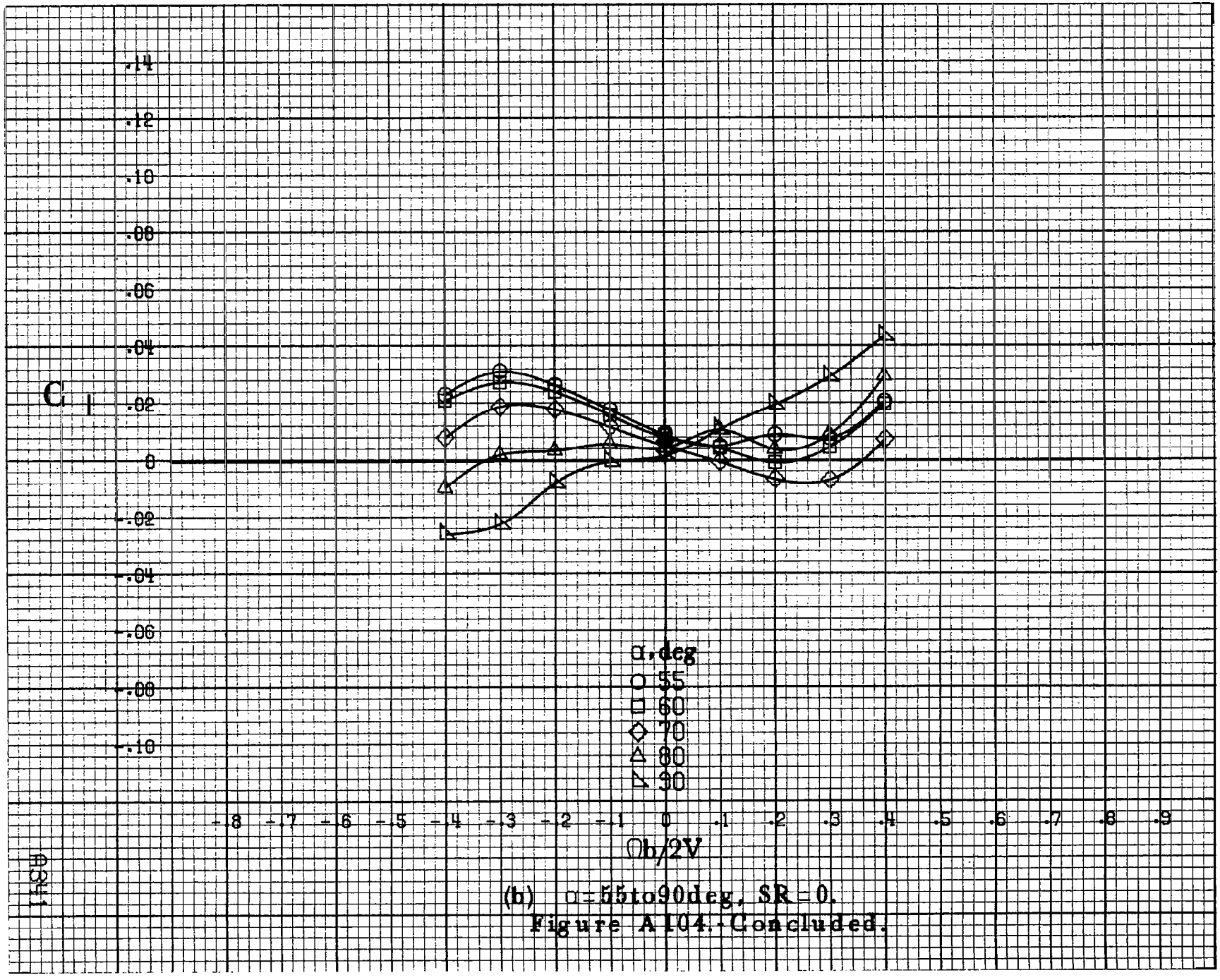

(b) α = 55 to 90 deg, SR = 0.

Figure A104.- Concluded.

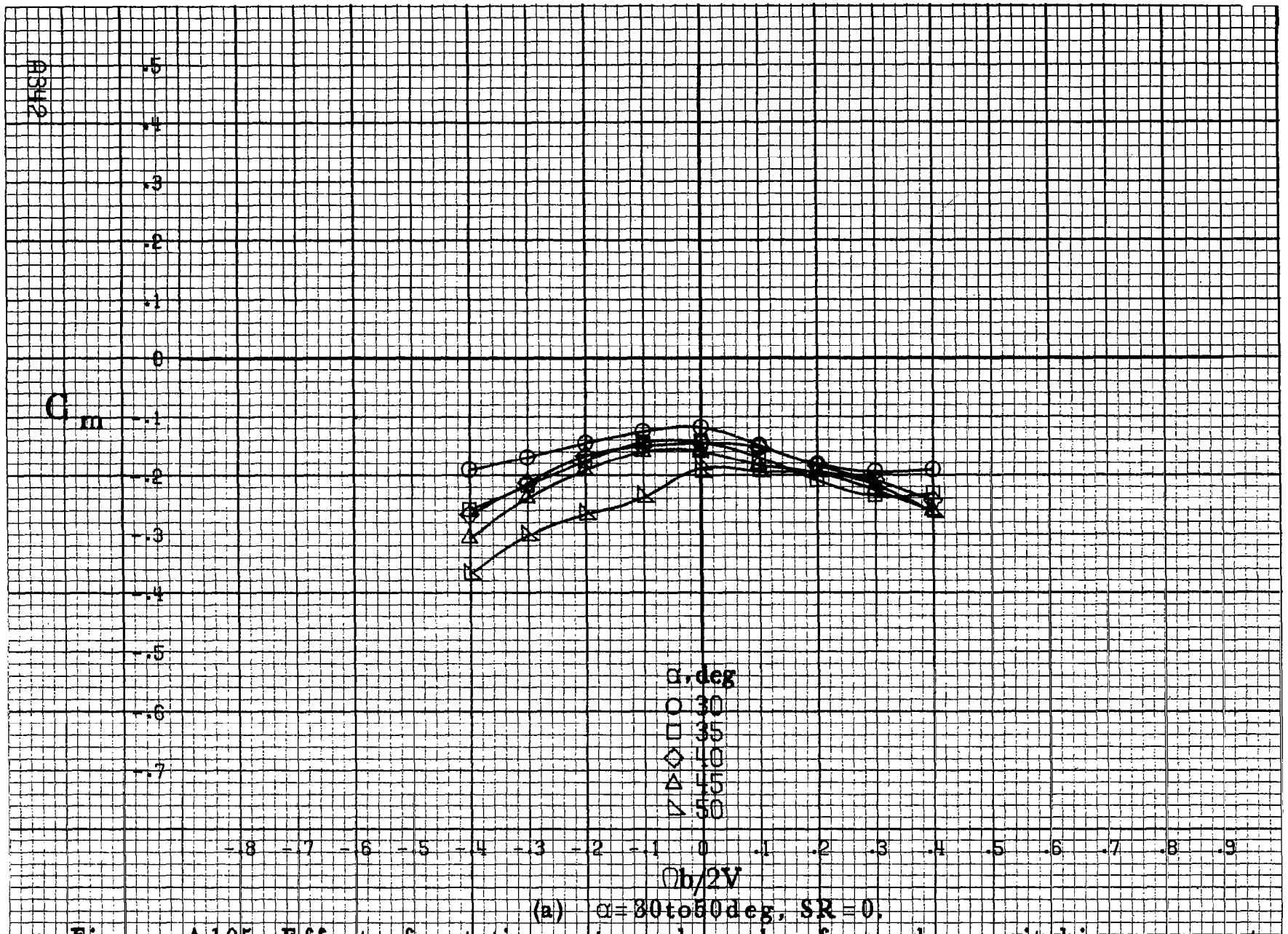

(a) $\alpha = 30$ to 50 deg, $SR = 0$.

Figure A105.- Effect of rotation rate and angle of attack on pitching-moment coefficient for basic configuration. $\delta_e = 0°$, $\delta_a = -20.0°$, $\delta_d = -6°$, $\delta_r = 30°$, $\beta = 0°$.

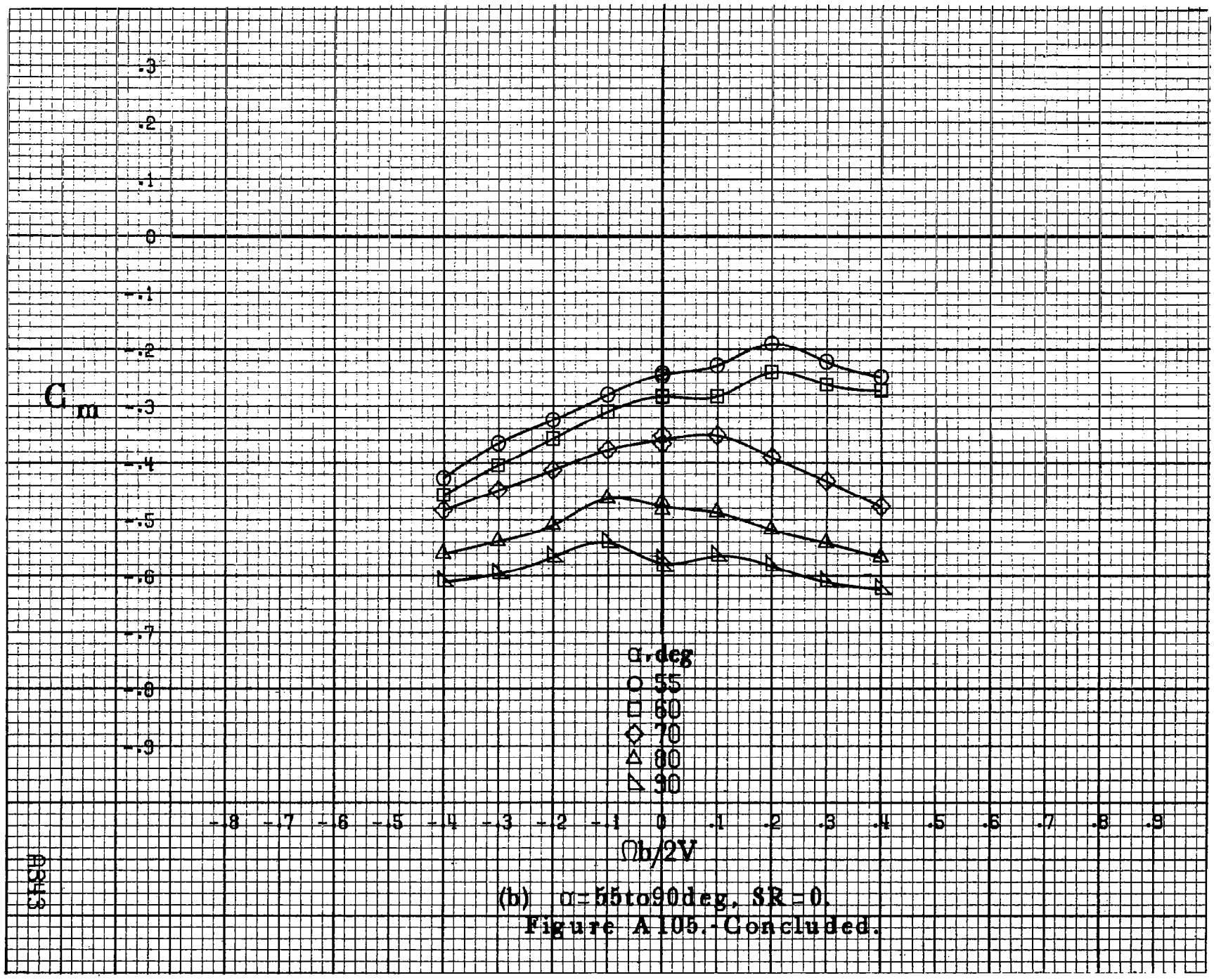

(b) $\alpha = 55$ to 90 deg, SR = 0.

Figure A105.- Concluded.

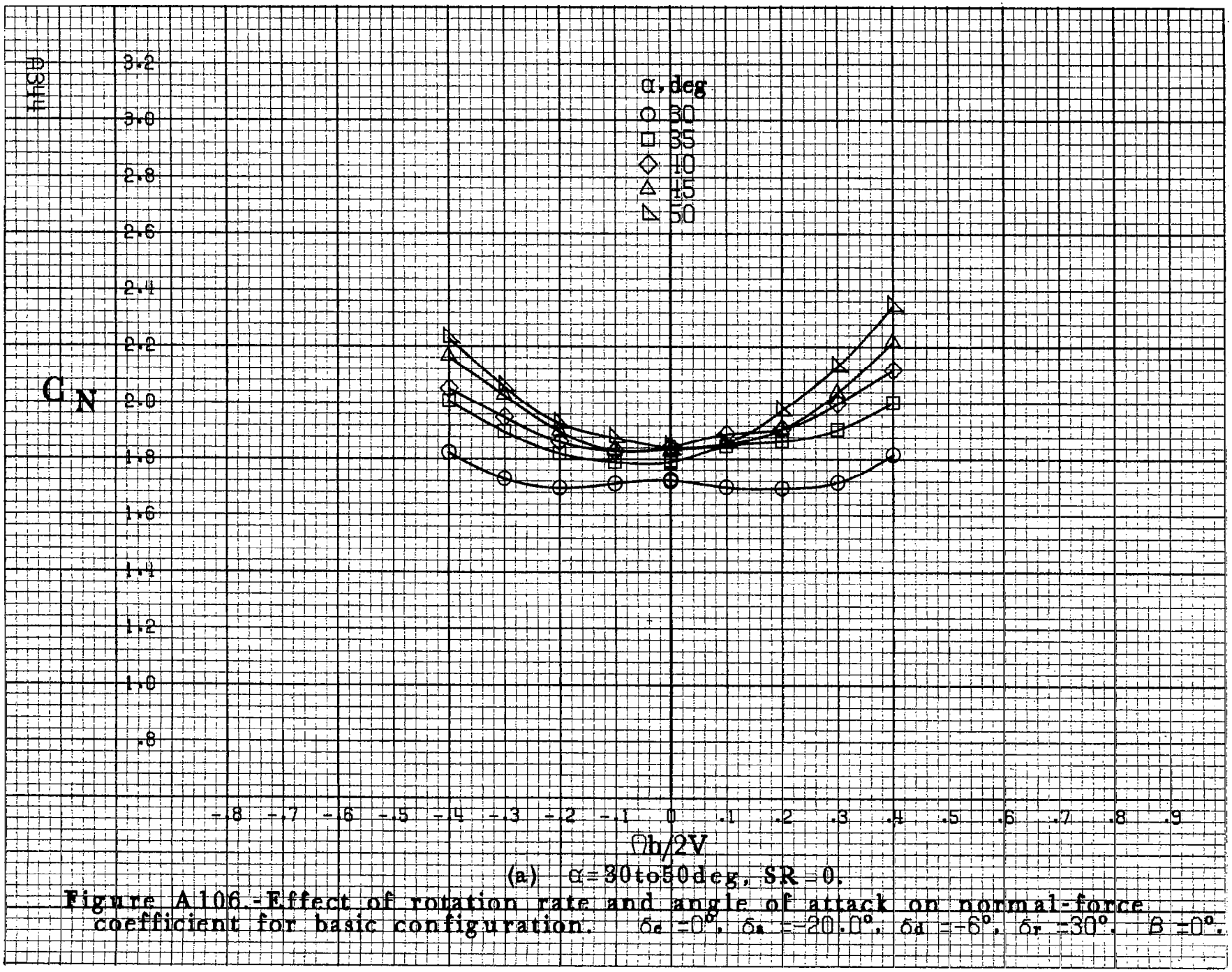

(a) $\alpha = 30$ to 50 deg, SR = 0.

Figure A106.-Effect of rotation rate and angle of attack on normal-force coefficient for basic configuration. $\delta_e = 0°$, $\delta_a = -20.0°$, $\delta_d = -6°$, $\delta_r = 30°$, $\beta = 0°$.

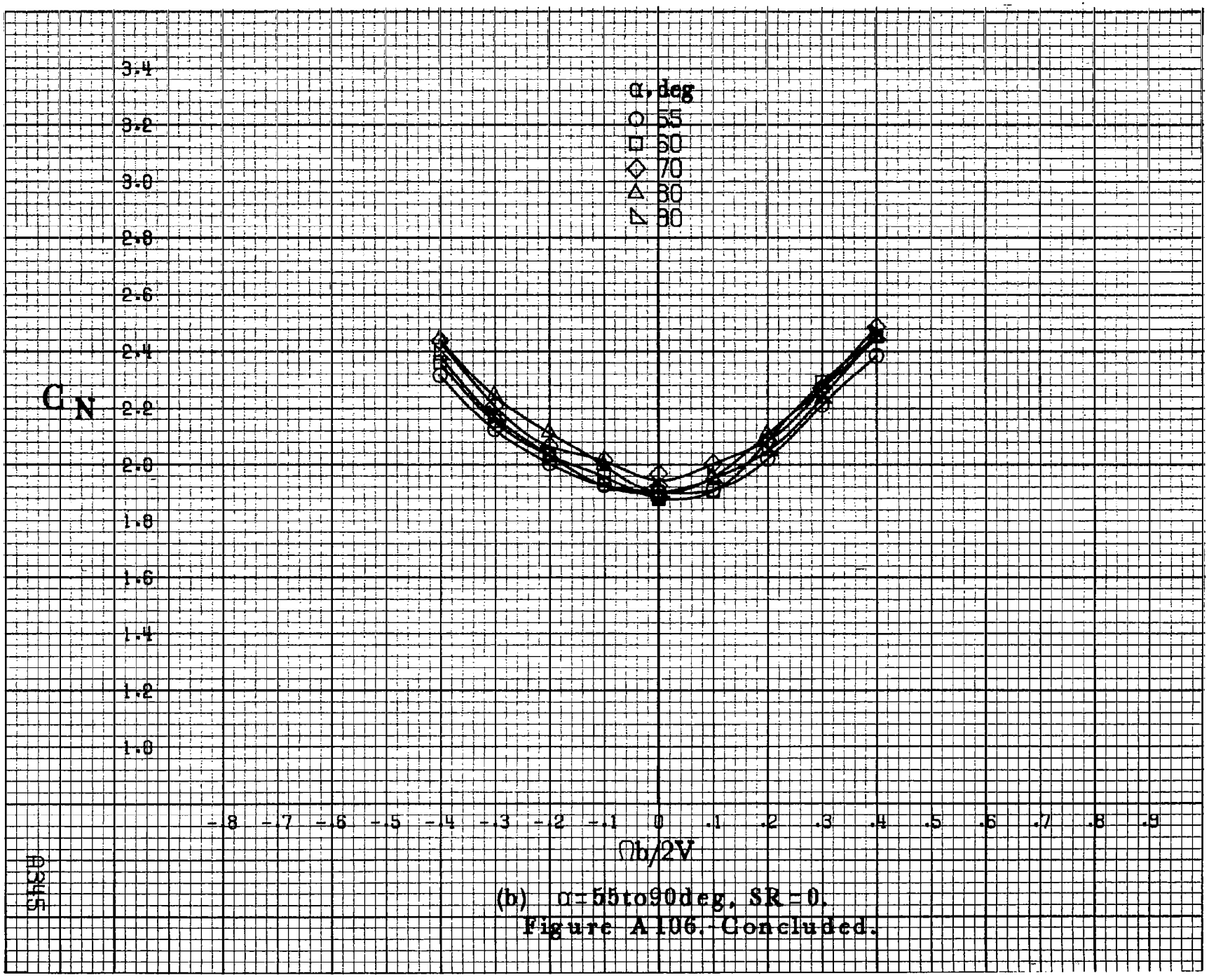

(b) α=55to90deg, SR=0.

Figure A106.-Concluded.

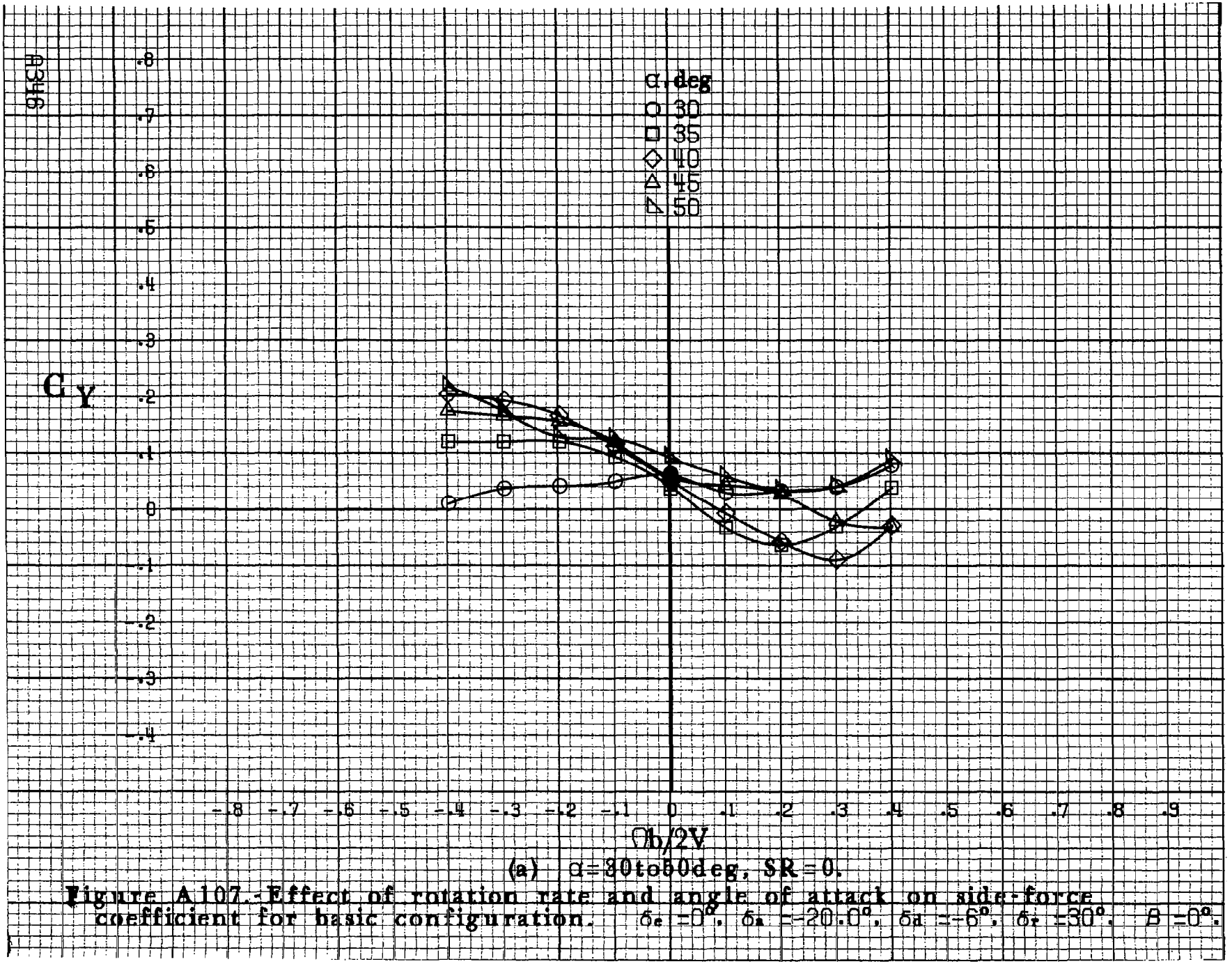

(a) $\alpha = 30$ to 60 deg, SR = 0.

Figure A107.- Effect of rotation rate and angle of attack on side-force coefficient for basic configuration. $\delta_e = 0°$, $\delta_{a_s} = -20.0°$, $\delta_a = -6°$, $\delta_r = 30°$, $\beta = 0°$.

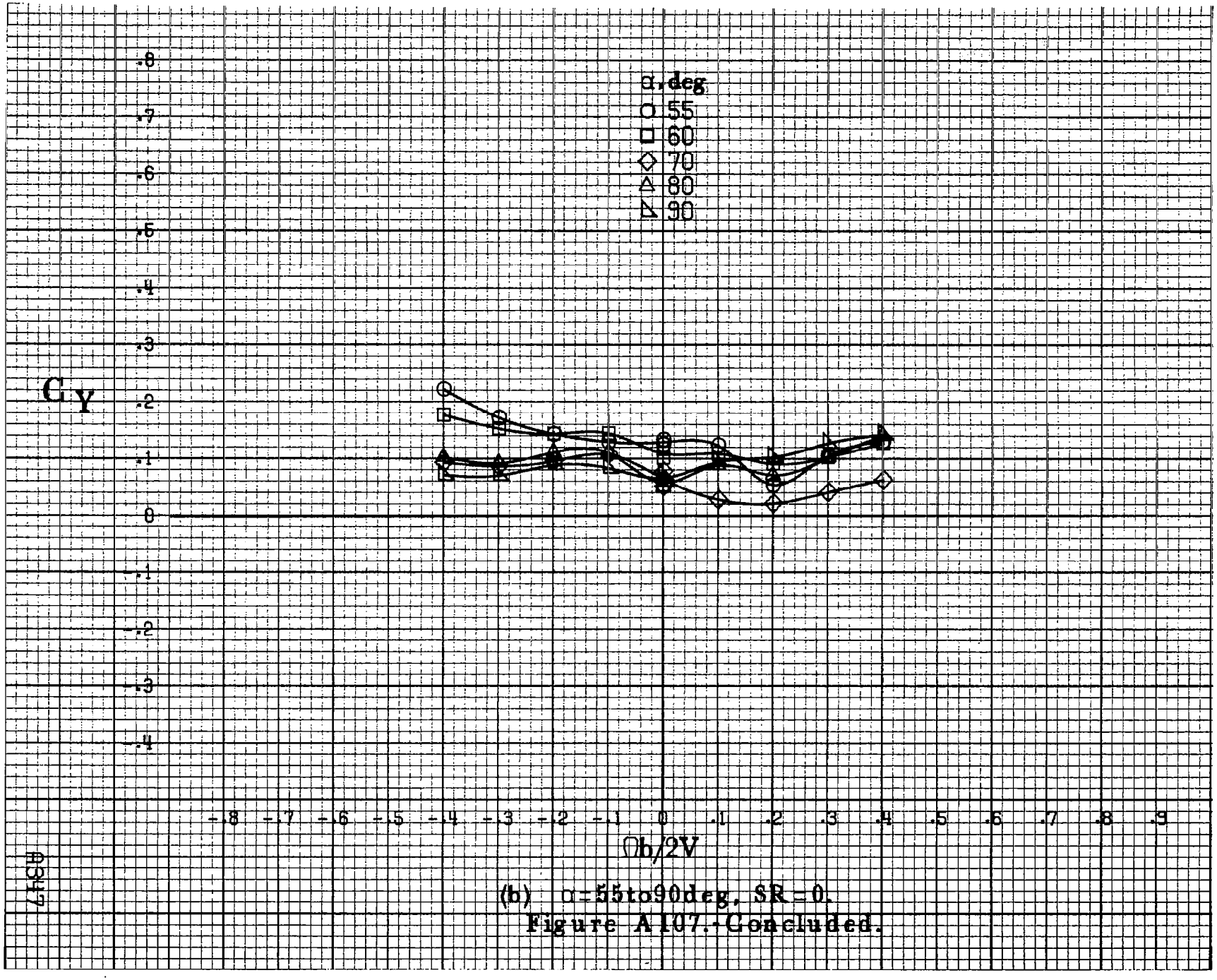

(b) α=55to90deg, SR=0.

Figure A107.-Concluded.

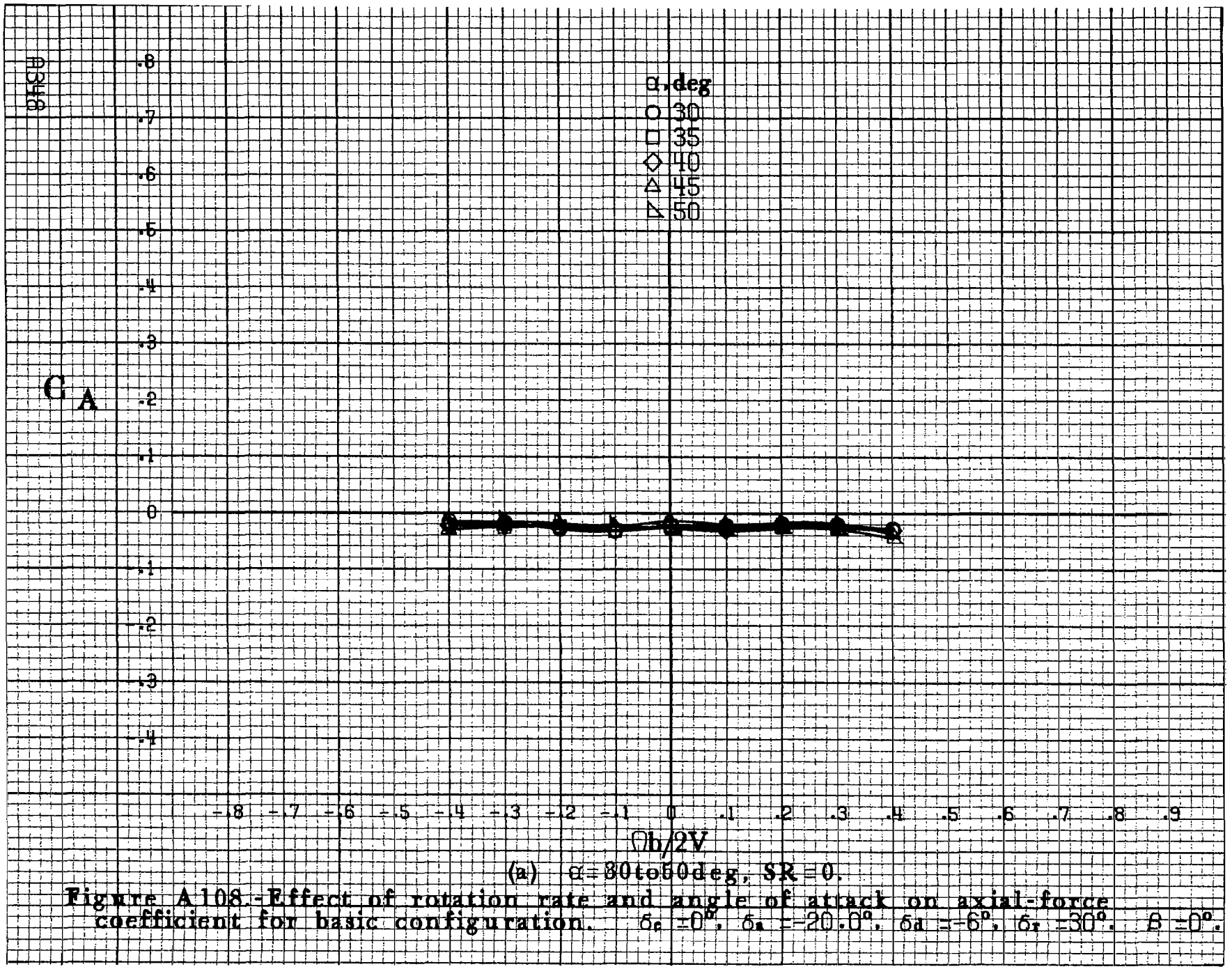

(a) $\alpha = 30$ to 50 deg, SR = 0.

Figure A108.- Effect of rotation rate and angle of attack on axial-force coefficient for basic configuration. $\delta_e = 0°$, $\delta_s = -20.0°$, $\delta_a = -6°$, $\delta_r = 30°$, $\beta = 0°$.

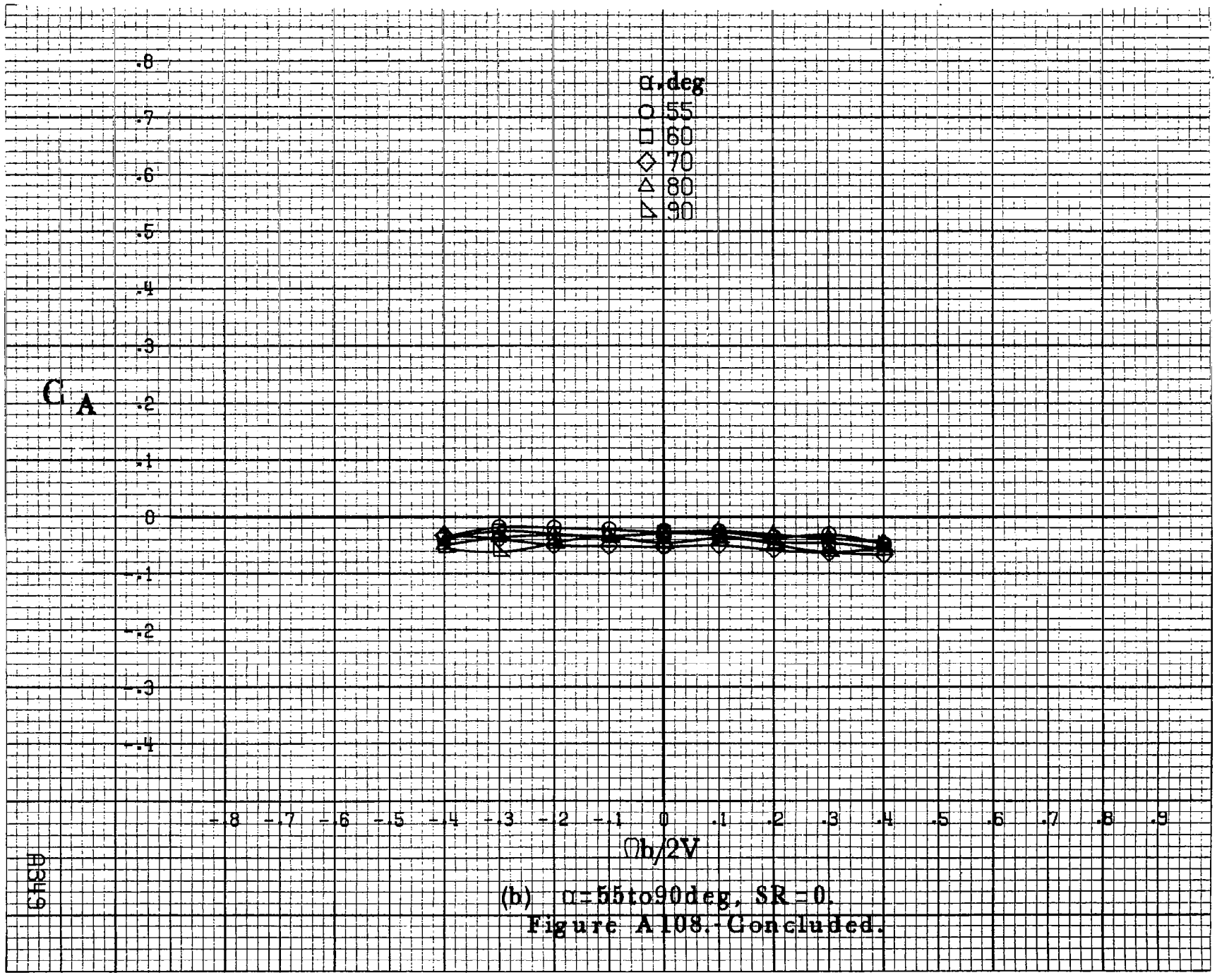

(b) α=55to90deg, SR=0.

Figure A108.- Concluded.

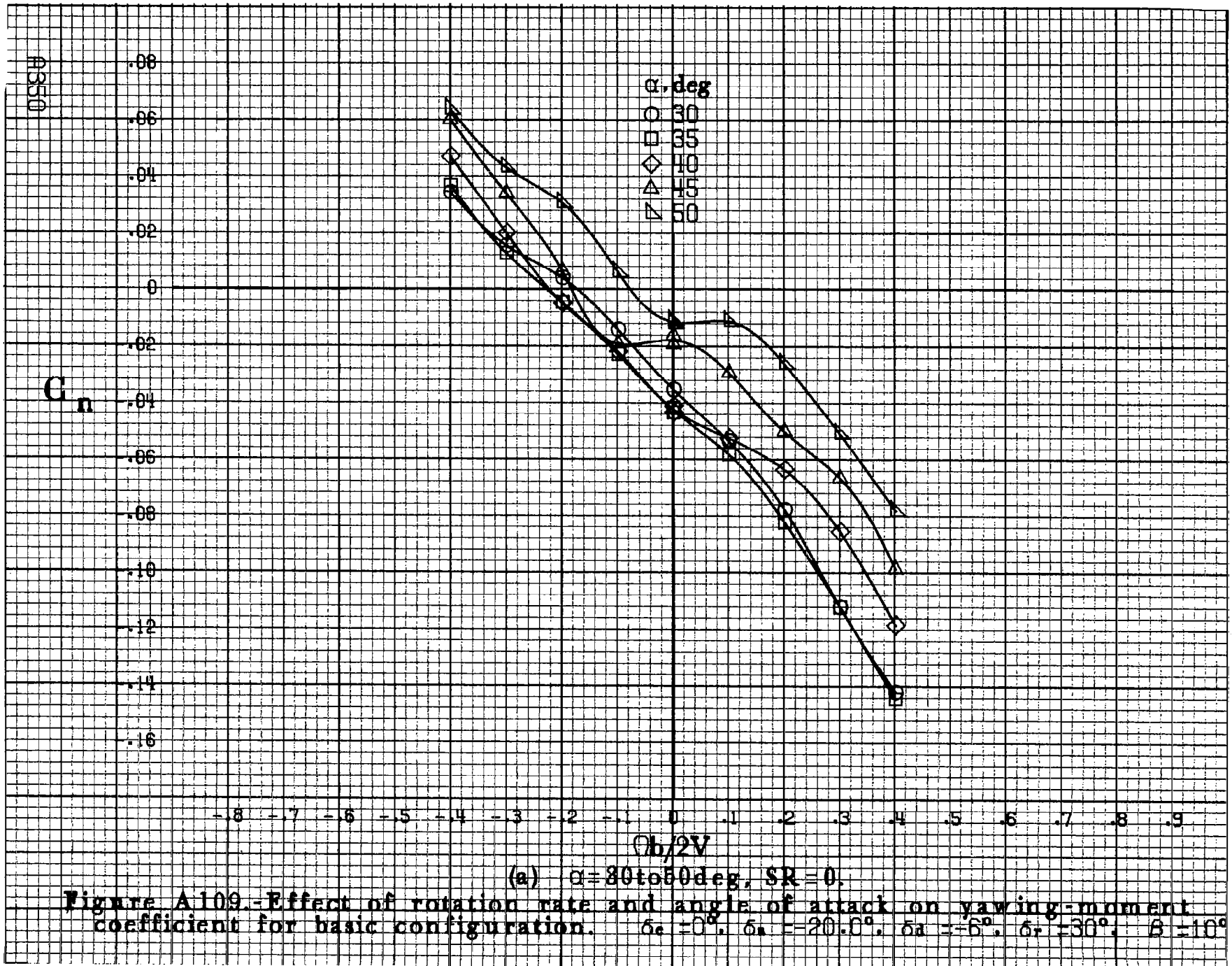

(a) $\alpha = 80$ to 50 deg, SR = 0.

Figure A109.- Effect of rotation rate and angle of attack on yawing-moment coefficient for basic configuration. $\delta_e = 0°$, $\delta_a = -20.0°$, $\delta_a = -6°$, $\delta_r = 30°$, $\beta = 10°$

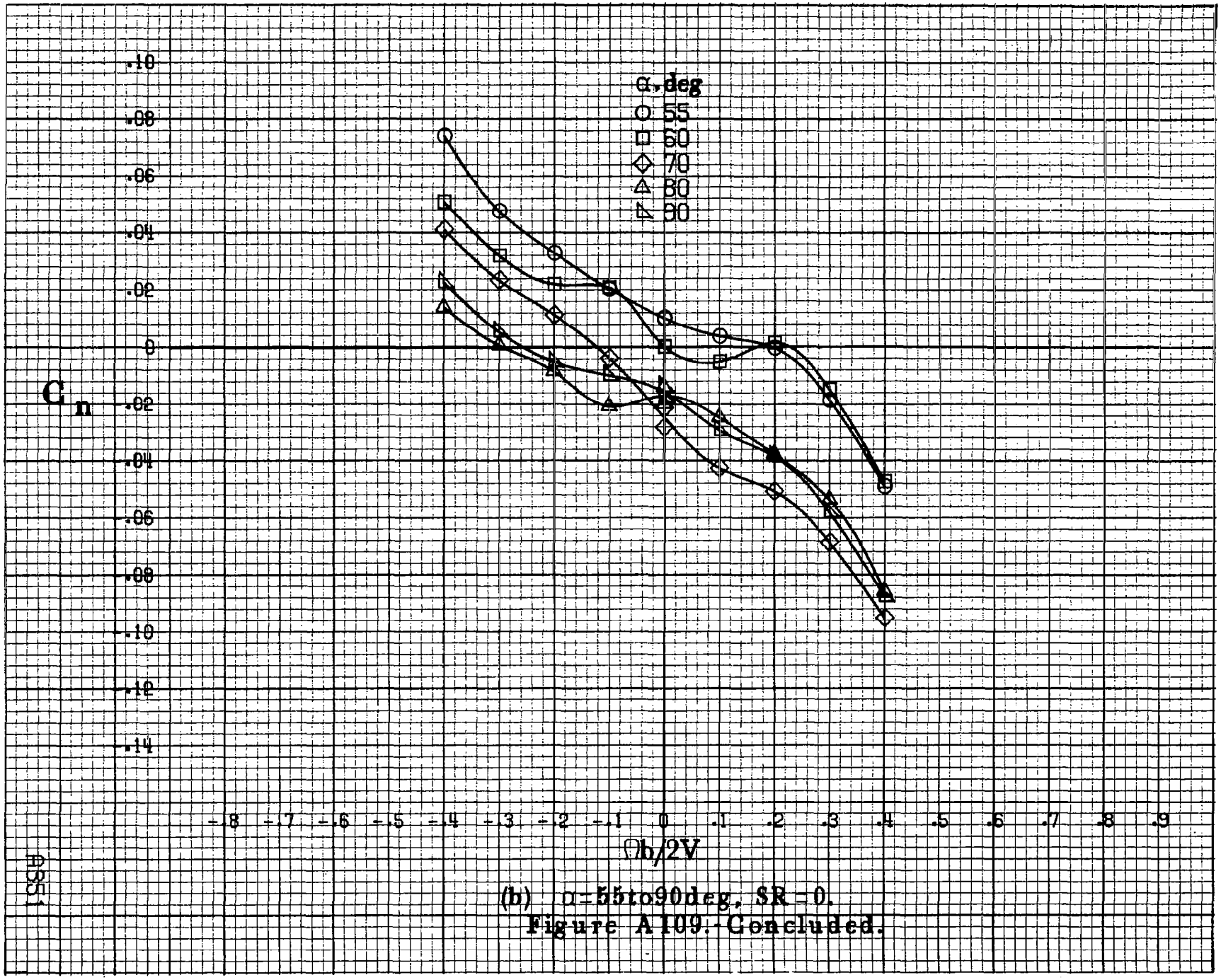

(b) $\alpha = 55$ to 90 deg, SR = 0.

Figure A109.- Concluded.

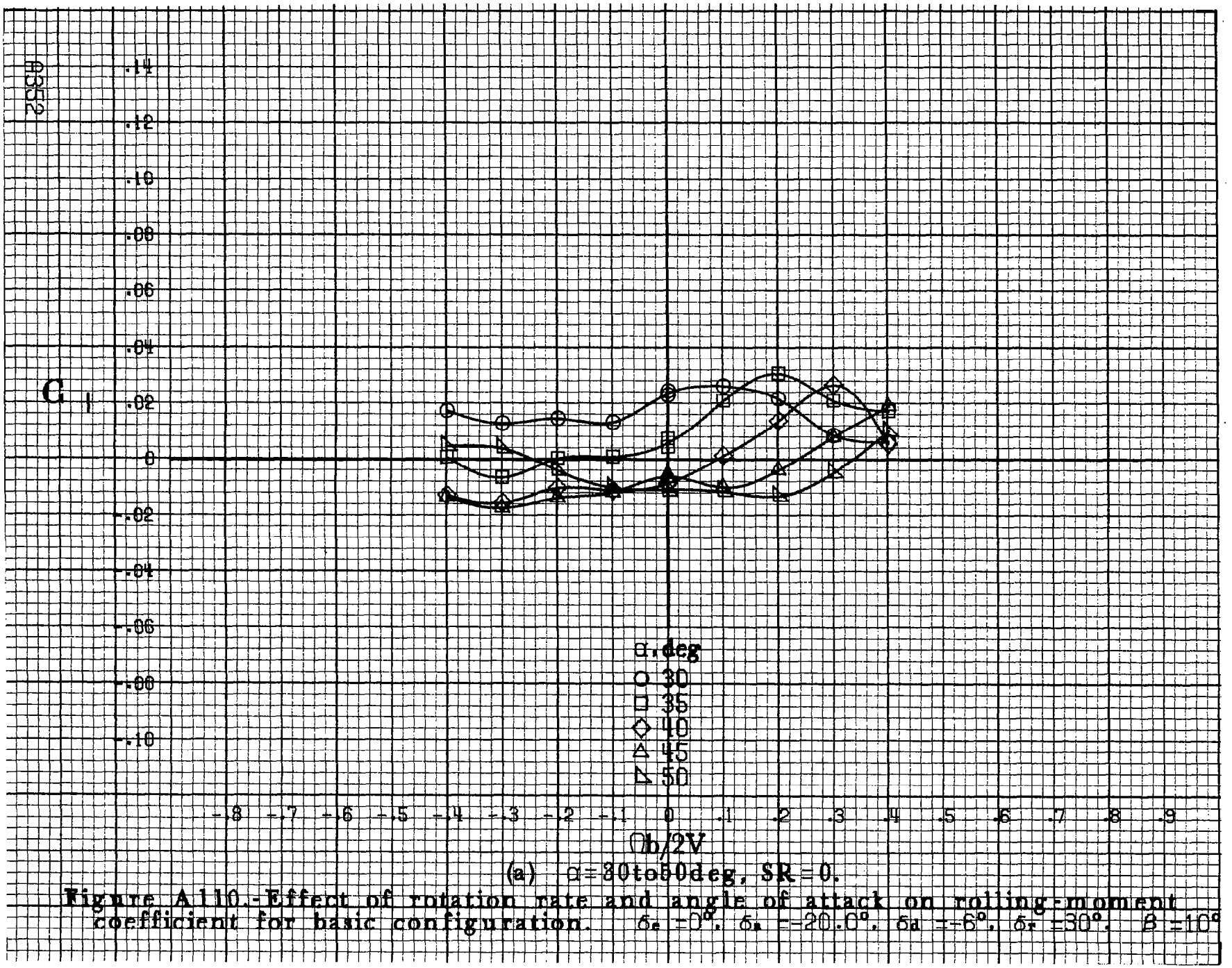

(a) $\alpha = 30$ to 50 deg, SR = 0.

Figure A110.- Effect of rotation rate and angle of attack on rolling-moment coefficient for basic configuration. $\delta_e = 0°$, $\delta_a = -20.0°$, $\delta_d = -6°$, $\delta_r = 30°$, $\beta = 10°$

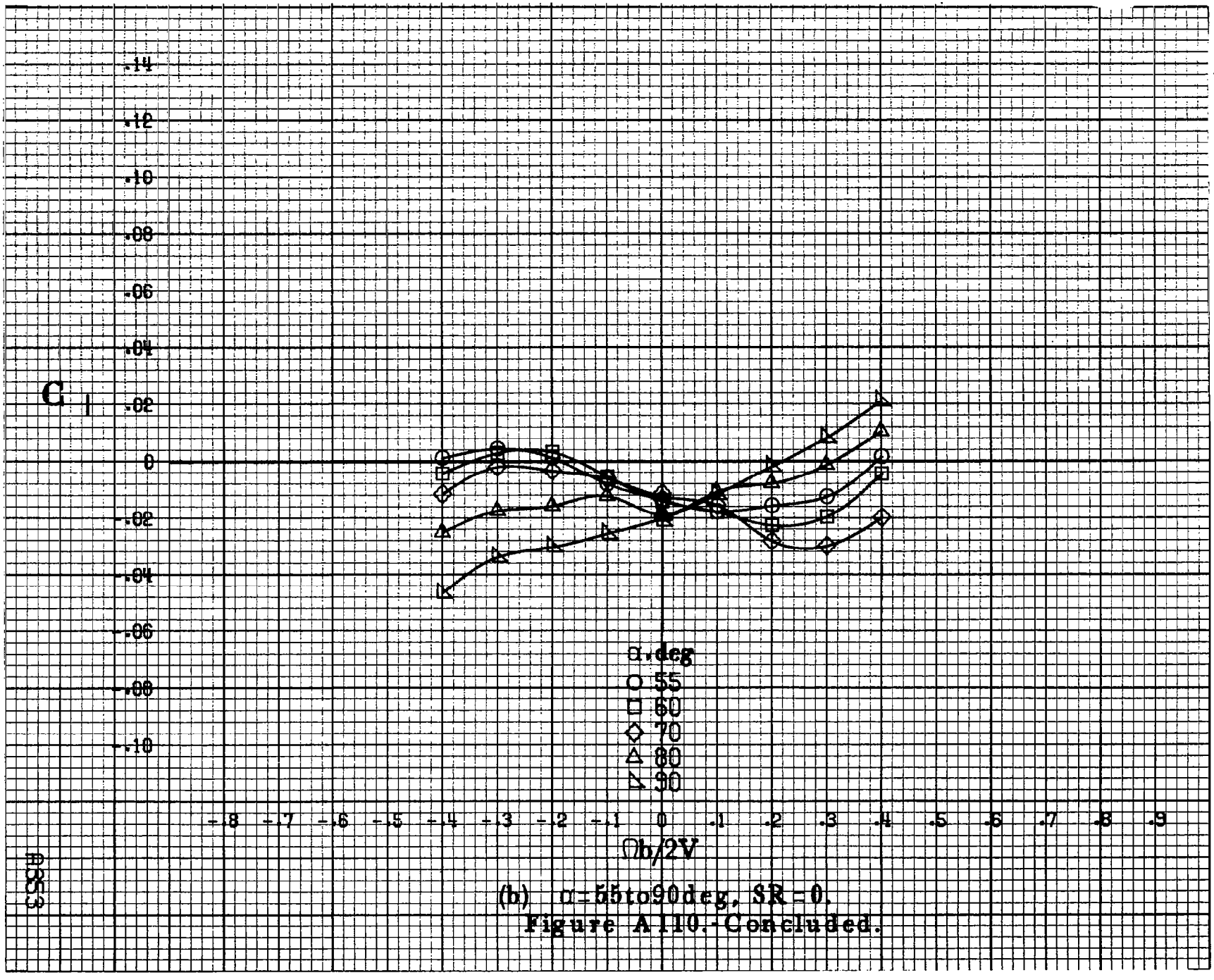

(b) $\alpha = 55$ to 90 deg, SR = 0.

Figure A110.- Concluded.

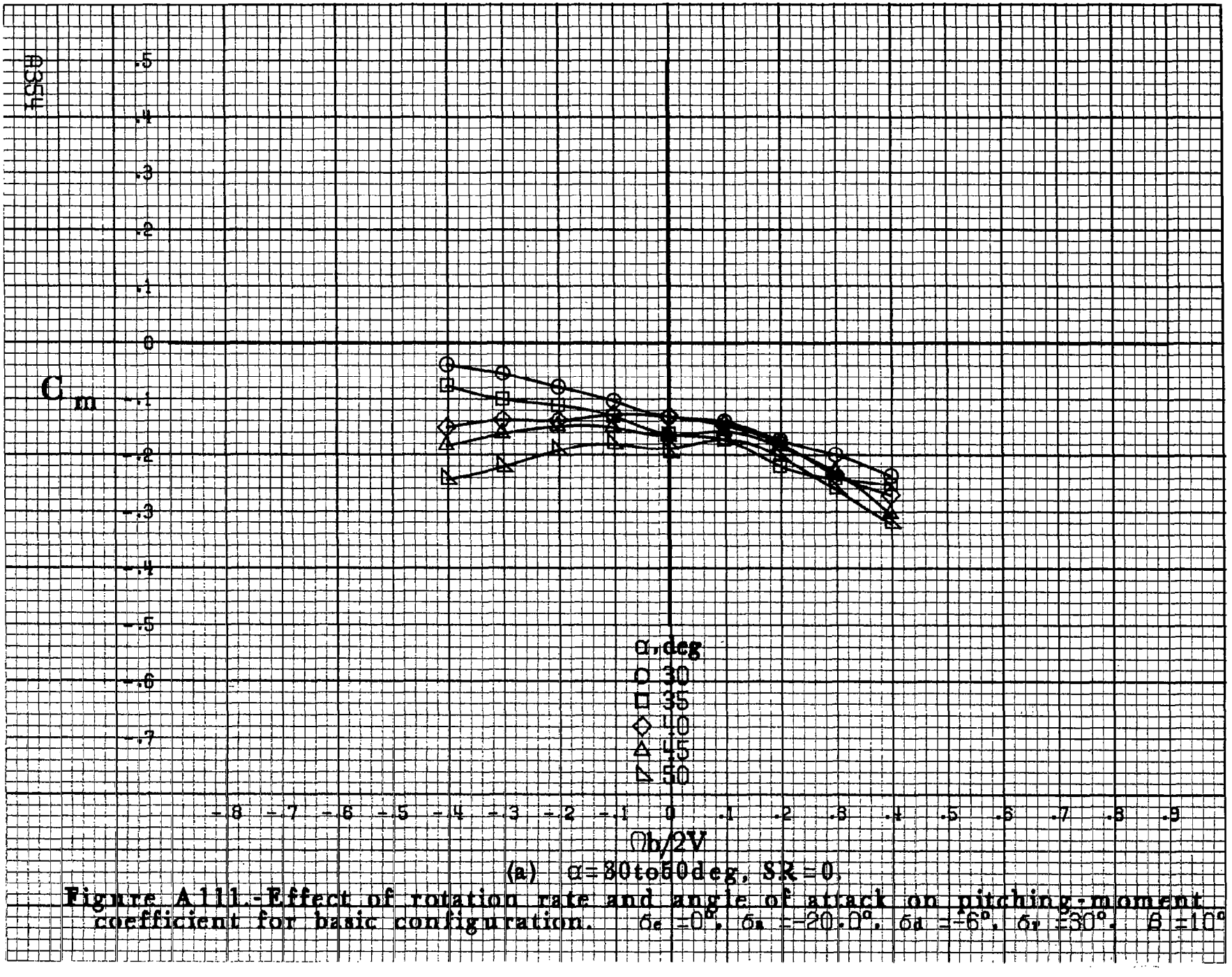

(a) $\alpha = 30$ to 60 deg, $SR = 0$.

Figure A111.-Effect of rotation rate and angle of attack on pitching-moment coefficient for basic configuration. $\delta_e = 0°$, $\delta_a = -20.0°$, $\delta_d = -6°$, $\delta_r = 30°$, $\beta = 10°$

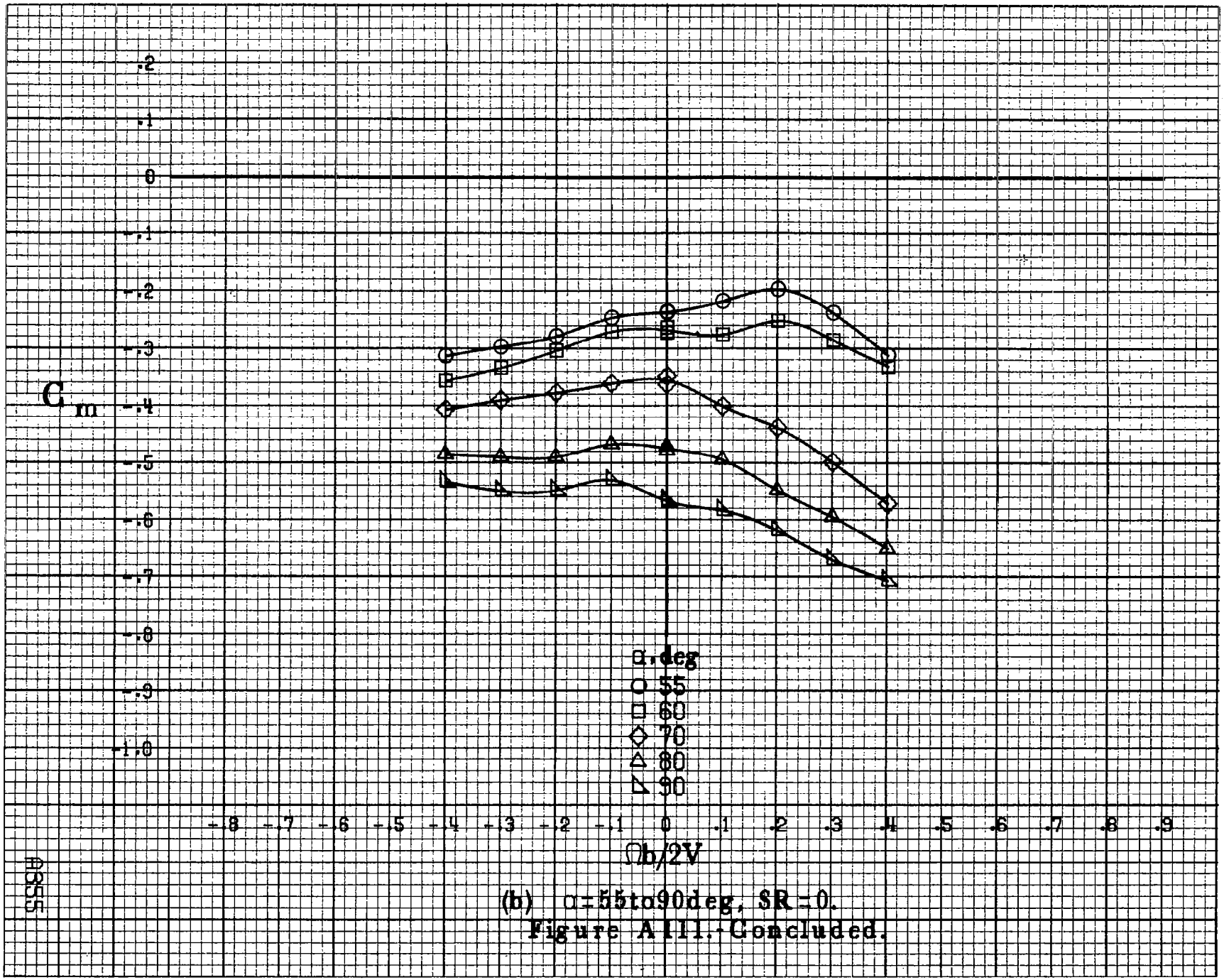

(b) α = 55 to 90 deg, SR = 0.

Figure A111.- Concluded.

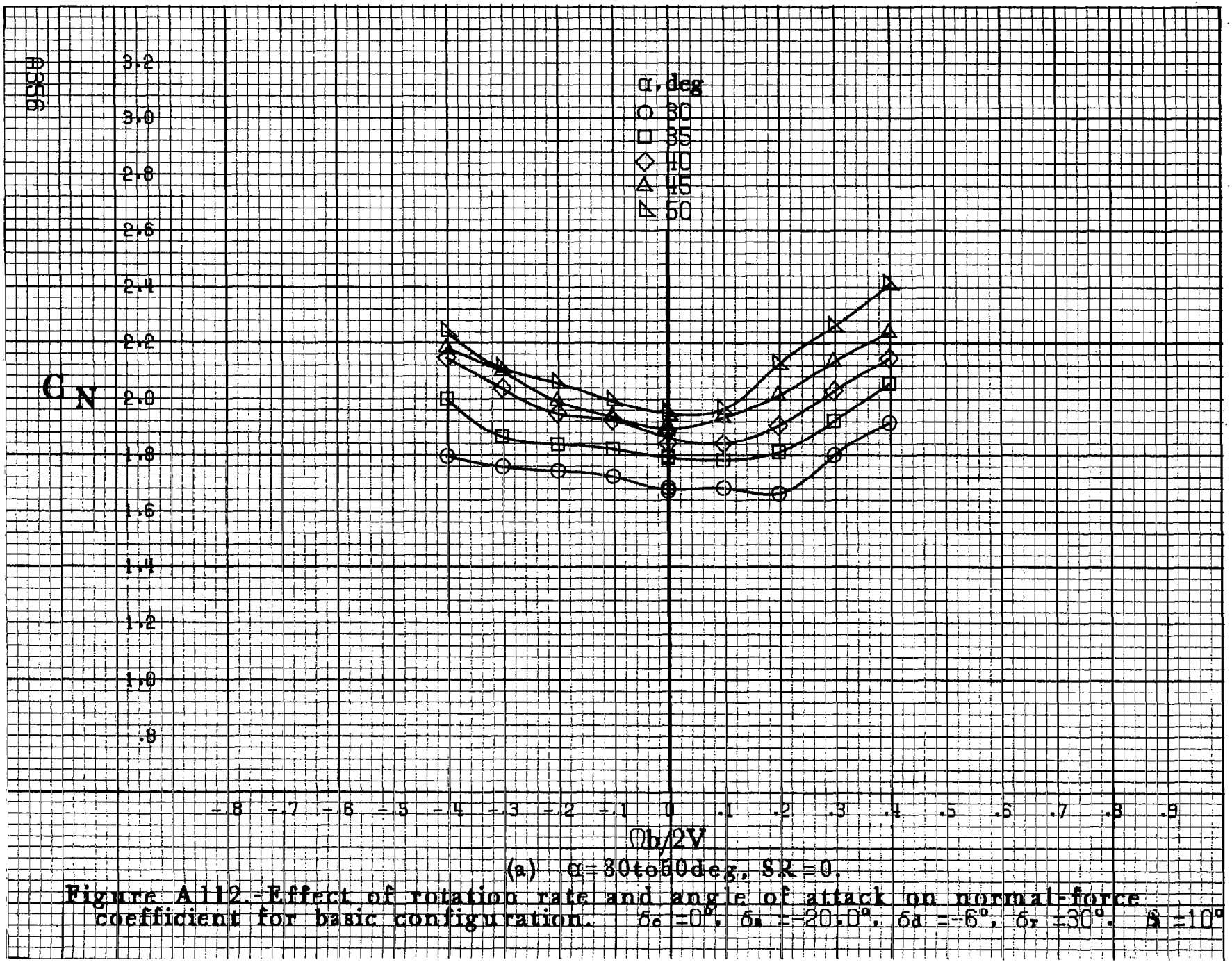

(a) $\alpha = 30$ to 50 deg, SR = 0.

Figure A112.-Effect of rotation rate and angle of attack on normal-force coefficient for basic configuration. $\delta_e = 0°$, $\delta_s = -20.0°$, $\delta_a = -6°$, $\delta_r = 30°$, $\beta = 10°$

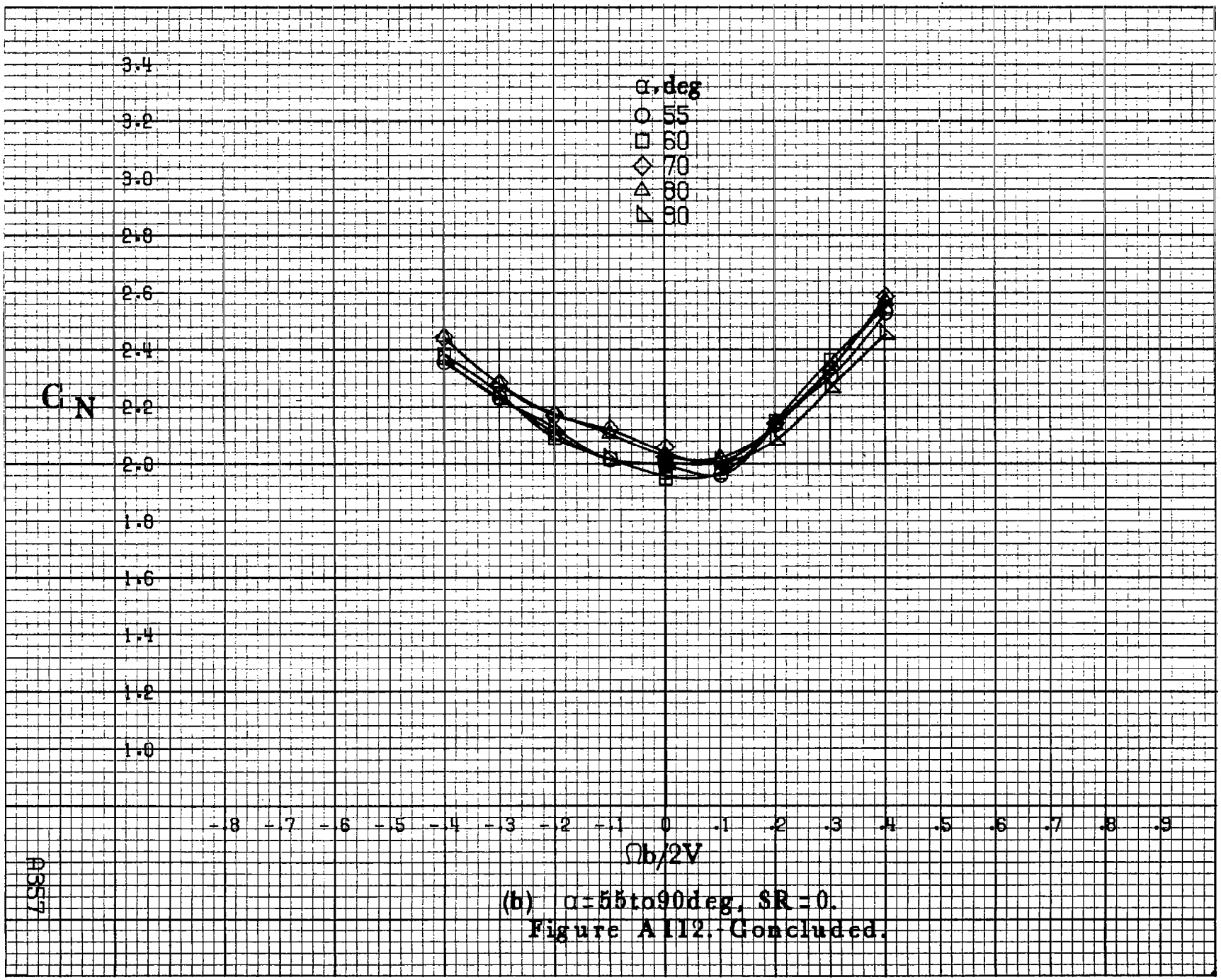

(b) α = 55 to 90 deg, SR = 0.

Figure A112. Concluded.

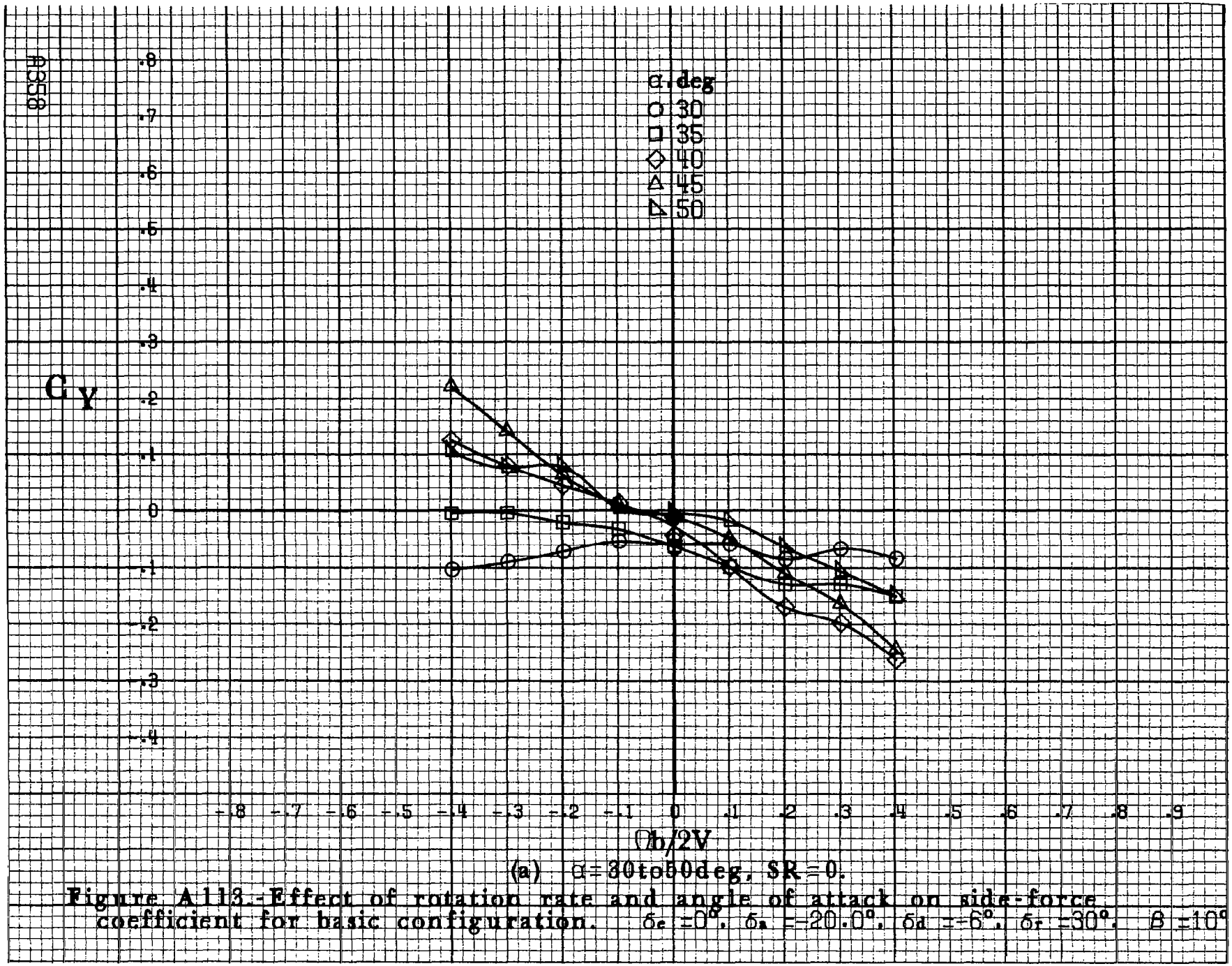

(a) $\alpha = 30$ to 50 deg, $SR = 0$.

Figure A113.-Effect of rotation rate and angle of attack on side-force coefficient for basic configuration. $\delta_e = 0°$, $\delta_s = -20.0°$, $\delta_a = -6°$, $\delta_r = 30°$, $\beta = 10°$

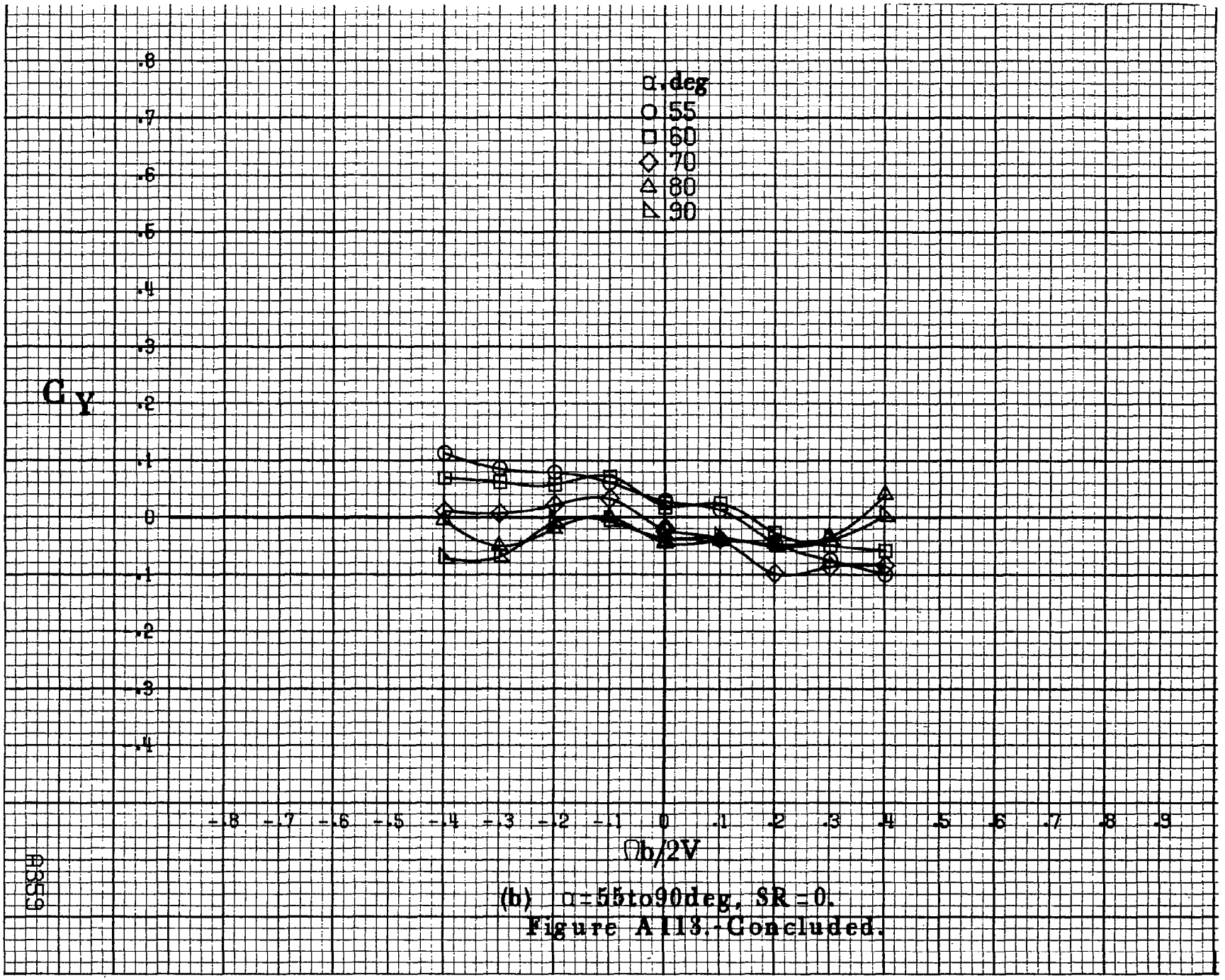

(b) α=55to90deg, SR=0.

Figure A113.-Concluded.

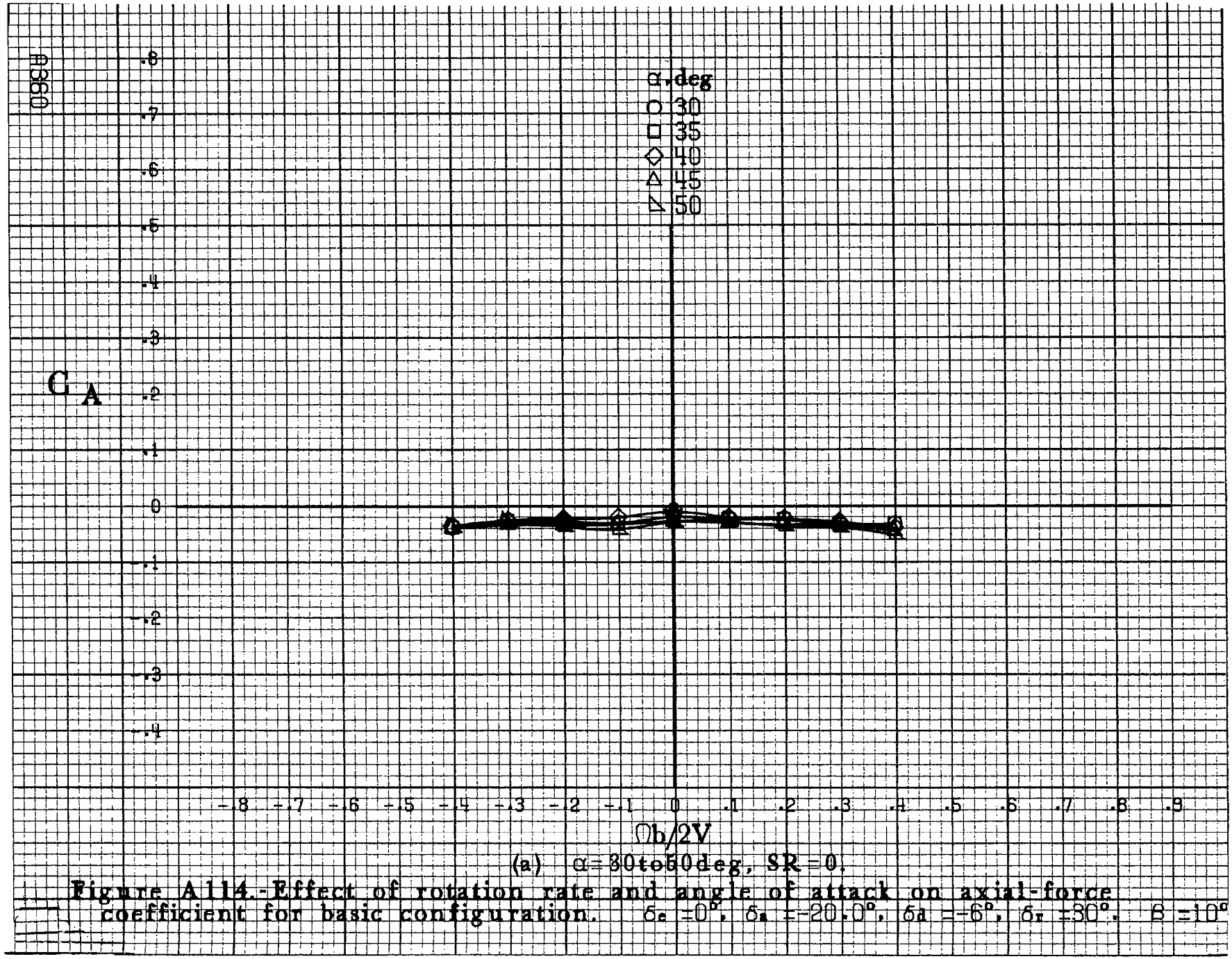

(a) $\alpha = 30$ to 60 deg, SR = 0.

Figure A114.-Effect of rotation rate and angle of attack on axial-force coefficient for basic configuration. $\delta_e = 0°$, $\delta_s = -20.0°$, $\delta_a = -6°$, $\delta_r = 30°$, $\beta = 10°$

(b) α=55to90deg, SR=0.

Figure A114. Concluded.

*U.S. GOVERNMENT PRINTING OFFICE: 1982 539-007/6 1-3

1. Report No.	2. Government Accession No.	3. Recipient's Catalog No.
NASA CR-3516		

4. Title and Subtitle	5. Report Date
ROTARY BALANCE DATA FOR AN F-15 MODEL WITH CONFORMAL FUEL TANKS FOR AN ANGLE-OF-ATTACK RANGE OF 8° TO 90°	May 1982
	6. Performing Organization Code
7. Author(s)	8. Performing Organization Report No.
Billy Barnhart	
	10. Work Unit No.
9. Performing Organization Name and Address Bihrle Applied Research, Inc. 400 Jericho Turnpike Jericho, New York 11753	11. Contract or Grant No. NAS1-16205
	13. Type of Report and Period Covered Contractor Report
12. Sponsoring Agency Name and Address National Aeronautics and Space Administration Washington, D.C. 20546	14. Sponsoring Agency Code 505-43-13-01

15. Supplementary Notes

Langley Technical Monitor: James S. Bowman, Jr.

Topical report

16. Abstract

Aerodynamic characteristics obtained in a rotational flow environment, utilizing a rotary balance located in the Langley spin tunnel, are presented in plotted form for a 1/12-scale conformal fuel tank equipped F-15 airplane model. The configurations tested included the build-up of airplane components and the basic airplane with various control deflections. Data are presented for all configurations without analysis for an angle-of-attack range of 8° to 90°, and clockwise and counter-clockwise rotations covering an $\Omega b/2V$ range from 0 to 0.4. Selected configurations are presented over an extended $\Omega b/2V$ range from 0 to 0.9. Analysis of these data is presented in another report.

17. Key Words (Suggested by Author(s))	18. Distribution Statement
Spinning Rotary balance High angle-of-attack wind tunnel data	Unclassified - Unlimited Subject Category 02

19. Security Classif. (of this report)	20. Security Classif. (of this page)	21. No. of Pages	22. Price*
Unclassified	Unclassified	378	A17

For sale by the National Technical Information Service, Springfield, Virginia 22161